INTRODUCTION OF FLUORINE INTO COALS USING N-FLUOROBENZENESULFONIMIDE.

Edward W. Hagaman and Suk Kyu Lee
Chemistry Division, Oak Ridge National Laboratory
Oak Ridge, Tennessee 37831-6201

Keywords: N-fluorobenzenesulfonimide, DCP/MAS ^{13}C NMR, fluorinated coal

INTRODUCTION

The selective introduction of fluorine into coals is under study as part of a program to define the chemical reactivity of coals through identification of reactive functional groups in the organic matrix of these solid fossil fuels. Recently, the number of reactive sites in coals as function of the strength of the organic indicator base has been determined by the C-methylation of O-methylated coals (1,2). The C-methylation was carried out by treatment of coal with carbanion bases and quenched with $^{13,14}C$ methyl iodide. The structural information derived from C-methylation of coals was limited to the number of reactive sites and an estimate of the methylene/methine site ratio (3). The generation of anions in coals is being repeated and quenched with *N*-fluorobenzenesulfonimide, **1**, (4,5), a versatile electrophilic fluorinating reagent, in order to chemically attach fluorine to the reactive carbon site. The ^{19}F nucleus provides the mechanism, dipole-dipole coupling, to selectively observe the ^{13}C nuclei in its immediate vicinity through the use of ^{1}H-^{13}C-^{19}F double cross polarization (DCP)/MAS ^{13}C NMR. In conjunction with MAS ^{19}F NMR and CP/MAS ^{13}C NMR experiments, the goal is the definition of the reactive sites in sufficient detail to discover the chemical basis for the C-H acidity of the original carbanions.

RESULTS AND DISCUSSION

O-methylated Illinois #6 coal was prepared by using tetrabutylammonium hydroxide and methyl iodide (2,6,7). The different anions of O-methylated Illinois #6 coal were prepared using fluorenyl lithium, *n*-butyl lithium, and lithium diisopropyl amine (LDA), respectively, in THF. Each of the coal anions prepared by different bases was quenched with 1 at -78°C. The reaction mixture was slowly warmed to RT and stirred for an additional 15 hours under Argon. After addition of saturated NH_4Cl, the solution was diluted with 5% NaOH solution in order to destroy the excess 1. The coal was collected by filtration, and successively washed with water, 1N HCl, water, and ethanol. The coal was extracted exhaustively with THF using a Soxhlet extraction apparatus and then dried under vacuum for 18 hours at 100°C.

The ^{19}F NMR spectrum of the fluorinated coal prepared using fluorenyl lithium and 1 shows a strong resonance at -123 ppm and a less intense resonance around -170 ppm (Figure 1). These resonances correspond to tertiary and secondary alkyl fluorides, respectively. The spectrum also contains a poorly resolved broad resonance at -100 ppm. Associated with this center band are first and second order side bands that indicate a very large static linewidth

for this band. The linewidth and chemical shift of this band are the signature of *gem*-difluorocarbon species.

The difference spectrum between the CP/MAS-^{13}C NMR spectra of the fluorinated coal prepared with fluorenyl lithium (Fig. 2a) and the O-methylated Illinois #6 precursor (Fig. 2b) is shown in Fig. 2c. Difference spectroscopy could show, in principal, the chemical shift reorganization due to the introduction of fluorine into the coal. In fact the difference spectrum is similar to the spectrum of fluorene, in the aromatic region, and indicates that the fluorenyl group is incorporated into the coal. The absence of the C(9) resonance of fluorene in the difference spectrum suggests the base is chemically attached to the coal network. The C(9) chemical shift will vary depending on the nature of the coal "substituent" at C(9), and will be distributed over a broad region. The remote aromatic carbons are less sensitive to the details of the bonding configuration at the sp^3 site. In control experiments it has been shown that physically absorbed fluorene can be completely removed by normal work-up procedures (Fig. 3). Hence, a fraction of the fluorenyl lithium reacts as a nucleophile and adds to O-methylated coal to give fluorenyl-coal linkages. These results support earlier work with [9-^{13}C]-fluorenyllithium which show reagent-derived fluorene is chemically bound to the organic coal matrix (3).

The CP/MAS ^{13}C NMR of a fluorinated coal produced using *n*-butyl lithium and 1 reveals that the *n*-butyl group is also chemically grafted into the coal. This is evident from comparison of the aliphatic region of the resolution enhanced spectrum (upper trace in Fig. 4a) of this material with the corresponding region in the spectrum of the precursor coal (Fig. 2b). The resonance of the methyl group of the *n*-butyl moiety is quite insensitive to the nature of the attachment and appears as the sharp peak at 13 ppm. The spectrum in Fig.2b does not show this resolved feature.

The CP/MAS ^{13}C NMR spectrum of the fluorinated coal produced using LDA and 1 is similar to that of the starting O-methylated Illinois #6 coal. The difference between these two spectra provides no evidence for sec-propyl amine resonances that would indicate nucleophilic addition of the base in the coal network.

While a necessary part of the background work to elucidate the chemical conversion occurring in the coal matrix the CP/MAS ^{13}C NMR spectra above do not reveal the fluorination chemistry the coal has undergone. This information is provided by the ^{1}H-^{13}C-^{19}F DCP/MAS ^{13}C NMR experiment (8). The DCP spectrum of the fluorinated coal prepared using fluorenyl lithium and 1 shows two kind of carbon resonances at 90-110 ppm and 150-170 ppm (Fig. 5). These resonances are assigned to alkyl fluoride carbons and aryl fluoride carbons, respectively. Aryl fluorides are formed by directed *ortho*-lithiation of activated aromatic rings (4).

The DCP/MAS ^{13}C NMR spectrum of the fluorinated coal prepared using *n*-butyl lithium and 1 (Fig. 4b) also shows aryl and alkyl fluoride resonance bands. The spectrum is similar to that of the fluorinated coal prepared with fluorenyl lithium and 1 (Fig. 5).

The DCP/MAS ^{13}C NMR spectrum of the fluorinated coal prepared using LDA and 1 shows only an aryl carbon resonance band.

ACKNOWLEDGEMENT

Research sponsored by the Division of Chemical Sciences, Office of Basic Energy Sciences, U.S. Department of energy under contract DE-AC05-84OR21400 with Martin Marietta Energy Systems, Inc.

REFERENCES

1. Hagaman, E. W., Chambers Jr., R. R., Woody, M. C., Anal. Chem., 1986, **58**, 387.
2. Chambers Jr., R. R., Hagaman, E. W., Woody, M. C., Smith, K. E., McKamey, D.R., Fuel, 1985, **64**, 1349.
3. Hagaman, E. W., Chambers, R. R., Woody, M. C., Energy & Fuels, 1987, **1**, 352.
4. Differding, E., Ofner, H., Synlett. 1991, 187.
5. Differding, E., Ofner, H., Synlett. 1991, 395.
6. Liotta, R., Rose, K., Hippo, E. J., Org. Chem. 1981, **46**, 277.
7. Liotta, R., Brons, G. J., Am. Chem. Soc. 1981, **103**, 1735.
8. Hagaman, E. W., Burns, J. H., Fuel in press.

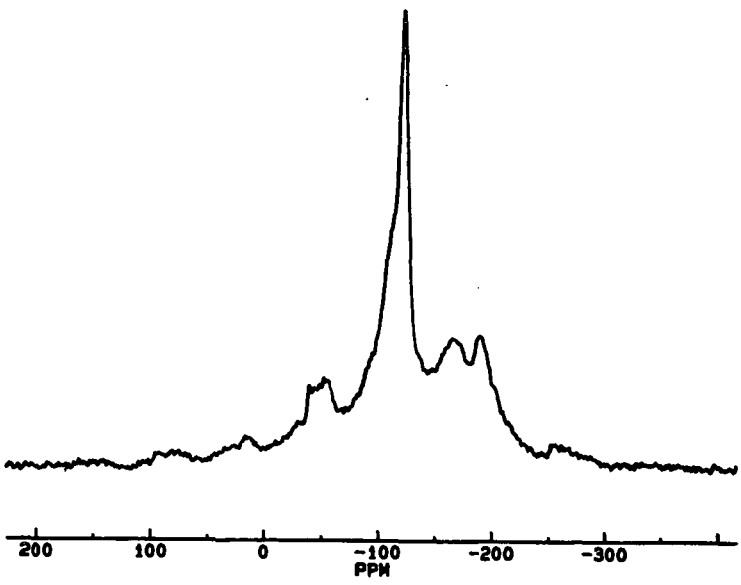

Fig. 1 MAS ^{19}F spectrum of a fluorinated coal by reaction of O-methylated Illinois # 6 coal with fluorenyl lithium and N-fluorobenzenesulfonimide.

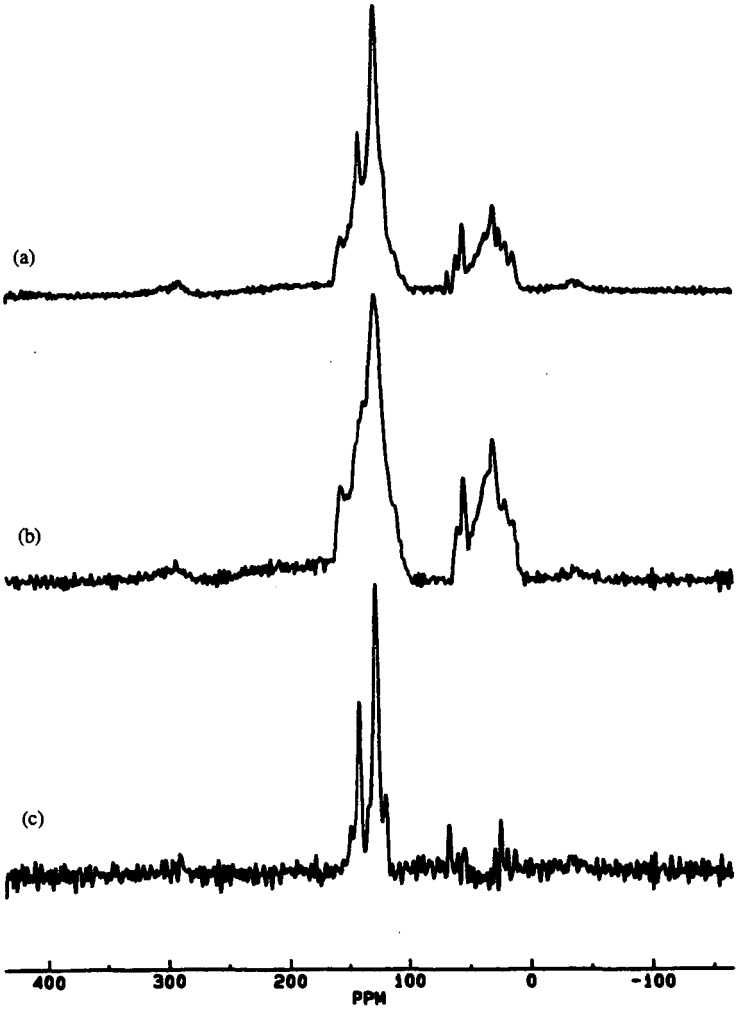

Fig. 2 (a) Resolution-enhanced CP/MAS ^{13}C spectrum of a fluorinated coal by reaction of O-methylated Illinois # 6 coal with fluorenyl lithium and N-fluorobenzenesulfonimide.
(b) Resolution-enhanced CP/MAS ^{13}C spectrum of O-methylated Illinois # 6 coal.
(c) Difference spectrum: (a) minus (b).

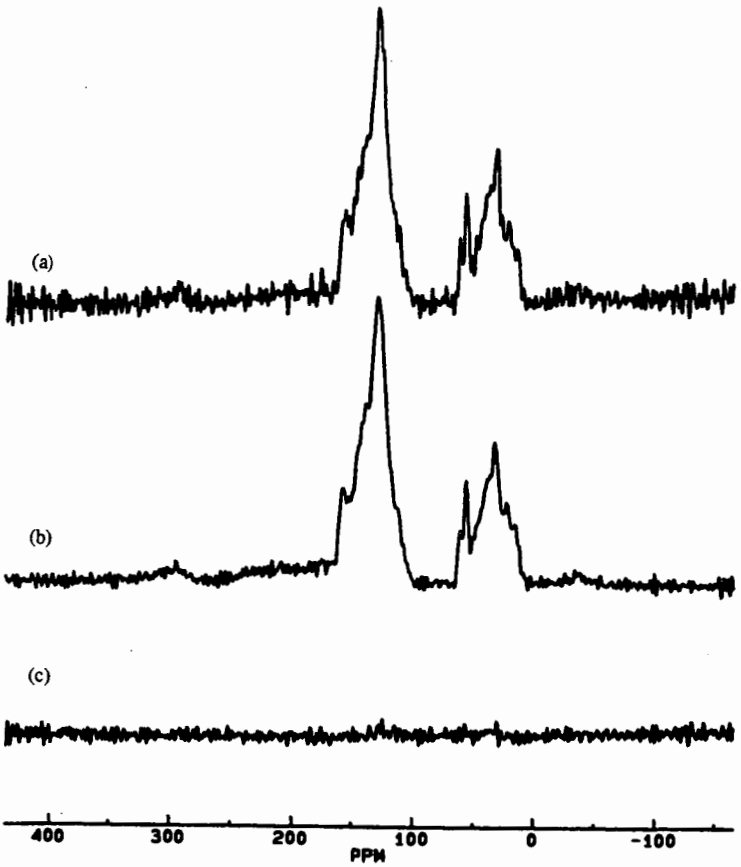

Fig. 3 (a) Resolution-enhancedCP/MAS ^{13}C spectrum of O-methylated Illinois # 6 coal which has been treated with fluorene and THF for 18hrs. and then succesively washed with 5% NaOH, H_2O, 1N HCl, H_2O, and ethanol followed by vacuum drying for 18hrs at 100 °C. (b) Resolution-enhanced CP/MAS ^{13}C spectrum of O-methylated Illinois # 6 APC coal. (c) Difference spectrum: (a) minus (b).

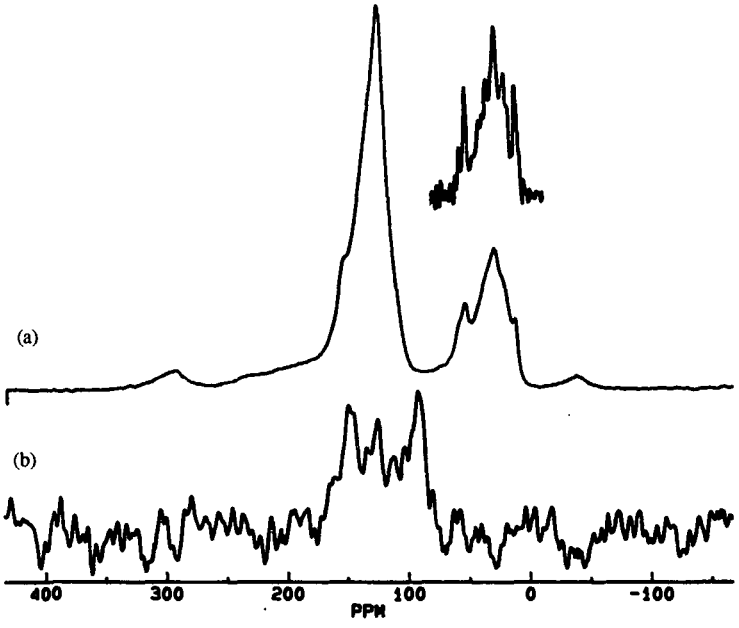

Fig. 4 (a) CP/MAS ^{13}C spectrum of a fluorinated coal by reaction of O-methylated Illinois # 6 coal with n-butyl lithium and N-fluorobenzenesulfonimide. The aliphatic region of the resolution-enhanced spectrum is plotted above the full spectrum.
(b) DCP/MAS ^{13}C spectrum of the same coal.

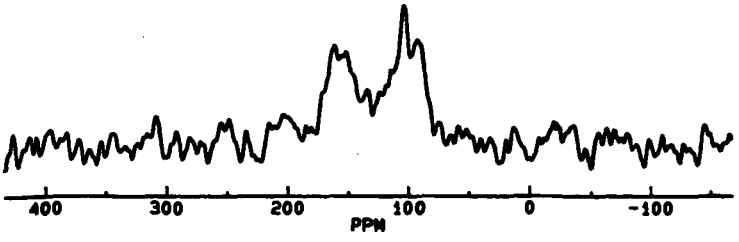

Fig. 5 DCP/MAS ^{13}C spectrum of a fluorinated coal by reaction of O-methylated Illinois # 6 coal with fluorenyl lithium and N-fluorobenzenesulfonimide.

NITROGEN XANES STUDIES OF FOSSIL FUELS.

Sudipa Mitra-Kirtley,[a] Oliver C. Mullins,[b] Jan Branthaver,[c] Jan van Elp,[d] and Stephen P. Cramer[d,e],
[a] Rose-Hulman Institute of Technology, Terre Haute, IN 47803,
[b] Schlumberger-Doll Research, Ridgefield, CT 06877,
[c] Western Research Institute, WY,
[d] Lawrence Berkeley Laboratory, Berkeley, CA 94720,
[e] University of California, Davis, CA 95616

Keywords: XANES, nitrogen, coals

All the major nitrogen chemical structures, present in coals of varying ranks have been quantitatively determined using nitrogen X-ray Absorption Near-Edge Spectroscopy (XANES). XANES spectra of these samples exhibit several distinguishable resonances which can be correlated with characteristic resonances of particular nitrogen chemical structures thereby facilitating analysis of these complicated systems. Aromatic nitrogen compounds abound in the coals; no evidence of saturated amine is found. Pyrroles, pyridines, pyridones, and aromatic amines are found in coal; of these, pyrrolic structures are the most prevalent. The low rank (high oxygen) coals have large quantities of pyridone and smaller quantities of pyridine; this suggests that with increasing maturation of coal, pyridone loses its oxygen and is transformed into pyridine. Aromatic amines are present at low levels in coals of all rank. Preliminary studies on kerogens and bitumens indicate the presence of pyrrole, pyridone, pyridine, and aromatic amine structures; some saturated amine may also be present. Other models containing multiple oxygen and nitrogen sites have been investigated and they may be present in bitumens and low rank coals in small quantities.

INTRODUCTION

Coal is a valuable natural resource. The origin of the organic part of coal stems from plant materials, which over geological time, become compacted, and mature into coal beds due to severe physical conditions such as heat and pressure. Heteroatoms such as nitrogen and sulfur present in fossil fuels pose major problems in the effective usage of the resource. Heteroatoms in coals often act as catalyst poisons; upon combustion of coal, heteroatoms evolve gases which are harmful to the environment. Heteroatoms also help in the determination of solubility and chemical properties of coal. Heteroatoms also provide markers to follow evolution of the chemistry of coal with maturation.

The rank of coal by definition is a measure of the degree of metamorphism of coal beds, higher rank indicating greater maturation. During the process of maturation, moisture and chemically bound oxygen are expelled from coal beds, and consequently, higher rank coals have lower oxygen and moisture content than lower rank coals. Aromaticity increases with maturation; carbon aromaticity can range from 90% in a high rank coal to 40% in a low rank coal. Oxygen, which is the major heteroatom present in coals, occur as furan analogues, phenolic analogues, and etheric groups. Sulfur is present in coals both in aromatic and saturated forms. X-ray Absorption Near-Edge Structure (XANES) spectroscopy has been used for the last ten years to successfully determine the major sulfur chemical forms present in coals(1-4). Thiophenic (aromatic) sulfur is the dominant type, followed by sulfidic (saturated) type of sulfur. Oxygen containing sulfur forms such as sulfoxides, sulfones and sulfates are also found in coals, as well as mineral pyritic sulfur(2,4).

Kerogens are the organic insoluble, and bitumens are the organic soluble fractions of oil shales. The maturation process is somewhat similar to coal maturation; however, the maturation process of kerogen results in the production of crude oil. The H:C ratio of both immature kerogens and bitumens is typically ~1.5. Most of the carbon exists in aliphatic forms, and nitrogen and oxygen are present in greater amounts than sulfur.

Nitrogen has been difficult to study in fossil fuels; the high molecular weight of coals hinder chromatographic measurements, and the low concentrations of nitrogen in coal make spectroscopic measurements difficult. X-ray photoelectron studies in coal

have been informative, but the limited energy resolution hinders determination of all major forms of nitrogen(5,6). Nitrogen studies have also been difficult in kerogens and bitumens; insolubility of kerogens and complex structures of both kerogens and bitumens exacerbate the analysis of their nitrogen chemistry. XANES methodology is direct and nondestructive and has already been successful in determining the different nitrogen chemical functionalities in coal (7,8) and petroleum asphaltenes(9).

The present study determines all principal nitrogen structures of coals of varying ranks; this study has also been extended to provide preliminary information about immature kerogens and bitumens. Pyrrole and pyridine are found in these samples; in addition, presence of pyridones and aromatic amines, and very small amounts of saturated amines are also found. In the low rank coals, there is less or no pyridine but considerable amounts of pyridone; in the high rank coals the pyridones lose the oxygen and become converted into pyridines. Aromatic amines, and very small amounts of saturated amines are found in both the immature kerogens and bitumens. The XANES spectra of the kerogens and bitumens suggest the presence of pyrroles, pyridones, pyridines, and aromatic amines, and perhaps small amounts of saturated amines. During the maturation process of oil shales while some biomarkers remain unaltered, several starting chemical functionalities in immature oil shales alter significantly in the production of crude oil. Our present data on the immature kerogens and bitumens suggest that there may be considerable quantities of pyridone present in them; in that case, these structures disintegrate upon reaching the crude oil stage, as our previous studies on petroleum asphaltenes(9) did not show any occurrence of pyridone structures.

EXPERIMENTAL SECTION

Our nitrogen XANES data have been collected at beamline U4B at National Synchrotron Light Source at Brookhaven National Lab; this beamline has been constructed by AT&T Bell Labs(10). We used a monochromator consisting of a grating of 600 lines/mm, and a multi-element fluorescent Ge detector(11). The pressure inside the beampipe leading to the sample chamber, as well as the sample chamber was on the order of 10^{-9}-10^{-10} torr; a cryopump and a turbo-molecular pump were used to maintain such high vacuum conditions. Samples were placed on nitrogen-free Scotch tape and were positioned inside the chamber by means of a load-lock system.

Our sample suite consisted of several coals, kerogens, bitumens, and nitrogen model compounds. The coals were obtained from Argonne National Laboratory Coal Sample Bank, IL(12), the kerogens and the bitumens were obtained from Western Research Institute, WY, and the model compounds from Aldrich Chemical Company. The models were used as received, without any further purification.

RESULTS AND DISCUSSIONS

Figure 1 plots the nitrogen XANES of several coals of varying ranks; the plots are in the order of increasing rank from the bottom to the top of the figure. Three principal regions are noticed, at ~400 eV, 402-405 eV, and 408 eV; the second region can be decomposed into three regions, at 402 eV, 403.3 eV, and 405 eV. The first resonance region at 400 eV varies considerably in intensity among the different coals, the intensity gradually increases as we move from a lower rank coal to a higher rank coal. The resonance feature at 402 eV, on the other hand, grows in intensity as we move from a higher rank to a lower rank coal. This suggests that as coal matures, the nitrogen structure identifiable with the 402 eV resonance feature transforms into a structure whose characteristic resonance is at 400 eV. The resonance feature at 403.3 eV in all the spectra varies less dramatically within different samples, and the 405 eV resonance intensity is rather small for all the plots.

Figure 2 shows the XANES plots of several kerogens and bitumens. Here we notice the three distinct resonance regions also observed in the coal plots, where the second region can be decomposed into three features. The peaks at 400 eV and ~403 eV are well pronounced in all the kerogen and bitumen spectra. the feature slightly shifted from 402 eV is very well pronounced in the bitumens, and the exact origin of such a peak is still under investigation.

XANES plots of a high rank coal, a low rank coal, a kerogen, a bitumen and analogues of five different nitrogen structures are shown in figure 3. The first resonance in the fossil-fuel spectra match well with the π^* resonance of pyridine, suggesting the presence of pyridine in these samples. The second resonance feature in the fossil-fuel spectra matches well with π^* resonance energy of the pyridone molecule. This suggests the presence of such structures in the fossil-fuel samples. The spectrum of a high rank coal has an intense pyridine peak, but a barely discernible shoulder for the pyridone signature; the opposite situation exists in the spectrum of the low rank coal, where the pyridine peak is absent, and a strong pyridone peak is present. This leads to the argument that as coals mature, oxygen is driven away, and the pyridone in a low rank coal loses its oxygen when it reaches a high rank stage and is transformed into pyridine(8). Among the kerogen and bitumen, the peak around 402 eV is relatively strong; this may be partly due to the presence of pyridone structures, as well as other oxygen nitrogen structures, and the issue is still under investigation. The kerogen and bitumen samples are immature, and considerable amounts of pyridone, as well as other oxygen containing molecules are not unexpected to be present in these samples. The third resonance in the fossil-fuel spectra corresponds in energy with the π^* resonance of the pyrrole molecule. The four fossil-fuel samples show intense pyrrole resonances, and the intensity is more or less uniform in all the four spectra. The smaller resonance feature at 405 eV in the fossil-fuel spectra can be attributed to the presence of aromatic amines, since the spectrum of an amine has a broad resonance in this region. The saturated amine spectrum shows an absence of a π^* resonance, but the presence of a σ^* resonance, which occurs at 408 eV. All the four types of fossil-fuel samples show resonances at this energy, which suggests that there may be some amount of saturated amine structures present in them.

Different nitrogen structures show π^* (or σ^*) resonances at well separated energies, as shown in figure 3. Several analogues of different structures of nitrogen have been studied previously(8,9), and it is found that all analogues belonging to the same structure exhibit π^* resonances at energies close to each other ($\Delta E \sim 0.5$eV), but well separated from the π^* resonances of the spectra of other structures ($\Delta E \sim 2$eV). This has been explained by means of the behavior of the lone pair of electrons at the nitrogen site in the molecule. When the electrons are involved in the π-cloud of the six-membered aromatic ring, as in pyrroles and pyridones, the nitrogen site is left slightly positive, and these structures show higher energy π^* resonances. In contrast, in pyridines, the lone pair of electrons are involved in the sp^2 orbital and the nitrogen site is left slightly negative; these structures show lower energy π^* resonances than pyrroles and pyridones.

A least-squares fitting program has been used in order to analyze the coal spectra. All the spectra of models and the coal samples were first normalized with respect to the respective step heights, and were then fit to a sum of several different Lorentzian peaks and an arc-tangent step. The peaks represent bound to bound electronic transitions, and the step represents transition to the continuum. Figure 4(a) shows a typical fitted spectrum of a nitrogen model compound (9-vinylcarbazole), and figure 4(b) shows the fitted spectrum of a coal (PITT). The first seven resonance features of the fossil-fuel spectra were identified to five different types of nitrogen; in order to maintain consistency, all the model and fossil-fuel spectra were fit with the same set of parameters. The relevant peaks were: 399.8 eV, $\Delta\nu$=0.8 eV (pyridine), 401.9 eV, $\Delta\nu$=0.97 eV (pyridone), 402.6 eV, $\Delta\nu$=1.3 eV and 403.7 eV, $\Delta\nu$=1.9 eV (pyrrole), 405.0 eV,

Δν=2.0 eV (aromatic amine), and 406.2 eV, Δν=1.4 eV and 407.9 eV, Δν=2.9 eV (all models including saturated amines). A continuum resonance was included to produce better fits to the data but were not used in our analysis procedure; its location was 412.8 eV, Δν=3.2 eV. The step was positioned at 408 eV, with a width of 1.5 eV. Average area values of the normalized peaks in the spectra of all analogues belonging to the same nitrogen structure were determined; these values were then used to analyze the coal spectra. For instance, the resonance at 400 eV in the fossil-fuel spectra was attributed to pyridine structure, and the pyridine contribution in the coal spectra was determined; in a likewise manner, other nitrogen contributions were also determined. Care was taken to subtract from the fossil-fuel spectra any secondary contribution arising from a different structure at the same energy as the π^* resonance of the primary structure in consideration. After determining secondary contributions from pyridines, pyridones, and pyrroles at 405 eV, the valley at this energy in the coal spectra was assumed to be "filled in" due to the presence of aromatic amine, and the aromatic amine contribution was determined. The 408 eV resonance was attributed as due to the presence of saturated amines.

Table 1 lists the percentages of the different nitrogen structures present in the coals. All the nitrogen in coals are aromatic in nature, with pyrrolic type being the most dominant. Substantial quantities of pyridinic structures are also found in the high rank coals. The low rank coals have smaller amounts of pyridine and larger amounts of pyridone, as opposed to the high rank coals; this leads to the argument that as coal matures from a low rank stage to a high rank stage, pyridone loses its oxygen and become transformed into pyridine structures. Small quantities of aromatic amine are found in all the coals.

We estimate the errors in the percentages listed in the above tables to be within 12%; there are several sources for such errors. First of all, the ratio of the intensity to the step height of different analogues of the same structure can vary significantly as seen previously, and an average value for the π^* area may introduce some errors. Secondly, the aromatic amine determination is not unique, since the aromatic amine analogues exhibit spectra with broad π^* resonances, and we have assumed that the valley at 405 eV in the fossil-fuel spectra is "filled up" due to the presence of aromatic amine in the fossil-fuel samples. Furthermore, the assignment of peaks in the fossil-fuel spectra to different nitrogen structures is somewhat arbitrary, and a slightly different position would perhaps generate a slightly different set of numbers. However, the trends would remain the same in the percentage values noted above.

CONCLUSIONS

Five different nitrogen structures have been determined by XANES methodology in several coals of different ranks. Coals have only aromatic nitrogen structures with pyrrolic types being the most dominant. Low rank coals have significant amounts of pyridone and smaller (or no) quantities of pyridine; as these coals mature over geological time to a higher rank stage, the pyridone structures lose their oxygen and become transformed to pyridine types. Aromatic amine is the other form of nitrogen found in these coals. The immature kerogens and bitumens have spectra similar to those of coals, although trends in the intensities of the different resonances among the different kerogen and bitumen spectra are not evident. The peak ~402 eV in the bitumen samples may arise from pyridone, as well as some other nitrogen structures; the matter is still under investigation

1)C. E. Spiro, J. Wong, F. W. Lytle, R. B. Greegor, D. Maylotte, and S. Lampson, Science, 226, 48 (1984)

2)G. P. Huffman, F. E. Huggins, S. Mitra Kirtley, N. Shah, R. Pugmire, B. Davis, F. W. Lytle, and R. B. Greegor, Energy and Fuels 3, 200 (1989)

3)M. L. Gorbaty, G. N. George, and S. R. Kelemen, Fuel, 69, 1065 (1990)

4)G. P. Huffman, S. Mitra Kirtley, F. E. Huggins, N. Shah, S. Vaidya, and F. Lu, Energy and Fuels, 5, 574 (1991)

5)P. Burchill, Intl. Conf. on Coal Science, (J. A. Moulijn, et al Eds.), Elsevier Science Publ.B. V., Amsterdam, (1987)

6)P. Burchill, and L. S. Welch, Fuel, 68, 100 (1989)

7)S. Mitra-Kirtley, O. C. Mullins, J. van Elp, and S. P. Cramer, Fuel, 72, 133 (1993)

8)O. C. Mullins, S. Mitra-Kirtley, J. van Elp, and S. P. Cramer, Appl. Spec., accepted.

9)S. Mitra-Kirtley, O. C. Mullins, J. van Elp, S. George, J. Chen, and S. P. Cramer, J. Am. Chem. Soc. 115, 252 (1993)

10) C. T. Chen, Nucl. Instrum. Methods Phys. Res., Sect. A 256, 595 (1987); C. T. Chen, and F. Sette, Rev. Sci. Instrum. 60, 1616 (1989)

11)S. P. Cramer, O. Tench, M. Yocum, H. Kraner, L. Rogers, V. Radeka, O. C. Mullins, and S. Rescia, X-Ray Absorption Fine Structure - Proc. 6th Intl. XAFS Conf., S. S. Hasnain Ed., Ellis Horwood Chichester, 640 (1991)

12)K. S. Vorres, Energy and Fuels, 4(5), 420 (1990)

Table 1. Percentages of different nitrogen structures found in coals of different ranks.

Samples	C	H	O	N	Pyridine	Pyridone	Pyrrole	Aniline
POC	91.81	4.48	1.66	1.34	18	8	66	8
UF	88.08	4.84	4.72	1.60	18	8	66	8
PITT	84.95	5.43	6.90	1.68	20	8	65	9
WV	85.47	5.44	6.68	1.61	20	16	55	9
UT	81.32	5.81	10.88	1.59	17	15	60	8
IL	80.73	5.20	10.11	1.43	20	19	54	7
WY	76.04	5.42	16.90	1.13	10	29	51	10
ND	74.05	4.9	19.13	1.17	2	42	50	6

*Mass fraction from K. S. Vorres, Users Handbook for the Argonne Premium Coal Sample Program, Argonne National Lab.
Normalized by nitrogen content

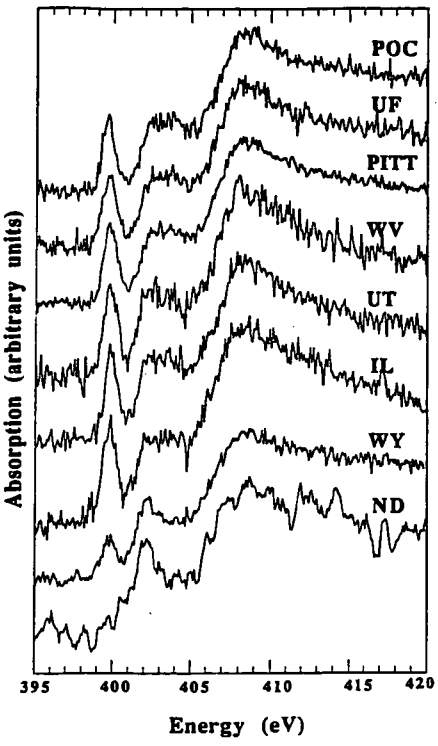

Figure 1. Nitrogen XANES of different coals. The plots are shown in order of coal rank, the higher rank being at the top.

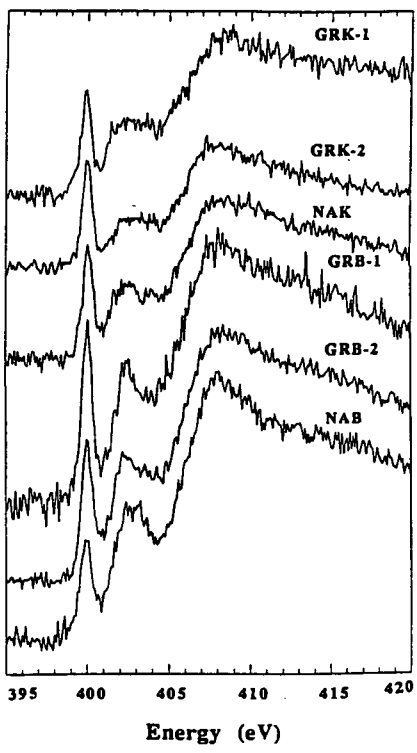

Figure 2. Nitrogen XANES of several kerogens and bitumens.

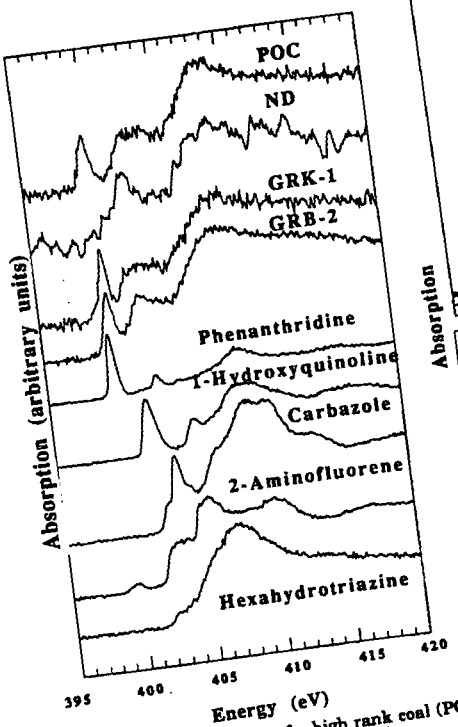

Figure 3. Nitrogen XANES of a high rank coal (POC), a low rank coal (ND), a kerogen (GRK-1), a bitumen (GRB-2), and five different nitrogen structures.

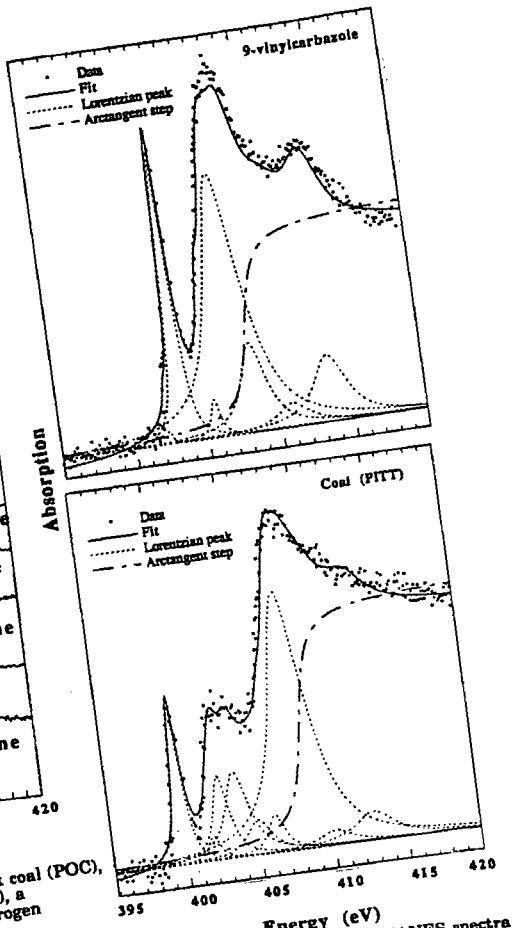

Figure 4. Least squares fit of the XANES spectra of a nitrogen model compound (9-vinylcarbazole) and a coal (PITT).

NUMERICAL MODELING OF NITROUS OXIDE FORMATION FROM CHAR COMBUSTION

Atsushi Morihara, Claes J. Tullin,
J. Derek Teare, Adel F. Sarofim and János M. Beér
Department of Chemical Engineering
and
Energy Laboratory
Massachusetts Institute of Technology
Cambridge, MA 02139

Keywords: coal, nitrous oxide and heterogeneous reaction

ABSTRACT

Growing scientific and public concerns over global warming and ozone layer depletion have led researchers to study the causes for the observed increase in ambient N2O concentrations. Man made sources, such as N2O emissions from fossil fuel combustion, have been implicated. However, the mechanism for N2O formation in coal combustion is not fully understood. It is especially difficult to deal with N2O formation since the reactions are complex. In this paper, a model for NO and N2O formation and destruction using a single particle model is discussed. The model is based on the experimental observation that the formation of N2O is dependent on the existence of both NO and O2 in the system. Numerical simulations, using the control volume method, show the effects of particle diameter and pressure. The results of the model are compared with experimental data, and show good agreement.

INTRODUCTION

Potential anthropogenic sources of N2O that have been investigated include fossil fuel combustion. Until recently, pulverized-coal combustion was implicated as the main source of N2O emission due to errors encountered in sampling. It is now known that emissions from these units are typically less than 10 ppm. Fluidized bed combustion (FBC) has emerged as an advanced method of energy production, but for current designs these units have been shown to emit more N2O than their pulverized-coal combustion counterparts[1].

In fluidized bed combustion, the emission of N2O formed from char decreases with increasing temperature, in contrast to the trend for char NO emissions that increase or pass through a maximum with increasing temperature[2][3]. The char nitrogen conversion to NO as a function of temperature has been determined by Yue using an analytical solution[4]. Yue's approach is based on first order kinetics. The complex N2O reactions, however,

preclude an analytical solution, and a numerical approach is indispensable for calculating the fraction of the char nitrogen converted to N2O.

The mechanism used in this paper is an extension of that developed by de Soete[5] in which it is postulated that (-CN) reacts with O2 to form (-CNO) and the (-CNO) next reacts with NO to form N2O. The (-CNO) can also dissociate to form NO.

FUNDAMENTAL EQUATIONS

The fundamental reactions leading to NO and N2O formation and destruction are considered to be:

$$O_2 + (-C) + (-CN) \xrightarrow{k_1} (-CO) + (-CNO) \quad (1)$$
$$(-CNO) \xrightarrow{k_2} NO + (-C) \quad (2)$$
$$(-CNO) + NO \xrightarrow{k_3} N_2O + (-CO) \quad (3)$$
$$NO + (-C) \xrightarrow{k_4} 1/2\,N_2 + (-CO) \quad (4)$$
$$N_2O + (-C) \xrightarrow{k_5} N_2 + (-CO) \quad (5)$$

NO and N2O are mainly reduced heterogeneously by carbon. The formation reaction rates of NO r_{NO} and that of N2O r_{N_2O} are given by:

$$r_{NO} = k_2[(-CNO)] \quad (6)$$
$$r_{N_2O} = k_3[NO]\cdot[(-CNO)] \quad (7)$$

The fractions of char-nitrogen transformed into NO and N2O has been shown to be roughly proportional to the fraction of carbon burnt[4]. The total nitrogen oxidization rate, f_N, is therefore equal to the product of N/C ratio and reaction rate of carbon oxidization, f_C:

$$f_N = r_{NO} + 2\cdot r_{N_2O} = \frac{N}{C} f_C \quad (8)$$

f_C in turn is calculated using reaction rate information from Smith[6]. By manipulating Eqs.(6), (7) , and (8), the concentration of (-CNO) can be shown to be:

$$[(-CNO)] = \frac{\frac{N}{C} f_C}{k_2 + 2\cdot k_3[NO]} \quad (9)$$

If we replace (-CNO) in Eqs.(6) and (7) by Eq.(9), the reaction rates of NO and N2O are given by:

$$r_{NO} = \frac{N}{C} f_C \cdot (1 - 2\alpha) \tag{10}$$

$$r_{N_2O} = \frac{N}{C} f_C \cdot \alpha \tag{11}$$

where

$$\alpha = \frac{k_3[NO]}{k_2} \cdot \left(1 + 2 \cdot \frac{k_3[NO]}{k_2}\right)^{-1} \tag{12}$$

If the NO concentration is small enough, Eqs.(10) and (11) become:

$$r_{NO} = \frac{N}{C} f_C \cdot (1 - 2 \cdot k_r[NO]) \tag{13}$$

$$r_{N_2O} = \frac{N}{C} f_C \cdot k_r[NO] \tag{14}$$

$$k_r = k_3 / k_2 \tag{15}$$

k_r is a function only of temperature. If the reaction rate of carbon oxidization is proportional to O2 concentration, then the rate of conversion of nitrogen in the char to N2O is proportional to the NO and O2 concentrations, and the rest of the nitrogen in the char is converted to NO.

CALCULATION

A material balance on a spherical shell in the carbon particle yields:

$$De_i \frac{1}{r^2}\left(r^2 \frac{\partial}{\partial r} C_i\right) + f_i(C_1, C_2 \cdots) = 0 \tag{16}$$

where Ci is the concentration of the i th species, where i can be O2, CO, CO2, NO, and N2O. De_i represents the effective diffusivity of component i calculated on the basis of Knudsen diffusion within the pores of the char particle. r is radial distance from the center of the particle. $f_i(C_1, C_2 \cdots)$ is the reaction term. The boundary conditions are given by:

$$-De_i \frac{\partial C_i}{\partial r}\Big|_{r=Rp} = k_m\left(C_i\Big|_{r=Rp} - C_i\Big|_{r\to\infty}\right) \tag{17}$$

where k_m is the external mass transfer coefficient and Rp is the particle radius[7][8].

Figure 1 shows the calculation cell of the particle, which is a portion of the spherical shell. To allow for the concentration of the reaction near the particle surface, the shell thickness decreases with increasing radius. The destruction and formation reactions are assumed to be uniformly distributed in a cell volume, and

diffusion between cells is formulated at each cell surface. For the exterior cell the diffusion to the surface is equated to the external mass transfer.

An example of a typical concentration profile is shown on the same figure. O2 is consumed near the surface of the particle. NO is also formed in this region, and it either diffuses towards the center of the particle where it reacts with the char or it diffuses to the surface where it escapes from the particle. As a result, the NO concentration in the particle is depleted at the center of the particle where the NO consumption reactions prevail, increases to a maximum nearer the surface where the NO is produced, and falls at the surface due to the NO diffusion out of the particle. N2O is formed at the same time as NO at a rate proportional to the local NO concentration. Part of the N2O is also destroyed in the particle by reaction with carbon. Because the N2O destruction rate is low the N2O concentration can increase with decreasing radius.

EXPERIMENTAL

Batch combustion experiments were performed in a small scale quartz glass bubbling fluidized bed reactor (inner diameter 57 mm). A bed of Silica sand (particle size 150-212μm), with a bed height of approximately 50 mm, was fluidized by a mixture 8 % O2 in helium. The composition and flow rate were controlled using mass flow controllers. The flow rate was set to 2.5 l/min NTP (273 K 1 atm). In each experiment, coal particles (diameter 4 mm) were burned. The concentrations of the combustion products, N2O, NO, O2 , CO2, CO, and CH4, were obtained using a FTIR spectrometer equipped with a MCT detector, and a low volume (223 cm^2) gas cell with variable path length, which was set to 7.25 m in the experiments discussed here. A detailed description of the reactor and experimental set-up can be found elsewhere[9].

The fractions of char nitrogen converted to NO and N2O as functions of carbon conversion can be calculated from the concentrations and gas flow rate. The instantaneous conversions to NO and N2O are given by:

$$f_{N_2O} = \frac{2[N_2O]}{\frac{N}{C}\Sigma([CO_2]+[CO]+[CH_4])} \tag{18}$$

$$f_{NO} = \frac{[NO]}{\frac{N}{C}\Sigma([CO_2]+[CO]+[CH_4])} \tag{19}$$

COMPARISON

The effect of particle radius on the fraction of fuel nitrogen converted to NO and N2O is shown in Figure 2. These calculations were performed by assuming a shrinking particle model. The calculated conversions to NO and N2O, which are functions of the shrinking sphere radius, are compared with the data. The conversion to NO decreases with increasing radius, while the conversion to N2O

increases. The calculated results show the formation and destruction of both NO and N2O . The ratio of N2O formation rate to total rate increases with increasing radius, since the NO concentration in the pore increases with increasing radius.

With the model in this way effectively validated by comparison with data at atmospheric pressure, it is reasonable to use it for prediction of behavior at higher pressures. For example, one can calculate the effect of decrease in the external mass transfer coefficient due to increase in pressure. The effect of this is shown in Figure 3. The conversions of the fuel nitrogen to NO and N2O can be shown, from consideration of the governing equations, to be functions of four dimensionless groups: three Thiele moduli $R_p\sqrt{k_{O_2}/D_e}$, $R_p\sqrt{k_{NO}/D_e}$, $R_p\sqrt{k_{N_2O}/D_e}$, and the Biot number $k_m R_p/D_e$, where k_{O_2}, k_{NO}, and k_{N_2O} are the rate constants for the reactions of O2, NO, and N2O with char, k_m is the external mass transfer coefficient, and D_e the effective diffusivity in the pores of the particle. Only k_m is a function of pressure since it is directly proportional to the bulk gas diffusivity, which in term is inversely proportional to pressure. The model can therefore be used to predict the effect of pressure by varying the Biot number. These results, for representative values of the Thiele moduli, are shown in Figure 3. The predicted results show that NO decreases with increased pressure, consistent with the limited available measurements.

Thus the model, based on comparatively simple formation and destruction mechanisms, yields good agreement between experimental data and the calculation results.

CONCLUSION

For the conditions studied (a Newland, Australia bituminous coal) as the char conversion increases, the conversion of char nitrogen to NO increases, approaching one in the limit, while that to N2O decreases with decreasing radius.

The results can be well modeled by assuming that, as the char is oxidized, the associated char nitrogen is converted to either N2O or NO, with the split depending on the local NO concentration, and that there is a subsequent partial reduction of the NO and N2O as these species diffuse through the porous char to the particle surface.

REFERENCES

1. M. D. Mann, M. D. Collings, and E. B. Botros "Nitrous Oxide Emissions in Fluidized-bed Combustion: Fundamental Chemistry and Combustion Testing." Prog. Energy Combust. Sci. 1992, Vol.18, pp. 447-461
2. Atsushi Morihara, Claes J. Tullin, Adel F. Sarofim and János M. Beér "Oxidization of Char Nitrogen: Extrapolation of Results from Fluidized Bed Reactors to Pulverized Coal Flames" 7 th Topic Oriented Technical Meeting, May 1993

3. Claes J. Tullin, Adel F. Sarofim and János M. Beér "NO and N2O Formation for Coal Combustion in a Fluidized Bed: Effect of Carbon Conversion and Bed Temperature" (Submitted to Energy & Fuel, April 1993)
4. G. X. Yue, F. J. Pereira, Adel F. Sarofim and Janós M. Beér, "Char Nitrogen Conversion to NOx in Fluidized Bed", Combustion Science and Technology, 1992. Vol. 83, pp. 245-256
5. G. G. de Soete "Heterogeneous N2O and NO Formation from Bound Nitrogen Atoms during Coal Char Combustion" Twenty-Third Symposium (International) on Combustion, 1990, pp. 1257-1264
6. I. W. Smith "The Combustion Rates of Coal Chars: A review" Ninth Symposium (International) on Combustion Institute, 1982, pp. 1045-1065
7. Octave Levenspiel "Chemical Reaction Engineering" Second Edition, John Wiley & Sons, Inc. pp. 357-401, 1972
9. Claes J. Tullin, Adel F. Sarofim and János M. Beér "Formation of NO and N2O in Coal Combustion: The Relative Importance of Volatile and Char Nitrogen" 12 th International Conference on Fluidized Bed Combustion, pp. 599-609, May 1993

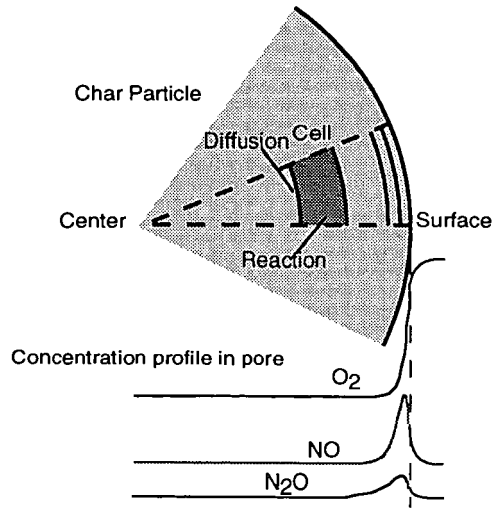

Figure 1 Calculation method and concentration profiles in the particle

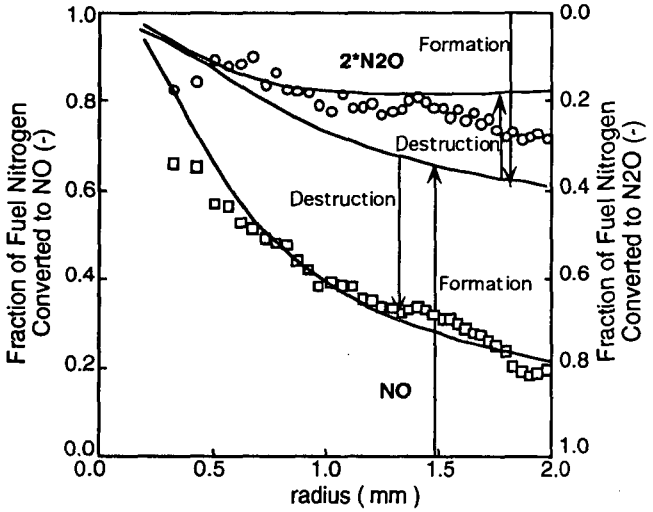

Figure 2 Effect of particle radius
on char nitrogen conversion rate to NO and N2O

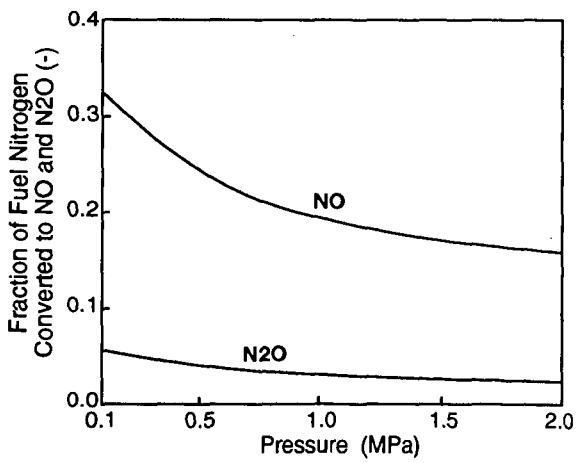

Figure 3 Effect of pressure on char nitrogen conversion rate to NO and N2O

Effect of Unleaded Fuel on Octane Requirements of Automobile Engines

R G Temple, Department of Chemical Engineering & Applied Chemistry, Aston University, Aston Triangle, Birmingham B4 7ET, UK.

J Ahmed, Energy Technology Support Unit, Harwell, Oxfordshire OX11 0RA, UK.

Unleaded fuels are increasingly supplanting lead-treated fuels throughout the world. Initiatives in the USA, in Europe and in many industrialised countries are leading to social and legislative constraints against the use of lead compounds as additives. Alternative gasoline formulations are being developed to restore the octane rating, which for more than fifty years has been boosted by lead. Initially, increased proportions of aromatics were included in the gasoline fraction, but these also have undesirable environmental consequences and substitute oxygenates (alcohols, ketones and ethers) are proving to be excellent octane boosters.

Apart from their octane rating benefits, the use of lead compounds has other consequences. Like certain other metals, lead provides some lubricant properties, eg with inlet and exhaust valve operation. Continuous provision of a miniscule layer of lead on metallic surfaces inside the combustion chamber proved inadvertently to be highly effective as a lubricant for adjacent surfaces sliding against each other at the very high frequency required. Using lead-free fuels may in the long-term alter the life of inlet and exhaust valves and valve stems and other engine components but no great concern on this matter has yet been heard. However a notable feature of the use of lead-free fuel is the progressive increase of octane requirement. Initially, ie, with a new engine, or with "clean" reconditioned surfaces, octane number is determined by the fuel formulation. Then with lead-free fuel a small but steady increase in octane requirement is noted. This has been attributed to the changed nature of combustion chamber deposits compared with the deposits from leaded fuels.

Combustion chamber deposits may affect octane requirements in three ways:

1) by occupying physical volume
2) by surface activity catalysing (or inhibiting) combustion reactions
3) by heat transfer effects due to changed thermal conductivity.

In our work at Aston we were most concerned with the physical properties of deposits studying the nature of the solid layers with scanning electron microscope to establish comparisons of porosity. Measurement of thermal conductivity was also undertaken since deposit surface temperature is almost certainly a key factor in knock-related reactions which determine octane requirements.

The nature of combustion chamber deposits

High boiling point hydrocarbons condense on the cooled walls and are partly burned off leaving a carbonaceous layer. With leaded fuels a layer of condensed lead compounds will cover and mingle with the carbonaceous layer. Lead oxide initially deposited will form lead salts - halides and sulphates. At low

temperatures, halides are favoured. As the engine warms up only the highest boiling hydrocarbons condense, leading to less carbonaceous material but the lead salts continue to build up, progressively increasing the deposit thickness. The deposit reduces heat transfer to the cooling water leading to increased deposit surface temperature. At this higher temperature lead sulphate formation is favoured.

Deposit removal

Volatilisation effects, which lead to some removal of deposit material, depends on engine operating conditions, higher chamber temperatures leading to greater deposit removal. Changes in chemical composition of deposits were similar to changes resulting from higher wall temperatures suggesting that the insulating effect of the deposit causes significant surface temperature increase as the deposit builds up.

Since engines are commonly run intermittently desposits will be formed in layers so that the deposit presents a stratified structure. Changes in chemical nature of the deposit would be expected as the total deposit layer increases in thickness.

As the deposit layer increases, internal temperature gradients will be set up and are likely to lead to flaking. Any mechanical or thermal shock will accelerate flake detachment. Flecking, or the detachment of small flakes, is also recognised on very thin deposit layers.

Deposit Adhesion

Adhesion of the deposit layers is partly chemical in nature. At higher temperatures the carbonaceous material will be oxidised forming a link between deposit and wall metal and then between successive deposit layers.

Deposits from Leaded Fuel

The introduction of lead into fuel is reported to lead to a four-fold increase in deposit weight. Dumont[1] showed that 25% of the resulting ORI (octane requirement increase) was due to volume effect and remainder to the insulating effect.

The carbonaceous portion of the deposit also depends on the type of crank-case oil and the amount of oil reaching the combustion chamber surfaces. Synthetic (polymer) lube-oils gave lower ORI values than conventional lube oils. However C^{14} tracer experiments have indicated that the fuel is responsible for 70% of the deposit.

Comparison of thermal conductivity

In our work we assessed thermal conductivities in a method designed to simulate *in situ* conditions. Every attempt was made to avoid disturbance of deposit with partial destruction of the porous structure. Heat Flow from a copper bar of larger radius than the piston was monitored as shown in fig 1. It was impracticable to ensure a completely flat contact surface owing to the irregular nature of the deposit surface.

The lower end of the copper bar was drilled to house four 0.75 kW cartridge heaters. Variable voltage input enabled several steady state readings to be obtained for calculation of effective thermal conductivity.

Assessment of permeability and porosity

These properties are important in relation to ORI since a porous deposit may trap residual combustible mixture enabling this to initiate subsequent precombustion reactions. It is also likely to trap exhaust gases discharging heat to the fresh incoming charge. Both phenomena are likely to contribute to ORI.

Permeability and porosity were measured using standard Lea & Nurse apparatus (fig 2).

Experimental Results

Lead-free fuel deposit was obtained on a car using US fuel over 1300 km of average operating conditions for a private passenger car. The leaded fuel deposit was from a similar engine in UK over 1480 km.

Thermal conductivity of the leaded-fuel deposit was 0.75 $Wm^{-1}K^{-1}$ while the lead-free fuel deposit showed a value of 0.5 $Wm^{-1}K^{-1}$. This lower thermal conductivity will naturally lead to higher surface temperature and increased tendency to induce knock. Furthermore the result of introduction of lead free fuel will be a progressive increase in octane requirement as the deposit builds up on piston head and combustion chamber walls, etc.

Volumetric effect of the deposit was also assessed. It is obvious that even a small change in deposit thickness alters compression ratio significantly. With a possible increase of compression ratio of around 0.25 units, lead-free deposits may well lead to an increased requirement of two octane numbers. Many researchers have reported deposits of much greater thickness.

Permeability and porosity effects are more difficult to quantify. The diffusion of reacting combustion chamber gases into the porous structure of the deposit will affect the influence of the nature of the solid surface on knock-inducing reactions and the relative areas of such surfaces available for contact with the gases. The lead-free deposit was shown microscopically to consist of a two-layer stratum, the outer layer more porous than the inner. Owing to this structure and the size of sample available it was not possible to make a meaningful comparison of deposit permeability.

The chemical nature of the deposits were compared by scanning electron microscope but it is impossible to make quantitative comparisons from the contrasting anlyses. Mineral constituents (barium, aluminium and zinc, etc) prominent in the lead-free deposit, presumably arise from processing catalyst residues.

The two-layer structure of the lead-free deposit is clearly visible but otherwise scanning electron microscope photographs merely confirm the contrasting porosity and grain structure of the deposits.

Conclusions

Quantitative conclusions are difficult because of diverse factors affecting engine combustion conditions. Driving behaviour, patterns of use, driving cycle, comparisons of acceleration, high-speed running and idling modes show wide variation across metropolitan, urban, and cross-country areas. These variations and engine size and load variations make precise prediction almost impossible.

However our work has confirmed that deposits from lead-free fuel do throw some light on the octane requirement increase resulting from the elimination of lead.

Further changes may now be expected as new unleaded fuel formulations replace the first generation of lead free fuels. The replacement of aromatics by oxygenates as octane improvers could well have a significant effect on deposit quality, quantity, and volume.

Reference

(1) Milkita J.J. and Sturgis, B.B. The Chemistry of Combustion Chamber Deposits. S.A.E. Journal 1957 65.

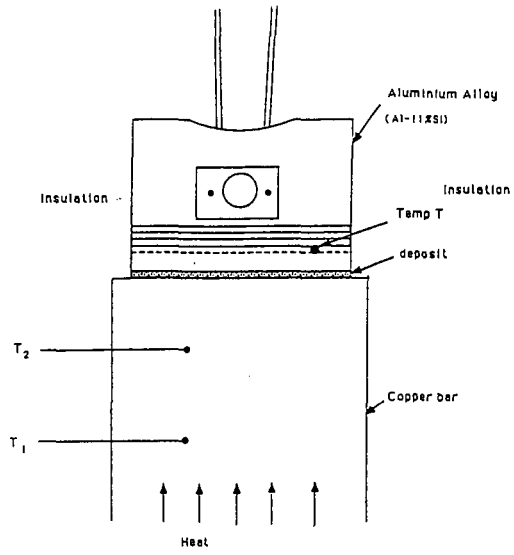

Figure 1. Measurement of Thermal Conductivity

Figure 2. Diagrammatic Presentation of Permeability Apparatus

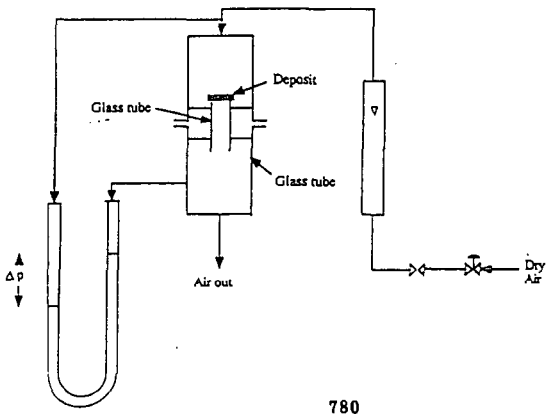

CHARACTERIZATION AND DEPOSIT FORMING-TENDENCY OF POLAR COMPOUNDS IN CRACKED COMPONENTS OF GASOLINE. IDENTIFICATION OF OXIDIZED SULFUR COMPOUNDS.

Pedro Martín, Lola De Lima and Aníbal Rojas*
Centro de Investigación y Apoyo Tecnologico INTEVEP s.a., Filial de PDVSA, Apartado 76343, Caracas 1070A, VENEZUELA.
*Escuela de Química, Facultad de Ciencias, Universidad Central de Venezuela, Apartado 47102, Los Chaguaramos, Caracas, VENEZUELA.

Keywords: FCC composition, ISD Deposit formation, Oxidized benzothiophenes

ABSTRACT

In order to evaluate the deposit forming-tendency of polar compounds in gasoline, one FCC component from a Venezuelan refinery was studied. The polar compounds were separated by column chromatography on alumina, using hexane, benzene, ethyl acetate and methanol as eluents, and their deposit forming-tendencies were determined by ISD apparatus. The ethyl acetate and methanol fractions showed high tendencies to form deposits. Identification of the different components of these fractions was intended by spectroscopic methods (IR, ^{1}H and ^{13}C-NMR and GC-MS) in subfractions obtained by further column and thin layer chromatographies. The main components were identified as mono- and dimethyl 2,3-dihydrobenzothiophene-S,S-dioxides in the ethyl acetate fraction, and mono- and dimethyl benzothiophene-S-oxides in the methanol fraction. This is the first report on the presence of this type of compound in gasoline components, and on their role as deposit-forming promoter.

INTRODUCTION

The role of oxidized compounds in deposit formation in the induction system of gasoline engines has been reported. This type of compounds have a natural affinity for metal surfaces and may react vigorously on the surface forming high deposit levels. Taniguchi (1) found that polar materials are implicated in Port Fuel Injector (PFI) deposit formation. Laboratory test showed that deposit formation was reduced when polar compounds were removed from unstable gasolines (2). Alcohol and catalytic cracked components in the fuel have been found to increase inlet valve deposits (3). The thermal descomposition of oxidized polar compounds, such as ketones, alcohols, carboxylic acids and others, contained in the fuel or formed by oxidation of fuel olefins increased of the ISD deposit formation (4).

This study reports the caracterization of two sulfur-rich and high polar fractions obtained by adsorption chromatography a cracked gasoline component and their contributions to deposit formation.

EXPERIMENTAL

Separation

The cracked gasoline component FCC-1 was subjected to acid-base extraction and adsorption chromatography on a column packed with neutral aluminum oxide, according to a previously described procedure (5). The material retained on the column was eluted with one gallon each of the following solvents: hexane, benzene, ethyl acetate and methanol. These fractions were evaporated under reduced pressure ($T<50^{o}C$) under an inert atmosphere.

Instrumentation

The carbon-13 and hydrogen-1 NMR spectra were recorded with a Brucker MSL-300 or an ACP-400 spectrometer at room temperature, using $CDCl_3$ as solvent and TMS as internal standard. Samples were contained in 5 mm i.d. nmr cells.

The mass spectra of the ethyl acetate fraction was obtained with a Hewlett Packard 5995A GC/MS apparatus, equipped with a 60 m x 0.32 mm i.d. (0.25 µm film) DB-1 Megabore column, programmed from 50-200^{o}C at 5^{o}C/min, using helium as carrier gas. The GC/MS of the methanol fraction was obtained with a Ruska Laboratories apparatus, equipped with a 30 m x 0.32 mm i.d (0.25 µm film) DB-5 column with the same temperature program.

Infrared spectra were recorded with a Perkin-Elmer model 1310. The samples were prepared as thin films on NaCl plates.

Total nitrogen and sulfur contents were determined by chemiluminescence and x-ray (ASTM D-2622) methods.

The subfraction R-1-D was analyzed by GC using a Hewlett Packard 5890A apparatus equiped with a sulfur-selective chemiluminescence detector (Sievers 350B) , under similar chromatographic conditions as those used for the GC/MS analyses.

In order to evaluate the deposit-forming tendency of the isolated fractions, 1000 ppm solutions of each fraction in the original FCC-1 sample were tested in an Induction System Deposit (ISD) apparatus (6). This apparatus simulates intake valve deposit formation. Fuels with a high deposit-forming tendency produce > 2 mg/100ml fuel.

RESULTS AND DISCUSSION

Ethyl acetate fraction.

The elemental analyses of the ethyl acetate fraction showed a high level of sulfur (2,9%) and a low level of nitrogen (0,2%). The ISD evaluation showed a high deposit-forming tendency (2,8 mg/100ml).

The IR spectrum of this fraction showed bands at 3600-3400, 2900-2800, 1750-1650 y 1150-1050 cm^{-1}, assignable to O-Hst, C-Hst (alifatic), C=Ost y C-Ost, respectively.

The ^{1}H-NMR spectrum showed strong signals at 8-7 ppm (ArC-**H**), 2-2,6 ppm (Ar-CH_3 and/or **H** of saturate cycles) and 1,5-0,8 ppm -(CH_2)- and lower intensity signals at 5-6 ppm =C-**H**, 3-3,5 ppm -**CH**-X (X=O or N or S=O) and/or -CH_2-C=O.

The ^{13}C-NMR showed very different kind of signals. The more important were located at 120-142 ppm (ArC and/or =C-H), 200-210 ppm (R-C=O , R-O-C=O and/or H-C=O), 172-170 ppm (HO-C=O), 62-64 ppm (HO-CH_2- and/or R-O-CH_2-), 50-55 ppm (-CH_2-C=O in saturated cycles, -O-CH_3 or -CH_2-S=O_x), 40-48ppm (-CH_2- y -CH saturates cycles) and 10-30ppm (-$(CH_2)_x$- and/or Ar-CH_3).

This fraction was subjected to adsortion chromatographic on a column packed with silica gel. The material retained on the column was eluted with mixtures of benzene, benzene-chloroform and cloroform-methanol, obtaining three fractions: R-1-A (7.7%), R-1-B (17.8%) and R-1-D (74.5%).

The subfractions R-1-A and R-1-B were identified as mixture of dimethylnaphtalenes and phtalic acid derivatives, respectively.

The carbon-13 NMR spectrum (Fig.1) of the major fraction R-1-D showed strong signals in the 50-53 ppm zone, assignable to -CH_2-C=O of saturated cycles, -O-CH_3 or -CH_n-S=O_x (n=1,2 and x=1,2). A DEPT experiment showed that these signals corresponded to -CH_2- groups. The GC analysis of this subfraction with a sulfur-selective detector showed the presence of sulfur compounds.

A detailed study of the carbon-13 NMR chemical shift data of this subfraction indicated the presence of 2,3-dihidrobenzothiophene, S,S-dioxide (7):

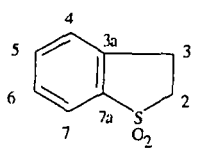

CARBON Nº	OBSERVED δ (ppm)	REPORTED δ (ppm)
2	50,6	50,6
3	25,4	25,3
4	128,7	128,8
5	133,4	133,4
6	127,3	127,2
7	121,3	121,5
3a	137,2	137,2
7a	138,9	138,9

The GC/MS chromatogram (Fig.2) showed ten strong signals. Only one of these peaks was identified as 2,3-dihidrobenzothiophene, S,S-dioxide (m/e 168) according to the NIST Library mass spectral data (Nº 12353) and in agreement with our ^{13}C-NMR results. The M^+ of the other signals: 182 (168+14) and 196 (168+14+14) suggested the presence of methyl- and dimethyl- 2,3-dihidrobenzothiophene, S,S-dioxide. Figures 3 and 4 show probable fragmentation ways of these compounds. Other compounds were identified as methyl and dimethyl indanones, present in minor concentrations.

Methanol fraction.

The elemental analyses of the methanol fraction showed the highest level of sulfur (3.5%) of all the obtained fractions and a low level of nitrogen (0,2%). The ISD evaluation showed also the highest deposit-forming tendency (6.1 mg/100ml).

The IR spectrum of methanol fraction showed bands at 3600-3400, 2980-2880, 1750-1650 and 1150-1050 cm^{-1}

assignable to O-Hst, C-Hst (alifatic), C=Ost and C-Ost or S=Ost, respectively.

The hydrogen-1 NMR spectrum showed strong signals at 8-7 ppm (ArC-**H**), 2-2,6 ppm (Ar-CH_3 and/or **H** of saturated cycles) and 1,8-1,0 ppm (-$(CH_2)_x$-), and lower intensity signals at 5-6 ppm (=C-**H**) and 3-4 ppm (-**CH**-X X=O or N or S=O and/or -CH_2-C=O).

The carbon-13 NMR spectrum showed many different types of signals. The more important were located at 115-158 ppm (ArC and/or -C=C-H), 200-210 ppm (R-C=O), 173,6 ppm (HO-C=O or RO-C=O), 76-64 ppm (-CH-OH), 50-53 ppm (-CH_2-C=O in saturated cycles and/or O-CH_3), and 12,7-20,9 ppm (-CH_2- and/or Ar-CH_3).

This fraction was subjected to adsorption chromatography on a column packed with silica gel. The material retained on the column was eluted with mixtures of clorophorm-methanol, obtained one major fraction R-2-B (73.3%).

The IR spectrum of this fraction showed a strong band located at 1060-1020 cm^{-1} attribute to S=Ost in sulfones. A detailed study of the carbon-13 NMR chemical shift data of this subfraction indicated the presence of 1- and 2-methyl benzothiophene, S-oxide and 1,2-dimethyl benzothiophene, S-oxide (Table 1).

The GC/MS analysis indicated 1- and 2-methyl benzothiophene, S-oxide (m/e 164) , confirming the previous carbon-13 NMR assignments (8). The M^+ of the others signals: 178 (164+14) suggested the presence of dimethyl benzothiophene, S-oxide. Fig. 5 show probable fragmentation ways for these compounds. Other compounds, present in minor concentrations, were identified as benzothiophene, methyl- and dimethyl-benzothiophenes.

To our knowledge, this is the first report demonstrating the presence of this type of compounds in gasoline fractions, and revealing the importance as promoter in the formation of deposit..

ACKNOWLEDGEMENT

The authors thank the Internal Market Coordination of Petróleos de Venezuela, S.A. (PDVSA) for financial support, Julio Medina and Ursula Ehrmann of Analusis and Evaluation Section of INTEVEP for the GC/MS spectra, Guillermo Rodriguez, head of the Fuels Section of INTEVEP for his support and comments on this work.

REFERENCES

1.- Taniguchi B., Peyla R., Parsons G., Hockman S. and Voss D.:"Injector Deposits-The Tip of Intake System Deposit Problems.", SAE Paper N^0 861534, 1986.

2.- Kim C., Tseregounis S. and Scruggs B.;"Deposit Formation on a Metal Surface in Oxidised gasolines.", SAE Paper N^0 872112, 1987.

3.- Bitting W., Gschwendtner F., Kohlepp W., Kothe M., Testvoet C. and Ziwica K.; "Intake Valve Deposit-Fuel Detergency requirements revisited.", SAE Paper N^0 872117, 1987.

4.- Martín P., Mc.Carty, F. and Bustamante D.; "Mechanism of Deposit Formation: Deposit Tendency of Craked Components by Boiling Range.", SAE Paper N^0 922217, 1992.

5.- Martín, P., Mc.Carty, F., Ehrmann, U., De Lima, L. and Rojas A.;"Characterization and Deposit-Forming Tendency of Polar Compounds in Cracked Components of Gasoline. General Scheme and Identification of Basic Fractions.", Fuel Science and Technology Int., 1993, in press.

6.- Dimitroff E. and Johnston A.; "A Bench Technique for Evaluating the Induction System Deposit Tendencies of Motor Gasolines.", Sae Paper No 660783, 1966.

7.- Genete P., Olivé J., Ung S., Faghi M., Easton J., Beierbeck H. and Saunders J.;"Carbon-13 Nuclear Magnetic Resonance Study of Benzothiophenes and Benzothiophene S-Oxides and S,S-Dioxides.", J. Org. Chem., 44(16), 2887-2892, 1979.

8.- Genete P., Grimaud J., Olivé L. and Ung N.;"Oxidation en Sulfoxydes de Benzothiophenes monosubstitues.", Bulletin de la Société Chimique de France, (3-4), 255-276, 1977.

Table 1. Carbon-13 NMR chemical shifts of subfractionsR-2-B fraction (Observed vs. Reported[7] values).

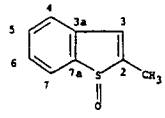

Carbon	Reported	Observed
2	150.6	149.8
3	128.7	128.7
4	127.6	127.5
5	132.0	131.9
6	123.7	123.7
7	126.1	126.0
3a	138.2	138.0
7a	144.8	145.2
2-Me	12.8	12.8

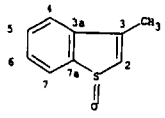

2	132.1	132.0
3	145.2	145.2
4	128.7	128.9
5	131.8	131.6
6	122.5	122.6
7	125.8	125.8
3a	138.5	138.3
7a	145.9	145.5
3-Me	14.1	14.0

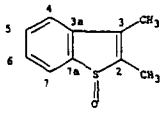

2	143.7	143.9
3	136.5	136.7
4	127.6	127.5
5	131.9	131.9
6	121.6	121.6
7	125.7	125.5
3a	139.9	139.8
7a	142.9	143.0
2-Me	10.6	10.4

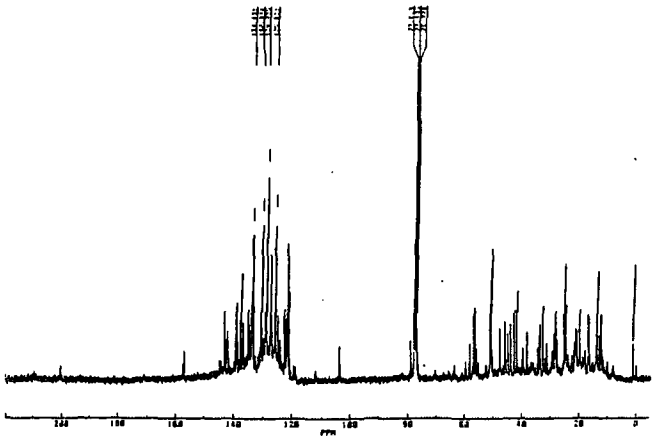

Fig.1 Carbon-13 NMR spectrum of fraction R-1-D.

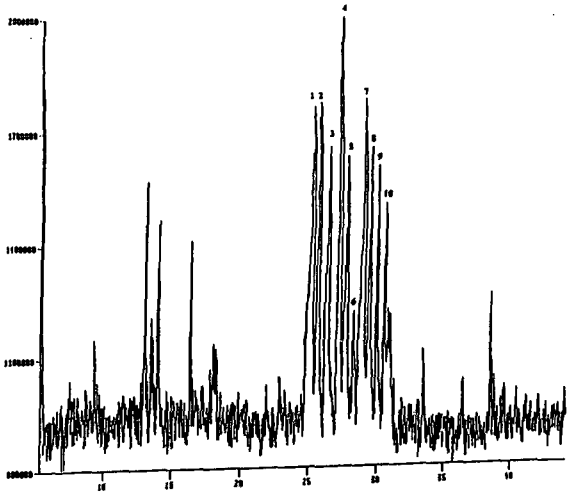

Fig.2 GC/MS chromatogram of fraction R-1-D.

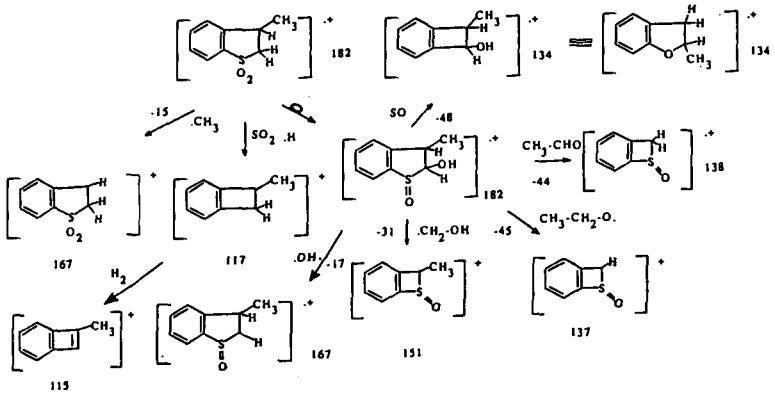

Fig.3 Probable mass fragmentation of methyl-2,3-dihidrobenzothiophene, S,S-dioxide.

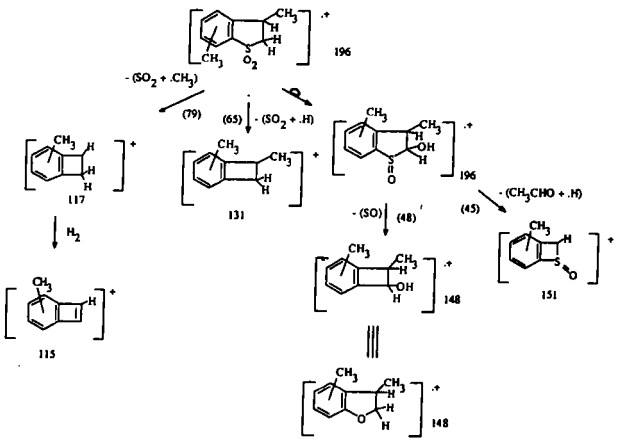

Fig.4 Probable mass fragmentation of dimethyl-2,3-dihidrobenzothiophene, S,S-dioxide.

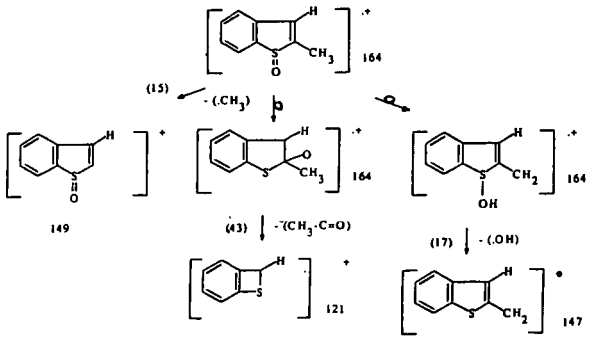

Fig.5 Probable mass fragmentation of methyl benzothiophene, S-oxide.

HYDROGEN SULFIDE: AN EFFECTIVE REAGENT FOR REDUCING THE ELEMENTAL MERCURY CONTENT OF LIQUID HYDROCARBONS.

by

Costi A. Audeh

Central Research Laboratory
Mobil Research and Development Corporation
P. O. Box 1025
Princeton, NJ 08543-1025

Abstract

Elemental mercury has been identified in various crude oils and in condensates associated with the production of natural gas. When these liquid hydrocarbons are distilled or further processed, the elemental Hg will appear somewhere in the downstream processes. In cases where downstream equipment contains metals which amalgamate with Hg, the presence of liquid elemental Hg can cause Hg induced stress corrosion which could cause equipment failure.

We have found that the Hg concentration in liquid hydrocarbons, exemplified by a natural gas condensate containing about 120 μg/Kg, i.e., parts per billion (ppb) Hg, can be reduced to 10-20 ppb. This is accomplished by contacting the condensate with a carrier gas containing 200-500 parts per million of hydrogen sulfide. Typically, the gas containing hydrogen sulfide is mixed with the hydrocarbon containing elemental Hg and passed downflow over a packed bed. Typical reaction conditions are 150°C at a pressure of about 250 psia and a gas to liquid volumetric treating ratio of less than 2:1.

Because the amount of Hg in the condensate used was in the ppb range, it was not possible to recover any HgS for positive identification. However, it is believed that because the stainless steel filter used to filter the treated product acquired a red deposit, and since Cinnabar is the red HgS salt, it is reasonable to conclude that HgS is the product of the reaction.

INTRODUCTION

Some crude oils [1,2] and natural gas produced in various geographic locations [3,4] contain elemental Hg. In many of the gas producing fields, condensate is also produced in association with the gas. Typically if the gas produced contains Hg, the condensate recovered also contains Hg.

In the U. S., condensates are a valuable source of light distillates for the gasoline market [5]. About 500,000 bbl/day of condensate are used as refinery feedstock [6] and about 15,000 bbl/day in steam cracking for ethylene production [7]. In either application, the Hg in the condensate will have to appear somewhere in the downstream processes. Thus, it would seem that the fate of the Hg will be of concern. This is especially so in the case of steam cracking for ethylene production where equipment made of aluminum is used for cryogenic separation of the cracked products. Any elemental Hg contained in the cracked products is undesirable and could cause Hg induced stress corrosion. Similarly, stress corrosion could also be induced in other process equipment constructed of metals that have the ability to form amalgams.

To prevent Hg carryover and thus the potential corrosion of susceptible process equipment, it is desirable to remove elemental Hg from condensate. In this paper, we report the results of laboratory experiments using hydrogen sulfide as the agent for converting Hg into HgS.

EXPERIMENTAL

1) Materials: a condensate containing about 120 μg/Kg, i.e., parts per billion (ppb) Hg. Nitrogen gas, methane gas, methane containing about 200 parts per million (ppm) hydrogen sulfide and carbon dioxide gas containing about 480 ppm hydrogen sulfide and about 2.5% methane.

2) Equipment: a down flow stainless steel reactor equipped with a mixing T, a preheat zone, temperature control, pressure control, a 1 ml section packed with 10-18 mesh Vycor chips, a 0.7 micron stainless steel product filter and appropriate liquid and gas flow controllers. Figure 1 is a schematic of the reactor and its ancillary systems.

3) Procedure:

   a) Unit start up: from room temperature the gas flow and liquid flow were started and set at the required flow rates. The reactor was heated until the required temperature was reached. After about 10 minutes of steady operation, the product was collected periodically and sampled for Hg analysis.

   b) Change of conditions: when changes in the process parameters or treating gas were made, the unit was not shut down. It was allowed to equilibrate at the desired conditions and after about 10 minutes of steady operation sampling/testing was resumed.

   c) Hg determination: this was performed using the Jerome Hg Analyzer, Model 301.

RESULTS AND DISCUSSION

Hg reacts with H_2S to produce HgS and H_2. Although the solubility of elemental Hg in various hydrocarbons [9] has been reported, that for HgS has not. However, the solubility of HgS in water is reported to be 2.8E-23 g HgS/liter of water [10]. Since, in general, inorganic salts are more soluble in water than in hydrocarbons, it would be expected that HgS will be less soluble in the hydrocarbon condensate used than it is in water. Thus, the solubility of HgS in the treated condensate is expected to be less than 2.8E-23 g HgS/ Kg of condensate. Any HgS formed would not dissolve to any measurable extent in the treated condensate and possibly, could be removed from the treated product by filtration. Changes in the concentration of Hg in the concentrate will indicate its removal and thus the measure of the effectiveness of this approach is the reduction in the concentration of elemental Hg in the treated condensate.

In the reaction of Hg with H_2S, each mol of Hg requires 1 mol of H_2S. Since the concentration of Hg in the feed is about 120 ppb, the amount of H_2S required to react with it will be very small. Thus we decided to use carrier gases containing small amounts of H_2S in this study. The gases chosen were methane and carbon dioxide. Methane is the major component of natural gas and natural gas usually contains small amounts of H_2S. Also, in natural gas processing typically CO_2 and H_2S are removed from the gas before it can be marketed. In such removal processes, the treating solutions are regenerated and the gases leaving the regenerators contain CO_2 and H_2S. With this in mind methane/H_2S and CO_2/H_2S mixtures were selected for this study.

"Treating" with Carrier Gas

To determine if "treating" the condensate in the presence of a carrier gas changes the Hg concentration, experiments in which nitrogen and methane without H_2S were conducted at different temperatures and flow rates. In all cases no significant changes in the Hg content of the treated condensate were observed. From these observations it was concluded that heating the condensate in the presence of a carrier gas does not reduce the Hg content of liquid hydrocarbons.

Treating the Condensate with H_2S in Methane

Based on the concentrations of the 2 reactants, 200 ppm H_2S in methane, and 120 ppb Hg in the condensate, it can be shown that H_2S is in a large molar excess at any reasonable treating ratio. For example, when 1 volume of the treating gas is used to treat 1 volume of the condensate, the H_2S is in about a 20 molar excess.

a) Effect of Temperature - At a gas to liquid treating ratio of 1:2.7, the treating efficiency increases as the treating temperature is raised. Table 1 shows our results. A plot of ln of the concentration of Hg, in ppb, in the treated liquid after treatment vs 1/T, in °K, Fig. 2, gives the straight line:

$$\ln ppb = 1089\ t + 0.95, \text{ where } t = 1/T.$$

b) Effect of Feed Ratio - To study the effect of feed ratio on the efficiency of Hg removal, we varied the rate at which the condensate was pumped and kept the flow rate of the treating gas constant. At 150°C, the temperature chosen for this study, we found that at a treating ratio of about 1:1, the concentration of Hg in the treated condensate approaches about 10 ppb. The results of this study are shown in Table 2.

Treating the Condensate with H_2S in CO_2

Not unexpectedly, H_2S/CO_2 was also effective in reducing Hg from the condensate. Table 3 shows our results. At 150°C and a treating ratio of 1:1, the concentration of of Hg in the treated condensate approached about 10 ppb.

This study was conducted at a constant temperature 150°C, and a constant gas flow rate, 23 ml/min, but at different condensate feed rates, 10-80 ml/min. Thus, from a plot of the reciprocal of the liquid hourly space velocity, LHSV, vs ln of the concentration of Hg, in ppb, in the treated condensate, Fig. 3, the rate equation, shown below, for the reaction between H_2S and Hg, can be derived.

ln ppb = -78.4 v + 4.75, where v = 1/LHSV

The slope of this equation gives the rate constant of the reaction in units of ln ppb Hg/hour.

Reaction Product

Because the amount of Hg in the condensate is in the ppb range, it was not possible to recover any HgS for positive identification. However, it is believed that because the stainless steel filter used to filter the treated product acquired a red deposit, and since Cinnabar is the red HgS salt, it is reasonable to conclude that HgS is the product of the reaction.

CONCLUSION

Laboratory results indicate that H_2S is an effective reagent for reducing the Hg content of hydrocarbon liquids. In this study, hydrocarbon liquids are exemplified by a condensate produced in association with natural gas and the H_2S is introduced in about 200-500 ppm in methane or carbon dioxide. At 150°C and about 180 seconds contact time, the Hg content of a condensate containing 120 ppb Hg can be reduced to about 10 ppb.

REFERENCES

1. Gorbunova, L. V., Filimonova, V. A., Aleshin, G. W., Glokhov, G.G. and Kamyanov, V. F., Petroleum Chemistry, U.S.S.R, Vol. 24, No. 1, p. 10, 1984.

2. Valkovic, V., "Trace Elements in Petroleum", Petroleum Publishing Company, Tulsa, Oklahoma, p.78, 1978.

3. Bodle, W. W., Attari, A. and Serauskas, R., Sixth International Conference on Liquefied Natural Gas, April 7-10, 1980, Kyoto, Japan.

4. Naklie, M. M., Deraton, L. A. and Kartiyoso, Iv., Oil and Gas Journal, Vol. 85, No.24, p.35, 1987.

5. Staff Report, Oil and Gas Journal, V. 84, No. 2, p. 71, 1986.

6. S. R. I. Chemical Economics handbook, 229.3000Z.

7. ibid., 300.5201A.

8. Kelley, K. K. Bur. of Mines Bull., 1937, No. 406, 52

9. Spencer, J. N. and Voigt, A., J. Phys. Chem. V. 72, p. 464, 1968.

10. Linke, W. F., "Solubilities" Volume 1, Van Nostrand, Washington, D. C., 1958, p. 1249.

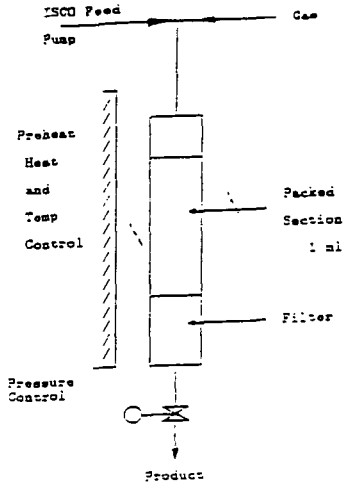

FIGURE 1

REACTOR FOR Hg REMOVAL

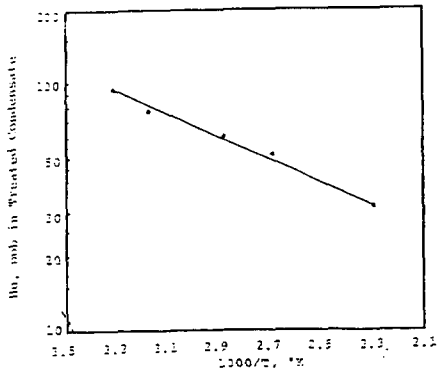

FIGURE 2

EFFECT ON FEED RATIO ON Hg REMOVAL

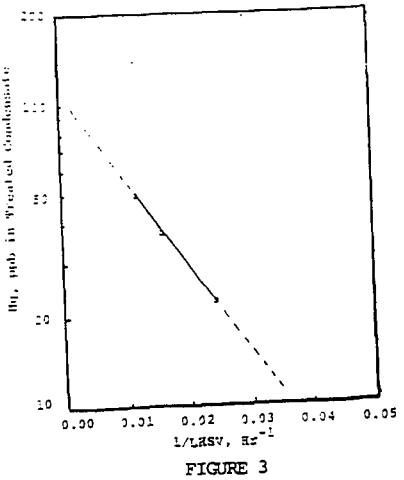

FIGURE 3

EFFECT ON FEED RATIO ON Hg REMOVAL

TABLE 1

Removal of Hg from Condensate (C) with H_2S in CH_4
Effect of Temperture

Gas: 200 ppm H_2S/balance CH_4
Packing: 1ml 10-18 mesh Vycor chips
Pressure: 220-260 psig

Temperature °C	Volume, ml/hr (C)	CH_4/H_2S	Hg in Product ppb	Hg Removed %
	Feed	-----	116	----
29	70	26	95	19
43	70	26	77	34
75	70	26	60	49
100	70	26	52	55
165	70	26	31	74

TABLE 2

Removal of Hg from Condensate (C) with H_2S in CH_4
Effect of Feed Ratio

Gas: 200 ppm H_2S/Balance CH_4
Packing: 1 ml 10-18 mesh Vycor chips
Pressure: 220 - 260 psig
Temperature: 150 °C

Volume, ml/hr (C)	CH_4/H_2S	Hg in Product ppb	Hg Removed %
Feed	----	116	----
80	26	52	54
60	26	34	70
52	26	28	78
40	26	23,20,21	82
13	26	<10	>90

TABLE 3

Removal of Hg From Condensate (C) with H_2S In CO_2
Effect of Condensate to Gas Ratio

Gas: 500 ppm H_2S/2.5% CH_4/balance CO_2
Packing: 1 ml 10-18 mesh Vycor chips
Pressure: 220-260 psig
Temperature: 150 °C

Volume, ml/hr (C)	CO_2/H_2S	Hg in Product ppb	Hg Removed %
Feed	----	116	----
80	23	50,47	58
60	23	38,36	68
40	23	17,21,19	84
20	23	<10,11,<10	>90
10	23	<10,<10,<10	>90

EFFECT OF LIGNITE PROPERTIES AND ASH CONSTITUENTS ON THE HYDROLIQUEFACTION BEHAVIOR OF THE TURKISH LIGNITES

M. Oner, E. Bolat, G. Yalin, S. Dincer
Yildiz Technical University
Chemical Engineering Department
Istanbul, TURKEY

Keywords: lignite properties, hydroliquefaction, ash

INTRODUCTION

In Turkey, coal represents major non-renewable energy resources since lignite and bituminous coal reserves are known to be around 8.1 billion tons and 1.4 billion tons, respectively. The high demand for imported fuel oil for energy requirement of Turkey has led to strong and sustained interest in the prospects for producing liquids from the coal resources. Due to the high sulfur (1-5 %), ash (10-50 %), moisture (10-40%) and low calorific value of Turkish lignites, coal liquefaction processes is believed to be one of the efficient way by converting them to clean liquid fuels and chemical feedstocks.

The purpose of this study was to develop correlations between physical , chemical and petrographic properties of representative Turkish lignites and liquefaction yield data obtained in tetralin, anthracene, creosote and vacuum residue oils, with or without catalyst, at 440 °C and 80 bar hydrogen pressure (cold charge).

EXPERIMENTAL

Materials and Procedure

Experiments were carried out by BE (Beypazari), CA (Can), EL (Elbistan), IL (Ilgin), KN (Kangal), KR (Karliova), SA (Saray), SE (Seyitomer), SO (Soma), TU (Tuncbilek), YA (Yatagan) lignites using tetralin, Tupras vacuum residue oil, anthracene and creosote oils as solvents. Creosote and anthracene oils used in this study were obtained from Karabuk Demir Celik Fabrikalari A.S. and vacuum residual oil (VR) was provided by Tupras, Turkey. Tetralin was supplied by Merck company and it was used as received. The creosote oil used has a carbon to hydrogen ratio of 1.24 (90.78% C, 6.12% H, and 0.70% N); anthracene oil has a carbon to hydrogen ratio of 1.27 (91.50%C, 6.01%H, and 0.75% N); vacuum residue oil has a carbon to hydrogen ratio of 0.64 (85.58%C, 11.06%H and 0.50%N). Two catalysts were used in these experiments. A commercially available alumina supported CoMo (3% CoO and 10% MoO_3 on Al_2O_3) was used in extrusion form having 2.6-3 mm diameter and bulk density of 0.5-0.6 kg/lt. In addition, a disposable catalyst, red mud (15.03% SiO_2, 35.96% Fe_2O_3, 21.04% Al_2O_3, 4.56% TiO_2, 9.3% Na_2O and 3.5% CaO) received as a waste by-product of Seydisehir Aluminum Company, having a grain size of 0.01 mm, was used. The elemental analysis for carbon, hydrogen and nitrogen was done by Beller Microanalysis Laboratories in Germany. The ash samples prepared at 800 °C were analyzed with Inducted Coupled Plasma (ICP) Leeman, Model PS1000 series.

The liquefaction experiments were carried out in a 250 ml magnetically stirred and electrically heated stainless steel autoclave manufactured by Ernst Haage. Based on the literature and evaluation of our previous work, the reaction temperature, pressure and reaction time for these experiments were chosen as 440 °C, 80 bar hydrogen (cold charge), respectively (1-3). Solvent/lignite or asphaltite ratio was chosen as 2 (db). At the completion of a liquefaction experiment, the autoclave was cooled overnight to room temperature and the gases were analyzed by Shimadzu Moduline GC-9A model gas chromatography. The liquid products and solid residue washed from the autoclave with toluene and fractionated by Soxhlet extraction into oil (hexane soluble

material); asphaltene (toluene soluble, hexane insoluble material); preasphaltane (tetrahydrofuran (THF) soluble, toluene insoluble material); and residue (THF insoluble material). The blank runs for all sets of experiments with no lignite present were carried out with all solvents to evaluate the reactivity of the lignite samples.

RESULTS AND DISCUSSION

The complete experimental data were reported in previous work (1-3). The characterization data for the lignites used are given in Tables 1 and 3. The experimental data used in this study are given in Figures 1-2.

The intercorrelation of experimental results and lignite characteristics was evaluated by simple linear regression analysis using Microstat Statistical Package program. By the application of simple linear regression, it was found that generally a good correlation did not exist between individual lignite properties and yield and conversion data. Only total sulfur content and xylene extract of lignites were observed to give partially acceptable correlations for the oil yields. The corrslation coefficient of experiments using tetralin as solvent is as follows:

$$O\ (\%\ daf) = 3.10\ S_t + 50.84$$
$$R^2 = 0.7024\ ;\ SEOE(\text{standard error of estimation}) = 4.45$$

The oil yields obtained in experiments using creosote oil and red mud catalyst were correlated with xylene extract content of lignites by the following regression equation

$$O\ (\%\ daf) = 1.980\ XEL + 29.39$$
$$R^2 = 0.560\ ;\ SEOE = 6.68$$

The effect of individual coal properties are not easily assessed as noted above. This is primarily due to the fact that the individual properties being highly cross-correlated hence they could not be independently varied. Therefore, the multiple regression analysis was employed and in order to improve the correlation coefficients unfitting lignites were eliminated. The equations developed with oil yield as the dependant variable are given in Table 4. The correlation coefficients indicated that a relationship existed between carbon, total sulfur and forms of sulfur, volatile matter, huminite plus exinite, and xylene extract of lignites with the oil yields obtained by using four differsnt solvents and two different catalysis. The highest correlation coefficient was obtained for experimental data using creosote oil as the solvent. For this case three equations were derived, using the pyritic sulfur, total sulfur and organic sulfur contents of the lignites. The R^2 values are 0.6819, 0.9727 and 0.7643 for S_p, S_t and S_o, respectively as shown in Equations 2-4. It is commonly believed that one of the factors contributing to the liquefaction yield is promotion by sulfur. However, the exact role of sulfur is not well understood. The organic sulfur is presumably present in coal as mercaptans, sulfides, thioethers. It is expected that thioethers are thermally cleaved at considerably low temperature to produce active coal fragments during the liquefaction reactions (4). Several workers have shown that conversion of coals of low sulfur content can be increased by from 5 to 18 percent through the addition of pyrite (5,6). It has been observed that during liquefaction, pyrite is reduced to pyrrohotite and hydrogen sulfide at roughly the same rate as the organic matter is converted to liquid products. Thus coals containing high proportions of pyritic sulfur will tend to form pyrrhotites with a high level of iron vacancies, which appear to promote liquefaction.

There is an indication that an increase in ash, huminite plus exinite, xylene extract and volatile matter contents of lignites help the hydroliquefaction process positively. On the other hand, as the negative coefficient before the elemental carbon content in Eq.5 indicates, increasing the elemental carbon content decreases the oil yield. As shown in equations 2-4 and 6-7, correlations were obtained when HU and

HU+EX contents of the lignite were used as the petrographic correlating parameter. The work undertaken by Given and coworkers in batch reactor showed that some coal macerals, including vitrinite, pseudovitrinite and liptinites are reactive while inertinite, as its name implies, is inert in coal liquefaction (7). The trend for increasing reactivity with increasing volatile matter content as given in Equations 2-4 was expected as volatile matter is known to be thermally easily liberated. Given also found that volatile matter had a direct correlation with conversion at 60 minutes and exhibited the highest correlation coefficient among the coal properties investigated (7). The oil yield increases as the xylene extract content of the lignite increases, as seen in Equations 1-4 and 7-8. The high partial correlation coefficients for xylene extract in Equations 2-4 indicate that it may be considered as a good correlation parameter for liquefaction reactions.

The equations 1, 6 and 8 show that increased ash content increases oil yield. It is known that the high ash coals are more easily hydrogenated than low ash coals because certain coal ash minerals catalyze the reactions (8-9). The observed relation between ash and oil yield data was further evaluated with respect to concentrations of ash constituents (g/100g of inorganic matter). In this study total Fe, Al, Si, Mg, Ca, Na and K concentrations were chosen as the independent variable, since the active form of the minerals has not been ascertained. There appears to be direct correlation between oil yield with Fe constituents but the dependance is not marked. The yield of oil data shows a tendency to increase with increasing Al, Ca and Mg content though with more scatter than in the case of Fe content. No detectable trends were observed with Si contents of ash. In this study, an examination of oil data for all samples studied did not reveal any statistically significant correlations with Na and K content of the ash. We have not included in this paper a thorough discussion for the effects of ash constituents on liquefaction yields because we are carrying out a detailed multiple regression analysis on that topic.

CONCLUSIONS

In this study, the oil yields of the Turkish lignites under same hydroliquefaction conditions in the presence of tetralin, creosote, anthracene and vacuum residue oils using a catalyst or not, were correlated total, pyritic and organic sulfur, volatile matter, elemental carbon, huminite, huminite plus exinite, xylene extract, ash and ash constituents of lignites using simple and multiple linear regression analysis. The derived equations indicated that although use of different lignite, solvents and catalyst resulted in different yield data , the oil yields exhibit almost similar dependencies on lignite characteristics. However, it should be noted that in order to strengthen the validity of these equations, the number of lignite sample studied should be increased. In any case, much more has to be done in order to correlate the liquefaction data with lignite properties.

REFERENCES

1. Oner, M., Bolat, E., Dincer, S., Energy Sources, 12, 407, 1990.
2. Oner, M., Bolat, E., Dincer, S., Energy Sources, 14, 81, 1992.
3. Bolat, E., Oner, M., Yalin, G., Dincer, S., Fuel Science and Technology International, 31, 55, 1992.
4. Miller, R. L., and Baldwin, R.M., Fuel, 64, 1235, 1985.
5. Alexander, B.F. and Anderson, R.P., Div. Fuel Chem. Amer. Chem. Soc., Prspr., 27(2), 18, 1982.
6. Bockrath, B.C. and Schroeder, K.T., in "New Approaches in Coal Chemistry", eds. B.P. Blaustein et al., ACS Sym. Series 169, 191, 1981
7. Given, P.H., Cronauer, D.C., Spackman, W., Lowell, H.L., Davis, A., and Biswas, B., Fuel, 54, 40, 1975.
8. Mukherjee, D.K., Choudhury, P.B., Fuel, 55, 4, 1976.
9. Guin, J.A., Tarrer, J.M., Lee, J.M., Van Brackie, H.F., Curtis, C.W., Ind. Eng. Chem. Proc. Des. Dev., 18(4), 631, 1979.

Table I

Analytical Data for Lignites Used

Lignite Sample	C (%daf)	H (%daf)	N (%daf)	S_t (%dry)	S_p (%dry)	S_o (%dry)	S_s (%dry)	VM (%daf)	FC (%daf)	ash (%dry)	H/C (Atomic)	XEL (%daf)
BE	64.90	5.61	2.19	5.69	2.88	2.33	0.48	35.61	64.38	49.88	1.04	3.83
CA	66.38	4.82	1.67	4.23	0.90	2.44	0.89	37.53	62.47	27.15	0.87	1.34
EL	65.95	4.97	2.48	5.82	3.33	2.22	0.27	54.78	45.22	28.19	0.90	5.04
IL	68.19	5.11	1.27	2.95	1.12	1.45	0.38	40.32	59.68	33.61	0.90	5.69
KN	67.66	4.52	2.78	5.63	3.15	1.93	0.55	62.93	37.07	38.50	0.80	5.22
KR	66.97	5.55	2.09	0.79	0.40	0.30	0.09	49.43	50.57	49.20	0.99	4.31
SA	61.32	4.73	1.60	4.97	0.15	1.25	3.57	48.21	51.79	59.99	0.93	12.62
SE	71.97	4.70	2.32	1.45	0.26	1.02	0.17	48.65	51.35	24.87	0.78	10.30
SO	64.10	5.62	1.47	0.80	0.41	0.34	0.05	39.69	60.30	55.51	1.05	2.02
TU	78.30	5.65	3.03	1.37	0.64	0.67	0.06	31.59	68.41	18.59	0.87	0.95
YA	63.65	4.87	1.59	5.11	1.72	2.98	0.41	44.41	55.59	25.35	0.92	6.90

BE: Beypazari; CA: Can; EL: Elbistan; IL: Ilgin; KN: Kangal; KR: Karliova; SA: Saray; SE: Seyitomer; SO: Soma; TU: Tuncbilek; YA: Yatagan; S_t: total sulfur; S_p: pyritic sulfur; S_o: organic sulfur; S_s: sulfatic sulfur; VM: volatile matter; FC: fixed carbon; daf: dry-ash-free; XEL: Xylene extract of lignites.

Table II

Maceral Group Analysis of Lignites

	Maceral Grup Analysis (volume %)					Organic Based Maceral Grup Analysis (volume %)		
Lignite	Huminite (HU)	Exinite (EX)	Inertinite (IN)	Pyrite	Clay	Huminite (HU)	Exinite (EX)	Intertinite (IN)
BE	77	6	4	3	10	88	7	5
CA	74	6	4	4	12	88	7	5
EL	69	5	11	3	12	81	6	13
IL	70	7	9	3	11	81	8	11
KN	54	4	7	3	32	83	6	11
KR	52	5	7	2	34	81	8	11
SA	71	6	7	2	14	85	7	8
SE	77	7	8	2	6	84	8	8
SO	62	3	9	2	24	84	4	12
TU	80	8	6	1	5	85	9	6
YA	77	6	5	4	8	88	7	5

Table III

Chemical Analysis of Ash (g/100 g organic matter)

Lignite	Si	Fe	Al	Mg	Ca	K	Na
BE	22.06	6.70	6.60	2.59	6.89	1.14	3.54
CA	8.24	3.26	5.55	0.13	1.18	0.27	0.12
EL	5.47	1.45	2.69	0.74	6.87	0.20	0.12
IL	9.36	2.88	6.88	0.96	3.75	1.60	2.06
KN	11.35	1.69	7.20	0.84	8.64	0.52	0.29
KR	33.26	3.70	3.97	0.81	2.34	2,44	0.42
SA	32.55	14.42	18.19	4.03	5.49	2.88	0.40
SE	9.02	6.87	1.94	1.12	2.18	0.13	0.34
SO	27.65	3.64	17.80	1.07	8.05	1.50	0.46
TU	5.48	2.29	3.52	0.47	0.37	0.27	0.03
YA	4.30	3.28	2.97	0.54	4.23	0.25	0.07

Table IV

Relations Between Oil Yield and Various Properties of Turkish Lignites

Solvent + Catalyst Used	Excluded Lignite	Derived Equation	
A.O.	SE, BE	$O\ (\%daf) = 20 + 0.44\ ash + 1.17\ XEL$ $R^2 = 0.7719 \quad R^2_{ash} = 0.5598 \quad R^2_{XEL} = 0.3501$	Eq (1) SEOE = 5.74
C.O.	SO, TU	$O\ (\%daf) = -247.4 + 1.41\ S_p + 0.18\ VM + 2.00\ XEL + 2.93\ (HU+EX)$ $R^2 = 0.9890 \quad R^2_{Sp} = 0.6819 \quad R^2_{VM} = 0.4644$ $R^2_{XEL} = 0.9890 \quad R^2_{(HU+EX)} = 0.6819$	Eq (2) SEOE = 1.36
		$O\ (\%daf) = -223.1 + 0.99\ S_t + 0.17\ VM + 1.79\ XEL + 2.66\ (HU+EX)$ $R^2 = 0.9991 \quad R^2_{St} = 0.9727 \quad R^2_{VM} = 0.9079$ $R^2_{XEL} = 0.9977 \quad R^2_{(HU+EX)} = 0.9967$	Eq (3) SEOE = 0.40
		$O\ (\%daf) = -216.1 + 2.32\ S_o + 0.20\ VM + 1.89\ XEL + 2.56\ (HU+EX)$ $R^2 = 0.9918 \quad R^2_{So} = 0.7643 \quad R^2_{VM} = 0.6376$ $R^2_{XEL} = 0.9800 \quad R^2_{(HU+EX)} = 0.9645$	Eq (4) SEOE = 1.17
TET	EL, SO	$O\ (\%daf) = 125.1 - 0.97\ C + 1.82\ S_p$ $R^2 = 0.9039 \quad R^2_C = 0.8697 \quad R^2_{Sp} = 0.5382$	Eq (5) SEOE = 2.12
VR	BE, KN	$O\ (\%daf) = 29.22 + 0.09\ Ash + 0.30\ HU$ $R^2 = 0.4800 \quad R^2_{ash} = 0.4169 \quad R^2_{HU} = 0.3999$	Eq (6) SEOE = 1.61
C.O.+CoMo	KR, KN	$O\ (\%daf) = -61.62 - 1.22\ XEL + 1.18\ (HU+EX)$ $R^2 = 0.5704 \quad R^2_{XEL} = 0.4904 \quad R^2_{(HU+EX)} = 0.3512$	Eq (7) SEOE = 5.70
C.O.+Red Mud	KR	$O\ (\%daf) = 25.25 + 0.20\ Ash + 1.67\ XEL$ $R^2 = 0.7908 \quad R^2_{ash} = 0.3286 \quad R^2_{XEL} = 0.7091$	Eq (8) SEOE = 4.42

A.O.: Antracene oil; C.O.: Creosote oil; TET: Tetralin; VR: Vacuum residue; CoMo: Cobalt Molybdenum catalyst.

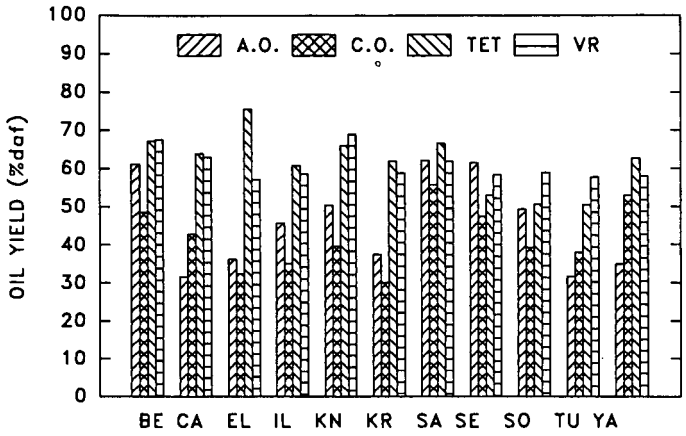

Figure 1. Effect of solvents on the oil yields of Turkish lignites; P = 80 bar (H_2, cold charge), T = 440 °C, reaction time = 1 hr.

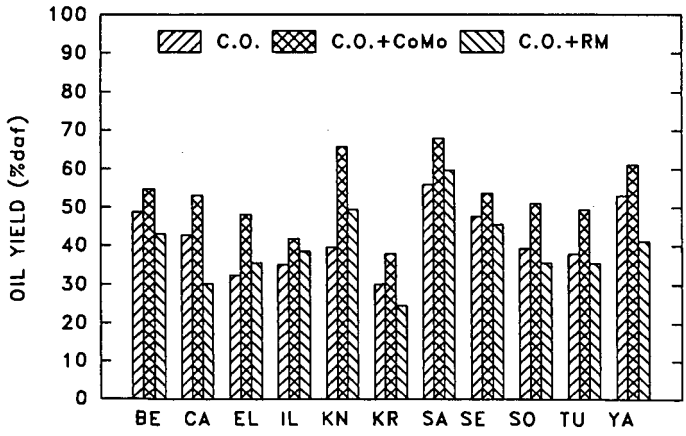

Figure 2. Effect of catalysts on oil yields of Turkish lignites; P= 80 bar (H_2, cold charge), T = 440 °C, reaction time = 1 hr.

FUNDAMENTALS OF HYDROTHERMAL PRETREATMENT OF SEWAGE & INDUSTRIAL SLUDGES: FEEDSTOCKS FOR CLEAN ENERGY.

M. R. Khan, C. Albert, R. McKeon, R. Zang*, S. DeCanio
Texaco R&D; P.O. Box 509, Beacon, NY 12508.
*Texaco AERD, White Plains, NY 10650.

Keywords: Sludge rheology, heating value, gasification.

Sludge rheology and slurry solids loadings are significant from pumping and slurry heating value standpoints. In this paper, we discuss the fundamental aspects of hydrothermal pretreatment of sludge which impacts the physical and chemical characteristics of the sludge. The fundamental work served as a basis of the development of a continuous 5 ton/day Process Demonstration Unit.

INTRODUCTION

Texaco Inc. has investigated techniques to prepare dewatered sewage, industrial and biological sludges as feedstocks for gasification/oxidation processes, as part of its waste gasification program.[1A] One of the most promising pretreatment methods has proven to be the hydrothermal treatment developed by Texaco R&D. A number of patents have been issued[1B-D]. The objective of this paper is to present the fundamental aspects of hydrothermal pretreatment of sludge. Based on extensive bench-scale and pilot-scale runs, a demonstration plant was built to process 6 dry tons per day of centrifuged sludge cake. The results of the inaugural run are presented.

The Texaco Gasification Process produces synthesis gas, principally carbon monoxide and hydrogen, from carbonaceous feedstocks by partial oxidation. One hundred commercial plants have been licensed to use this technology over the last thirty years and the synthesis gas generated has been used for end-products ranging from hydrogen, ammonia and alcohol to electric power. The feedstocks have included natural gas, distillate oils, petroleum coke, and coal.

The proposed technical standards for the use/disposal of sewage sludge (40 CFR Part 503) cover the following options: incineration, agricultural and non-agricultural land application, marketing and distribution, monofilling, and surface disposal. Most large treatment plants would prefer incineration, land application, or marketing/distribution. However, the first option could be limited to plants with existing incineration facilities and the next two, the so-called "beneficial use" options, could be limited by land availability and assurances of pathogen reduction. Solids handling is a significant operating cost for municipal wastewater treatment plants. As an example, Greater Chicago spent over half of its 1990 operating and maintenance budget on solids processing and disposal. These costs will increase at all plants because new regulations and public concerns are limiting old options. Ocean dumping is banned, landfills are closing, and the public is demanding that sewage

sludge be put to beneficial reuse.[3,4]

Obviously, there is a market for new sludge management technologies. Recently, wastes have been considered for gasification because they are a good source of hydrocarbons and cost less than traditional feedstocks. Gasification research and development is conducted by Texaco at its Montebello Research Laboratory in Los Angeles, California. Montebello was established in 1945 and has three 15 to 25 ton per day pilot units. In 1988, under a Hazardous Waste Reduction Grant from the State of California Department of Health Services, a demonstration at Montebello proved that low-Btu hazardous waste could be gasified safely with coal and with little impact on thermal efficiency.[1] The successful testing of hazardous wastes showed that gasification would be an environmentally-acceptable method of disposal for other high-volume, low-hazard wastes such as sewage sludge.

In order to maintain the highest efficiency in gasification there is a need to limit the amount of water carried in the feed. The high viscosity of partially-dried sludge limits its suitability as a feedstock, yet too much water in a less viscous slurry decreases its heat content. It was observed that even after complete drying, sewage sludge had a tendency to reabsorb water and did not form a good slurry for gasification. This phenomenon is known to occur with low-rank coals, so developments in this area were investigated. Several steam and hot water processes were developed to thermally dewater low-rank coal. The first of these was the Fleissner process patented in 1927.[5] When coal is heated various oxygen functional groups are decomposed releasing carbon dioxide and water from the coal structure. The tendency to reabsorb moisture is reduced so that the slurring characteristics are similar to higher rank coals.[7]

EXPERIMENTAL

Bench-Scale Results/Discussion: Bench-scale and pilot tests were begun at the Texaco Research Center at Beacon, New York to investigate various techniques to improve the physical, chemical and transport properties of sludge.[4,6] An indicator viscosity for all feedstocks was established at 1000 centipoise to allow comparisons of different pretreatment methods.

The Texaco Research Center at Beacon conducted extensive autoclave and other testings including pilot plant runs to demonstrate that hydrothermal pretreatment of sludge can significantly improve the physical/chemical properties of sludge. Hydrothermal treatment of sludge is somewhat similar to that of low-grade coals; however, there are significant differences between the pretreatment of coal and sludge. The viscosity of the product can be greatly reduced depending on the conditions used during pretreatment.

Figure 1 shows the influence of heat-treatment temperature on the

oxygen content of the sludge. The greater the pretreatment temperature the lower the sludge oxygen content. However, the overall solids loading for a pumpable slurry is increased as a function of pretreatment temperature. Figure 2 shows the similar trends for a different sludge. The sludge was mixed with coal after the former was hydrothermally pretreated (for the data shown in Figures 1 and 2).

Figure 3 shows the influence of sludge pretreatment on the various functional groups of (dried or hydrothermally treated) sludges. The treated sludge contains significantly lower oxygenated functional groups compared to the feed sludge. Similar results were also noted for an industrial sludge (Figure 4).

Figure 5 shows the typical "Coalification" curve as applied to sludge as a function of sludge pretreatment temperature. The sludge O/Cx100 versus atomic H/C ratio of various sludges are plotted in this Figure along with various other fossil fuels feedstocks. It is interesting to note that the as the pretreatment temperature of sludge is increased, a pathway is followed by sludge which is similar to the pathway followed by geological maturation of various fossil fuels.

Process Demonstration Unit Results: Based on these results, it was decided that construction of a larger process demonstration unit was justified. Burns and Roe Industrial Services Company was retained to provide detail design and construction services for a trailer-mounted PDU with a capacity of 900 kg/h or 6 dry tons per day at 25% solids. The process is shown schematically in Figure 6. The effect of PDU Hydrothermal treatment on the viscosity of the slurry is shown in Figure 7. The dramatic effect is qualitatively similar to our pilot test results (not shown) and demonstrates that the pilot-scale and bench-scale results can be achieved in a commercial unit.

CONCLUSION

Hydrothermal Pretreatment Process, developed based on fundamental investigation, converts sewage and industrial sludges into attractive feedstocks for gasification/combustion and offers municipalities an environmentally-acceptable alternative to other disposal options.

REFERENCES

1. A) Davis, L.A., Miranda, J.E., Amrheim, M., "Pilot Plant Demonstration Gasification of Petroleum Production, RCRA Exempt, Low Btu, Hazardous Wastes." Final Report Contract No. 88-90359, June 1990.
   B) Khan, M., US Patent 5,188,740; Zang, R., Khan, M. 5,188,741.
   C) Khan, M, McKeon, R., European Patent No. 93300425.1
   D) Zang, R., and Khan, M. European Patent No. 93300800.5
   E) Khan, M. Zang, R., Albert, C., European Patent No. 92310995.3,
2. Canelli, B. A., et al. "Improved Centrifugal Dewatering," AC91-042-004 Water Environment Federation, October 1991.
3. Khan, M. R., McMahon, M.A., and DeCanio, S. J., "Estimating the Heating Value of Sewage Sludge: A New Correlation," Chapter 12 in Clean Energy from Waste and Coal, Edited by Khan, M. R., ACS Symposium Series No. 515, American Chemical Society, Washington, DC, 1992.
4. McMahon, M. A. and Khan, M. R., "Preparing Pumpable Mixtures of Sewage Sludge and Coal for Gasification," Chapter 13 in Clean Energy from Waste and Coal, Edited by Khan, M.R., ACS Symposium Series No. 515, American Chemical Society, Washington, DC, 1992.
5. Fleissner, H., "Drying of Coal," US Patent 1,632,828 July 21, 1927 and 1,678,078 July 31, 1928.
6. Zang, R. B., and Khan, M. R., "Gasification of Sewage Sludges," presented to New York Water Pollution Control Association Annual Meeting, January, 1991.
7. Khan, M. R., and Potas, T., "Hot-Water Upgrading of Low-Grade Coal: Fundamentals and Slurry Rheology," Preprints, Fuel Chemistry Division of ACS, American Chemical Society Annual Meeting, Atlanta, Georgia, 1991.

Figure 1. Relationship Between Heat-Treatment-Temperature and Slurry Solids Loading as a Function of Sludge Oxygen Content.

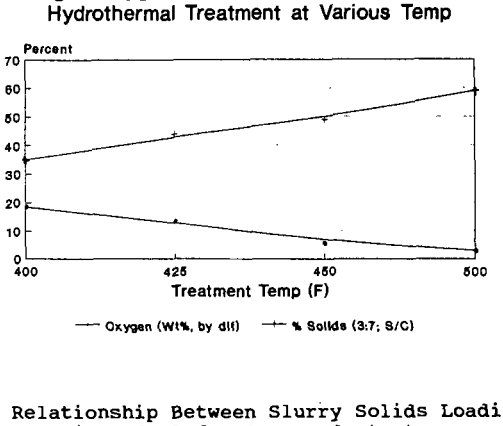

Figure 2. Relationship Between Slurry Solids Loading as a Function of Sludge Oxygen Content.

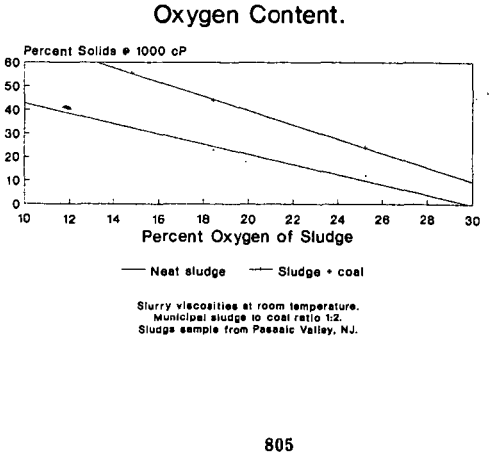

Figure 3. FT-IR Analysis of a Municipal Sludge

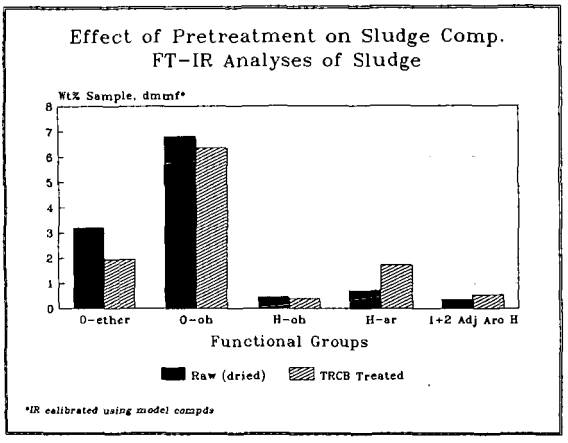

Figure 4. FT-IR Analysis of an Industrial Sludge

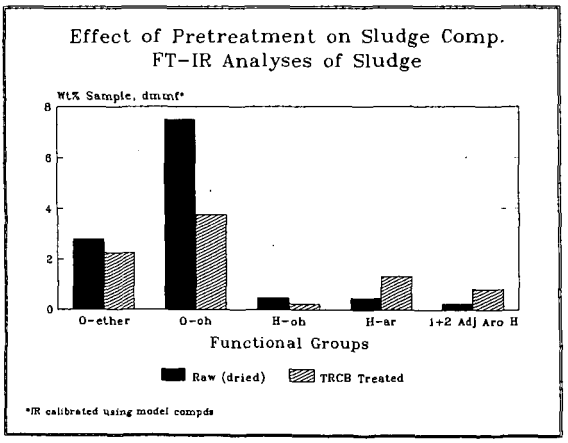

Figure 5. "Coalification" Curve: Atomic O/C Ratio Versus Atomic H/C Ratio

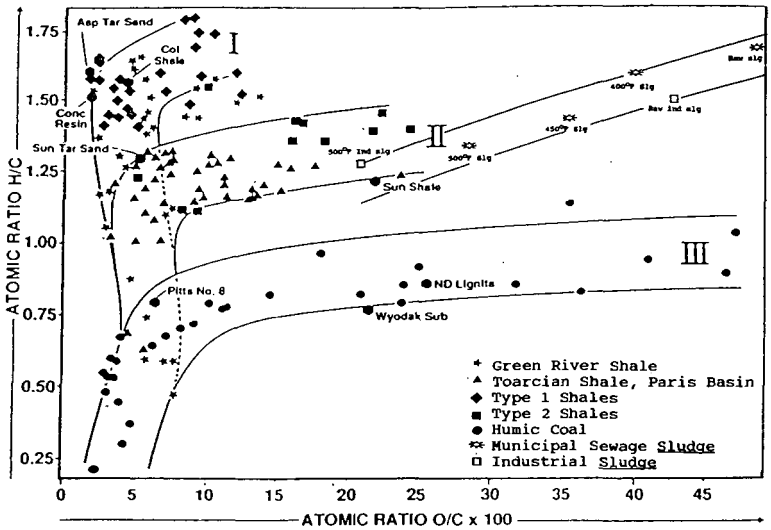

Figure 6.

Texaco Hydrothermal Treatment

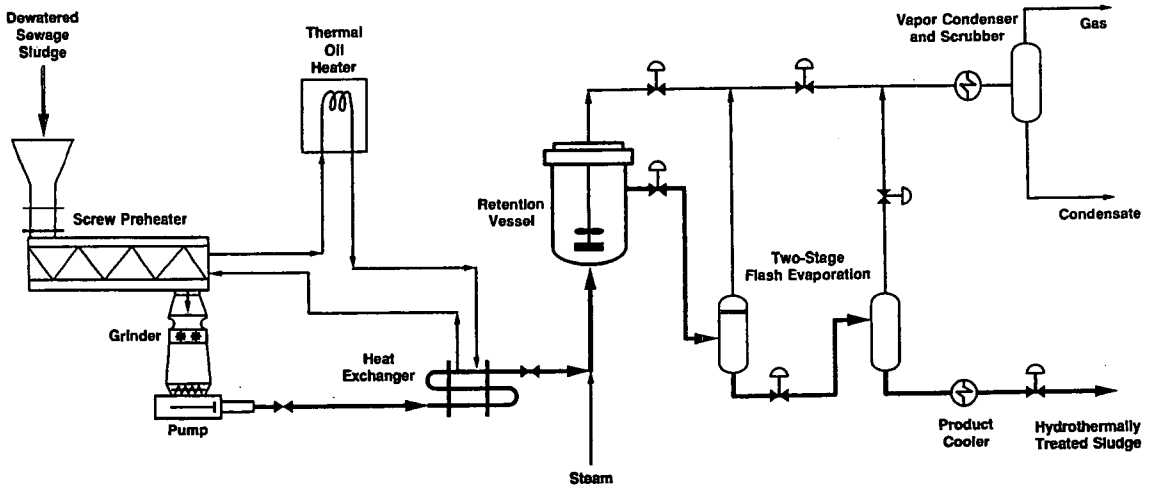

Figure 7.

TEXACO HYDROTHERMAL PDU RESULTS

Sludge:Coal 1:2; Slurry Rheology

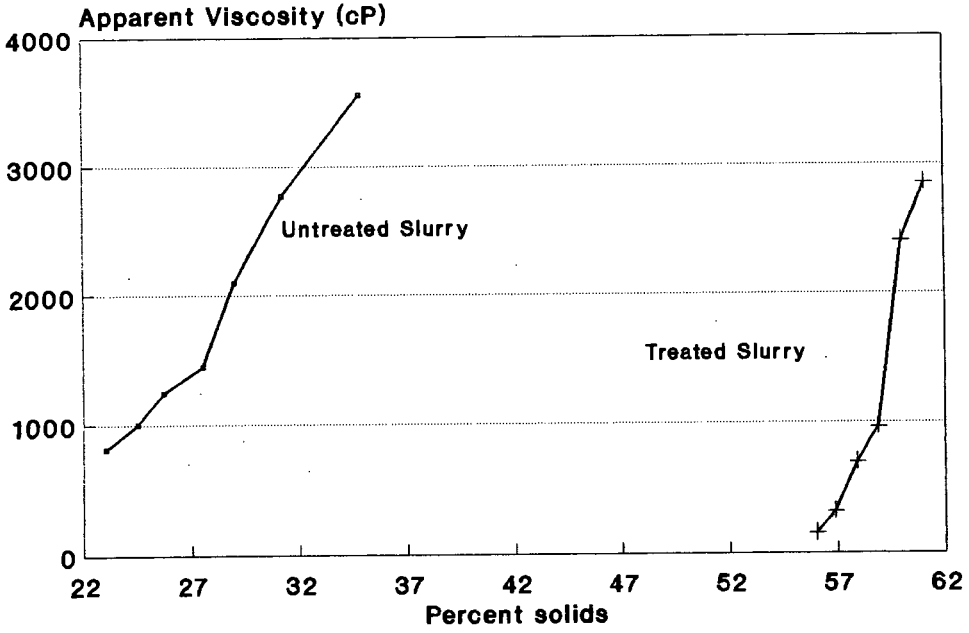

COLIQUEFACTION OF WASTE PLASTICS WITH COAL

M. Mehdi Taghiei, Frank E. Huggins, and Gerald P. Huffman

Consortium for Fossil Fuel Liquefaction Science
233 MMR Bldg., University of Kentucky, Lexington, KY 40506

Keywords: plastic wastes, coliquefaction, superacid catalysts.

ABSTRACT

Polyethylene (PE), poly(ethylene terephthalate) (PET), mixtures of PE and PET with different coals,and actual plastic wastes from such items as milk jug and soft drink bottles were liquefied in a tubing bomb reactor. Comparative experiments were performed at 400-450°C for times of 15-60 min. at a cold hydrogen pressure of 800 psi. The experiments used two types of catalysts: highly dispersed iron based catalysts and an HZSM-5 zeolite catalyst. Saturated oil, consisting of mainly straight chain alkanes and minor alkenes, and some light hydrocarbon gases were produced from liquefaction of both the plastic and the plastic-coal mixtures. Using PE, PET, and samples prepared from waste milk jugs and soda bottles alone with the HZSM-5 catalyst, 100% conversion with oil yields of 86 to 92% were obtained. Using coal/plastic mixtures with a highly dispersed iron catalyst, which gives excellent results for coal alone, somewhat lower conversions (53-91%) and oil yields (26-83%) were obtained. Further studies are in progress to explore the optimum conditions for direct liquefaction of plastic wastes and coal, and to examine the effect of a variety of potential superacid catalysts such as zeolite and highly dispersed sulfated metal oxides (e.g. Fe_2O_3/SO_4^{2-} and Fe_2O_3-ZrO_2/SO_4^{2-}).

INTRODUCTION

In recent years, disposal of plastic wastes has become an increasingly serious environmental concern. Due to an ever increasing volume of plastic products, sanitary landfills can no longer continue to be the major means for plastic wastes disposal. Plastics recycling appears to be a possible alternative solution and has potential for high growth. However, the recycling of plastics that takes place currently is not due to industry initiatives, but because of government edicts. In the United States, laws are in effect in states such as California, Oregon, and Wisconsin that require plastic bottles to be made of at least 25 wt% of recycled plastic. Similar laws in other states and federal laws are likely to follow. In Germany, the law requires that 80% of plastic wastes must be recycled by 1995. France has just recently passed a similar law.

In 1990, about 0.4 million tonnes of plastics in the form of soft drink bottles entered the municipal waste stream, of which 31.5% was recovered. However, out of seven million tonnes of total plastic wastes in the same year, only 3.7% was recycled (Figure 1)[1]. Conventional plastic recycling always faces the problem of contaminated and mixed plastic scrap, which cause difficulties in the recycling. The potential exists for impurities to diffuse into products packaged in recycled containers. Aside from toxic concerns, these impurities could also damage the processing equipment. Further, the equipment conversion or replacement costs in order to use reclaimed plastics are high and may not be economical for a small plastic molding industry. In addition to all these obstacles in the way of using recycled resin in industry, the average price of virgin high-density polyethylene in the U.S. is currently 30 cents per pound, while the price of recycled high density polyethylene is 32-33 cents per pound[2]! Conventional pyrolysis, as an alternative for plastic waste recycling, usually results in unsaturated and unstable oils of low yield and low value that can be used only for combustion.

Considering current conditions and expected future trends, of all the options that exist for plastics recycling, liquefaction of plastic and rubber wastes should be considered seriously for efficient and economical plastics recycling. Liquefaction of plastic wastes can not only provide a solution for plastics disposal, but can also generate an environmentally acceptable transportation fuel. The current rate of plastic waste materials that are disposed in the United States each year constitutes a potential hydrocarbon resource from which over 80 million barrels of oil per year could be produced. Moreover, coliquefaction of plastic wastes and coal could yield synergistic effects. Unfortunately, very few investigations have been conducted in this area and much work needs to be done to develop liquefaction strategies for recycling plastic wastes.

EXPERIMENTAL

In our preliminary experiments, a medium density polyethylene (PE), poly(ethylene terephthalate) (PET), mixtures of PE and PET with different coals, and actual plastic wastes from such items as milk jug and soft drink bottles were liquified in a one stage tubing bomb reactor in a fluidized sand bath using two different catalysts. This set of experiments is designed to investigate the effect of catalysts on the total yield and product distribution in the liquefaction process. The tubing reactor is first charged with feed materials and pressurized to 800 psi with hydrogen (cold). The reactor is then connected to an agitation apparatus and heated to desired temperature in a fluidized sand-bath while being agitated with a vertical motion at 400 cycles per min. during the reaction period. The liquefaction products from these experiments were determined by Soxhlet extraction with toluene, tetrahydrofuran (THF), and pentane. Comparative experiments were

performed for coliquefaction of mixtures of a medium density polyethylene (PE) and Blind Canyon coal and iron ion-exchanged Beulah lignite. The experiments used two types of catalysts: highly dispersed iron based catalysts and an HZSM-5 zeolite catalyst.

The quality of the oil products was examined using chemical analysis and gas chromatography. Extensive characterization studies are being carried out on the source materials, liquefaction products, and catalysts. A variety of analytical techniques are being used in these studies, including x-ray absorption fine structure (XAFS) spectroscopy, Mossbauer spectroscopy, x-ray diffraction (XRD), and transmission electron microscopy (TEM) for catalyst characterization.

RESULTS AND DISCUSSION

Saturated oils, consisting mainly of straight chain alkanes and minor alkenes, and some light hydrocarbon gases were produced from the liquefaction of both the plastic and the plastic/coal mixtures. The total conversion and oil yield for these experiments are listed in Table I. Using PE, PET, and samples prepared from waste milk jugs and soda bottles alone with the HZSM-5 catalyst, 100% conversion with oil yields of 86 to 92% were obtained. Using coal/plastic mixtures with a highly dispersed iron catalyst that gave excellent results for coal alone, somewhat lower conversions (53-91%) and oil yields (26-83%) were obtained. It is found that a mixture of iron ion-exchanged Beulah lignite[3] and polyethylene (in a ratio of 25:75) exhibits higher conversion than mixtures of 50:50 and 75:25 of these two components, but lower than that for pure polyethylene. Catalytic liquefaction experiments were carried out both with and without the presence of the solvent. Polyethylene in the presence of HZSM-5 catalyst on the other hand, exhibited higher conversion than either the polyethylene alone or mixture of polyethylene and superfine iron oxyhydroxide, implying synergistic effects. The quality of the oil products was examined using gas chromatography in collaboration with the UK Center for Applied Energy Resources (CAER) and the results for oil and gases produced during liquefaction of polyethylene are shown in Figures 2 and 3, respectively.

Further detailed studies are in progress to explore and establish the optimum conditions for direct liquefaction of waste plastics and coal, including the effect of temperature, pressure, reaction time, and coal/waste plastic ratio. The effect of a variety of potential superacid catalysts such as zeolite and highly dispersed sulfated metal oxide (e.g. Fe_2O_3/SO_4^{2-} and Fe_2O_3-ZrO_2/SO_4^{2-}) is also being investigated.

Acknowledgement
The authors would like to thank Mr. Robert Keogh and Dr. Burt Davis for their generous collaboration during the experimental portion of this work at the UK CAER. We also would like to acknowledge the support provided for this work by the U.S. Department of Energy as a part of the research program of the Consortium for Fossil Fuel Liquefaction Science.

References

1- Characterization of Municipal Waste in the United States; Washington, D.C.; U.S. Environmental Protection Agency.
2- Graff, Gordon; Modern Plastics, **1992,** 45.
3- Taghiei, M. Mehdi; Huggins, Frank E.; Ganguly, B; and Huffman, Gerald P.; Energy and Fuels, **1993,** in press.

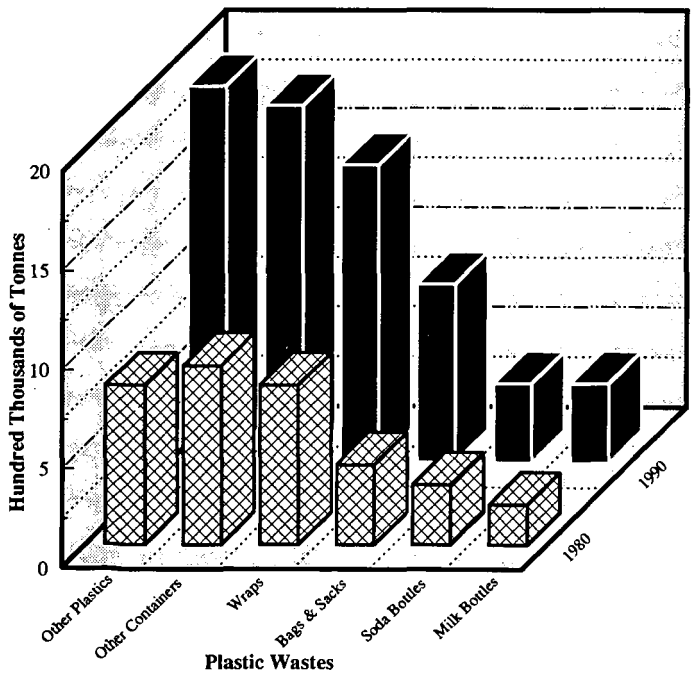

Figure 1. Characterization of Municipal Waste in the United States

Table I. Experimental results obtained from liquefaction of plastics, and coliquefaction of plastic/coal mixtures.

Sample	Additives	Temperature(C)	Total Conv.%	Oil Conv.%
PET	HZSM-5	420	100	92
PE	HZSM-5	420	100	88
PET	HZSM-5	400	100	90
Milk jug	HZSM-5	420	100	86
Coke Bottles	HZSM-5	420	100	93
lignite:PE 1:3	Fe-exch.+DMDS	450	91	83
lignite:PE 1:2	Fe-exch.+DMDS	450	67	51
lignite:PE 1:1	Fe-exch.+DMDS	450	53	40
PE	Tetralin	450	100	33
BC Coal:PE 1:1	Tetralin	450	70	42
BC Coal:PE 1:1	30Å FeOOH+DMDS	450	48	26
PE	30Å FeOOH+DMDS	420	100	76

PE = polyethylene, PET = Polyethylene Terephthalate, DMDS = Dimethyl Disulfide
BC = Blind Canyon coal, Fe-exch. = Iron ion-exchanged Beulah lignite

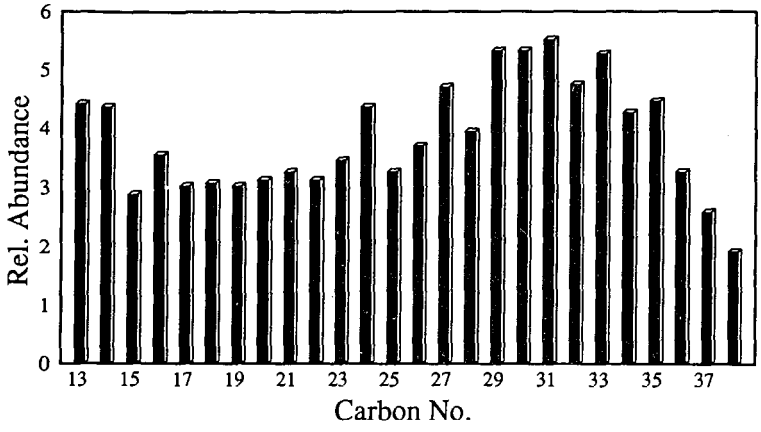

Figure 2. Pentane soluble products distribution of polyethylene

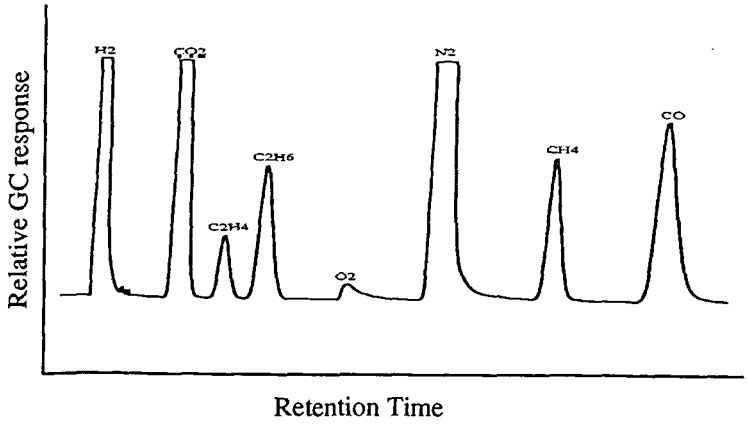

Figure 3. GC chromatogram of gaseous compounds produced during liquefaction of polyethylene

COLIQUEFACTION OF COAL AND POLYMERS TO LIQUID FUELS

L.L. Anderson and W. Tuntawiroon
Department of Chemical and Fuels Engineering
University of Utah
Salt Lake City, Utah 84112

Coal is our most abundant fossil fuel , but presently supplies only about 24 percent of our total energy. Petroleum provides over 40 percent of our energy, but recently, over one-half of our petroleum demand has been satisfied by imports. This situation constitutes both a strategic and an economic problem which could be partially alleviated by liquefaction of coal. A serious environmental problem is the disposal of polymer wastes such as polyethylene, polystyrene, polypropylene and used rubber tires. Over 22 million tons of plastic wastes are disposed of annually in landfills [1] and over 75 percent of discarded used tires are similarly treated (242 million tires in 1992).[2] Such waste polymers contain a large fraction of hydrogen which is needed to convert coal to high quality liquids. Coliquefaction of coal and waste polymers has the potential for supplying liquid fuels which could reduce our need on imported crude oil and refined products and at the same time, alleviate an environmental disposal problem.

Several others have studied the coliquefaction of coal with polymeric materials. Only a few will be mentioned here but they are significant relative to our research. W. Hodek combined coal with several plastic polymers with the idea of using coal as a hydrogen donor[3]. Using polyethylene, polystyrene, dechlorinated PVC, and "Trabant resin" in combination with coal, Hodek found coal to be a good hydrogen donor but the reaction rate was low. He also observed that some plastics formed condensation products in his experiments. Both Williams et al.[4] and Farcasiu[5] utilized rubber tire material to obtain liquid products. Farcasiu used tire rubber in combination with coal and found the quality of liquids produced from coal/polymer combinations higher than for products from thermal coal liquefaction in tetralin. Heptane soluble liquids (oil) represented over 80 percent of the products. This fraction was high in hydrogen (9.7 weight percent) and had low heteroatom content. Williams et al. used only pyrolysis to convert "automotive tyres" to products but nearly 60 percent of the charged rubber material was converted to gases and liquids. Temperatures were relatively high compared with conventional coal liquefaction processes (maximum yields were obtained at 720°C, the highest temperature studied). Molecular weights for the liquid "oil" fell between 100 to 1600 with the maximum number between 300 and 400. As with many pyrolysis processes, higher temperature treatments caused a shift in the molecular weights of the liquids to higher values.

Experimental

Coliquefaction experiments were conducted in tubing reactors (volume = 29 ml) which were heated in a fluidized sand bath. Reactions were conducted on dry coal and polymer mixtures or pure samples with shaking at 160 rpm and with hydrogen at 2000 psi. Pure polyethylene (PE), polystyrene (PS), and a commingled plastic mixture (mostly high density PE) obtained at a local recycling center were used with a high volatile bituminous coal (DECS-6-Blind Canyon, Utah, obtained from the Penn State Coal Sample Bank). Coal was ground to -100 mesh and plastics were ground to -8+25 mesh. In the case of commingled plastic, the bottles and containers were washed to remove contaminants and labels before size reduction by cutting and shaving. Final size reduction was done by grinding in a kitchen flour mill (stainless steel). Polyethylene and polystyrene were obtained from Aldrich Chemical Company. Analytical data for the coal and commingled plastic are given in Tables 1 and 2. In Table 3, trace element analyses for coal and commingled plastic waste (CPW) are given.

Table 1

Proximate Analysis of Coals and Plastic Waste
(weight percent, as received)

	Coals		Commingled Plastic
	DECS-6	DECS-17	Waste
Fixed Carbon	47.31	44.9	0.45
Volatile Matter	42.4	45.0	99.7
Ash	5.6	6.3	1.8
Moisture	4.7	3.7	0.06

Table 2.

Ultimate Analysis of Coals and Commingled
Plastic Waste (weight percent, as received)

	Coals		Plastic Waste
	DECS-6	DECS-17	
Carbon	81.7	82.05	86.3
Hydrogen	6.2	6.2	14.0
Nitrogen	1.6	1.4	.05
Sulfur	0.4	0.44	0.22
Oxygen (by diff.)	10.1	9.94	--

Table 3

Trace Element Analyses for Coals and Commingled Waste Plastic (ppm, wt. basis):

	Coals (Blind Canyon, Utah) DECS-6	DECS-17	Commingled Plastic Waste
Cr	6.0	6.0	0.77
Cd	--	--	0.19
Cu	9.0	9.0	--
Ni	<2.0	--	0.4
Pb	--	--	3.2
Zn	4.	3.0	--

Results and Discussion

We have extensively studied the liquefaction of Blind Canyon coal, which has a low pyrite content. Hydroliquefaction of this and other coals of similar rank gives high yields of liquid products at temperatures near 400°C. At higher temperatures, liquid yields decrease as more gases are produced. To determine if coliquefaction could be accomplished experiments were done using different combinations of coal and polyethylene (PE) and coal and polystyrene (PS). In Figure 1 results for total conversion of PE and coal show that highest conversion was obtained at 400°C for PE but little difference was observed for coal/PE at 350 and 400°C. Polystyrene was easier to convert to liquids and gases than was PE as shown in Figure 2. Conversion of PS only at 400°C gave nearly 90 percent conversion. In contrast to polyethylene, polystyrene liquefaction gave highest yields at 300°C (Figure 3). Polystyrene conversion differed from polyethylene in another important respect; gas production. At 300°C a 50:50 mixture of coal and polystyrene gave a conversion of 71.5 percent with most of the product as a liquid (62.3% of the total sample weight). However, at 400°C the conversion dropped to 58%, but the drop in liquids was even greater (to 15%). Coal/polyethylene liquid yields were essentially identical at 350 and 400°C (33.1% and 33.3%, respectively).

Commingled plastic waste (CPW) contained some polystyrene, and other plastics, but the most abundant polymer in this waste was high density polyethylene (HDPE). CPW was composed of many large and small drink bottles, soap containers, prescription drug containers, etc. Colors included black, transparent, red, orange, green and blue. This material was by far the most difficult to convert to liquids soluble in THF. As shown in Figure 4 the conversion values for commingled plastic was much lower than for either PS or PE. From the trend shown at different temperatures it appears that higher temperatures may be required to obtain satisfactory liquid yields. Other results not shown in Figure 4 have been obtained for 50/50 coal/CPW at 450 and 500°C. At these higher temperature, total conversions were 28 percent with liquid yields of 23 percent at 450°C and 35 percent with a liquid yield of

26 percent at 500°C. CPW/coal/waste rubber tire material (WRT) were reacted at 450°C (33/33/33) and gave only slightly higher conversion and liquefaction (36 percent and 32 percent, respectively). Even higher temperatures and/or suitable catalysts will obviously be required to obtain higher conversion and liquefaction values.

From work by others using waste rubber tire material (WRT) it has been observed that high yields of liquids and gases can be obtained. We also reacted WRT with coal and with coal/CPW. Table 4 gives results at 350°C using a catalyst, ammonium tetrathiomolybdate (1% of total feed weight) for coal only and mixtures of coal and WRT. Although simple mechanical addition of the catalyst was no better than hydroliquefaction without catalyst, impregnation from aqueous solution improved the liquefaction (from 56% to 79% for 60/40 coal/WRT).

Table 4

Results for hydroliquefaction of Blind Canyon Coal (DECS-17 and Waste Rubber Tire Material Using 1% (weight % of total feed) Ammonium tetrathiomolybdate. (Temperature = 350°C)

% Coal in feed	% WRT in feed	Catalyst addition	Yields, (wt. %) Liquids (THF Sol.)	Gas
100	0	none	36	2
60	40	Impregnated	79	2
50	50	Impregnated	65	2
50	50	Mechanically added	55	1
60	40	none	56	2

Reaction of coal and plastic materials, especially commingled plastic waste (CPW) has so far given only marginal results. Even for relatively long reaction times (1 hour) and temperatures up to 500° C liquid yields are less than we have obtained for hydroliquefaction of coals. Further work and characterization of the liquid products will be necessary to improve the conversion of coal/plastic streams to high quality liquid products.

Summary

Hydroliquefaction of coal, polyethylene, polystyrene and waste rubber tire material individually gives good conversion and liquefaction yields. Combinations of these materials gave less satisfactory results as far as liquid yields were concerned. Catalyst application (molybdenum) enhances the reaction to increase liquid yields and to produce higher quality liquids.

Acknowledgement

The financial support for this work by the U.S. Department of Energy through the Consortium for Fossil Fuel Liquefaction Science and the University of Utah is gratefully acknowledged.

References

1. Franklin Associates, Ltd., Characterization of Plastic Products in Municipal Solid Waste. Final Report February 1990; prepared for the Council for Solid Waste Solutions.
2. Hearing before the Subcommittee on Environment and Labor and Subcommittee on Regulation, Business Opportunities, and Energy of the Committee on Small Business: House of Reprsentatives, Apr. 18, 1990. Scrap Tire Management and Recycling Opportunities; Serial No. 101-52.
3. Hodek, W., "Low Temperature Pyrolysis of Plastic Waste in the Presence of Coal," Internat. Conf. Coal Sci. Proc., 1991, pp. 782-785.
4. Farcasiu, M., "Another Use for Old TIRes," 1993, ChemTech. January, pp. 22-24.
5. Williams, P.T., S. Besler, and D.T. Taylor, "The Pyrolysis of Scrap Automotive Tyres" 1990, *FUEL*, Vol. **69**, pp. 1474-1482.

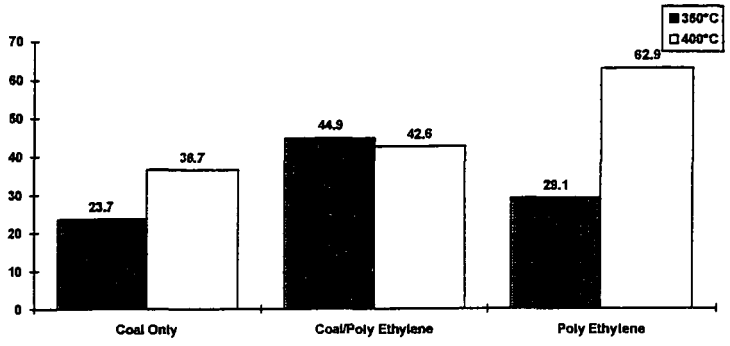

Figure 1. Coliquefaction yields for Blind Canyon Coal and PE (50/50) at two temperatures. Values are total conversion.

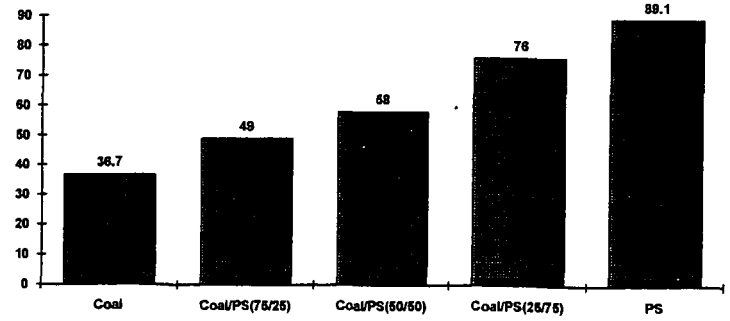

Figure 2. Coliquefaction conversion (liquids + gases) for Blind Canyon Coal and PS at 400°C (weight percent).

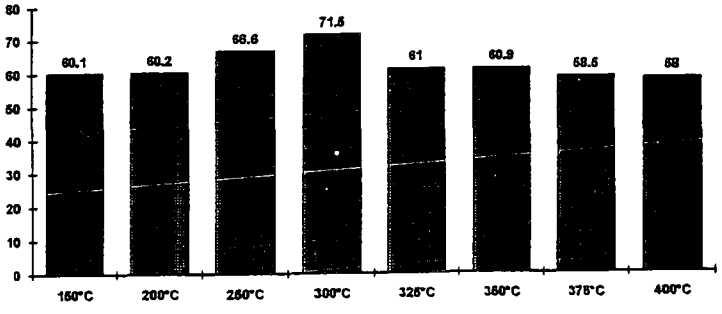

Figure 3. Coliquefaction yields (liquids + gases, weight percent) for Blind Canyon Coal and PS (50/50) different temperatures.

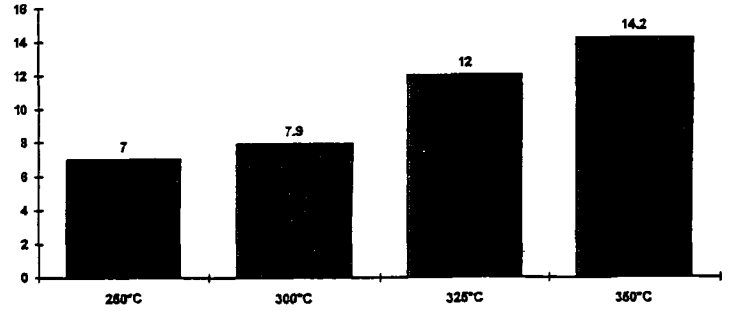

Figure 4. Coliquefaction yields (liquids + gases, wt percent) for Blind Canyon Coal and Commingled Plastic waste (50/50) at different temperatures.

MICROSCALE SIMULATION OF HIGH PRESSURE THERMAL AND CATALYTIC CONVERSION PROCESSES IN COAL AND WASTE POLYMERS WITH ON-LINE GC/MS

Kui Liu, Emma Jakab, William H. McClennen and Henk L. C. Meuzelaar

Center for Micro Analysis and Reaction Chemistry
University of Utah, Salt Lake City, Utah 84112

Keywords:(on-line TG/GC/MS, coal, rubber, hydropyrolysis)

INTRODUCTION

Over 279 million automotive tires are discarded in the United States each year.[1] These used tires cause serious environmental problems since they are non-biodegradable, occupy considerable land-fill space, and emit noxious fumes when burned. One of the promising approaches to deal with used rubber is the co-processing of it with coal to produce hydrocarbon liquids for use as fuels and specialty chemicals. Recently there have been numerous studies on co-processing of tire rubber and coal since depolymerized rubber has good solvent properties and the carbon black which constitutes of about 20-30% of the rubber is a good catalyst for depolymerization and possibly enhanced coal liquefaction.[2,3,4,5] Monitoring sample weight loss as a function of temperature with on-line analysis of the evolved products during the co-processing reactions is necessary to elucidate mechanisms and kinetics of the key conversion reactions. Due to the high pressure and high temperature required by some of the most interesting processes, it is difficult to continuously monitor the weight loss and reaction intermediates without interrupting the reactions.

On-line analysis techniques for high pressure conversion reactions have been reported previously,[6,7] but these systems did not monitor total weight loss vs reaction temperature. They also were not applied directly to coal conversion studies because of the strong potential for plugging of sample orifices with pulverized coal.

Microscale simulation of coal conversion reactions has been performed by high pressure thermogravimetry with on-line combined gas chromatography and mass spectrometry (TG/GC/MS). It requires only a small sample size and can be operated at high temperature and pressure. The weight loss and low molecular weight products can be monitored vs reaction temperature. Analysis of pyrolysis and hydropyrolysis of coal, rubber and coal with tire rubber, with or without catalyst, by high pressure TG/GC/MS are reported here.

EXPERIMENTAL

High Pressure TG with On-Line GC/MS

The system as shown in Figure 1 consists of the high pressure TG instrument, pressure reduction line, vapor sampling inlet, short GC column and MS detector. A Cahn high pressure TG-151 was used as the reactor. The reactor vessel was made from a quartz tube which is corrosion resistant and has no known catalytic effect on the reaction. This reactor can be operated up to 1000 psi with temperatures up to 1000 C and heating rates ranging

from 0 to 25 C/min. The experiments in this study were operated at 900 psi with a heating rate of 10 C/min up to 600 C followed by a 10 min hold of the final temperature. The reagent gas was either helium or hydrogen. The quartz crucible used for holding the sample was modified as shown in Figure 1. The modified crucible with an open hole at the bottom greatly increased the sensitivity of the GC/MS detection since the vapor products go directly into the quartz sampling tube, which reduced the amount of sample necessary. The coal and tire rubber used were 60 mg each. The pressure of the reactor was kept constant by a back pressure regulator. During operation the reagent gas is flowing continuously through the reactor at 500 ml/min (ambient). A 1 m x 50 μm i.d. fused silica capillary is used as a pressure reduction line, which carries vapor products to the ambient pressure sampling device. A novel automated vapor sampling (AVS) inlet developed at the University of Utah (U.S. Patent No. 4,970,905), provides automated, repetitive vapor sampling for the GC column. Samples were taken each 73 seconds. The AVS inlet was connected directly to a 2m x 150 μm i.d. fused silica capillary column coated with methyl silicone (CP-SIL-5CB). The short column was operated isothermally at 90 C and provided rapid separation of the vapor products. The separated products were detected by a small quadruple MS system, the Hewlett Packard model 5971A MSD operating at 70 eV electron energy.

Materials

Blind Canyon (DEC-6), Utah coal (-100 mesh) from the Penn State sample bank was employed in this study. The proximate analysis of the coal is listed in Table I. The experimental procedure for impregnating coal with catalyst is described by Anderson et al.[8] The catalyst used in the experiments was 1% Fe as iron chloride hexahydrate [$FeCl_3 \cdot 6H_2O$] promoted with 0.05% Mo as ammonium tetrathiomolybdate [$(NH_4)_2MoS_4$]. The used tire rubber was scraped, cut into small pieces and then ground into fine particles in a cryogenic grinder with liquid nitrogen. The weight ratio of coal to rubber for the mixture was 1:1.

RESULTS AND DISCUSSION

The thermal decomposition of Blind Canyon coal, tire rubber and the mixture of coal and rubber was studied at high pressure under various conditions as seen in Table II. The thermogravimetric profiles are shown in Figure 2 indicating the different course of decomposition of the samples. The complex structure of coal resulted in continuous volatile product evolution up to the final temperature of the experiment (600 C) whereas the flat weight curves of rubber above 500 C suggest that only the relatively inert carbon black and inorganic filling are left and the organic components have been completely devolatilized. Although the volatile evolution of rubber is shifted to somewhat lower temperature in hydrogen atmosphere, the TG profile similarity in helium and hydrogen atmospheres is apparently due to the high inherent hydrogen content of rubber. The effect of hydrogen is clearly visible in the coal decomposition, where a significant increase in volatile product evolution can be observed above 500 C. Adding liquefaction catalyst to the coal and coal + rubber samples increases the total weight loss (Table II) by about 3-4% and the volatile evolution occurs at lower temperature. The effect of rubber on the coal decomposition is not apparent solely by looking at the thermogravimetric results.

Figure 3 shows the average mass spectra of the volatiles evolved from 350 to 600 C from coal and rubber as well as coal + rubber with and without catalyst in hydrogen

atmosphere. The spectrum of the high volatile bituminous coal is dominated by alkene (m/z 41, 55, 69, 83, etc.), and alkane (m/z 43, 57, 71, 85, etc.) fragment ion series as well as aromatic hydrocarbons (m/z 78, benzene; m/z 91, toluene fragment) and phenols (m/z 94, phenol; m/z 107, cresol fragment). The rubber spectrum shows the formation of unsaturated hydrocarbon ions from the butadiene segments of rubber (e.g., m/z 67, methyl butadiene fragment) and aromatic hydrocarbons originating from the styrene moieties (e.g., m/z 91, toluene fragment; m/z 104, styrene). It should be noted that the oil additive of rubber may also release aromatic products. The spectra of the coal + rubber mixture (ratio 1:1) resemble the rubber spectrum at first sight because the rubber releases higher amounts of organic volatiles than the coal. The evaluation of average mass spectra is further complicated by the formation of several common products from coal and rubber (e.g., alkyl aromatics and alkenes). In spite of these difficulties it can be seen that the intensity of several ions is not additive and the presence of catalyst changes the product distribution. More detailed information can be obtained about the effect, of the rubber and catalyst on the coal hydropyrolysis by using the time resolved data.

As discussed in the experimental section, samples were taken every 1.22 minutes from the volatiles evolved from the TG furnace and analyzed by MS after separation on a short GC column. The total ion intensity profile of coal obtained by this method can be seen in Figure 4a indicating that the maximum rate of decomposition occurs at 480 C. Enlarging one sampling period, the total ion curve shows the separation of several compounds within the 1.22 min interval (Figure 4b). Although the resolution is insufficient in the low MW range due to the relatively high column temperature (90 C), the extracted single ion chromatograms can be used for further analysis. Figures 4c and d show the abundance of characteristic alkene (m/z 55) and alkane (m/z 57) fragment ions revealing the increase of alkene/alkane ratio with decreasing carbon atom number. The intensity profile of a typical alkyl phenol fragment ion (m/z 107) indicates (Figure 4c) that not only different MW compounds (cresol vs. xylenol), but certain isomers (ethyl phenol vs. dimethyl phenol) can be separated on the short column.

The hydropyrolysis of tire rubber results in the formation of a large variety of products, as shown by the total ion current profile in Figure 5a. Figures 5b, c and d display the intensity profiles of three ions representing the three types of products. The butadiene segment of rubber releases primarily butene (m/z 56), exceeding the yield of butadiene, apparently due to the hydrogen atmosphere and high pressure applied. Styrene (m/z 104) is the major product of the polystyrene segments. Various alkyl, alkenyl, alkadienyl benzenes are released containing both building elements of the rubber polymer; m/z 117 (C_3H_4-benzene) represents a characteristic alkenyl benzene fragment ion in Figure 5d. M/z 104 ion is formed from several compounds beside styrene (Figure 5c). The evolution of styrene starts at lower temperature than the formation of other alkenyl benzenes as shown by the intensity profile of m/z 104 expanded to the whole temperature range in Figure 5c. Although the simple thermogravimetric curve does not reveal the complex reaction route, the different evolution profiles of products suggest a multiple step decomposition mechanism.

The most important products of the thermal decomposition of Blind Canyon coal were presented above. The next Figure (Figure 6) shows the effect of hydrogen reactant gas and a liquefaction catalyst on the evolution profiles of four characteristic products of coal. The TG curve of coal (Figure 2) exhibits two main decomposition regions in hydrogen atmosphere (350-520 C and above 520 C). The rate of volatile evolution up to 520 C is similar in

hydrogen and helium suggesting that hydrogen does not promote the devolatilization significantly in this temperature range. This assumption is confirmed by the intensity profiles of the individual ions in Figure 6. Although there are some variations in the evolution curves the overall difference does not seem to be significant in the lower temperature range. However, the formation of alkyl aromatic products (m/z 92, toluene and m/z 142, methyl naphthalene) is greatly enhanced at high temperature in hydrogen atmosphere. The liquefaction catalyst applied in hydrogen atmosphere increases the yield of each product. Some increase is observed in the high temperature release of alkyl aromatics in comparison with the uncatalyzed coal experiment in hydrogen. Furthermore, the catalyst promotes the formation of alkanes (m/z 43 propyl fragment of C_3-C_9 alkanes) and phenol (m/z 94) as well as methyl naphthalene at lower temperatures.

The mixture of coal and tire rubber (ratio 1:1) was used for simulation of their co-processing under high pressure in hydrogen atmosphere. Figure 7 compares the evolution profiles of m/z 92 and m/z 94 from coal, rubber and the mixture. The absolute intensities cannot be evaluated due to the different experimental conditions; therefore the intensities are scaled for equal height. The toluene evolution profile of the mixture (Figure 7a) appears to be the sum of the individual components. Other hydrocarbons exhibit similar behavior, however, it should be emphasized that this is not a quantitative comparison.

The spectra of both coal and rubber contain the m/z 94 ion, however, it represents two different compounds, phenol and heptatriene, respectively. Due to the chromatographic separation, the intensity profile of each product can be monitored separately in the mixture, as seen in Figure 7b. The heptatriene evolution occurs at about the same temperature from the rubber and the mixture. The rate of phenol formation from coal shows two maxima in hydrogen atmosphere (at about 450 C and 550 C). The presence of rubber significantly promotes the release of phenol in the lower temperature range (350-520 C).

CONCLUSIONS

Simulation of thermal and catalytic coal conversion processes was carried out in inert helium vs hydrogen atmospheres using a high pressure thermobalance coupled on-line to a GC/MS. The weight loss curves and the intensity profiles of products show that the volatile evolution of Blind Canyon coal significantly increases above 500 C in hydrogen atmosphere in comparison with helium due to the release of alkyl benzenes and alkyl naphthalenes. The Fe, Mo liquefaction catalyst increases not only the yield of alkyl aromatics, but enhances the formation of aliphatic hydrocarbons and phenols in the lower temperature range (350-520 C).

The presence of tire rubber appears to promote the phenol formation at 350-520 C, but the evolution profiles of other products seems to be additive in the mixture of coal and rubber. However, further experiments are required to reveal the effect of rubber on the yield of the individual products of coal.

ACKNOWLEDGEMENTS

We would like to thank Professor Larry L. Anderson and W. Tuntawiroon (University of Utah) for providing us with the samples of catalyst impregnated coal. We also acknowledge the U.S. Department of Energy through the Consortium for Fossil Fuel Liquefaction Science and the State of Utah who financially supported this research.

REFERENCES

1. Hearing before the Subcommittee on Environment and labor and Subcommittee on Regulation, Business Opportunities and Energy of the Committee on Small Business: House of Representatives, April 18, 1990. *Scrap Tire Management and Recycling Opportunities*, Serial No.101-52.
2. Farcasiu, M.; Smith, C. M. *Fuel Chem. Preprints. Am. Chem. Soc.* 35 (1990), 404.
3. Farcasiu, M.; Smith, C. M.; Hunter, E. A. *Proc. 1991 Conference on Coal Science*, IEA Coal Research Ltd. (Ed.), Butterworth: Heinemann Ltd., 1991, p. 166.
4. Farcasiu, M.; Smith, C.M. *Prepr. Pap. Am. Chem. Soc. Div. Fuel Chem.* 37 (1992), 472.
5. Farcasiu, M. *Chem TECH*, January (1993), 22.
6. Huai, H.; Tsai, C.H.; Shabtai, J.S.; Meuzelaar, H.L.C., *Prepr. Pap. Am. Chem. Soc. Div. Fuel Chem.* 37 (1992), 925.
7. Dworzanski, J.P.; Chapman, J.N.; Meuzelaar, H.L.C., *Prepr. Pap. Am Chem. Soc. Div. Fuel Chem.* 37 (1992), 424.
8. Anderson, L.L.; Yuen, W.H.; Jaturapitpornsakul, J., *Prepr. Pap. Am. Chem. Soc. Div. Fuel Chem.* 38 (1993), 142.

Table I. Proximate Analysis of Blind Canyon (DEC-6) Coal

	as received
Moisture (wt.%)	4.73
Volatile matter (wt.%)	42.40
Fixed carbon (wt.%)	47.31
Ash (wt.%)	5.56

Table II. Weight Loss Data from High Pressure TG

	Fe, Mo Catalyst	Reactant Gas	Weight Loss, %
Coal	No	He	36.6
Coal	No	H_2	54.7
Coal	Yes	H_2	57.9
Rubber	No	He	66.6
Rubber	No	H_2	67.5
Coal + Rubber	No	H_2	57.7
Coal + Rubber	Yes	H_2	61.8

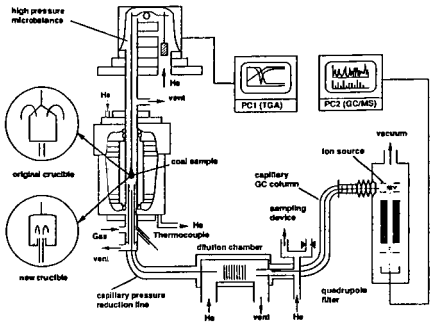

Figure 1. Schematic of the TG/GC/MS system.

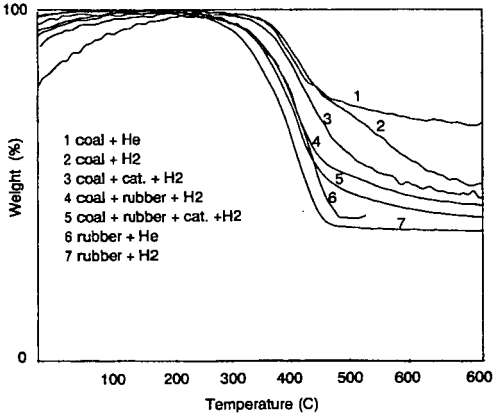

Figure 2. TG curves of coal and rubber under various conditions at high pressure (900 psi).

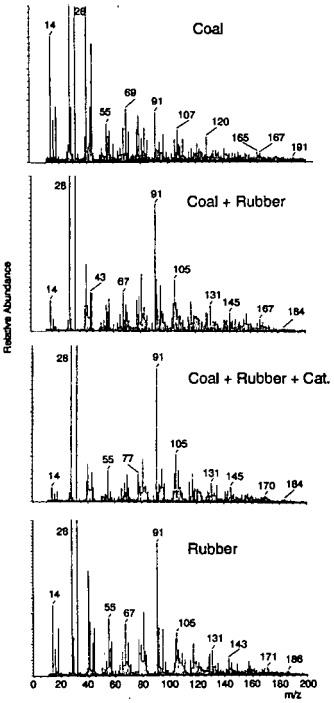

Figure 3. Average mass spectra of hydropyrolysis products of coal, rubber and coal + rubber with and without catalyst from 350 C to 600 C. (m/z 14, 28, 32, 40 are background peaks.)

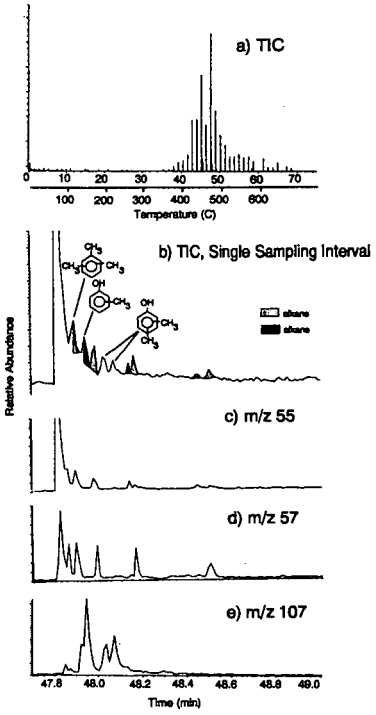

Figure 4. Thermal decomposition of coal in helium atmosphere. Total ion intensity a) in the whole temperature range; b) in a single sampling interval. Ion intensity of c) m/z 55, alkene; d) m/z 57, alkane; e) m/z 107, cresol fragment.

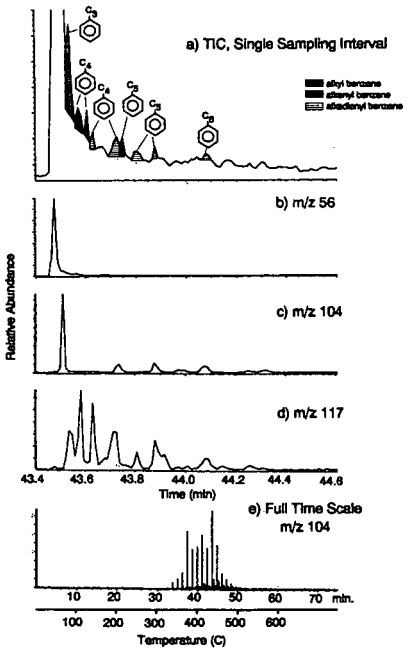

Figure 5. Decomposition of rubber in hydrogen atmosphere. a) Total ion intensity; ion intensity of b) m/z 56, butene; c) m/z 104, styrene; d) m/z 117, C_3H_7-benzene fragment; e) m/z 104 in the whole temperature range.

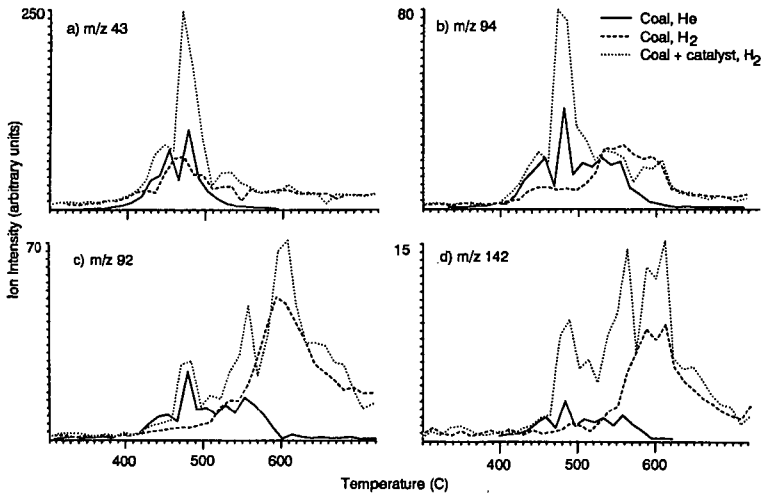

Figure 6. Effect of hydrogen and catalyst on evolution profile of coal decomposition products. a) m/z 43, propyl fragment, b) m/z 94, phenol; c) m/z 92, toluene; d) m/z 142 methyl naphthalene.

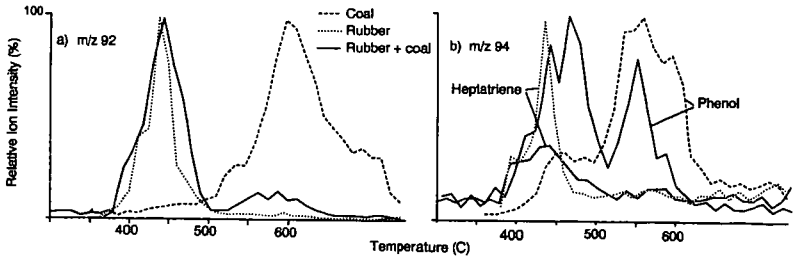

Figure 7. Evolution profile of a) m/z 92, toluene; b) m/z 94, phenol and heptatriene from the hydropyrolysis of coal, rubber and the mixture of coal and rubber.

A PROCESS TO RECOVER PLASTICS FROM OBSOLETE AUTOMOBILES BY USING SOLVENTS AT AMBIENT PRESSURE*

by
Bassam J. Jody
Edward J. Daniels
Patrick V. Bonsignore
Norman F. Brockmeier

Argonne National Laboratory
Argonne, Illinois

INTRODUCTION

Recycling of the metal content of obsolete vehicles has been actively pursued since the 1950s [1]; today, obsolete automobiles are the single largest source of scrap iron. They contribute over 25% of the 36 metric tonnes (40 million short tons) of ferrous scrap recovered annually by the secondary metals industry and used in the production of finished steel products. They also contribute over one million metric tonnes (1.1 million short tons) of nonferrous metallic scrap a year for recycling. For each ton of metals recovered, about 500 lb of nonmetallic residue or waste is co-produced. Auto shredder residue (ASR) is a very heterogeneous mixture of solids and liquids. Table 1 lists most of the materials that are commonly present in the ASR. Figure 1 shows the relative concentration of the major constituents.

We have developed and tested in the laboratory a three-step process to separate thermoplastics, and other potentially recyclable products, from ASR [2]. The process involves a drying step followed by a mechanical separation step to concentrate the thermoplastics by separating the polyurethane foam and the fines, which are mostly metal oxides and other inert materials that are smaller than 0.62 cm (0.25 in.) in size. The concentrated plastics stream is then treated with organic solvents at ambient pressure and elevated temperatures to dissolve the desired plastics. The basic process is described in detail in Reference [2]. The salient features of the process are described below.

THE ARGONNE ASR-RECYCLING PROCESS

The Argonne process consists of three steps: drying, mechanical separation to concentrate the plastics, and solvent extraction of the plastics. The drying process is by indirect heating (i.e., steam coil) only. Flame or sparks could potentially set the material on fire. Drying at lower temperatures will minimize the evaporation of organic species along with the moisture, thereby avoiding a potential environmental problem that may require scrubbing or wastewater treatment.

The mechanical separation of polyurethane foam and fines (< 0.62 cm in size) from ASR is necessary for many reasons. First, the foam can be recovered as a potential product. Second,

* Work supported by U.S. Department of Energy, Assistant Secretary for Conservation and Renewable Energy, under Contract W-31-109-Eng-38.

the plastics in the remaining fraction can be concentrated (this results in smaller and less expensive equipment for the solvent-extraction operation and in lower solvent losses because fewer nonplastic materials that can absorb solvent [foam] or be wetted by it [dirt] will be present). Third, the presence of the fine, nonplastic particles will contaminate the extracted plastics unless excessive and costly filtration of the fine particles from the solution is performed. The mechanical separation was accomplished in the laboratory by using a fluidized column fitted with screens [2]. In the design of a 200-lb/day pilot plant, the plan is to use a trommel combined with a modified air classifier. Tests were conducted on several types of commercially available full-scale separation equipment. The trommel was selected because its of acceptable performance, moderate cost, and widespread use in the shredding industry.

An evaluation of the plastics-rich stream that remained after the separation of the foam and the fines, identified acrylonitrile-butadiene-styrene (ABS), polyvinyl chloride (PVC), polypropylene (PP), and polyethylene (PE) as potential candidates for recovery and recycling. ABS was targeted because of the high market value of the virgin resin and because of its good solubility characteristics in several mild organic solvents at low and moderate temperatures. PVC was selected because its chlorine content could be an obstacle if the stream is to be processed for its energy or chemical value (incineration, pyrolysis). In addition, reasonably clean PVC can also be used for making numerous products with flexible specifications. PVC, however, is susceptible to degradation upon thermal cycling; among the first signs of degradation is the appearance of a blackish color. PP was targeted for recovery because it is present in large quantities and its use by the automotive industry is on the rise. Moreover, because it is soluble only at high temperatures, it can be recovered with little contamination, except for the PP, which dissolves under very similar conditions. At this point, the economic values of PE and PP are not sufficient to justify their separation.

To minimize the contamination of the recovered plastics, the first step in the extraction process was to use a mild solvent (such as hexane) to extract the automotive fluids (see Table 1) without dissolving the targeted plastics. The "oils" recovered in the process have heating values between 16,000 and 178,000 Btu/lb. However, the hexane also extracts the PCBs that may be present in the ASR.

After the "oils" are extracted, the extraction of the plastics at ambient pressure was tested by using two methods. In the first method, selective solvents were used to extract individual plastics in series [2]. In the second method, a solvent was used to dissolve all of the plastics of interest, and then the mixed plastics were separated by using different solvents. Each method has advantages and disadvantages. For example, in the first method, the ABS and the PVC can be recovered without being exposed to the high temperature required for the recovery of PP and PE. However, the extraction steps occur in large reactors. In the second method, only one extraction has to be done in a large vessel. The separation of the mixed plastics can be conducted in smaller reactors. In addition, the second method enables more efficient cascading of the heat between the stages to minimize the energy requirement of the process. All of the plastics will, however, be exposed to the high temperature and will experience a higher number of thermal cycles. Therefore, the potential degradability of some of the products is higher. Products generated by both methods are under evaluation. The economics of both methods is also being studied.

Figures 2, 3, and 4 are the infrared spectra of recovered ABS, PVC, and PP/PE samples, respectively.

PROCESS ECONOMICS

Table 2 summarizes the key parameters used in and the results obtained from a preliminary economic study that we have recently completed. The results indicate that a three-year payback is realistically possible. This study assumed that the plant will charge no tipping fees for accepting the ASR and will pay no fees for the disposal of the nonmagnetic fines. It was, however, assumed that the recovered oil will be disposed of as a hazardous waste. No revenues were assumed for the material left after the extraction process is completed, even though it has a heating value of about 3,000-5,000 Btu/lb and is virtually dry, PCBfree, and nearly chlorine-free.

CONCLUSIONS

The work done so far on the process demonstrated that the process is technically feasible and potentially economical. The process uses all commercially available equipment, even though it can benefit from a better system for the mechanical removal of foam and fines. The economic competitiveness of the process is dependent on the market value of the recovered foam and the recovered plastics.

REFERENCES

[1]. Jody, B.J., and E.J. Daniels, "Automobile Shredder Residue: Treatment Options", Hazardous Waste & Hazardous Materials, Vol. 8, Number 3, pages 219-230, 1991.

[2]. Daniels, E.J., B.J. Jody, and P.V. Bonsignore, "Alternatives for Recycling of Auto Shredder Residue", the Journal of Resource Management and Technology, Vol. 29, Number 1, pages 14-26, March 1992.

Table 1. Composition of ASR

Recyclables	Energy Value*	Inerts
Thermoplastics	Gasoline	Glass
Foams	Brake fluid	Dirt
Fibers	Engine oil	Sand
Metal chunks	Transmission oil	Gravel
Rust	Grease	Moisture
Wires	Wood chips	
	Thermosets	
	Rubber	
	Tar	
	Paper	

* Heating value is about 2,500-7,000 Btu/lb.

Table 2. Economic Analysis of the Argonne Plastics-Recycling Process

Item	Description/Value
Plastics product form	Pellet
Process type	Precipitation
Raw material source	ASR
Feed (MM PP)	183
Plastic output (MM PP)	25
Capital investment (MM)	7.5
Operating pressure (atm)	1
Costs (cents/lb)	
Variable	11
Fixed	8
Subtotal mfg. cost	19
Depreciation (20%)	5
Charge for ROI + wk cap	6
Netback Req'd (ex SAR)	30
Annual Realization (MM$)	+1.6*
Payout time (yr)	3

* Value is determined on the basis of assumed values for the recovered materials of $0.25/lb for foam and PVC, $0.05/lb for PP&PE, and $0.40/lb for ABS.

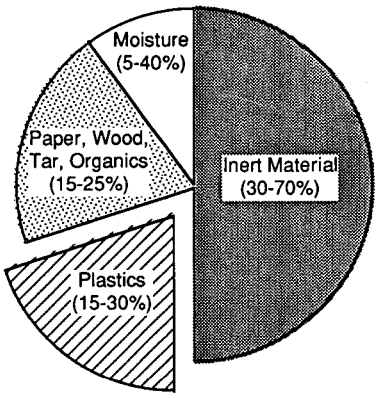

Figure 1. Approximate Composition of ASR

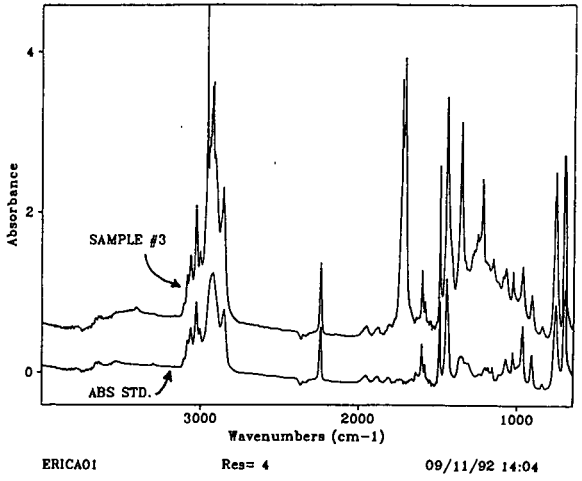

Figure 2. Infrared Spectra of Recovered ABS and Commercial-Grade ABS

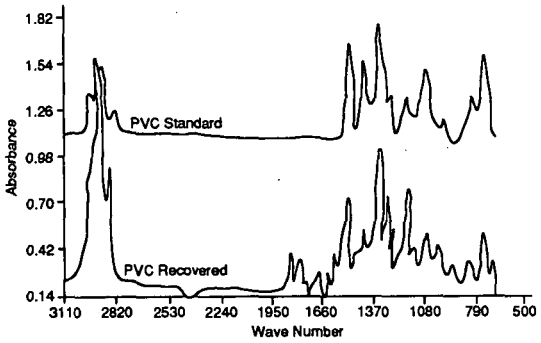

Figure 3. Infrared Spectra of Recovered PVC and Commercial-Grade PVC

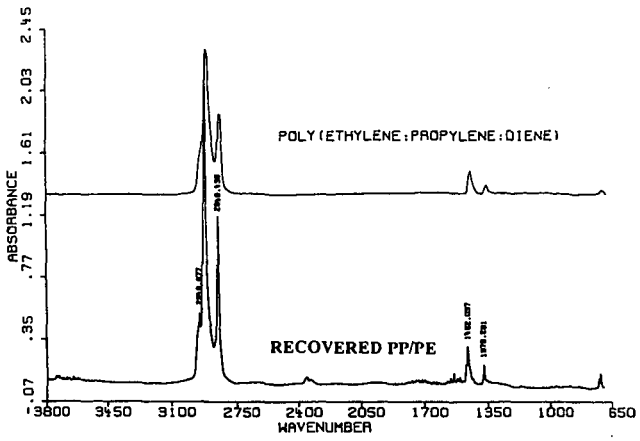

Figure 4. Infrared Spectra of Recovered PP/PE and PP/PE-Diene

TREATMENT TECHNOLOGY FOR AUTO FLUFF

Michael C. Mensinger and Amir Rehmat
Institute of Gas Technology
Chicago, IL 60616

Satish C. Saxena and N. S. Rao
University of Illinois
Chicago, IL 60612

INTRODUCTION Auto fluff is the non-metallic material that remains after junked automobiles are stripped and then shredded to recover their metal (primarily ferrous) and other valuable components. The composition of auto fluff varies, however, it is generally comprised of scrap metal (wire, molding, etc.), plastic, vinyl, leather, cloth, sponge, foam, glass, and other non-combustibles. In addition, traces of lead, cadmium, chromium, and mercury are present along with organic compounds, such as oil, antifreeze, transmission and brake fluids, and polychlorinated biphenyls (PCB).

It is estimated that each year, the 200 or so automobile shredders[1] in the U.S. generate as much as 3 to 4 million tons of auto fluff.[2] Currently, most auto fluff is sent to municipal landfills or is stored on the site of the auto shredder facilities. The presence of PCBs and heavy metals in auto fluff render some samples hazardous wastes according to the U.S. Environmental Protection Agency (EPA) Toxicity Characteristic Leaching Procedure (TCLP). These materials must be stored in specially designed land- or monofills. The reduction of existing landfill capacity, mounting disposal costs and more stringent legislation on auto fluff disposal have spurred the development of alternative methods of disposing or reducing the volume of material that must be landfilled.

TWO-STAGE AGGCOM COMBUSTOR The Institute of Gas Technology (IGT) is developing the two-stage fluidized-bed/cyclonic agglomerating (AGGCOM) combustor (Figure 1) for treating soils and other materials, such as auto fluff, that are contaminated with both organic and inorganic compounds. The AGGCOM combustor combines the fluidized-bed gasification and cyclonic combustion technologies that have been developed at IGT over many years. The AGGCOM combustor efficiently destroys organic compounds and encapsulates inorganic contaminants within benign, glassy agglomerates suitable for disposal in ordinary landfills.

The first stage of the combustor is a sloping-grid, agglomerating fluidized-bed reactor that can operate under either substoichiometric or excess air conditions. In addition to the sloping grid, the first stage incorporates a central jet and classification section. Fuel gas and air enter the central jet while only air is admitted through the grid and classifier. The contaminated waste material is admitted directly into the fluidized bed. With a unique distribution of fuel and air, the bulk of the fluidized bed is controlled at a temperature of 1500° to 2000°F, while the central spout temperature can be varied from 2000° to 3000°F. This feature is key to the combustor's ability to produce benign agglomerates. Upon introduction of contaminated wastes into the bed, the organic fraction is immediately volatilized and partially combusted. The inorganic fraction undergoes melting and subsequent agglomeration.

Volatilized organic compounds are destroyed in the second stage of the AGGCOM combustor. This second stage is a cyclonic combustor, which provides intense mixing to ensure complete combustion of these organic compounds. Either secondary air or a mixture of fuel gas and air is fed to this stage to maintain a temperature in the range of 1800° to 2400°F. The destruction and removal efficiency (DRE)

of organic contaminants in the AGGCOM system is expected to exceed 99.99% (99.9999% for PCBs, dioxins, etc.). Fine particulates collected in the cyclonic stage are returned to the fluidized-bed stage for assimilation in the agglomerates.

EPA SITE PROGRAM A multiyear program is currently underway at IGT to develop a data base for application of the AGGCOM technology at Superfund sites. The program is sponsored by the U.S. EPA Superfund Innovative Technology Evaluation (SITE) program, IGT's Sustaining Membership Program, and the Gas Research Institute. The program includes soil agglomeration tests in a 6-inch diameter fluidized-bed bench-scale unit (BSU), the design, construction, and operation of a 6-ton/day AGGCOM pilot plant, and the utilization of the pilot plant data to assess the commercial viability of the technology. The primary objectives of the program include 1) determining the operating conditions in the fluidized bed that, for a given contaminated soil, will enhance the capture and encapsulation of inorganic contaminants within the glassy matrix, 2) identifying operating conditions in both AGGCOM stages for the destruction of organic contaminants with a DRE to exceed 99.99%, and 3) minimizing utility requirements by maximizing process heat recovery.

The batch BSU tests with commercially available top soil were successfully completed; conditions required to produce soil agglomerates were determined. Samples of agglomerated soil were shown to be essentially non-leachable per the TCLP. Construction of the AGGCOM pilot plant has been completed and testing is underway.

AUTO FLUFF TESTS IGT conducted an experimental program to determine the operating conditions necessary for combusting auto fluff and for agglomerating the inorganic fraction of auto fluff. The University of Illinois (Chicago, UIC) participated in the program as a subcontractor to IGT. A bulk sample of auto fluff was obtained from a local auto shredder. Physical and chemical analyses of the bulk sample of auto fluff were determined (Table 1).

Fluidization tests were conducted with as-received and ground (-½ inch) auto fluff and with auto fluff ash generated in the fluidized-bed combustor at UIC. The objective of the tests was to determine the fluidization characteristics of the auto fluff and ash. The raw and ground auto fluff did not fluidize well. The ash from the fluidized-bed combustion test behaved like discrete particles and the results from this test were considered more representative of the fluidization expected in the BSU. A minimum fluidization value (U_{mf}) of 1.5 ft/s (0.45 m/s) was selected as the best compromise for both raw fluff and combusted ash.

Feeding of the ground auto fluff to the BSU with existing equipment was also difficult. The 1½-inch screw was not capable of discharging auto fluff from the 6-inch diameter feed hopper. After much modification and testing, IGT and UIC developed an auger-stirred feed hopper that could effectively meter auto fluff into a horizontal pocket feeder. With air assist, this feed system could consistently feed up to 15 lb/h of auto fluff into the BSU.

The combustion/agglomeration tests were conducted in the BSU with natural gas as the secondary fuel. The bottom of the BSU is fitted with a sloping-grid gas distributor, including venturi discharge, and central burner jet for generating the hot zone. Cyclones are installed downstream of the BSU to collect fine particles elutriated from the fluidized bed. A product gas scrubber is also used to capture fine particles not removed by the cyclones. The BSU is equipped with external electric heaters for achieving temperatures up to 2000 °F and a feed gas preheater.

Three auto fluff combustion/agglomeration tests were conducted in the BSU. Each test consisted of several set points in an attempt to identify conditions required to agglomerate the inorganic fraction of auto fluff. The operating conditions were temperatures of 1560 ° to 1950 °F, superficial fluidization

velocities of 2.3 to 4.6 ft/s (about twice the U_{mf}), and auto fluff feed rates of 3.0 to 4.9 lb/h. Auto fluff agglomerates (Figure 2) were produced in two of the tests.

Three auto fluff combustion tests were also conducted in the UIC 6-inch diameter fluidized-bed reactor. The test conditions were temperatures of 1250° to 1590°F, fluidization velocities of 2.1 to 3.8 ft/s, and excess air of 12 to 99 percent. On-line gas analyzers indicated that auto fluff was not consistently fed to the bed by the screw feeder. The CO concentration increased and decreased in the range of 100 to over 5000 ppm during auto fluff feeding.

A sample of the ground auto fluff was analyzed for priority trace elements including chlorine. Raw ground auto fluff and the agglomerated auto fluff were subjected to the TCLP test. The trace element analysis and TCLP results are shown in Table 2. The results show that this sample of raw auto fluff has considerable cadmium, chromium, lead, and mercury contents and exhibits a toxic character per the TCLP test (see Cd and Pb concentrations). However, the leachability of the agglomerated auto fluff sample was significantly less than that of the raw fluff and the sample passed the TCLP test.

CONCLUSIONS The results of the bench-scale batch fluidized-bed agglomeration tests demonstrate that the inorganic fraction of auto fluff can be agglomerated via IGT's sloping-grid technology. The leachability of auto fluff agglomerates is less than that of raw auto fluff; the agglomerates pass the TCLP test. Product gas analyses of fluidized-bed combustion of auto fluff indicate that a second stage of cyclonic combustion is required to reduce the CO content to acceptable levels. The chlorine content of auto fluff may require the addition of sorbents to the fluidized bed to reduce HCl emissions to acceptable levels.

ACKNOWLEDGMENTS The authors gratefully acknowledge the funding of this research project by IGT's Internal Research and Development program. The efforts of Mr. Robert Schlusser in conducting the BSU tests are also acknowledged.

REFERENCES 1. "Detroit - The day of the throw-away car is over," Jack Keebler, Automotive News, March 4, 1991, p. 36.
2. "Process Recovers More From Junked Cars," Irwin Stambler, R&D Magazine, January 1993, p. 14.

Table 1. PHYSICAL AND CHEMICAL CHARACTERISTICS OF AUTO FLUFF

Material	wt % (dry)
Scrap Metal	8.8
Hard Plastic	11.8
Sponge	6.5
Rubber	2.5
Vinyl+Leather	12.3
Carpet+Cloth	3.8
Other Fluffy	39.5
Wood+Cardboard	4.1
Glass	2.7
Dirt+Other	8.0
Total	100.0
Calorific Value, Btu/lb (dry),	7810

Proximate Analysis	wt %
Moisture Content	24.1
Volatile Matter	39.8
Ash	32.8
Fixed Carbon	3.3
Total	100.0

Ultimate Analysis	wt % (dry)
Ash	42.77
Carbon	39.77
Hydrogen	4.58
Nitrogen	0.92
Sulfur	0.25
Oxygen (by diff.)	11.76
Total	100.00

Table 2. TRACE ELEMENT ANALYSES AND TCLP RESULTS ON AUTO FLUFF SAMPLES

Sample	Raw Auto Fluff		Agglomerated Auto Fluff	TCLP Limit
	-- μg/g --	---------- TCLP Leachate Concentration, mg/L ----------		
Arsenic	11	<0.002	<0.05	5
Barium	12	2.1	0.85	100
Cadmium	160	1.5	<0.05	1
Chromium	280	<0.05	0.65	5
Lead	100	7.1	2.8	5
Mercury	1.6	<0.005	<0.001	0.2
Selenium	5.8	0.016	<0.002	1
Silver	<6.0	<0.20	<0.05	5
Chlorine	7700	--	--	--

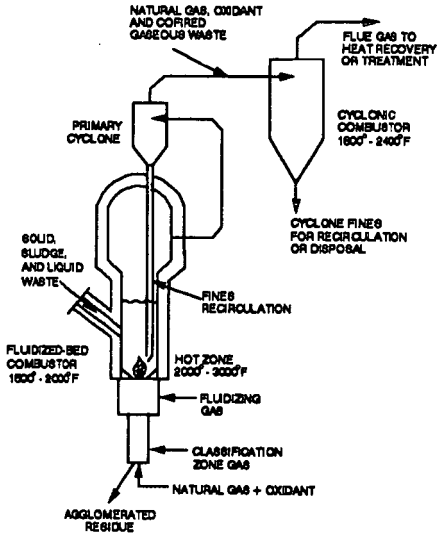

Figure 1. IGT's AGGCOM COMBUSTOR

Figure 2. AGGLOMERATED AUTO FLUFF

THERMOGRAVIMETRIC AND FREE RADICAL EVIDENCE FOR IMPROVED LIQUEFACTION OF COAL WITH WASTE TIRES.

M. M. Ibrahim and M. S. Seehra, Physics Department
P.O. Box 6315, West Virginia University, Morgantown, WV 26506-6315.

Keywords: coal, tire, coprocessing, free radicals.

ABSTRACT:

Thermogravimetry and in-situ electron spin resonance spectroscopy of free radicals are used to investigate the coprocessing of blind canyon coal with waste tire rubber (Goodyear Vector) and with polystyrene and polyethylene. Temperature-programmed thermogravimetry shows improved conversion and the data of free radical density versus temperature to 500°C, under vacuum and flowing H_2 gas conditions, show that waste tires act as good hydrogen donors. These findings suggest improved liquefaction of coal with waste rubber. Similar experiments of coprocessing of coal with polystyrene and polyethylene shows enhanced hydrocracking indicated by a large increase in the free radical densities above 350°C.

INTRODUCTION:

The free radicals in coals as monitored by electron spin resonance (ESR) spectroscopy are an integral part of the coal structure since their characteristic properties vary systematically with coal rank and coal macerals [1,2]. As coals are subjected to pyrolysis, new free radicals are generated due to coal depolymerization whose intensities vary in a systematic fashion with pyrolysis temperature in bituminous coals [3-5]. In the process of direct coal liquefaction, hydrogenation of the products of coal pyrolysis must occur resulting in the capping of the free radicals by transferred hydrogen [6-8]. Therefore a decrease in the free radical density upon hydrogenation is indicative of the liquefaction process. Consequently ESR spectroscopy is an important experimental technique for coal conversion studies if the experiments can be carried out in-situ under the practical conditions of high temperatures and pressures used in coal liquefaction. Recently we have developed such an ESR apparatus in which in-situ experiments for temperatures up to 600°C can be carried out under various atmospheres such as vacuum, flowing gases and H_2 pressures up to 700 psi [9]. In the work reported here, we have employed this apparatus to investigate the coprocessing of coals with waste tires and we provide definite evidence of significant enhancement of coal hydrogenation facilitated by the tire polymers. These results are supportive of the increased coal liquefaction yield in the presence of waste tires reported first by Farcasiu and Smith [10] and more recently by Liu et al [11]. Similar experiments on the coprocessing of coal with polyethylene and polystyrene show a rapid increase in the free

$$N = \left(\frac{N_T\ T}{298}\right)\ \frac{m_c}{m_T M} \qquad \text{------ (1)}$$

where N_T is the measured free radical density at any temperature T and (T/298) corrects for the Curie law variation of the free radical density relative to room temperature (298K), m_c is the mass of coal at room temperature, m_T is the mass of the mixture at any temperature, and M is the total mass at room temperature. For the ESR measurements in sealed configuration only the Curie law corrections are applied. From Figs. 3 and 4, for measurements in sealed and under hydrogen flow configurations, it is clearly evident that above ~ 400°C, the tire polymer has considerable effect in reducing the coal free radical densities. The following points are noteworthy.

At the lower temperatures of around 100°C, there is a slight increase in N due to the effect of tire. Above 400°C, the N values in the presence of tire are suppressed by a factor of two to three and the presence of H_2 appears to provide additional suppression of the free radical density. In Figs 5 and 6 the variation of free radical densities with temperature is shown for the coal mixed with polyethylene or polystyrene. Here, above 350°C there is very rapid increase of free radicals compared to the coal alone. Since a large mass loss occurs in this temperature, the mass corrected free radical densities show a very large effect. The free radical densities shown in Figs 5 and 6 include plots for both with and without the application of mass correction. In either case, we see enhanced hydrocracking in the coprocessing of coal with polymers and beyond 450°C, the increase in N is by a factor of 3 to 6.The importance of these results is discussed next.

In a recent paper Shin et al [12] have reviewed the effect of hydrogen on the free radicals and it is argued that in addition to the generally accepted view of the capping of the free radicals by hydrogen in the hydrogenation process, hydrogenolysis can also occur in the initial stages of the reaction (Hydrogenolysis should increase N whereas hydrogenation should lower N). The results presented in Figs. 3 and 4 show an initial increase in N at lower temperatures due to the coal-tire interaction and this may be due to hydrogenolysis. The rapid decrease in the free radical density at the higher temperatures in Figs. 3 and 4, is most likely due to hydrogenation facilitated by the transfer of hydrogen from tire polymers to coal fragments. The liquefaction experiments of Farcasiu and Smith [10] carried out 425°C and those of Liu et al [11] at 400°C also indicate increased conversion of coal in coprocessing with waste tires. Our results also indicate that significant coal liquefaction occurs in the presence of tires and that the tires act as excellent hydrogen donors. The polyethylene and polystyrene mixed with coal, on the other hand, promote rapid hydrocracking of coal.

radical densities beyond ~350°C indicating enhanced hydrocracking of coal with these polymers. These results are described below.

EXPERIMENTAL RESULTS AND DISCUSSION

The ESR studies reported here were carried out on a Blind Canyon coal obtained from the Penn State Coal Bank. The analysis of this coal as well as details of the x-band high temperature ESR cavity system were given in a recent paper [9]. The tire polymer used in these experiments was chipped from a used tire (Goodyear Vector) and it was mixed with the coal in 1:1 ratio with mortar and pestle. Two samples of tire were cut from the central portion and from the rim of the tire and are referred to as tire(C) and tire(R) respectively. Polyethylene (spectrophotometric grade) and polystyrene (mol. wt. ~2500) were obtained from Aldrich Chemical company Inc. Polymers were mixed 1:1 with coal for TG and ESR measurements. For ESR, experiments were carried out under vacuum conditions (sealed tube) and in flowing H_2 gas at a flow rate of 100cc/m [8,9]. We also measured the weight loss in thermogravimetry in flowing H_2 gas (100cc/m) at a heating rate of 10°C/m using a Mettler TA3000 system .

Fig. 1 shows the remaining weight (%) as a function of temperature for the Blind Canyon coal, the tire and the tire coal mixture in a flowing H_2 experiment. Most of the weight loss due to release of volatiles occurs between 300 and 500°C and it is clearly evident that the coal-tire mixture has the highest weight loss. There is a no significant difference between the samples cut from the central or rim part of the tire in the variation of remaining weight with temperature. If we use the weight loss due to volatiles as the percentage conversion, then at 500°C, the percentage conversions for coal, tire and coal-tire respectively are about 32%, 48% and 66%. The presence of tire polymers has clearly enhanced the percentage conversion of coal. Fig 2. shows the plots of remaining weight (%) as a function of temperature for the polyethylene and polystyrene and for coal mixed with these polymers. For these cases also we see that the weight loss in the mixture is greater than a simple addition of weight loss of coal and polymer alone. Note also that in the mixture the major weight loss occurs at temperatures different from that for the individual polymers indicating strong reaction of polymers with coal.

For the ESR experiments, samples were either vacuum sealed in the ESR tube at room temperature followed by measurements at elevated temperatures or measurements were done in flowing H_2 gas [8,9]. Only a single ESR line is observed from the coal sample and no ESR signal was observed from the tire or polymers as determined in a separate experiment up to 500°C. In Fig. 3 we show the temperature variation of the free radical density N for the coal and the coal-tire(R) mixture in sealed configuration and in Fig 4. for hydrogen flow configuration. For measurements in hydrogen flow the values of N plotted are determined by the equation(1):

In summary, the results presented here on the free radical density of coals during coprocessing with tire and polymers suggest that tire polymers lower the free radical densities and act as good hydrogen donors. On the other hand polyethylene and polystyrene promote rapid hydrocracking of coal. Both of these findings are positive indicators for improved liquefaction of coals coprocessed with waste tires and polymers.

ACKNOWLEDGMENTS

This research was supported in part by the U.S. Department of Energy through CFFLS under Contract No. DE-FC22-90PC90029.

REFERENCES

1. Retcofsky, H. L.; Stark, J. M.; Friedel, R. A. Anal. Chem. 1968, 40, 1699-1704.
2. Silbernagel, B. G.; Gebhard, L. A.; Dyrkacz, G. R.; Bloomquist, C. A. A. Fuel 1986, 65, 558-565.
3. Seehra, M. S.; Ghosh, B.; Mullins, S. E. Fuel 1986, 65, 1315-1316.
4. Seehra, M. S.; Ghosh, B. J. Anal. Appl. Pyrolysis 1988, 13, 209-220.
5. Fowler, T. G.; Bartle, K. D.; Kandiyoti, R. Fuel 1987, 66, 1407-1412.
6. Neavel, R. C. Fuel 1976, 55, 237-242.
7. Petrakis, L. and Grandy, D. W. "Free Radicals in Coals and Synthetic Fuels" 1983 (Elsevier Science Publication Co. N.Y.).
8. Ibrahim, M. M.; Seehra, M. S. Energy & Fuels 1991, 5, 74-78.
9. Ibrahim, M. M.; Seehra, M. S. ACS Fuel Div. Preprints 1992, 37, 1131-1140.
10. Farcasiu, M.; Smith, C. ACS Fuel Div. Preprints 1992, 37, 472-479.
11. Liu, Z.; Zondlo, J. W.; Dadyburjor, D. B. (private communication).
12. Shin, S.-C.; Baldwin, R. M.; Miller, R. L., Energy & Fuels 1989, 3, 71-76.

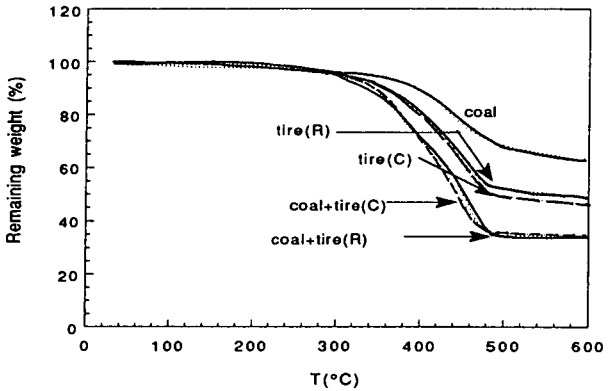

Fig 1. Remaining weight as a function of temperature for coal and coal tire mixtures (1:1 by weight). Tire(C) and tire(R) are cut from the central and rim portions of the tire. All measurements were done in flowing hydrogen.

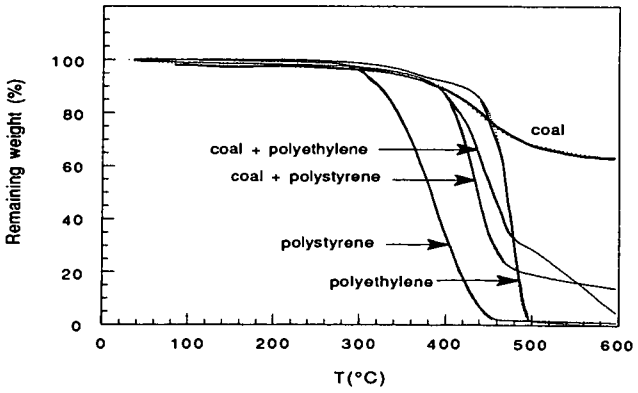

Fig.2. Remaining weight as a function of temperature for coal and coal mixed with polyethylene and polystyrene(1:1 by weight) Measurements were done under hydrogen flow.

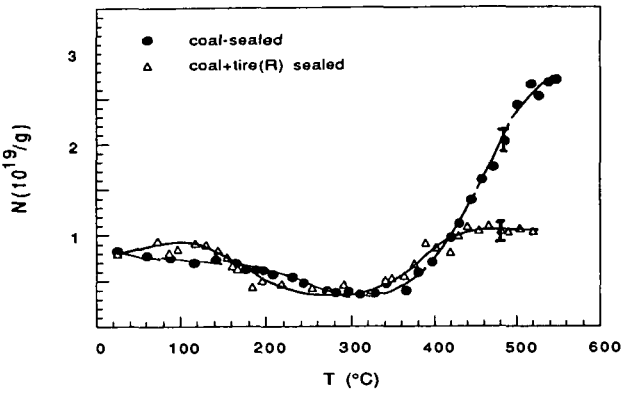

Fig 3. Variation of free radical densities with temperature for coal, and coal mixed with tire(R) (1:1 by weight). Samples were evacuated and sealed. No corrections for mass changes were applied.

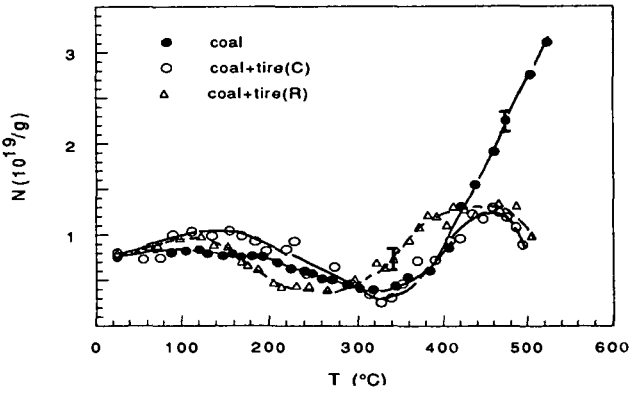

Fig. 4. Variation of free radical densities with temperature for coal and coal tire mixtures (1:1 by weight). Measurements were done under hydrogen flow. Free radical densities are corrected for changes in mass.

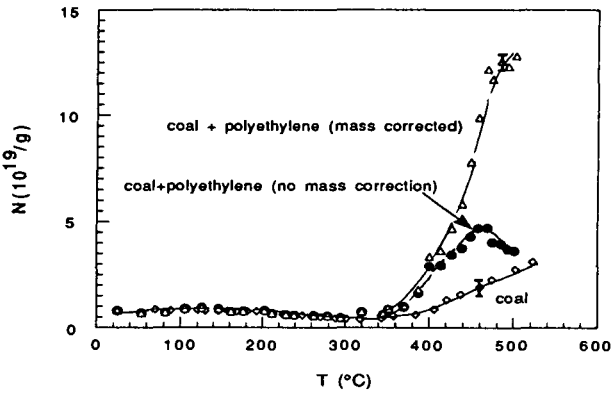

Fig 5. Variation of free radical densities for coal and coal mixed with polyethylene (1:1 by weight). For the mixture, N is plotted both with and without the mass correction.

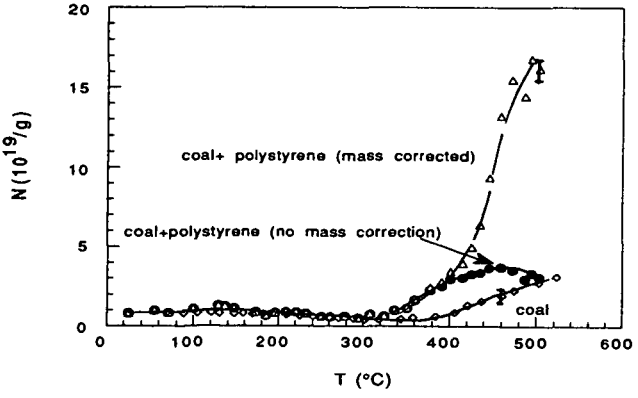

Fig 6. Variation of free radical densities for coal and coal mixed with polystyrene (1:1 by weight). For the mixture, N is plotted both with and without the mass correction.

THIS PAGE INTENTIONALLY

MADE BLANK

PAPER WITHDRAWN

FROM PROGRAM

ETHANOL FROM BIOMASS BY GASIFICATION/FERMENTATION

E. C. Clausen
J. L. Gaddy
Department of Chemical Engineering
University of Arkansas
Fayetteville, AR 72701

Keywords: Biomass, Gasification, Ethanol Fermentation

ABSTRACT

Bacteria have recently been isolated from natural sources that produce ethanol from CO, H_2 and CO_2. This paper describes a unique process for producing liquid fuel from biomass by gasification, followed by fermentation of the synthesis gas to ethanol. This process offers the advantage of very high yield (140 gal/ton), since the lignin and pentose fractions of the biomass can also be readily utilized. This presentation describes laboratory experiments with the culture and discusses bioreactor designs for this mass transfer limited fermentation.

INTRODUCTION

The United States currently imports about 20 percent of its total energy requirements of about 70 quads annually. As petroleum reserves decline and prices rise, the U.S. must develop alternative energy resources.

The nation has about 1.5 billion tons of biomass residue and wastes that could be used as an energy source (Sitton *et al.*, 1979). These residues could furnish 10 quads, or about 15 percent of our energy requirements, if converted at a 50 percent efficiency. In addition, if energy crops were grown on idle arable rangeland and forestland (about 200 million acres), another 25 quads could be produced (Clausen *et al.*, 1977). Therefore, the U.S. could supply half of its energy needs from renewable biomass and wastes.

Lignocellulosic matter may be used as a solid fuel and burned directly to produce energy. However, efficiencies are low and handling problems are serious. Consequently, biomass must be converted into gaseous or liquid forms of energy to be utilized in conventional energy processes. The major components of cellulosic biomass are hemicellulose, cellulose and lignin. The compositions of the biomass resources vary; however, most materials contain 15-25 percent hemicellulose, 30-45 percent cellulose, and 5-20 percent lignin. The carbohydrates may be hydrolyzed to sugars and fermented to ethanol or they may be converted into methane by anaerobic digestion. These technologies are under development and may become economical in the future.

Biomass may also be gasified to yield a low Btu gas consisting of H_2, CO, CO_2, and N_2. Technology for pyrolysis or gasification of biomass has been under intensive development during the last two decades (Stasson and Stiles, 1988). Large scale demonstration facilities have been tested (Fisher *et al.*, 1976) and small scale commercial facilities are now in operation. A major advantage of gasification of biomass is that all the carbohydrate and lignin are converted into energy forms, whereas the lignin is not converted by hydrolysis or digestion.

The problems with the application of biomass gasification have not been technical, but economic. The product from gasification is a heat source, which is very cheap today. Therefore, even nominal capital and operating costs for gasification cannot be justified with such low income. If the components of synthesis gas were converted into a higher value fuel product, biomass gasification could become a viable alternative energy technology.

BIOLOGICAL PRODUCTION OF ETHANOL FROM BIOMASS SYNTHESIS GAS

Synthesis gases, consisting of CO, H_2 and CO_2, may be produced from biomass according to the approximate reaction (Alden *et al.*, 1991):

$$\underset{\text{biomass}}{8CH_2O + (4N_2)} \rightarrow 6CO + 2CO_2 + 8H_2 + (4N_2) \qquad (1)$$

There are many gasifier designs that have been demonstrated and are commercially available. Gas composition is a function of the amount of air or oxygen necessary to generate the heat for pyrolysis of the biomass, as well as the type of gasifier and the moisture content of the biomass. Steam may also be added to adjust the hydrogen concentration. If oxygen is used, nitrogen is eliminated.

The components of synthesis gas may be converted into ethanol by certain anaerobic bacteria according to the equations (Klasson *et al.*, 1990a; 1990b; 1992; Barik *et al.*, 1988):

$$6CO + 3H_2O \rightarrow CH_3CH_2OH + 4CO_2 \qquad (2)$$

$$6H_2 + 2CO_2 \rightarrow CH_3CH_2OH + 3H_2O \qquad (3)$$

Equations (2) and (3) may be combined with Equation (1) to give

$$8CH_2O + O_2 + (4N_2) \rightarrow 2.33CH_3CH_2OH + 3.33CO_2 + H_2O + (4N_2) \qquad (4)$$

Since nearly all the biomass (including the lignin, but not the ash) can be converted into gas by Equation (1), yields of ethanol of about 50 percent of the total biomass are possible (135 gal per ton). This compares to yields of only about 30 percent for enzymatic or acid hydrolysis/fermentation processes.

Synthesis gas compositions from biomass are variable, depending upon the raw material, temperature and process used. Typical compositions show a CO:H_2 ratio of about one with CO and H_2 compositions of about 35 percent (Borgwardt *et al.*, 1991; Alden *et al.*, 1991). Yields of gas of about 90 percent are common. Gas composition can also be tailored for fuels production (Collaninno and Mansour, 1988).

Fuel ethanol production from grain is about one billion gallons per year and expected to increase steadily as oxygenated fuels usage is mandated in many metropolitan areas. Prices have been as high as $1.85 per gallon, but have stabilized at about $1.20 per gallon (wholesale gasoline price plus tax credit of $0.54 per gallon) in recent years. The potential market for fuel ethanol is 10 billion gallons annually, at a 10 percent blend with gasoline. Higher percentages are, of course, possible and pure ethanol is marketed in Brazil. Therefore, the market for this product is quite large and the price is sufficient to support commercialization.

The biological process for producing ethanol from synthesis gas would be quite simple. The process would consist of an exchanger to cool the hot gases, a biological reactor, and a separator for ethanol purification. The cool gases would be passed through a liquid phase reactor where a culture of the desired microorganism is maintained. The microorganism would carry out the reaction to produce ethanol, converting only the CO, H_2, or CO_2 present. The reactor would be operated at mild temperature (95°F) and atmospheric pressure. Higher pressure may be desirable to enhance gas mass transfer and can be used where the synthesis gas may be at elevated pressure. Ethanol would be removed in the aqueous phase from the reactor and recovered by extraction and distillation. Separation of ethanol from water is standard commercial technology.

The advantages of biological reactions, over chemical reactions, include operation at atmospheric conditions, which generally provides a more energy efficient process. Also, microorganisms give high yields (>95 percent), with only small amounts of raw materials used for growth and maintenance. Microoganisms are also quite specific in producing a single product, with only small quantities of by-products formed and requiring relatively simple recovery processes. Resistance to toxicity from substances that degrade other catalysts can often be developed in biological systems. Finally, the biocatalyst is continually regenerated in the biological process, which allows more dependable and consistent operation than catalytic processes.

PURPOSE

The purpose of this paper is to present information on a unique bioprocess for the conversion of biomass to ethanol by gasification/ fermentation. Following gasification of the biomass, CO, CO_2 and H_2 in synthesis gas are converted to ethanol using *C. ljungdahlii*. Data are presented for this fermentation, including results from both batch and continuous reactors. In addition, the effects of the sulfur gases H_2S and COS on growth, substrate uptake and product formation are presented and discussed.

MICROBIOLOGY OF ETHANOL PRODUCTION

The bioconversion of the gases, CO_2, CO, and H_2, by anaerobic bacteria has been known for many years and recently demonstrated in our laboratories as having commemrcial potential (Clausen and Gaddy, 1985; Klasson *et al.*, 1990b; 1992). Several bacterial species are capable of converting these gases into acetate, which is an intermediate in many biological pathways. However, only one bacterium has been shown to produce ethanol from the components of synthesis gas.

In 1985, Barik *et al.* (1985) isolated a bacterium from animal waste that was capable of converting CO, CO_2 and H_2 to ethanol and acetate by the equations:

$$6CO + 3H_2O \rightarrow C_2H_5OH + 4CO_2 \quad (2)$$
$$2CO_2 + 6H_2 \rightarrow C_2H_5OH + 3H_2O \quad (3)$$
$$4CO + 2H_2O \rightarrow CH_3COOH + 2CO_2 \quad (5)$$
$$2CO_2 + 4H_2 \rightarrow CH_3COOH + 2H_2O \quad (6)$$

This strain was found to be a new bacterial species and named *Clostridium ljungdahlii* (Vega *et al.*, 1989a). Under normal conditions, the "wild strain"

produced approximately 20 moles of acetate per mole of ethanol (Barik *et al.*, 1988). However, by manipulating the culture and employing low pH and minimal nutrients, the culture has been found to be capable of producing only ethanol, with minimal amounts of acetate (Klasson *et al.*, 1992).

A kinetic analysis was performed on the data to determine kinetic parameters for growth and CO uptake. The following models were obtained with $P_{CO}^{L} \leq 1.1$ atm:

$$\mu = \mu_m = 0.04\ h^{-1} \quad (7)$$

and

$$q = q_m = 42.7\ \text{mmol CO/g cell}\cdot\text{h} \quad (8)$$

If the specific uptake rate of CO is converted to a carbon mass basis, a value of 0.22 g C/g cell•h is obtained for q_m, which is comparable to the rate of glucose uptake by *Saccharomyces cerevisiae* with a q_m of 0.27 g C/g cell•h (Vega, 1985). This rate indicates that *C. ljungdahlii* has reaction rates equivalent to other organisms that are used for commercial fermentations.

Culture Manipulation

As was shown in Equations (1,2,5,6) both ethanol and acetate are produced from the fermentation of CO, CO_2 and H_2 by *C. ljungdahlii*. Early results with the culture showed that acetate was the predominant product, with ethanol:acetate ratios of 0.1 or lower typically found in the "wild" strain. Many researchers have studied solvent/acid formation in clostridial cultures, reporting that factors including medium manipulation, decreased pH and the addition of reducing agents have brought about solvent formation in favor of acid production.

Research with *C. ljungdahlii* has shown that lowering of the pH to 4 - 4.5 coupled with a nutrient limited medium brings about a drastic shift in product formation in favor of ethanol (Phillips *et al.*, 1992). Figure 1 shows ethanol and acetate production from synthesis gas using *C. ljungdahlii* in the CSTR at reduced pH and with a specially designed nutrient limited medium. As is noted, ethanol concentrations exceeding 20 g/L with corresponding acetate concentrations of only 2 - 3 g/L are obtained. The cell concentration in these studies was approximately 1.5 g/L. Thus, an increase in ethanol concentration coupled with high product ratios were obtained by lower reaction pH in combination with employing a specially designed nutrient medium.

BIOREACTOR DESIGN

The choice of a suitable reactor for gas-liquid reaction or absorption is very often a question of matching the reaction kinetics with the capabilities of the proposed reactor. In the case of biological systems, special care must be taken to insure the viability of the biocatalyst at the operating conditions. The specific interfacial area, liquid holdup and mass transfer coefficients are the most significant characteristics of a reactor, and special schemes have been devised to maximize mass transfer. Mechanically agitated reactors, bubble columns, packed columns, plate columns, spray columns, gas-lift reactors, etc. are examples of various kinds of contacting systems employed in these type of processes.

The rate of disappearance of CO from the gas phase can be related to the partial pressures in the gas and the liquid phase and the cell concentration, X, by the equation:

$$-\frac{1}{V_L}\frac{dN_{CO}^{G}}{dt} = \frac{K_L a}{H}\left[P_{CO}^{G} - P_{CO}^{L}\right] = \frac{X\, q_m\, P_{CO}^{L}}{K_P' + P_{CO}^{L} + \left[P_{CO}^{L}\right]^2/W'} \qquad (9)$$

Under mass transfer limiting conditions, P_{CO}^{L} approaches zero so that the rate of disappearance of CO is proportional to the gas phase CO concentration. As the cell concentration, X, reaches a value at which mass transfer is controlling, the concentration of carbon monoxide in the liquid becomes zero and the reaction rate is controlled by the rate of transport of the substrate into the liquid phase. Thus, both high cell concentrations and fast gas transport are necessary to minimize reactor size. High cell concentrations may be obtained in the reactor by employing a cell recycle system in which the cells are separated from the effluent and returned to the reactor. Fast mass transfer can occur by employing increased pressure or solvents to increase CO solubility.

The Use of Cell Recycle in the CSTR

A cell recycle apparatus was used in conjunction with a standard CSTR as a method to increase the cell concentration inside the reactor. This is particularly important since total product formation with *C. ljungdahlii* has been shown to be proportional to the cell concentration inside the reactor.

Figure 2 shows the product concentration profile for the CSTR with cell recycle. In this experiment, the cell concentration increased (with agitation rate and gas retention time increases) from approximately 800 mg/L to over 4000 mg/L The maximum in the previous CSTR study without cell recycle was 1500 g/L. The CO conversion was consistently around the 90 percent level after 150 h of operation. The corresponding H_2 conversion, on the other hand, averaged 70 percent up to a time of 500 h. At this time, the H_2 conversion fell, probably due to an accumulation of CO in the liquid phase. The ethanol concentration ranged from 6 g/L at the beginning of the study to 48 g/L after 560 h of operation. The corresponding acetate concentrations at these times were 5 g/L and 3 g/L, respectively. The ratio of ethanol to acetate ranged from 1.2 g/g to 16 g/g. Thus, very high ethanol concentrations are possible and acetate production is nearly eliminated with high cell concentrations.

High Pressure Operation

As was mentioned previously, elevated pressure may be used to increase the rate of mass transfer of CO into the liquid phase. A high pressure system (both CSTR and trickle bed reactor) has been constructed in the University of Arkansas laboratories. The system has a maximum operating pressure of 5000 psig and can be used for both photosynthetic and non-photosynthetic bacterial systems. The system is presently being used to gradually acclimate *C. ljungdahlii* to increased pressure.

CONCLUSIONS

The anaerobic bacterium *Clostridium ljungdahlii* has been shown to be effective in converting CO, CO_2 and H_2 to ethanol. Rates of carbon uptake by *C. ljungdahlii* comparable to the rate of carbon uptake by the yeast *Saccharomyces cerevisiae* have been obtained. A CSTR cell recycle system has been shown to be effective in permitting the cell concentrations necessary for high concentrations of ethanol. An ethanol concentration of 47 g/L with a corresponding acetate concentration of 3 g/L has been attained. *C. ljungdahlii* has been shown to be tolerant of H_2S or COS in concentrations exceeding typical levels in synthesis gas.

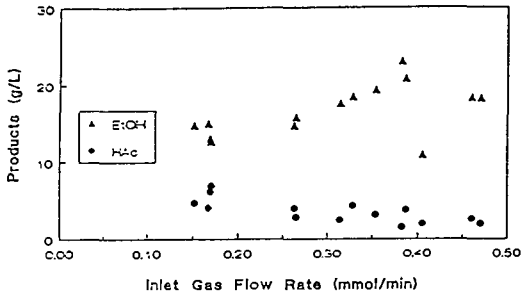

Figure 1. Product concentrations from growth of *C. ljungdahlii* in designed medium in the CSTR.

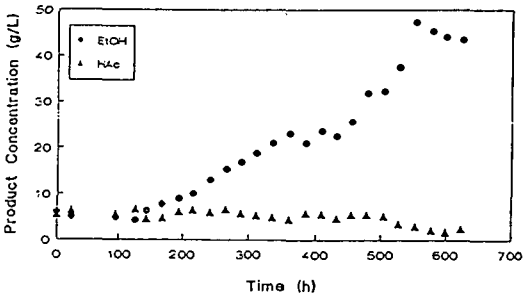

Figure 2. Product concentration measurements for *C. ljungdahlii* in the CSTR with cell recycle.

LIST OF REFERENCES

Alden, H., E. Bjorhman, and L. Waldheim, *Energy from Biomass and Wastes* IGT (March, 1991)

Barik, S., S. Prieto, S.B. Harrison, E.C. Clausen, and J.L. Gaddy, (1988), "Biological Production of Alcohols from Coal Through Indirect Liquefaction," *Appl. Biochem. Biotechnol.*, 18, 18, 363

Barik, S., R.E. Corder, J.L. Vega, E.C. Clausen, and J.L. Gaddy, (1985), "Biological Production of Liquid Fuels and Chemicals from Coal Synthesis Gas," Proceedings of the Coal-Liquid Fuels Technology Symposium.

Borgwardt, R.H., M. Steinberg, E.W. Grohse and Y. Tang, *Energy from Biomass and Wastes*, IGT (March, 1991).

Clausen, E.C. and J.L. Gaddy: "Biological Conversion of Coal Synthesis Gas," Annual Report, U.S. DOE-Morgantown Energy Technology Center, (May 1985).

Clausen, E.C., O.C. Sitton, and J.L. Gaddy, (1977), "Converting Crops into Methane," *Chem. Eng. Prog.*, 73.1, 71.

Collaninno, J. and Mansour, (1988), *Proc. Energy from Biomass and Wastes* IGT.

Fisher, T.F., M.L. Kasbohm, and J.R. Rivero, "The PUROX System," *Proc. of Nat'l Waste Proc. Conf.*, Boston (May 1976).

Klasson, K.T., M.D. Ackerson, E.C. Clausen, and J.L. Gaddy, "Bioconversion of Synthesis Gas into Liquid or Gaseous Fuels," *Proceedings Int'l Symp. on Biol. Proc. of Coal*, EPRI and DOE, Orlando (May 1990a).

Klasson, K.T., B.B. Elmore, J.L. Vega, E.C. Clausen, and J.L. Gaddy, (1990b), "Biological Production of Liquid Fuels from Synthesis Gas," *Applied Biochem and Biotech.*, 24/25, 857.

Klasson, K.T., M.D. Ackekrson, E.C. Clausen, and J.L. Gaddy, "Bioliquefaction of Coal Syntehsis GAs," presented at the San Francisco ACS Meeting (April 1992).

Phillips, J.R., K.T. Klasson, E.C. Clausen, and J.L. Gaddy, "Biological Production of lEthanol from Coal Synthesis Gas: Medium DevelopmentStudies," presented at the 14th Symposoum on Biotechnology for Fuels and Chemicals," Gatlinburg, TN (May 1992)

Sitton, O.C., G.L. Foutch, N.L. Book, and J.L. Gaddy, (1979), "Ethanol from Agricultural Residues," *Chem. Eng.Prog.*, 75.12, 52.

Stasson, H.E.M. and H.N. Stiles, (1988), *Proc. Energy from Biomass Wastes*, IGT.

Vega, J.L. (1985), M. S. Thesis, University of Arkansas.

Vega, J.L., S, Prieto, B.B. Elmore, E. C. Clausen, and J.L. Gaddy, (1989a), *Appl. Biochem. Biotechnol.* 20/20, 781.

IDENTIFYING POTENTIAL BINDING AGENTS FOR UTILIZATION OF WASTES AND RENEWABLE RESOURCES AS FUELS OR MATERIALS

Kenneth E. Daugherty
Chemistry Department
University of North Texas
P.O. Box 5068
Masters Hall, Room 5
Denton, Texas 76203

The following is a procedure developed at the University of North Texas for identifying potential binding agents for the utilization of wastes and renewable resources as fuel materials. This procedure is being used for other materials which will be described in the extended paper for book publication.

The goals were to find six low-cost, environmentally acceptable binders for preparing pellets of densified refuse derived fuel (RDF). The binders had to be capable of being used with RDF to produce a pellet that could be produced in a more stable fashion than with water alone. The pellet produced had to be chemically and biologically stable and had to be capable of being stored for up to six months prior to being used as a fuel.

Over 100 potential binders were considered including glues, natural starches and celluloses, adhesives, waste liquors, fly ashes, dusts, hydraulic cements, reaction cements precipitation cements, etc.

The densification fabrication technique used must remove the pores between the RDF particles (accompanied by shrinkage of the component), combined with growth together and strong bonding between adjacent particles. The following criteria must be met before densification of the RDF can occur:

* A mechanism for material transport must be present
* A source of energy to activate and sustain this material must be present.

The primary mechanisms for transport are diffusion and viscous flow. Heat is the primary source of energy, in conjunction with energy gradients due to particle-particle contact and surface tension.

Much progress in understanding densification techniques has been achieved since 1935. Now densification is studied by plotting density or shrinkage data as a function of time and by actual examination of the microstructure at various stages of densification by using scanning electron microscopy, transmission electron microscopy, and lattice imaging.

Densification mechanisms may include vapor phase, solid phase, liquid phase, and reactive liquid phenomena. Probably the most applicable of these to RDF are solid phase mechanisms, although other forces are undoubtedly present. Diffusion will be important. The differences in free energy or chemical potential between the free surfaces of particles of RDF and free points of contact between adjacent particles will be important. The control of temperature and particle size for densified RDF will probably be extremely important, but control of time less important. Particle size distribution may be of critical importance. Particle shape will also be important.

Other processes are also available to achieve densification, deposition of a solid phase, or strong bonding. These types of processes include hot pressing, reaction densification, chemical vapor deposition, liquid particle deposition, and cementitious bonding. All of these processes were considered during the course of this project and in the pilot-plant phase. The application of pressure during densification of RDF might provide the following processing and property advantages:

- Reduction of densification time,
- Reduction of densification temperature,
- Minimization of residual porosity, and
- Higher strengths than can be achieved through pressureless densification, due to the minimization of porosity and grain growth

The RDF was obtained from Madison, Wisconsin; Ames, Iowa; and Monroe County, New York. It was determined in our laboratory that the three sources of RDF were similar and behaved in approximately the same way to binders. The RDF was minus one inch in particle size. The RDF was first dried in the oven for several hours to remove as much moisture as possible at 100°C. Once dried, the RDF was suitable for preparation with binders and follow-up tests.

The preparation involves the weighing of a desired quantity of the dried RDF, usually 30 to 40g, and adding to it 5 percent by weight of water. For those binders that are in liquid form, no water is added. All of these components are mixed and the binder-RDF mixture chopped and reduced in particle size with a food processor. The RDF/binder mixture is then placed into a stainless steel die and formed into pellets by a Carver laboratory pellet press using 5,000 lb of pressure. The pellets produced range in weight from 1 to 1.5g. The process of making the pellets takes about 30-45 minutes. After the pellets are produced, various tests are conducted according to design protocols and a binder rating system.

For example, the durability test is conducted in order to determine the durability of the pellets when subjected to handling. Two pellets are weighed by difference and placed into a ball mill jar with then ceramic stones. The jar is allowed to tumble for ten minutes. After this specified time, the two largest remaining pieces are reweighed. The percent durability is calculated using the following formula, with 100% being the ideal:

$$\% \text{ Durability} = \frac{\text{weight of largest RDF pieces}}{\text{weight of RDF pellets}} \times 100$$

Another example is the water sorability test, which helps to determine the quantity of water that the pellets absorb within a given time frame (in this case, 24 hours). The pellets should absorb as little water as possible in order to further enhance their endurance potential. Two pellets are weighed into a petri dish (W_w) and their weight obtained by difference (W_p). Twenty-five milliliters of water are added, and the pellets are allowed to absorb water for one hour. Actually, the pellets remain on each side for 30 minutes in order to ensure equal water absorption, thus resulting in a total of one hour. The pellets are then placed into a desiccator with a constant 100% relative humidity and maintained for 24 hours; and the petri dish is then placed into an oven at 100°C to dry. Following the 24 hour period in the environmental chamber, the pellets are removed and reweighed (W_t). The percent absorbed water is calculated using the following formula, with the lower percentage being most favorable:

$$\% \text{ Absorbed Water} = \frac{W_t - W_w}{W_p} \times 100$$

The overall study was divided into two sections, a preliminary study and a laboratory study. The preliminary study was designed to reduce the number of binders that would be investigated in the laboratory study to approximately 50. In order to accomplish this, a series of protocols was developed for the preliminary study and the laboratory study in order to evaluate the potential binders discussed previously. The protocols were subjected to peer review early in the project and modified in some instances.

The preliminary study was divided into two parts. They were binder cost and environmental acceptability, rated at 60 points and 40 points, respectively, for a total of 100 points. Cost was considered to be the more important aspect of a suitable binder. This is because the RDF is a low-cost binder with a low-cost material. This would only make sense if the binder could be used in very low concentrations, and none of our studies indicated that this was possible. The environmental acceptability part was broken into three segments - toxicity, odor, and emissions - rated at 10 points, 10 points and 20 points, respectively.

The laboratory study was divided into 11 segments; binder dispersability, binder Btu content, binder ability to wet, binder ash content, pellet weatherability (including in the ice box at 32°F and in the environmental chamber at 110°F), pellet water sorability, pellet caking, pellet ignition temperature, moisture content, durability, and aerobic stability. These were considered to be in two parts, the first four segments being binder properties and the last seven segments being pellet properties. The binder properties were rated at 7 points per segment, and the pellet properties were rated at 9 points per segment (with the exception of weatherability, which was rated at 9 points each for the ice box test and the environmental chamber test).

The above concepts were also subjected to peer review, and comments generally favored this approach. Protocols for each study were developed and will be discussed in the extended paper.

Worksheets were prepared listing point values for the various binder and pellet properties identified previously. The sheets are arranged in order from the binder having the highest rating to the binder having the lowest rating. In some cases, binders with low preliminary study ratings were tested in the laboratory study, in order to evaluate different types of binders.

The top six binders were carbon black, calcium hydroxide, free lime, cement kiln dust, limestone and lignite fly ash. Further pilot plant work at Jacksonville Naval Air Station in Florida indicated that calcium hydroxide was the best binder. The above procedure, with some modifications, is being used with other solid waste problems. These will be briefly discussed in the extended paper.

PCFB GASIFICATION OF BIOMASS

ANDERS L. HALLGREN, INGEMAR BJERLE,
LARS A. CHAMBERT
University of Lund
Chemical Center
Dept. of Chem.Eng. II
Box 124, S-221 00 Lund
Sweden

Keywords: pressurized circulated fluidized bed biomass gasification; hot gas filtering; hot gas alkali removal

INTRODUCTION

Gasification technology is and has been widely used in different ways of commercial fuel gas production. Coal gasification technology has shown to have potential also in biomass gasification although it must be kept in mind that coal and biomass show quite different behavior in thermochemical processes. The technology has been applied to biomass gasification and numerous research efforts are referred to in the literature. These represent in many ways a firm theoretical base [1,2].

Nevertheless, additional comprehensive information is needed for taking the technology of pressurized biomass gasification into industrial scale applications. However, the real commercial impact in power generation is yet to be seen mainly because of perhaps immature biomass pretreatment and conversion technology, lacking hot gas cleaning solutions and of course depending on relatively low oilprices. A successful commercial development of the technology is needed and how fast this is going to take place is crucial for the introduction of biomass based power production.

Research activities in the United States

Considerable efforts and substantial resources have been invested in studying pressurized gasification. A small selection of the recent efforts is presented below [3,4].

The Institute of Gas Technology (IGT) in Chicago (IL) has been conducting research with an oxygenblown, fluidized-bed gasification reactor designed to operate at pressures up to 3.5 MPa. IGT has carried out a comprehensive test matrix with the Renugas process development unit with funds from the U.S. Department of Energy (DoE). These tests have been completed to determine the effects of various process variables in order to obtain parametric information for process optimization with refuse derived fuels (RDF) and other biomass feedstocks.

On the Maui island of Hawaii the Pacific International Center for High Technology Research (PICHTR), Hawaii Natural Energy Institute of the University of Hawaii, Hawaiian Commercial Sugar Company, The Ralph M. Parson Engineering Company, and IGT are planning a demo-scale plant for biomass (bagasse) gasification. The start of operation is scheduled for the second half of 1993 and the experimental program will be supported by the US Department of Energy. The IGT Renugas process is going to be applied, i.e. the pressurized air-blown fluidized bed gasifier. Apart from the main fuel bagasse other biomass and wastes such as eucalyptus wood chips, RDF, and agricultural wastes will be used as well.

The University of Missouri-Rolla has been investigating the technical feasibility of using a metal fired-tub heat-exchanger to provide heat for a fluidized-bed gasifier. This concept allows the production of medium-energy gas or synthesis gas without the use of oxygen. The gasifier is a stainless steel reactor fitted with an internal heat exchanger bundle consisting of thirty stainless steel U-tubes. Hot combustion flue gases, which could be produced by burning a portion of the product gas or other fuels such as char, are passed through the heat exchanger. Extensive series have been conducted in order to determine the effect of various process variables. Wood feed rates ranged from 45 kg/h to 180 kg/h producing a product gas with a higher heating value ranging from 14.6 to 21.6 MJ/Nm^3.

Battelle-Columbus Laboratories (BCL), Columbus (Ohio) has conducted research on a medium-energy gasification process which involved an indirectly heated dual fluidized bed gasifier by circulating low density, incandescent sand to the gasifier. Entrained sand and any non-reacted char leaving the gasifier are separated from the gas product in a cyclone. The char and sand are fed into a fluidized-bed, air-fired, combuster where the char and supplementary fuel are burned. The BCL gasification process is capable of operations at temperatures up to 870°C and pressures slightly above atmospheric. The gasifier has been tested with a number of biomass feedstocks including hard and soft wood chips, sawdust, hogged fuel and bark strips at wood feed rates as high as 960 kg/h. The gas product higher heating value has been ranging from 16.0 to 19.1 MJ/Nm^3 and the carbon conversion to gas in the gasification reactor varied from 50 to over 90 % for wood containing 3-34 % moisture.

Research activities in Europe

A commercial application of gasifiers developed in Finland is the A. Ahlström Oy PYROFLOW circulating fluidized-bed gasifier. A maximum thermal output of 35 MW is accomplished using not only waste wood as the main fuel but also peat is a well-suited feedstock. The PYROFLOW gasifier consists of a refractory-lined cylindrical vessel and a refractory-lined cyclone. A fluidized-bed of hot sand is operated in a circulating mode where dry waste wood is entering the bed through the side of the reactor.

The German company Lurgi GmbH has been involved in developing and designing commercial gasifiers applicable for various feedstocks ranging from coal to biomass, wastes and RDF. The circulating fluidized-bed gasification system is commercially available for the production of low-energy gas. The gas produced is suitable for a number of processes and particular interesting for the paper and pulp industry, where sufficient bark and wood-waste are produced without costly transportation and distribution overheads to partly substitute oil and gas.

Besides the applied biomass gasification technology, basic research has been reported in the literature from different places in Europe. However, the topics covers a broad scientific spectrum which is sometimes difficult to overview. Research groups at VTT in connection with universities in Finland represent a forward position in this field and additionally the University of Saragossa (Spain) should be mentioned in this context. Lately here basic research was successfully conducted in catalytic steam gasification of biomass and wastes sponsored by the governmental funds.

Research activities in Sweden

The biomass gasifiers built in Sweden so far have been, with few exception, atmospheric updraft/ downdraft or fluidized bed gasifiers for the production of burnable gases for district heating systems and the paper pulp industry. One of the exceptions is the Studsvik MINO-plant which was planned for the production of synthesis gas from wood through pressurized oxygen gasification. Comprehensive research efforts were made with the MINO plant and gave the Studsvik Energy, Thermal Processes Laboratory a leading position in gasification technology [5].

During the last years the power industry in Sweden has shown a growing interest in the gasification technology and particularly in biomass gasification. Through combined cycle applications good possibilities are supposed to be given in producing environmentally favourable power at high efficiency. In the light of 10 GW nuclear power generation in Sweden phasing out after the year 2010, it has been shown that Sweden has a potential of 33-53 TWh/year of electricity from biomass based gas turbine systems.

Taken in connection with Sweden's traditionally genuine knowledge in the field of thermochemical processing and particularly in the gasification technology, abundant opportunities should be available for successfully implementing biomass based power generation.

The PCFB biofuel gasifier at Lund Institute of Technology (LIT)

The pressurized gasifier is intended to be a small flexible test rig which will offer adequate scientific results and constitute the link between lab-scale developments and industrial scale application. The pilot plant will to a certain degree be operated parallel to the Sydkraft biomass gasifier at Värnamo for evaluation and confirmation of the test results. The gasifier at LIT is constructed as a circulating

fluidized bed and the intentions are to study gasification of different biomass feedstocks at pressures up to 2.5 MPa and at temperatures between 600 - 1050°C.

The objective of the test program is to investigate the influences of the process parameters on each other and on the product distribution and composition. This will be done in as realistic circumstances as possible regarding pressure intervals, temperature and residence time intervals. In addition to studying the gasification process as such, investigations will be made regarding finishing treatments of the gas products at elevated temperatures and pressures. Examples of such treatments will be dust separation at high temperatures, desulfurization, tar cracking, catalytic ammonium dissociation, and hot gas alkali removal.

APPARATUS

The equipment which is going to be used can be characterized as a process development unit (PDU). The PDU consist of four main parts; feeder, circulating fluidized bed (CFB), hot gas filter, and a reactor for catalytic treatment of dust free gas. The warm parts, i.e. the gasification reactor, the hot gas filter, and the catalytic reactor are concentrically placed inside an outer pressure vessel consisting of three vertical tubes of 0.5 m in diameter. The gas pressure inside these tubes is suppose to balance the process gas pressure. The pressure vessel also contains electric heating elements and insulation. A schematic diagram of the apparatus is shown in Figure 1.

The feeding system

A well defined portion of the feeded biomass is transported with screws into a pressure chamber where the feeded material together with the gas are compressed by means of a hydralic piston. From this chamber the biomass is screwed into the reactor inlet. This setup will demonstrate batch compression followed by continuous feeding into the reactor. Similar technical design has scarcely been seen reported in the literature or in studying patents, hence, the feeder construction might offer novel solutions in pressurized feeding systems.

The gasifier

The gasifier is constructed as a circulating fluidized bed (CFB) gasifier with options to operate it as a bubbling bed gasifier. Great attention has been paid to give the experimental setup a broad range of flexibility for modifications. The reactor will have a diameter of 40.9 mm and an approx. height of 3 meter. This makes it possible to operate the CFB at fluidizing velocities and residence times that are comparable with those of industrial scale applications.

Flow conditions typical to CFB with small diameters have been reported in the literature [6]. A large amount of basic work regarding analyses of flow dynamics have been made with small scale equipment at atmospheric pressure and at various temperatures

Figure 3 shows the primary range of operation at 950 °C and at the pressure interval 0.4 - 2.0 MPa. Calculations have been done in order to find the influences of various fluidization velocities on the total gas production and fuel/air consumption. As can be noted in the diagram, the calculated maximum gas production is 42.24 Nm^3/h at an air and fuel feed of 22.78 Nm^3/h and 18 kg/h respectively.

A fluidization velocity of 1.0 m/s is the calculated minimum velocity in order establish reasonable fluidization in the gasifier of diameter 40.9 millimeter. Accordingly, the maximum calculated fluidization velocity is 2.0 m/s in the pressure interval mentioned above.

The reactor consist of an inner and an outer tube with an annular space in between. The feed including bed material is introduced directly into the inner gasifier. Solid material will be separated from the gas phase with a low pressure axial cyclone at the top of the reactor. The separated solid materials are forced down through the annular space between the inner and outer reactor tube. At the bottom, material re-introduction into the riser at minimum acceleration losses and increased circulation is possible due to the design of the gas inlet distributor. The material recirculation is supposed to be governed by the height of the material in the return tube. High transport density and good mixing of the feed material and the separated solid materials are wanted in order to insure

gasification and gas quality.To demonstrate the function of these parts will propably show major practical significance in industrial scale applications.

The hot gas filter
Before the hot gas from the gasifier enters the filter element is cooled down to a temperature between 300-800°C depending on given circumstances. The gas is cooled by letting it pass a spiral shaped tube heat exchanger containing water at 2.0 MPa and 212°C.

The hot gas filter element consists of a sintered granular ceramic material. The filter is 1 meter long and have outer diameter of 60 mm and is designed as a single conventional industrial filter. The potential of the filter will be tested with respect to the function within a broad temperature interval for the optimization of future plants gas turbine inlet gas temperature.

The catalytic reactor
The catalytic reactor will be used for investigations concerning adsorption of alkali/trace metal elements, tar cracking, ammonia reduction, and H_2S . The reactor is of a downdraft type and consists of a stainless steel tube filled with the catalytic material. As for the gasifier and the hot gas filter, the catalytic bed reactor is concentrically placed inside an outer pressure vessel containing electric heat elements for heating up to approx. 1000°C.

EXPERIMENTAL

Background
Pyrolysis, thermal dissciation of an organic material in an oxidizing free atmosphere, is a thermal precursor to gasification. Gasification of solid materials is normally regarded as the combination of pyrolysis followed by heterogeneous and homogenous chemical reactions of chars, tars, and primary formed gaseous components.

In pure pyrolysis sufficient energy must be added for the conversion while in gasification adequate or at least part of the energy required for the reactions is internally produced mainly through oxidation of the pyrolysis products. Consequently, additional indirect heating can be kept at a minimum and sub-stoichiometric amounts of of air, oxygen, and water vapor produce burnable gaseous products.

Through varying different parameters, e.g. temperature, pressure, and material residence time, the gasification reactions can be influenced in the desired direction that establish different spectra of the gas product composition. The equibrilium composition of the gas product for an adiabatic air/biomass conversion at different air to fuel ratios is indicated in Figure 4.

The experimental program
Sawdust from wood and forest wastes in the first phase of the experimental program. Possibly other feedstocks such as RDF and agricultural wastes will be taken into account as feedstocks in future research programs.

A complete survey of the gasification products, including closing material balances, as well as scientific adequate gasification investigations are judged possible. The basic properties of the reactor will be studied including monitoring the flexibility influenced by different process conditions. In addition to general gasification studies the experimental program, based on two years, will focus on the following subjects:

- influences from the inherent moisture and the particle size distribution of the solid biofuel on product distribution and composition
- qualitative/quantitative analyses of the distribution of alkali/trace element metals in the gasification products
- influences from dolomite and other additives in the bed material
- tar and ammonia cracking as a function of the type catalysts.

Apart from the experimental program, verifications of dynamic modelling work of the reactor function will be carried out.

SUMMARY

A pilot plant biomass PCFB-gasifier is being installed at the Chemical Center in Lund. The official project start-up was in February 1992 after a one-year extensive feasibility study with involvement's from design consultants and Sydkraft AB. However, the financial issue wasn't completely solved until late April 1992 which delayed the actual project start-up to the beginning of June 1992.

The purpose of the project is to establish realistic conditions for thermal gasification of biofuel and gas cleaning, and to study the various parameters involved in the process and how they influence each other.

Project status May 1993

A first version of a comprehensive literature survey has been concluded. This survey will be published and available through Nutek.

After a very busy investment period we are now escalating our efforts in assembling the pilot plant. A first pressurized test series with the biofuel feeding system has been successfully completed. Fluidization and feeding tests will be continued during the summer of 1993. Due to problems involved with the delivery of certain parts and materials, the experimental program start-up is delayed The first phase of the experimental program will be implemented during the second half of 1993 and 1994

ACKNOWLEDGMENTS

This project is finacially supported by the National Board for Industrial and Technical Development (NUTEK), Sydkraft AB, and the Swedish Energy Development Corporation (SWEDCO).

REFERENCES

1. Rensfelt, E., "Practical Achievements in Biomass Gasification" paper presented at BioEnergy 84, June 18-21 1984, Gothenburg, Sweden.

2. Bridgewater, A.V., "An overview of thermochemical biomass conversion technologies", in Wood:fuel for thought. Proceedings of the conference held at Bristol (UK) 23-25 Oct.1991

3. Schiefelbein, G. F., "Biomass Thermal Gasification Research : Recent Results from the United States DOE's Research Program", Biomass 19 (1989) 145-159.

4. Trenka, A.R, Kinoshita, C.M., Takahashi, P.K., Phillips, V.D., Caldwell , C., Kwok, R., Onishak, M., Babu, S.P.,"Demonstration plant for pressurized gasification of biomass feedstocks". 15th Annual Conference on Energy from Biomass and Wastes, Washington DC, March25-29 1991.

5. Rensfelt, E., Waldheim, L., Blackadder, W.H., "Gasification research and development 1980-1990 by Studsvik", internal report STUDSVIK-EP--91/5, April 30, 1991.

6. Mori, S., et al, "Turbulent fluidization phenomena", Nagoya Inst. of Technology, Showa, Nagoya; Mitsubishi Gas Chemical Co Ltd, Matsuhama, Niigata; CFB Conference II, Compiagne 1988.

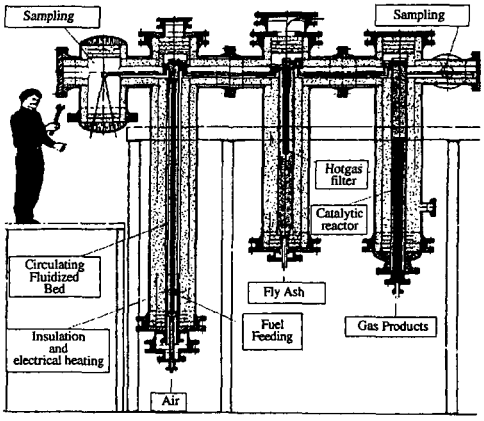

Figure 1. Schematic diagram of the LIT/PCFB gasifier

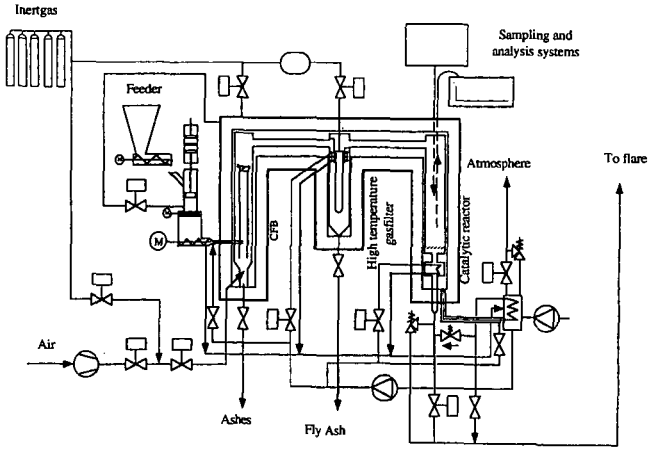

Figure 2. The process layout for the LIT/PCFB gasifier system

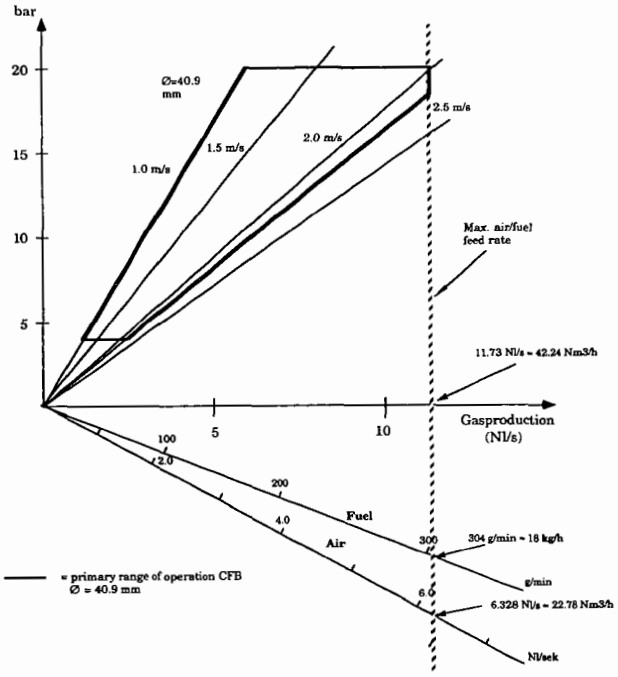

Figure 3. Test rigg range of operation as a function of the fluidization velocity.

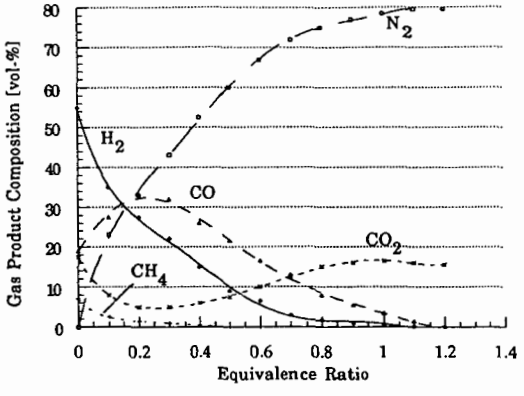

Figure 4. Gas product composition for adiabatic air/biomass conversion versus the air to fuel ratio at 0.1 MPa.

Genetic Engineering for Productivity in the Fermentation of Xylose to Ethanol

Xu, Jie; Das, Anu; Erbe, Jarrod; Hall, L.M. & Taylor, K.B.
Department of Biochemistry, The Fermentation Facility, The University of Alabama at Birmingham, University Station, Birmingham, AL 35294

Keywords: xylose, fermentation, ethanol, genetic engineering

INTRODUCTION

With the increased awareness of the limitations in the world supplies of petroleum came an increased interest in gasoline extenders and additives. The use of ethanol as an extender on a national scale is associated with advantages (1,2): the security of fuel sources; a more favorable foreign trade balance; and the renewability of the raw materials for production. Although ethanol can be produced either from a petroleum component or by fermentation, the latter source is the only one associated with all of the advantages above. The most attractive raw materials for ethanol production in this country are corn sugar, and sugar derived from wood and crop residues (lignocellulosic materials). Corn ($98-$104 per ton), (2) can be competitive only in special circumstances, such as government subsidy. However, lignocellulosic material ($20-$70 per ton) could be competitive, if the technical limitations associated with processing and fermentation could be overcome. Although the approximate price of corn-derived ethanol is currently $1.20 per gallon, it is estimated that the cost of fuel ethanol from lignocellulosic materials should be $0.60-$0.80 per gallon (3).

The most productive and cost effective processing of lignocellulosic material currently consists of mild acid hydrolysis to release a fraction containing primarily xylose (15%-40% of dry weight) followed by strong acid treatment to release the glucose (30%-60%), (4,5,6). The sugars are then fermented, usually separately, to ethanol. However, there are two steps in particular that limit the productivity and increase the cost of this process: the hydrolysis of cellulose and the fermentation of xylose. The most promising solution to the former problem is enzymatic hydrolysis, but currently the enzymes remain too expensive and the hydrolysis is incomplete. The problem with xylose fermentation results from a poor overall yield. It is estimated that the efficient conversion of xylose would reduce the cost of ethanol by about $0.40/gal (7).

A number of both yeasts and bacteria will convert xylose to ethanol and other products (8,9,10), but most of the attention has been given to three yeast strains: *Pachysolen tannophilus, Candida shehatae,* and *Pichia stipitis*. Yeast has the advantages of growing in a simple, inexpensive medium; growing at a low pH to minimize contamination; and being the subject of much past experience. Although both bacteria and yeast generally convert D-xylulose to hexose (as the phosphate esters) and convert the hexose to ethanol by the classic fermentation pathway, they differ with respect to the methods used to convert D-xylose to D-xylulose. Most bacteria carry out the conversion with a single enzyme, xylose isomerase; whereas most yeast reduce the xylose to xylitol with xylose reductase and subsequently reoxidize it to xylulose with xylitol dehydrogenase.

The principal limitation to the ethanol yield in the yeast fermentation is the accumulation of xylitol in molar amounts equal to

or exceeding that of ethanol (11). Furthermore, the accumulated xylitol is not further utilized. Fermentation under micro-aerobic conditions reduces the amount of xylitol (12,13) accumulated, but the oxygen also promotes the further oxidation of ethanol.

The ethanol yield has been improved by the addition to the medium of fatty acids (14), polyethylene glycol (15), azide (16), or acetone (17). In addition mutants with increased yield have been reported (18,19,20). However, none of these strategies seems to have become widely used in practice. Xylose isomerase has been utilized in the fermentation to facilitate the conversion of xylose to xylulose (21), but neither the equilibrium of the reaction nor the pH optimum of the enzyme is favorable (22). Several workers have described strains of *Saccharomyces cerevisiae* (23,24) and *Schizosaccharomyces pombe* (25) into which the xylose isomerase gene has been cloned, but the productivity was low presumably because of low levels of transport systems, xylulokinase, transketolase, and transaldolase.

The most important unanswered questions deal with the causes of xylitol accumulation and its non-utilization. Several investigators have attributed xylitol accumulation to the fact that the majority of the xylose reductase activity requires NADPH, whereas the xylitol dehydrogenase requires NAD (26,27). However, if this nucleotide imbalance were the only cause, the utilization of xylose would quickly stop, because of the low concentration of intracellular nucleotides.

The poor xylitol utilization is inconsistent with its status as an intermediate. Although the utility of oxygen and acetone in xylitol conversion, as well as its redox status, indicates that an electron acceptor is necessary, xylitol still accumulates to a very significant extent and the utilization of extracellular xylitol remains very poor in the presence of oxygen.

The present work was undertaken to provide answers to these questions and to utilize the answers to design and implement a strategy of metabolic and genetic engineering to develop a strain of *Pachysolen tannophilus* to ferment xylose efficiently.

RESULTS

Whole, resting cells of *Pachysolen tannophilus* converted xylose to ethanol (yield, 1.11 mole/mole) but did not convert xylitol (28). However, a cell-free extract, prepared by French pressure cell and low-speed centrifugation, produced ethanol from both xylose (yield, 1.1 mole/mole) and xylitol (yield, 1.64 mole/mole; theor, 1.67 mole/mole). These results supported the hypothesis that the cell permeability to xylitol limits its utilization and the fact that nystatin, amphotericin B, and filipin; all agents that increase the cell-membrane permeability of yeast and fungi (29,30), increased the rate 40-fold.

In order to simplify the investigation of the requirements for xylose metabolism the putative pathway was separated into two parts by the inclusion of xylose isomerase (Spezyme GI, Finnsugar Biochemicals, Inc.) in the incubations with the fractions of the cell-free extract. Preliminary experiments showed that ethanol formation from xylose by the crude cell extract was stimulated 9-fold by added xylose isomerase.

In the Presence of Xylose Isomerase the activity of the HMW fraction, prepared by gel filtration of a soluble fraction of the cell-free extract, was restored by the addition of both ADP and NAD^+ (Table 1). Although NAD^+ stimulated ethanol formation in this preparation (fraction A), its complete removal required treatment three times with

gel filtration and once with charcoal (fraction B, Table 1).

In contrast to our previous results with xylitol (28) xylose is metabolized in the absence of oxygen, and xylose is metabolized by soluble fractions of the cell-free extract from which the membranes and organelles have been removed by centrifugation.

Although the addition of NAD^+ and ADP restored the production of ethanol from xylose by the HMW fraction, in the presence of xylose isomerase, their addition failed to restore ethanol formation from xylose by the same fraction in the absence of xylose isomerase. In addition, the inclusion of $NADP^+$, NADPH, or ATP in addition to NAD^+ and ADP, as well as the inclusion of a variety of other coenzymes and metal ions in the presence of NAD^+, $NADP^+$ and ADP failed to restore activity.

Because of the fact that added NADPH was rapidly consumed by the HMW fraction in the absence of xylose and the fact that, at higher concentration (>100 μM), both NADPH and $NADP^+$ inhibited ethanol formation from xylose by the unfractionated cell extract, three NADPH generation systems were tested to maintain a constant supply of the reduced coenzyme at low concentration: partially purified transhydrogenase from *E. coli K-12*, NADP-linked isocitrate dehydrogenase from porcine heart, and NADP-linked alcohol dehydrogenase from *Thermoanaerobium brockii*. Although transhydrogenase activity ineffective in the restoration of ethanol production, both the NADP-linked isocitrate dehydrogenase and the alcohol dehydrogenase stimulated the formation of ethanol from xylose by about 60 and 80 fold respectively (Table 2).

A number of factors contribute to the causes of xylitol accumulation. Certainly the fact that xylose reductase requires NADP whereas xylitol dehydrogenase requires NAD (nucleotide imbalance) is one of the factors. Another is certainly the fact that extracellular xylitol is not normally utilized by whole cells.

In experiments containing purified cell-free fraction, xylose isomerase, NAD and ADP, xylitol was produced during xylose metabolism (Table 3). Furthermore, the gas chromatographic assay for ethanol contained an additional peak that had the same retention time as acetaldehyde. Therefore, some of the NADH generated by glyceraldehyde phosphate dehydrogenase is reoxidized in the generation of xylitol, presumably from xylulose by xylitol dehydrogenase. The addition of $NADP^+$ had little effect on the amount of ethanol made from xylose, but it increased the xylitol accumulation by 2.5-fold; increased the xylose consumption by 2-fold; and eliminated the acetaldehyde peak (Table 3). Therefore, most of the xylitol is generated by xylose reductase in these extracts containing all of the cofactors and presumably in the whole cells.

Xylose is reduced to xylitol with electrons from the pentose-hexose cycle, but the poor coupling of the rate with the rate of xylitol dehydrogenase causes xylitol to accumulate faster than it is utilized. The intracellular xylitol leaks out of the cell and becomes diluted in the medium, from which it is not reutilized because the transport back into the cell is limiting. The intracellular xylitol can be metabolized, if oxygen is present. Thus oxygen is required for optimum xylose metabolism.

The logical strategy for process improvement according to the results above would be the transformation and expression of the gene for xylose isomerase in one of the xylose-fermenting yeasts. However, it would also be necessary to inhibit both the xylose reductase and xylitol dehydrogenase, in order to prevent xylitol accumulation. However, the transformants should be able to ferment xylose to ethanol

anaerobically.

The genetic engineering strategy to accomplish these objectives takes advantage of homologous recombination in yeast, at least in *Saccharomyces cerevisiae*, in which genetic material with homologous DNA sequences will insert in the homologous gene with high frequency. Therefore, the desired genetic construct will contain the gene of interest, xylose isomerase plus a suitable promoter, flanked on either end with DNA sequences homologous to those for xylose reductase or those for xylitol dehydrogenase. These constructs should take advantage of the high frequency of recombination to increase the transformation frequency as well as inactivate the target gene.

In preliminary experiments a gene conferring antibiotic resistance, e.g. kanamycin, will be used in place of the xylose isomerase gene because the feasibility of the strategy and the optimal experimental conditions can be determined with an easily selectable marker. The successfully transformed strain should be resistant to the antibiotic and be unable to grow on xylose. In subsequent experiments the gene for antibiotic resistance will be put in tandem with the gene for xylose isomerase. In the latter case the successfully transformed strain should be antibiotic resistant and grow anaerobically on xylose.

The identification of and the determination of the sequences for xylose reductase and xylitol dehydrogenase in *Pachysolen tannophilus* require a probe with an homologous DNA sequence. The gene for each of the two enzymes from *Pichia stipitis* has been identified and sequenced (31,32), and part of the amino acid sequence of xylose reductase from *Pachysolen tannophilus* is known (33). A homologous probe for the *Pachysolen* gene for xylose reductase has been designed and constructed by back translating the amino acid sequence of a region that is highly homologous with the *Pichia* sequence according to the most frequent codon usage of *Pachysolen*. This probe was made radioactive and used to test binding to whole *Pachysolen* DNA, a restriction enzyme digest of *Pachysolen* DNA, and to the DNA from clones from a xylose-induced cDNA library of *Pachysolen* DNA. The positive results from each experiment are being tested further with this and similar probes, and the appropriate DNA will be sequenced to identify the limits of the coding sequences and the promoter for the gene.

Literature Cited

1. Lynd L. R. Appl. Biochem. Biotechnol. 1990, 24/25, 695-719.
2. Wyman, C. E., and Hinman, N. D. Appl. Biochem. Biotechnol. 1990, 24/25, 735-753.
3. Lynd L. R., Cushman, J. H., Nicholas, R. J. and Wyman, C. E. Science 1991, 259, 1318-1323.
4. Whistler, R. L., Bachrach, J. and Bowman, D. R. Arch. Biochem. 1948, 19, 25-33.
5. Weihe, H. D., and Phillips, M. J. Agr. Res. 1940, 60, 781-786.
6. Rosenberg, S. L. Enz. Microb. Technol. 1980, 2, 185-193.
7. Hinman, N. D., Wright, J. D., Hoagland, W and Wyman, C. E. Appl. Biochem. Biotechnol. 1989, 20/21, 391-401.
8. Skoog K., and Hahn-Hagerdal, B. Enzyme Microb. Technol. 1988, 10, 66-80.
9. Toivola, A., Yarrow, D., van den Bosch, E., van Duken, J. and Scheffers, W.A. Appl. Environ. Microbiol. 1984, 47,1221-1223.
10. Nigram J. N., Ireland, R. S., Margaritis, A. and Lachance, M. A. Appl. Environ. Microbiol. 1985, 50, 1486-1489.
11. Taylor, K. B., Beck, M. J., Huang, D. H. and Sakai, T. T. J. Ind. Microbiol. 1990, 6, 29-41.
12. du Preez, J.C., Prior, B. A. and Monteiro, A. M. T. Appl. Microbiol. Biotechnol. 1984, 19, 261-266.
13. Debus, D., Methner, H., Schulze, D. and Dellweg, H. Appl. Microbiol. Biotechnol. 1983, 17, 287-291.
14. Dekker, R. F. H. Biotechnol. Bioeng. 1986, 6, 605.
15. Hahn-Hagerdal, B. Joensson, B. and Lohmeier-Vogel, E. Appl. Microbiol. Biotechnol. 1985, 21, 1173-175.
16. Hahn-Hagerdahl, B., Chapman, T. W. and Jeffries, T. W. Appl. Microbiol. Biotechnol. 1986, 24, 287.
17. Alexander, N. Appl. Microbiol. Biotechnol. 1986, 25, 203-207.
18. Jeffries, T. W. Enz. Microb. Technol. 1984, 6, 254-258.
19. Lochke, A. H. and Jeffries, T. W. Enz. Microb. Technol. 1986, 8, 353-359.
20. Lee, H. James, A. P. Zahab, D. M. Mahmourides, G., Maleszka, R. and Schneider, H. Appl. Environ. Microbiol. 1986, 51, 252-1258.
21. Gong, C. S., Chen, L. F., Flickinger, M. C. Chiang, L. C. and Tsao, G. T. Appl. Environ. Microbiol. 1980, 41, 430-436.
22. Olivier, S. P. and du Toit, P. J. Biotechnol. Bioeng. 1986, 28, 984-699.
23. Sarthy, A. V. Appl. Environ. Microbiol. 1987, 53, 1996.
24. Batt, C. A. Carvallo, S., Easson, D. D., Jr., Akedo, M. and Sinskey, A. J. Biotechnol. Bioeng. 1986, 28, 549.
25. Chan, E. C., Ueng, P. P. and Chen, L. Biotechnol. Lett. 1986, 8, 231.
26. Bruinenberg, P. M., DeBot, P. H. M., Van Dijken, J. P. and Scheffers, W. A. Eur. J. Appl. Microbiol. Biotechnol. 1983, 18, 287-292.
27. Bruinenberg, P. M., DeBot, P. H. M., Van Dijken, J. P. and Scheffers, W. A. Appl. Microbiol. Biotechnol. 1984, 19, 256-260.
28. Xu, J. and Taylor, K. B. Appl. Environ. Microbiol. 1993, 59, 231-235.
29. Bolard, J. Biochim. Biophys. Acta 1986, 864, 226-234.
30. Sutton, D. D., Arnow, P. M. and Lampen, J. O. Proc. Soc. Exp. Biol. Med. 1961, 108, 170-175.

31. Takuma, S. Nakashima, N. Tantirungkij, M., Kinoshita, S., Okada, H., Seki, T.. and Yoshida, T. Appl. Biochem. Biotechnol. 1991, 28, 327-40.
32. Kotter, P., Amore, R., Hollenberg, C. P. and Ciriacy, M. Current Genet. 1990, 18, 493-500.
33. Bolen, P. L., Bietz, J. A. and Detroy, R. W. Biotechnol. Bioeng. Symp. 1985, No 15, 129-148.

Table 1. Effects of Sephadex column and charcoal treatment of the high speed supernatant fraction (HSSF)[a]

Fraction	Additional Components		EtOH mg/ml
HMW	-	-	<0.01
HMW	-	NAD^+	<0.01
Fraction A[b]	ADP	-	0.12
Fraction A	ADP	NAD^+	0.64
Fraction B[c]	ADP	-	<0.01
Fraction B	ADP	NAD^+	0.62

[b]Fraction A, the HMW fraction of the high speed supernatant fraction has undergone two consecutive gel filtration treatments.
[c]Fraction B, Fraction A was treated with charcoal.

Table 2. Restoration of ethanol formation from xylose in the HMW fraction of the crude cell extract in the presence of an NADPH generation system[a]

Reaction Mixture	Substrate	EtOH Made mg/ml
None	Xylose	<0.01
IC[a] + ICDH[a]	none	0.057
IC + ICDH	Xylose	0.710
cPen-OH[a] + ADH[a]	none	0.016
cPen-OH + ADH	Xylose	0.925
TH[b] + NADPH (0.1 mM)	Xylose	<0.01

[a]IC, sodium isocitrate; ICDH, $NADP^+$-linked isocitrate dehydrogenase; cPen-OH, cyclopentanol; ADH, $NADP^+$-linked alcohol dehydrogenase; TH, transhydrogenase preparation.

Table 3. Comparison of the ratio of formation of ethanol to xylitol by different systems[a]

	Xylose Used μmole	Xylitol Made μmole	EtOH Made μmole	Ratio
Whole Cell				5.75[a]
Crude Extract				3.63[a]
HSSF				0.63[a]
Fraction B[b] + XI[b] + ADP + NAD^+	15.4	7.9	11.0	1.39
Fraction B + XI + ADP + NAD^+ + $NADP^+$	29.1	19.9	9.7	0.49

[a]Xu and Taylor (1993a).
[b]Same as in Table 1; XI, xylose isomerase.

COPROCESSING OF CELLULOSIC WASTE AND COAL

H. Jung, J. W. Tierney and I. Wender
Chemical and Petroleum Engineering Department
University of Pittsburgh
Pittsburgh, PA 15261

Introduction

Paper and other cellulosic wastes constitute more than half of landfill volumes. These materials could be a significant energy source[1]; it is the object of this work to find ways of converting these huge volumes of waste to liquid transportation fuels.

It is well known, of course, that coal can be converted to liquid fuels. There are a number of ways of achieving this. A major route from coal to liquid fuels is by direct liquefaction in the presence of hydrogen or hydrogen donor solvents. Experiments have also demonstrated that cellulosic materials and biomass can be converted to oil in the same way[2, 3]. However, there has been little or no work on the coprocessing of coal and these wastes. We call this route A.

Another way to converting coal to liquids is via the so-called COSTEAM process which involves the treatment of coal with carbon monoxide or synthesis gas ($CO + H_2$) in the presence of water and an alkali compound as catalyst[4, 5, 6]. Again, it has been demonstrated that cellulosic wastes can be converted to liquids in the same manner[7, 8]. However, as far as we know, there has been no work on coprocessing coals with these wastes via the COSTEAM process, which works particularly well with low rank coals such as lignite and subbituminous coals. Most of our coprocessing experiments are being carried out with cellulosic wastes and these coals. We call this route B.

Experimental

Route A (hydrogen and/or hydrogen donor solvents with a molybdenum catalyst)

Wyodak subbituminous coal, obtained from the Argonne Coal Sample Bank, and ordinary copy paper (6.7% moisture and 7.2% ash) were used in this study. Three grams (either coal, paper or a mixture of both), slurried with 12 g of tetralin and 5000 ppm of $Mo(CO)_6$ plus 10,000 ppm of sulfur, were charged in a horizontally shaken 45cc microautoclave with an initial hydrogen pressure of 1000 psig. The reactions were carried out at two different temperatures (325°C and 400°C) for one hour with reaction pressures of about 1800 psig and 2300 psig, respectively.

The nonvolatile products were recovered with THF and then filtered through a cellulose thimble. The filtered materials (THF insolubles) were then extracted with boiling THF. The conversion to THF-solubles was calculated from THF insolubles on an maf basis. THF was removed by rotary evaporation and the product was fractionated into pentane-solubles (oil) and pentane-insolubles (asphaltenes). Since, in the case of H_2-tetralin runs, pentane-solubles include the tetralin, some of which reacted during the reaction and some was lost during the product analysis, only asphaltenes were accurately measured. As a result, the oil and gas fraction was calculated by subtracting the recovered asphaltenes from the total converted. Gases were collected and analyzed by a GC equipped with a Porapak Q column and a 5A molecular sieve

column using a carrier gas with the composition of 8.5% H_2 and 91.5% He.

Route B (CO and H_2O with an alkali catalyst)

Severe mass transfer limitations were experienced in a microautoclave for CO-H_2O runs so that reactions in CO-H_2O environments were carried out in a 300cc autoclave. A total of 8 g of reactants mixed with 24 g of water and 1.02 g of Na_2CO_3 were used with 580 psig (cold) of CO. The reactor was heated to 400°C in about 50 minutes and was held for one hour while stirring at 1400 rpm. Due to the significant amount of water, pressures up to 4200 psig were registered. The reactor was then cooled to below 200°C in 10 minutes. Figure 1 shows a typical history of the temperature and pressure during a run in a CO-H_2O environment.

The same product analysis procedure was employed in Route B runs, except that oil fractions and gas fractions could be measured because the pentane solubles were free of tetralin. The oils were directly calculated from pentane solubles and the gas fraction by subtracting the oils from the oil and gas fraction which was determined from the asphaltene content.

Results and Discussion

Route A (H_2-tetralin system)

Table 1 lists the results at 400°C using a molybdenum catalyst with added sulfur. As expected, conversion of the paper is almost complete. It has been reported that only 90% of a caustic type of lignin was converted under similar conditions with no added catalyst[9]. The conversion of paper yielded only about 10% of high molecular weight asphaltenes with a large yield of oil and gas. Wyodak coal is also converted in high yield but with significant amounts of asphaltenes. Since conversions and yields of oil and gas are very high for paper, the conversion and yield of coal in the coprocessing runs were calculated with the assumption that addition of coal has no influence on paper conversion. As shown in Table 1, the conversion of coal was increased to 91.7% when the 33 wt% of paper was coprocessed, up from 86% of conversion when coal was reacted alone. However, the yield of oil and gas remained unchanged. Addition of paper evidently increased the conversion of coal. Increase in the amount of paper to 50 wt% in the coprocessing does not seem to increase this effect.

It has been proposed that the thermal depolymerization of lignin forms phenoxy radicals, which then cause scission of carbon-carbon bonds in coal[9]. Cellulose in paper can also form phenoxy radicals which may assist the liquefaction of coal in our coprocessing runs. It has also been hypothesized that, at temperatures as high as 400°C, phenoxy radicals polymerize or recombine so that their enhancing effect is minimal[9]. This may help explain the finding that the same oil and gas yield of coal was obtained in the coprocessing as that of coal alone.

Reactions were carried out at a lower temperature (325°C) and the results are listed in Table 2. Even at the lower temperature, paper gave high conversion (88.9%) and high oil and gas yields (77.2%). However, there was a decrease in conversion of coal when the reaction temperature was decreased to 325°C. Both the coal conversion and the yield of oil and gas from the coprocessing run are almost same as those from coal alone at 325°C, suggesting that the effect of paper is small at 325°C. This result is surprising since a synergistic effect of lignin during lignin-coal coprocessing is reported to be the most pronounced in this temperature range[9].

Route B (CO-H_2O system)

The results of runs in CO-H_2O environments with Na_2CO_3 catalysts at 400°C are summarized in Table 3. The paper conversion was almost as high as that in the H_2-tetralin case. However, the product contains more high molecular weight asphaltenes. The same trend is observed for the coal only run in COSTEAM. As stated earlier, there were severe mass transfer limitations in a microautoclave when reactions were carried out in a CO-H_2O environment. For example, the conversion of coal in a microautoclave at 400°C was about 32% in a CO-H_2O environment while that in a 300cc autoclave with stirring was 84%.

It should also be pointed out that the amount of oil (pentane solubles) can be quantitatively measured in CO-H_2O runs since no hydrogen-donor solvent was used. As can be seen in Table 3, most of the product from paper is gas, suggesting the reaction conditions are so severe that most of the liquid product formed light gaseous materials.

Addition of paper to coal provided only a slight increase in coal conversion ($\sim$1%). However, the coprocessing of paper with coal decreased the amount of asphaltenes to half of that produced from coal alone and almost doubled the amount of oils from coal. With the CO-H_2O route, the coprocessing of paper and coal yielded higher quality products. It is also possible that coal may, to a certain extent, prevent liquid formed from paper from reacting further to form gases.

It has been proposed that the pathway for conversion in the CO-H_2O system utilizing an alkali catalysts includes a formate intermediate[4,5].

$$M^+OH^- + CO \rightarrow HCOO^-M^+ \quad (1)$$

$$coal + HCOO^-M^+ \rightarrow coal(H)^-M^+ + CO_2 \quad (2)$$

$$coal(H)^-M^+ + H_2O \rightarrow coal(H_2) + M^+OH^- \quad (3)$$

$$HCOO^-M^+ + H_2O \rightarrow M^+OH^- + CO_2 + H_2 \quad (4)$$

Both the formate ion and water supply hydrogen to coal radicals, while reactions (1) and (4) complete the water-gas shift reaction to generate gaseous hydrogen. Table 4 shows the results of gas analyses for the runs listed in Table 3. As can be seen, about 78% of the CO is converted by the water-gas shift reaction to form hydrogen and CO_2 with a small amount of light hydrocarbons.

Since our experiments were carried out in a batch mode, the system pressures at room temperature after reaction were higher than the initial pressure of pure CO (580 psig) due to the water-gas shift reaction (water is condensed at room temperature). From the gas composition data with the final pressure at room temperature, the total conversion of CO can be calculated and is listed in Table 4. The total conversion of CO includes conversion to supply H_2 to coal and a water-gas shift reaction conversion. The difference between the total moles of CO converted and the moles of hydrogen produced gives the moles of hydrogen consumed by the reactants (coal and paper). The moles of consumed hydrogen thus calculated are also listed in Table 4. As can be seen, the total conversions of CO are all about 78%, regardless of the type of reactants. However, more hydrogen is consumed for coal conversion than for paper conversion. An intermediate amount of hydrogen is consumed by the mixture of coal and paper. According to the reaction pathway proposed, one mole of CO_2 should be produced for every mole of CO converted. However, the amount of CO_2 produced is less than the amount of CO converted. Even when the water-gas shift reaction was carried out in the absence of the reactants, the amount of CO_2 produced was smaller than H_2, suggesting that a significant amount of CO_2 is

dissolved in the aqueous phase. In the paper runs, larger amounts of CO_2 were produced than from coal runs, suggesting that a large portion of gas produced from paper is CO_2.

Summary

Based on an exploratory study of coprocessing of paper and subbituminous Wyodak coal, the following conclusions were drawn. A possible desirable effect of paper in coprocessing was observed in both the H_2/tetralin/Mo system and the CO/H_2O/alkali system at 400°C. More specifically, the conversion of coal was increased due to the addition of paper in the H_2/tetralin/Mo system, but the quality of the product seems to be unchanged. However, very little increase in coal conversion was observed when coprocessing in the CO/H_2O/alkali system, while the product quality of coal was significantly improved (more oil and less asphaltenes). No effect of paper was observed at 325°C in the H_2/tetralin/Mo system.

Acknowledgements

The authors gratefully acknowledge financial support from the U.S. Department of Energy under grant number DE-FG22-91PC91304.

Literature Cited

1. Anderson, L. L. and D. A. Tillman, "Fuels from Waste," p 10, Academic Press, New York, 1977.
2. Mill, I. J. and S. K. Fellows, Fuel, 64, 1246 (1985).
3. Stray, G., P. J. Cassidy, W.R. Jackson, F. P. Larkins, and J. F. Sutton, Fuel, 65, 1524 (1986).
4. Appell, H. and I. Wender, Div. Fuel Chem. Preprints, Amer. Chem. Soc. 12(3), 220 (1968).
5. Ross, D. S. and J. E. Blessing, Fuel, 57, 379 (1978).
6. Fu, Y. C. and E. G. Illig, Ind. Eng. Chem. Process Des. Dev., 15, 392 (1976).
7. Appell, A. P., I. Wender, and R. D. Miller, U.S. Bur. Mines, Tech. Prog. Rep. 25, May 1970.
8. Schuchardt, U. and F. A. P. Matos, Fuel, 61, 106 (1982).
9. Coughlin, R. W. and P. Altieri, Fuel, 65, 95 (1986).

Table 1. Liquefaction in the H_2/tetralin/Mo system at 400°C for 1 hour.

Reactant	Conversion (%)	Asphaltenes (%)	Oil and Gas (%)
paper	98.6	10.2	88.4
coal	86.0	39.9	46.1
coal (50%) + paper (50%)	91.7[a]	44.0[a]	47.7[a]
coal (67%) + paper (33%)	91.7[a]	46.0[a]	45.7[a]

a: conversion and yield with respect to coal.

Table 2. Liquefaction results in H_2/tetralin/Mo system at 325°C.

Reactant	Conversion (%)	Asphaltenes (%)	Oil and Gas (%)
paper	88.9	11.7	77.2
coal	35.9	21.6	14.3
coal (67%) + paper (33%)	37.7[a]	25.3[a]	12.4[a]

a: conversion and yield with respect to coal.

Table 3. Liquefaction results in the $CO/H_2O/Na_2CO_3$ system at 400°C for 1 hour.

Reactant	Conversion	Asphaltenes	Oil and Gas	Oil	Gas
paper	96.6	15.2	81.4	7.0	74.4
coal	84.2	42.8	41.4	15.1	26.4
coal(50%)+ paper(50%)	85.3[a]	22.9[a]	62.4[a]	38.1[a]	24.3[a]

a: conversion and yield with respect to coal.

Table 4. Gas compositions after 1 hour of run in $CO/H_2O/Na_2CO_3$ system at 400°C (initial pressure of CO=580 psig).

reactant	final pressure (psig)	CO	H_2	CO_2	CH_4	C_2-C_6	CO conversion (%)	H_2 consumption (mole)
paper	950	14.2	37.8	47.1	0.9	0.1	77.1	0.078
coal	863	14.9	37.5	46.3	1.4	0.3	78.0	0.113
coal + paper	913	13.5	38.2	47.0	1.3	0.3	78.5	0.090

Figure 1. Typical heating and cooling for coal conversion (Route B).

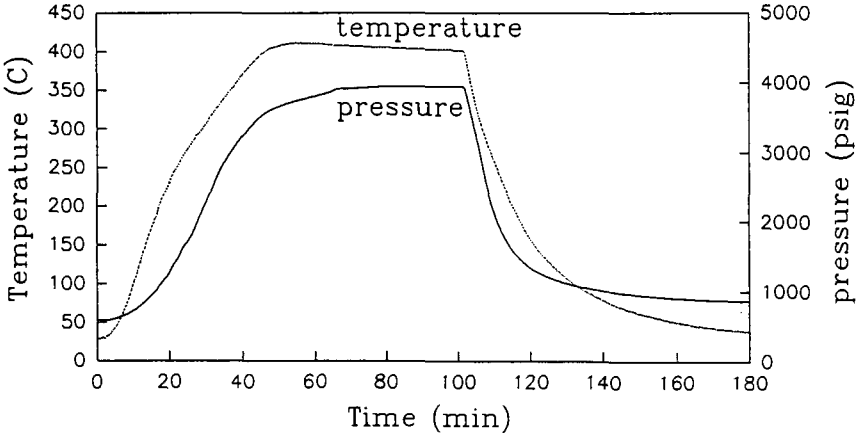

VOLATILE FATTY ACIDS PRODUCTION BY ANAEROBIC FERMENTATION OF URBAN ORGANIC WASTES

C. Sans, J. Mata-Alvarez
Department of Chemical Engineering
University of Barcelona, E-08028.
F. Cecchi, P. Pavan.
University of Venice, I-30123.

KEYWORDS

Volatile fatty acids, methyl ethyl esters, organic fraction of the municipal solid waste

ABSTRACT

During six months of experimentation, a plug-flow system without recirculation was employed to study the volatile fatty acids (VFA) production by means of anaerobic fermentation of urban organic wastes. Results showed an important VFA production at mesophilic range of temperature (37°C). Particulary, VFA concentration in the outlet sludge went from 11.8 g/L at 2 days of retention time up to 23.1 g/L at 6 days of retention time.

INTRODUCTION

One of the biotechnologies developed in the last years to utilize municipal solid wastes (MSW) for useful energy and materials recovery is the anaerobic digestion. Particulary, the anaerobic fermentation of the organic fraction of the municipal solid wastes (OFMSW) mainly to acetic, propionic, butyric and valeric acids has been studied. The volatile fatty acids obtained can be recovered and used to produce methyl or ethyl esters which, considering their elevate octane number (between 103-118), could be advantageously used as additive for gasoline (D'Addario et al., 1992). An alternative possibility would be the production of biogas in a second step of the anaerobic digestion. The resulting sludge from the fermentation could be converted in an optimal soil amendment after a composting step. All these possibilities makes the alternative particulary interesting.

The main studies described in the literature about the steps for the production of esters from MSW are the ones made by Antonopoulos in the U.S.A and D'Addario and co-workers in Italy (Antonopoulos and Wene, 1989; D'Addario et al., 1992). However, further research is necessary in order to study the feasibility of the process.

This work shows and discusses the results obtained using the OFMSW to produce volatile fatty acids in a tubular pilot-scale reactor at mesophilic temperature. The influence of operational parameters, such as hydraulic and solid retention time and organic loading rate, on the hydrolytic-acidogenic phase of the anaerobic digestion has also been investigated.

MATERIALS AND METHODS

Experimental device

The research was carried out with a pilot-plant, located in the experimental facilities of the University of Venice in Treviso (Italy). The plant can be divided in two sections. In the first section, the substrate is introduced into a 80 litters tubular reactor from the feed tank by an archimedean screw. The retention time of the sludge in the reactor can be controlled changing the turn of the screw. In the second section, the sludge coming out from the reactor goes to a separation area where part of the liquid phase is separated from the outlet sludge. VFA will be extracted from the liquid phase. The concentrated sludge can be partially recycled to the feed tank by a recycling archimedean screw and partially discharged.

Substrate

The substrate used for the experimentation was a mixture of the OFMSW coming from the mechanical selection plant of San Giorgio di Nogaro (Udine, Italy), and source sorted OFMSW coming from the food market of the city of Treviso (Italy). Tables 1 and 2 show the most important characteristics of both types of refuses. Initially, the substrates were mixed in a way to obtain a feed substrate with a total solids (TS) content around 20 % and a total volatile solids (TVS) content around 60 %TS, adding water for diluting purposes when necessary. The feeding mixture was prepared three times a week and kept in the feeding tank. The archimedean screw carried the substrate daily inside the digester at the desired loading rate, by controlling the time and rate of running of the screw, which determined the hydraulic retention time.

Analytical methods

The digestion process was monitored following the analytical procedure according to the Standard Methods for the examination of water and wastewater (1985). Total volatile fatty acids (TVFA) were carefully monitored in the feed, in the outlet sludge and in each valve of the reactor, when possible. TVFA were determined by a gas-chromatographic method (Chromatograph Vega serie 6000 Carlo Erba). Conditions of this analysis were: Capillary column type Nukol, length 15 m, internal diameter 0.53 mm; Injector temperature, 200°C; Detector -flame ionization- temperature, 220°C; Air pressure 120 kPa, H_2 pressure 70 kPa; Temperature program (isotherm): 106°C; Duration, 6 minutes; Carrier pressure 30 kPa.

RESULTS AND DISCUSSION

During six months of continuous operation, the acidogenic process was studied at different working conditions in the mesophilic (37±2°C) range of temperature. Table 3 shows the operational parameters and results obtained in the 4 different mesophilic periods experimented.

The start-up of the digester was performed at mesophilic temperature for almost one month. During the first period (period 1), solid recirculation was operated, in a way to work with a solid retention time (SRT) > hydraulic retention time (HRT). But, due to different technical problems

mainly at the separation and recirculation stage, the complete control of the solids retention time was not possible, although it can be considered close to 8 days. Taking into account the difficulties found during the first period of operation it was decided to eliminate solid recirculation system in the next periods experimented. Hydraulic and solid retention times studied were 2, 4 and 6 days (periods 2, 3 and 4, respectively). The screw of the reactor operated discontinuously. This particularity and the obliqual disposal of the digester caused separation of the liquid phase back to the feed box and desiccation of the sludge inside de digester. Thus, in order to avoid these problems, the reactor position was changed and placed horizontally during period 4 and for the rest of the periods studied. The influence of reactor design on the results during this period were sufficiently important to present them separately (period 4.1: obliqual reactor; period 4.2: horizontal reactor, see Table 3).

Figure 1 shows the VFA production with retention time of periods 1-4. The TVFA concentration in the outlet sludge obtained when working at SRT > HRT = 2 days, that is, with solid recirculation (period 1) was 19.5 g/L. This concentration is quite superior compared with the one obtained in period 2 (mean value 11.8 g/L, see Table 3), when working at SRT = HRT = 2 days without solid recirculation. The solid recirculation implied the presence of acidogenic inoculum in the feeding mixture which increased bacterial activity and substrate degradation in the reactor. Another result that supports this conclusion is the higher ammonia concentration in the outlet sludge of period 1, compared with period 2 (360.3 mg/L and 101.3 mg/L, respectively). This indicates a major protein mass degradation in the working conditions of the first period. The TVFA concentration obtained in period 3 (HRT = SRT = 4 days) increased respect period 2 (18.3 g/L and 11.8 g/L, respectively), which could indicate that retention time of 2 days (period 2) was not enough for an optimal degree of substrate degradation. This hypothesis is confirmed by the acid concentration reached in period 4.2 (HRT = SRT = 6 days), when correction in digester disposal was already done. There were obtained 23.1 g/L of volatile fatty acids in the outlet sludge, which determine the increasing profile of VFA production with retention times (see Figure 1). The optimal bacterial activity in period 4.2 was also reflected in the ammonia concentration, which was higher when acid concentration was maximum (486.7 mg/L in the digester sludge of period 4.2).

Figure 2 shows the yields obtained in the different mesophilic periods studied. Important yields were obtained when solid recycling was applied (period 1): yield expressed in percentage of TVFA produced per TS of the feeding mixture reached 9.3 % and in percentage of TVS reached almost 15 %, which can be considered an optimal result, taking into account the high organic loading rate operated (66.9 kgTVS/m^3d) and the kind of substrate utilized for the digestion. When there was no solid recycle (periods 2, 3 and 4.2) yields increased with increasing retention time (see Figure 2). Maximum values were obtained at 6 days of retention time and those were 7.8% TS, 13.9% TVS and 12.1% TCOD.

TVFA concentration obtained in the sludge samples from the first valve of the tubular reactor where quite high for the four mesophilic periods: the concentration increased with retention time from 9 g/L in period 2 up to 13.4 g/L in period 4.2. This is because acidogenic bacteria are fast-growing bacteria, with minimum doubling times around 30 minutes (Mosey, 1983) and are capable of fermenting the soluble fraction of the organic refuse to produce a mixture of VFA in a short interval of time. Maximal VFA concentration in the first valve was obtained in period 1, when solid recycling was operated (17.8 g/L), that is, with acidogenic inoculum in the feeding mixture.

The stability parameters -pH and alkalinity- were always within the optimal ranges: pH in the reactor varied between 4.77 (period 2) and 5.97 (period 4.1) but mean value never reached values that could inhibit the acidogenic process, that is, pH values below 4.5 (Zoetemeyer et al., 1982). ΔTA in the outlet sludge kept always quite high and between 11.6 and 19.5 $gCaCO_3/l$, as well as ammonia concentration (between 81.2 mg/L and 486.7 mg/L, see Table 3), so the system was always optimally selfbuffered.

CONCLUSIONS

This work shows that the acidogenic fermentation of the organic fraction of the municipal solid waste in a tubular reactor and at pilot scale level, is an optimal process for the obtention of volatile fatty acids. These fatty acids are the row material of valuable products, like methyl-ethyl esters or alkane.

In mesophilic conditions, the production of VFA increased with the retention time up to a production of 23.1 g/L for 6 days of retention time. No inoculation of the substrate was necessary as VFA concentration was already important at short retention time (first valve of the tubular reactor). The yields obtained can be considered as optimal (15% expressed as TVFA, % TVS fed), considering the high values of loading rates employed (66.9 $KgSV/m^3d$) and the mixture of urban wastes utilized as substrate for the digestion. The acidogenic process, in the working conditions studied, is stable, considering the parameters pH, alkalinity and ammonia. Furthermore, the ammonia concentration in the reactor sludge has revelled as a good indicator of the bacterial activity.

REFERENCES

Antonopoulos A. & Wene, E.G. (1988). "Bioconversion Of Municipal Solid Waste and Recovery of Short-Chain Organic Acids for Liquid Fuel Production". Energy and Environmental System division, Energy from Municipal waste Program.

D'Addario, E., Pappa, R., Pientrangeli, B., Valdiserri, M. (1992). "The acidogenic digestion of the organic fraction of municipal solid waste for the production of liquid fuels".

Mosey, F.E. (1983). "Mathematical modelling of the anaerobic digestion process: regulatory mechanisms for the formation of short-chain volatile acids from glucose". Wat. Sci.Tech. Vol. 15, pp. 209-232.

Standard Methods for the Examination of Water and Wastewater, 16th Edition, 1985.

Zoetemeyer, J.C. Van der Heuvel and A. Cohen (1982). "pH influence on anaerobic dissimilation of glucose in an anaerobic digester". Water Research, Vol 16, pp 303-311.

Table 1: Main characteristics of the OFMSW coming from the mechanical selecting plant of San Giorgio di Nogaro (Italy).

PARAMETERS	AVER.	MAX.	MIN.	STD	SAMPL.
TS, g/Kg	647.2	832.4	472.2	89.3	45
TVS, g/Kg	300.8	487.5	212.4	65.1	33
TVS, % ST	45.4	62.4	35.8	6.9	33
TCOD, % ST	51	76	23	15	22
TKN, % ST	1.36	1.79	1.06	0.22	22
P, % ST	1.41	1.82	1.02	0.30	10
TC, % ST	22.05	26.80	18.94	2.78	6

Table 2: Main characteristics of the source-sorted OFMSW coming from the market of the city of Treviso (Italy).

PARAMETERS	AVER.	MAX.	MIN.	STD	SAMPL.
TS, g/Kg	163.9	353.3	69.42	58.5	115
TVS, g/Kg	153.6	568.3	54.7	82.5	88
TVS, % ST	90.0	95.3	52.8	16.8	87
TCOD, % ST	112	133	84	64	44
TKN, % ST	2.07	3.07	1.21	6.39	45
P, % ST	2.57	5.45	0.82	6.26	43
TC, % ST	43.21	48.80	34.25	15.16	19

Table 3: Working conditions and averaged results obtained at steady state conditions in the 5 periods studied at mesophilic conditions.

PERIOD	1	2	3	4.1	4.2
HRT, d	1.8	1.9	3.8	4.9	4.6
SRT, d	-	2.0	4.0	6.0	6.0
OLR, KgSV/m³d	66.9	85.2	42.3	33.9	38.5
Feed:					
TS, g/Kg	198.5	248.3	244.9	285.9	285.5
TVS, g/Kg	122.2	159.0	159.2	155.7	160.4
STS, g/Kg	32.7	38.6	35.2	34.2	34.6
SVS, g/Kg	27.2	32.9	27.9	27.8	28.7
TCOD, gO_2/Kg	188.0	199.5	192.7	179.5	196.7
SCOD, gO_2/Kg	33.7	41.7	37.9	30.9	32.1
pH	5.92	6.11	6.19	6.39	6.06
ΔTA, $gCaCO_3$/l	2.9	4.0	2.9	3.4	3.6
TVFA, mg/L	2902	2645	7651	4722	4361
Sample valve 1:					
STS, g/Kg	27.7	61.2	64.3	38.9	55.3
SVS, g/Kg	20.2	42.7	47.3	27.8	36.6
pH	5.33	4.77	5.68	5.21	5.69
ΔTA, $gCaCO_3$/L	10.7	12.3	9.0	9.0	13.0
NH_4-N, mg/L	223.4	40.6	177.6	49.0	100.7
TVFA, mg/L	17822	9061	12782	7375	13372
Sample exit reactor:					
TS, g/Kg	230.4	255.2	304.0	419.5	303.6
TVS, g/Kg	125.5	153.9	188.2	214.5	152.7
STS, g/Kg	24.1	58.4	71.4	45.3	36.5
SVS, g/Kg	17.0	40.6	48.5	29.3	25.0
TCOD, gO_2/Kg	161.2	212.6	237.9	247.8	214.8
SCOD, gO_2/Kg	22.1	39.8	52.6	28.6	38.8
pH	5.57	5.08	4.98	5.97	5.72
ΔTA, $gCaCO_3$/L	11.6	14.7	17.2	16.2	19.5
NH_4-N, mg/L	360.3	101.3	81.2	255.4	486.7
TVFA, mg/L	19524	11780	18265	13000	23110

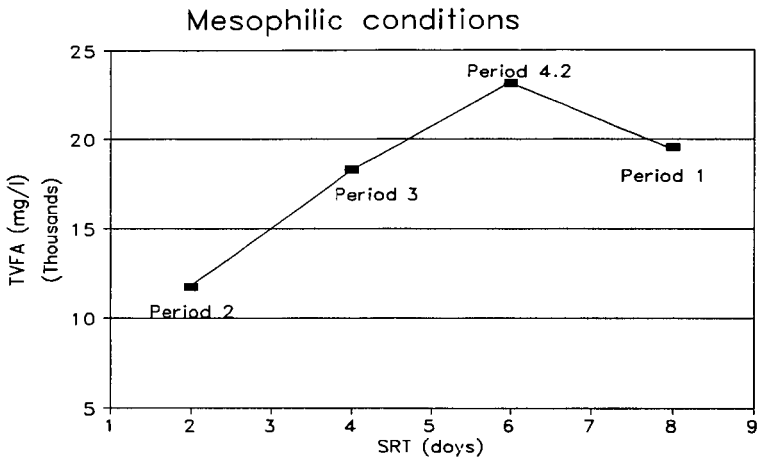

Figure 1: Variation of TVFA production in the outlet sludge with solid retention time in mesophilic conditions.

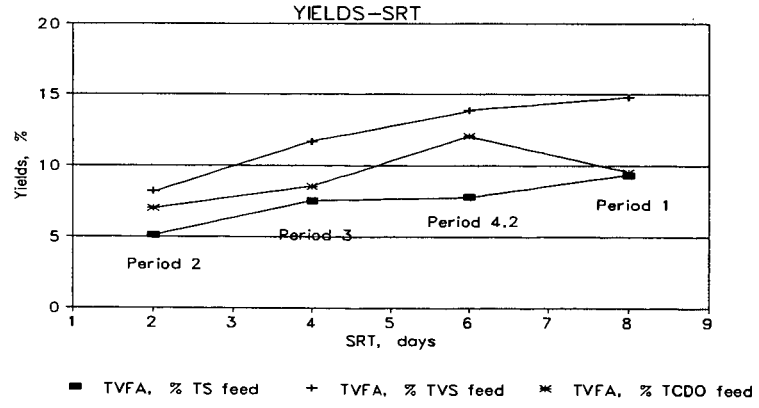

Figure 2: Yields obtained in the four mesophilic periods studied.

THE COPROCESSING OF FOSSIL FUELS AND BIOMASS FOR CO_2 EMISSION REDUCTION IN THE TRANSPORTATION SECTOR

Meyer Steinberg
Brookhaven National Laboratory, Upton, NY 11973

INTRODUCTION

Research is underway to evaluate the Hydrocarb process for conversion of carbonaceous raw material to clean carbon and methanol products. These products are valuable in the market either as fuel or as chemical commodities. As fuel, methanol and carbon can be used economically, either independently or in slurry form, in efficient heat energies (turbines and internal combustion engines) for both mobile and stationary single and combined cycle power plants. When considering CO_2 emission control in the utilization of fossil fuels, the coprocessing of those fossil fuels with biomass (which may include, wood, municipal solid waste and sewage sludge) is a viable mitigation approach. By coprocessing both types of feedstock to produce methanol and carbon while sequestering all or part of the carbon a significant net CO_2 reduction is achieved if the methanol is substituted for petroleum fuels in the transportation sector. Biomass removes CO_2 from the atmosphere by photosynthesis and is thus a prime feedstock for mitigation of CO_2 emission from mobile sources. Since the availability of biomass will, in most cases, determine the amount of petroleum that can be displace, it is essential to obtain maximum yield in the conversion process.

Basic Hydrocarb Process

The basic Hydrocarb Process would use carbonaceous feedstock or combination of feedstocks to produce, in addition to pure carbon, the coproducts, hydrogen, methane or methanol. The process which combines 3 basic steps; (1) a hydropyrolyzer (HPR) in which the carbonaceous material is hydrogasified with a recycled hydrogen-rich gas to form a methane-rich gas (2) a methane pyrolyzer (MPR) in which methane is decomposed to carbon and hydrogen and (3) a methanol synthesis reactor (MSR) in which the CO is catalytically combined with hydrogen to form methanol (MeOH or CH_3OH) and the remaining hydrogen-rich gas is recycled to the first step (HPR). The principal distinguishing features of the process are that the hydropyrolysis is an exothermic reaction which does not require internal heating, the methane pyrolysis is an endothermic process which does require heating and the recycled hydrogen-rich gas conserves the energy balance in the process.

Process Simulation Computer Model

A Hydrocarb process simulation computer model was developed based on well-known thermodynamic data taking into account equilibrium among the gaseous species CH_4, CO, CO_2, H_2, and H_2O and carbon in the solid phase. This detailed model allows the complete determination of the mass and energy balances around each reactor and around the entire process for various feedstock types and for various pressure and temperature conditions in each of the reactors. From numerous computer runs we cite here only two configurations which are most relevant to CO_2 emissions reduction. In one configuration we obtain a net zero CO_2 emission and in the other configuration we maximize the production and utilization of methanol as transportation fuel and substantially reduce CO_2 emission although not to zero.

Hydrocarb Methanol as an Alternative Transportation Fuel

An analysis can also be made with respect to CO_2 emissions when considering methanol displacing gasoline as a transportation fuel. About 30% of the U.S. anthropogenic CO_2 emission comes from the transportation sector which is about equal to emissions from stationary sources. EPA has estimated that 1.54 gallons of methanol can displace 1 gallon of gasoline in automobiles on a mileage per unit energy basis. Gasoline emits 9 Kg CO_2 per gallon. For maximum Hydrocarb methanol production configuration, the CO_2 emitted is 4 Kg CO_2 per gallon of gasoline displaced. There is thus a 55% reduction in CO_2 emission by the use of Hydrocarb methanol in displacing gasoline. Hydrocarb methanol can yield from 80% to 130% greater reduction in CO_2 emission than the other conventional biomass gasification plant for methanol production.

Cost Estimates

The following is a summary of the conclusions of a preliminary economic study of alternate fuel options. The preliminary capital cost estimate was determined based on a comparative analysis with a Texaco Coal gasification process plant assuming that equal gas througput through the gasifier will have the same capital cost when escalated to 1992 dollars. Credit was taken for elimination of the air separation plant and half credit for acid gas removal which are not needed in the Hydrocarb plant. A reasonable plant capacity handling 5000 dry metric tons of biomass per day (DMT/day) selected mainly by the deliverability and cost of biomass from an area of a fast rotational crop tree plantation (bundled willow). The economic parameters assumed for methanol production based on the maximum yield of methanol option and results in a production cost of $0.405/gallon methanol.

An equivalent gasoline price and incremental cost of gasoline displaced has also been calculated. The U.S. national average gasoline price toward the end of 1989 was $1.12 per gallon. Taking into account methanol displacement, production cost, taxes, markups and distribution cost, the incremental cost of gasoline displaced is equal to $1.01/gallon or 11¢/gallon less than the national average.

A further cost comparison was made with other biomass derived alcohol production processes. Comparing ethanol produced by acid and enzymatic hydrolysis, methanol produced by steam-oxygen gasification and ethanol produced by fermentation. Hydrocarb methanol for a 5000 DMT/day biomass plant costs from 50% to 75% less, on a lower heating value (LHV) basis, than the other ethanol or methanol processes as reported in the literature..

CONCLUSION

The Hydrocarb process has the potential, if the development objectives are achieved, to produce alternative transportation fuel from indigenous resources at lower cost than any other biomass conversion process. Our comparisons suggest the resulting fuel can significantly displace gasoline at a competitive price while mitigating CO_2 emissions and reducing ozone and other toxics in urban atmospheres. This general conclusion could also apply to stationary power generation in peaking and combined cycle power generation plants.

GAS RECOVERY AND UTILIZATION FROM MUNICIPAL SOLID WASTE LANDFILLS

Todd A. Potas
RUST Environment & Infrastructure
3033 Campus Drive, Suite 175
Minneapolis, MN 55441
(612) 551-1001

INTRODUCTION

Landfill gas recovery and utilization can be a viable energy resource. This gas, which is composed mostly of methane, carbon dioxide and minor amounts of non-methane organic compounds (NMOCs), is generated by anaerobic degradation of the municipal solid waste (MSW) in place. Although landfills are required to place a clay cap over the MSW to contain the gas generated, as well as to minimize environmental exposure to any other biological and chemical hazards, the cap can be breached by many mechanisms, including; gas migration through and around the cap, leachate migration, rain water erosion and heavy equipment activities. Therefore, MSW gas will eventually migrate out of landfills and be emitted to the atmosphere. Air emissions of NMOCs and methane from landfills are of concern, as there are over 6000 active MSW landfills nationwide as of 1987 with the potential to emit annually over 283,000 tons of NMOCs and over 12 million tons of methane (1). In addition, there are over 32,000 closed solid waste disposal facilities in the United States, many of these facilities having received MSW (2).

Gas recovery systems installed at landfills have been proven to effectively capture high quality gas (greater than 500 Btu/cubic foot). New Source Performance Standards (NSPS) for new and existing MSW landfills have thus been proposed by the US Environmental Protection Agency which outline minimum control requirements for gas recovery and subsequent combustion or utilization of the NMOCs in the landfill gas. These rules are proposed as 40 CFR Parts 51, 52 and 60, Standards of Performance for New Stationary Sources and Guidelines for Control of Existing Sources: Municipal Solid Waste Landfills; Proposed Rule, Federal Register, May 30, 1991.

Landfills required to comply with this proposed rule will be any new or operating landfill with the potential to emit more than 167 tons of NMOCs/yr (150 Megagrams/year) and closed landfills that have accepted waste since November 8, 1987. Assuming an average gas generation potential of 230 cubic meters/megagram (7374 cubic feet/ton) and an average NMOC concentration of 8,000 ppm NMOC (as hexane) in the landfill gas, any landfill that has or is accepting over 50,000 tons of MSW/year (45,400 Megagrams/yr) or that has a total of 750,000 tons of MSW in place would be required to comply with the proposed rule (1). A landfill of this size will generate approximately 280,000 cubic feet of landfill gas per day or, assuming 500 Btu/cubic foot in the gas, 5.8 MMBtu/hr. Testing the actual NMOC concentrations and gas flow rate from the landfill to show that the landfill gas emissions are actually under the threshold is possible and the procedures to show this are also outlined in the NSPS.

Landfills of the size mentioned will be required to show that their emissions are below 167 tons/year threshold of NMOCs by source testing, or the minimum gas collection and combustion requirements of the pending NSPS, which is referred to as "Best Demonstrated Technology" (BDT) to control the NMOC emissions, must be implemented. BDT is the combination of an active gas collection system and a combustion device with 98% NMOC combustion efficiency. Figure 1 shows a diagram of a model landfill with an active gas collection system, an energy recovery unit and two types of combustion flares (open and enclosed) (3). The diagram also shows other necessary ancillary equipment for gas recovery and utilization, such as a slurry cut-off wall, a leachate collection system and perimeter vents. A landfill with the equipment illustrated would be expected to comply with the proposed NSPS.

DISCUSSION

The minimum requirement for complying with the proposed rule in terms of simplicity of operation is an active gas collection system and an open flare. Candle flame type open flares are relatively inexpensive to install and operate. However, it is not possible to accurately sample air emissions from open flares. In addition, the open flare has no defined residence time at temperature and is aesthetically unpleasant due to the sight of the candle flame. Open flares are also difficult to control and can be subject to flame out during high winds. Therefore, it is difficult to predict the air emissions from open flares over an extended period of time, although the open flare is a dramatic improvement over venting landfill gas directly to the atmosphere.

Alternatively, enclosed flares; 1) provide for stack emissions measurement, 2) have a defined residence time, and 3) keep the flame hidden. This is due to the defined combustion chamber created by the stack of an enclosed flare. They also provide better mixing and temperature control in the combustion chamber, assuring more complete combustion. Therefore, the enclosed flare can be expected to perform with more dependability in keeping air emissions to a minimum than an open flare.

A deficiency of both types of flares is that they do not make use of the landfill gas as a fuel (energy) source. There are two major types of heat engine electrical generation systems that are capable of utilizing landfill gas for electrical power generation. The two types are reciprocating internal combustion engines and gas turbines. There are several advantages and disadvantages to each utilization option.

Reciprocating Engines

Reciprocating engines are popular due to their flexibility, low capital cost, low gas pressure and small size (base units start at 0.8 MW (1200 HP)). It is easy to add and subtract units with variations in the landfill gas generation or the size of the collection system and they operate with iow maintenance costs. In addition, when the reciprocating engines are operated at low operating pressure (12 - 30 psi), there is less gas compression condensate to handle and treat than if operating at high operating pressure (60 - 160 psi). The disadvantage of reciprocating engines are their relatively low combustion efficiencies as compared to turbines; 80% for internal combustion engines compared to 99+% for gas turbines. This results in low overall efficiencies for power generation and relatively higher air emissions for the same amount of gas combusted.

Gas Turbines

Gas turbines have the advantage of being highly efficient systems for electrical power generation, which results in relatively low air emissions. However, these two advantages come at the expense of several disadvantages; high capital and operating cost, limited flexibility, larger base capacity and higher maintenance costs than reciprocating engines, and the creation of large amounts of gas condensate. The gas compression condensate must often be treated as a hazardous waste. In addition, the turbines need a dependable gas source to operate efficiently. Both types of systems, turbines and reciprocating engines, are most efficiently operated when a flare is used as a back-up and/or as a supplemental combustion source to respond to fluctuations in landfill gas generation.

Air Emissions Comparison

The air emissions generated from the landfill operations are obviously of highest concern when the landfill gas is vented directly to the atmosphere. The addition of an active gas collection system and combustion control system of the types mentioned above relieve this concern dramatically. Once installed, the emissions from an active gas collection system itself are near non-existent due to the negative pressure maintained in the system and the relatively non-porous landfill cap. Only infrequent cases of gas well maintenance or isolated landfill gas pockets breaching the cap would likely cause any significant amount of emissions. Minor amounts of volatile organic compound (VOC) emissions are generated from condensate water collected from gas collection system pumps, exposed manholes and vents, water storage tanks and turbine or reciprocating engine compressors, as the water will contain a small percentage of soluble and insoluble VOCs.

A comparison of the emissions from the three combustion sources discussed, enclosed flares, reciprocating interal combustion engines and gas turbines, is shown in Table 1. Data for the table was generated from averaged actual compliance stack testing using the number of tests shown in the title block for each type of unit tested. The emissions data shown as referenced for each type of combustion system is from reference (3). Data has been included for both low pressure and high pressure reciprocating internal combustion engines. The enclosed flare data can be used to estimate the emissions for an untested open flare, assuming well-maintained operation and temperature control.

There are several points to note when comparing the emissions data for the landfill gas combustion units discussed.

1) The sulfur dioxide emissions for the turbines and the reciprocating engines were quite low, just as they are for natural gas combustion. This is expected as landfill gas is typically low in sulfur, usually below 200 ppm in total sulfur compounds. Sulfur dioxide was not measured in the test data shown for the enclosed flare. The reference information shows an average value of 0.006 lbs/MMBtu for flares, reciprocating engines or turbines.

2) Carbon monoxide (CO) emissions were found to be relatively high for the reciprocating engines and the enclosed flares, while being low for the gas turbines. This

can be an important consideration if the landfill is located in a metropolitan area which is non-attainment for CO. The turbine option is, therefore, a good possibility for many metropolitan areas of the United States.

3) Nitrogen oxides (NOx) emissions were higher for the reciprocating engines compared to the gas turbines and the enclosed flare. The reference data showed the same trend, although the NOx emissions for the actual reciprocating engine tests averaged over 3 times higher than for the reference data. It is unknown why this was the case.

4) The NSPS for new and existing MSW landfills has indicated that the VOC destruction efficiency for the flare, the reciprocating engine and the gas turbine is expected to be greater than 98%, if the systems are operating properly at appropriate operating temperatures. Note the low or not detected VOC emission values for the three combustion systems shown in Table 1.

5) In general, the actual test data matched the reference information quite well, especially the general trends of the data comparing the various sources. The largest deviation of the actual data from the reference data was the higher NOx and CO emissions for the reciprocating engines than shown in the referenced data. Consideration for the carbon monoxide emissions and nitrogen oxide emissions, which could be of major significance in metropolitan areas of non-attainment for CO and ozone must be taken into account concerning air quality compliance issues.

References

1. Federal Register, Standards of Performance for MSW Landfills, Vol. 56, No. 104, May 30, 1991.

2. Federal Register, 53 FR 33324, August 30, 1988.

3. Air Pollution Engineering Manual, Air and Waste Management Association, edited by A.J. Buonicore and W.T. Davis, Van Nostrand Reinhold, pages 863-73, New York, 1992.

TABLE 1
EMISSIONS DATA FOR LANDFILL GAS COMBUSTION AND UTILIZATION SYSTEMS

3.8 MW TURBINES (44 MMBtu/hr) (2 turbines tested - 6 tests conducted)				
	NOX	**SO2**	**CO**	**VOC**
Average	0.098	0.015	0.006	0.008
Maximum	0.118	0.035	0.010	0.009
Minimum	0.044	0.00	0.004	0.005
Gas Turbine[a] Reference Data	0.053	0.006	0.025	NA
1200 HP High Pressure Reciprocating Engines (9.3 MMBtu/hr) (1 engine tested - 4 tests conducted)				
	NOX	**SO2**	**CO**	**VOC**
Average	0.536	0.013	0.704	0.098
Maximum	0.763	0.018	0.818	0.111
Minimum	0.361	0.007	0.552	0.082
1200 HP Low Pressure Reciprocating Engines (9.3 MMBtu/hr) (6 engines tested - 19 tests conducted)				
	NOX	**SO2**	**C0**	**VOC**
Average	0.734	0.073	0.519	0.060
Maximum	0.936	0.204	0.685	0.075
Minimum	0.429	0.008	0.236	0.050
Internal Combustion[a] Reference Data	0.222	0.006	0.518	NA
78 MBtu/Hr Enclosed Flare (2 flare tested - 6 tests conducted)				
	NOX	**SO2**	**CO**	**VOC**
Average	0.019	NM	0.089	ND
Maximum	0.020	NM	0.106	ND
Minimum	0.017	NM	0.059	ND
Enclosed Flare[a] Reference Data	0.01	0.006	0.116	NA

NOTES:
ND - Not Detected NM - Not Measured NA - Not Available

All Data is Listed as Lbs/MMBtu
VOC Data listed as Total Hydrocarbon Emissions
[a]Reference: Air Pollution Engineering Manual, AWMA, 1992.
Calculations assume 1 Ft^3 of LFG = 500 Btu. Assumed efficiency for turbine was 43%. Assumed efficiency for reciprocating engines was 32%.

FIGURE 1

DIAGRAM OF A MSW LANDFILL WITH GAS COLLECTION AND RECOVERY SYSTEMS

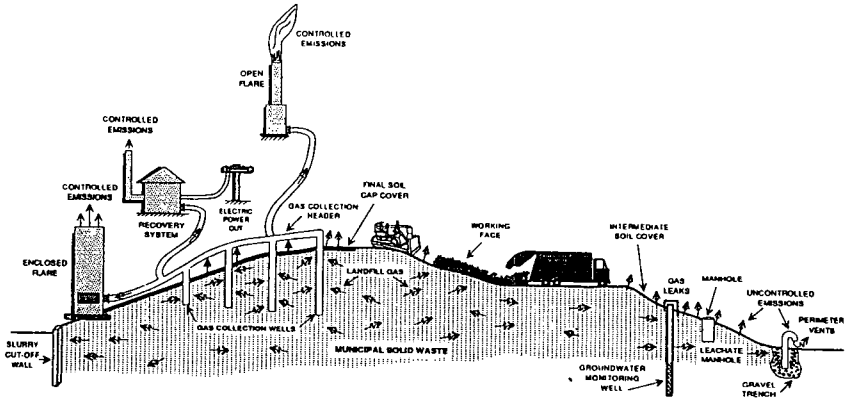

USE OF WASTES FOR FUELS AND CHEMICALS

Robert Clyde
Clyde Engineering, POB 740644
New Orleans, LA 70174

KEYWORDS: Soil, Fungi, Toxic metals

INTRODUCTION

Fibers from old cardboard boxes have high surface area for immobilization of cells which can degrade spilled fuels and produce other chemicals. When Celite is entrapped in the fibers, even more area is provided. A device for supplying oxygen quickly to cells is described.

SOILS AND LAGOONS

Shulman (1) describes how the military has contaminated soils in many parts of the world with jet fuel and TNT. Wood preserving sites have also contaminated soils with chlorinated compounds. These toxic materials are getting into drinking water. White rot fungus degrades these toxic materials but it needs air to grow. When grown on sawdust and buried, it doesn't do a good job for lack of air even when tilled once a week, but when grown on old cardboard boxes, air is entrapped in the corrugations. Landfills consist of 12% cardboard boxes (2) so these are readily available. White rot fungus is sensitive to larger amounts of TNT (3) but on the inside of the corrugations it is protected. The boxes can also be weighted and put into lagoons. A device for putting fungi on boxes is shown in Fig. 2

Supplying air or oxygen for growing fungi is a problem because of low solubility (about 10 ppm). When holes are put in the valleys (Fig.1) of the corrugations and rotated in a half full device, liquid is carried up into the vapor space and falls down through the holes. Mass transfer to droplets is 10-15 times that to a flat surface (4). A US patent (5) covers cells on rotating fibers.

TAXOL FOR CANCER

Taxol can be obtained from the bark of a yew tree but this kills the tree which grows very slowly. Scientists in Montana (6) have found a fungus that produces taxol. In the same article, the National Cancer INstitute has said it has "tremendous implications" for taxol production and Prof. Demain from MIT has said a problem would be to supply oxygen. A device as described in the previous section would supply oxygen much faster. Many women die of breast cancer and taxol is effective against other cancers too.

TOXIC METALS

Lead and six valent chromium are very toxic. Over 100 cities exceed the limit of 15 ppb of lead. When Zymomonas mobilis was grown on Tyvek fiber from DuPont, it removed lead and chromium in a few seconds. A control with nutrient but no Zymomonas did nothing. Large amounts of metals were removed and small amounts also (21 ppb to 3). Lead was analyzed with a Hitachi Z-8100 polarized Zeeman atomic absorption spectrometer with a graphite furnace. A lab corrugator has been made from an old washing machine wringer so other fibers can be corrugated. Patent 4,530,763 describes uranium removal. For valuable metals like silver, brushes between the discs remove the cells as in patent 4,600,694.

ETHANOL

Old cars and trucks still use leaded gasoline but ethanol has high octane and doesn't need lead. Old newspapers can be hydrolyzed to sugar and the sugar fermented to ethanol in 10-15 minutes as described by Clyde (7). Wayman (8) describes this as "remarkable." Bringi and Dale (9)put yeast on a single fiberglas disc and got "high rates of mass transfer...at low agitator speeds." They rotated at 90 rpm but we have found that 20-30 works well so less power is used for agitation. Ingram (10) puts the Zymomonas gene into E.coli so cellulose can be fermented. E.coli grows on fibers too. Old newspapers can be alternated with plastic (similar to the grooves in the ceiling below fluorescent lights) as in Fig. 2. There are health problems with MTBE. It gets into the blood.

CALCIUM MAGNESIUM ACETATE

Salt causes much damage to roads and bridges. CMA can be made with Clostridium on rotating fibers (11). Mathews makes calcium magnesium propionate (12)

COAL

Beer at MIT (13) sprays CMA into burning coal to remove most of the sulfur. Clostridium also converts syn gas to chemicals.

RICE HULLS

Rice hulls are wasted but can be used for growing cells to degrade chemicals or produce chemicals.

LACTIC ACID

Fast food containers are filling up landfills. Lactic acid can be made with a rotary biological contactor half full with air in the top. Polymers of lactic acid are biodegradable.

OTHER APPLICATIONS

Pseudomonas putida grows on fibers as in example 6 of patent 4,530,763. At a meeting of the American Society of Microbiol. in New Orleans, Jackson (talk Q216) degraded toluene,Frackman removed cadmium (Q78) and Babu degraded cyanide (Q312). When an RBC with circular discs is rotated and a light shone in the top, the light hits a thin moving film as in patent 4,446,236. In other photo reactors, colored solution blocks the light. Titania can be entrapped in the fibers. Drops are also made from polyurethane foam as in patent 4,333,893. Scientists at Tufts University gave talk 151c at the Miami AIChE meeting describing putting nutrient down between small polyester discs in a zig zag fashtion as in Fig. 3 and a well known company in New Jersey does the same. When cells are immobilized on rotating discs, however, the nutrient makes a large circle before going through holes to the next disc as in Fig.4.

REFERENCES

1. Shulman,S. The Threat at Home. Beacon Press, Boston (1992)
2. EPA Journal, July/Aug. '92 pg.8
3. App. Env. Micro. Sept.'92 pg.3199
4. Perry's Chem. Eng. Handbook 6th ed. 18-38
5. 4,407,954
6. Science 260,pg.154,5 and 214-216
7. FUEL 70,1225,6
8. Process Biochem. June '89 pg. 88-91
9. Biot. Progress 6,205-209
10. App. and Env. MIcro.Apr.'91 893-900 and patent 5,000,000
11. Calcium Magnesium Acetate. Ch.16, book by Elsevier.
12. Ind.Biopr.March '93 pg.2
13. Meeting on CMA in Boston sponsored by D.Wise, NE Univ.

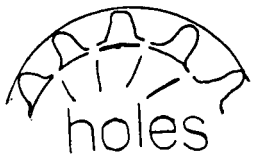

Fig.1

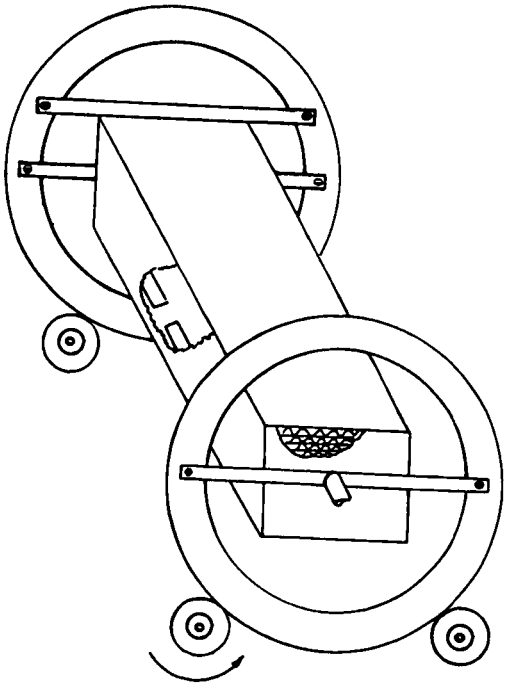

Fig.2

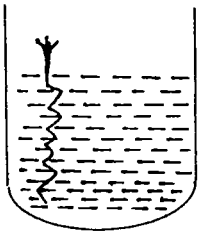

Fig. 3

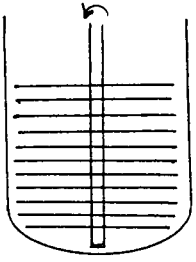

Fig. 4

A MULTIPLE-PRODUCT APPROACH TO THE PROCESSING OF USED TIRES

M. A. Serio, M. A. Wójtowicz, H. Teng, D. S. Pines and P. R. Solomon
Advanced Fuel Research, Inc.
87 Church Street, East Hartford, CT 06108

Keywords: scrap tires, activated carbon, pyrolysis

ABSTRACT

The disposal of used tires by landfilling is becoming an increasingly serious problem in the U.S. From an environmental and economic standpoint, a better solution is to reprocess tires into valuable products such as activated carbon, other solid carbon forms (e.g., carbon black), and liquid and gaseous fuels. A process design is proposed which involves pyrolysis of tires, activation of the solid residue, partial combustion of liquids to produce carbon black, and the use of the high-BTU gas for process heat. The activation of the solid residue is done using CO_2, which produces CO and activated carbon. The CO_2 is regenerated and the lost carbon is recovered using the Boudouard reaction to produce CO_2 and finely divided carbon. The latter material may be used as a substitute for carbon black. A preliminary assessment of the process is presented.

INTRODUCTION

Scrap tires present formidable disposal problems. The very same properties that make them desirable as tires, notably their durability, also make their disposal and reprocessing difficult. Tires are well known to be virtually immune to biological degradation. The disposal of 280 million tires generated each year in the U.S. by landfill is increasingly becoming an unacceptable solution [1]. The tires take up large amounts of valuable landfill space and also present fire and health hazards. Recently, a large mountain of tires caught on fire in Canada with widespread environmental consequences due to the oils and gases generated from the decomposing tires. A better solution from an environmental and economic standpoint is to thermally reprocess the tires into valuable products [2]. Large-scale efforts employ tires either as a fuel (Oxford Energy Corporation, Modesto, CA) or as a filler for asphalt (Rubber Asphalt producers, Phoenix, AZ). These two technologies annually consume about 5-6 million tires. However, tire burning has had repeated problems with feeding the tires and slagging, while the rubber asphalt costs 40% more than conventional material. RW Technology, Cheshire, CT, has also tried to convert tires into other plastic products, but the market niche is small and the process is unreliable.

Three features underlie the problem of converting used tires and other waste polymers into useful, marketable products. The first problem is the low level of understanding of the chemistry and physics of tires during thermal degradation. Secondly, even if the thermal degradation processes were well understood, they would have to be monitored carefully to maintain product quality. The tire feedstock varies with time, and the process engineer must be able to monitor reactions and respond to changing conditions as necessary. Finally, the technology must produce a high yield of a product with a viable market. The best solution to disposing of waste tires is to develop a chemical process to convert the tires into another commodity material.

The proposed solution is to thermally reprocess the used tires into activated carbon, other solid carbon forms (e.g., carbon black, graphite, or carbon fibers) and/or liquid and gaseous fuels. The process is based on pyrolysis of tires and the key to its successful development is understanding and controlling the chemistry of low temperature carbonization so that the yield and physical properties of the products can be optimized.

Pyrolysis has been widely used for converting solid fossil fuels, e.g., coal, into liquid and gaseous hydrocarbons, a process which results in a solid char residue. Used automotive tires contain polymeric aromatic structures which are similar to those of coal in some respects. Not surprisingly, typical elemental compositions of both materials are also similar (rubber -- 88% C, 8% H, 2% O, 0.5% N, 1.5% S; and coal -- 82% C, 5.5% H, 8% O, 1.7% N, 2.4% S). Coal pyrolysis has been extensively studied [3-5] but investigations of tire pyrolysis are rarely reported in the open literature.

The most commonly used vulcanized tire rubber is a styrene-butadiene-copolymer (SBR) containing about 25 wt.% styrene [6]. A typical composition of tire rubber is: 60-65% SBR, 29-31% carbon black, 1.9-3.3% zinc oxide, 1.1-2.1 sulfur, ~ 2% extender oil, and ~ 0.7% additives (wt.%, as received) [6, 7]. In most cases, tire pyrolysis studies were performed under inert conditions [6, 8, 9]. Pyrolysis may also be carried out in mildly oxidizing atmospheres, such as steam and carbon dioxide, to improve the quality of pyrolytic products [9-11].

Tire pyrolysis experiments have usually been conducted in the 773-1173 K temperature range [6-8]. Similar to coal pyrolysis, the principal products from thermal degradation of tires are gases, liquid oils and solid carbon residues. The following yields of tire pyrolysis are typical (on an as-received basis): 33-38 wt.% char, 38-55 wt.% oil, and 10-30 wt.% gas. The product yields are affected by the pyrolysis conditions, such as pyrolysis temperature and heating rate. The literature on the analysis of products from tire pyrolysis is summarized below.

Gas Analysis -- Gases produced from tire pyrolysis are mainly hydrogen, carbon dioxide, carbon monoxide, methane, ethane and butadiene, with lower concentrations of propane, propene, butane and other hydrocarbon gases [6].

Oil Analysis -- The yield of oil from tire pyrolysis is high (~50 wt % of initial tire rubber), reflecting the potential of tire rubber to act as a substitute for fossil fuel and chemical feedstocks. The oils have high aromaticity, low sulfur content, and are considered relatively good fuels [11]. The molecular weight range for the oils is up to 1600, with an average molecular weight between 300 and 400 [6]. Infrared analysis of the oils indicates the presence of alkanes, alkenes, ketones or aldehydes, aromatic, polyaromatic and substituted aromatic groups [6]. The derived oils may also be an important source of refined chemicals, because it has been reported that they contain high concentrations of valuable chemical feedstocks, such as benzene, toluene and xylene [6].

Carbon Residue Analysis -- The carbon residue could become a marketable product if its properties were similar to those of manufactured carbons. The simultaneous production of valuable solid products and gaseous and/or liquid fuels from what is currently a waste material would make tire pyrolysis economical if a large supply is readily available. This situation exists in many regions of the U.S.

As mentioned before, tire pyrolysis performed in an inert environment can produce 33-38 wt. % of carbon residue. It has been reported that the char yield increases with decreasing pyrolysis temperature and decreasing heating rate [6]. The surface area of the tire char also depends on pyrolysis temperature and heating rate. The surface area of a tire char produced by pyrolysis in an inert gas usually ranges from 30 to 90 m^2/g [6-8].

Basically, there are two uses of tire chars: as a reinforcing filler and as an adsorbent. Commercial carbon black is usually used for filling polymers and vulcanizates. Use of tire char as an end product for the tire and printing ink industries has been reported to be unsatisfactory [6, 8]. This is due to the high ash content of tire char. Chars from tire pyrolysis contain as much as 15 wt. % of ash, with the majority of this ash being zinc oxide [8]. A means of removing the ash from tire char is an important issue in the process of producing useful carbon black from the solid residue from waste tires. An alternative approach, which is advocated in the current study, is to use the solid residue to produce activated carbon for which the ash content is less critical. High-quality carbon black can be made from the liquid products, which are absolutely ash-free, and finely divided carbon can additionally be obtained from the CO produced during char activation.

Carbon as an adsorbent is usually evaluated by its surface area, and this is why an activation process is necessary to produce salable activated carbons from tire char. To develop a high internal surface area, char can be activated by mild oxidation with steam or carbon dioxide at high temperatures . The slow kinetics of carbon gasification in steam and CO_2 allow gas molecules to diffuse into the micropores and enlarge the existing surface area. The activation process usually follows hydrocarbon pyrolysis performed in an inert environment, but it is possible to accomplish pyrolysis and activation in one stage by pyrolyzing under mildly oxidizing conditions [7].

Ogasawara et al. [7] carried out the pyrolysis and activation of tires in one stage. The carbon residue from 1 hour of steam activation at 1173 K was found to have a surface area of 1260 m^2/g,

while pyrolysis in helium yielded char with a surface area of 87 m^2/g. The carbon residue produced from this "wet method" is as good as the commercial activated carbon in terms of surface area, but the carbon yield was only 9 wt. % of the starting tire material. Therefore, a method to increase char yield from tire pyrolysis is one of the most important issues in making activated carbon from waste tires. In a recent study [12], a high surface area activated carbon (> 800 m^2/g) was produced in relatively high yields from pyrolysis of tires at temperatures up to 1173 K, followed by CO_2 activation at the same temperature. The surface area of this carbon is comparable with that of commercially available activated carbons.

The objective of the present study is to propose and carry out preliminary assessment of a process leading to the conversion of waste tires into marketable products such as activated carbon or carbon black. Some quantities of gaseous and liquid fuels can also be produced. Process flexibility, in terms of the type and amounts of particular products, is a desirable feature in view of high variability of markets. This work is based on the results of a recent laboratory study of scrap-tire reprocessing [12].

PROCESS DESCRIPTION AND DISCUSSION

A schematic of the proposed process is shown in Figure 1. A stream of scrap tires enters the pyrolyzer where it is contacted with a recycle stream of pyrolysis gas. Mixing used tires with other waste material and solid-waste pretreatment are optional features of the process and they are discussed below. The pyrolyzer operates at approximately 1173 K, and the product streams are fuel gas, which also contains pyrolysis liquids, and char. The pyrolysis liquids are separated from the gas in a condenser, and they are subjected to partial combustion in an oil furnace to produce carbon black. The high-BTU gas is combusted to supply the process heat requirements. The solid product does not have sufficient surface area to make it commercially attractive and thus needs an activation step. Char activation is carried out using CO_2 at approximately 1173 K, which results in CO_2 reduction to form carbon monoxide. The consumed CO_2 is regenerated in a Boudouard reactor with simultaneous formation of finely dispersed carbon (Boudouard carbon). The net result of the process is the conversion of used tires into three marketable products: activated carbon, carbon black, and Boudouard carbon. The particular elements of the process scheme are described in more detail below. Pyrolysis and char-activation units constitute the heart of the process and their integration is very much a novelty in the proposed scheme. Carbon-black and Boudouard-carbon production will be integrated into the process by adapting existing technologies.

Feed-Stream Preparation -- The tires are first shredded and then possibly combined with another waste stream. The use of mixed wastes would improve the appeal and the number of sites where a plant could be installed. This feature, however, increases the complexity of the design as well as the operating costs. The amount of size reduction required for scrap tires does not appear to be excessive. In fact, higher char activation efficiencies were reported when coarser waste material was used (~170 mg pieces versus -50 mesh particles) [12]. The size of scrap tire material that would be optimal for the process is still to be determined. Since shredding costs are high (at least $0.20/kg), there is an economic incentive to make the tire pieces as large as possible. For smaller particle sizes, pretreatment with O_2 was found to increase char yields and surface areas [12]. Pretreatment with chlorine would probably have a similar effect but would also likely have negative consequences from the associated HCl formation.

Pyrolysis and Char-Activation Units -- While a rotary kiln reactor has been successfully used for pyrolysis of tires, this is not likely to be the optimal solution for a high throughput system [8]. A kinetic analysis of tire pyrolysis indicates that the process is relatively fast and can be completed in under a second at 873 K. This fact would allow the use of an entrained-flow reactor, which is quite appropriate for high-throughput applications. Unfortunately, only relatively small particles can be fed into such a reactor, mainly due to heat-transfer limitations. For larger pieces of tire material, a fluidized-bed reactor operating at a lower temperature can be used. In either case, a hot cyclone is desirable to separate char particles from the oils. According to scheme presented in Figure 1, char activation by CO_2 takes place in a separate reactor. This has the advantage of allowing the oxides of carbon to be cycled between the activation step (producing CO) and a disproportionation step (producing CO_2 and carbon). In this way, CO_2 is periodically consumed (activation) and regenerated (disproportionation); both CO and CO_2 stay relatively pure in this scheme.

Another possibility is to use a moving-bed countercurrent system. While solids throughput would necessarily be lower, this disadvantage would be offset by combining the pyrolysis and char-activation stages in a single reactor. In this scheme, tire pieces would be fed into the reactor at the top and CO_2 at the bottom (Figure 2). A temperature of about 1173 K would prevail at the bottom of the reactor so that the char would be progressively pyrolyzed and then activated as it moves through the reactor. Such a design, shown schematically in Figure 3, simplifies the process of feeding the tire pieces and eliminates the requirement for a hot cyclone since the oil and char come out of opposite ends of the reactor. The moving-bed concept has been employed in the large-scale gasification of coal at a plant in North Dakota which is producing synthetic pipeline gas [13]. There are some differences between the two schemes, however. The tire-processing unit would operate under atmospheric pressure since there is little or no advantage in producing activated carbon at an elevated pressure. Secondly, the coal gasification system is internally heated by introducing oxygen at the bottom and partially combusting a portion of the coal. In the tire-processing reactor, the pyrolysis gases which come off the top of the unit would be combusted externally and the hot exhaust gases (mostly CO_2 and H_2O) would be introduced into the bottom of the reactor for char activation. The reactor would be insulated to prevent heat losses. The disadvantages of a single-reactor scheme of Figure 3 are: (1) the pyrolysis gas has a lower heating value due to dilution with the flue gas; and (2) if Boudouard carbon is to be produced, a fairly complex separation step is required to recover pure CO from the pyrolysis gas (Figure 4). Previous work has demonstrated that the final product is not very sensitive to the conditions under which pyrolysis is carried out [12]. This allows for greater design flexibility and for the possibility to consider several feasible schemes.

It was demonstrated that activation using an 8% CO_2/He mixture at 1173 K for 3-10 hours was sufficient to obtain high surface area chars [12]. This residence time could be reduced by raising the temperature, increasing the CO_2 partial pressure, or by using steam rather than CO_2. The char activation chemistry can be represented by the following two reactions:

CO_2 activation: $CO_2 + C \text{ -----> } 2\,CO$ (the Boudouard reaction)

steam activation: $H_2O + C \text{ -----> } CO + H_2$

Both reactions are endothermic and the equilibrium becomes more favorable as the temperature increases. The use of steam would offer advantages in terms of a higher reaction rate and a higher surface area product. The use of CO_2 would increase the production of CO from the activation step. The CO could then be subjected to the reverse Boudouard reaction for the production of finely divided carbon [14-17].

Carbon-Black Production -- The oils resulting from tire pyrolysis can be used to produce carbon black since their properties are known to be similar to those of the petroleum fraction used in carbon-black production [11]. In the oil-furnace process, a highly aromatic feedstock is converted to carbon black by partial combustion and pyrolysis at 1673-1923 K in a refractory-lined steel reactor. The carbon-black properties which are important in reinforcement-material applications (e.g., in tires) are the particle size and structure (degree of agglomeration into three-dimensional networks). These properties are controlled by the nozzle design, reaction-chamber geometry, temperature, residence time, and turbulence intensity [18]. An example of a carbon-black furnace is shown in Figure 5. As an alternative to carbon-black production, tire pyrolysis oil can be used for its fuel value, although further processing to remove aromatic components would be required. The conversion of the oil stream to carbon black is a more attractive option for a number of reasons: (1) a solid product is easier to store and handle; (2) the value of the solid product is higher than any possible fuel uses; (3) little or no upgrading of the material is required; (4) possible transportation fuel uses would require upgrading because of the relatively high aromatic content of oil; and (5) since carbon black is required to make tires, the production of carbon black from the oil is a form of tire recycling and is more practical than trying to recover the original carbon black.

Boudouard-Carbon Production from CO -- This process step was recently discussed by Walker [14] as a part of his coal-processing scheme. The temperature of the Boudouard reactor is maintained at 773-800 K and the carbon product is ash-free and of a particle size much smaller than can be obtained by grinding [19]. In fact, the particle size of the Boudouard carbon is small enough to burn completely in a Diesel engine [20]. The Boudouard carbon is similar to carbon black (except for

having a zero hydrogen content) and in some cases can probably be substituted for carbon black. The envisaged applications of this product include its use as a colorant or lubricant.

The Energy Balance -- The fuel gases produced during pyrolysis can be used to provide process heat for the pyrolysis and activation stages. Some heat can also be recovered from the manufacturing of carbon black by partial combustion of the oil; an additional amount of heat will be generated by the production of Boudouard carbon from CO. Preliminary estimates show that the process outlined in Figure 1 will be self-sufficient from an energy standpoint. The net yields of the products depend on the degree of activation required in the production of activated carbon. A high degree of activation would correspond to a larger amount of Boudouard carbon produced from the CO stream.

Process Economics -- A preliminary cost analysis for the process indicates that the proposed tire-reprocessing scheme could be profitable. The following estimates have been used: the cost of scrap tires -- about $0.20/kg (tire-disposal charge: $0.01-0.35/kg; transportation: ~ $0.04/kg; size reduction: $0.20-0.60/kg); the typical pyrolysis yields -- 35% char, 20% gas, and 45% oils; 50% carbon loss during char activation; selling prices for the activated and Boudouard carbons of $2.22/kg and $0.67/kg, respectively; zero profit from the high-BTU gas and oils which would be used mainly to provide the process heat requirements. These figures lead to a net income of ~ $0.30 per kilogram of the original tire material. Of course, more detailed economic analysis needs to be performed, but even the above simplified and fairly conservative treatment demonstrates the high commercial potential of the proposed approach. It should be pointed out that, in most cases, the raw material costs for the project will be negative due to increasingly high tire-disposal charges.

For the sake of comparison, the cost of scrap-tire incineration without heat recovery is about $0.04-0.07/kg [21]. The cost of burning used tires for energy generation is 1.5-5.1 times higher than the corresponding cost for coal, depending on whether whole or ground tires are used [21]. Depolymerized scrap rubber (DSR) can also be used as liquid fuel but, in general, depolymerization is difficult and involves extensive high-pressure treatment. Clearly, reprocessing of waste tires into fuels does not seem to be an economically attractive option.

Pyrolysis processes can be made somewhat more profitable. Nippon Zeon estimated that the break-even cost of its tire-pyrolysis pilot plant was $0.25 per tire [22]. According to a different estimate [23], a plant processing 81,000 tons of scrap tires per year could be made profitable, based on sales of reclaimed products. As mentioned before, pyrolysis processes involving direct carbon-black recovery suffer from difficulties related to ash removal and, generally, low final-product quality. Asphalt rubber is probably the most competitive tire-derived product currently available on the market. Although nearly twice as expensive as regular asphalt pavement, asphalt rubber has already demonstrated superior performance and durability. According to legislation passed in 1991, the use of asphalt rubber may be required in 5% of new pavement as early as in 1994, with a projected increase to 20% by 1997 [24]. Unfortunately, the estimated total demand for this product is still at about 2% of the amount of scrap tires available [21]. It can be concluded, therefore, that a large market exists for other technologies targeted at scrap-tire reprocessing into useful products.

CONCLUSIONS

A preliminary process design was developed in which scrap tires are used as the input and in which activated carbon, carbon black (or fuel oil), Boudouard carbon and fuel gas are produced as the output. The proposed technology has the potential to convert an unmitigated waste stream of tires into marketable products (activated carbon, Boudouard carbon and carbon black). Tire-derived activated carbons could be used, for example, in waste-water treatment, stabilization of landfills and in the recovery of organic solvents and vapors. The Boudouard carbon may have a variety of uses which are yet to be explored; they include the manufacture of colorants and lubricants. The liquid stream can be utilized in the production of carbon black and/or fuel oil. The oil-derived carbon black can be reused in tire manufacturing, which forms a recycle loop for this material. Since the typical feedstocks for activated carbon and carbon black are either coal or petroleum, the proposed technology would obviate the need to deplete these resources. The process allows a high degree of flexibility in the relative amounts of each product to reflect changes in the feed stream and market conditions. Another advantage of the system is the production of both activated carbon and carbon black from used tires, with inorganic material ending up in the product with a high tolerance for this

component. Finally, following additional research, the proposed technology should be able to find applications in reprocessing other polymer wastes found in American industry (e.g., end cuttings from automobile hoses or products which do not pass quality control).

ACKNOWLEDGEMENTS

The financial support of the National Science Foundation under Grant No. ISI-9060297 is gratefully acknowledged. The Project Officer was Dr. Edward Bryan.

REFERENCES

1. New York Times, May 9, 1990, p. D1.
2. Schulman, B.L. and White, P.A., "Pyrolysis of scrap tires using the Tosco II process -- a progress report," Solid Wastes and Residues: Conversion by Advanced Thermal Processes (J.L. Jones and S.B. Radding, Eds.), ACS Symposium Series #76, 274 (1978).
3. Solomon, P.R., Hamblen, D.G., Carangelo, R.M., Serio, M.A., and Deshpande, G.V., Energy and Fuel 2, 405 (1988).
4. Serio, M.A., Hamblen, D.G., Markham, J.R., and Solomon, P.R., Energy and Fuels 1(2), 138 (1987).
5. Suuberg, E.M., Peters, W.A., and Howard, J.B., 17th Symp. (Int) on Combustion, The Combustion Institute, Pittsburgh, PA, 117 (1979).
6. Williams, P.T., Besler, S., and Taylor, D.T., Fuel 69, 1474 (1990).
7. Ogasawara, S., Kuroda, M., and Wakao, N., Ind. Eng. Chem. Res. 26, 2552 (1987).
8. Petrich, M.A., "Conversion of Plastic Waste to Valuable Solid Carbons", Final Report of a Project in the Innovative Concepts Program, U.S. DOE, Jan., 1991.
9. Torikai, N., Meguro, T., and Nakamura, Y., Nippon Kagaku Kaishi 11, 1604 (1979).
10. Funazukuri, T., Takanashi, T., and Wakao, N., J. Chem. Eng. Japan, 20, 23 (1987).
11. Merchant, A. and Torkelson, J.M., "Pyrolysis of Scrap Tires", Chemical Engineering Dept., Northwestern U., Spring, 1990.
12. Teng, H., Serio, M.A., Bassilakis, R., Morrison, P.W., Jr. and Solomon, P.R., "Reprocessing of used tires into activated carbon and other products," ACS Div. of Fuel Chem. Prepr. 37(2), 533-547 (1992).
13. Penner, S.S., Coal Gasification: Direct Application and Synthesis of Chemicals and Fuels, DOE/ER-0326 (1987).
14. Walker, David G., ACS Div. of Fuel Chem. Prepr. 36(3), 1129 (1991).
15. Watanabe, O., Tokunosuke, N., Bull. Inst. Phys. Chem. Research (Tokyo) 8, 288-292 (1929).
16. Donald, J.H., "An Annotated Bibliography of the Literature and Patents Relating to the Production of Carbon by the Decomposition of Carbon Monoxide," Mellon Institute of Industrial Research, Pittsburgh, PA (1956).
17. Hadley-Coats, Lyndon and D.G. Walker, "Boudouard Carbon: An Alternate to Gasoline and Diesel Oil," International Journal of Energy Research, 12, 2443-2451 (1988).
18. Austin, G.T., Shreve's Chemical Process Industries, 5th Edition, McGraw-Hill, New York (1984).
19. Soehngen, E.E., "The Development of the Coal Burning Diesel in Germany," Report FE/WEPO 3387-1, Purchase Order No. 3387, U.S. Energy Research and Development Administration (1976).
20. Essenhigh, H., "Coal Combustion," Coal Conversion Technology (C.Y. Yen and S. Lee, Eds.), Addison - Wesley Pub. Co., Reading, MA , 171-312 (1979).
21. Paul, J., "Rubber Reclaiming," Encyclopedia of Polymer Science and Engineering (H.F. Mark, N.M. Bikales, C.G. Overberger and G. Menges, Eds.), John Wiley & Sons, New York, vol. 14, 787-804 (1988).
22. Saeki, Y. and Suzuki, G., Rubber Age 108, 33 (Feb. 1976).
23. Bracker, G.P., Conserv. Recycl. 4(3), 161 (1981).
24. Clark, C., Meardon, K. and Russell, D., Scrap Tire Technology and Markets, Noyes Publications (1993).

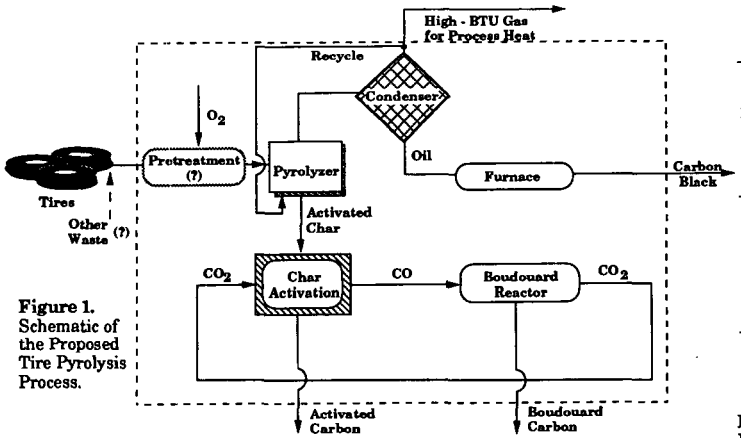

Figure 1. Schematic of the Proposed Tire Pyrolysis Process.

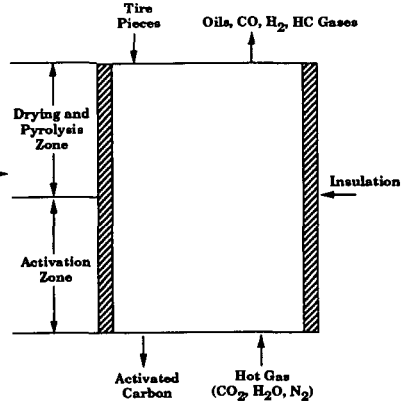

Figure 2. Schematic of the Countercurrent Moving-Bed Reactor Concept which Combines Tire Pyrolysis and Activation into a Single Unit.

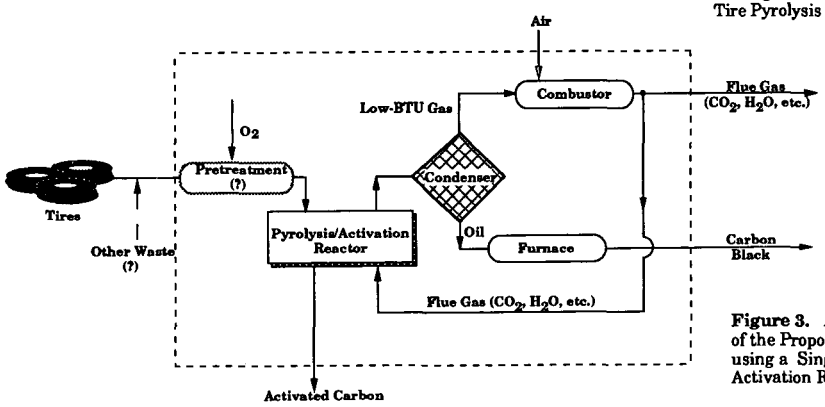

Figure 3. A Schematic Representation of the Proposed Tire-Pyrolysis Process using a Single Pyrolysis/Char-Activation Reactor.

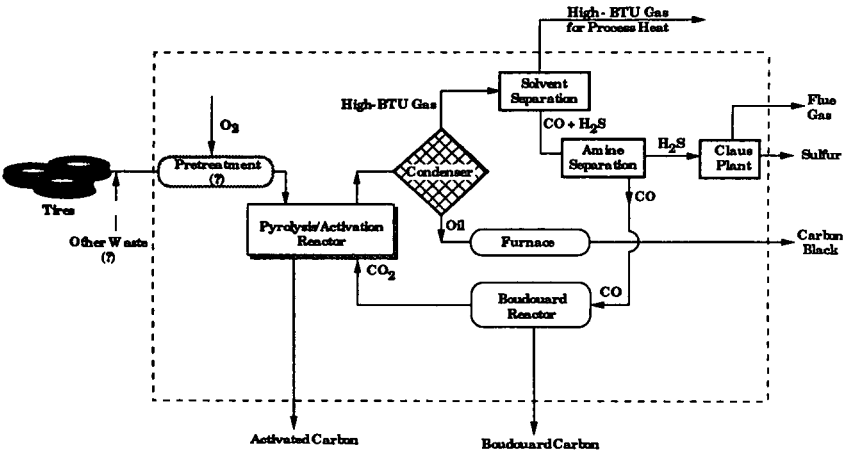

Figure 4. A Schematic Representation of the Proposed Tire-Pyrolysis Process using a Single Pyrolysis/Char-Activation Reactor and CO Separation from the Pyrolysis Gas.

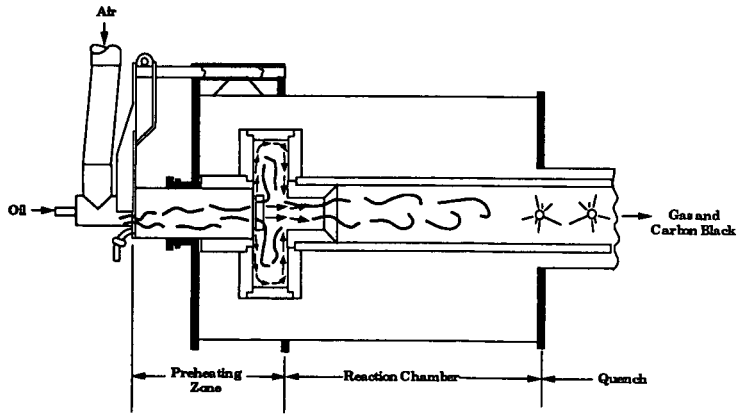

Figure 5. Flow Chart, Carbon Black Furnace Process. [*Chem. Week* 88 (24) 79 (1962)].

DERIVATION OF ADSORBENT CARBONS FROM OIL SHALE RESIDUES

U.M. Graham[1], E. Ekinci[2,3], A. Hutton[4], F. Derbyshire[1], T. Robl[1], M.L. Stewart[1], and A.M. Rubel[1].

[1] University of Kentucky, Center for Applied Energy Research, 3572 Iron Works Pike, Lexington, KY
[2] Istanbul Technical University, Department of Chemical Engineering, Ayazaga, Istanbul, Turkey
[3] Marmara Research Center, Department of Chemical Engineering, Gebze, Kocaeli, Turkey
[4] University of Wollongong, Department of Geology, Wollongong NSW, Australia

Keywords: Oil Shale, Adsorbent Carbons, Pyrolysis, Steam Activation

Introduction

Active adsorbent carbons can be derived from the pyrolysis residues of low-ash oil shales. Besides producing liquid fuels, oil shales, like coal, may be utilized as a source material to produce high-value added products. This utilization also leads to the reduction of waste material.

Oil shale is a sedimentary rock which contains sufficient organic matter (Kerogen) which produces oil and gas when pyrolyzed. In the past, oil shale research has predominantly focussed on maximizing the liquid hydrocarbon yield [1-3]. The primary goal was to produce a substitute for naturally occurring petroleum. These efforts have proven the commercialization of oil shale to be very difficult. Shale oil is simply not, economically, a reasonable substitute for crude oil. Based on current market forces, which suggest the continuation of low crude oil prices and high supply, oil shale commercialization does not appear to be a near-term prospect. To make oil shale more competitive, the development of new high value products needs to be examined.

After pyrolysis, as much as half of the carbon remains in the retorted (spent) shale. This carbon-rich product is generally considered a waste material. Its disposal represents an economic and environmental problem. It is, therefore, important that the pyrolyzed shale be utilized, either in the retorting process as a source of energy, or as a source of new products. The former strategy is the basis for the development of the KENTORT II technology for Eastern US oil shales [4,5]. This technology completely utilizes the carbon on the pyrolyzed shale by incorporating integrated gasification and combustion steps. The latter strategy, the utilization of the spent shale carbon for new products, is the focus of this study.

In previous work it was shown that a range of materials can be manufactured from oil shale residues, including cement and asphalt additives [6,7]. However, the utilization of carbon-rich residues of oil shales as precursor materials for the production of adsorbent carbons has not been examined. The objective of this project is to fabricate adsorbent carbons from low-ash oil shale residues. The production of high-value solids such as adsorbent carbons, in addition to oil, would make the economics of oil shale development more attractive.

Experimental Procedures

Two oil shales from the Turkish Goynuk [8] and the Australian Alpha [9] deposits were selected for this study based on the following criteria: (1) low ash contents and; (2) high oil yields upon retorting. The oil shales were pyrolyzed at 550 °C under a continuous flow of nitrogen. Proximate

and ultimate analyses of the raw and spent shale materials are illustrated in Table 1. The N_2-swept fixed bed pyrolysis experiments were performed in a 1.5 inch stainless steel reactor. The reactor conditions are discussed in detail elsewhere [10]. During pyrolysis, the alginite-rich, low-ash oil shales were observed to form a macroporous network of charred carbonaceous material. Heating stage microscopic (HSM) examination allowed the observation of the spatial relationships between macropores generated by the volatilization of alginite macerals and the char and minerals that stabilize the macrostructure. The HSM apparatus utilized in this study consists of a Zeiss Universal polarized light microscope, a heating stage, and temperature and gas flow controllers.

After pyrolysis, the spent shale was activated in a steam reactor (gasifier) at 880 °C. Water was pumped through a 1/16 inch capillary and entered the reactor below the shale distributor plate, where it is released into the hot zone as superheated steam. The steam passed through the shale zone and exits the reactor, where it is condensed.

Surface area measurements were performed on the samples to investigate porosity development resulting from both the pyrolysis and steam retorting processes. Standard nitrogen adsorption using a static volumetric flow process was used, employing an Autosorb-6 sorption system at a temperature of 77 °Kelvin. All surface area measurements were calculated using the standard BET equation [11] between relative pressures of 0.05-0.25. Micropore volume approximations were calculated using the Dubinin-Radushkavich equation [12] over a linear region of the D-R plot. Samples were outgassed under vacuum at a temperature of 200 °C prior to analysis.

Scanning electron microscopic (SEM) examination of the pyrolyzed and steam activated samples, using a Hitachi S-2700 (magnification up to x 10^4), allowed a comparison of the morphological features.

Samples of the shale carbons were monitored for their gas adsorption characteristics using thermogravimetry/mass spectroscopy (TG-MS). A temperature programmed adsorption/desorption (TPA/D) analysis was performed using H_2S, NH_3 and NO gases as adsorbates.

Results and Discussion

Pyrolysis Induced Porosity

The pyrolysis induced porosity (PIP) in the retorted shale corresponds to a BET surface area of only 8 - 10 m^2/g for both shales (Table 2). However, this framework provides excellent accessibility for steam to infiltrate the chars at 880 °C during activation. The HSM experiments showed that the bulk of the macropores formed when alginite macerals volatilized. These large elongated macropores are inherited from the structure of alginite and vitrinite (desmocollonite) macerals (Figure 1). The temperature at which constituents boiled in these macerals occurred in the HSM experiments at 467 °C. The extensive macroporosity of the carbon-rich pyrolysis residues (from Goynuk and Alpha) indicates these shales to be promising precursors for adsorbent carbons. This is based on the abundant macropores in the chars contributing to an intricate infrastructure that readily allows steam and/or catalyst metals to infiltrate. The action of steam is expected to cause extensive micropore development in the chars. The validity of this working hypothesis was examined by enhancing the inherent porosity (PIP) by catalyzed and uncatalyzed steam treatments at 880 °C.

Steam Induced Porosity

The purpose of the pyrolysis experiments was to provide spent (pyrolyzed) shale for steam activation experiments. The steam induced porosity (SIP) was generated using run times from one to ten hours. The SEM study of the steam treated chars reveled a much rougher surface compared to the pyrolyzed char (Figure 2). The increase in microporosity was documented by the substantial increase in BET surface area of the steam treated samples (Table 2). The SIP was more pronounced after mineral matter removal by acid treatment. This was probably due to the removal of minerals blocking pore entrances. Studies of the effects of steam retorting the spent shale showed that the overall surface area could be increased up to 110 fold by retorting under extremely slow steam flow conditions for prolonged periods of time (up to 10 hours). However this resulted in an extensive loss of carbon. Steam activation at 880 °C for four hours, using steam flow rates of 2 grams/minute, developed a BET surface area of around 400 m^2/g with a 43% loss of carbon (Table 2). An inverse relationship was observed between overall surface area and carbon yield from the retort. The percent carbon loss and the relatively high mesopore volumes of the carbons may be dependent on the high reactivity of the shale precursors, or the presence of finely dispersed mineral matter, both of which has jet to be determined. Preliminary studies on the effects of catalytic metals ($ZnCl_2$; $CaCl_2$) finely dispersed on the shale surface during activation indicated some improvement over simple steam activation (Table 2).

Adsorbent Carbons from Oil Shale Precursors

Samples of the carbons from shale precursors were monitored for their gas adsorption characteristics using TG-MS. Both the Goynuk and Alpha derived carbons showed higher adsorptive capacities for H_2S and SO_2 than a commercially available carbon. The TPA/D profile for the steam activated Goynuk sample using H_2S as adsorbate indicated the adsorption capacity of the Goynuk carbon material at 70 °C was 0.06 g/g of carbon. The adsorption capacity was based on the weight gain during adsorption, weight loss during desorption, and the identification of H_2S as the only desorbed gas (Figure 3). Samples of shale-derived carbon also demonstrated significant adsorptive capacity for NO and NH_3 (Figure 4), indicating potential uses of shale derived adsorbents as industrial gas scrubber carbons.

Synopsis

Adsorbent carbons can be produced from the pyrolysis residues of the Turkish Goynuk and Australian Alpha oil shale samples. Both materials have low ash contents and produce high oil yields upon retorting at 550 °C. During pyrolysis, a macroporous network of charred carbonaceous material forms. The development of the pyrolysis induced pores (PIP), and that of the macrostructure stabilizing char and mineral matter, were observed using a heating stage microscope. The PIP in the retorted shale corresponds to a BET surface area of only about 10 m^2/g, but provides sufficient access for steam to infiltrate the char during activation at 880 °C. The steam induced porosity (SIP) corresponds to a BET surface area of 300-400 m^2/g at 43 % burn off. The steam activation treatment results in increased gas adsorption capacities: the Goynuk and Alpha derived carbons showed promising adsorptive capacities for NO, NH_3 and H_2S compared to a commercial carbon. The carbon-rich pyrolysis residues of the two shales under investigation have shown excellent potential as feedstocks for the production of adsorbent carbons. Utilization of the retorted or spent shale can not

only result in new high-value added products, but can also lead to the reduction, and hence regulation, of a waste material.

Acknowledgements The authors appreciate the analytical support of G. Thomas, M. Moore, and M. Spears. We like to thank S. Carter, C. Lafferty, J. Hower and R. Rathbone for helpful discussions.

1 Richardson J.H., Huss E.B., Ott L.L., Clarkson J.E., Bishop M.O., Gregory L.J., and Morris C.J. Lawrence Livermore National Laboratory, UCID-19548, (1981).
2 Gwyn J.E., Roberts S.C., Hinds, Jr. G.P., Hardsty D.E. and Johnson G.L. Thirteenth Oil Shale Symposium Proceedings, Golden, CO, April., (1980).
3 Cummins J.J. and Robinson W.E. Amer. Chem. Soc., Div. Fuel Chem., Prepr., 21 (6), p. 94, (1976).
4. Carter S.D., Robl T.L, Rubel A.M., and Taulbee D.N. Fuel, 69, p.1124, (1990).
5. Carter S.D., Robl T.L., Taulbee D.N., and Rubel A.M. Fuel 70, p.1347, (1991).
6. Speight J.G. The Chemistry of Petroleum. Second Edition. Marcel Dekker Inc., New York (1991).
7. Riedhammer M. Zement-Kalk-Gips, 38, No. 7. p. 359, (1985)
8. Putun E., Akar A., Ekinci E. and Bartle K.D. Fuel, 67, p. 1106 (1988).
9. Duffy G.J., Udaja P., and Shao-Xin L. Fuel, 69, p. 1134, (1990)
10. Rubel A.M. and Coburn T.T. In Proceedings of the 1981 Eastern Oil Shale Symposium, Kentucky Energy Cabinet, Lexington, KY, p. 21, (1981).
11. Brunauer S., Emmett P.H., Teller E. J. Amer. Chem. Soc.,p. 6309, (1938).
12. Dubinin M.M. and Radushkavich L.v. Proc. Acad. Sci. USSR, Vol. 55, p. 331, (1947).

Table 1 Ultimate and Proximate Analyses for Goynuk and Alpha

	Goynuk Raw Shale	Goynuk Spent Shale	Alpha Raw Shale	Alpha Spent Shale
C wt%	54.7	49.9	76.6	73.1
H wt%	8.3	1.8	9.9	3.2
N wt%	1.4	1.7	1.1	1.7
S wt%	2.8	2.2	1.3	2.9
Moisture wt%	12.1	3.2	0.9	1.2
Ash wt%	17.2	41.6	4.4	15.6
Volatiles wt%	60.1	16.7	87.7	33.4
Fixed C wt%	10.9	38.2	10.1	49.4
BTU/lb		9150		13400

Table 2 BET - Surface Area Development for Goynuk and Alpha Shales

Sample		BET	BET 1 h *	BET 4 h **
Goynuk:	Pyrolysed	8.8		
Goynuk:	Steam Activated		180	350
Goynuk:	Steam Activated/ZnCl2-Catalyst		190	400
Goynuk:	Steam Activated/ Acid Washed		210	370
Alpha:	Pyrolysed	10		
Alpha:	Steam Activated		170	280
Alpha:	Steam Activated/ ZnCl2-Catalyst		170	310
Alpha:	Steam Activated/ Acid Washed		200	350

* 1 hour steam treatment using steam flow rates of 2 grams/minute
** 4 hour steam treatment using steam flow rates of 2 grams/minute
BET-surface area (calculated using standard BET equation [9])
Steam Activation at 880 C
Acid Washing with 0.5 molar HCl for 1 hour.

Figure 1 SEM micro-photograph showing PIP after steam pyrolysis of the Goynuk oil shale. The elongated cavities formed after volatilization of the alginite maccrals. Char and mineral matter stabilize the macro-structure.

Figure 2 SEM micro-photograph showing SIP after steam activation of Goynuk shale char. Flaky surface with abundant macropores is depictured.

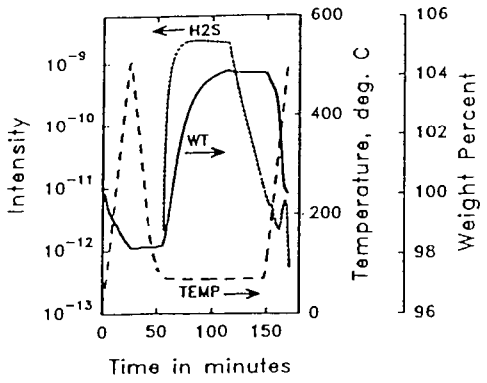

Figure 3 Temperature programmed adsorption/desorption analysis of the Goynuk adsorbent carbon. The carbon was activated at 880 °C using steam using $ZnCl_2$ catalyst. Mineral Matter was reduced after steam activation using 0.5 molar HCl.

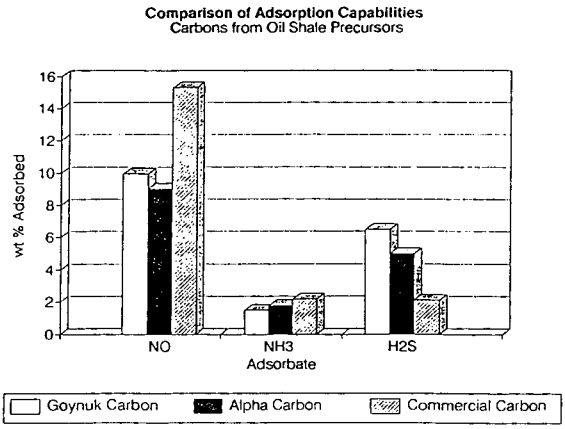

Figure 4 Comparison of the adsorption capabilities of Goynuk and Alpha derived adsorbent carbons with a commercial carbon. Goynuk and Alpha carbons have a BET surface area of about 350 m^2/g. BET surface area of the commercial carbon corresponds to 450 m^2/g.

CHARACTERIZATION OF CONCRETES FORMULATED WITH BLENDS OF PORTLAND CEMENT AND OIL SHALE COMBUSTION ASH

James T. Cobb, Jr. and C. P. Mangelsdorf

School of Engineering, University of Pittsburgh
Pittsburgh, Pennsylvania 15261

Keywords: oil shale, combustion ash, Portland cement concrete

ABSTRACT

Previous experimental studies of the use of oil shale combustion fly ash in Portland cements have been reported by Germany, Israel, China, Jordan and the United States. In the current study seventeen samples of a standard concrete mix (49% coarse aggregate, 30% fine aggregate, 13% cement and 8% water) were prepared, containing various percent substitutions of Portland cement with oil shale fly ash from the pilot combustor of Occidental Oil Shale Company and commercial additives, and tested for unconfined compressive strengths. An increase in strength, consistent with observations in Israel and China, was found with substitution at 15%. Four standard mechanical tests were carried out preliminarily with the formulation with 45% substitution and a commercial additive, which gave a 90-day compressive strength of 5310 PSI. The freeze-thaw tests were confounded by poor coarse aggregate performance. The samples containing oil shale ash had less resistance to scaling than those containing no ash. Three zero-slump materials containing oil shale ash were investigated, again preliminarily. Three samples of compressed/autoclaved ash/lime paste ranged up to 2870 PSI. One of two samples of concrete masonry unit reached 1590 PSI. A sample of light-weight concrete, containing 40% fly ash, set up quickly, was hard and strippable in one day and had a density of 40 lb/ft^3.

INTRODUCTION

As a portion of a broader study of the beneficial use of ash from the combustion of oil shale from deposits owned by the Occidental Oil Shale Company in the western United States, the replacement of portions of Portland cement in standard concrete and of fine aggregate in zero-slump formulations by fly ash from a pilot plant combustor were evaluated at the University of Pittsburgh. Elements of this portion of the study include:

- a literature survey, identifying similar studies that have been carried out in several other countries, particularly in Israel and China;
- production of seventeen batches of concrete, containing oil shale combustion fly ash, and the measurement of the compressive strength of each over time;
- determination of two mechanical properties of a particular concrete, produced by one of the better formulations;

- a preliminary evaluation of zero-slump products containing oil shale combustion fly ash, specifically the preparation and examination of three samples formulated as brick, two samples as concrete masonry units and one sample as light-weight concrete.

LITERATURE

Previous experimental studies of the use of oil shale ash in cements have been carried out in the Federal Republic of Germany, the United States, Israel, China, the (former) USSR and Jordan. The work in the FRG and in the USSR has been reported only in German [1-6] and Russian [7-9], respectively. A review article by the Israelis [10] provides an excellent and comprehensive description of work in that country, as well as of the work in the Federal Republic of Germany and the United States. Four papers describing the Chinese work in English [11-14] are rather extensive, but they can be found only in a publication with, unfortunately, very limited circulation. The Jordanian paper is easily available and very informative [15].

ASH PROPERTIES

Three samples of fly ash from the Occidental Oil Shale pilot combustor were used in this study. The combustion temperature and percentages of shale and coal being fed to the pilot unit during the period of collection of each sample were:

Sample Period	Temperature (°F)	% Shale	% Coal
3	1550	54	46
4	1594	54	46
6	1500	65	35

Samples of the fly ash from Sample Periods 3 and 4 were analyzed by the Coal By-Products Utilization Laboratory (CBUL) of the ND Mining and Mineral Resources Research Institute at the University of North Dakota. Elemental compositions and LOI (Loss on Ignition) of these two samples, which relate to those found for other ashes were:

	SOURCE OF OIL SHALE ASH					
Comp.	FRG[10]	Israel[10]	China[12]*	Jordan[15]	Samp. 3	Samp. 4
CaO	16-60%	44.5	1.29	39.7	18.4	17.4
SiO_2	12.25	19.0	60.64	35.4	50.4	45.2
Al_2O_3	9-12	8.3	20.09	3.8	12.6	10.9
Fe_2O_3	6-7	4.3	11.89	2.0	4.6	4.5
MgO	1.4-2.0	0.7	0.83	4.0	6.6	6.6
SO_3	9-10	8.5	0.61	4.0	7.47	6.59
L.O.I.		11.3	0.55	7.3	0.38	0.24

* 860°C ash

The relatively high magnesia content of the fly ash from Sample Periods 3 and 4 does not appear to be a cause for concern. It is likely present in a bound form inside the ash particles. This is strongly suggested by CBUL's results, which determined that the expansiveness of the fly ash was almost an order of magnitude lower then the ASTM C618 Specification for both Class C and Class F fly ash.

CBUL also reported particle size distributions for which between 78 and 87 percent passed a #325 sieve. The fly ash thus meets the ASTM C618 Specification that at least 66 percent must pass this sieve to be a Class C or Class F fly ash.

CONCRETE FORMULATION AND COMPRESSIVE STRENGTHS

The basic concrete formulation used for seventeen test batches of ash-containing concrete, made during this study, was a standard mix of:

- 49 percent coarse aggregate;
- 30 percent fine aggregate;
- 13 percent Type 1 Portland cement;
- approximately 8 percent water.

[All formulation percentages throughout this paper are on a weight basis.] The water content was adjusted to provide a slump of two inches. Six batches also contained a workability (water-reduction) additive. Two of these six batches also used Type 3 Portland cement in place of Type 1 Portland cement.

Several trends were noted from a comparison of the 3-day, 7-day, 14-day and 28-day compressive strengths of cylinders (6 inches in length and 3 inches in diameter) formed from these seventeen batches. At low levels of Portland cement replacement (15 percent), oil shale fly ash behaves as a workability (or water reduction) agent and leads to a 9 percent higher compressive strength than that of standard concrete. This enhancement is lost by 30 percent replacement, which leads to a 9 percent lower compressive strength than that of standard concrete. The addition of the workability agent restores the high strengths, even at 45 percent replacement where it leads to a 9 percent higher compressive strength than that of standard concrete. Type 3 Portland cement does not appear to be effective in building compressive strength.

It is difficult to make direct comparisons to the work of other investigators because of differences in methodologies. The Germans, for example, make a special "oil shale cement" containing 27 percent oil shale ash and 73 percent Portland cement. It has compressive strengths up to 8800 PSI (60.8 MPa) at 28 days [10]. The Israelis make and compare pastes of Portland cement and oil shale. Portland cement pastes (water to cement ratios of 0.3 to 0.6) at 20 days reach 10,660 PSI (73.5 MPa), while oil shale ash pastes reach only 2830 PSI (19.5 MPa), when it has a water to cement ratio of 0.8 to 1.0 (which gives it the same consistency as the Portland cement paste). However, in making cement blends (Portland and oil shale ash together), the Israelis found that Portland cement replacement by 15 to 25

percent oil shale ash yielded concrete with slightly increased strength [10]. The Chinese report 28-day strengths as high as 11,200 PSI (77 MPa) with ash/Portland cement blends. They also found an increase in strength at replacements up to 25 percent [14]. The Jordanians, on the other hand, saw a drop in compressive strength when ash was added to Portland cement. Their paste strengths were much lower, peaking at 6530 PSI (45 MPa) for pure Portland cement paste at 28 days at a water/cement ratio of 0.4 [15].

MECHANICAL PROPERTIES OF CONCRETE

Two sets of concrete forms were prepared for physical testing. The first set, a control sample, was prepared with the basic concrete recipe without fly-ash replacement, while the second set with 45% fly-ash replacement (fly ash from Sample Period 3), was prepared with the workability agent (12 oz per 100 lb cement + ash) mixed with the cement separately.

The 17-day compressive strength of the standard formulation was 4010 PSI, while that for the ash-containing formulation was 5050 PSI. The length change test (ASTM C157-86) showed that from Day One to Day Seven the average shrinkage was 0.0023 inches for ash-containing specimens, compared to 0.0133 inches for specimens of standard concrete.

The abrasion test (ASTM C944-80) was performed on six two-inch-high cylinders, cut from two six-inch-in-diameter cylinders. One cylinder was standard concrete and the other was fly ash-containing concrete. The cut surfaces were abraded. The results are:

Specimen	Loss by Abrasion (Gram)			Average Loss
X-1-1	0.7	0.5	0.6	0.60
X-1-2	0.5	0.5	0.6	0.53
X-1-3	0.8	0.9	1.0	0.90
X-15-1	0.7	0.8	0.8	0.77
X-15-2	1.0	1.1	1.3	1.13
X-15-3	0.9	0.8	0.8	0.83

The freeze/thaw (ASTM C666-84) and deicing tests (ASTM C672-84) were performed by CBUL, using test specimens prepared at the University of Pittsburgh. The freeze-thaw tests were confounded by poor coarse aggregate performance. The samples containing oil shale ash had less resistance to scaling than those containing no ash.

The Chinese report that, for pastes in which 35 to 40 percent of the Portland cement has been replaced by shale ashes, sulfate resistance increases by 166 percent and the bleeding ratio drops nearly to zero. Other physical properties of the oil shale-containing cements appear to the Chinese to be comparable to cements containing coal fly ash [12].

ZERO-SLUMP MATERIALS

Compressed/Autoclaved Ash/Lime Pastes

Three two-sample sets of short, compressed cylinders (2.5 inches in diameter and 2 inches high), using fly ash from Sample Period 7, were prepared by R. I. Lampus Company, a member of the National Precast Concrete Association (NPCA) from Springdale, Pennsylvania (a suburb of Pittsburgh). The specimens had the following formulations:

	Percentage		
Specimen ID Number	Lime	Ash	Ash + Sand
1	8	--	92
2	10	90	--
3	15	85	--

An optimum amount of water (10 percent based upon dry weight) was added for maximum compaction. The cylinders were autoclaved at the University of Pittsburgh for eight hours at 170 psi (350°F) to obtain calcium silicate bonding. The compressive strengths achieved were 1500, 2130 and 2870 PSI respectively.

Concrete Masonry Units

Eight sets of zero-slump concretes, similar in formulation to concrete masonry units, were prepared at the University of Pittsburgh, two of them containing oil shale combustion fly ash. In all cases, cylinders four inches high and two inches in diameter were fabricated and then allowed to set at room temperature in a humid environment for five hours. Next, they were heated to 150°F at one atmosphere with steam over a two-hour period and then cured at 150°F and one atmosphere for twelve hours within a steamed environment before being cooled to room temperature.

The first set of four cylinders was prepared with fly ash partially substituting for Portland cement. The following formulation was used:

- 1119.8 grams sand;
- 136.9 grams Portland cement (Type 1);
- 63.0 grams oil shale fly ash;
- 49.3 grams water.

The particle size distribution of the sand was adjusted to an optimal one by screening and blending. The final sand blend was 14 percent greater than 4 mesh, 20 percent in the range of 4 to 8 mesh, and 66 percent less than 8 mesh. The cylinders were formed by pressing the concrete into the molds, followed by ten seconds of vibration at 900 CPM with a handheld unit. Release from the molds was difficult and the average compressive strength of the final product was very poor. The molds were oiled for future tests to make release more easily accomplished.

The second, third, fourth, fifth and sixth sets of four cylinders each (twenty in all) were made without fly ash substitution. Their purpose was to test various formulations and preparation techniques. An air entrainer was added for the fourth and fifth tests. For the sixth set the sand particle size distribution was set by screening and blending, according to the method suggested in the Technical Bulletin No. 5 of the National Concrete Masonry Association. All twenty cylinders were rodded, rather than vibrated. The oversized, handheld vibrator, used for the first set, tended to eject portions of the mix from the cylinders. The maximum compressive strengths of these cylinders after curing was 2000 PSI. It should be noted that the three-day strength of commercial concrete block is between 2000 and 2400 PSI.

The seventh and eighth sets of four cylinders each were prepared with 1344 grams sand, 150 grams water and either 240 grams Type 1 Portland cement (seventh set) or 168 grams Type 1 Portland cement and 72 grams oil shale fly ash (eighth set). The average compressive strength of the vibrated, cured cylinders was 1590 PSI for both sets.

Light-Weight Concrete

The third, and final, zero-slump product line that was examined was light-weight concrete. This material generally has a very low density (down to 25 lb/cubic foot) and a correspondingly low compressive strength (down to 60 PSI). It is used for fireproofing and insulation in structures. The "foaming approach" to produce this material, applied in this project, uses a foaming agent in the concrete mix. The agent introduces and stabilizes air bubbles during mixing at high speed. A sample of oil shale ash was provided to Elastizell Corporation of America in Ann Arbor, Michigan. A test using 60 percent Type 1 Portland cement and 40 percent oil shale ash yielded a well-mixing, quick-setting formulation, which resulted in a hard, strippable product in one day. The cast density of the sample was 40.3 lb/ft^3. Elastizell concluded that, based upon this limited investigation, oil shale combustion fly ash is a viable addition to light-weight concrete mixes.

CONCLUSIONS

The literature survey, conducted within the framework of this project, identified fifteen articles on the use of oil shale combustion ash in cement. These come from Israel, China, Jordan and the (former) USSR.

The ash from the combustor tests with 54 percent shale/46 percent coal is moderate in both CaO and MgO. The MgO is bound inside the particles and does not negatively impact the soundness of the ash.

Standard concrete with 15 percent substitution of Portland cement with ash shows an improvement in compressive strength at the same consistency (slump) of the wet mix, as standard Portland cement concrete. The addition of a wettability agent allows an additional 30 percent replacement without a drop in compressive strength below that of standard Portland cement concrete.

A first exploratory set of four physical tests were applied to the concrete which had 45 percent of the Portland cement replaced by ash, along with the addition of a wettability agent.

Preliminary specimens of three zero-slump products were prepared -- compressed/autoclaved ash/lime paste, concrete masonry units and light-weight concrete. The properties of the first product were sufficiently interesting that one manufacturer entered into direct negotiations with Occidental Oil Shale Company to test this product further. The second and third products met or exceeded one or more basic minimum standards, the third sufficiently so that one manufacturer desired to continue further testing. It is regrettable that Occidental Oil Shale Company has ceased operation, thus halting work in this promising area.

ACKNOWLEDGEMENTS

The Occidental Oil Shale Company provided the funds to carry out this preliminary study. Mr. Amin Tomeh prepared the seventeen batches of ash-containing concrete and conducted the tests of compressive strengths at the University of Pittsburgh.

REFERENCES

[1] Wuhrer, J., Zement-Kalk-Gips, April 1949, Pages 61-65, 89-93.
[2] Wuhrer, J., Zement-Kalk-Gips, March 1950, Pages 45-48.
[3] Rohrbach, R., Zement-Kalk-Gips, 22 (7), 1969, Pages 293-296.
[4] Rechneier, H., Zement-Kalk-Gips, 23 (6), 1970, Pages 249-253.
[5] Rapp, G., Betonwerk + Fertigteil-Technik, 50 (7), 1984, Pages 468-473.
[6] Mathauer, W., Betonwerk + Fertigteil-Technik, 50 (9), 1984, Pages 613-619.
[7] Puzyrev, Yu. A., Tekhnol. Izgot. i Svoistvanov. Kompozits. Stroit. Mater., L., 1986, Pages 63-68. Referenced in Ref. Zh., Khim. 1987, Abstr. No. 7M415.
[8] Remnev, V. A., Issled. po Str-vu Stroit. Teplofiz. Dolgovech. Konstruktsii, Tallin, 1987, Pages 75-85. Referenced in Ref. Zh., Khim. 1988, Abstr. No. 8P95.
[9] Puzyrev, Yu. A., A. B. Klyuev and I. I. Zinchenko, Intensif. Tekhnol. Protsessov v Pr-ve Sbor. Zhelezobetona, L., 1988, Pages 92-97. Referenced in Ref. Zh., Khim. 1989, Abstr. No. 11M340.
[10] 8entur, A., et al., Proceedings of the Second International Conference on Fly Ash, Silica Fume, Slag and Natural Pozzolans in Concrete, Madrid, Spain, April 21-25, 1986, SP 91-37, American Concrete Institute, Pages 779-802.
[11] Guangshu, T., et al., Proceedings of the International Conference on Oil Shale and Shale Oil, Colorado School of Mines 21st Oil Shale Symposium, Beijing, China, May 16-19, 1988, Pages 547-551.
[12] Zhongpu, H., and X. Qihai, Document of Reference 11, Pages 552-558.
[13] Guangshu, T., et al., Document of Reference 11, Pages 559-564.
[14] Zhimin, Wang, et al., Document of Reference 11, Pages 565-572.
[15] Smadi, M., A. Yeginobal, and T. Khedaywi, Magazine of Concrete Research, 41 (148), September 1989, Pages 183-190.

Utilization of Coal-Tar Pitch in Insulating-Seal Materials

Janusz Zieliński
Technical University of Warsaw
Branch at Płock
Institute of Chemistry
Płock, Poland

George Górecki
Ardrox, Incorporated
921 Sherwood Drive
Lake Bluff, IL 60044

Substances obtained from coal, in light of their physicochemical properties, can find a number of interesting applications. Among these substances are tars and coal-tar pitch. Collin (1) has described a variety of applications using coal-tar pitch (see Fig. 1). The majority of these applications, however, are realized only in a narrow scope. At the industrial level, pitch is most often treated as a by-product of the process of continual distillation of coal-based tar. One path that leads to the improvement of thermal and rheological properties of bitumens derived from coal is their modification by means of the addition of polymers. This creates the possibility of attaining greater utility from coal-tar pitch. One example is the improvement of binder quality in insulating-seal materials. This capability permits, in a relatively straightforward manner, the application of coal-tar pitch on a large scale. We feel that, in addition to the applications of pitch described by Collin, it is important to understand that pitch can be used as a binder or as a base substance in insulating-seal materials for the building, road construction and machinery industries.

Compositions based on petroleum asphalts are examples confirming the usefulness of this approach. The literature pertaining to the modification of petroleum bitumens by polymers is very extensive, the majority of which has been published in patents. For the most part, these works deal with the physical modification of asphalts by means of plastics, with the intention of obtaining homogeneous mixtures (2-6). Polymers produce diverse changes in the properties of petroleum bitumen. This is related mostly to an increase in stability and durability of the bitumen's physico-colloidal structure (7).

On the other hand, combining coal-tar pitch with polymers has generated a significantly smaller level of interest. Nevertheless, various types of polymers have been utilized to modify the properties of tars and coal-tar pitch. These polymers provided the means of attaining homogeneous and stable compositions. In particular, the goal of these works was to obtain binders used in the building of roads (8) and in tar-based lacquers (9). At present, the mechanisms for the composition of coal-tar pitch/polymer mixtures has not been elucidated. Neither has the interaction between these two types of constituents been distinctly explained. In both petroleum-asphalt/polymer compositions and pitch-polymer arrangements, it is accepted that homogeneity is the uniform dispersion of (a) polymer particles and (b) elements of resinous asphaltene pitch in its oil phase. Mutual interactions between the continuous phase of the bitumen (low molecular weight oils and resins) and the polymer as well as between the polymer and the dispersed phase of the pitch (resinous and asphaltenic substances, beta- and gamma- forms) determine the final physico-colloidal structure of the composition (7). Compared to petroleum asphalts, coal-tar pitch comprises relatively small amounts of the continuous phase. It is therefore appropriate to enrich coal-tar pitch with additional plasticizing substances.

The goal of the investigations was to determine the pitch-polymer composition which would fill the role of the matrix, having as a basis high-molecular weight insulating-seal materials. The investigations were carried out in two stages.

In the first stage, problems relating to the attainment of homogeneous and stable compositions made from the chosen types of polymers, plasticizers and coal-tar pitch were investigated. The first stage is outlined in Fig. 2. In the second stage, the formulations of the compositions were established. These mixtures were able to define beneficial characteristics for bituminous insulating-seal materials.

The following materials were studied:

1. Normal coal-tar pitch at its softening point of 87°C as well as the contents of components insoluble in toluene (21.45%).

2. Polymers. Atactic polypropylene (aPP, molecular weight: 32,600); isotactic polypropylene (iPP, MW: 220,000) with an isotactic index above 95%; polyvinyl chloride (PVC, MW: 139,000); polystyrene (PS, MW: 304,000); styrene-butadiene rubber latex containing 24.5% combined styrene and 59% rubber substances.

3. Plasticizers. Dibutyl phthalate; anthracene oil; furfurol extract.

4. Fillers. Milled chalk; talc; colloidal silica.

The following determinations were performed on the obtained compositions:

1. Fragility point (Fraass).

2. Softening point (Pierscien and Kula).

3. Penetration and stability at elevated temperatures according to the Tube Test (10). The stability index was determined from the mutually relative densities of upper and lower layers of samples heated to 150°C for 4 days.

4. Adhesion. Concrete, glass, wood and aluminum were used as substrates.

5. Flow along vertical surfaces.

6. Resistance to freezing.

7. Elasticity at negative temperatures, as low as -20°C.

8. Aging tests. Twenty cycles, where one cycle lasted 48 hr and involved exposure to UV radiation, artificial rain and heating to 70°C and freezing to -25°C.

In the case of compositions made up of coal-tar pitch and polymers, certain intrinsic factors play a particular role with regard to obtaining mixtures which are homogeneous and which will not delaminate. These factors include: temperature, the time needed to reach homogeneity and the order of addition of components. Another important factor is the elimination of circumstances which may destroy the polymers.

The polymers that were examined differed in structure and characteristics. Beneficial properties were attained only in the case where pitch was combined with polar PVC. Mixtures containing 10% w/w PVC in pitch were homogeneous and stable. The addition of PVC increased the softening point to 114°C, with a concurrent lack of improvement in elasticity.

In the cases involving other polymers, the results were not as fruitful. Differences in the chemical make-up and the colloidal structure of pitch and PP prevented the attainment of mixtures that did not delaminate. In order to obtain homogeneous mixtures of pitch and PS, a temperature range of 260-310°C was required. This led to the destruction of the polymer and provided no changes in the properties of the pitch.

Plastification of pitch by means of oil fractions that are coal-based (anthracene oil) and petroleum-based (fuel oil, furfurol extract), as well as artificially-produced dibutyl phthalate obtained from industry was studied. It was demonstrated that the most beneficial changes in properties were obtained using dibutyl phthalate at 25-30% w/w. The dibutyl-phthalate-modified pitch provided new qualities in pitch-plasticizer binders. For example, the fragility point

(according to Fraass) of pitch-phthalate mixtures is -24°C. Mixtures of pitch and furfurol extract or anthracene oil at 20-25% w/w provided similar improvements.

In order to be eventually applied as base substances for insulating-seal materials, two-component mixtures of pitch-polymer and pitch-plasticizer required further modification. This was made possible by improving their mechanico-rheological properties. The three-component systems were comprised of coal-tar pitch, polymers and plasticizers. The best properties were obtained by compositions having 25% w/w dibutyl phthalate relative to pitch and 5-8% w/w PVC relative to pitch-plasticizer binder. Phthalate was used as plasticizer because it efficiently enabled the elimination of the elastomeric properties of PVC in a pitch environment.

The compositions were also modified with styrene-butadiene rubber in order to impart resistance to elevated temperatures and to provide high elasticity at negative temperatures. The following composition provides advantageous properties: coal-tar pitch (58.6% w/w), phthalate (22%), PVC (7.4%), styrene-butadiene rubber latex (7.4%). The fragility point of this mixture was -36°C and the softening point was 58°C. The penetration at 25°C was about 100 x 10^{-4} m and the stability index was 0.4%. These properties permitted the mixture to behave like an insulating-seal material.

The second part of the investigation involved determining the formulation of the final mixture, which had coal-tar pitch as a fundamental component. The composition was defined by standard specifications used for dilatant putties and hydroinsulation linings used in the building industry. As a rule, fillers and adhesion agents comprise materials of this type. The influence of the types and amounts of fillers (milled chalk, talc, colloidal silica) as well as that of adhesive media (balmy rosin, coumarone-indene resin) on the properties of butadiene-styrene pitch-phthalate-PVC-latex mixtures was studied. It was found that, regardless of the choice of filler, the most beneficial changes in applied properties were attained with filler mixtures containing chalk or talc with colloidal silica in a mass ratio of 4:1. Testing was performed by examining levelling at higher temperature, vertical flow at 60°C, resistance to freezing at -10°C and -20°C. At the same time, the amount of filler in the entire substance, depending on the application, should be 15-30% w/w. On the other hand, balmy rosin, in quantities of 2-3% w/w, was used as the adhesive agent. The rosin increases cohesion between the binder and the fillers. This provides an increase in the breaking strength (>0.1 MPa).

The results of the investigation provided the optimal formulations, which are listed in Table I. These compositions have many practical applications, such as the filling of horizontal slits in concrete as well as strengthening the bonds between metal-glass and wood-glass interfaces. Other applications include bituminous dilatant putties, sealing vertical surfaces in building elements, and hydroinsulating linings (1-3 mm thickness) formed by the hot rolling method, for use in the building industry.

The thermomechanical, rheological and practical properties of these compositions are comparable to the properties of analogous mixtures based on petroleum asphalts. In some instances, the properties of the pitch-based mixtures exceed those of the petroleum-based ones (e.g., adhesion to concrete, metallic or glass substrates). Modified pitch-polymer compositions can be used in general and specialized building applications. Examples include the construction of roads, airports, underground objects. Other examples can be found in the machine industry, where these mixtures are used as materials to prevent water penetration and to deaden vibrations.

References

1. G. Collin, Production and Application of Coal-Tar Pitch, International Conference on Structure and Properties of Coals, 154, 1991.

2. US Patent 4,430,464, 1984.

3. UK Patent 1,457,999, 1976.

4. J. Zieliński, Erdol u. Kohle, Erdgas, Petrochemie, **42**, 456, 1989.

5. G. Collin and M. Zander, Erdöl u. Kohle, Erdgas, Petrochemie, **39**, 517, 1986.

6. J. Zieliński and A. Bukowski, Ropa a Uhlie, **29**, 404, 1987.

7. J. Zieliński, The Studying of Structure and the Properties of Bitumen-Polymer Compositions, Wyd. Politechniki Warszawskiej, Seria Chemia, 1991.

8. Z. Stompel, et. al., Koks, Smoła, Gaz, **33**, 24, 1989.

9. J. Kozakiewicz, et. al., Polimery, **37**, 534, 1992.

10. G. Zenke, Bitumen, 1, 11, 1973.

TABLE I - OPTIMAL QUANTITIES of COMPONENTS

Component	Sealing Compound (% w/w)	Sealing putty (% w/w)	Pitch-polymer lining (% w/w)
Coal-tar pitch	56.10	48.90	48.30
Dibutyl phthalate	18.70	16.30	16.10
PVC	6.50	5.70	7.10
Styrene-butadienerubber latex	6.50	5.70	7.10
Talc	9.76	--	17.10
Milling chalk	--	17.00	--
Colloidal silica	2.44	4.30	4.30
Balmy rosin	--	2.10	--

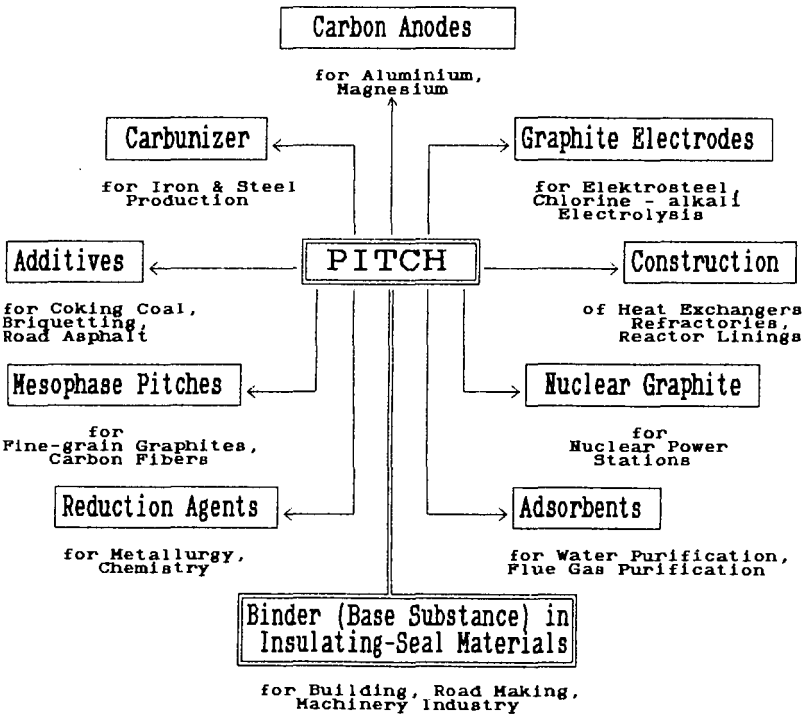

Fig.1. Application of Coal-Tar Pitch [G.Collin]

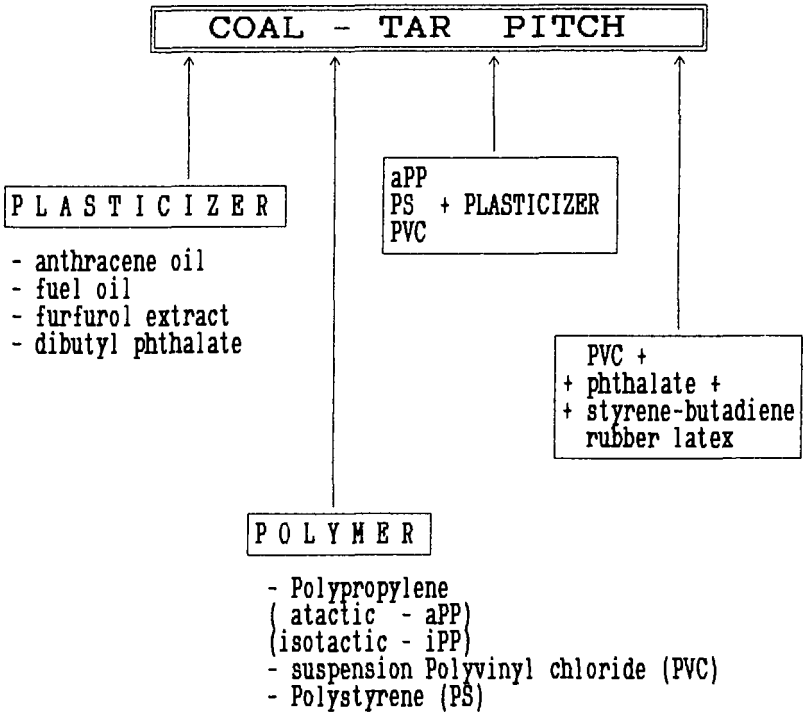

Fig. 2. Essential directions of investigation concerning modification of properties of coal-tar pitch

BRIQUETTING ANTHRACITE FINES FOR RECYCLE

Salustio Guzman
Research and Development Laboratories
QIT-Fer et Titane Inc., P.O. Box 560, Sorel
Quebec, Canada, J3P 5P6

John T. Price
Energy Mines and Resources Canada
Energy Research Laboratories, CANMET
555 Booth Street, Ottawa, K1A 0G1

Keywords: Anthracite fines, Briquetting, Recycle

ABSTRACT

Pennsyvania anthracite is employed at QIT as reductant in electric arc furnaces, for the production of metal iron and Titanium dioxide rich slag from ilmenite. Fines are generated at the drying stage of anthracite, prior feeding to the electric arc furnaces, and represent approximately 3.4 % of the annual amount of anthracite used at QIT.

The size of these anthracite fines make them unsuitable for their direct use at the electric arc furnaces, because during feeding, they would be lost to the wet gas scrubbers. Briquetting of anthracite fines allows recycle of these materials for smelting ilmenite at QIT.

The paper presents results of a laboratory study for briquetting anthracite fines with a pitch binder, on the physical properties and chemical composition of the briquettes and, also discusses the proposed plant flowsheet for briquetting.

QIT's metallurgical operations in Quebec consist of an open pit mine located in the Allard Lake region, 500 miles north of Montreal, where an ilmenite ore is extracted and, the operations in Sorel where, the ore is beneficiated before smelting in electric arc furnaces. Smelting produces a titanium dioxide rich slag which is used as feed stock by pigment producing companies, and liquid iron metal which is processed further for production of different grades of pig iron, production of steel billets at QIT's steel plant and, production of iron and steel powder products at QIT's metal powders plant QMP.

Smelting at QIT in electric arc furnaces, consists of a carbothermic reduction of iron oxides present in the ilmenite in a molten bath. The reducing agent employed for smelting is Pennsylvania anthracite which is delivered to Sorel by boat.

The anthracite reductant prior to feeding to the electric arc furnaces is dried in three rotary louvre type driers, which use the arc furnace fuel gas (85 % CO and 15 % H2) produced from the iron oxide reduction. The drying operation removes 8 to 8.5 % moisture from anthracite as received at Sorel.

Fines are generated in the drying stage and are entrained in the gas exiting the driers. Fines represent approximately 3.4 % weight of the total annual amount of anthracite used at QIT, which is separated from the gas by cyclones and wet gas scrubbers.

Typically anthracite fines contain 75.38 % fixed carbon, 5.7 % volatile matter, 0.68 % sulfur 18.92 % ash, and 79 % of the particles are bigger than 38 microns. The relative high ash content in the fines relative to the 9.6 - 10 % ash content in dry anthracite, is consistent with the fact that, coal fines in general are associated with higher ash content.

The laboratory experimental work was carried out at the Energy Research Laboratories of CANMET in Ottawa. A batch laboratory size twin roll briquetting machine manufactured by K. R. Komarek, model B-100 was employed for the tests, this machine is equipped with, 130 mm diameter and 50 mm width rolls, and produces pillow shape briquettes with 12 x 12 x 40 mm dimensions.

The only binder tested was type II roofing asphalt, because this carbonaceous binder is compatible with the nature of anthracite reductant.

The experimental range of conditions for briquetting were: 5 - 14 % wt binder, and 6880 - 13760 pounds briquetting pressure, as summarized in Table 1.

Good quality green briquettes were produced for 10 and 12 % binder additions at 6800, 10320 and 13760 pounds of pressure, with more than 90 % of the initial mixture weight briquetted with the 12 x 12 x 40 mm target size.

Green briquettes with the best drop and abrasion resistance properties, were produced for 12 % binder addition and 10320 pounds pressure, these briquettes, withstood 9 ft drop tests without breakage while, the rest of the briquettes withstood only 6 ft or less high drop test.

The green briquettes containing 10, 12 and 14 % binder additions were crushed, for producing briquetted anthracite material smaller than the original 12 x 12 x 40 mm briquette size produced. A roll crusher was employed for crushing the briquettes, and the particle size distribution ranges from 1.13 cm (3/8") to 130 microns (100 mesh), as shown in Figure 1.

The + 10 mesh fraction of crushed green briquettes were subject to abrasion tests, employing an ASTM tumbler for coal, which procedure was modified to accommodate to the coarse granulometry and smaller weight of the crushed samples. Once again, the crushed green briquettes containing 12 % binder addition and briquetted with 10320 pounds of pressure, exhibited the highest abrasion resistance, with only 16.6 % decrease in the average particle size from 6420 microns before to 5355 microns after tumbling while, larger average particle size reductions ranging from 29.4 to 37.2 % are experienced after tumbling the + 10 mesh fraction of crushed briquettes containing 10 % binder additions.

In summary, use of 12 % type II asphalt roof binder and 10320 pounds briquetting pressure constitute, the optimum experimental conditions for producing briquettes with desirable drop and abrasion resistances, necessary to withstand handling and transport within the feeding system for recycle at QIT, for crushed or non crushed briquettes produced from anthracite fines.

The successful completion of the laboratory testing has led to the proposal of a flowsheet for briquetting anthracite fines, as illustrated by the schematic flowsheet shown in Figure 2. It is estimated that, a 5 metric tonnes per hour briquetting plant would be more than sufficient for processing the anthracite fines generated at QIT.

TABLE 1

EXPERIMENTAL CONDITIONS FOR BRIQUETTING ANTHRACITE FINES

ROLLS SPEED (RPM)	AUGER RATE (RPM)	BRIQUET. FORCE (LBS)	MOISTURE CONTENT (% WT)	BINDER CONTENT (% WT)	FINES WEIGHT (g)
1.818	32.25	10320	3	5	7077
1.818	32.25	10320	3	7	7077
1.818	32.25	10320	3	9	7077
1.818	32.25	10320	7	5	7000
1.818	32.25	10320	7	7	7000
1.818	32.25	10320	7	9	7000
1.818	32.25				
1.818	32.25	6880	3	12	7077
1.818	32.25	10320	3	12	7077
1.818	32.25	13760	3	12	7077
1.818	32.25	6880	3	10	7077
1.818	32.25	10320	3	10	7077
1.818	32.25	13760	3	10	7077
1.818	32.25	6880	3	12	7077
1.818	32.25	10320	3	12	7077
1.818	32.25	13760	3	12	7077
1.818	32.25	6880	3	14	7077
1.818	32.25	10320	3	14	7077
1.818	32.25	13760	3	14	7077

FIGURE 1

PARTICLE SIZE DISTRIBUTION OF CRUSHED BRIQUETS

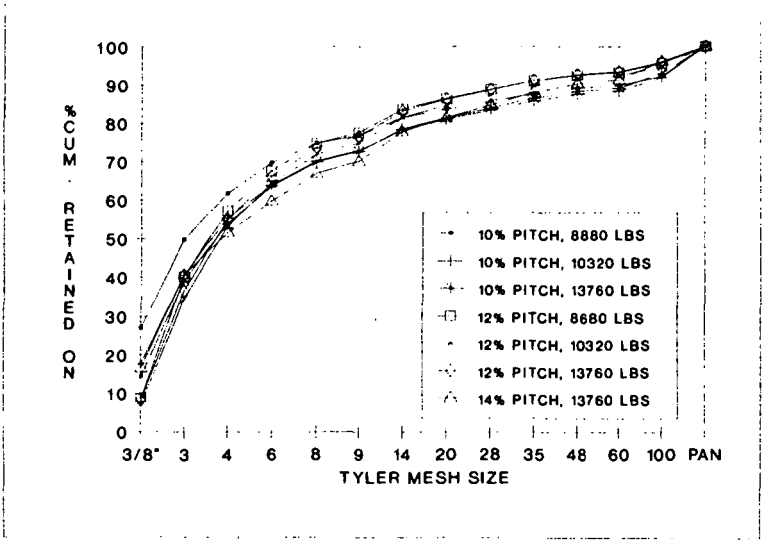

FIGURE 2

ANTHRACITE FINES BRIQUETTING

SCHEMATIC OF PROPOSED FLOWSHEET

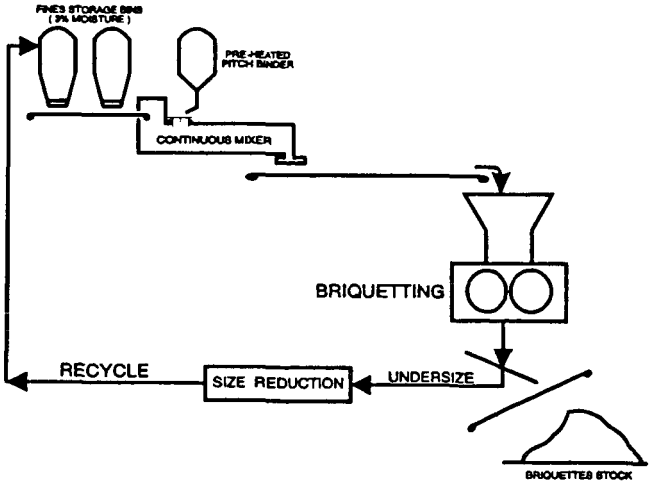

ASH UTILIZATION IN WATER QUALITY MANAGEMENT

T. Viraraghavan
Faculty of Engineering, University of Regina
Regina, Saskatchewan, Canada, S4S 0A2

ABSTRACT

The potential for water pollution involving heavy metals and organics exists especially when wastewater treatment is either inadequate or non-existent. This paper reviews a number of investigations where coal ashes have been studied for the removal of organic matter (COD), color, organic compounds such as phenol, and heavy metals. Results of experimental studies conducted at the University of Regina, on the adsorption of 1) phenol and 2) heavy metals such as cadmium, chromium, mercury, copper, nickel and zinc by fly ash, are presented. The use of fly ash in sludge management is also examined.

Keywords: coal ash utilization, water treatment, wastewater treatment

INTRODUCTION

Increased reliance on coal as an energy source has led to significant by-product management problems of storage or disposal. These by-products include slag, bottom ash and fly ash. Commercial uses of coal ashes are limited and this paper examines the application of these by-products in water pollution control.

USE OF FLY ASH IN WATER TREATMENT

Ballance et al. used fly ash as a coagulant aid in water treatment (1). Fly ash from four sources and in certain proportions was found by the authors to assist in the chemical coagulation of turbid water and in the settling of chemically induced floc. A denser sludge was produced from coagulation with fly ash and alum than with alum alone. Laboratory tests using Neyveli lignite fly ash showed that it aids in the settling of turbid water when used along with alum (2).

USE OF COAL ASHES IN WASTEWATER TREATMENT

The use of bottom ash and fly ash in removing contaminants from wastewater (on-site and municipal) is examined with special reference to removal of COD, color, organic compounds, and heavy metals.

On-site Wastewater Treatment

Bottom ash was considered as an alternative medium for the mound type soil absorption systems used in on-site wastewater treatment. Laboratory work carried out at West Virginia University showed that the bottom ash filter had the ability to reduce BOD and SS (3, 4). Three bottom ash mound systems built in Monogalia County, West Virginia based on this work were reported to be operating well (5). Laboratory studies on four different recirculating filters using pea gravel, medium sand, bottom ash and fly ash-bottom ash mixture showed that there was no significant difference in the performance of different media with respect to reduction in COD and SS (6). A 23-month study examined 11 filters - five bottom ash filters, five sand filters treating septic tank effluent and one bottom ash filter treating aerobically treated effluent. The study data showed that sand media filters resulted in a higher quality effluent; noticeable improvement in the performance of all the filters was observed in the last five-month period with effluent BOD in the 10-14 mg/L range (5). The Southern Illinois Power Co-op used unscreened bottom ash in a single intermittent filter treating septic tank effluent. The filter

operation was monitored from January 1981 to April 1982; the average effluent BOD and SS values were 7 and 8 mg/L respectively (7). Detailed studies on a bottom ash recirculating filter treating septic tank effluent from a residence showed that the system performed consistently and produced an effluent with average BOD and SS less than 12 mg/L (8).

Municipal Wastewater Treatment

Batch tests showed that unsieved fly ash (6% carbon) removed in 24h 19 to 56% of COD, and 0 to 77% of ABS from secondary effluent depending upon the adsorbent dose (9). This study also showed that COD removal increased with an increase in the carbon content of fly ashes tested (9). Deb et al. found that the removal of COD is logarithmically related to three parameters - 1) time of mixing, 2) initial COD and 3) concentration of fly ash (10). Nelson and Guarino found that removals of COD, BOD and SS by the addition of fly ash to a municipal plant effluent were not appreciable (11). The investigations by Eye and Basu showed that fly ash was capable of reducing COD of a secondary effluent by about 30 percent at a fly ash concentration of about 1600 mg/L when the initial COD is around 60 mg/L and removal of SS containing fly ash by coagulation with lime was very efficient (12).

Removal of color. The removal of Metomega Chrome Orange GL, a commercial textile dye from wastewater was found to be nearly 99% under optimal conditions (pH = 3.0 and temperature =30°C) using fly ash as an adsorbent (13); the sorption data fitted the Langmuir isotherm model. The removal of Omega Chrome Red ME (a popular chrome dye) from its aqueous solution by adsorption on a mixture of fly ash and coal was studied; a 100% removal of the dye was achieved at 10 mg/L, 30°C, and 2.0 pH, using a 1:1 ratio of fly ash and coal (14). The equilibrium data was reported to fit well with the Langmuir model of adsorption.

Removal of organics. Fly ash was successfully used to recover phenol from industrial wastewater, by lagooning the mixture of fly ash and wastewater; phenol was reduced from 4500 mg/L to 280 mg/L (15). Fly ash was also used to remove TNT in both batch and column systems; in column systems 90% removal of TNT was reported (16). Bhargava et al. examined the removal of a detergent in a fixed-bed continuous flow fly ash column and developed a relationship for the design of such systems (17). Using 1000 mg/L of fly ash containing 23.27% carbon, 74% removal of ABS was obtained with a two-hour contact time (18). Khanna and Malhotra examined the kinetics and mechanism of phenol removal by fly ash and provided data for the design of phenol-fly ash adsorption systems (19). Jain et al. showed that the adsorption plot of oxalic acid from aqueous solution by fly ash has two linear components each following the Langmuir isotherm (20). Banerjee et al. examined the use of fly ash as a sorbent in the treatment of alcohols, aldehydes, ketones and aromatics (21). This study showed that immobilization of organic pollutants is feasible by adsorbing the contaminants onto fly ash. The residual carbon content was found to play a significant role in the adsorption process. Percent reductions of the aromatic compounds were found to be much higher compared to other functional groups such as alcohols, aldehydes and ketones.

Removal of heavy metals. Gangoli et al. performed batch tests by contacting 40 g of fly ash with 1 L of an aqueous solution of chromium (22). They concluded that the removal of hexavalent chromium using fly ash involved a chemisorption mechanism associated with the bonding between active alumna sites and the chromate anion. Grover and Narayanaswamy carried out batch experiments to study the effects of contact time, pH and fly ash dosage on the removal of hexavalent chromium (23). They explained the equilibrium data for chromium uptake by fly ash at different pH values on the basis of the Freundlich adsorption isotherm. They found that there was an improved adsorption of chromium at a pH less than 2.5. Yadava et al. (24) investigated the removal of cadmium by fly ash at different conditions by varying the

contact time, temperature and pH. They found that the removal of cadmium from aqueous solutions by adsorption on fly ash increased with time and that equilibrium is attained in 2 hours. On studying the kinetics of adsorption of cadmium on fly ash using the Lagergren equation, they concluded the adsorption process to be first order. They found that the adsorption of cadmium on fly ash could be explained by the Langmuir equation. Their results showed that an increase in temperature from 20°C to 40°C decreased the adsorption of cadmium on fly ash from 96.07% to 83.78%. The removal of cadmium by fly ash increased from 11.85% to 89.82% on increasing the pH of cadmium solution from 4.0 to 8.5. The ability of a homogenous mixture of fly ash and wollastonite (1:1) to remove Cr^{6+} from aqueous solution by adsorption was investigated by Panday et al. (25). Maximum removal was observed at pH 2.0 and 30°C. Studies were conducted to investigate the removal of copper from the metal cleaning wastes by adsorption on fly ash; these studies showed that adsorption can significantly increase copper removal (26). The removal of Cu^{2+} by adsorption on fly ash was found by Panday et al. to be concentration, pH and temperature dependent (27). Adsorption was found to be endothermic; the maximum removal was observed at pH 8.0. Prabhu et al. showed that fly ash was a good adsorbent for the removal of zinc from aqueous solutions; maximum removal was obtained in the pH range of 3 to 4 (28). They found that adsorption fitted the Freundlich isotherm. Studies by Gashi et al. showed that fly ash showed good adsorptive properties of removal of lead, zinc, cadmium and copper from effluents of battery industry and fertilizer industry (29). Removal efficiencies were greater than 70%. Adsorption studies carried out to estimate heavy metal removal using fly ash on wastewater at Varnasi, India showed that removal was in the following order: Pb>Zn>Cu>Cr>Cd>Co>Ni>Mn (30). Adsorption of Cu^{2+}, Ni^{2+}, Cd^{2+}, Pb^{2+}, Zn^{2+} and Ag^{+} on fly ash was investigated by Weng and Huang and they found that the process was spontaneous and endothermic (31). Sen and De found that fly ash was found to have a good adsorption capacity for Hg^{2+}; they reported that the adsorption conformed to Freundlich model (32). They found that the equilibrium time for adsorption was three hours and that the optimum pH range was 3.5 to 4.5. Fly ash was found to be a good adsorbent for the removal of lead; an equilibrium time of two hours and a pH of 5.0 was found to be most effective for the removal of lead (33).

USE OF FLY ASH IN SLUDGE MANAGEMENT

Eye and Basu concluded, based on their investigation, that fly ash could be a useful agent in conditioning sludge prior to vacuum filtration (12). Helm et al. concluded that mixtures up to 10% wastewater sludge with fly ash appeared suitable for use in highway embankments and other structural fills (34). Kincannon et al. showed that an admix of municipal wastewater sludge with fly ash could produce a dry, deodorized and sterile product with a potential for use as a soil conditioner (35).

RESEARCH AT THE UNIVERSITY OF REGINA

Batch studies were conducted to evaluate the use of fly ash in the removal of cadmium, chromium, copper, nickel, zinc, mercury and phenol from municipal wastewater. The fly ash used in the study was obtained from unit #2 of the Poplar River Power Station of the Saskatchewan Power Corporation. The fly ash generated from the combustion of lignite was collected from the first bunker of the power station's electrostatic precipitators. The wastewater used in the study was collected from the City of Regina Municipal Wastewater

Treatment Plant, before the wastewater enters the primary sedimentation tanks. The first study related to cadmium and chromium; the second study was conducted with copper, nickel and zinc; the third study was on mercury removal and the fourth related to phenol. For the studies, the wastewater was spiked with the respective heavy metals to raise their concentrations to approximately 1 mg/L. Batch (kinetic and adsorption isotherm) studies were conducted using a Jar Test Apparatus. Adsorption studies were conducted at various pH values and the best pH for maximum adsorption was chosen. Isotherm studies were conducted at 5°C, 10°C, 15°C and 21°C for heavy metal removal. Methods outlined in "Standard Methods" (36) were followed for the analysis. Batch studies showed that fly ash removed 93% of the cadmium in the wastewater in the pH range 7 to 8, and 44% of the chromium in the wastewater in the pH range 2 to 3 in an equilibrium time of 3 hours (37). The adsorption of cadmium and chromium on fly ash was found to be exothermic. Isotherm analysis of the data showed that the adsorption of cadmium on fly ash was described by the Langmuir isotherm at 5°C, 10°C, 15°C, and 21°C whereas the adsorption of chromium on fly ash followed the Freundlich isotherm at 5°C, 10°C and 15°C and Langmuir isotherm at 21°C. Removals of copper, zinc and nickel attained equilibrium in two hours (38). Removals of the three metals were found to reach maximum values in the pH range 3 to 3.5. It was found that the adsorption capacity of fly ash with respect to these three heavy metals generally decreased with an increase in temperature. Removals of copper, nickel and zinc were approximately 73%, 33% and 59% respectively at 21°C at a pH of 3.0 to 3.5. The adsorption of the three metals on fly ash generally followed the Langmuir isotherm. It was found that a contact time of two hours was necessary for the adsorption of mercury from wastewater to reach equilibrium (39). The optimum pH was found to be between 5.0 and 5.5. The adsorption isotherm data were described adequately by both the Langmuir and the Freundlich models. In the case of the adsorption of phenol from wastewater by fly ash, it was found that the removal of phenol was optimum at a pH of 5.0 in an equilibrium time of five hours. The adsorption data was adequately described by the Langmuir isotherm.

ACKNOWLEDGMENTS

The author would like to thank the Natural Sciences and Engineering Research Council of Canada (NSERC) for funds provided to the project by way of an operating grant to the author.

REFERENCES

1. R.C. Ballance, J.P. Capp and J.C Burchinal. Fly Ash as a Coagulant Aid in Water Treatment. Report of Investigation 6869. Washington, DC: U.S. Department of the Interior, Bureau of Mines, 1966.
2. S. Torrey. Coal Ash Utilization: Fly Ash, Bottom Ash and Slag. Park Ridge, NJ: Noyes Data Corporation, 1978, p. 62.
3. C.R. Schriner. Use of Bottom Ash as a Medium for the Construction of a Septic Tank Effluent Disposal System. Morgantown, WV: Department of Civil Engineering, West Virginia, 1979.
4. N. Oshkoohi. Use of Bottom Ash as Media for the Construction of a Septic Tank Effluent Disposal System. Morgantown, WV: Department of Civil Engineering, West Virginia, 1979.
5. S.P. Dix, M. Usmen and A.W. Babcock. "Bottom Ash Analysis for Effluent Treatment." Orlando, FL: Proceedings of the Seventh International Ash Utilization Symposium, 1985, pp. 517-529.
6. D.J. Ralph, D.H. Vanderholm and W.D. Lembke. "Recirculating Sand Filters for Onsite Sewage Treatment in Areas with Soils Unsuitable for Seepage Fields." New Orleans, LA: Paper presented at the 1979 Winter Meeting of the American Society of Agricultural Engineers, 1979.
7. D.L. Hill. Evaluation of Bottom Ash from Southern Illinois Power Company for Use as

Filter Media. Marion, IL: Memorandum, Illinois Environmental Protection Agency, June 1983.
8. M.A. Usmen and S.A. Dix. "Use of Bottom Ash as Filter Aggregate for Septic Tank Wastewater Treatments." Istanbul, Turkey: Proceedings of the Third Symposium on Environmental Management for Developing Countries, 1986.
9. G.E. Johnson, L.M. Kanka and J.H. Field. "Use of Coal and Fly Ash as Adsorbents for Removing Organic Contaminants from Secondary Municipal Effluents." Industrial and Engineering Chemistry - Process Design and Development, Vol. 4, No. 3, July 1965, pp. 323-327.
10. P.K. Deb, A.J. Rubin, A.W. Launder and K.H. Mancy. "Removal of COD from Wastewater by Fly Ash." W. Lafayette, IN: Engineering Bulletin, Purdue University Extension Series 121, 1966.
11. M.D. Nelson and C.F. Guarino. "The Use of Fly Ash in Municipal Waste Treatment." Journal of Water Pollution Control Federation, Vol. 41, No. 11, Part 1, November 1969, pp. 1905-1911.
12. J.D. Eye and T.K. Basu. "The Use of Fly Ash in Wastewater Treatment and Sludge Conditioning." Journal of Water Pollution Control Federation, Vol. 42, No. 5, Part 2, May 1970, pp. R125-R135.
13. G.S. Gupta, G. Prasad and V.N. Singh. "Removal of Color from Wastewater by Sorption for Water Reuse." Journal of Environmental Science and Health, A. Vol. 23, No. 3, 1988, pp. 205-217.
14. G.S. Gupta, G. Prasad and V.N. Singh. "Removal of Chrome Dye from Aqueous Solutions by Mixed Adsorbents: Fly Ash and Coal." Water Research, Vol. 24, No. 1, 1990, pp. 45-50.
15. K. Lorenz. "Secondary Treatment of Power-Plant Phenol Waste with Fly Ash and Cinders." Gesubdb. Ing. Vol. 75, 1954, p. 189.
16. V. Solin and M. Kustka. "The Treatment of Wastewaters Containing TNT by Sprinkling on Ashes." Scientific Papers from Institute of Chemical Technology, Prague, Vol. 2, 1958, p. 247.
17. R. Bhargava, R.P. Mathur and P. Khanna. "Removal of Detergent from Wastewater by Adsorption on Fly Ash." Indian Journal of Environmental Health, Vol. 16, No. 2, April 1974, pp. 109-120.
18. K.H. Mancy, W.E. Gates, J.D. Eye and P.K. Deb. "The Adsorption Kinetics of ABS on Fly Ash." Lafayette, IN: Proceedings of the 19th Industrial Waste Conference, Purdue University, 1965, pp. 146-160.
19. P. Khanna and S.K. Malhotra. "Kinetics and Mechanism of Phenol Adsorption on Fly Ash." Indian Journal of Environment Health, Vol. 19, No. 3, July 1977, pp. 224-237.
20. K.K. Jain, G. Prasad and V.N. Singh. "Application of Langmuir Isotherm for Oxalic Acid Adsorption by Fly Ash and Activated Carbon." Indian Journal of Chemistry, Vol. 19A, No. 2, February 1980, pp. 154-156.
21. K. Banerjee, P.Y. Horng, P.N. Cheremisinoff, M.S. Sheih and S.L. Cheng. "Sorption of Selected Organic Pollutants by Fly Ash." West Lafayette, IN: Proceedings of 43rd Industrial Waste Conference, Purdue University, 1988, pp. 397-406.
22. N. Gangoli, D.C. Markey and G. Thodos. "Removal of Heavy Metal Ions from Aqueous Solution with Fly Ash." Chicago, IL: Proceedings of the Second National Conference on Complete Water Reuse, May 1975, pp. 270-275.
23. M. Grover and M.S. Narayanaswamy. "Removal of Hexavalent Chromium by Adsorption on Fly Ash." Journal of the Institution of Engineers (India), Vol. 63, Part EN 1, October 1982, pp. 36-39.
24. K.P. Yadava, B.S. Tyagi, K.K. Panday and V.N. Singh. "Fly Ash for the Treatment of Cd (II) Rich Effluents." Environmental Technology Letters, Vol. 8, 1987, pp. 225-234.
25. K.K. Panday, G. Prasad and V.N. Singh. "Removal of Cr (VI) from Aqueous Solutions by Adsorption on Fly Ash-Woolastonite." Journal of Chemical Technology and Biotechnology, Vol. 34A, 1984, pp. 367-374.

26. T.J. Cha, G.R. Steiner and C.L. McEntyre. "Removal of Complex Copper-Ammonia Ions from Aqueous Wastes with Fly Ash." Journal of Water Pollution Control Federation, Vol. 5, No. 9, 1978, pp. 2157-2174.
27. K.K. Panday, G. Prasad and V.N. Singh. "Copper (II) Removal from Aqueous Solutions by Fly Ash." Water Research, Vol. 19, No. 7, 1985, pp. 869-873.
28. P.V.S.S. Prabhu, M.S. Narayanaswamy and T.S.S. Narasa Raju. "Adsorption of Zinc from Aqueous Solutions by Fly Ash." IAWPC Technical Annual, Vol. 8, 1981, pp. 46-52.
29. S.T. Gashi, N.M. Daci, X.M. Ahmeti, T.J. Selimi and E.M. Hoxha. "Removal of Heavy Metals from Industrial Wastewaters." In: Chemistry for Protection of the Environment 1987 (ed. L. Pawlowski et al.). Amsterdam: Elsevier Publishers, 1988.
30. A. Mathur, S.K. Khare and D.C. Rupainwar. "Removal of Heavy Metals from Main Sewer-Water of Varnasi City by Adsorption on Fly Ash and Blast Furnace Slag." Journal of Industrial Pollution Control (India), Vol. 5, No. 2, 1989, pp. 52-57.
31. C.H. Weng and C.P. Huang. "Removal of Trace Heavy Metals by Adsorption and Fly Ash." Arlington, VA: Proceedings of the 1990 ASCE Environmental Engineering Specialty Conference, 1990, pp. 923-924.
32. A.K. Sen and A.K. De. "Adsorption of Mercury (II) by Coal Fly Ash." Water Research, Vol. 21, No. 8, 1987, pp. 885-888.
33. A. Mathur and D.C. Rupainwar. "Removal of Lead from Polluted Waters by Adsorption on Fly Ash." Asian Environment, Vol. 10, No. 3, 1988, pp. 19-25.
34. R.B. Helm, G.B. Keefer and W.A. Sack. "Environmental Aspects of Compacted Mixtures of Fly Ash and Wastewater Sludge." Proceedings of the 4th International Ash Utilization Symposium, St. Louis, MO, March 1976, pp. 396-421.
35. D.F. Kincannon, A.F. Gaudy, Jr., W.F. Scriminger and W. Ricketts. "Some Effects of Western Coal Fly Ash on Municipal Sewage Sludge." Proceedings of the Fifth International Ash Utilization Symposium, Atlanta, Georgia, February 1979, pp. 898-903.
36. Standard Methods for the Examination of Water and Wastewater. Washington, DC: American Public Health Association, 1985.
37. G.A.K. Rao. Adsorption of Cadmium and Chromium from Wastewaters by Peat and Fly Ash, M.Sc. Thesis, University of Regina, Regina, Saskatchewan, Canada, 1989.
38. M.M. Dronamraju. Removal of Copper, Nickel and Zinc from Wastewater by Adsorption Using Peat and Fly Ash, M.Sc. Thesis, University of Regina, Regina, Saskatchewan, Canada.
39. A. Kapoor. Adsorption of Mercury from Wastewater by Peat, Fly Ash and Bentonite, M.Sc. Thesis, University of Regina, Regina, Saskatchewan, Canada.

REUSE OF PRETREATED COAL GASIFICATION WASTEWATER AS COOLING TOWER MAKEUP

Prof. M.S.Nie*, Prof. B.Z.Wang**, and Eng. Y.G.Zhao***
* Dept. of Science & Technology, Ministry of Construction, Beijing, 100835, China
** Water pollution Control Research Center, HACEI, Harbin, 150006, China
*** Northeast Coal Gasification Design & Research Institute, Shenyang, 110026

GOALS AND OBJECTIVES

Coal gasification wastewater, containing various high concentrated organic and inorganic contaminants, reuse and recycling is practiced in coal gasification plant for two primary purposes: to reduce wastwater discharge amount and to protect environment. Cooling systems are major consumers in many coal gasification plants. Therefore, reuse of pretreated coal gasification wastewater as cooling tower makeup may bring considerable saving in fresh water consumption and protection of environment.

It is possible to find a feasible approach for the reuse of coal gasification wasteweter with large amount discharge and various high concentrated pollutants. Some tests of pretreated wastewater for industrial cooling have been reported [1,2,3] . However, the reuse of the wastewater as cooling tower makeup presents both operating and environmental problems, especially in severe biological fouling and organic emissions.

The principal goals of the research project are to develop an advanced process for the treatment and reuse of gasification wastewater. Another object is to test alternative treatment method that may be necessary for

execution of gasification wastewater zero discharge.

WASTEWATER PRODUCTION AND PRETREATMENT

Wastewater tested in this study was the effluent from Lurgi fixed-bed gasification and coal cooking plant. Raw gasification wastewater pretreatment process for removing tar, phenolic compounds and ammonia was performed by a pliot. facility [4]. Flotation cell is used to remove residual suspended tars. Phenols and ammonia in the wastewater are reduced by an improved solvent extraction system with steam stripping [6] In the process, di--isopropyl ether is used as the solvent. 98% (fixed- bed gasification) and 95% (coal coking) phenol removal efficiecy and less than 100 mg/l phenol in effluent are obtained at a wastewater-to- solvent ratio of about 10: 1. After extraction, the wastewater is directly pumped to steam stripping colum. By separating distillate, 98% recovery efficiecy of ammonia and 99% recovery efficiecy of the solvent dissolved in the wastewater are obtained.

The next step of the pretreatment involves biological oxidation and dualmedia filtration to remove organic contaminants and suspended solids.

Table 1 and 2 show the average composition of the fixed--bed gasification and coal coking wastewater before and after each of these pretreatment respectively. As shown in table 1 and 2, after these pretreatment, the wastewater characterization doesn't meet the national discharge criteria . As shown in the late, it can be reused as makeup in an evaporative cooling tower.

TABLE 1 AVERAGE WASTEWATER CHARACTERISTICS FOLLOWING EACH PRETREATMENT STEP (FIX-BED GASIFICATION)

Constituent*	Raw Wastewater	Solvent Extraction Effluent	Steam Stripping Effluent	Activated Sludge and Filtration Effluent
COD	38500	20800	2900	670
BOD_5	15600	--	1518	40
Phenol	2450	48	36	0.42
Ammonia	1300	1250	210	163
Sulfide	48	38.4	18.4	14.4
Cyanide	3.5	0.27	0.04	0.013
pH	9.77	9.18	8.7	7.6
Oil	8328	273	40	23
Fatty acid	85	43.7	1.5	0.067

* All concentrations in mg/l except pH

TABLE 2 AVERAGE WASTEWATER CHARACTERISTICS FOLLOWING EACH PRETREATMENT STEP (COAL COKING)

Constituent*	Raw Wastewater	Solvent Extraction Effluent	Steam Stripping Effluent	Activated Sludge and Filtration Effluent
COD	25000	13500	2783	510
BOD_5	2970	--	1025	38
Phenol	1285	70	45	0.51
Ammonia	1520	1515	180	185
Sulfide	23	14.8	4.87	4.4
Cyanide	9.86	9.36	9.6	6.48
pH	9.08	9.10	8.4	7.18
Oil	300	170	110	74.7
Fatty acid	81.6	38.9	0.24	0.11

* All concentrations in mg/l except pH

COOLING TOWER EXPERIMENTAL PROCEDURES

Two series (phase 1 and 2) were conducted by using fixed-bed wastewater showing in Table 1. A series (phase 3) was conducted by using coal coking wastewater showing in Table 2. The most significant difference between phase 2, 3 and phase 1 was biocide addition which was used to control biological fouling. Another difference between phase 2, 3 and phase 1 was filtration which was used to reduce Suspended Solid in the cooling water. A schematic of the test cooling tower system is presented in Figure 1. The cooling tower design parameters are as the following liquid-to-gas ratio 1:830 m^3/m^3, flow per unit area of packing sufac: 11.8 m^3/m^2 . The design cooling range of 10 ℃ to 15 ℃ and 10 cycles of concentration were maintained in each of the three tests. A 300 l/h cooling water circulation rate, a 6l/h pretreated wastewater makeup rate, and a blowdown rate of approximately 10% of the makeup were kept in order to maintain 10 cycle operation. In addition to hydraulic control, during day-to-day operation of both segments of all phase tests, the cycles of concentration were monitored using the concentration of sodium ions. All three tests were run for 350 hours.

As shown in Figure 1, the blowdown water was pumped into an evaporator, in which the water was futher concentrated by 10 times and condensate was return to the basin. Therefore only opproximately 1 % of the wakeup was discharged. Cooling water in the tower basin is pumped through a test heat exchanger wich can be used for measuring the steel corrosion both of carbon and stainless steel and monitoring fouling and heat transfer performance. The test heat exchanger was equipped with carbon stell tube, and operated with tube-side fluid velocity of 1. 0 m/sec. The shell side was heated by steam.

During phase 2 and 3 the biocid (ClO_2) and bypass filtration were added. The biocid was added every six hours with dosage of 20 mg/l (calculated on tatol cooling water volum). The flow rate of bypass filtration was 8 l/h.

COOLING TOWER TEST RESULTS

Characterization of Water. The average makeup and cooling water analysis results for all phase 1. 2 and 3 are presented in Table 3. The most significant difference between phase 1 and phase 2. 3 was the concentration of

suspended solids. TSS of phase 2, 3 was significantly reduced 1/2 comparing with phase 1. This is likely due to the biocide addition which led to reduced bacterial population. In phase 1, without biocide, the counts of total bacteria in the cooling water was 8.2×10^{7} /ml. In both Phas 2 and 3, used ClO_2 as biocid, the counts was less 1.5×10^{4}/ml. It appears that ClO_2 is a effective biocide for cooling tower operating with pretreated coal gasification wastewater as makeup.

TABLE 3 ANALYSIS RESULTS OF WATER FROM THE TESTS

Constituent*	Fixed-bed gasification				Coal cooking	
	Phase 1		Phase 2		Phase 3	
	Makeup	CW	Makeup	CW	Makeup	CW
COD	697	3787	669	4828	510	4211
BOD_5	40	88.4	38	248	36	250
Phenol	0.4	1.2	0.42	1.6	0.51	1.7
Ammonia	155	1020	155	1015	185	400
Alkalinity	175	825	195	445	115	325
Calcium	4.16	24.3	19.5	90	12	62.5
Sodium	57.1	588	61.8	583	42.6	423
Magnesium	4.19	8.35	2.56	22.2	3.51	31.6
TSS	48	1840	40	540	110	780
TVSS	0.52	0.53	0.53	0.25	0.52	0.54
TDS	830	5156	916	6718	1448	11942
TVDS	536	3642	548	4242	960	7586
pH	7.1	8.62	7.8	8.7	7.78	8.9
Conductivity	0.0132	0.0876	0.013	0.074	0.034	0.138

* All concentrations in mg/l, conductivity in ms

System Fouling. Figure 2 illustrates the rates of fouling and heat transfer coefficient loss in carbon steel tubes observed in all three test phases. All tests showed that the heat transfer coefficent loss was zero after 200 hours. Figure 2 showed the HTC during first 200 hours for each test. As shown in Figure 2 both the rate of fouling and heat transfer coefficient loss in phase 1 were greater than that in phase 2 and 3. It is indicated that the use of ClO_2 as biocide tested in phase 2 and 3 was beneficial for the reduction of biofouling, because the use of biocide (ClO_2) can control the extent of biological deposition that happened in phase 1. Calculating on the basis of the Kern-Seaton Model [6], the limit of fouling thermal resistance for phase 2 and 3 tests was 3.324×10^{-4} and 5.86×10^{-4} $m^2\cdot h\cdot ℃$ /Kcal respectively. The relationship between fouling thermal resistance (R) and time (t) is as follwing:

For the pretreated fixed-bed gasification wastewater

$R = 3.324 \times 10^{-4} (1-e^{-0.0086t})$ $m^2 \cdot h \cdot ℃ /kcal$

For the pretreated coal coking wastewater

$R = 6.86 \times 10^{-4} (1-e^{-0.0078t})$ $m^2 \cdot h \cdot ℃/kcal$

Corrosion. Corrosion rates in the cooling tower system were determined using weight loss coupons. Table 4 presents a summary of the corrosion rate during the all three bases tests. As showing in Table 4, the highest corrosion rate always occured at heat exchanger outline where the temperature of cooling water was the highest. The corrosion rates for carbon steel varied from 0.0036-0.037 mm/y for the various locations, and for stainless steel varied from 0.0002-0.0014 mm/y.

TABLE 4 CORROSION RATES DURING THE TESTS (mm/y)

Metallurgy	Location	Phase 1	Phase 2	Phase 3
Carbon steel	Basin	0.0036	0.0066	0.0078
Carbon steel	HE inlet	0.0164	0.0144	0.0039
Carbon steel	HE outlet	0.0385	0.0182	0.0280
1Cr18Ni9Ti SS	Basin	0.0019	0.0014	0.0014
1Cr18Ni9Ti SS	HE inlet	0.0005	0.0002	0.0010
1Cr18Ni9Ti SS	HE outlet	0.0024	0.0014	0.0014

Based on measuring corrosion rates from each of these tests, corrosion wasn't a significant problem for reusing pretreated gasification wastewater as makeup. These low corrosion rates indicated that the pretreated wastewater from fixed- bed gasification or coking were suitable for makeup to a cooling tower without the addition of corrosion inhibitors. This is likely due to that some organic materials (phenols and cycnide et al.) in the wastewater act as inhibitors.

CONCLUSIONS

Several conclusions can be drawn from the data collected during the three Phases of cooling tower reuse testing with pretreated Lurgi fixed- bed gasification and coal coking wastewater. Use of these wastewater as direct makeup to a cooling tower resulted in a high level of biological activity, which influenced the fouling and heat tranfer performence of the equipment in test process. The steel corrosion both carbon and stainless steel in these operations were not high which would be acceptable in a commercial use.

The Phase 2 and 3 indicated that reuse pretreated gasification wastewater was suitable for makeup to a cooling

tower with the biocide (ClO_2) addition. The limit of fouling thermal resistance of the Lurgi fixed- bed gasification and coal coking wastewater was 3.24×10^{-4} and $5.86 \times 10^{-4} m^2.h.℃$ /kcal repectively; the highest carbon steel corrosion was 0. 0182 and 0. 028 mm/y respectively and the highest stainless steel corrosion were 0. 0014mm/y for both. All those results well meet the national criteria of China. These results have led us to conclude that Lurgi fixed- bed gasification and coking wastewater, after removal tar, extraction phenol, stripping ammonia, biological oxidation and dualmedia filtration treatment, will make a suitable cooling tower makeup at ten cycles of concentration with the addition of biocide (ClO_2) and without the addition of corrosion inhibitors. The study also showed that the reuse of this streams were beneficial both for water resource saving and reducing environmental pollution due to the reduction of wastewater discharge.

REFERENCES

1. Sheila J. Galegher, et al. Pilot- Scale Treatment and Cooling Tower Reuse of Gasification Wastewater. DOE/FE/60181-132, 1985.
2. Sheila J. Galegher, et al. Evaluation of Treated Gasification Wastewater As Cooling Towe Makeup. DOE/FE/60181-130, 1985.
3. W. G. Willson, et al. Pilot- Scale Treatment of Gasification Wastewater and Reuse in A Cooling Tower. DOE/FE/60181-74, 1985
4. 《The Report for Pilot Scale Extraction and Stripping Tests for Gasification wastewater 》. Northeat Coal Gasification Disign & Research Institute, 1990.
5. China Patent. 91104418. 3
6. Donalc. Kern and Ralph E. Seaton, Surface Fonling, Chem. Engi. Pro. 1959 Vol. 55. No. 671-73.

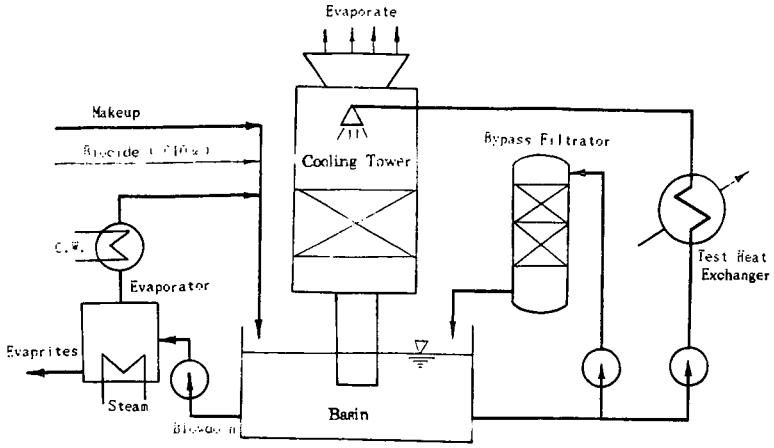

Figure 1 — Schematic of the Test Cooling Tower System

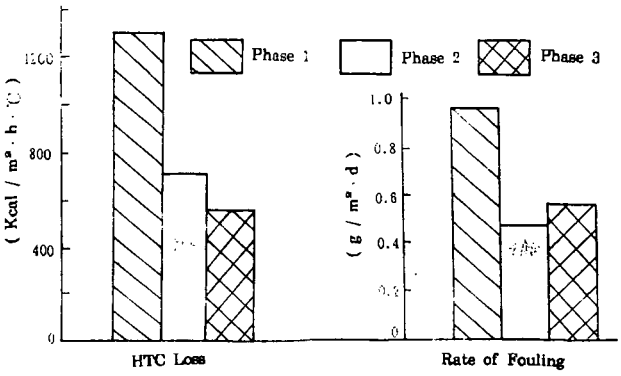

Figure 2 — Results of Average Fouling and Heat Transfer Coefficient Loss in Carbon Steel Tube

RETORTING POTENTIAL OF LIGNITE OVERBURDEN FROM CLAY MINING

J.C. Hower, U.M. Graham, R.F. Rathbone, and T.L. Robl

University of Kentucky
Center for Applied Energy Research,
Lexington, KY 40511-8433

Keywords: Lignite, Pyrolysis, Oil Yields

Lignite is found in the Eocene formations in the Gulf Coast Province from Texas north to Kentucky and east to Georgia. Commercial development of the lignite as an energy resource is currently confined to Texas and Louisiana where mine-mouth power plants are large consumers of lignite. The lignite in other Gulf Coast Province states is not mined as a product at the present time.

Lignite is present in the eight-county Jackson Purchase region of Kentucky at the northern end of the Mississippi embayment. The Claiborne Formation, the primary lignite-bearing formation in Kentucky, is dominated by clay deposits with associated lignites and sands. The lignite and clay bodies were deposited as narrow elongate deposits, which resulted from the filling of oxbow lakes over periods of 500 to 1500 years. The axis of the fluvial depositional system migrated east then back to the west over the course of the Claiborne deposition.

The lignite sample was obtained from the Eocene Claiborne Formation, Milburn 7½ minute quadrangle, Carlisle County, Kentucky. Lignite is removed as overburden in the mining of ball clay from the Eocene of Kentucky's Jackson Purchase region, but is not currently mined as an energy resource but rather is a waste product. About 160 kt of clay was mined in 1991 (Kentucky Department of Mines and Minerals) with an estimated 40 kt of lignite moved in the process. The high moisture, low heating value lignite has not been competitive as an energy resource due to its proximity to the higher quality bituminous coals in the nearby Illinois Basin and, more recently, to the import of Powder River Basin coals into the lower Ohio River Valley. In this study, we examine potential uses of the lignite which could provide the opportunity to develop it as an added resource along with the clay.

Results and Discussion

Petrography of the Lignite

The petrography of the lignite is rather typical of other lignites from the region in having a high percentage of detrital macerals: humodetrinite and liptodetrinite (Table 1). Petrographic analysis of those macerals is difficult owing to their fine (generally less than 10 μm) size and consequent difficulty of resolution in either white-light or blue-light microscopy. Blue-light excitation is an aid in resolving some liptinite macerals in complex mixes. Liptinite macerals

in this and other Kentucky lignite samples evolve mobile constituents in the form of the maceral fluorinite. The reflectance of lignite is typically measured on ulminite. The low percentage of ulminite in this lignite limited the number of measurements. Ulminite reflectance was determined to be 0.21%, consistent with previous samples from the same mine. The petrology of the Eocene lignites in the Jackson Purchase region was discussed by Hower et al. (1990).

Pyrolysis of the Lignite Sample

The lignite sample was retorted in N_2-swept fixed bed experiments. The production of oil from a waste overburden, such as the present lignite, would make the economics of clay mining in this region even more attractive. Accordingly, the lignite sample was first ground to a grain size of 18 x 20 mesh and fed into a retort to establish the lignite's oil yield potential. The N_2-swept fixed bed experiments were performed in a 1.5 inch stainless steel reactor. Oil vapors and sweep gas passed through a 100 micron filter at the base of the reactor. Heating rate was 4° C/minute with a maximum bed temperature of 550 °C. The reactor conditions are discussed in detail by Rubel and Coburn (1981). The objective of this part of the research was to obtain the oil yields of the lignite sample. Results of the retorting experiments indicate that 11.7 wt % oil may be obtained during pyrolysis.

The oils derived from the lignite are very waxy. Large amounts of water were also captured during the retorting of the lignite sample. Because most of the water was released before the sample was heated to above 150 °C it may be concluded that only small amounts of structural water were released by clay minerals which occur as ash components within the lignite sample.

The processed lignite sample was analyzed for carbon, hydrogen, nitrogen, and sulfur using automated LECO elemental analyzers. Ultimate and proximate analyses of the retorted lignite sample are illustrated in Table 2. The majority of the moisture was released during pyrolysis. After pyrolysis the retorted lignite sample was found to have very high fixed carbon values [Table 2].

Heating Stage Microscopic Examination of the Lignite Sample.

The heating stage microscope (HSM) apparatus utilized in this study consists of a Zeiss Universal polarized light microscope, a heating stage, and temperature and gas flow controllers. A polished shale sample was positioned in the heating chamber and could be observed at any time using a polarized light microscope. The sample chamber consists of three quartz plates which help to channel the preheated N_2-gas flow above and below the sample for optimum temperature control. The hot stage was equipped with a monitor and video camera for real time observations. Most importantly, the HSM -apparatus allowed the *in situ* observation of the pyrolysis process of the lignite sample.
Because the HSM-study permitted the use of larger lignite particles than those used in the reactor, the retorted parts were big enough to preserve the spatial relationships between the charred macerals, mineral matter and macro-pores that were generated during oil evolution.

Observations of the process induced macroporosity in the retorted (spent) lignite sample were made possible using a scanning electron microscope (SEM; Hitachi 2700-S), which allowed a magnification of the sample by $x10^4$ times. Structural changes in the retorted lignite sample are documented in Figure 1 and Figure 2. The SEM results indicate that volatilization of macerals causes a complex network of macropores to develop which typically have the shape and size of the macerals in the raw lignite. A multitude of cracks also formed throughout the lignite sample (Figure 1), which probably aid in the escape of the oil vapors. Prior to pyrolysis, cracks were not observed in the lignite sample (Figure 1).

Not all of the macerals contribute to the oil phase when heated in the retort. The pyrolysis residue was primarily composed of uniformly reflecting isotropic semi-coke and unreacted inertinite macerals, primarily sclerotinite. Semi-coke with the texture of the huminite maceral textinite was observed. Other huminite macerals, and perhaps a portion of the liptinite component, are preserved as a porous semi-coke with little preservation of the original morphology. Anisotropic semi-coke, perhaps as a retrograde product of evolved liquids, was a rare component. Pyrrhotite was observed, but silicates are the more common mineral form in the residue.

Summary and Conclusions

Lignite is presently removed as overburden in the mining of ball clay in the eight-county Jackson Purchase region of Kentucky rather than mined as an energy resource. Although this is mainly due to the fact that higher quality bituminous coals are mined locally, the removal of the lignite causes both environmental and economical concerns. This lead to the objective of this study to examine potential uses of the lignite to be utilized as an added resource along with the clay. Liquid product recovery after pyrolysis of the lignite indicates that this waste product contains 11.7 wt % of oil. Furthermore, a carbon-rich solid remains after pyrolysis. Upon retorting the lignite was observed to have formed an intricate network consisting of variously sized pores and charred carbonaceous material. Heating stage microscope (HSM) observations helped to establish the spatial relationships between process induced pores and char. In addition, the HSM-experiments allowed the precise determination of the boiling temperature when constituents in the macerals start to vaporize. The development of a porous structure in the carbon-rich pyrolysis residue of the lignite under investigation may indicate the lignite's potential as source material for the production of adsorbent carbons. Utilization of the lignite in the production of liquid fuels, and possibly as carbon precursor, may help in the regulation of a waste material.

Acknowledgements The Authors would like to thank G. Thomas, M. Moore, and M. Spears for analytical and technical support.

References

1 Hower, J.C., Rich, F.J., Williams, D.A., Bland, A.E., and Fiene, F.L., 1990, Cretaceous and Eocene lignites, Jackson Purchase, Kentucky: Int. Journal of Coal Geology, v. 16, p. 239-254.

2 Rubel, A.M. and Coburn, T.T., 1981, Eastern Oil Shale Symposium, Kentucky Energy Cabinet, Lexington, KY, p. 21

Table 1 Maceral Composition of the Lignite

Maceral	Sample 91999 (W. KY)
Textinite	0.7
Ulminite	3.5
Humodetrinite	35.1
Gelinite	0.4
Corpohuminite	5.5
Fusinite	3.3
Semifusinite	0.3
Sclerotinite	1.1
Inertodetrinite	0
Exinite	6.3
Resinite	2.3
Suberinite	1.6
Liptodetrinite	39.1
Alginite	0.8

Table 2 Ultimate and Proximate Analyses of Raw and Pyrolyzed Lignite Sample

	91999	91999	91999	91999p	91999p	91999p
	as rec.	dry	daf	as rec.	dry	daf
Moisture	10.97					
Ash	19.11	21.16		3.21		
Volatile Matter	51.30	57.62	73.36	35.53	36.71	
Fixed Carbon	18.60	20.89	26.64	21.64	22.36	35.33
Carbon	50.00	56.16	71.50	39.60	40.91	64.67
Hydrogen	6.03	5.39	6.86	56.11	57.97	91.59
Nitrogen	0.96	1.08	1.37	2.15	1.85	2.92
Oxygen	11.85	14.70	18.73	1.07	1.11	1.75
Sulfur	1.08	1.21	1.54	0.52	0.90	1.43
Heating value (Btu/lb)	8690			1.41	1.46	2.31
Heating value (MJ/kg)	20.26					

91999 = lignite raw sample 91999p = pyrolyzed lignite sample

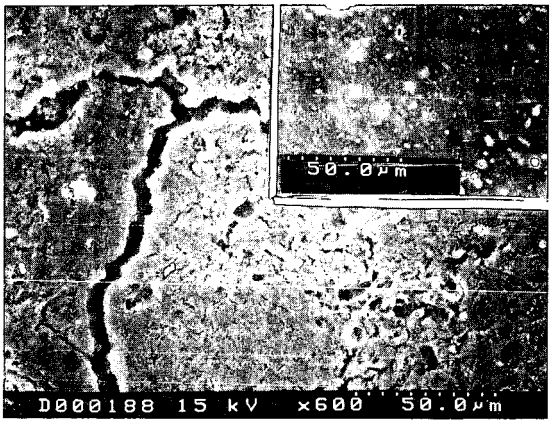

Figure 1 SEM-microphotograph of a polished section of the lignite sample. The insert presents the raw lignite sample before the heating stage microscope (HSM) experiment. The polished lignite surface shows only minimal signs of cracks or pores. The main photo shows the surface of the lignite sample after pyrolysis in the HSM. The surface is characterized by abundant cracks of various sizes and large amounts of elongated macropores.

Figure 2 Magnification of lignite sample shown in SEM-microphotograph of Figure 1. Macropores develop during pyrolysis. The spatial relationship among macropores, and that of the macrostructure stabilizing char and mineral matter are preserved during the HSM experiments.

Fractionation of Coal Extracts with Bacterial Enzymes.

Leonard L. Matz
Matz & Associates
3061 Bishop Road
Appleton, NY 14008

ABSTRACT: Common and novel bacterial enzymes or *de novo* synthesized unique organic ethers reacted with Coal extracts yielding coal breakdown products. The diphenyl ether was synthesized *de novo* from methyl benzoate and 1-Diphenyl-1,3-butanedione preparation of the di-cation of butanedione with the aid of sodium hydride (NaH). After synthesis of 2,6-Diphenyl-4-methoxypyridine and other less common ethers, dissolution of coal fractions yielded various levels of carbon fragments. Ether extraction of Coal (Illinois No. 6) resulted in release of aromatic and short chain fractions. Enzymatic dissolution of Coal and ether extracts also yielded identifiable carbon fragments. Specific enzymatic dissolution of Coal with pure flavin containing enzymes remains a goal. This approach involves: 1-more complete kinetic characterization of the proposed NADPH Reductase/comproportionation system, 2-initial experimentation into flavodoxin components common to both the Nitrogenase system and the electron transport system of *Azotobacter vinelandii*, 3-the degree of complementarity between these systems judged by component interaction and immunologic cross reactivity.

INTRODUCTION: *De novo* synthesized ethers reacted with Coal Extracts yielding breakdown products (1). A novel pyridine ether (I) synthesized *de novo* from 1-Phenyl-1,3-butanedione and methyl benzoate and two more common pyridine ethers (II & III) solubolized dried Coal Extracts (Fig.1).

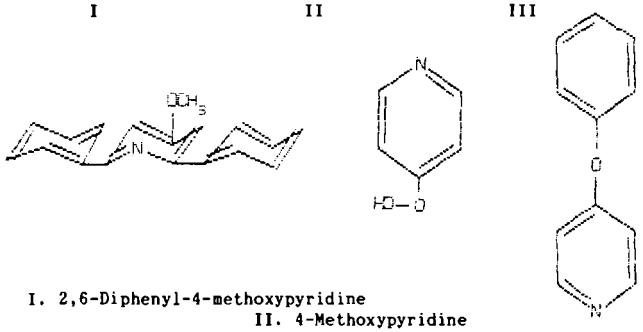

I. 2,6-Diphenyl-4-methoxypyridine
II. 4-Methoxypyridine
III. 4-Phenoxypyridine

Fig 1. Organic Structures

The purpose of these experiments, in general, is to differentiate the ultrastructure from that of living structure such as the bacterial spore. In particular, unlike bacterial spores that possess easily discernible pore sizes, coal is much more difficult to approximate because of its local regions of heterogeniety. That is unlike bacterial spores, different regions of the coal ultrastructure apparently differ markedly from other domains of the ultrastructure. Interaction of the pyridine ethers with the coal structure can considerably curtail interpretation. However, the study reported above

describing the abbreviated exposure of 4-methoxypyridine pyridine to coal assumes limited if not exclusionary chemical reaction with the coal. The ultrastructure of coals is susceptible to study using small molecular weight organic molecules that are not susceptible to alternation by the interior of the coal pores. In these experiments commonly accepted organic molecules that are very resistant to alternation in such organic milieu, ethers. Theoretically these molecules can be used as molecular sieves to approximate the size of coal pores. Unfortunately, the pyridine ethers are somewhat unreasonable solvent because they react with the coal ultrastructure after prolonged periods of time. Generally, however, the ethers and the enzymes reactions with the coal were understandable and provided valuable data.

RESULTS:

1,5-Diphenyl-1,3,5-pentanetrione 1,5-Diphenyl-1,3,5-pentanetrione, the enolate carbanion of 1-phenyl-1,3-butanedione, formed after proton extraction with sodium hydride in the aprotic solvent, 1,2-dimethoxy ethane (monoglyme). Condensation of this carbanion with methyl benzoate yielded the triketone, 1,5-diphenyl-1,3,5-pentanetrione. This aroylation apparently involves the di-anion of the B-diketone which forms in a

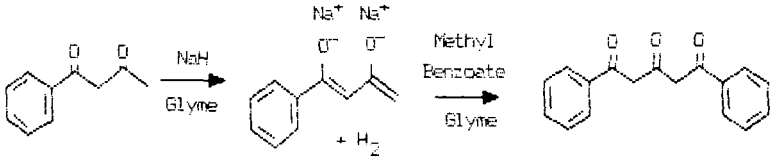

Fig. 2. Synthesis of 1,5-Diphenyl-1,3,5-pentanetrione

"step-wise" extraction of its a-hydrogens. The terminal a-hydrogen is not the first extracted from the b-diketone, but is only extracted after mono-anion formation and in the presence of methyl benzoate. The terminal a-hydrogen is, however, the site of reaction of the b-diketone with the carbonyl carbon of the ester. The methoxide group of the ester, neutralized by the Na+ counter ions, then leaves the condensation product. Exposure to air with its incipient moisture and neutralization of the reaction mixture with 6N HCl provide the protons for neutralization of the carbanions present and formation of the triketone.

This reaction occurs with a high degree of efficiency yielding 80-90% product (86.9%). Apparently once formed, the di-anion is quite reactive and the reaction is evidently highly selective for the terminal carbon of the dianion. As expected, the symmetric triketone formed, was soluble in diethyl ether, but its solubility varied considerably depending on the pH of the reaction mixture.

These differences could be a reflection of minor changes in the structure of the triketone. The spectral data substantiates that they are not reflective of impurities present. Variation of the color, crystalline form and melting points of the triketone which substantiate similar earlier observations are also suggestive of small variations in the structure of the triketone. Because of the H-bonding, various keto-enol tautomeric forms can be envisioned and as pH changes occur in the solvent all of these forms are undoubtedly present in the solution. At low pH values the triketone is probably found as a doubly H-bonded enolic structure (Formula 4), at intermediate pH values as a mono-H-bonded structure (Formula 2) and at high pH values as a keto form (Formula 1) with little H-bonding.

2,6-Diphenyl-4H-pyran-4-one The triketone can be protonated in concentrated sulfuric acid in the 1-or 5-keto position leading to the formation of enolic

triketones. The triketone is then cyclized by the formation of an intramolecular acetal. Upon dehydration the pyran is completed yielding the 2,6-

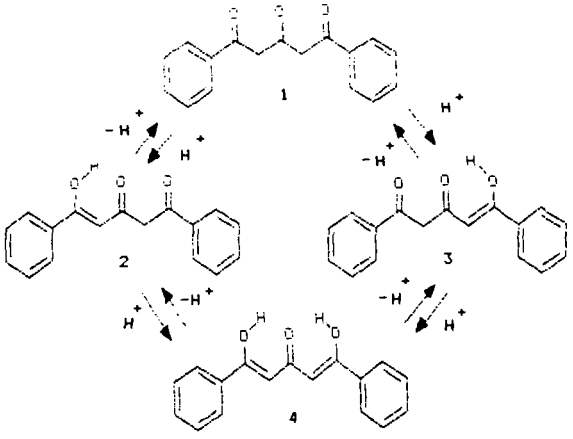

Fig. 3. Hydrogen Bonding of 1,5-Diphenyl-1,3,5-pentanetrione

diphenyl-4H-pyran-4-one. The reaction occurs with great efficiency (89-91%) suggesting that the stability of the 6-membered ring in the product is the selecting factor in the formation of the pyran derivative.

2,6-Diphenyl-4(1H)-pyridinone This pyridinone was produced by the cyclization of the 1,5-diphenyl-1,3,5-pentanetrione with liquid ammonia. Because of the high pH of the reaction milieu, which causes the enolization of the ketone groups, the addition product is the primary amine-enol or dienol intermediate.

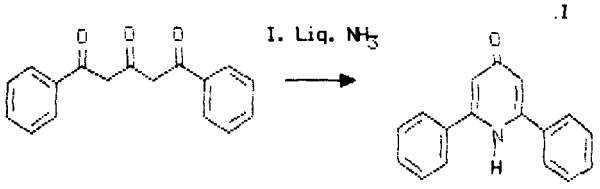

Fig. 4. Synthesis of 2,6-Diphenyl-4(H)-pyridinone

Cyclization by addition of the primary amine to the other terminal carbon of the pentanetrione chain then readily occurs (Table 1).

This di- or trienolic structure is then dehydrated to form the highly conjugated diphenyl-pyridine derivative with its quinoid-like pyridine ring. Noteworthy in this synthesis is the modification of the original synthetic procedure by addition of the dehydrating agent, sodium sulfate, to the reaction milieu. The combination of the anhydrous ethanol and sodium sulfate promoted the reversible dehydration of the product and gave an increase in yields of 32.3-35.4 to 66.6-75.1%.

Table 1. Physical Properties of Synthetically Prepared Precursors and Ethers

This addition had little effect on the physical properties of the product. The yields were also increased from a literature value of 45% to an average value of 70% in our experiments. Also, sodium sulfate added in only the second step was equally effective. In the presence of this additional dehydrating agent, the efficiency of the reaction is quite high. Because the product pyridinone is highly conjugated investigators have obtained its UV spectrum. This property and the electronic configuration around the heterocyclic nitrogen, suggest that the molecule may be

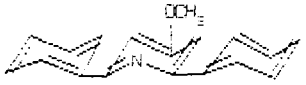

Fig. 5. 2,6-Diphenyl-4-Methoxypyridine (A)

planar even though this would involve an eclipsed conformation of the phenyl rings (A) and the pyridinone. Steric hindrance would not preclude this possibility, since the phenyl rings could move freely about the carbon to connecting them to the heterocyclic ring. The heterocyclic ring is of a quinoid not benzenoid configuration which disallows enol formation of the keto group in the C-4 position. The highly conjugated nature of the pyridinone allows little stereochemical analysis of the molecule which contains no asymmetric carbon, but the presence of two chiral centers during the closure-dehydration mechanism suggests specificity of the protons lost from the C-3 and C-5 positions as dehydration occurs. The formation of the double peak feature at 3090 and 3140 cm-1 not found in the original triketone, is evidence of the presence of the heterocyclic This coincides with the loss of some of the carbonyl intensity and features. This is also strongly suggested by the loss of IR features from 900-1299 cm-1. The NMR spectrum also reveals the downfield migration of the non-aromatic protons of the triketone to the C-3 and C-5 protons of the heterocyclic ring. The signal for these protons occurred within the signal for the three terminal protons of each phenyl ring of the pyridinone. It could be observed when using a sweep width of 250 instead of 500 Hz. The proton of the heterocyclic nitrogen was not observable even at a chemical shift of 15 ppm. Mass spectral analysis revealed a molecular peak at 247 me units and the usual fragments associated with the molecule. The synthesized pyridinone possessed the literature values of the physical properties. In addition, the physical properties of the triketone and pyran were considerably different. These results suggest because of their interdependence that the structural parameters attributed to these isolates are consistent and reputable.

Enzymatic Properties

Enzymological Purification of NADPH:Flavodoxin Oxidoreductase Ten to fifteen mgs of purified reductase remained after purification of 220 times from the 250,000 x g supernatant. Gel filtration of the FLD reductase succeeds only on large diameter pore size gels, i.e., Sepharose 2B or 4B or Ultragel-32. This suggests either a very large molecular weight enzyme, complexation of the enzyme with other proteins, or polymerization of a small molecular weight enzyme into large aggregates. Spectra of the flavin group of the enzyme undergo reduction by light and EDTA. The absorption spectrum of Flavodoxin Oxidoreductase that contains a FAD residue as a prosthetic group is sensitive to EDTA reduction in light.

Enzymological Properties Purified FLD reductase shows little selectivity of substrates and reaction rates appear entirely dependent on the redox potential of the substrate. Progress curves of $FLDH_2$ formation are biphasic and suggest an initial rapid rate of $FLDH_2$ formation (0-2 ms) and a second more persistent $FLDH_2$ formation (2-12 ms) (Table 2). Double reciprocal plots of either rates are straight lines over a limited range of substrates concentration (15-50 mM FLD_{Av}). The initial rate of formation of $FLDH_2$ resides within the reduction rate range described for the other electron acceptors. The Km of $FLDH_2$ formation is also quite comparable to that of the other electron acceptors (Table 2). The change of K_m at 2 ms

Table 2. Enzyme Parameters and Kinetic Constants of the Enzymatic Reduction/Comproportionation of FLD_{Av} and the Me-FLD_{Av}.

of K_m at 2 ms is consistent with the idea that the affinity of the FLD for the FLD reductase changes as the $FLDH^*$ concentration increases. If this is the operative mechanism of FLD_{Av} reduction that is quite consistent with the fluorescent data, it suggests that NADH reduces FLD then the $FLDH_2$-NAD^+ complex reduces FLD_{Av}.

Enzymological Reactivity

Spectrophotometric Assay: The enzymatic reduction of both FLD and N_3-CH_3-FLD straight forwardly demonstrates the primary formation of $FLDH^*$ and its analogue. The initial velocity (v_0) was 10% larger for substituted flavodoxin indicating that it is a better substrate. The formation of N_3-CH_3-$FLDH^*$ also remains more sustained producing 32% of the possible N_3-CH_3-$FLDH^*$ in the first 10 ms of reduction. During the same period 16% $FLDH^*$ undergoes reduction. Second order rate equations facilitated quantitation of these kinetic differences.

Product Formed Graphic representation of the hydroquinone formation (Reaction 1) exhibits a shift from one constant (k_{1a}) to another (k_{2a}) as the reaction proceeds. The duration of the initial kinetic parameters varies greatly from native to substituted flavodoxin. The modification of the initial rate (slope) occurs more quickly and completely with FLD. This modification accelerated by ionic strength, causes further displacement of the 5 mM Tes, line toward the x-axis at 25 mM Tes. Contrariwise, these ionic strengths don't affect the secondary kinetic constants because the slopes remain constant. The dFLDH*/dti is about as large at 25 mM Tes. Its formation is linear throughout the observed reduction.

Enzymological Properties of NADH:Ferricyanide Dehydrogenase: Topological and ultrastructural membrane features accrued during comparison of walled, *Staphylococcus aureus*, and wall-less, *Acholeplasma laidlawii*, bacterial membranes. Osmotic lysis of protoplasts of these organisms produced membrane vesicles or large membrane fragments, but alumina grinding or sonication of these protoplasts or cells produced much smaller particles whose morphologic origin was difficult to determine. Disrupted membranes from either organism were covered with ribosomes from 15 to 30 nm diameter adhering almost exclusively to the inside of the vesicles or fragments.

An NADH dehydrogenase possessing a specific activity 3-5 times that of membrane bound enzymes was obtained by extraction of *A. laidlawii* membranes with 9.0% ethanol at 43° C. This dehydrogenase contained only trace amounts of iron (suggesting an uncoupled respiration), a flavin ratio of 1:2 FAD to FMN, and 30-40% lipid, which could explain its resistance to sedimentation. It efficiently utilized ferricyanide, menadione and dichlorophenol indophenol as electron acceptors, but not O_2, ubiquinone Q10 or cytochrome c. Lineweaver-Burke plots of the dehydrogenase were altered to linear plots of the dehydrogenase were altered to linear functions upon extraction with 9% ethanol. In comparison to other respiratory chain-linked NADH dehydrogenases in cytochrome containing respiratory chains, this dehydrogenase was characterized by similar K_m's with ferricyanide, dichlorophenol indophenol, menadione as electron acceptors, but considerably smaller V_{max}'s with ferricyanide, dichlorophenol indophenol, menadione as electron acceptors, and smaller specific activities. Some kinetic properties of the dehydrogenation, the uniquely high glycolipid content and apparently uncoupled respiration at Site I characterized this NADH dehydrogenase from this truncated respiratory chain.

DISCUSSION:

Studies revealed hydrogen bond activation of alkyl-aryl ethers (I) toward cleavage by formation of its mono- then di-anion and combination with methyl-benzoate. These reactions provide good yields due to the driving force of the charged molecular species. Our yields provide excellent conditions for continued synthesis of ether precursors. Unfortunately, the inefficiency of the diphenyl-chloropyridine and the phenyl-ether synthetic steps limited the total yields of ethers.

Current thinking now suggests that coal is an elastomer in which strong internal hydrogen bonding gives it high internal glass transition temperatures. The same acidic hydrogen donors and basic hydrogen receptors that provide strong hydrogen bonds in the bulk structure populate the surface of coal powders. A dominant property of this molecule is the H-bonding capacity of the 2,6-diphenyl-1,3,5-pentanetrione. A variety of physical properties reflected this dominating molecular effect during isolation procedures.

REFERENCES:

1. Matz, L. L. & Buchanan, D. H. Synthesis and Characterization of Pyridine and 2,6-Diphenylpyridine Ethers, *C&E News*, 1990, 69, 69.
2. Ryan, M. D., Noker, P. E. & Matz L. L. Immunologic Properties of Glycolipids from Membranes of *Acholeplasma laidlawii*. Infect. Immun. 1976, *12*, 799.
3. Weiner, D. W. & Matz, L. L. Topologic and Ultrastructural Features of Membrane from *Acholeplasma laidlawii*. Microbios 1976, *15*, 7.
4. Jinks, D. C. & Matz, L. L. Purification of the Reduced Nicotinamide Adenine Dinucleotide Dehydrogenase from Membranes of *Acholeplasma laidlawii*, Biochim. Biophys. Acta. 1976, *452*, 3041.
5. Matz, L. L. *NADPH Dehydrogenases of Terminal Electron Transport Systems, Emerging Technologies for Hazardous Waste Management*; Tedder, W. D., Ed; Hazardous Waste Mansgement; ACS Press, Washington, D.C., 1993, 2, pp .
6. Matz, L. L. *Flavodoxin Hydroquinone-(1,5-Dihydroflavin)-as the Energy Source for Biological Nitrogen Fixation by Azotobacter vinelandii*; Himmel, M. E., Overend, R. P. & Baker, J. O., Ed.; Bioconversion for Fuels; ACS Press: Washington, D.C., 1994, 1; pp .

SUMMARY:
1,5-Diphenyl-1,3,5-pentanetrione was cyclized to form 2,6-Diphenyl-4(1H)-pyridinone with liquid ammonia. The resulting ether, 2,6-Diphenyl-4-methoxypyridine, from substitution of the keto (C-4 position) of the pyridinone, was used to extract Coal. Several extraction treatments of Coal based upon enzymatic treatment of extracted coal are foreseen.

Table 1. Physical Properties of Synthetically Prepared Precursors and Ethers

Name	Recrystallization Solvent	Color	Mp (Bp)	% Yd
1,5-Diphenyl-1,3,5-pentanetrione	95% Ethanol	Yellow	107-109	57.7
2,6-Diphenyl-4(1H)-pyridinone	Benzene	Cream	176-179	66.6
2,6-Diphenyl-4-chloropyridine	95% Ethanol	White	83-84	86.3
2,6-Diphenyl-4-methoxypyridine	Methanol	White	79-80	46.3
4-Methoxypyridine	Distilled Water	Clear	41-45	
4-Phenoxypyridine	Distilled Water	Clear	78-79	

Table 2. Enzyme Parameters and Kinetic Constants of the Enzymatic Reduction/Comproportionation of FLD_{Av} and the Me-FLD_{Av}.

Properties	FLDH		N_5-CH_3-FLDH	
	5 mM Tes pH=7.4	25 mM Tes pH=7.4	5 mM Tes pH=7.4	50 mM Tris pH=9.5
$(FLDH^{\cdot}/FLDH_2)$ of Final Product	$\frac{10.55_{\mu M}}{4.06}$	$\frac{12.75}{1.70}$		
$dFLDH_2/dt_i=v_o$	0.53 nmol	0.33	0.58	0.26
$dFLDH^{\cdot}/dt_i$	0.10	0.15	0.58	0.26
k_{1a}	$8.58 M^{-1}sec^{-1}$	5.86	8.04	2.89
k_{1b}	$2.75 M^{-1}sec^{-1}$	1.94	3.34	1.52
k_2*	$60.60 M^{-1}sec^{-1}$	318.00	31.37	30.00
K_{sq}	$0.10 M^{-1}sec^{-1}$	1.60	0.39	0.34

APPLICATION OF SELECTIVE LEACHING TECHNIQUE FOR MAJOR, MINOR, AND TRACE ELEMENT ANALYSIS IN COAL

Catherine O'Keefe, Kurt Eylands, and Debra Pflughoeft-Hassett
Energy & Environmental Research Center
University of North Dakota
Grand Forks, North Dakota 58202

Keywords: selective leaching technique

INTRODUCTION

The abundance and association of major, minor, and trace inorganic constituents in coal must be determined to predict their fate during combustion and gasification. In addition, the inorganic composition of coal influences the properties of the ash produced that, in turn, affects the usability of ash. The adverse effects of the inorganic components (ash-forming species) on coal utilization system performance include the formation of fine particulate that is difficult to collect, ash fouling and slagging, and conversion and erosion. Recently, selected metals that are present in coal were identified as air toxics. The 1990 Amendments to the Clean Air Act identified 189 hazardous air pollutants, including many trace metals. Therefore, the fate of trace metals considered to be air toxics is increasing in importance. Knowledge of the abundance and association of inorganic constituents is necessary in predicting the inorganic species behavior in coal in a given process. Chemical fractionation, in combination with other analytical techniques such as computer-controlled scanning electron microscopy (CCSEM), is used in models to predict the formation and ash deposition properties.

The inorganic components in the higher-rank coals (anthracite and bituminous) are primarily present in mineral phases. Whereas, the inorganic components in low-rank coals can be associated as discrete mineral phases, coordinated metal ions, and cations bound to carboxyl groups or in clays (1). The major mineral phases found in coal include aluminosilicates, carbonates, sulfides, and sulfates. Much of the Si, Al, and K is found in the aluminosilicate minerals such as clay minerals, with Si also found in quartz. Clays may also adsorb some trace elements such as Cs, Li, and Rb. Sulfide minerals such as pyrite can contain the trace elements arsenic, cadmium, cobalt, chromium, copper, mercury, manganese, molybdenum, nickel, lead, and selenium (2, 3). Carbonate minerals such as calcite, siderite, dolomite, and ankerite contain magnesium, calcium, and iron, but may also have trace amounts of manganese, strontium, and barium present.

The organic coal portion of coal consists of carboxylic acid, phenolic hydroxyl, mercapto, and imino groups which are able to bond with several trace elements. Cations of sodium, calcium, magnesium, potassium, barium, iron, manganese, strontium, and zinc bond to the carboxyl group to produce carboxylate salts (3). The trace elements are generally associated with both the organic and the mineral matter. In the mineral portion of coal, the trace elements can be found as discrete minor minerals, as replacement ions in minerals, or adsorbed on clays (2).

This paper discusses the application of a selective leaching technique known as chemical fractionation to coal. The method described is a modification of a leaching method by Miller and Given (4). Chemical fractionation is used to determine the distribution of elements among the organic and mineral phases in coal based on the differences in solubilities of coal constituents in three separate, stirred solutions: deionized water, 1 M ammonium acetate (NH_4OAc), and 1 M hydrochloric acid (HCl) as shown in Figure 1. A representative 140-gram sample of coal is ground to -200 mesh (< 74 micrometers) and then vacuum dried to a constant weight. A 35-gram portion of coal is ashed at 750°C and the ash content is determined. A sample is analyzed for the major, minor, and trace elements. The remainder of the coal is then subjected to successive extraction treatments. The first extraction treatment uses 4 mL of deionized water per gram of coal and is stirred in a covered beaker at room temperature for 24 hours. The sample is vacuum-filtered and

rinsed with deionized water. About 35 grams of the coal residue is removed and dried for ash content determination, and an analysis on the ash for the major, minor, and trace elements is performed by energy-dispersive x-ray fluorescence (EDXRF) utilizing direct excitation and three secondary excitation conditions (aluminum, titanium, and germanium). The filtrate is then acidified and transferred to a 125-mL volumetric flask, made up to volume, and stored for further analysis by inductively coupled plasma emission spectroscopy (ICP) and atomic absorption (AA).

Four mL of 1 M NH_4OAc per gram of coal is then added to the beaker containing the remaining 70 grams of coal residue. The sample is stirred and heated at 70°C for 24 hours. The sample is then vacuum-filtered and rinsed with deionized water. The filtrate is acidified and saved. The 1 M NH_4OAc extraction procedure is repeated two additional times. The filtrates from the three successive NH_4OAc extractions are combined, transferred to a 500-mL volumetric flask, made up to volume, and stored for analysis by AA. About 35 grams of residue coal is removed and dried. The residue coal is used for determination of the ash content, and major, minor, and trace constituents are determined on the ash by EDXRF.

To the remaining coal residue, 4 mL of 1 M HCl per gram of coal is added, stirred, and heated at 70°C for 24 hours. The sample is vacuum-filtered and rinsed with deionized water. The filtrate is acidified and saved. The 1 M HCl extraction procedure is repeated once more. The filtrate from both HCl extractions is combined, transferred to a 300-mL volumetric flask, made up to volume, and stored for analysis by AA. The coal residue is then dried. A portion of the dried coal residue is used for ash content determination, and the remainder is ashed and analyzed by EDXRF for the major, minor, and trace elements.

RESULTS AND DISCUSSION

The chemical fractionation procedure uses deionized water to extract the water-soluble minerals, such as halite (NaCl) and thenardite (Na_2SO_4). The cations associated on ionic exchange sites of carboxylic acids in the organic portion of coal are removed by ammonium acetate. Hydrochloric acid extracts elements that are associated with acid-soluble minerals, such as calcite ($CaCO_3$), dolomite ($CaMg[CO_3]_2$), and siderite ($FeCO_3$), and organic coordination complexes. The elemental constituents remaining in the residue presumably are associated with the insoluble minerals, such as clays (aluminosilicates), quartz (SiO_2), and pyrite (FeS_2).

Table 1 summarizes the chemical fractionation results obtained from five coals ranging in rank from lignite to bituminous. The ash produced by ashing (at 750°C) the chemical fractionation residues was analyzed using a Fisons 770 EDXRF system, and the mass balance was completed by normalizing to zero silicon loss. The results indicate that sodium is the only element that is consistently and appreciably extracted in the water treatment. The sodium is probably present in the coals as sodium chloride (halite), and sodium sulfate (thenardite), and, in the Beulah coal, may be present in the water inherent in the lignite.

Calcium, magnesium, and sodium in all five coals, along with some potassium in two of the coals, are removed primarily in the ammonium acetate extraction. These elements are usually found in salts of organic acids in coals. They may also be found in minerals such as gypsum which is soluble in both water and ammonium acetate, or they may be associated with ion-exchange sites in clays.

The hydrochloric acid leaching extracted a majority of the iron and aluminum that was removed during the chemical fractionation process. Much of the remainder of the calcium and magnesium that was left after the ammonium acetate leaching was removed by the hydrochloric acid extraction. These elements were probably associated with the carbonate minerals calcite and dolomite which are acid-soluble. A small amount of titanium in two of the coals was also leached out of the coal during the hydrochloric acid extraction. The hydrochloric acid extraction removes elements that exist in organic coordination complexes such as Al^{3+} and Fe^{3+} and in acid-soluble minerals such as carbonates.

The bituminous coals differed from the lignite and subbituminous coals in that less sodium and magnesium were extracted, indicating an association of sodium with the insoluble mineral fraction of the coal. A larger portion of the aluminum remains in the bituminous coals than in the lignite or subbituminous coals, suggesting that the aluminum is not associated with a coordinate site, or that there is a better developed crystalline structure of the clays such as illite and montmorillonite.

The iron in all of the coals is located in the acid-soluble or the insoluble fractions. Computer-controlled scanning electron microscopy (CCSEM) analysis of the coals indicates the percent of pyrite to be as follows: Beulah - 30%, Black Thunder - 11%, Rochelle - 2%, Illinois No. 6 - 36%, and Pittsburgh No. 8 - 13%. This indicates a direct relationship between the pyrite content and the iron content after leaching. The iron leached by HCl can be attributed to the dissolution of siderite ($FeCO_3$). This is the most evident in the Rochelle subbituminous coal.

The weathering of Pittsburgh No. 8 has caused some minerals such as pyrite to oxidize. Therefore, the oxidized iron was removed in the hydrochloric leaching, but aluminum was not because aluminum is not readily oxidized. The aluminum was removed in the lignite and bituminous coals, due to aluminum being organically associated.

Arsenic and mercury, according to Norton and others (5) and Ciocco and others (6), are strongly associated with pyrite and other sulfide minerals. Finkelman (7) and Galbreath and others (8) also have indicated that mercury is present in coal as a sulfide. Chromium is reported to be associated with clay minerals (9). Table 2 indicates that arsenic is primarily removed by hydrochloric acid, while only a small portion of chromium is removed. However, the majority of mercury and chromium are not leached out and are associated with the insoluble fraction of coal, indicating an association with pyrite or silicates.

SUMMARY

Few water-soluble minerals were found in the coals studied. The water-soluble minerals are likely limited to halite (NaCl); gypsum ($CaSO_4 \cdot 2H_2O$), found in the Pittsburgh No. 8 and Illinois No. 6 coals; and sylvite (KCl), found in the Beulah and Illinois No. 6 coals. A small amount of iron was removed from the bituminous coals, most likely from hematite (Fe_2O_3).

High levels of calcium, magnesium, and sodium were removed by ammonium acetate (NH_4OAc). These elements are associated with ion exchange sites of the carboxylic acids in the organic portion of the coal. The lower-grade coals studied contained more organically associated elements.

Iron, calcium, and magnesium are the most commonly removed elements in the acid leaching. The loss of these elements can be attributed to the dissolution of calcite ($CaCO_3$), dolomite ($CaMg[CO_3]_2$), and siderite ($FeCO_3$). The Illinois No. 6 coal had very few elements removed by HCl, indicating few carbonate minerals in the coal and the probable association of mercury and chromium with pyrite and silicates. The calcium present was either in the form of gypsum ($CaSO_4 \cdot 2H_2O$), an accessory element in clays, or organically associated.

In order to predict the behavior of the inorganic portions of the coal during combustion, it is necessary to know how the elements are distributed between the organic and inorganic portions of the coal. The chemical fractionation process helps to define this distribution. The organically associated elements will be freed during the earliest stages of combustion and will react with the inorganic phases as combustion continues. This will have an effect on fouling and slagging within the boiler, reducing plant efficiency. By thorough characterization and careful selection of coals, coal-burning plants can increase efficiency and, in some cases, reduce pollution containing trace elements.

REFERENCES

1. Benson, S.; Holm, P. "Comparison of Inorganic Constituents in Three Low-Rank Coals," *Ind. Eng. Chem. Prod. Res. Dev.* **1985**, *24*, 145-149.

2. Martines-Tarazona, M.; Spears, D.; Tascon, J. "Organic Affinity of Trace Elements in Austrian Bituminous Coals," *Fuels* **1992**, *71*, 909-917.

3. Swaine, D.J. "The Organic Association of Elements in Coals," *Organic Geochemistry* **1992**, *18* (3), 259-261.

4. Miller, R.N.; Given, P.H. *Ash Deposits and Corrosion Due to Impurities in Combustion Gases*, Bryers, R.H., Ed.; Hemisphere Publishing Corp.: Washington, DC, 1977; p 39.

5. Norton, G.A.; Markuszewshi, R.; Buttermore, W.H. "The Removal and Control of Trace Elements in Coal and Coal Wastes," *In* Proceedings of the International Conference on Elemental Analysis of Coal and Its By-Products; 1991, p 270-288.

6. Ciocco, M.V.; Morsi, B.I.; Araujo, G.; Chiang, S.H. "Trace Elements Removal Using a Selective Coal Agglomeration Process," *In* Proceedings of the Ninth Annual International Pittsburgh Coal Conference; 1992, p 299-305.

7. Finkelman, R.B.; Stanton, R.W. "Identification and Significance of Accessory Minerals from a Bituminous Coal," *Fuel* **1977**, *57*, 763-768.

8. Galbreath, K.C.; Brekke, D.W. "Feasibility of Combined Wavelength-Dispersive/Energy-Dispersive Computer-Controlled Scanning Electron Microscopy for Determining Trace Metal Distribution," *In* Draft Proceedings of the Trace Elements Workshop: Trace Element Transformations in Coal-Fired Power Systems; Scottsdale, Arizona, 1993.

9. Wiese, R.G., Jr.; Muir, I.; Fyfe, W.S. "Trace Element Siting in Iron Sulfides from Coal Determined by Secondary Ion Mass Spectrometry," *Energy Source* **1990**, *12*, 251-264.

TABLE 1

Chemical Fractionation Results

Coal — Beulah — Lignite

Elements	Initial, ppm	% Removed by H_2O	% Removed by NH_4OAc	% Removed by HCl	% Remaining
Aluminum	8,100	0	0	33	67
Iron	8,400	0	0	20	80
Titanium	270	0	0	9	91
Calcium	18,000	0	74	24	2
Magnesium	4,600	0	87	6	7
Sodium	5,800	13	87	0	0
Potassium	230	7	43	3	47

Coal — Black Thunder — Subbituminous

Elements	Initial, ppm	% Removed by H_2O	% Removed by NH_4OAc	% Removed by HCl	% Remaining
Aluminum	8,400	0	26	42	32
Iron	1,800	0	0	75	25
Titanium	400	0	0	0	100
Calcium	9,900	0	72	28	0
Magnesium	3,000	0	64	35	1
Sodium	290	27	62	8	3
Potassium	140	0	48	0	52

Coal — Rochelle — Subbituminous

Elements	Initial, ppm	% Removed by H_2O	% Removed by NH_4OAc	% Removed by HCl	% Remaining
Aluminum	8,300	0	0	18	82
Iron	4,600	0	0	96	4
Titanium	2,000	0	0	0	100
Calcium	8,800	0	64	35	1
Magnesium	2,900	0	57	37	6
Sodium	450	11	76	5	8
Potassium	230	0	0	0	100

Coal — Illinois No. 6 — Bituminous

Elements	Initial, ppm	% Removed by H_2O	% Removed by NH_4OAc	% Removed by HCl	% Remaining
Aluminum	15,900	0	0	0	100
Iron	21,100	9	0	0	91
Titanium	610	0	0	2	98
Calcium	5,900	19	74	0	7
Magnesium	750	3	6	0	91
Sodium	1,400	47	17	3	33
Potassium	1,800	2	2	2	94

Coal — Pittsburgh No. 8 — Bituminous

Elements	Initial, ppm	% Removed by H_2O	% Removed by NH_4OAc	% Removed by HCl	% Remaining
Aluminum	12,300	0	0	0	100
Iron	5,200	4	0	39	57
Titanium	580	0	0	0	100
Calcium	330	15	63	10	12
Magnesium	3,300	0	13	15	72
Sodium	420	11	23	0	66
Potassium	1,200	0	0	0	100

TABLE 2

Illinois No. 6 Filtrate Analysis by AA

Elements	% Removed by H_2O	% Removed by NH_4OAc	% Removed by HCl	% Remaining
Arsenic	<7	7	68	18
Chromium	1	1	26	72
Mercury	<24	5	<3	68

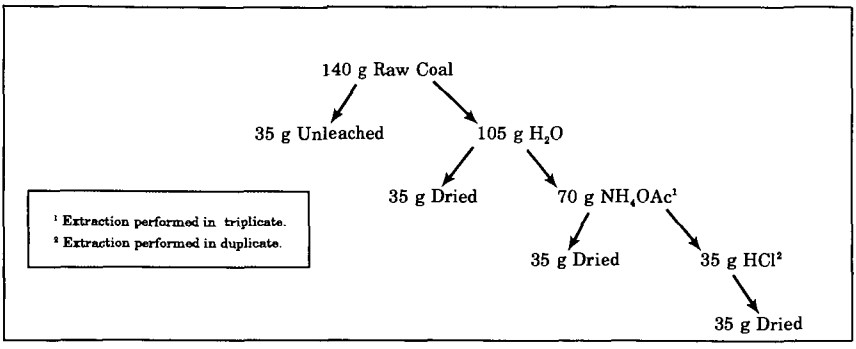

Figure 1. Chemical fractionation procedure.

UTILIZATION OF SPENT OIL SHALE IN A FLUIDIZED BED PROCESS

Asmund Vego, Scott D. Carter and John L. Stehn
Center for Applied Energy Research, University of Kentucky
Lexington, Kentucky 40511-8433

Keywords: Oil shale, Pyrolysis, Gasification, Desulfurization and Combustion

Abstract

The Center for Applied Energy Research (CAER) is currently developing the KENTORT II oil shale retorting process for eastern U.S. oil shales. This is a fully integrated multi-stage fluidized-bed retorting process, which is designed to maximize extraction and utilization of the organic and inorganic components of the shale. After pyrolysis, the spent shale undergoes gasification for generation of hydrogen sulfide and synthesis gas. Combustion of the previously pyrolyzed and gasified shale generates the heat necessary to drive the process.

Introduction

Testing of the KENTORT II retorting concept was initiated in 1986 in a 3.8-cm diameter fluidized bed reactor,[1] and further evaluation was performed in a fully integrated 7.6-cm diameter unit.[2,3] The KENTORT II process is currently being scaled up to a 15.2-cm diameter 23-kg/hr process demonstration unit (PDU). Recent cold flow studies in a full scale model and information from the successful 7.2-cm diameter system provided design data for the PDU.[4,5]

A detailed discussion of the rationale behind the KENTORT II design has been published previously.[6] The primary motivation behind the design was the complete utilization of the spent shale from the pyrolysis step. This is currently not the case for two of the world's largest processors of oil shale, however. The Petrosix process in Brazil currently discards pyrolyzed shale, and this accounts for nearly 50% of the energy losses from the system.[7] The Estonian oil shale industry also discards pyrolyzed shale, and because of the nature of the shale and the process, this results in environmental problems at the shale disposal site.[8] So it is important for process efficiency and sound environmental practices that the pyrolyzed shale be sufficiently utilized within the retorting process. In addition to in-process utilization of spent shale, it may be possible for spent shale to be employed as feedstock for the production of construction materials. Raw Michigan Antrim oil shale is currently in use for the production of portland cement, but it has been suggested that spent shale would be suitable also.[9]

While fluidized bed pyrolysis of oil shale is an efficient method of quickly generating relatively large yields of crude shale oil, substantial amounts of residual carbon and sulfur remain in the spent shale. Traditionally, direct combustion of the char from pyrolysis has been reserved as the method for utilizing the residual carbon. This technique presents two problems when applied to Eastern shales. First, char from fluidized bed pyrolysis contains more carbon than required to provide heat for the retort. It would be necessary to remove substantial amounts of energy from the reactor in order to deplete all the carbon in this manner. Second, the sulfur to carbon weight ratio of pyrolyzed shale is large, which if combusted could produce prohibitive amounts of SO_2.

Steam gasification of the excess carbon from the char represents an alternative to direct combustion. Tests at the CAER have shown that fluidized bed pyrolysis char gasifies readily at 800

°C and 1 atmosphere steam partial pressure.[1] Under these conditions over 40% of the carbon in the pyrolyzed shale was gasified following 30 minutes mean char residence time. Steam fluidization enables also steam/ FeS_x reactions to go nearly to completion. Studies have shown that 90% sulfur removal can be achieved at residence times greater than 30 minutes and temperatures less than 600 °C.[10] Therefore, introduction of an intermediate gasification step between pyrolysis and combustion provides means for attaining total carbon utilization as well as removing substantial amounts of sulfur prior to combustion.

Process Description

The heart of the KENTORT II process (Figure 1) consists of four fluidized bed vessels. The four zones are configured in cascade, where the shale undergoes pyrolysis, gasification/desulfurization, combustion and cooling. The pyrolysis, gasification and cooling sections are aligned vertically and share a common fluidizing gas. Combustion takes place in the fourth bed which is placed adjacent to the other three, and the fluidizing gas is supplied separately. The main body of the KENTORT II unit is constructed from 316 stainless steel. Because of the combination of extreme temperature and corrosive environment in the gasification and combustion section, these sections have been aluminized to prevent scaling and spalling of the reactor material.[5] Aluminizing is a process where aluminum diffuses at high temperature onto the surface of a base metal for a minimum dept of 100 microns, producing an aluminum-rich alloy on the surface. The different sections of the unit are separated by gas distributors which are sandwiched between flanges. The total height of the unit is about 6 meters.

Shale Handling Systems

A screwfeeder is used to meter the shale into the pyrolysis section at a rate of 23 kg/hr. The screwfeeder is supplied by a 140-kg capacity sealed feed hopper. Additional shale can be loaded into the hopper during operation, so truly continuous operation can be achieved. Processed shale at about 400 °C leaves the unit trough an overflow port in the cooling zone. The spent shale is collected in a sealed bin, which may be emptied out during a run to permit lengthy periods of operation. Fines recovered from the pyrolysis cyclone are feed to the combustor by an air lift.

Shale Conveying System

J-valves with corresponding liftpipes provide a conveying system for shale recirculation from the gasification section to the pyrolysis and combustion sections. Solids are transported in a lean phase through the liftpipes, using nitrogen as the carrier gas in the pyrolyzer liftpipe and air as carrier gas in the combustor liftpipe. Nitrogen is used to meter the flow of solids through the J-valves and into the liftpipes. Recirculation rates of up to 90-kg/hr to the pyrolysis section and 225-kg/hr to the combustion section can be achieved simultaneously.

Start-Up System

A propane burner (Figure 2) is used to heat the fluidizing air for the combustor during start-up. By circulating solids among the zones, most of the heat required for preheating is provided by the burner. A superheater upstream of the cooling zone provides the rest of the energy needed to preheat the system. Air, rather than steam, is used during most of the preheating period so that the amount of steam condensate is kept as small as possible. Once steady state conditions are approached, the energy provided by the burner and superheater is reduced or eliminated completely.

Pyrolysis Section

Raw shale is fed over-bed to the pyrolysis section, and a mixture of steam and product gases from the gasification stage below serves as the fluidizing medium. Heat is provided to the pyrolysis section by a combination of fluidizing gas and recirculating solids from the hotter gasification section. The pyrolysis zone has a vertical baffle which splits the section into two equally sized beds. The purpose of the baffle is to narrow the particle residence time distribution by creating two beds in series. By narrowing the particle residence time distribution, greater chemical conversion can occur per unit reactor volume. The operational conditions for the pyrolyzer are: temperature, 500-550 °C; mean shale residence time, 3 minutes; bed depth, 30.5 cm.

Gasification Section

Shale from the pyrolysis section is transferred to the gasification/desulfurization zone by a gravity feed downcomer. The bed depth is designed to be adjustable between 38-76 cm so that solid residence time may be adjusted from 30-60 minutes. Like the pyrolyzer, the gasifier is baffled to narrow the particle residence time distribution. The gasification section is heated by hot solids from the combustion section entering the lower part of the bed, and the operational temperature is from 750 to 850 °C. Steam from the cooling zone below is used as the fluidizing medium.

Cooling Section

A downcomer transfers shale from the gasifier to the cooling section which also serves to preheat the steam that fluidizes the gasification bed. The cooling zone is the primary exit point for solids from the reactor. An overflow outlet in the wall of the vessel creates a 38-cm deep bed.

Combustion Section

The combustor provides the heat required for the pyrolysis and gasification sections of the KENTORT II retort. The gasification and the combustion zones are closely aligned to facilitate the transfer of solids. To minimize mixing of the gas streams, however, the pressure between the two vessels is balanced. The bed depth is 30.5 cm, although this is adjustable by regulating the height of the standpipe. Carbon-containing shale recycled from the gasification section via a pneumatic lift pipe, is the primarily fuel for the combustor. Fines recovered from the pyrolysis cyclone are also fed into the combustor to provide additional fuel. Air is used for fluidization in the combustor.

Oil Collection System

Gases and vapors from the pyrolyzer enter a cyclone for fines removal. A combination convection/liquid-injection heat exchanger then cools the vapor stream to 150 °C which causes an oil aerosol to develop. This aerosol is trapped by an electrostatic precipitator (ESP) which contains approximately 10 m^2 of collection surface area and includes two, two-stage Penney-type collection cells in series to ensure high collection efficiency. Downstream of the ESP, a shell-and-tube condenser is then used to condense steam and light oil that remain. Light oil and water from the condenser are separated, and the water is sufficiently treated to be fed back into the steam generator. Mist collection, further cooling and more mist collection are performed before the gas stream is sampled by an on-line gas chromatograph and mass spectrometer.

Combustion Flue Gas System

Fines are removed from the combustion gas stream by a cyclone before the gas is cooled to approximately 250 °C and released to the ventilation system.

Fines and water are removed from a small portion of the gas stream for analysis by on-line combustion gas analyzers which provide a continuous measure of all major flue gas components.

Discussion

The KENTORT II process utilizes pyrolyzed shale to generate valuable by-products such as elemental sulfur and synthesis gas. The shale is also used to facilitate the operation of the retort by providing the energy to drive the process and the means to transfer this energy throughout the process by recirculating the shale itself. The pyrolysis step of the process actually represents a small fraction of the whole system. It is the additional processing of the shale to extract process heat and by-products that occupies much of the unit. Since fluidized bed pyrolysis is so efficient, the combustion and gasification zones do not make the process any larger than current commercial units which only pyrolyze the shale.[7,8] There is, of course, a point of diminishing returns relating to the carbon utilization of the shale. An objective of the testing with the 23-kg/hr PDU is to evaluate carbon burn-off as a function of gasification and combustion conditions. Once this is complete, an economically-based determination of the optimal carbon burn-off can be made.

It is important from an environmental point of view that the pyrolyzed oil shale be sufficiently processed so that its acid leaching potential upon disposal is not high. The iron disulfide (pyrite and marcasite) content of eastern U.S. shale is high which can lead to acid drainage if these minerals are not converted to FeS (pyrrhotite).[11] Fluidized bed pyrolysis only results in partial conversion of the disulfide to the monosulfide so either combustion or gasification or both, as in the case of the KENTORT II process, is needed so that the conversion is enhanced by the oxidization of the iron. The advantage of using gasification rather than combustion to accomplish this is that H_2S is produced which can be readily scrubbed and converted to elemental sulfur, whereas SO_2 control technology is relatively expensive and inefficient.

The use of the processed shale to transfer heat increases process efficiency in two ways. First, the volumetric heat capacity of shale is high compared to gases which means that large volumes of gas are not needed to heat the system. Second, by using the shale, which is present in the system anyway, rather than an added heat-transfer material, the need for a step to separate the shale from the heat carrier is eliminated. The properties of the shale will dictate the extent to which pyrolyzed shale can be used as the heat carrier. The shales of the eastern U.S. are fairly refractory and can be processed at high temperatures with relatively little decrepitation. The Western shales on the other hand lose their strength when subjected to normal combustion or gasification temperatures because of their high carbonate content; therefore, processes which have been designed for Western shale that combust the spent shale utilize combustion temperatures of less than 700°C.[12]

Summary

A 23-kg/hr integrated fluidized bed Process Demonstration Unit (PDU) called the KENTORT II, has been built at the Center for Applied Energy Research. The PDU effectively utilizes the organic and inorganic components of eastern U.S. oil shales through pyrolysis, gasification/desulfurization and combustion. Autothermal operation is achieved by combustion of the residual carbon following pyrolysis and gasification. Heat is transferred among the different sections of the unit by recirculation of hot combusted solids. The main product from the KENTORT II is a high yield of liquid hydocarbons from the pyrolyzer, and important by-products include elemental sulfur (from hydrogen sulfide gas) and synthesis gas.

Acknowledgements
This work was supported in part by the Morgantown Energy Technology Center, USDOE, under Cooperative Agreement DE-FC21-90MC27286 (such support does not constitute an endorsement by the USDOE of the views expressed in this article).

References
1. Rubel, A.M and Davis, E., "Evaluation of the Gasification Potential of Kentucky Oil Shale Char Produced Under High Yield Fluid Bed Conditions," 1987 Eastern Oil Shale Symposium Proceedings, Univ. of Kentucky, Lexington, Ky.

2. Carter, S.D., Robl, T.L., Rubel, A.M., and Taulbee, D.N., "Processing of Eastern U.S. Oil Shale in a Multistaged Fluidized Bed System," Fuel, 1990, 69, 1124.

3. Carter, S.D., Robl, T.L., Taulbee, D.N., and Rubel, A.M., "Testing of an Irati Oil Shale in a Multistaged Fluidized Bed System," Fuel, 1991, 70, 1347.

4. Vego, A., Carter, S.D., Stehn, J.L. and Neathery, J.K., "Scaleup of the KENTORT II Process, Cold Flow Modeling of the 50-lb/hr. retort", 1991 Eastern Oil Shale Symposium Proceedings, University of Kentucky, Lexington, KY.

5. Carter, S.D., Rubel, A.M., Robl, T.L., and Taulbee, D.N., "The development of the KENTORT II Process for Eastern U.S. Oil Shale", Final Report for U.S. Department of Energy, Cooperative Agreement NO: DE-FC21-86LC-11086.

6. Carter, S.D., "The KENTORT II Concept: A Process Description," 1987 Eastern Oil Shale Symposium Proceedings, Univ. of Kentucky, Lexington, Ky.

7. Lisboa, A.C., Novicki, R.E., and Piper, E., "Petrobras Boosts Oil Shale Fines Processing," 1989 Eastern Oil Shale Symposiumn Proceedings, University of Kentucky, Lexington, Ky.

8. Urov, K., 6th Australian Workshop on Oil Shale, 1991, Univ. of Queensland, St. Lucia, Brisbane, pp. 25-31.

9. Schultz, C.W., Lamont, W.E., and Daniel, J., "The Use of Devonian Oil Shales in the Production of Portland Cement," 1991 Eastern Oil Shale Symposium Proceedings, Univ. of Kentucky, Lexington, Ky.

10. Carter, S.D. and Taulbee, D.N., "Fluidized Bed Steam Retorting of Kentucky Oil Shale," Fuel Processing Technology, 1985, 11, 285.

11. Robl, T.L., Barron, L.S., Schram, W., and Thomas, G., 1988 Eastern Oil Shale Symposium Proceedings, IMMR88/101, University of Kentucky, Lexington, Ky.

12. Lewis, A.E., Braun, R.L., and Diaz, J.C., 17th Oil Shale Symposium Proceedings, 1984, Colorado School of Mines, pp. 1-16.

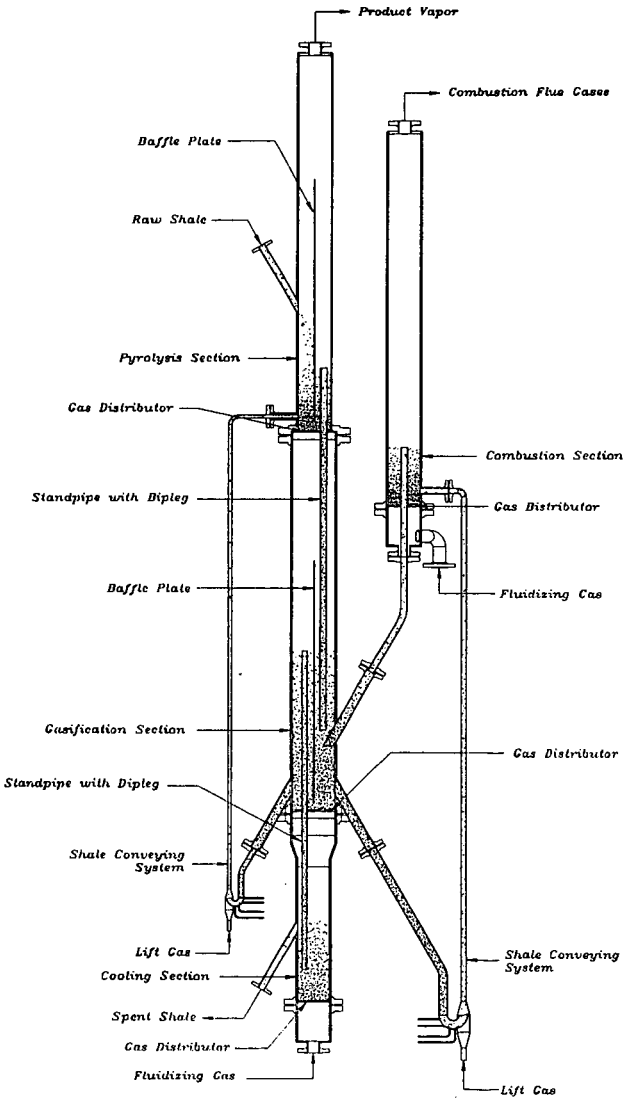

Figure 1. KENTORT II Reactor with Internals

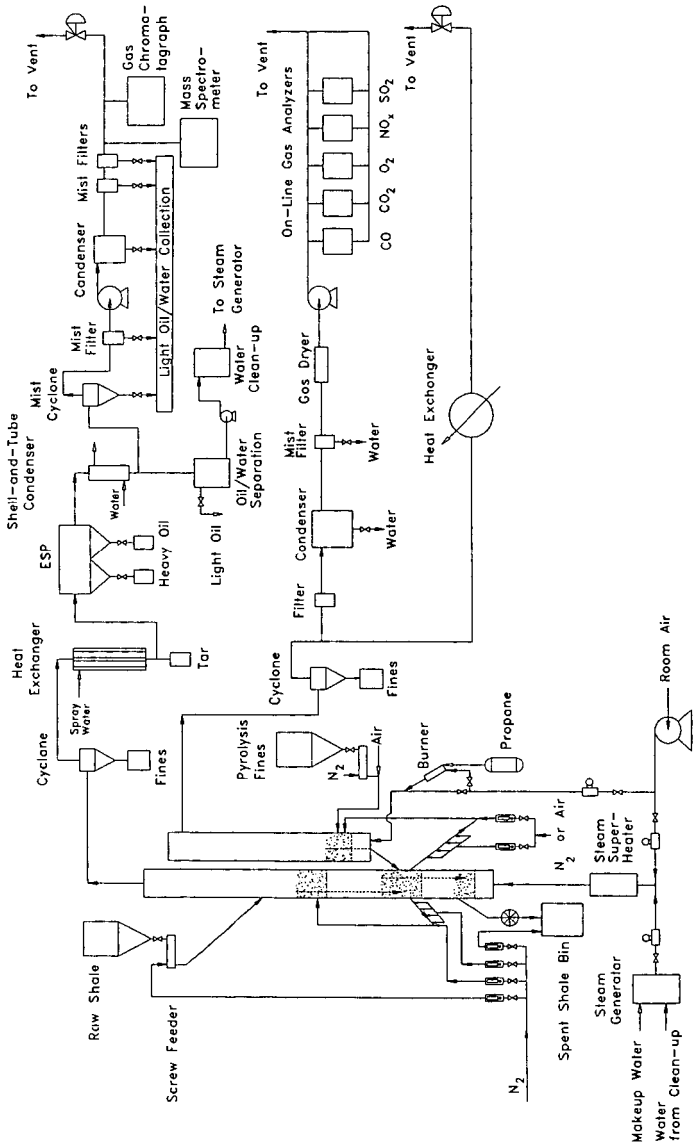

Figure 2. Simplified Flow Diagram of the 23-kg/hr KENTORT II Retort

ROLE OF BIOFUELED GAS TURBINES IN SOIL REMEDIATION

Joseph T. Hamrick
Aerospace Research Corporation
5454 Aerospace Rd.
Roanoke, VA 24014

Keywords: Biomass Fuel, Gas Turbines, Power Generation, Soil Remediation

INTRODUCTION

Clean up of soils polluted with metals pose difficult and expensive problems in many places around the world. Remediation has ranged from vitrification of the polluted soil to disposal in landfills. Dr. Rufus L. Chaney, reference 1, has proposed "Green Remediation" as a means of treatment. "Green Remediation" relies on the ability of plants to accumulate metals from the soil. Upon reaching maturity the plants can be harvested and burned with subsequent recovery of the metals from the ash. Some specifics of growth, species selection, and various aspects of agronomic management are covered in reference 1. It is the purpose of this presentation to introduce the prospect of using a biomass fueled gas turbine power generating system as a remediation vehicle in conjunction with growth of metal accumulating plants some of which have been given the name "Hyperaccumulators". The biofueled gas turbine power generating system is described and various aspects of its use are presented in references 2, 3, & 4.

BACKGROUND INFORMATION

The use of metal accumulating plants as fuel was first brought to the attention of Aerospace Research Corporation by Dr. Barry Noval and Lionel Gillston of Energy Products Enrichment, Inc. of Norristown, Pa. They suggested a multiple use of the biomass fueled gas turbine in which operation with metal accumulating plants would produce an ash-ore product that could be smeltered to recover the metal. In areas where the contaminated land could not support full time operation, nonpolluted land growing crops such as sweet sorghum together with sawmill waste, demolition waste, and clean municiple waste could be used.

Conversations with Dr. Robert P. Bosshart of Horsehead Resource Development Company, Inc. of Palmerton, Pa. revealed that there is considerable interest within that company in use of metal accumulating plants to clean up contaminated soil. Soils in the Palmerton area where zinc smelters are located have become contaminated over the years. One problem is that much of the contaminated land is too steep to cultivate by conventional methods. An estimated 1000 acres of level land may be available for use in a remediation program. Sixty to eighty percent of the fuel needed for an economical biomass fueled gas turbine installation would have to come from other sources.

Throughout the U.S. and the world there are large land areas that have become contaminated with metals such as lead, copper, zinc, cadmium, arsenic, and nickel and may be candidates for phytotreatment. While it may be desirable in some cases to delay installation of phytotreatment systems until more research is performed on candidate metal accumulators, there are many locations where biomass fueled power generation systems may be installed and economically operated with marginal accumulators. Under the Public Utilities Regulatory Policies Act power companies are required to purchase the power at their avoided energy costs. Growth, harvesting, transportation, storage, and processing of the biomass fuel and ash disposal constitute the main differences in the biomass fueled gas turbine power generating systems and those now in operation and use with petroleum and gaseous fuels around the world.

GROWTH OF METAL ACCUMUULATORS

As pointed out in reference 1, the metal accumulators may be specific in their tolerance for the contaminating metals. The selection of species will require agronomic expertise and will involve soil analysis, not only from standpoint of metal contamination but also from standpoint of alkalinity and nutrient content. A mixture of plant species may be required to accommodate multiple contaminants and erosion control. It is pointed out in reference 1 that few hyperaccumulators are available which generate substantial biomass. A low level accumulator which generates substantial biomass may achieve the same metal uptake for a given area as a hyperaccumulator with low biomass production. The higher biomass production would improve the economics of power generation. In climates with short frost free seasons it may be necessary to grow a variety of crops to support a power system. For example, bagasse from sorghum which constitutes substantial biomass for fuel after the sweet juice is extracted is seasonal. However, elemental analysis of sweet sorghum bagasse show the presence of chromium, barium, nickel, zinc, and copper among the lighter metals. Therefore, it is a good accumulator candidate. It can be grown in combination with hyperaccumulators as well as high producing legumes and grasses.

TRANSPORTATION AND STORAGE

Transporting and storage of biomass presents an economic problem because of its low density. For that reason it is important that hauling distances be short and storage operations be well planned. Legumes and grasses can be round baled and stored in the field near roads where they can be picked up and hauled to the point of use. The bales can be capped with plastic or left exposed to the weather. Both practices are followed throughout the United States. The storage of sweet sorghum is more complex. It is estimated that the harvesting and processing of sweet sorghum can be stretched out over a period of approximately six months in single crop climates. Mixing of varieties and staggered plantings will be required. The six month estimate is based upon information contained in references 5 and 6. The bagasse remains of the sorghum have to be dried and put in covered storage to prevent deterioration from fermentation. Providing covered storage for the large amounts of bagasse that would be required for year round use may not be practical. In tropical areas where year round growth of sweet sorghum is possible, the storage problem is minimal.

PROCESSING

Densification of legumes and grasses is necessary for feeding into the pressurized combustion chamber. Densifying involves grinding, pelleting, and crumbling. Efficient machines are commercially available for accomplishment of all three tasks. The pelleting process requires steam which can be supplied by a waste heat boiler heated by the turbine exhaust gases. Use of some of the generated electricity will also be required. Extraction of the juice from sweet sorghum may be accomplished by grinding or squeezing through rolls. The product from either process is referred to as bagasse. Bagasse from grinding can be dried and with little further screening or grinding be fed into the combustor. The bagasse from squeezing retains its identity as a stalk and must be subjected to substantial grinding before drying and feeding into the combustor. The sweet juice can be reduced to syrup with heat from the gas turbine exhaust. Storage of the syrup will allow year round operation of an ethanol plant. The seed head on the sorghum can also be used in ethanol production.

DISPOSAL OF THE ASH

The ash generated in the combustion chamber passes with the hot gases to a cyclone filter. The ash falls to the bottom of the cyclone where it is recovered, and the cleaned hot gases are ducted to the turbine. The cleaned gases normally contain 35 to 50 parts per million of particles that are on the order of 2 micrometers or less in diameter. The heavy metal content of the particles and any hazard potential will have to be evaluated. It is expected that particles containing heavy metal constituents will be more completely filtered due to higher density.

Biomass ash normally contains a commercially recoverable amount of potassium oxide which reacts with water to form highly soluble potassium hydroxide. Leaching of the potassium hydroxide while leaving the generally insoluble heavy metal oxides in the ash is one approach to recovery of the potassium.

The metal content of the ash will depend upon the variety and types of plants being used as a fuel as well as the condition of the soil in which the plant is grown. If the metal can be economically recovered and the residue from the recovery process is free of contaminating metal, the ash may be returned to the soil. If it is uneconomical to recover the metal, the most economical disposition probably will be into a qualified landfill.

ECONOMIC CONSIDERATIONS

The objective in using biofueled gas turbine power generating systems in soil remediation is to reduce clean up costs or to turn a profit if possible. The payment received for the generated power is the key factor. The avoided energy costs for power that public utilities are required to pay in complying with the Public Utilities Regulatory Policies Act will not normally be adequate to allow economical use of fuels other than waste products such as sawdust. Utilities with power plants located near coal mines generally have avoided energy costs less than 2¢/kw hr. with a charge to customers of 5¢ to 8¢/kw hr. Businesses generally pay a demand penalty in addition. Paper mills in coal producing areas are large users of sawdust and bark in their boilers. With 1993 prices for coal it is more economical for paper mills to switch to coal when the price of sawdust approaches $28 per ton on a bone dry basis. To compete with coal would require production of approximately ten tons of dry biomass per acre at $280.00 per acre. To meet a production goal of ten dry tons per acre probably would require harvesting a summer crop of sweet sorghum plus a winter cover crop in the northeastern part of the U.S. where there is an identified need for remediation. Unless there is a very large acreage, for example, five thousand acres of land to be remediated, reliance upon waste products for supplemental fuel probably would be the most economical approach.

In addition to bagasse, the sweet sorghum in the northeastern part of the U.S. would produce approximately 1.5 tons of sugar per acre which is equivalent to approximately 130 gallons of ethanol. The heat from the gas turbine exhaust can be used for processing the ethanol. An industrial user of power that has land to be remediated may well profit from generation of its own power with sale of the excess to a utility.

SUMMARY

Of the methods available to effect soil remediation phytotreatment of contaminated soils promises to be the most economical. The number of years required to accomplish the task will depend upon the skillfulness in soil management, the

variety of plants used, and the severity of the contamination. The ability to turn a profit with burning of the biomass in a gas turbine power generating system will depend upon the payment received for the power produced, payment for by-products, operating costs, cost of biomass production, and availability of waste for alternate fuel. By-products will consist primarily of potassium and the metal of contamination. In the case of sweet sorghum, ethanol produced from the sweet juice would be a major by-product. Biomass waste from sawmills and demolition can fill in during seasonal lulls in crop production.

REFERENCES

1. Cheney, Rufus L. "Revival Field", A Test of "Green Remediation", Soil Microbial Systems Laboratory USDA - Agricultural Research Service, Beltsville, MD 20705.

2. Hamrick, Joseph T., Biomass Fueled Gas Turbine Development, ACS Symposium Series 515 Clean Energy from Waste and Coal, M. Rashid Khan, Editor Aug. 25 - 30, 1991 American Chemical Society, Washington, D.C.

3. Hamrick, Joseph T., Worldwide Role of Gas Turbine Power Generation with Biomass Fuels, Volume 4 No. 4 World Resource Review, International Journal Dec. 1992, 7501 Lemont Suite 335, Woodridge, IL 60517-2661.

4. Hamrick, Joseph T., The Biomass Fueled Gas Turbine; One Answer to Global Warming, Global Gas Turbine News, May 1992, International Gas Turbine Institute, American Society of Mechanical Engineers, 6085 Barfield Road Suite 207, Atlanta, GA 30328.

5. Parrish, David J. and Cundiff, John S., Long-term Retention of Fermentables During Aerobic Storage of Bulked Sweet Sorghum, Departments of Agronomy & Agricultural Engineering, Virginia Tech April 1985.

6. Gascho, Gary J., The Potential Length of the Harvest Period For Sweet Sorghum, Agronomy Department, Coastal Plain Experiment Station, University of Georgia, Tifton, GA, April 1983.

From a literature search in 1992 by Dr. Shu-I Tu and associates of the Plant and Soil Biophysics Research Unit of the North Atlantic Area Regional Research Center of the U.S. Department of Agriculture the following individuals have been working on the selection of plant varieties with unique abilities to accumulate certain metals: R.B. Clark of University of Nebraska, E.A. Brams of Prairie View A&M University in Texas (university information number is 409-857-3812), D.R. Parker of the University of California at Riverside (department phone number is 907-787-5116), Dr. Grunes and collaborative with ARS at Ithaca, NY (607-255-3003), and V.V. Baligar with ARS at Beckley, WV (center information number is (304-252-6426). G.N. Richard at the University of Montana at Missoula (campus information number is 406-243-0211) has been working on the influence of cations pyrolysis of wood. The assistance of Dr. Shu-I Tu is appreciated.

MATHEMATICAL ANALYSIS OF A MSW ROTARY INCINERATOR

James T. Cobb, Jr. and K. Banerjee

Department of Chemical & Petroleum Engineering
University of Pittsburgh
Pittsburgh, Pennsylvania 15261

Keywords: municipal solid waste, incineration, mathematical model

ABSTRACT

A computerized mathematical model of a refractory-lined rotary kiln combustor with a vertically well-mixed bed has been developed. Bed height varies with horizontal distance as fuel is consumed. The kiln contains a pyrolysis zone, followed by a combustion zone. A kinetic model for cellulose pyrolysis simulates the thermal destruction of MSW in the first zone. The combustion of particles in the second zone follows a shrinking-core model. Model behavior is in good agreement with the performance of commercial units.

INTRODUCTION

A number of the waste-to-energy facilities operating in the United States utilize a rotary kiln combustor as the principal treatment unit in their systems. The barrel of the kiln may be either refractory-lined or water-walled. Waste is fed to the kiln from a receiving system and the products of combustion are treated and released. The combustion gases are polished in a secondary combustor, cleaned of acidic components and particulates, and sent to a stack. Bottom ash is cooled, mixed with fly ash, stabilized and landfilled.

Because of the concerns for full burnout of the combustibles in the feed, the destruction of toxic organics, the segregation and collection of toxic metals, and the efficient collection of energy, developers and operators of MSW kiln combustors must have a thorough understanding of the operation of each element of their waste-to-energy facilities and of the integration of these elements. The mathematical model described in this paper has been constructed and tested to assist in better understanding the operation of the rotary kiln combustor at the heart of many such facilities.

KINETIC MODEL

Incineration is a complex physical and chemical process [1]. Waste fed to the rotary kiln first is demoisturized and heated. When it reaches its reaction onset temperature, pyrolysis, sublimation and other solid volatilization reactions occur under starved-air conditions. After these are complete, the char remaining is oxidized under excess-air conditions. For manageability of the final kiln combustor model developed in this study, a simple kinetic model for cellulose pyrolysis has been adopted to describe the pyrolysis of waste in the starved-air region of the kiln [2]. In addition, the assumption has been made that the surface oxidation of char in the

excess-air portion of the kiln is rapid and is largely controlled by the mass transfer of oxygen through the bed.

The kinetic model for the pyrolysis of cellulose is based upon experimental work in the temperature range of 300°C to 1000°C. In its simplest version, the model assumes that cellulose decomposes directly to each reaction product, *i*, by a single, independent reaction pathway,

$$\text{cellulose} \xrightarrow{k_i} \text{product } i$$

and that the kinetics of this process can be modeled by a unimolecular first-order reaction having a rate constant that may be written in the Arrhenius form,

$$\frac{dV_i}{dt} = k_i \, exp\left(\frac{-E_i}{RT}\right)\left[V_i^* - V_i\right]$$

where V_i is the percent yield of gas *i* at any time t, V_i^* is the ultimate (maximum) yield of gas *i*, and k_i and E_i are kinetic parameters. These parameters were correlated with gas-phase pyrolysis products, observed by experimentation, including light hydrocarbons, alcohols, aldehydes, acids, H_2, H_2O, CO, CO_2 and tar.

Two modifications of the kinetic model were required before it could be applied to MSW incineration. First, the rate expressions had to be rewritten so as to account for the decomposition of tar to smaller gaseous species. In order to achieve this, it was assumed that the tar decomposed in the same proportion as the ultimate yields of the various species. A modified ultimate yield was therefore defined according to,

$$V^*_{m,i} = V_i^* + \frac{V_i^*}{\sum_{i=1}^{n} V_i^*} V^*_{tar}$$

were n is the number of gaseous species evolved during pyrolysis. Secondly, the discrete rate equations were combined, using the modified ultimate yields, to achieve a mass balance.

To reach the char surface and combust the carbon there, the oxygen is assumed to diffuse through the bed to the individual char particles and then through the inert ash layer to the surface of the carbon. The carbon core shrinks as the combustion reaction proceeds. However, the total particle radius remains constant due to the formation of the ash layer, with an accompanying increase in particle porosity. Although the model can account for a particle size distribution of char, for the purpose of this study a uniform particle size has been considered. A mass balance is performed on selected individual particles throughout the bed, using a shrinking core modeling technique [3] to calculate the burning rate of the particles.

KILN COMBUSTOR MODEL

Previous mathematical models for rotary combustors have been developed and described by Essenhigh and Kuo [4], Gorog [5], Ghoshdastidar et al. [6], Jang and Acharya [7], Silcox et al. [8], Ghezzi et al. [9], Wormeck and Pershing [10], Lemieux et al. [11] and Sethi and Biswas [12].

In this study the kiln is divided into two active zones - a first zone for pyrolysis and a second zone for combustion. The model for the pyrolysis zone relies upon the following assumptions:

- bed height decreases linearly with distance along the kiln's centerline;
- the bed is well mixed in the vertical direction;
- only convective heat transfer from the gas to the bed is considered; the kiln wall is assumed to be refractory-lined, thus no heat is transferred through the barrel;
- the temperature in the product gas above the bed is constant throughout this zone of the kiln; its value is calculated by the method of Tillman [1];
- both the solid and gas regions operate in the plug-flow regime.

The model for the combustion zone is based upon the model for zirconium combustion, developed by Lemieux et al. [11] The bed depth and the uniform temperature throughout the bed are set at the values obtained at the exit of the pyrolysis zone. The model determines the burning rate of the char and calculates the char mass flow profile across the combustion zone. The bed is axially divided into slices of uniform surface oxygen concentration and each axial slice is divided vertically into segments of uniform oxygen concentration and particle size. A mass balance is performed on the slices in the vertical direction, yielding an ordinary differential equation describing diffusion of oxygen through a porous solid, with boundary conditions at the wall-solid and gas-solid interface. The particle burning rate (calculated as defined earlier) is combined with equations used to describe oxygen transport through the bed. Oxygen is assumed to be at a uniform concentration at each bed depth location, and the particles are assumed to be small enough that oxygen is at a uniform concentration in the gas surrounding each particle. The resulting finite difference equations are solved using a tridiagonal matrix algorithm.

The residence time of char in the kiln was calculated according to [13],

$$\theta = \frac{0.19L}{NDS}$$

where Θ is expressed in minutes, L is the kiln length, D, the kiln diameter, N, the number of revolutions of the kiln per minute and S is its inclination to the horizontal.

The complex three-dimensional nature of the kiln, with variations in the x, z and ϕ directions necessitates simplifications to enable a solution of the model equations. The bed height, t_b, is that corresponding to the one required for a bed with the same cross-sectional area and the same area exposed to the gas as in the

actual kiln. It is reasonable to assume that the bed height remains constant in the burnout zone because char constitutes but a small fraction of the solids in this zone.

RESULTS FROM USING THE MODEL

Physical parameters required by the model were derived from the MSW incineration facility located at McKay Bay, a suburb of Tampa, Florida [14]. The sources of values of the various fundamental parameters required by the model are detailed in Reference 15. This reference also includes a discussion of the method used to solve the set of ordinary differential equations that constitute the pyrolysis model and the tridiagonal matrix, which is derived from the linear finite difference equations that constitute the combustion model. The FORTRAN code is also provided.

The cellulose and char mass flow profiles for a base case where the McKay Bay facility is operating at 77% of its design capacity are shown in Figures 1 and 2. Three distinct regions exist in Figure 1, which shows the results of the pyrolysis model. A significant portion of the kiln length is taken up by the heatup zone in which the MSW is raised to the reaction onset temperature. This is achieved by auxiliary fuel usage. Farther down the kiln is a short reaction zone in which pyrolysis of the waste occurs. This zone is characterized by a fall in the cellulose mass flowrate and a concomitant increase in that of the char. The third zone, where the pyrolysis model shows a constant char flowrate, and is in reality the burnout zone, is more appropriately described in Figure 2 by the results of the combustion model. Note that the abscissa has been shifted between Figures 1 and 2, such that the origin for Figure 2 is placed at the beginning of the burnout zone.

Bed temperature profiles through the heatup and reaction zones are shown in Figure 3 for the base case (9,400 kg waste/hr) and a case of further reduction in flow (4,500 kg waste/hr). This is an example of the use of the model to conduct parametric studies. Figure 3 indicates that the bed temperature is fairly insensitive to changes in the MSW feedrate. This could perhaps be justified by recalling that the bed is fairly well mixed and also that at a constant fuel-air ratio the flame temperature remains constant due to a balance between the reactive heat input and the convective heat removal. In operating incinerators the bed temperatures have been observed to be markedly different for different solids feedrates. This could result if the fuel-air ratio is not held constant during such experiments. Then again, incorporation of the radiative component of heat transfer could result in temperature profiles which match the actual trends better.

Another example of a parametric study is shown in Figure 4, which examines the relatively significant effect of bed porosity (0.54 void fraction - the base case - vs. 0.675 void fraction) on the rate of combustion in the burnout zone. Higher values of porosity reduce the length of this zone because the oxygen has better access to the char.

CONCLUSIONS

The mathematical model of a rotary kiln MSW combustor successfully predicts important aspects of its overall performance and several trends involving parametric variations in its operation. The size of the heatup zone, the size of the reaction zone, and the carbon burnout are quite accurate. However, temperature responses to changes in the MSW feedrate and the size of the burnout zone do not conform strictly to operational experience.

The current model, as well as improved future versions, should prove helpful in the analysis and design of waste-to-energy facilities employing this technology. The analysis of bed porosity has already shown that this parameter is a key factor in the performance of the burnout zone. Analysis of the heatup zone suggests that, because this region appears to require a major portion of the incinerator, preheat of the MSW feed by exiting flue gases might increase kiln capacity.

REFERENCES

[1] Tillman, D. A., et al., Incineration of Municipal and Solid Hazardous Wastes, Academic Press, 1989, p. 21.

[2] Hajalogol, M. R., et al., Ind. Eng. Chem. Process Des. Dev., 21, 457, 1982.

[3] Levenspiel, O., Chemical Reaction Engineering, John Wiley & Sons, 1977, p. 466.

[4] Essenhigh, R. H., and T. J. Kuo, Second Incineration Conference, Chicago, IL, 1965.

[5] Gorog, J. P., et al., Metall. Trans., **13B**, 153, 1982.

[6] Ghoshdastidar, P. S., et al., ASME National Heat Transfer Conference, Denver, CO, 1985.

[7] Jang, D. S., and S. Acharya, AIChE Annual Meeting, New Orleans, LA, 1988.

[8] Silcox, G. D., and D. W. Pershing, AIChE Annual Meeting, New Orleans, LA, 1988.

[9] Ghezzi, U., et al., Proceedings of the Intersociety Energy Conversion Engineering Conference, Piscataway, NJ, 1988.

[10] Wormeck, J. J., and D. W. Pershing, Proceedings of the ASME National Heat Transfer Conference, Houston TX, 1988.

[11] Lemieux, P. M., et al., Waste Management, **9**, 125, 1989.

[12] Sethi, V., and P. Biswas, JAPCA, **40**, 42, 1990.

[13] Theodore, L., and Reynolds, Introduction to Hazardous Waste Incineration, John Wiley & Sons, 1987, p. 248.

[14] Waste Management, Inc., Fact Sheet and Project Description of the McKay Bay Refuse-to-Energy Facility, Tampa FL, 1985.

[15] Banerjee, K., MS Thesis, University of Pittsburgh, 1990.

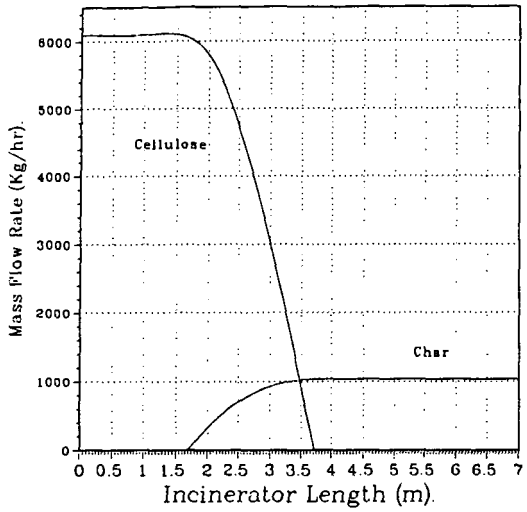

Figure 1. Mass Flow Profiles for the Base Case

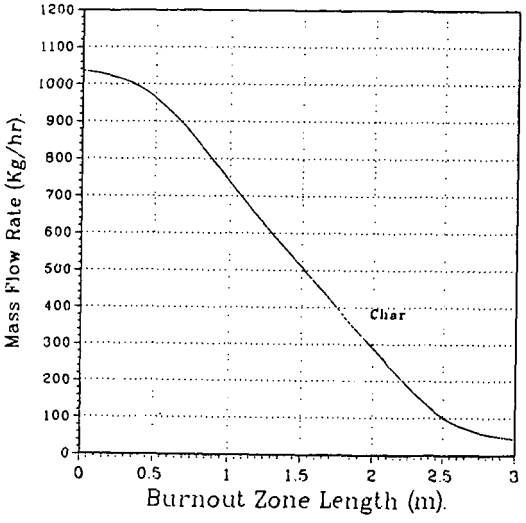

Figure 2. Char Mass Flow Profile in the Burnout Zone

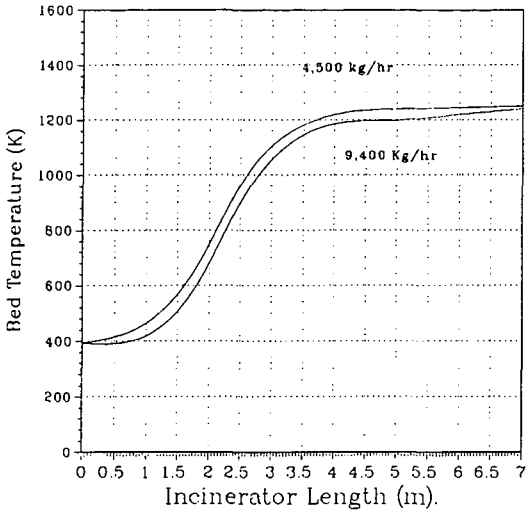

Figure 3. Bed Temperature Profiles

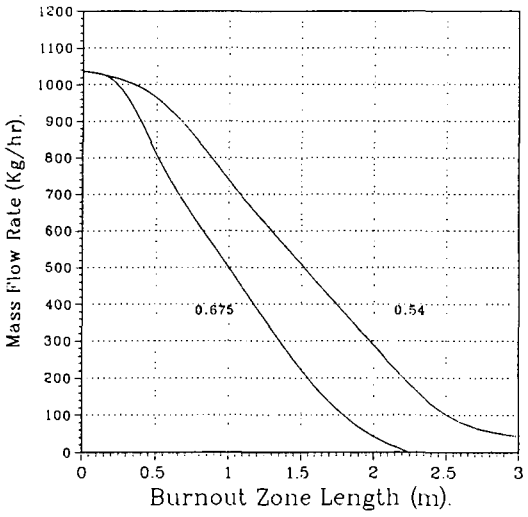

Figure 4. Effect of Bed Porosity

ENERGY AND MASS BALANCE CALCULATIONS FOR INCINERATORS

C.C. Lee and G.L. Huffman
U.S. Environmental Protection Agency
Risk Reduction Engineering Laboratory
Cincinnati, Ohio 45268

ABSTRACT

An estimate of an energy and mass balance within an incinerator is a very important part of designing and/or evaluating the incineration process. This paper describes a simple computer model which is used to calculate an energy and mass balance for a rotary kiln incinerator. The main purpose of the model is to assist EPA permit writers in evaluating the adequacy of the data submitted by incinerator permit applicants. The calculation is based on the assumption that a thermodynamic equilibrium condition exists within the combustion chamber. Key parameters which the model can calculate include:

- Theoretical combustion air;
- Excess air needs for actual combustion cases;
- Flue gas flow rate; and
- Exit temperature.

INTRODUCTION

Although there are many potential hazardous waste treatment technologies, current data indicate that no other treatment technology is as universally applicable as incineration to treat the many different types of hazardous waste. A recent survey showed that more than 80% of the technologies used to remediate Superfund sites are incineration-related technologies (Lee, 6/90). As a matter of fact, incineration has been considered to be a proven technology in many of the regulations developed under the various environmental laws enacted to cover the treatment/disposal of the different types of solid wastes; for example:

(1) Hazardous, medical and municipal waste as regulated under the Resource Conservation and Recovery Act (RCRA);

(2) Industrial and municipal sludge waste as regulated under the Clean Water Act;

(3) Pesticide waste as regulated under the Federal Insecticide, Fungicide and Rodenticide Act (FIFRA);

(4) Superfund waste as regulated by the Superfund Amendments and Reauthorization Act (SARA); and

(5) Toxic substances as regulated under the Toxic Substances Control Act (TSCA).

In addition, incineration facilities are subject to the regulations under the Clean Air Act and numerous State and local requirements.

One of the key factors necessary to ensure the safe incineration of various wastes is for a permit writer to fully understand the incineration process and to adequately check or specify permit conditions at an incineration facility that has come under his or her scrutiny. However, this not an easy task for the following reasons:

- In many cases, the incineration facility is site-specific and process-specific. In other words, different incinerators use different destruction processes and different pollution controls.
- In reviewing a permit application, a permit writer often is confronted with the complex and highly uncertain task of determining whether data submitted are adequate or accurate. For example, if an applicant's data show that his incinerator can reach a certain temperature by burning certain wastes at certain combustion air levels, the question is, "Are the claimed data dependable?"
- In issuing a permit, a permit writer needs to make decisions regarding how to approve or how to specify permit conditions which, for obvious reasons, involve costs and the personnel needed for that industry to comply with the final permit.

The Risk Reduction Engineering Laboratory (RREL) of EPA's Office of Research and Development in Cincinnati has been supporting EPA's RCRA permit writers regarding how to appropriately evaluate a permit application. One of the products from this support effort has been the development of the Energy and Mass Balance Model for Incinerators. The model was intended to assist a permit writer in quickly evaluating whether or not an incineration applicant's claimed data are based on sound engineering principles and are dependable. However, the model involved many complex submodels and are compiled in a computer diskette. Presently, a user cannot see the detailed steps which are built into the software in order to edit the calculation procedures to serve his own specific calculational needs. To overcome this model disadvantage, the authors used the model concept and wrote a program on Lotus 1,2,3 to compare the calculated results with an actual case for which measurement data were available. The results will show that the calculated data are reasonably consistent with the actual trial burn data.

STATEMENT OF THE PROBLEM

A Ciba-Geigy rotary kiln incinerator was chosen as the basis for the calculation. The schematic of the Ciba-Geigy incinerator is shown in Figure 1 (EPA 9/86).

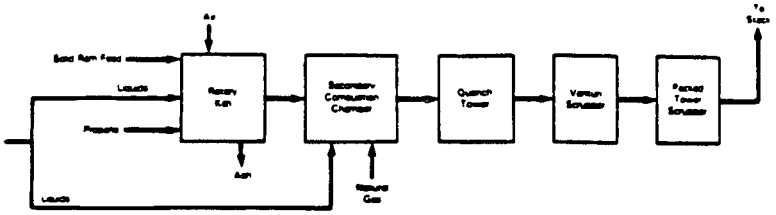

Figure 1. Process Flow Diagram of Ciba-Geigy Incinerator

Ciba-Geigy sponsored a trial burn on November 12-17, 1984. The measured data was later summarized in an EPA report (EPA 9/86) and key aspects of it appear below.

Equipment Information:

- Type of unit: Private incinerator-Rotary kiln with secondary chamber, Vulcan Iron.
- Capacity: 50 tpd (tons per day) with 10% excess capacity (30 x 10^6 Btu/h for each burner)
- Pollution control system: Quench tower, Polygon venturi scrubber (25-in. pressure drop), and packed tower scrubber.
- Waste feed system:
  - Liquid: Hauck Model 780 wide range burners (kiln and secondary burners)
  - Solid: Ram feed
- Residence time: 5.05 s (kiln); 3.09 s (secondary chamber)

Test Conditions:

- Waste feed data: Hazardous liquid and nonhazardous solid wastes usually burned; for this run, only, synthetic hazardous liquid waste was tested
- Length of burn: 6 to 9 h (2-h sampling time)
- Total amount of waste burned: 480 gal (liquid) and 0 lb (solid)
- Waste feed rate: 4 gpm (liquid); 0 lb/h (solid)

- POHCs (Principal Organic Hazardous Constituents) selected and concentration in waste feed:

Name	Concentration, %
Hexachloroethane	4.87
Tetrachloroethene	5.03
Chlorobenzene	29.52
Toluene	60.58

- Btu content: 15,200 Btu/lb
- Ash content: Not measured
- Chlorine content: 20.8% (calculated)
- Moisture content: Not measured

Operating Conditions:

- Temperature: Range 1750° - 1850°F (kiln); 1950° - 2050°F (Secondary chamber)
- Average 1800°F (kiln); 2000°F (Secondary chamber)
- Auxiliary fuel used: Natural gas
  - Primary kiln 1200 scfh natural gas; Secondary chamber 900-1300 scfh
- Airflow:
  - Primary air to kiln: 2200 cfm
  - Secondary air to kiln: 1400 cfm
- Flue gas oxygen content: 10.3%

ENERGY AND MASS BALANCE CALCULATIONS [For Primary Chamber (Kiln) Only]

a. Given Conditions

a1.	Waste feed rate (gpm):	4 gpm	
	Assume that 1 gal =	5 lb	
	Waste feed rate in lb/hr:		1200 lb/h
a2.	Fly ash (% of waste feed):		0 (assumed)
a3.	% of ash due to unburned carbon:		0 (assumed)
a4.	Ash quench temperature:	undefined	
a5.	Exit temperature:	unspecified	
a6.	Reference temperature:		70°F
a7.	Radiation loss (assumed):	(5%)	0.05 (5%)
a8.	Excess air rate (EAR)[assumed]		0.885 (i.e., 88.5% XSair)
a9.	Humidity at 60% RH and 80°F	0.0132 kg H_2O/ kg-dry-air	0.0127 lb H_2O/ lb-dry-air
a10.	Standard volume:	24.04 scm/ kg-mole	386.9 scf/lb-mole
a11.	Water latent heat:	2460 kJ/kg	1057 B/lb
	Heat capacity (specific heat):		(where B = Btu)
a12.	Ash	0.83 kJ/kg-C	0.25 B/lb-F
a13.	Flue gas:	1.09 kJ/kg-C	0.26 B/lb-F
a14	Water:	2.35 kJ-kg-C	0.49 B/lb-F

a15. 1kcal/g=	4187	kJ/kg	1799 B/lb
	2.33	kJ/kg	1 B/lb
	1	kJ/kg	0.43 B/lb
	1.06	kJ	1 B
	1	m	3.28 ft
a16. Natural gas (NG): (heat of combustion)	13.3	kcal/g	23932 B/lb

	POHC ratio	waste lb/h	ΔHc kcal/g	B/lb	Mixture B/h
Hexachloroethane, C_2Cl_6	0.0487	58.44	0.46	828	4.84E+04
Tetrachloroethene, C_2Cl_4	0.0503	60.36	1.19	2141	1.29E+05
Chlorobenzene, C_6H_5Cl	0.2952	354.24	6.60	11876	4.21E+06
Toluene, C_7H_8	0.6058	726.96	10.14	18246	1.33E+07
Water, H_2O		0		0	
Waste		0		0	
Fuel		0		0	
		0		0	
	1.0000	1200.00			1.76E+07

Therefore, the heat value of the POHC mixture = 14,667 B/lb

a17. Natural gas (NG): (heat of combustion)	13.3	kcal/g
a18. Total waste heat input:	1.76E+07	B/h

a19. Chemical analysis:

	Σ C's	Σ H's	Σ Cl's	Σ O's	Σ Molecular Weight, M
C_2Cl_6	24.00	0	213	0	237.00

		lb/h
C's/M	0.1013	5.92
H's/M	0.0000	0.00
Cl's/M	0.8987	52.52
O's/M	0.0000	0.00
	1.0000	Σ = 58.44

C_2Cl_4	24.00	0	142	0	166.00
C's/M	0.1446				8.73
H's/M	0.0000				0.00
Cl's/M	0.8554				51.63
O's/M	0.0000				0.00
	1.0000				Σ = 60.36

C_6H_5Cl	72.00	5	35.5	0	112.50
C's/M	0.6400				226.72
H's/M	0.0444				15.74
Cl's/M	0.3156				111.78
O's/M	0.0000				0.00
	1.0000				Σ = 354.24

C_7H_8	84.00	8	0	0	92.00
C's/M	0.9130				663.72
H's/M	0.0870				63.24
Cl's/M	0.0000				0.00
O's/M	0.0000				0.00
	1.0000				Σ = 726.96

Fuel (natural gas, CH_4) to kiln: 1200 scf/h
Fuel density = Molecular Wt/std volume (a10): 0.04135 lb/scf
Fuel weight flow rate = fuel density x fuel volume flow rate
= 49.62 lb/h

CH_4	12.00	4	0	0	16.00
C's/M	0.7500				37.22
H's/M	0.2500				12.40
	1.0000				49.62

H_2O in fuel: 0

a19. Fuel heat input = weight rate x HHV: 1.188+06 Btu/h
a20. Total Heat In = Waste Input (a18) + Fuel Input (a19): 1.88E+07 Btu/h
Total average heating value = a20/(waste + fuel): 15,045 Btu/lb

*****Test data was 15,200 Btu/lb*****

a21. Chemical analysis summary (in lbs/hr):

	W & F analysis	F: fuel	unburned carbon	W: waste feed	total combustible feed	Fraction of combustible feed
C:		37.2		905	942.2	0.7540
H:		12.4		79	91.4	0.0731
Cl:				216	216	0.1729
O_2:				0	0	0.0000
N_2:				0		
S:				0		
H_2O				0		
Ash:				0		
Fly ash: (unburned carbon becomes ash):				0		
		49.6		1200	1249.6	1.0000

b. Theoretical Combustion Air

b1. Calculation of oxygen needs
$C+O_2 \rightarrow CO_2$
O_2=C*32/12=2.67*C= 2.67(942.2)= 2516 lb/hr
H left over after Cl's reaction (HLO)
HLO=H-Cl/35.5= 85.32 lb/hr
$H_2+0.5O_2 \rightarrow H_2O$
O_2=HLO*0.5*32/2= 682
$S+O_2 \rightarrow SO_2$ O_2=S*32/32 0
- Bound O_2 0

b2. Theoretical oxygen (Th. O_2) 3198 99.94 mole/h
b3. Th. nitrogen, N_2=(Th.O_2)*3.76*28/32 10521 375.77 mole/h
b4. Theoretical dry air = Theor. O_2+N_2: 13719 475.71 mole/h

b5. Humidity: 0.0127

b6. Water due to humidity = b4*b5 174

b7. Actual theor. air=dry theor. air+its H_2O 13893

b8. Theor. reactants=actual theor. air+feed 15143 lb/hr

b9. Theoretical air combustion products:
CO_2=C*44/12: 3455 lb/hr 78.52 mole/h
SO_2=S*64/32 0 0.00

b10. H_2O=HLO*18/2:	768	42.66
N_2=(Th.O_2)*3.76*28/32	10521	375.77
HCl=Cl*36.5/35.5	222	6.08
b11. H_2O in feed:	0	0.00
Fly ash:	0	0.00
Ash:	0	0.00
b12. H_2O due to humidity:	174	9.67
N_2 with waste:	0	0.00
b13. Theor. combustion products:	15140 lb/hr	513 mole/h
b14. Check (b8=b13):	15143 lb/hr	
b15. Combustion dry gas=CO_2+SO_2+HCl+N_2:	14198 lb-dry-gas/hr	
b16. Combustion gas H_2O: (b10+b11+b12)	942 lb H_2O/hr	
	15140 lb/hr	

c. Actual Combustion Air:

Excess air rate, EAR (a8): 0.885 (assumed)

c1. O_2, additional=EAR*(Th.O_2):	2830
c2. N_2, additional=EAR*(Th.N_2):	9311
c3. Actual Excess dry air:	12141
c4. Excess H_2O (b5xc3):	154 lb/h

c5. Actual dry air= theor. air+Additional O_2 and N_2 25860 lb-dry air/h

c6. H_2O associated with actual air = (b5xc5 or b12+c4): 328 lb H_2O

c7. Actual air=dry air+H_2O in air: 26188 lb-air/h=908 lb-mole/h (c5+c6)

c8. Air flow rate = std. volume (a10) x lb-mole/h=351305 scf/h =(a10 x c7): =5855 scf/min

*****Test data was 3600 cfm*****

Total water vapor in flue gas

• With waste (a21):	0 lb/h
• Due to combustion (b10):	768
• Humidity (c4+b12):	328
• Quenching water:	0

c9. Total water vapor in flue gas = 1096 lb/hr

c10. Actual reactants=actual dry air+feed + H_2O in combustion air (a21+c7)= 27438 lb reactant/hr =27438 lb product/hr

Actual Combustion Products (i.e., Flue Gas):

c11. O_2 leftover in products = 2830 lb/hr
Additional O_2 = c1:
c12. O_2 content in flue gas = 0.1031 = 10.31%
c11 ÷ c10:
**** Test data was 10.3% ****

d. Calculation of Exit Temperature from Kiln

d1. Total heat in=Waste Heat Input (a18) + Fuel Heat Input (a19)=a20: 1.88E+07 B/h
d2. Overall heat loss (assumed as 5%, see a7): 0.0940E+07

Unburned carbon:
d3. Unreleased heat (due to unburned carbon): 0.0000E+00

Trial #1
Assumed exit temp.: 1500°F
Reference temp.: 70°F

d4. Temp. difference (ΔT): 1430°F
d5. Heat in dry flue gas=mCpΔT =[c10-c9)xa13xd4] 0.9794E+07B/h
d6. Heat in water = mCpΔT =(c9xa14xd4): 0.0768E+07
d7. Total latent heat = (c9xa11): 0.1158E+07
d8. Heat in ash = mCpΔT=(a2xa12xd4): 0.0000E+00
d9. Total heat accounted for= (d2+d3+d5+d6+d7+d8): 1.2660E+07

d10. Net heat balance = (a20-d9)=(d1-d9): 0.6140E+07B/h

Trial #2
Assumed exit temp.: 2500°F
Reference temp.: 70°F

d11. Temp. difference (ΔT') 2430°F
d12. Heat in dry flue gas=mCpΔT' =[(c10-c9)xa13xd11]: 1.6643E+07
d13. Heat in water=mCpΔT' =c9xa14xd11): 0.1305E+07
d14. Total latent heat=(c9xa11): 0.1158E+07
d15. Heat in ash=mCpΔT'=(a2xa12xd11): 0.0000E+07
d16. Total heat accounted for=(d2+d12+d13+d14+d15): 2.0046E+07b/h
d17. Net heat balance=(a20-d16): -0.1246E+07b/h

d18. Using the interpolation method to estimate kiln temperature, we have:

x1	1500°F	0.6140E+07 B/Hr	y1	
	x	0.00E+00	y	y=0
x2	2500	-0.1246E+07	y2	

$$(x-x1)/(0-y1)=(x2-x1)/(y2-y1)$$
$$x=x1-y1(x2-x1)/(y2-y1)$$

d19. x= 2331°F

*****Test data was 1800°F (average kiln exit temperature)*****

SUMMARY OF CALCULATED RESULTS AND MEASURED RESULTS

Based on the calculations contained herein and information provided by the trial burn results, a summary of key data are provided in the following Table:

SUMMARY OF CALCULATED AND TRIAL BURN RESULTS

	Calculated Results	Measured Results
• O_2 content in Flue Gas	10.31%	10.3%
• Heating Value	15,045 Btu/lb	15,200 Btu/lb
• Exit Kiln Temperature	2331°F	1800°F (average)
• Air Flow Rate	5855 scfm	3600 cfm

CONCLUSIONS

The above Table shows that the differences between the calculated and the measured results are small with the exception of the kiln exit temperature and the air flow rate. The calculated value of the air flow rate is about 63% greater than the trial burn (measured) value. The difference is due to the fact that the measured air rate values neglected to account for the amount of air in- leakage which has to occur in any actual (negative pressure) kiln combustion operation. The measured data relative to oxygen content shows that the calculated air in the system (the 5855 scfm amount) is reasonable because the oxygen content measured downstream of the kiln matches the calculated oxygen concentration (the 10.3%). The calculation, therefore, confirms that the air needed is much more than the 3600 cfm measured value (which, of course, proves that air in-leakage phenomena does occur). The fact that the measured kiln exit temperature is also much lower (about 530°F lower) than the calculated kiln exit temperature indicates that the assumed amount of heat loss (the 5% figure) is probably too low.

It is hoped that these example calculations will assist those who must design incinerators or those who must know how to evaluate their performance (such as governmental permit writers, consultants and public interest groups).

REFERENCES

(EPA, 9/86), "Permit Writer's Guide Test Burn Data: Hazardous Waste Incineration," EPA/625/6-86/012, September 1986.

(Lee, 6/90), "Review of Mobile Thermal Technologies for Solid Waste Destruction," C.C. Lee, G.L.Huffman and D.A. Oberacker. Presented at the 83rd National Meeting of the Air and Waste Management Association, Pittsburgh, Pennsylvania, June 24-29, 1990.

AN INVESTIGATION OF THE EFFECT OF COAL PRETREATMENT ON LIQUEFACTION BEHAVIOR

C.J. Brannan[a], C.W. Curtis[a] and D.C. Cronauer[b]
[a]Chemical Engineering Department, Auburn University, Alabama 36849;[b] Amoco Oil Company, Naperville, Illinois 60566

The effect of coal pretreatment on thermal and catalytic liquefaction behavior was examined in this study. Black Thunder coal, a subbituminous coal from Wyoming, was used untreated and after pretreatment with SO_2. SO_2 pretreatment involved crushing and sizing the coal and then contacting the coarse fraction with aqueous SO_2 to remove alkali and alkaline metals. This treatment was followed by a gravity separation to recover the fraction with the lowest ash content.[1] Analysis of these coals presented in Table 1 indicates that the SO_2 treatment of Black Thunder coal doubles the amount of sulfur in the coal but halves the amount of ash present.

In this study, the effect of different slurry-phase catalyst precursors, most of which were oil-soluble, on the liquefaction behavior of both the untreated and SO_2 pretreated coal was examined. The first set of experiments was performed without a solvent but with the addition of a probe hydrogenation species, pyrene. The second set of experiments was performed with selected catalysts and pyrene but with using a solvent in the liquefaction reactions. The solvents chosen were a non-donor solvent, 1-methylnaphthalene, a coal-derived solvent, V1074, and a hydrogen donor solvent, 9,10-dihydroanthracene. The last set of experiments evaluated the combination of two types of coal pretreatment, in which the untreated and SO_2 treated Black Thunder coals were preswelled prior to liquefaction reactions. The swelling solvents chosen were methanol, isopropanol, tetrahydrofuran and dimethylsulfoxide on the basis of the research performed at Amoco in conjunction with this work.[2] The liquefaction reactions were performed thermally and catalytically. Ni octoate was chosen as the catalyst because of its demonstrated activity while 1-methylnaphthalene was chosen as the reaction solvent because of its apparent noninteraction with the coal and pyrene system which would allow the effect of preswelling as a pretreatment method to be clearly demonstrated.

EXPERIMENTAL

Catalyst Screening Test. The catalytic activity of a number of different catalysts for coal conversion of untreated and SO_2 treated Black Thunder coal and pyrene hydrogenation was evaluated with and without solvent. The system without solvent was composed of 1.5 g pyrene, 20 wt% coal and a nominal 600-700 ppm of active metal from the catalyst precursor based on the coal feed. The coals used were untreated Black Thunder coal and SO_2 treated Black Thunder coal which were obtained from Amoco. Proximate and ultimate analyses for both coals are given in Table 1. The catalyst precursors tested were molybdenum naphthenate (Shepherd Chemical), iron naphthenate (Aldrich), nickel naphthenate (Shepherd Chemical), nickel octoate (Shepherd Chemical), chromium 2-ethylhexanoate (Strem Chemical), and vanadium naphthenate (Strem Chemical). The reactions were performed using ~20 ml stainless steel tubular reactors at 410° for 30 min and were agitated horizontally at 450 cpm. The pyrene reaction products were analyzed by gas chromatography using a Varian Model 3400, a J&W DB column and flame ionization detection. Pyrene conversion and hydrogenation were used to compare the effect of the catalyst and coal pretreatment on the hydrogenation reactions. Pyrene hydrogenation is defined as the moles of hydrogen required to form the liquid hydrogenation products from pyrene as a percentage of the moles of hydrogen required

to form the most hydrogenated product, perhydropyrene. Coal conversion to THF solubles was also determined.

The reaction systems with solvent employed these different solvents: 9,10-dihydroanthracene, 1-methylnaphthalene, and V1074, a coal derived solvent from the Wilsonville Coal Liquefaction Research and Development facility. The coals used were untreated and SO_2 treated Black Thunder coals. The catalysts employed with the different solvents were nickel octoate, cobalt naphthenate and chromium naphthenate with 9,10-dihydroanthracene; nickel octoate with V1074; and nickel octoate and chromium naphthenate with 1-methylnaphthalene. The reaction conditions used were 410 °, 1250 psig H_2 at ambient temperature, 30 min reaction time, 1.33 g maf coal, 0.67 g pyrene, 2.00 g of solvent, and catalyst loading of 600 to 700 ppm of active metal based on coal feed. The reactors were the same as previously described. The pyrene reaction products and coal conversion were obtained as stated earlier.

Coal Swelling Reactivity Test. For the coal swelling reactivity test, four swelling solvents were used: methanol, isopropanol, tetrahydrofuran, and dimethylsulfoxide, all of which were obtained from Fisher Scientific and were used as received. Untreated and SO_2 treated Black Thunder coals were swelled prior to reaction by introducing 2 g of coal to a swelling tube along with 7 ml of swelling solvent. After 2 hr the amount of coal swelling that occurred was determined by measuring the height of the coal and comparing that to the height of the coal prior to swelling. The coal remained in the swelling solvent for a total of 24 hr, after which the solvent was removed from the coal and dried for 7 hr at room temperature; the weighed coal was placed in the liquefaction reactor and then reacted at 410° for 30 min under well-agitated conditions. Each reaction contained a nominal 1.33 g of maf coal, 2.00 g of 1-methylnaphthalene as solvent, 0.67 g of pyrene, and any residual swelling solvent remaining in the coal for those reactions performed with prior solvent swelling. Hydrogen gas was introduced at 1250 psig at ambient temperature. Reactions were performed thermally and catalytically; the catalyst used was nickel octoate introduced at a level of 600 to 800 ppm of active metal

DISCUSSION OF RESULTS

Effect of Catalyst Precursors on Coal and Pyrene Conversion. Liquefaction reactions were performed with untreated and SO_2 treated Black Thunder coals without a solvent using pyrene as a probe hydrogenation species. The amount of coal conversion, pyrene conversion and pyrene hydrogenation (HYD) achieved with the different catalyst precursors is presented in Table 2. With each catalyst precursor when no solvent was present, the coal conversion was higher with the SO_2 treated coal than with the untreated. In the reactions with Mo naphthenate, the amount of coal conversion was almost doubled, while Fe naphthenate, Ni naphthenate, and Ni octoate showed substantial improvements with the SO_2 treated coal. The catalyst precursors that had the least effect on coal conversion for untreated Black Thunder coal were Mo naphthenate and Cr 2-ethylhexanoate which yielded average coal conversions of 48.1 and 48.0%, respectively.

Pyrene conversion varied considerably depending upon the type of catalyst precursor present and the amount of sulfur present in the system (Table 2). Pyrene conversion for the untreated coal system was greatest with Ni octoate and Ni naphthenate while Mo naphthenate, Fe naphthenate, Cr 2-ethylhxanoate and V naphthenate showed low activity. The presence of the additional sulfur in the SO_2 treated coal affected some of the activity for pyrene conversion for the different catalysts. Mo naphthenate increased substantially from 3.4% in the untreated system to 26.3% in the SO_2 treated system. Cr 2-ethylhexanoate doubled in pyrene conversion but still showed low activity. Ni octoate was active with the SO_2 treated coal just as it was with the untreated coal. The primary hydrogenation product from pyrene observed with all of the catalyst precursors was dihydropyrene

(DHP) while the more active catalysts also yielded tetrahydropyrene (THP) and hexahydropyrene (HHP) as the reaction products.

When solvents were used in the liquefaction reaction in the presence of catalysts precursors, interactions between the solvent and catalyst precursor became apparent. For example, Ni octoate was used with all three solvent systems; for both untreated and SO_2 treated Black Thunder coal, the hydrogen donor solvent, 9,10-dihydroanthracene (DHA), produced the highest coal conversion, followed by coal-derived V1074 with the nondonor, 1-methylnaphthalene (1-MN), yielding the least conversion. The reactions with Cr naphthenate in DHA yielded coal conversions of ~77 and ~79% for untreated and SO_2 treated coals while in 1-MN the conversions with Cr naphthenate were ~53 and ~52%, respectively. Pyrene conversions tended to vary rather substantially and appeared to be influenced by the specific interactions of the solvent with the catalyst and probe pyrene molecule. The highest conversions of pyrene were observed with Ni octoate in 1-MN, but nearly twice as much pyrene conversion was obtained with SO_2 treated coal than with untreated coal. The primary hydrogenation products from pyrene in the reactions with the solvents were DHP; only minor amounts of THP were formed when DHA was solvent while neither THP nor HHP was formed with the other two solvents.

Effect of Solvent Preswelling on Liquefaction Reactions. Four swelling solvents, THF, methanol, isopropanol, and DMSO, were employed to preswell untreated and SO_2 treated coals. The swelling of the SO_2 treated and untreated Black Thunder coals ranked as methanol $\simeq$ isopropanol $<$ THF $<$ DMSO. DMSO swelled the untreated coal by 100% so that the volume of the coal doubled. The other swelling solvents, methanol, isopropanol and THF, swelled the untreated coal by 16 to 42% with THF being the most effective among the three. Methanol and isopropanol remained in the coal in similar amounts which ranged from 0.9 to 1.3 g for 1.6 to 1.7 g of coal. THF showed more inclusion in the coal leaving between 1.45 to 1.7 g in 1.6 to 1.7 g of coal while DMSO left between 3.1 to 4.3 g in 1.62 g of untreated coal.

All of the swelling solvents increased the volume of the SO_2 treated coal more than they did for the untreated coal, although the swelling ranking was the same. Again DMSO remained strongly absorbed in the coal after removal of the swelling solvent with amounts ranging from 4.0 to 5.7 g. By contrast, nearly 2.0 g of THF and about 1.0 g of either methanol or isopropanol was retained in an equivalent amount of coal.

Liquefaction reactions were performed thermally without a catalyst and with Ni octoate. Ni octoate was chosen as the catalyst because of its demonstrated high activity for coal conversion. Table 3 presents the change in coal volume upon swelling, coal conversion and pyrene conversion for both untreated and SO_2 treated coals. The addition of Ni octoate increased the amount of coal conversion achieved regardless of swelling solvent or no swelling solvent. Likewise, pyrene conversion was increased with Ni octoate present in the reaction medium.

The preswelling solvent which showed the most improvement for coal conversion compared to no preswelling for thermal reactions of untreated coal was isopropanol and THF for the SO_2 treated coal. Methanol yielded the greatest improvement in the reactions with Ni octoate for both untreated and SO_2 treated coals. By contrast, DMSO, which was the most effective swelling solvent and had the highest incorporation into the coal, was most detrimental for coal conversion. The SO_2 pretreated coal reacted with Ni octoate was more adversely affected by DMSO than the untreated coal.

Pyrene conversion varied according to the reaction condition. For untreated Black Thunder coal systems, the highest pyrene conversion was achieved with Ni octoate with methanol and without preswelling solvent. For the SO_2 treated Black Thunder coal systems, the highest pyrene conversion was obtained with Ni octoate and no preswelling solvent followed by Ni octoate with DMSO as preswelling solvent. Product distributions achieved from pyrene with coal preswelling yielded DHP

as the primary product for reactions with Ni octoate and occasionally with the thermal reactions depending upon the type preswelling solvent. Some HHP was formed with the Ni octoate systems depending again upon the preswelling solvent.

SUMMARY

SO_2 pretreatment of Black Thunder coal enhanced the liquefaction behavior of the coal in the presence of different catalytic agents regardless of whether a solvent was present or not. A hydrogen donor solvent, 9,10-dihydroanthracene, promoted increased coal conversion compared to nondonor and coal-derived solvents. Pyrene conversion and hydrogenation were highly dependent upon the catalyst type and upon the presence of sulfur in the system. For Mo naphthenate the sulfur in SO_2 treated Black Thunder coal with solvent present promoted pyrene conversion while for Ni octoate, the sulfur was detrimental to pyrene conversion. The presence of solvent in the liquefaction reaction tended to level the amount of pyrene conversion although 1-methylnaphthalene had a lesser effect than did the other two solvents.

Swelling coal prior to liquefaction reactions had a more positive effect with untreated Black Thunder coal than with the SO_2 treated as shown in Table 4. The only swelling solvent that was detrimental to coal conversion for the untreated coal was DMSO while for the SO_2 treated coal only methanol showed an improvement in coal conversion. Hence, coal preswelling was most effective for untreated Black Thunder coal.

NOMENCLATURE

% HYD	=	percent hydrogenation	maf	=	moisture and ash free
1-MN	=	1-methylnaphthalene	PYR	=	pyrene
DHA	=	dihydroanthracene	THF	=	tetrahydrofuran
DHP	=	dihydropyrene	THP	=	tetrahydropyrene
HHP	=	hexahydropyrene			

ACKNOWLEDGEMENTS

We thank the Department of Energy for support of this work under Contract No. DE-AC22-91PC91051. We also sincerely appreciate the strong support of our staff: Janice Johnson, Patricia Sandlin, Frank Bowers, and Joseph Aderholdt.

REFERENCES

1. Cronauer, D.C., Quarterly Report for "Advanced Liquefaction Using Coal Swelling and Catalyst Dispersion Techniques," July-September 1992; Contract No. DE-AC22-91PC91051.
2. Cronauer, D.C., Personal Communication, 1993.

Table 1. Proximate and Utimated Analysis of Untreated and SO_2 Treated Black Thunder Coals[a]

Proximate Analysis[b]			Ultimate Analysis[c]		
	Untreated	SO_2 Treated		Untreated	SO_2 Treated
% Moisture	11.2	9.9	% Carbon	69.7	70.5
% Ash	5.4	3.1	% Hydrogen	4.9	5.0
% Volatile Carbon	44.5	41.7	% Nitrogen	0.9	0.9
% Fixed Carbon	38.8	45.3	% Sulfur	0.4	0.8
Total	100.0	100.0	% Ash	6.1	3.4
Btu/lb	10606	10993	% Oxygen (by difference)	18.0	19.4

[a]CommercialTesting and Engineering Co., Birmingham, AL
[b]As Received
[c]Dry Basis

Table 2. Effect of Catalyst Type on Coal and Pyrene Conversions Using Untreated and SO_2 Treated Black Thunder Coal With and Without Solvents[a]

Catalyst	Untreated Black Thunder Coal			SO_2 Treated Black Thunder Coal		
	% Coal Conversion	% Pyrene Conversion	% Pyrene HYD[b]	% Coal Conversion	% Pyrene Conversion	% Pyrene HYD
No Solvent						
None	59.6±0.9	1.6±0.1	1.0±0.1	57.5±11.5	1.3±0.4	0.8±0.3
Mo Naphthenate	48.1±1.8	3.4±1.7	1.1±0.6	85.7±2.1	26.3±2.5	9.2±0.9
Fe Naphthenate	54.2±11.2	1.4±0.1	1.0±0.3	63.4±2.8	4.9±4.2	2.1±1.6
Ni Naphthenate	62.7±10.9	13.1±6.8	5.7±1.5	73.9±5.7	15.8±0.4	5.7±0.1
Va Naphthenate	64.4	4.2	2.0	66.1±1.8	3.9±0.7	1.9±0.3
Ni Octoate	73.8±6.0	25.6±0.1	9.1±0.0	84.4±7.6	21.9±2.0	7.8±0.7
Cr 2-Ethylhexanoate	48.0±7.9	1.2±0.3	0.8±0.2	54.8±1.5	3.3±1.6	1.5±0.6
Solvent: 1-Methylnaphthalene						
None	49.3±0.8	3.5±1.1	2.1±0.6	47.3±1.1	1.5±1.1	0.7±0.7
Ni Octoate	70.7±4.1	6.8±0.3	2.3±0.1	76.3±4.2	12.5±3.5	4.2±1.2
Cr Naphthenate	52.7±1.8	0.0±0.0	0.0±0.0	51.7±1.1	0.0±0.0	0.0±0.0
Solvent: V1074						
Ni Octoate	81.5±0.9	6.8±4.3	2.4±1.6	82.1±3.0	2.0±2.8	0.7±0.9
Solvent: 9,10-Dihydroanthracene						
Ni Octoate	87.0±1.7	4.4±1.1	2.1±0.3	92.4±5.0	3.7±1.4	1.8±0.5
Co Naphthenate	83.2±0.1	2.1±0.2	1.3±0.1	85.9±0.8	2.7±0.4	1.6±0.3
Cr Naphthenate	76.8±4.2	4.0±0.0	2.6±0.0	78.6±5.7	2.9±1.3	2.0±0.9

[a]Reaction Conditions: 410°C, 30 min, 1250 psig H_2 at ambient temperature, agitated at 450 cpm.
[b]HYD = hydrogenation

Table 3. Effect of Solvent Preswelling on Reactions of Untreated and SO_2 Treated Black Thunder Coal in 1-Methylnaphthalene[a]

Catalyst	Swelling Solvent	Untreated Black Thunder Coal			SO_2 Treated Black Thunder Coal		
		Change in Volume (% ΔV)	Coal Conversion (%)	Pyrene Conversion (%)	Change in Volume (% ΔV)	Coal Conversion (%)	Pyrene Conversion (%)
None	None	NA	49.3±0.8	3.5±1.1	NA	47.3±1.1	1.5±1.1
Ni Octoate	None	NA	70.7±4.1	6.8±0.3	NA	76.3±4.2	12.5±3.5
None	THF	34.2±7.0	59.7±8.9	0.0±0.0	87.6±2.7	58.0±9.5	0.0±0.0
Ni Octoate	THF	41.3±0.6	77.0±0.1	2.4±0.1	97.4±3.7	72.5±5.8	2.2±0.4
None	Methanol	26.7±0.8	53.9±2.8	1.0±0.3	38.4±2.3	41.8±2.4	1.5±0.1
Ni Octoate	Methanol	18.6±0.6	85.5±0.1	10.9±0.4	31.6±7.4	78.6±1.1	4.9±0.8
None	Isopropanol	16.9±5.5	61.7±1.1	0.8±1.1	45.0±0.0	56.4±3.0	1.6±0.1
Ni Octoate	Isopropanol	16.3±3.8	77.6±1.1	2.2±0.4	32.3±6.4	73.9±5.1	3.9±0.6
None	DMSO	111.7±3.7	29.3±4.0	1.2±0.5	176.5±26.2	29.8±3.2	1.3±0.4
Ni Octoate	DMSO	102.4±9.5	63.6±3.6	5.0±0.8	171.6±11.9	50.1±9.5	7.1±1.1

[a] Reaction Conditions: 410°, 30 min, 1250 psig at ambient temperature agitated at 450 cpm.

Table 4. Comparison of the Effect of Swelling Solvents on the Liquefaction of Untreated and SO_2 Treated Black Thunder Coal

Swelling Solvents	Untreated Black Thunder Coal Percent Change in					SO_2 Treated Black Thunder Coal Percent Change in				
	Coal Conversion		Pyrene Conversion		Swelling Index	Coal Conversion		Pyrene Conversion		Swelling Index
	Thermal	Ni Octoate	Thermal	Ni Octoate	(ΔV%)	Thermal	Ni Octoate	Thermal	Ni Octoate	ΔV %
THF	+10.5	+6.3	-3.5	-4.5	37.3	+10.7	-3.8	-10.4	-10.4	88.1
Methanol	+4.6	+14.8	-2.5	4.1	21.3	-5.5	+2.4	-7.6	-7.6	35.6
Isopropanol	+12.5	+6.9	-2.7	-4.6	17.0	+9.1	-2.4	-8.7	-8.7	38.6
DMSO	-20.0	-7.2	-2.4	-1.9	110.0	-17.6	-26.2	-5.5	-5.5	175.0

COMPARISON OF LOW-SEVERITY COAL PRETREATMENTS FOR SUBSEQUENT CATALYTIC LIQUEFACTION

Ramesh K. Sharma and Edwin S. Olson
University of North Dakota
Energy & Environmental Research Center
Grand Forks, ND 58202-9018

ABSTRACT

Coal can be effectively solubilized by treatment with carbon monoxide reductant in an aqueous solvent (COsteam process). In recent work with U.S. and Australian low-rank coals, sodium aluminate was demonstrated to improve the conversions in the CO/H_2O system and in water/hydrogen donor solvent mixtures. In this paper, the catalytic hydrotreatment of the solubilized low-severity products from sodium aluminate-catalyzed and uncatalyzed CO/H_2O reactions of a Wyodak subbituminous coal are compared. Catalytic hydrogenations of the THF-soluble fractions obtained from the two low-severity products were performed with a conventional cobalt–molybdenum catalyst as well as two clay-supported iron catalysts at 425°C for 3 hours in the presence of 1000-psi (cold) H_2O pressure. Liquefaction with the cobalt–molybdenum catalyst gave 68% conversion to heptane solubles for both the sodium aluminate and the uncatalyzed low-severity reaction intermediates. In contrast, the supported iron catalysts gave much higher conversions for the intermediate from the sodium aluminate-catalyzed reaction compared to those from the uncatalyzed reaction. These results have important implications for multistage liquefaction processing schemes.

Keywords: liquefaction catalysts, coal solubilization catalysts

INTRODUCTION

Carbon monoxide and water have been utilized in the liquefaction of coal since 1921, when Fischer and Schrader demonstrated the effectiveness of this process (1). Improvements in the COsteam process have increased conversions to soluble products, but extensive depolymerization and hydrogenation of the coal macromolecules require further catalytic hydrotreatment of the COsteam product. The goal of the University of North Dakota Energy & Environmental Research Center (EERC) coal science group is the development of new homogeneous catalysts for the CO reaction. These catalysts are expected to aid in solubilization and preliminary reduction of low-rank coals to a high-quality intermediate product that can be easily catalytically converted to distillate fuels with low heteroatom content.

Catalysis of the first stage of coal liquefaction involves improving the rates of bond cleavage reactions leading to improved solubility and of preliminary reduction reactions so that oils and asphaltenes are produced without extensive retrogressive reactions. The catalysts should be able to interact effectively with the colloidal coal matter, to generate soluble products at moderate temperature. Thus various inexpensive and disposable inorganic agents that are soluble in the reaction vehicle or solvent are being investigated. Sodium aluminate catalyzed the solubilization of Australian coals in the CO/H_2O system and in water/hydrogen donor solvent mixtures (2, 3). Previous work at the EERC demonstrated that aqueous sodium aluminate was also effective for Wyodak subbituminous coal (4). High conversions comparable to those obtained with hydrogen donor solvents and hydrogen sulfide

were obtained. This paper compares the suitability of the intermediates from catalyzed and uncatalyzed CO/H_2O reactions as a feed for catalytic hydrogenation.

EXPERIMENTAL

Catalyst Preparation

An Amocat-1A cobalt–molybdenum catalyst was presulfided by heating with a small amount of sulfur and 1000 psi of hydrogen in a 15-mL rocking microreactor heated at 350°C for 3 hours. The clay-supported iron catalysts were obtained from Universal Fuel Development Associates, Inc. and were in situ sulfided by adding a small amount of elemental sulfur with the catalyst prior to hydrotreating.

Coal Solubilization

A slurry consisting of 5.0 g of coal (as-received Wyodak-Clovis Point), 2.5 mmole of $NaAlO_2$ (if desired) dissolved in 3.0 g of water and 5.0 g of tetralin (solvent) was placed in a 70-mL Parr reactor. The reactor was evacuated and charged with 1000 psi (initial) of carbon monoxide gas. The reactor was heated to 400°C in a rocking autoclave (initial heatup time = 11 minutes) and left at this temperature for 30 minutes. The reactor was cooled to room temperature, and the gases were removed. The products were distilled to remove water. The remaining slurry was extracted with THF. The THF-insoluble product was dried under vacuum and weighed. The percent conversion was calculated on the basis of the coal (maf) that did not appear in the THF-insoluble fraction. The extract was evaporated to remove THF. The resulting low-severity products from sodium aluminate-catalyzed (SA-LSW) and uncatalyzed reactions (U-LSW) contained the original tetralin as well as the solubilized coal material. These were stored under nitrogen for further catalytic hydrotreating.

The composition of THF-soluble products was determined by adding an aliquot of this product to a large excess of heptane with vigorous stirring. The heptane-insoluble product was separated by centrifugation, washed with heptane, dried in vacuo at 50°C, and weighed. The heptane-soluble product was evaporated to remove heptane and kept for further analyses. The heptane-soluble yield was calculated with the following equation:

$$\%\ \text{heptane solubles}^* = \%\ \text{conversion} - \%\ \text{heptane insolubles}$$

(* = includes gas and water)

Catalytic Hydrotreatment of Low-Severity Intermediates

A slurry consisting of 3 g of SA-LSW or U-LSW, 10 wt% of desired catalyst, and 2 wt% of sulfur (if needed) was placed in a 70-mL Parr reactor. The reactor was evacuated and charged with 1000 psi (initial) of hydrogen gas. The reactor was heated to 425°C in a rocking autoclave (initial heatup time = 15 minutes) and left at this temperature for 3 hours. At the end of the reaction, the reactor was cooled to room temperature, and the gases were removed. The product slurry was extracted with THF. The THF-insoluble product was dried under vacuum and weighed. The THF-insoluble fraction was used to determine the amount of coke formed due to retrogressive reactions during hydrotreatment. The extract was diluted to 250 mL with THF. A 4-mL aliquot of the THF-soluble was mixed with 1 mL of solution of internal standard (a mixture of 2,2,4-trimethylpentane and n-octadecane in dichloromethane) and analyzed by gas chromatography (GC). The remaining THF-soluble fraction was evaporated to remove THF, and the dark oil was added to a large excess of heptane and stirred. The heptane-insoluble product was separated by centrifugation, washed with heptane, and dried in vacuo at 50°C. The percent conversion was calculated on the basis of

the heptane-insoluble product that was converted to heptane-soluble product (oils). The conversion and yield data are given in Table 1.

RESULTS AND DISCUSSION

The advantage of using a solubilization stage in coal processing is that almost all of the inorganic material present in the coal can be eliminated prior to catalytic hydrogenation over a supported catalyst. Thus the calcium deactivation that has seriously affected catalytic liquefaction in the low-rank coals can be avoided. Aqueous solubilization reactions that utilize carbon monoxide as the reductant gas have been extensively investigated in this and other laboratories over many years (5-7). Basic catalysts have been employed to achieve higher conversions. The CO/H_2O reduction has been shown to be superior to hydrogen for the first stage of liquefaction. A number of candidates for improving the conversion in CO/H_2O were reported by Jackson and others (2, 3). Aqueous sodium aluminate gave good conversions of brown coal to oils at temperatures of 350° to 400°C. The mechanism for sodium aluminate activation of carbon monoxide to produce an effective reducing intermediate is still under investigation.

Investigations of homogeneous catalysts for coal liquefaction at the EERC (4) verified that sodium aluminate is also effective in improving the CO/H_2O liquefaction of low-rank western U.S. coals. High conversions to THF solubles were obtained for the Wyodak subbituminous coal (89%). This was substantially higher than that obtained in a similar CO/H_2O reaction with no added sodium aluminate (78%). Conversion of the Wyodak to THF solubles in a CO/H_2O liquefaction experiment with sodium hydroxide catalyst was substantially lower (72%).

A mixed solvent containing an organic solvent with lower vapor pressure (tetralin) was also used for the CO/H_2O reaction. Solubilization reactions of the Wyodak coal were performed in a water-to-tetralin wt/wt ratio of 0.6, both with and without sodium aluminate, at 400°C for 30 minutes with 1000 psi of cold initial CO pressure. Compared with water only, the operating pressure as well as conversions to THF-soluble products was significantly lower for the mixed solvent system. The sodium aluminate-catalyzed reaction gave 79% conversion to THF solubles, whereas the uncatalyzed reaction gave only 63% conversion. The lower yields for the mixed solvent in both catalyzed and uncatalyzed reactions may have resulted from the lower water concentration. The dependence of the conversions on the CO and water partial pressure was previously described (8). It should also be pointed out that the lower fluid density in the mixed solvent reactions may have resulted in a lower conversion. Higher conversions can be obtained by longer reaction times or higher temperatures, but minimal processing severity was desired for generating the intermediates needed for this study.

The yield of heptane solubles from the sodium aluminate-catalyzed reaction (CO/water/tetralin system) was the same (30% heptane solubles) as that obtained in uncatalyzed reactions in the same system (31% heptane solubles). Since the conversions were higher for the sodium aluminate-catalyzed reactions, the heptane-insoluble fraction is larger for the sodium aluminate-catalyzed reactions. Thus the two products do not have the same composition with respect to the solubility fractions.

Development of an economical process for liquefaction of low-rank coals requires an evaluation of the suitability of the soluble COsteam products as a feed for catalytic

hydrogenation. The catalytic hydrogenation is required for depolymerization to a distillable product with higher hydrogen content and low heteroatom content. The evaluation of product quality was determined by carrying out hydrogenations with both a conventional supported cobalt–molybdenum catalyst as well as two dispersed iron sulfide catalysts. In these tests, the THF-soluble low-severity products from the sodium aluminate-catalyzed (SA-LSW) and the uncatalyzed CO/H_2O reactions (U-LSW) were catalytically hydrotreated with 10 wt% of the catalyst at 425°C for 3 hours in hydrogen (1000 psi cold). Since the compositions of the U-LSW and SA-LSW were not identical, the percent conversion was measured as the percentage of heptane insolubles converted to heptane solubles in the hydrogenation of each intermediate with each catalyst. The conversion data and product yields are given in Table 1.

The thermal (noncatalytic) hydrogenation of the SA-LSW product converted 24% of the heptane-insoluble fraction to heptane solubles. Thermal hydrogenation of the U-LSW product gave a similar conversion to heptane solubles (26%).

The supported cobalt–molybdenum catalyst was presulfided in hydrogen sulfide/hydrogen (10% H_2S). Hydrogenation of the SA-LSW with the presulfided cobalt–molybdenum catalyst resulted in a high conversion (68%) of the heptane-insoluble fraction to heptane solubles. Hydrogenation of the U-LSW with this catalyst also gave a high conversion to heptane solubles (67%).

In contrast to the molybdenum catalyst results described above, the results obtained with sulfided iron catalysts demonstrated significant differences for the hydrogenation of the low-severity products obtained from the sodium aluminate-catalyzed and the uncatalyzed reactions. An iron/alumina-pillared montmorillonite catalyst was sulfided in situ by adding elemental sulfur to the reactants. The hydrogenation of SA-LSW with this catalyst gave a 62% conversion to heptane solubles. A conversion of only 47% was obtained with the U-LSW product. The very large increase in conversion to heptane-solubles in the SA-LSW experiment clearly demonstrates that the use of sodium aluminate catalyst in the CO/water pretreatment solubilization stage had a beneficial effect on the quality of the low-severity product.

This improvement in the hydrotreatability of the low-severity product as a result of sodium aluminate catalysis was further demonstrated by a different sulfided iron catalyst. This catalyst was prepared by the impregnation of triiron complex on an acid-washed montmorillonite. Sulfidation was performed in situ with elemental sulfur, and reaction conditions were the same as before. The reaction with the SA-LSW gave an excellent conversion to heptane solubles (67%), which compared favorably with that produced by the molybdenum catalyst. As in the reactions with the pillared clay-supported iron sulfide catalyst, the reaction of this clay-supported iron catalyst gave a much lower conversion (56%) with the U-LSW.

CONCLUSIONS

The low-severity products from CO/H_2O reactions obtained with and without sodium aluminate were compared in hydrogenation tests with three catalysts as well the thermal noncatalytic reaction. The thermal reaction gave poor conversions to heptane solubles for both low-severity products. A significant difference in the conversions of the two low-severity products to heptane solubles was found for two clay-supported iron catalysts. The sodium

aluminate-catalyzed CO/H_2O reaction gave a product with much higher potential for hydrotreating than that obtained from the uncatalyzed CO/H_2O reaction. In contrast, a commercial cobalt–molybdenum catalyst gave about 68% conversion for both low-severity products. Thus the very effective hydrogen-activating molybdenum sulfide catalyst was able to compensate for the lower quality of the uncatalyzed reaction product. If the economics of coal liquefaction and catalyst recovery demand the use of the inexpensive and disposable iron catalysts, the use of sodium aluminate in a pretreatment solubilization step will be very important in increasing the yields obtained in the subsequent catalytic hydrogenation step.

ACKNOWLEDGMENTS

The support of the U.S. Department of Energy is gratefully acknowledged.

REFERENCES

1. Fischer, F.; Schrader, H. *Brennstoff Chem.* **1921**, *2*, 257.

2. Jackson, W.R.; Lim, S.C.; Stray, G.J.; Larkins, F.P. *In* Proceedings of the 1989 International Conference on Coal Sciences, Tokyo, Dec. 1989, Vol. II, pp 815-818.

3. Hughes, C.P.; Sridhar, T.; Lim, C.S.; Redlich, P.J.; Jackson, W.R.; Larkins, F.P. *In* Proceedings of the Australian/USA Workshop on Low-Rank Coals; EERC publication, 1991, p 65.

4. Sharma, R.K.; Olson, E.S. *Prepr. Pap.–Am. Chem. Soc., Div. Fuel Chem.*, **1992**, *37 (2)*, 992.

5. Appell, H.R.; Wender, I.; Miller, R.D. *Prepr. Pap.–Am. Chem. Soc., Div. Fuel Chem.* **1969**, *13*, 39-44.

6. Sondreal, E.A.; Knudson, C.L.; Schiller, J.E.; May, T.H. *In* Proceedings of the 9th Biennial Lignite Symp., DOE/GFERC/IC-77/1, 1977, pp 129-158.

7. Ross, D.S.; Green, R.K.; Monsani, R.; Hum, G.P. *Energy & Fuels* **1987**, *1*, 287.

8. Appell, H.R.; Wender, I.; Miller, R.D. "Liquefaction of Lignite with Carbon Monoxide and Water" *in* Symposium on Technology and Use of Lignite; Bismarck, ND, May 12-13, 1971, Bureau of Mines Informational Circular 8543, 1971, pp 32-39.

Table 1

Catalytic Hydrotreating of Low-Severity Products
from CO/H_2O Liquefaction of Wyodak Coal

Reaction Time = 3 hr, H_2 = 1000 psi (cold),
Low-Severity Product wt = 3 g, Catalyst wt = 0.3 g

Low-Sev. Product	Catalyst	Sulfur (%)	Temp. (°C)	Heptane Insol.	%-Conv. to Heptane Sol.
U-LSW	---	---	---	0.49	---
U-LSW	None	None	425	0.36	26
U-LSW	APC-Fe_3[a]	(2)	425	0.26	47
U-LSW	K-10/Fe_3[b]	(2)	425	0.22	56
U-LSW	Co–Moly	(2)	425	0.16	67
SA-LSW	---	---	---	0.61	---
SA-LSW	None	None	425	0.48	24
SA-LSW	APC-Fe_3[a]	(2)	425	0.23	62
SA-LSW	K-10/Fe_3[b]	(2)	425	0.20	68
SA-LSW	Co-Moly	(2)	425	0.20	68

[a] Catalyst washed with ethanol prior to drying and calcination.
[b] Triiron was supported on K-10 in ethanol.
SA-LSW = Sodium aluminate-catalyzed low-severity product.
U-LSW = Uncatalyzed low-severity product.

PARAMETRIC EVALUATION OF LOW TEMPERATURE CO PRETREATMENT OF SUBBITUMINOUS COAL

S. C. Lim, R. F. Rathbone, A. M. Rubel, F. J. Derbyshire, E. N. Givens
University of Kentucky, Center for Applied Energy Research,
3572 Iron Works Pike, Lexington, KY 40511-8433

Keywords: Coal liquefaction, carbon monoxide, pretreatment

Abstract
Thermal CO pretreatment of subbituminous coal in aqueous media at 250-300°C produces a water-insoluble product having a higher hydrogen content, lower oxygen content, increased solubility and higher volatility. Both the conversion and water-gas-shift (WGS) reactions are catalyzed by OH^-, $CO_3^{=}$ and HCO_3^-, although under some conditions significant WGS reaction is not accompanied by comparable modification to the coal structure. Turnover numbers in the NaOH-catalyzed WGS reaction in excess of 100 were observed. Thermal, optical and chemical characterization data on the modified coal is presented. Improved liquefaction conversion and oil yields of the pretreated material were observed relative to the corresponding untreated coal.

Introduction
Earlier work has shown that pretreating coal can impact on its performance in subsequent processing to provide higher yields and better product slates.[1] Pretreatment can contribute toward lowering the processing costs of converting coal to liquid fuels. The application of CO in conversion of coal in aqueous media was pioneered by Fischer and Schrader[2] and later revived by Appell and co-workers.[3] They found that the CO/H_2O system is effective for converting low-rank coals to liquid products via the WGS reaction along with removal of heteroatoms (particularly oxygen).[4]

Previously, we reported that pretreating a subbituminous coal with CO in an aqueous media at 300°C produces a material which has a higher atomic H/C ratio, lower oxygen content, higher pyridine solubility and a liquefaction reactivity comparable to untreated coal.[5] As an extension of the preceding study, the effect of temperature, NaOH concentration and CO pressure on pretreatment was evaluated and the effect of adding different salts (NaOH, Na_2CO_3, $NaHCO_3$) on the reaction was studied. In addition, the liquefaction of the pretreated coal was determined.

Experimental
Coals - Ultimate analyses of Clovis Point and Black Thunder Wyodak coals, that had been ground to -200 mesh, riffled and stored in tightly sealed containers, are given in Table 1.
Procedures - Microautoclave coal pretreatment and liquefaction experiments were performed in 25 ml reactors which, after loading and pressurizing, were submerged in a fluidized sand bath at reaction temperature and agitated vertically at a rate of 400 cycles per minute. After quenching, gaseous products were collected and analyzed. In coal pretreatment experiments solid and liquid products were scrapped and washed from the reactor with water and then filtered and air dried at 4°C. These products were separated into the THF insoluble, THF soluble/pentane insoluble (PA+A), and pentane soluble fractions. The difference between the weight of coal charged to the reactor and the sum of the THF insolubles plus PA+A is reported as oil+gas+water (OGW).

In the liquefaction experiments solid/liquid products were separated into THF insoluble, PA+A, and pentane soluble (oil+water) fractions. Conversions and product yields are reported on a moisture and ash free (maf) basis assuming complete recovery of ash in the THF insolubles. Further details of the experimental work-up procedure have been reported elsewhere.[5] Larger scale coal pretreatments were performed in a 1-liter stirred autoclave by adding 80 ml. of water to the reactor which was sealed and pressurized with CO to 800 psig. The reactor was heated to 310 ± 5° C and a slurry containing 150 g dry coal in an additional 120 ml water, containing the required amount of NaOH or Na_2CO_3, was injected into the hot reactor. After approximately 7-8 minutes, the temperature of the reactor had returned to the reaction temperature. After 1 hour the reactor was cooled and depressurized and the solid product was removed from the reactor and separated in the manner described above.
Analysis - Optical microscopic techniques are discussed elsewhere.[5] Both as-received and CO-pretreated Black Thunder coal were analyzed simultaneously by thermogravimetry/differential thermal analysis/ differential thermogravimetry (TG/DTA/DTG) on a Seiko TG/DTA 320. The conditions were: heating rate of 10°C/min from ambient temperature to 120°C; a 15 min hold at 120°C to remove surface moisture; a heating rate of 10°C/min from 120°C to 600°C; He sweep rate of 200 ml/min; and constant sample volume weighing approximately 20 mg.

Results and Discussion
CO Pretreatment - Experiments to define the effects of temperature, CO pressure, and NaOH concentration on conversion and product distribution were organized in a 2^3 factorial format as shown in Table 2. The experiments were organized around low and high levels for each of the independent variables, i.e., temperatures of 250°C and 300°C, starting CO pressures of 300 and 800 psig, and NaOH molar concentrations of 0.021 and 0.33. Results from these experiments show that the yield of THF soluble product is substantially higher at 300°C than at 250°C, irrespective of the initial CO pressure and NaOH concentration. From the magnitude of the THF conversions at 300°C, there appears to be an interactive effect of NaOH concentration and CO pressure. THF conversions for three of these four runs are in excess of 23 wt% while the other at 300 psig CO and 0.021M NaOH gave a somewhat lower THF conversion. The magnitude of the THF soluble products at 250°C is quite small but uniform and fail to show any definite trend in their distribution. The effectiveness of the CO-pretreatment at the lower NaOH concentrations is encouraging since it shows that the base concentration can be reduced.

The results observed earlier[5] plus those reported here show that humic acids (HA) are observed only at 300°C and at CO pressures (cold) of 400 psig or less. Likewise, at 300 psig CO, HA is favored by increasing NaOH concentration. This agrees with previous studies which showed that the HA yield is dependent primarily on reaction temperature, pH and reaction time.[6] HA appears to diminish as PA+A increases and its disappearance parallels an increase in the H/C ratio in the water insoluble product.

In most cases, especially at higher CO pressures, coal dissolution reports to the PA+A fraction rather than the OGW fraction. However, as our previous results on Clovis Point Wyodak coal showed, treatment at low CO pressures, such as in the presence of 200 psig CO or in the absence of CO, i.e., in N_2, results in formation primarily of OGW

product.[5] The resulting pretreated products have lower H/C ratios, i.e., 0.72 and 0.75 in the presence of 200 psig CO and in the absence of CO, respectively, relative to coal, which has a H/C ratio of 0.83. The H/C ratio for the 800 psig CO-pretreated product was 0.92. The products prepared at low CO pressures are significantly more intractable with pyridine compared to products prepared at 800 psig CO. The pyridine extract yields (wt. maf basis) were 4% for untreated coal, 6% for coal treated in the absence of CO (in N_2), 9% for coal treated with 200 psig CO, and 60% for coal treated with 800 psig CO. Optical microscopy showed that the coal treated at 800 psig CO pressure underwent significant modification relative to the original coal.

In general, temperature appears to have little impact on the extent of the WGS reaction. The maximum WGS conversion obtained in this series was 88%, which experimentally confirms that the reaction is not thermodynamically limited. However, CO conversion appears to plateau at approximately 50% in the higher temperature and pressure experiments. Extending the reaction period to two hours increased CO conversion by only 5%. Similar limitations on CO conversions have been reported in the reaction with NaOH to make sodium formate.[7]

Hydrogen that is generated by the WGS reaction and then apparently consumed in the reaction is higher at 800 psig CO (18-20 mg/g maf coal) than observed at 300 psig (ca. 10 mg/g maf coal). This disappearance or "consumption" of hydrogen that occurs at 250°C has not been correlated to either coal reconstruction or an increase in the H/C ratio in the product. We are investigating whether this hydrogen is being "stored" in one of the WGS reaction intermediates (e.g. Na formate, formic acid, etc.) as proposed by Elliott[8] and others.[9] Unquestionably, base catalyzes the disappearance of CO and formation of H_2 by the WGS reaction. The molar ratio of CO converted per mole of NaOH initially present in the experiments with 0.021M NaOH varies between 96 and 183:1, while for those experiments at 0.33M the ratio varies from 9 to 12:1. Although WGS conversions are higher at the lower pressures, turnover numbers increase at higher CO pressures.

Comparative conversions and product distributions from CO pretreatment in 0.33M solutions of NaOH, Na_2CO_3 and $NaHCO_3$ are shown in Table 3. Even though the pH of the starting $NaHCO_3$ (pH ~ 8.5) solution is significantly lower than that of the NaOH or Na_2CO_3 solutions (pH >13), they all catalyze the WGS reaction to a similar extent. Likewise, the relative THF solubilities as well as the optical microscopic properties of the water insoluble products are quite similar. Clearly, HCO_3^- is effective in promoting both the WGS reaction and the corresponding pretreatment of coal.

The volatilization of the water insoluble product is considerably higher than for the coal itself as shown by TGA (Figure 1a). In addition, the temperature of maximum volatilization decreases from 442°C for untreated coal to 432°C and 429°C for Na_2CO_3 and NaOH treated samples, respectively (Figure 1b). This suggests a reduced molecular weight distribution.

Liquefaction - CO-pretreated coals gave better THF conversion than untreated coal under mild liquefaction conditions (see Table 4). The increased conversion from both the NaOH and Na_2CO_3 catalyzed water insoluble products reported almost exclusively to the PA+A fraction. Catalyzed liquefaction in the presence of both NiMo/alumina (Shell 324)

and nanometer size iron oxide (Nanocat®) provided even sharper differentiation of the pretreated coal versus the untreated coal as shown in Table 5. The NiMo catalyst added at a level of 0.1 wt% Mo on dry coal increased oils+water conversion by 10 wt% and iron oxide added at a level of 1 wt% on dry coal increased conversion by 5 wt% and oils+water conversion by 7 wt%. All of the pretreated coal runs show a decrease in gases production and a lower H_2 consumption than for untreated coal. Presumably, the lower oxygen content in the pretreated coal would reduce the water portion of the oils+water fraction.

Conclusions

Temperature is the dominant independent variable in the CO-pretreatment of subbituminous coal with a significant interactive effect at 300°C between CO-pressure and NaOH concentration. NaOH concentrations as low as 0.021M were found to be effective in promoting both the WGS reaction and in pretreating the coal. $NaHCO_3$ was found not only to be effective in promoting the WGS reaction but also in giving water-insoluble product that is comparable to water-insoluble product from NaOH and Na_2CO_3 catalyzed CO-pretreatment. The volatility of the product increases versus untreated coal. In addition, the temperature decreases at which maximum volatilization occurs. Catalyzed liquefaction of CO-pretreated coal gives increased THF conversion and oil yield plus better H_2 utilization compared to untreated coal.

Acknowledgement

Financial support was provided by the Commonwealth of Kentucky and the U.S. Department of Energy under contract number DE-AC22-91PC91040.

References

1. Serio, M. A., P. R. Solomon, E. Kroo, R. Bassilakis, R. Malhotra and D. McMillen, *Preprints, Am. Chem. Soc. Div. of Fuel Chem.*, **1990, 35(1)**, p. 61; Deshpande, G. V., P. R. Solomon and M. A. Serio, *Preprints, Am. Chem. Soc., Div. of Fuel Chem.* **1988, 33(2)**, p. 310; Matturo, M. G., R. Liotta, and R. P. Reynolds, *Energy and Fuels*, **1990, 4**, p. 346; Warzinski, R. P., and G. D. Holder, Preprints, Am. Chem. Soc., Div. of Fuel Chem. **1991, 36(1)**, p. 44.
2. Fischer, F. and Schrader, H., *Brennstoff-Chem.*, **1921, 2**, p. 257
3. Appell, H.R., and Wender, I., *Preprints, Am. Chem. Soc., Div. of Fuel Chem*, **1968,12(3)**, p. 220.
4. Ross, D.S. et al., *Energy and Fuels*, **1987, 1**, p. 292; Stenberg, V.I. et al., *Preprints, Am. Chem. Soc., Div. of Fuel Chem*, **1984, 29(5)**, p.63.
5. S.C. Lim, R.F. Rathbone, E.N. Givens and F.J. Derbyshire, *Preprints, Am. Chem. Soc. Div. of Fuel Chem.* **1993, 38(2)**, p. 618
6. Fischer, F., et al., *Ges. Abhandl. Kenntnis Kohle*, **1920, 5**, p. 360; Brooks, J.D. and Sternhell, S., **1958**,*Fuel*, **37**, p.124.
7. Sirotkin, G.D., *Zhur. Prikbad Khim*, **1953, 26**, p. 340
8. D. C. Elliott and L. J. Sealock, Jr., *Ind. Eng. Chem. Prod. Res. Dev.* **1983, 22**, p 426.
9. Hartman, K.O. and Hisatsune, I.C., *J. Phys. Chem.*, **1966, 70**, p.1281; Royen, P. and Ehrhard, F., *Erdol Kohle*, **1953, 6**, p.195

Table 1. Ultimate Analysis of Wyodak Coals		
	Clovis Point	Black Thunder
Composition, wt% maf		
Carbon	71.0	73.9
Hydrogen	4.9	5.2
Nitrogen	1.3	1.3
Sulfur	1.1	0.6
Oxygen, by difference	21.7	19.0
Ash, wt% dry coal	6.94	6.12
H/C Ratio	0.83	0.84

Table 2. Product Distribution from CO Pretreatment of Black Thunder Coal[a]

Condition[b]	LLL	HLL	LHL	HHL	LLH	HLH	LHH	HHH
Temp, °C	250	300	250	300	250	300	250	300
CO, psig[c]	300	300	800	800	300	300	800	800
NaOH, mol/l	0.02	0.02	0.02	0.02	0.33	0.33	0.33	0.33
THF Conv	5	16	6	23	7.4	26	9	32
PA+A	3	8	2	18	7.5	18	9	29
Humic Acids	-	1	-	-	-	4	-	-
O+G+W	2	7	4	5	-	4	-	3
WGS Shift[d]	58	56	36	41	n.a.[e]	88	45	45
H_2 Consump, mg/g maf coal[f]	10	9	18	20	n.a.	6	20	20

a. 25 ml reactor; 1 hour reaction time; 2 grams dry coal; 20-22 wt% moisture; 3.25 g water/g maf coal; all conversions and yields based upon maf coal.
b. L = low, H = high; sequence: temperature, CO pressure, NaOH concentration.
c. CO pressure (cold).
d. WGS Conv(%) = $([CO_{in}]-[CO_{out}])/[CO_{in}]$
e. n.a., not available
f. H_2 Consump (mg/g maf coal)= $[H_2(\text{from WGS})]-[H_2(\text{final})]$

Table 3. Effect of Na Salt on CO-Pretreatment of Wyodak Coal[a]			
Catalyst	NaOH	Na_2CO_3	$NaHCO_3$
Coal[b]	BT	BT	CP
THF Conv.	32.0	37.2	36.0
Product Distribution, wt% maf coal			
PA+A	29.0	29.5	31.1
Oils+Gas+Water	3.0	5.7	4.9
WGS Reaction[c]	45	47	51
H_2 Consump,g/g maf coal[d]	20	22	24
Pyridine Solubles[e]	60	56	n.a.[f]

a. Conditions: 800 psig CO with 5.5 ml of 0.33M Na salt solution, 300°C, 1 hr.
b. BT is Black Thunder Wyodak coal; CP is Clovis Point Wyodak coal.
c. WGS Conv(%) = $([CO_{in}]-[CO_{out}])/[CO_{in}]$
d. H_2 Consump (mg/g maf coal)= $[H_2(\text{from WGS})]-[H_2(\text{final})]$
e. Wt% of water-insoluble product.
f. n.a. not available

Table 4. Liquefaction of Base Promoted CO-Pretreated Coal[a]			
	Na_2CO_3	NaOH	Untreated
THF Conversion	80.4	80.4	74.7
Product Distribution, wt% maf coal			
PA+A	53.4	50.6	43.9
Oil+water	24.3	30.0	26.1
Gases	2.7	2.0	4.7
H_2 Consump, mg/g maf coal	17.8	18.6	21.4
Total H_2 Consump, mg/g maf coal[b]	27.3	27.1	34.2

a. 400°C, 2 g dry coal/2 g tetralin, 1 hr, 800 psig H_2 (cold), 25 ml reactor.
b. Includes hydrogen from tetralin solvent.

Table 5. Catalyzed Liquefaction of CO-Pretreated Coal[a]				
	Pretreated Coal[b]		Untreated Coal	
	Shell 324[c]	Nanocat[d]	Shell 324[c]	Nanocat[d]
Added Fe, wt% dry coal	-	1.0	-	1.0
Added Mo, wt% dry coal	0.1	-	0.1	-
THF Conv, wt% maf coal	84	86	83	81
Product Distribution, wt% maf coal				
PA+A	43	52	49	50
Oils+Water	39	32	29	25
Gases	2	2	5	6
Total H_2 Consump, mg/g maf coal[e]	31	29	34	34

a. Liquefaction conditions: 400°C, 2 g dry coal/2 g tetralin, 1 hr, 800 psig H_2 (cold), 25 ml reactor.
b. Pretreated coal prepared in 1-liter autoclave with 0.19M Na_2CO_3 (3.7 wt% maf coal), 800 psig CO, 310±5°C.
c. NiMo/alumina (2.8 wt% Ni, 12.4 wt% Mo) ground to -100 mesh; dimethyldisulfide added to provide a S/added metal(s)(mol/mol) ratio of 2.
d. 63 wt% Fe.
e. Includes hydrogen from tetralin solvent.

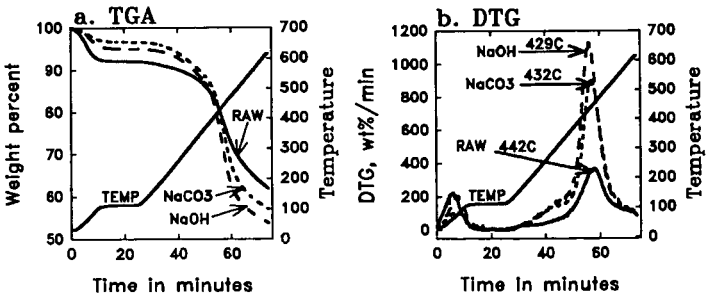

Figure 1a,b. Thermal analysis of CO-pretreated coals.

IMPROVED LIQUEFACTION OF LOW RANK COALS BY REDUCTION OF RETROGRESSIVE REACTIONS

Michael A. Serio, Erik Kroo, Sylvie Charpenay and Peter R. Solomon
Advanced Fuel Research, Inc.
87 Church Street
East Hartford, CT 01608, USA

KEYWORDS: Coal liquefaction, Low rank coals, Retrogressive reactions

INTRODUCTION

Direct coal liquefaction processes have recently been based on a two stage processing approach: coal dissolution followed by upgrading of the solubilized products. While low rank coals offer the potential of high oil yields because of their small aromatic ring cluster size, low rank coals are more difficult to liquefy in the first (solubilization) stage (1,2) under conditions optimized for bituminous coals. For example, Whitehurst and co-workers (3-5) demonstrated that low rank coals produce low conversions in short contact times in a donor solvent (see Fig. 1) or for long times in a non-donor solvent. For low rank coals and lignites, it appears likely that crosslinking reactions associated with oxygen functional groups (6,7) occur before the homolytic cleavage reactions, and if not controlled can limit the maximum conversion of coal to liquids. This paper discusses three approaches which have been used to either study or mitigate these reactions in an effort to improve liquefaction yields from low rank coals. 1) catalytic pretreatment; 2) demineralization and cation-exchange; 3) hydrothermal pretreatment and water addition.

RESULTS AND DISCUSSION

Catalytic Pretreatment

Impregnated Catalysts - For low rank coals, the use of a pretreatment at 350°C with an impregnated MoS_2 catalyst and H_2 shows a vastly superior product slate in subsequent liquefaction at 425°C (8-14). The improvement is especially noticeable for the low rank coals where short contact time liquefaction alone produces large residues (3-5). Results obtained at Advanced Fuel Research, Inc. (AFR) (15-17) confirmed the observations of Derbyshire and co-workers (8-14). Data for a Wyodak subbituminous coal (PSOC-1401) are presented in Fig. 2. The figure compares liquefaction data (10 min at 425°C) for no preliquefaction, preliquefaction at 275°C (with H_2 and catalyst) and preliquefaction at 350°C (with H_2 and catalyst). The results show that preliquefaction at 350°C does have a positive effect on the total yield and product quality in liquefaction (much lower residue) while preliquefaction at 275°C causes a negative effect (higher residue).

A number of tests were performed on the preliquefaction products to identify the chemistry, including FT-IR analysis of the Wyodak coal preliquefaction residue (15-17). The preliquefaction step produces the following changes in the residue: 1) decreases the carbonyl (1700 cm^{-1}) and hydroxyl regions (3400 cm^{-1}) (presumably carboxyl loss); 2) decreases the aliphatic hydrogen (2900 cm^{-1}); and 3) substantially increases the aromatic hydrogen (750-850 cm^{-1}). Our initial conclusion from the FT-IR data on the residual is that it is the reduction in the carboxyl concentration which is most important to the improvements brought about by preliquefaction, and this reduction requires the catalyst but not the solvent and probably not the hydrogen. The increase in aromatic hydrogen appears to be due to the adduction of naphthalene.

The evolutions of the volatile products of pyrolysis are related to the functional group composition of the sample, so TG-FTIR analysis provides a good complement to the FT-IR functional group analysis. Since the FT-IR analysis showed the carbonyl region to change drastically in preliquefaction, we considered the CO_2 evolution which is probably associated with the thermal decomposition of the carboxyl groups (15-17). When a comparison was made of the CO_2 evolution from a number of residua, the major changes were observed for catalytic preliquefaction at 350°C with hydrogen or nitrogen. Here a drastic reduction is observed in the CO_2 evolution at all temperatures. This result is consistent with the major chemical change in the carboxyl groups observed from the FT-IR results. The nitrogen thermal case shows much less of a change.

Since the preliquefaction showed a significant role of carboxyl groups, model compounds with aryl carboxyl groups were studied. The starting reaction mixture used was 50% naphthalene, 25% of 1-napthoic acid and 25% of 2-napthoic acid (weight basis). The FT-IR spectra of the starting reaction mixture and the residue after preliquefaction indicated that there is a strong loss in the carbonyl and hydroxyl bands during the preliquefaction in the presence of the catalyst. A blank run was done without the catalyst which indicates that the catalyst is necessary to cause extensive decarboxylation.

Recently, a set of experiments was done with fresh Argonne Wyodak coal impregnated with a molybdenum sulfide catalyst prepared by the incipient wetness technique (18). This was a repeat of earlier work done by Derbyshire and co-workers (8-14) and Solomon and co-workers (15-17) discussed above, except for the substitution of the Argonne Wyodak coal for the PSOC 1401 Wyodak coal. The results are shown in Fig. 3 for freshly opened and aged samples. This treatment did not show an improvement of the liquefaction yields for the fresh Argonne Wyodak coal samples. It was concluded that this different behavior toward catalyst impregnation may be due to aging of the PSOC 1401 Wyodak coal, which was presumably absent for the Argonne coal. Consequently, similar experiments were done with a sample of the latter coal which had been stored in a dry box, but where no care was taken to exclude air. The liquefaction results for the aged samples, with and without catalyst are also shown in Fig. 3. As expected, the yield of THF solubles was reduced by aging of the coal and these yields were subsequently improved by catalyst addition. However, a surprising result was that the addition of catalyst to the aged samples gave yields that were even higher than for the fresh coal or the catalytically treated fresh coal. Similar results have recently been reported by Schobert and coworkers for an air dried DECS-8 Wyodak subbituminous coal (19). The results for gas evolution from these samples during pretreatment and liquefaction are given in Fig. 4. The catalyst reduces the amount of CO_2 evolved during the pretreatment stage for both the fresh and oxidized coals. However, only in the case of the oxidized coals did the reduction in early CO_2 (and, presumably, the associated crosslinking reactions) lead to improvements in liquefaction yields.

A possible explanation for the above results is as follows. The mild oxidation of the coal due to aging may create positively charged sites which attract the tetrathiomolybdate anions during the impregnation process, which leads to better dispersion of the catalyst.

Ion-Exchanged Catalysts - To increase yields with fresh coals there are two approaches which can be pursued: a) to find a better catalyst to be impregnated onto the coal matrix; or b) to find a technique to get better - if possible atomic - dispersion of the catalyst. There has been a significant effort in the literature in pursuit of both approaches, however, a reliable and simple technique resulting in atomic dispersion of an active catalyst still needs to be found.

Ion exchange experiments have demonstrated that, around neutral pH, the coal surface is negatively charged, thus preventing anions from adsorption or ion exchange (20). This can be overcome in acidic media but any acidic treatment will result in removal of cations - an effect leading to enhanced liquefaction itself (21-25). This would obscure the effect of a catalyst. In order to circumvent this problem our approach was to first react the coal with trivalent cations

(Fe^{+3}) and thus produce locally positively charged sites (18). After this pretreatment, the tetrathio-molybdenate anions could be anchored to these positions. This technique worked very well and it was also found that the catalyst activity thus prepared depended on the Fe/Mo ratio. Since no H_2 pressure was applied in the liquefaction, H_2 evolution could be observed occasionally, but only in cases of catalyzed liquefaction. The occurrence of H_2 thus was the indicator of catalytic activity in the system towards hydrogenation-dehydrogenation with the actual H_2 concentration depending on the ratio of the two reaction rates. Table 1 shows a comparison of the time resolved liquefaction yields for a catalyzed versus uncatalyzed run for one of the most active formulations (1.4% Fe/0.6% Mo). The advantage of the catalysis is more evident at earlier reaction times, as would be expected.

Modification of Liquefaction Chemistry by Demineralization or Cation-Exchange

Coal modifications to remove cations - Crosslinking has also been observed to be influenced by the presence of alkali metals, whose removal increases pyrolysis tar yields (26) and fluidity (27). These results would indicate that the role of carboxyl groups, as indicated above, is important, but it is the carboxylate (cation exchanged carboxyls) which are the key agents in retrogressive reactions for low rank coals. The role of calcium in reducing liquefaction yields from low rank coals has been suggested in previous work by Whitehurst et al. (4), Mochida et al. (28), and Joseph and Forrai (29). It is also consistent with work which shows an effect of calcium on reducing pyrolysis tar yields (26,30-33). The role of calcium may be to provide a nascent crosslink site in the coal by allowing coordination of groups like carboxyl and hydroxyl which are prone to such reactions. Otherwise, these sites would be more likely to coordinate with water (through hydrogen bonding) then with each other.

The preparation of modified low rank coals was studied systematically by Serio et al. (21-25). The following coal modifications were tested: raw, vacuum dried, treated with ammonium acetate, acid-demineralized and methylated. Each of the latter three modifications was effective in removing ion-exchanged cations. The results of liquefaction experiments with the coals and modified coals are summarized for the Zap lignite in Fig. 5. The results for the Wyodak subbituminous coal (not shown) are similar to those for the Zap lignite (22). The results show that the decrease in crosslinking, as implied by the reduction in CO_2 yield (Fig. 5b), roughly correlates with the increased liquefaction yields (soluble products, Fig. 5a). The trends in CO_2 yield (inverse correlation) and solubles from liquefaction (positive correlation) generally parallel the results from pyrolysis for the tar yield (Fig. 5c). The extent of retrograde reactions for low rank coals (lignite, subbituminous) is significantly reduced by methylation and demineralization. However, these treatments do not have much impact on bituminous coal, presumably because of the lack of exchangeable cations. A similar beneficial result has recently been observed by Miller et al. (34) in liquefaction studies with the Argonne Wyodak coal treated with methanol/HCl.

TG-FTIR analyses were run on the modified coals to see whether changes occurred in the gas evolutions. The results indicated that the demineralization and methylation processes both decrease the evolution of CO_2 and H_2O between 200°C and 400°C where crosslinking occurs, suggesting that the high tar and liquid yields produced by these two treatments are a result of reduced crosslinking which is accompanied by reduced evolutions of CO_2 and H_2O.

Coal Modifications to Add Cations - Recent work at AFR has involved preparation of ion-exchanged (barium, calcium, and potassium) coals starting with demineralized Argonne Zap, and Wyodak samples (21, 25). The exchange was done at two different pH levels (8 and 12.5) in order to effect exchange of carboxyl groups and carboxyl plus phenolic groups, respectively. These modified samples were subjected to functional group analysis as KBr pellets with FT-IR, programmed pyrolysis with TG-FTIR, and donor-solvent liquefaction experiments. The results of sample characterization by programmed pyrolysis at 30°C/min to 900°C or solvent extraction/solvent swelling experiments in pyridine are summarized in Table 2 for the Zap lignite.

These results show that demineralization tends to increase the tar yields and decrease the gas yields, which is consistent with the previous work discussed above. Similar results were observed for the Wyodak coal (21). Table 2 also shows a decrease of the tar yield with the extent of ion-exchange with the metal cations, and a corresponding increase in the total amount of gas evolution. The liquefaction results for the different samples are shown in Table 3. The data in Tables 2 and 3 show that the yields of both the pyrolysis tar and toluene solubles from liquefaction decrease with the extent of ion-exchange, i.e., in the order of (demineralized) > (ion-exchanged at pH 8) > (ion-exchanged at pH 12.5). This result indicates that having the carboxyl or phenolic groups in the salt form makes it easier to crosslink the coal structure during pyrolysis or liquefaction reactions. The ability of cations to coordinate polar groups is probably an important aspect of their role in retrogressive reactions. The ability of both monovalent and bivalent cations to act as initial crosslinks in the structure is supported by data on the volumetric swelling ratios (VSR) in pyridine and the yields of pyridine extractables, also shown in Table 2. The values of the VSR are lower for the bivalent cations at high pH. At pH 8, the values of the VSR for the monovalent and bivalent cations are more similar, though lower than the values for either the raw or demineralized coals. Consequently, the evidence indicates that the monovalent cations can also act as crosslinking agents, although this must occur through electrostatic rather than colavent interactions. It makes sense that valency would be less important in the normal state of the coal or at pH=8 since, for steric reasons, cations are unlikely to be exchanged on more than one carboxyl or ortho-dyhydroxy site.

Hydrothermal Pretreatment and Water Addition

Hydrothermal Pretreatment of Coal - Water pretreatment of coal at elevated temperatures, has been studied previously as a means to increase the yields of liquid products from extraction (35,36), pyrolysis (36-38), or liquefaction (39,40) of coal. Selected results from work done at AFR with Zap coal are shown in Fig. 6 (37,39). The data show that the sharp increase of pyrolytic tar yield, as a result of short time water pretreatment, is accompanied with decreased pyrolysis CO_2 evolution. This is in harmony with our previous conclusions about the correlation between decomposition of oxygen functionalities and crosslinking, namely the water pretreatment apparently removes precursors which would otherwise lead to crosslinking under liquefaction conditions. The pyrolysis data for the water pretreated samples show a close similarity for water pretreatment to accelerated aging of the coal (38). However, the toluene solubles of a subsequent liquefaction are reduced opposite to our expectations (see Fig. 6d). Another observation was that, specifically in this short pretreatment time range, occasionally negative oil yields were observed (39). Since the oils are measured by weight difference a likely explanation is that the solvent is forming adducts with the pretreated samples. The water pretreatment step appears to sensitize the coal to this problem.

Pyrolysis and Liquefaction of Moisturized Coal Samples - Remoisturization of vacuum dried Zap and Wyodak was done in the attempt to understand if moisture uptake for low rank coals is a reversible process and to see if moisture influences the role of the cations. The remoisturized samples were analyzed by programmed pyrolysis with TG-FTIR. Preliminary results show that the moisture content can be restored to values which are close to those of the raw coals, especially for Zap (21,25).

The detailed results for the pyrolysis and liquefaction experiments are given in Ref. 21. In general, pyrolysis tar yields and the toluene solubles yields from liquefaction for the remoisturized samples were similar to those for the vacuum dried samples. It appeared that the liquefaction results were more sensitive to the presence of moisture, although the increases in asphaltene yields were generally balanced by decreases in oil yields. A possible explanation for the difference is that most of the moisture is depleted early in the pyrolysis process, whereas the moisture is retained in the reactor during liquefaction and can exist in a liquid phase under the right conditions.

Water Addition to Liquefaction Experiments - It is also known from our results (21) and the literature (41) that the moisture is associated with cations in raw coals. Consequently, an investigation was made to determine if the deleterious effects of cations could be mitigated by adding water to the donor solvent liquefaction system. Results from experiments with raw and demineralized Zap at three different temperature levels are given in Table 4. At temperatures near or below the critical temperature of water (374 °C), it appears that there is a profound beneficial effect of added water for the raw coal (note the significant reduction in CO_2 evolution). Conversely, there is a significant deleterious effect of added water for the demineralized coals. The ability of water to interact with cations and affect the course of the thermal decomposition behavior is consistent with results that have been observed in hydrothermal treatment of coal, which mimics the geological aging process in many respects.

CONCLUSIONS

The conclusions from this study are as follows:

- Catalytic pretreatment (Mo impregnation following by heating to 350 °C for 30 min.) prior to liquefaction leads to increased yields for low rank coals which have not been protected from aging, but is not effective for pristine coals, like the Argonne Premium Coals.

- For the latter coals, an ion-exchange technique in which the coal is first treated by Fe^{+3} cations followed by treatment with Mos_4^{-2} anions was found to be effective in increasing yields in a two-step liquefaction process (pretreatment at 350 °C, 30 min. followed by liquefaction at 400 °C, 30 min).

- The extent of retrogressive reactions for low rank coals in pyrolysis and liquefaction is significantly reduced by removal of cations exchanged on carboxyl groups, based on experiments where the coal has been ion-exchanged (using NH_4^+), acid demineralized (using HCl/HF) or methylated.

- The addition of monovalent (K^+) or bivalent (Ca^{+2}, Ba^{+2}) cations to acid demineralized coals at pH 8 significantly increases the extent of retrogressive reactions in pyrolysis and liquefaction (liquid yields are reduced). The effect is even more pronounced at pH 12.5.

- The ability of cations to act as initial crosslinks in the coal structure through electrostatic or covalent interactions is believed to be an important aspect of their role in promoting retrogressive reactions.

- Since the moisture in low rank coals is associated with the cations, the presence of liquid water during pyrolysis (as in hydrothermal treatment) or liquefaction can help to mitigate these reactions.

- The benefits of catalytic pretreatment for low rank coals may also be a result of the interaction of the catalyst with the cations present in these coals. It has been reported that alkaili metals reduce the effectiveness of Mo catalysts in coal liquefaction (10), suggesting that an interaction does occur.

- The evolution of CO_2 from carboxylate groups appears to be the key indicator of retrogressive reactions in pyrolysis or liquefaction of low rank coals. The removal of the cation, the association of the cation with water or the association of the cation with a highly dispersed catalyst can inhibit the crosslinking events which are normally associated with the decomposition of these groups.

ACKNOWLEDGEMENTS

This work was supported by the U.S. D.O.E. Pittsburgh Energy Technology Center under Contract Nos. DE-AC22-88PC88814, DE-AC22-89PC89878, DE-AC22-91PC91026 and Grant No. DE-FG05-92ER81324. The methylated coal samples were prepared at SRI International (Menlo Park, CA).

REFERENCES

1. Neavel, R.C., Phil. Trans., R. Soc. Lond., **A300**, 141, (1981).
2. Talib, A., Neuworth, M. and Tomlinson, G., Working Paper No. 84W00279, The Mitre Corp., VA, (1984).
3. Derbyshire, F.J. and Whitehurst, D.D., Fuel, **60**, 655, (1981).
4. Whitehurst, D.D., Mitchell, T.O., and Farcasiu, M. Coal Liquefaction, The Chemistry and Technology of Thermal Processes, Academic Press, NY (1980).
5. Whitehurst, D.D., in "Coal Liquefaction Fundamentals," Ed. D.D. Whitehurst, ACS Symposium Series, **139**, 133 (1980).
6. Suuberg, E.M., Lee, D., and Larsen, J.W., Fuel, **64**, 1668 (1985).
7. Solomon, P.R., Serio, M.A., Deshpande, G.V., and Kroo, E., Energy & Fuels, **4**, (1990); also see, Deshpande, G.V., Solomon, P.R., and Serio, M.A., ACS Div. of Fuel Chem. Preprints, **33**, (2), 310, (1988).
8. Derbyshire, F., Davis, A., Epstein, M., and Stansberry, P., Fuel, **65**, 1233, (1986).
9. Derbyshire, F.J., Stansberry, Terrer, M.-T., Davis, A., and Lin, R., Proc. 1985 International Conf. on Coal Science, Sydney, Australia, pp 169-172.
10. Davis, A. Derbyshire, F.J., Finseth, D.H., Lin, R., Stansberry, P.G., and Terrer, M.-T., Fuel, **65**, 500 (1986).
11. Derbyshire, F.J., Davis, A., Lin, R., Stansberry, P.G., Terrer, M.-T., Fuel Processing Technology, **12**, 127, (1986).
12. Davis, A., Schobert, H.H., and Derbyshire, F.J., "Enhanced Coal Liquefaction by Low Severity Catalytic Reactions", Technical Progress Report for the period Mar. to May, 1987, U.S. DOE/PETC Contract No. DE-FG22-86PC90910, (6/1987).
13. Davis, A., Schobert, H.H., and Derbyshire, F.J., "Enhanced Coal Liquefaction by Low Severity Catalytic Reactions", Technical Progress Report for the period June to Aug. 1987, U.S. DOE/PETC Contract No. De-FG22-86PC90910, (9/1987).
14. Derbyshire, F.J., Davis, A., Epstein, M., and Stansberry, P.G., ACS Div. of Fuel Chem. Preprints, **31**, (4), 308, (1986).
15. Solomon, P.R., Deshpande, G.V., Serio, M.A., and Kroo, E., "Advanced Liquefaction by Temperature Staged Reactors", Final Report for DOE Contract No. DE-AC01-88ER80560, (1989).
16. Solomon, P.R., Serio, M.A., Deshpande, G.V., Kroo, E., Schobert, H., and Burgess, C., ACS Div. of Fuel Chem. Preprints, **34**, (3), 803, (1989).
17. Solomon, P.R., Serio, M.A., Deshpande, G.V., Kroo, E., Schobert, H., and Burgess, C., Chemistry of Catalytic Preliquefaction, in "Recent Advances in Coal Science", ACS Symposium Series, (H. Schobert, K. Bartle, and L. Lynch, Eds.), pp 193-212, (1991).
18. Serio, M.A., Kroo, E., Charpenay, S., and Solomon, P.R., "Advanced Liquefaction by Catalytic Reduction of Low Temperature Crosslinking," Final Report under DOE Grant No. DE-FG05-92ER81324 (May 17, 1993).
19. Saini, A.K., Song, C. and Schobert, H.H., ACS Div. of Fuel Chem. Preprints **38** (2), 593 (1993).
20. Abotsi, G.M.K., Bota, K.B., Saha, G., Energy and Fuels **6**, 779 (1992).
21. Serio, M.A., Kroo, E., Teng, H., Charpenay, S. and Solomon, P.R., , Fifth Quarterly Report, U.S. DOE Contract No. DE-AC22-91-PC91026 (1992).
22. Serio, M.A., Solomon, P.R., Bassilakis, R., and Kroo, E., "Fundamental Studies of Retrograde Reactions in Direct Liquefaction", Final Report for DOE Contract No. DE-

AC22-88PC88814, (1991).
23. Serio, M.A., Solomon, P.R., Kroo, E., Bassilakis, R., Malhotra, R., and McMillen, D., ACS Div. of Fuel Preprints, **35** (1), 61 (1990.
24. Serio, M.A., Solomon, P.R., Kroo, E, Bassilakis, R., Malhotra, R. and McMillen, D."Studies of Retrogressive Reactions in Direct Liquefaction," 1991 proceedings, Int. Conf. on Coal Science, New Castle, England, pp. 656-659 (Sept. 1991).
25. Serio, M.A., Kroo, E., Teng., H., Solomon, P.R., "The Effects of Moisture and Cations on Liquefaction of Low Rank Coals," ACS Div. of Fuel Chem. Preprints, **38** (2), 577 (1993).
26. Tyler, R.J. and Schafer, H.N.S., Fuel, **59**, 487, (1980).
27. McCollon, D.P., Sweeny, P.G. and Benson, S.H., "Coal/Char Reactivity", 5th Quarterly Technical Progress Report, April to June, 1987, UNDERC.
28. Mochida, I., et al., Fuel **62**, 659, (1983).
29. Joseph, J.T. and Forrai, T.R., Fuel **71**, 75 (1992).
30. Morgan, M.E. and Jenkins, Fuel, **65**, 757, (1986).
31. Morgan, M.E. and Jenkins, Fuel, **65**, 764, (1986).
32. Morgan, M.E. and Jenkins, Fuel, **65**, 769, (1986).
33. Womat, M.J., and Nelson P.F., Energy and Fuel, **6** (2) (1992).
34. Miller, R.L., Armstrong, M.E., and Baldwin, R.M., ACS Div. of Fuel Chem. Prepr., **34**, (3), 873, (1989).
35. Bienkowski, P.R., Narayan, R., Greenkorn, R.A., Choa, K.W., IEC REs., **26**, 202, (1987).
36. Graff, R.A., and Brandes, S.D., Energy & Fuels, **1**, 84, (1987).
37. Serio, M.A., Solomon, P.R., Kroo, E., and Charpenay, S., "Water Pretreatment of Coal," ACS Div. of Fuel Chem. Preprints, **36** (1), 7, (1991).
38. Serio, M.A., Kroo, E., Charpenay, S., and Solomon, P.R., "Hydrous Pyrolysis of Four Argonne Premium Coals," ACS Div. of Fuel Chem. Preprints, **37**, (4), 1681, (1992).
39. Serio, M.A., Kroo, E., and Solomon, P.R., "Liquefaction of Water Pretreated Coals," ACS Div of Fuel Chemistry Preprints, **37**, (1), 432, (1992).
40. Ross, D.S., Hirschon, A., Tse, D.S., and Loo, B.H., ASC Div. of Fuel Chem. Prepr., **35**(2), 352, (1990).
41. Schafer, H.N.S., Fuel, **59**, 295 (1980).

Table 1. Time Resolved Liquid Yields (DAF WT %) from Liquefaction Experiments with Raw and Fe/Mo Exchanged (1.4% Fe/Mo) Argonne Wyodak Coal.

Reaction Time (minutes)	Raw Vac. Dried Coal			1.4% Fe/Mo Exchanged Coal		
	Toluene Solubles			Toluene Solubles		
	Total	Oils	Asphaltenes	Total	Oils	Asphaltenes
0	3	-4	7	12	6	6
10				34	12	22
20				48	14	34
30	50	8	42	57	14	43
40				57	15	42
50				62	22	40
90	62	33	29	66	29	37

Notes: Pretreatment done at 350 °C, 30 min.; Liquefaction done at 400 °C, 30 min.; Tetralin/Coal = 6/1

Table 2. Results From Characterization of Vac Dry Modified Zap Samples By Programmed Pyrolysis And Solvent Swelling/Pyridine Extraction.

Coal	Pyrolysis Products (wt.% ,daf)					Solvent Swelling/ Pyridine Extraction	
(type/preparation)	Tars	CO_2	CO	H_2O	CH_4	V.S.R.[a]	P_s[b]
Fresh	7	8.9	14.7	14.3	2.2	2.7	5
Demin.	20	4.8	10.4	8.4	2.7	3.1	20
Demin. + K^+ (pH8)	11	8.6	9.9	16.0	1.9	2.0	10
Demin. + Cs^{++} (pH8)	10	8.6	13.5	10.3	2.4	1.8	3
Demin. + Ba^{++} (pH8)	6	11.7	15.8	18.6	2.6	2.1	6
Demin. + K^+ (pH12.5)	5	9.9	12.4	13.5	1.6	1.7	2
Demin. + Ca^{++} (pH12.5)	4	8.2	22.6	12.6	2.0	1.1	2
Demin. + Ba^{++} (pH12.5)	3	10.5	24.1	15.5	2.6	1.1	1

Notes: a = Volumetric Swelling Ratio in Pyridine; b = Pyridine Extractables (daf)

Table 3. Liquefaction Results of Vac Dry Modified Zap Samples.

	Toluene Solubles (wt.%, daf)			Gas (wt. %, daf)		
	Total	Oils	Asphaltenes	CO_2	CO	CH_4
Fresh	26	12	14	4.3	0.24	0.25
Demin.	52	26	26	1.1	0.43	0.27
Demin. + K^+ (pH8)	30	11	19	7.7	0.27	0.17
Demin. + Ca^{++} (pH8)	25	13	12	2.7	0.30	0.22
Demin. + Ba^{++} (pH8)	37	25	12	7.3	0.40	0.20
Demin. + K^+ (pH12.5)	17	5	12	5.0	0.24	0.27
Demin. + Ca^{++} (pH12.5)	*	*	3	0.7	0.04	0.08
Demin. + Ba^{++} (pH12.5)	15	15	0.5	0.3	0.27	0.02

* Yields Calculated by Difference were Negative. Solvent Incorporation is Suspected.

Table 4. Effect of Added Water on Liquefaction of Raw and Demineralized Argonne Zap Coal.

Temp. Level (°C)	Water Addition	Toluene Solubles wt.%, daf		CO_2 Yields wt. %, daf	
		Raw	Demin.	Raw	Demin.
350	yes	13	0	0.0	1.1
	no	1	27	5.4	2.4
375	yes	23	19	2.4	1.5
	no	11	40	5.2	2.2
400	yes	31	24	5.2	0.8
	no	30	58	4.1	4.2

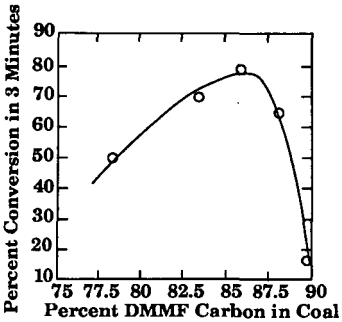

Figure 1. Rank Dependence of Short Contact Time Liquefaction Yields (3).

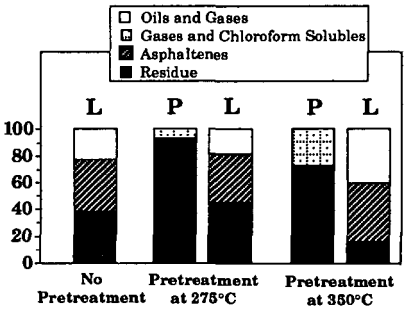

Figure 2. Product Distributions for Preliquefaction and Liquefaction Comparing Results for No Preliquefaction, Preliquefaction at 275°C and Preliquefaction at 350°C. P = Preliquefaction; L = Liquefaction. *Liquefaction Conditions* - 425°C, Mo, Catalyst, Naphthalene Solvent, Hydrogen Atmosphere (10 min). Preliquefaction Conditions - Mo, Catalyst, Naphthalene Solvent, Hydrogen Atmosphere (275°C-30 min., 350°C - 60 min.).

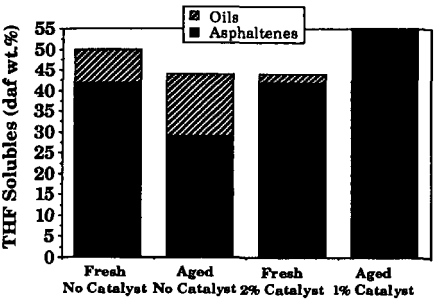

Figure 3. Effect of Coal Aging and Molybdenum Catalyst Impregnation on THF Solubles Yields from Liquefaction of Argonne Wyodak Coal in Tetralin (Pretreatment done at 350°C, 30 min; Liquefaction done at 400°C, 30 min).

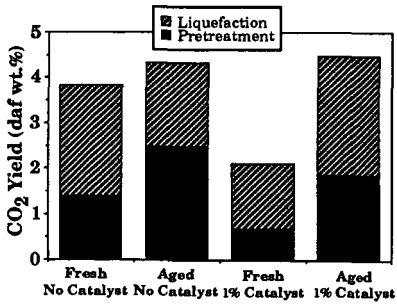

Figure 4. Effect of Coal Aging and Molybdenum Catalyst Impregnation on Total CO_2 Evolution from Pretreatment (350°C, 30 min) and Liquefaction (400°C, 30 min) of Argonne Wyodak Coal.

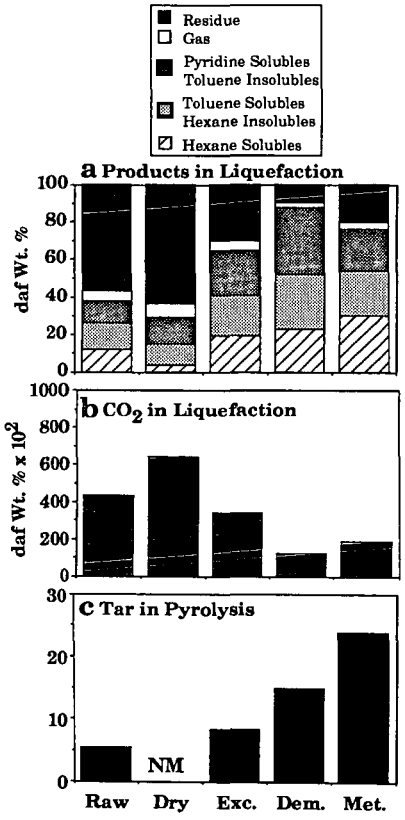

Figure 5. The Variation in Product Distributions for Zap Lignite with Coal Treatment. a) Products in Liquefaction, b) CO_2 in Liquefaction and c) Tar in Pyrolysis. NM = Not Measured.

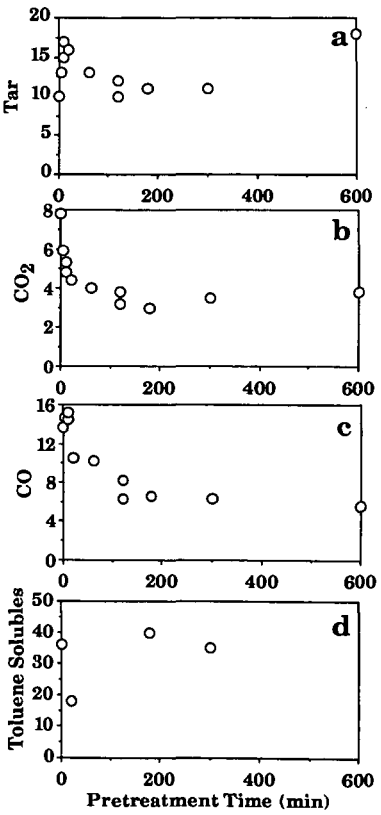

Figure 6. Results from Analysis of Zap Residues Produced by Water Pretreatment at 350°C, 4000 psig for a Range of Pretreatment Times. (a-c) Data on Pyrolysis Gas Yields from TG-FTIR Analysis; (d) Data for Toluene Solubles Yield from Donor Solvent Liquefaction. All Results are Given on a DAF Basis.

Enhancing Low-Severity Catalytic Liquefaction of Low-Rank Coal by Adding Water

Chunshan Song*, Ajay K. Saini and Harold H. Schobert

Fuel Science Program, 209 Academic Projects Building
The Pennsylvania State University, University Park, PA 16802

Keywords: Coal, Liquefaction, Dispersed MoS_2 catalyst, Water addition, Low-rank coal

INTRODUCTION

As a part of an on-going program for investigating the effects of thermal and catalytic pretreatments on coal structure and reactivity in liquefaction, the present study seeks to explore the effects of water in low-severity catalytic liquefaction of low-rank coal. The motivation of the present study comes from our recent work on the influence of mild pretreatments, drying and oxidation, of Wyodak subbituminous coal on its catalytic liquefaction [Saini et al., 1993; Song et al., 1993]. In that work we found that adding a small amount of water equivalvent to the original moisture content (28.4 wt%) back to the vacuum-dried or air-dried coal restored over 90 % of the conversion of the fresh raw coal in non-catalytic runs at 350 °C with and without solvents. This fact strongly suggests that the negative impact of drying on thermal (uncatalyzed) liquefaction reactions is largely due to the removal of water. Another fact that puzzled us is that the conversions of fresh raw coal in the non-catalytic runs and catalytic runs with either tetralin or 1-methylnaphthalene (1-MN) solvent are very similar to each other, although the catalytic runs of the vacuum-dried or air-dried coal afforded significantly higher conversions than the corresponding thermal runs. These two facts prompted us to examine the effects of water addition in catalytic coal liquefaction. This paper reports on the dramatic improvement of coal conversion upon addition of a small amount of water in low-severity liquefaction of Wyodak subbituminous coal using a dispersed molybdenum sulfide catalyst at 350 °C for 30 min.

EXPERIMENTAL

The coal used was a Wyodak subbituminous coal, which is one of the Department of Energy Coal Samples (DECS-8) maintained in the DOE/Penn State Sample Bank. It was collected in June 1990, ground to ≤ 60 mesh, and stored under argon atmosphere in heat-sealed, argon-filled laminated foil bags consisting of three layers. It contains 32.4 % volatile matter, 29.3% fixed carbon, 9.9 % ash and 28.4 % moisture, on as-received basis; 75.8% C, 5.2% H, 1.0% N, 0.5% S and 17.5% O, on dmmf basis. The as-received fresh sample is designated as raw coal. Vacuuum-drying (VD) of the coal was conducted in a vacuum oven at 100 °C for 2 h. Air-drying (AD) was done in an oven maintained at 100 °C for 2-100 h, or at 150 °C for 20 h, with the door partially open. For the loading of dispersed catalyst, ammonium tetrathiomolybdate (ATTM) was used as precursor, which is expected to generate molybdenum sulfide particles on coal surface upon thermal decomposition at ≥ 325 °C. ATTM was dispersed on to coal (1 wt% Mo on dmmf basis) by incipient wetness impregnation from its aqueous solution. The impregnated coal samples were dried in a vacuum oven at 100 °C for 2 h.

The liquefaction was carried out at 350 or 400 °C for 30 minutes (plus 3 minutes heat-up time) with an initial (cold) H_2 pressure of 7 MPa (1000 psi) in 25 ml tubing bomb microreactor. We conducted three types of reactions including solvent-free runs, the runs in the presence of a hydrogen donor tetralin solvent, and the runs with a non-donor 1-methylnaphthalene solvent, using 4 g of coal and 4 g of solvent, and optionally, added water. The wt ratio of added water to dmmf coal was kept constant (0.46) for both thermal and catalytic runs with added water. After the reaction, the gaseous products were analyzed by GC, with the aid of gas standards for quantitative calibration of GC responses of CO, CO_2, and C_1-C_4 hydrocarbon gases. The liquid and solid products were separated by sequential Soxhlet extraction into oil (hexane soluble), asphaltene (toluene soluble but hexane insoluble), preasphaltene (THF soluble but toluene insoluble), and residue (THF insoluble). The conversions of coal into soluble products were determined from the amount of THF-insoluble residues. More experimental details may be found elsewhere [Song and Schobert, 1992; Saini et al., 1993]. In order to obtain highly reliable data, almost all the experiments were duplicated or triplicated. The deviations in conversions and product yields are generally within ± 2 wt%. Most results reported here are average of two runs.

RESULTS AND DISCUSSION

Tables 1, 2 and 3 show the results for liquefaction of the coal at 350 °C with and without added water in the absence of any solvent (Table 1) and in the presence of a non-donor 1-methylnaphthalene (1-MN) solvent (Table 2) and a hydrogen-donor tetralin solvent (Table 3). Tables 4 and 5 show the results for thermal (non-catalytic) and catalytic runs, respectively, at

higher temperature (400 °C) with and without added water. The data include coal conversion, total yields of gaseous products by two different methods, yields of CO, CO_2, and C_1-C_4 hydrocarbon gases determined by GC, yields of oil, asphaltene, and preasphaltene obtained from Soxhlet extraction, consumption of gas-phase H_2, and net hydrogen transfer from solvent where appropriate. These results are grouped and discussed below.

Effect of Water Reflected by the Influence of Drying

For the thermal (non-catalytic) runs, both vacuum-drying and air-drying decreased coal conversion significantly, as compared to the run of the raw coal. Original fresh raw coal contains 28.4 wt% water. To see whether the changes caused by the drying is reversible or irreversible, we added a small amount of water equivalent to the original moisture content, to the dried coal. The liquefaction results showed that adding water back to the vaccum-dried and air-dried coals restored over 90% of the conversion of the fresh raw coal. The coal conversion levels always follow the order of solvent-free < 1-methylnaphthalene < tetralin; the use of the raw coal always give the highest conversion. In the absence of water, there were some differences between the vacuum-dried and air-dried coals, with the latter affording higher conversion when a solvent was used. When water is added back, the differences between the two types of dried coals become much smaller.

These trends reveal that the major effect of drying on thermal liquefaction is associated with the effect of water. Under the conditions of vacuum-drying at 100 °C for 2 h, most of the changes caused by drying are reversible, as can be seen by the over 90% restoration of coal conversion. The other effects of drying and oxidation may include the changes in pore structure (Suuberg et al., 1991; Vorres et al., 1992), surface characteristics (Song et al., 1993), and, if oxidation involved, the change in functionality (Saini et al., 1993). These kinds of changes may be irreversible if high severity conditions were used for drying. However, when water is added back, the differences caused by using different drying methods, largely diminish. In other words, decrease in conversion caused by some undesirable changes during drying is largely compensated by the desirable effect of water addition.

The results for uncatalyzed runs in Tables 1 to 3 demonstrate that the presence of water promotes the conversion of the coal, increases oil yields, and significantly enhances the oxygen removal as CO_2. Adding water also resulted in small but consistent decrease in the yield of CO. This is considered to be due to water gas shift reaction: $CO + H_2O = CO_2 + H_2$. However, the increase in CO_2 yield upon H_2O addition is much more than the decrease in CO on a molar basis, indicating the occurence of other reactions between water and species in or from coal, which led to substantial increase in CO_2 formation.

Positive Effect of Added Water in Catalytic Liquefaction at 350°C

For all the catalytic runs listed in Tables 1 to 3, regardless how the coal was pre-dried or undried, all the ATTM-loaded coals were dried in vacuum at 100 °C for 2 h before use. In the runs testing the effect of water addition, we added a small amount of water (H_2O/dmmf coal = 0.46, wt ratio). It is clear from Table 2 that adding water to the catalytic reactions at 350°C dramatically promoted the coal conversion from 29-30 wt% for the vacuum-dried or air-dried coals to 62-63 wt% in the solvent-free runs, and from 43 to 66 wt% for the fresh raw coal. Therefore, the present results demonstrate that dispersed MoS_2 catalyst and a small amount of water can act in concert to strongly promote coal conversion at 350 °C. In fact, the use of ATTM with added water at 350 °C without solvent (Table 1) or with 1-MN solvent (Table 2) resulted in coal conversion level (63-66 dmmf wt%) that is much higher than that (30-38 wt%) from the non-catalytic runs at much higher temperature, 400 °C (Table 4).

For the solvent-free runs, the increased coal conversion upon water addition is mainly manifested by the significant gain in asphaltene and preasphaltene yields (Table 1). In the presence of either a H-donor tetralin solvent or a non-donor 1-MN solvent, the enhanced conversions are largely due to the increase in the yields of preasphaltene and oil, and this trend was most apparent with 1-MN solvent (Table 2).

With respects to the effect of water associated with influence of drying, it also appears that dispersing ATTM on vacuum-dried coal gives higher conversion upon water addition, as compared to loading ATTM on air-dried coal. The extents of increase in conversion due to water addition are also higher with the former than with the latter. These results show that for water-aided catalytic liquefaction at 350 °C, less oxidation of the coal sample can lead to higher conversion.

The use of catalyst generally decreased the yield of CO_2 in the runs of the dried coals without added water. Similar to the thermal runs, adding water to the catalytic runs also decreased the CO yield and significantly enhanced the formation of CO_2. The increasing extent in CO_2 yield is much higher than the decrease in CO yield, indicating the contribution of the reactions between water and coal species, other than water gas shift reaction, to the increased CO_2 formation.

Negative Effect of Added Water in Catalytic Liquefaction at 400°C

In order to examine the effect of added water in relation to the influence of reaction temperature, we also carried out the liquefaction experiments at 400°C. In uncatalyzed runs, adding water resulted in moderate increase in oil yields and coal conversion (5-7 wt%) with 1-MN solvent and without solvent, and small increase in coal conversion with tetralin

solvent. The changes in coal conversion with solvents are much larger at 400 °C than at 350 °C, but conversion always increases in the consistent order of none < 1-MN < tetralin.

As can be seen by comparing Table 5 with Table 4, the trends for the water effect in catalytic runs at 400 °C are different from those in non-catalytic runs. In the absence of added water, the solvent-free run of the vacuum-dried and ATTM-impregnated coal afforded highest conversion, 85 wt%, and highest oil yield, 46 wt%. The run with 1-MN solvent gave the lowest conversion, 71 wt%. Relative to the solvent-free run, the use of H-donor tetralin solvent at 400 °C did not display any advantage in terms of coal conversion and oil yields. Given the fact that water acts as a very good promotor for coal conversion at 350 °C (Tables 1-3), it is surprising to note from Table 5 that adding water to the catalytic runs at 400 °C decreased coal conversion substantially in the runs with 1-MN and without solvent. We conducted duplicated runs under the three different conditions at 400 °C, and confirmed a reproducible trend for the negative impact of water on the catalytic reactions at 400 °C. The solvent-free run suffered large decrease in coal conversion from 85 to 62 wt%. The run with tetralin displayed less sensitivity to the water, with slight but consistent decrease in conversion in duplicated runs from about 84 to 80 wt%.

These results show that the catalytic activity is significantly lower in the presence of water at 400 °C, indicating that water is detrimental for liquefaction at higher temperature. The action of water at 400 °C may be inferred through the following comparative examination. The highest oil yield and the highest conversion in the solvent-free run with no added water indicate that dispersed molybdenum catalyst exhibited maximum activity in activating molecular H_2, namely dissociation of H_2 on catalyst surface, and in transfer of the active H atom to the coal-derived free radicals and other coal species when there is no externally added solvent. Relative to the solvent-free catalytic run, the decrease in conversion and H_2 consumption upon addition of 1-MN may be attributed to the decrease in partial H_2 pressure, additional difficulty in mass transport of H_2 to the catalyst surface in the presence of solvent, and competitive adsorption of aromatic 1-MN molecules on catalyst surface. The same trends also applies to the run using tetralin, but the negative impact of tetralin to mass transport of H_2 gas is largely compensated by hydrogen donation from benzylie hydrogens in tetralin. As a result, oil yield decreased but conversion did not decrease as much as oil yield. Relative to the runs with added 1-MN, the added water initially occupied less space and therefore the partial H_2 pressure should be higher during the water-added but solvent-free run. Such a inferenee indicates that the presence of water deactivated the catalyst. The conversion decrease due to water addition was also accompanied by significant reduction in gas-phase H_2 consumption, from 2.8 to 1.4 in solvent-free runs, and from 1.8 to 0.7-0.9 in the runs with a solvent (Table 5). It should also be noted that the enhanced formation of CO_2 upon water addition seems to be unaffected at higher temperature, suggesting the enhanced CO_2 formation is caused by thermal reaction between added water and coal species.

The Desirable and Undesirable Functions of Water at 350 and 400 °C

Little is reported in literature about the effects of water on the catalytic coal liquefaction using dispersed catalyst. However, for non-catalytic coal conversion such as pyrolysis, liquefaction and coprocessing, hydrothermal pretreatments of coal has been reported to be beneficial in terms of increased conversion, or oil yield (Graff and Brandes, 1987; Bienkowski et al., 1987; Ross and Hirschon, 1990; Pollack et al., 1991; Serio et al., 1991; Tse et al., 1991). Siskin et al. (1991) have suggested that the presence of water during coal pretreatment will facilitate depolymerization of the macromolecular structure to give an increased proportion of liquids by cleaving important thermally stable covalent cross-links in the coal structure. On the other hand, Tse et al. (1991) suggested that the pretreatments of low rank coals in the presence of water should minimize retrogressive reactions such as crosslink formation by phenollic compounds such as catechol and lead to higher conversion or a better quality product. The present results for thermal runs are consistent with those in literature. However, there is no comparable literature data for the desirable and undesirable effects of water addition in catalytic liquefaction. Ruether et al. (1987) reported that in uncatalyzed systems, a substantial water partial pressure at fixed H_2 partial pressure increases the conversion of Illinois #6 bituminous coal, but in the runs using 0.1% dispersed Mo catalyst at 427 °C for 60 min, highest conversions are obtained without added water. How water affects the catalytic reaction is not clear. The present results suggest that water promotes coal liquefaction with dispersed MoS_2 catalyst at 350 °C (Tables 1 to 3), but has less promoting effect to thermal reaction at 400 °C (Table 4) and can deactivate or passivate the catalyst at 400 °C (Table 5).

CONCLUSIONS

Water can be excellent promoter or undesirable inhibitor for coal conversion in catalytic liquefaction, depending on the reaction systems and conditions. For catalytic liquefaction at 350°C, adding a small amount of water has a dramatic promoting effect on coal conversion, but a significant inhibiting effect of water is observed for catalytic runs at 400 °C. It appears that water and dispersed molybdenum sulfide catalyst can act in concert to promote coal conversion and oil production at 350 °C, but water can passivate the catalyst at 400°C. The remarkably high conversion level at low-temperature (350 °C) achieved with the co-use of ATTM and added water may give rise to new opportunities for developing novel low-severity catalytic liquefaction processes with significantly reduced oprational costs.

ACKNOWLEDGEMENTS

This work was supported by the U.S. Department of Energy, Pittsburgh Energy Technology Center. The authors wish to thank Drs. M.J. Baird and M.A. Nowak of DOE PETC for their support, and Mr. D. Glick and Dr. A. Davis of PSU for providing the coal sample.

REFERENCES

Atherton, L.F. Chemical Coal Beneficiation of Low-Rank Coals. Proc. 1985 Int. Conf. Coal Sci., pp. 553-556.

Bienkowski, P.R.; Narayan, R.; Greenkorn, R.A.; Chao, K.C. Ind. Eng. Chem. Res., 1987, 26, 202.

Cronauer, D.C.; Ruberto, R.G.; Silver, R.S.; Jenkins, R.G.; Davis, A.; Hoover, D.S. Liquefaction of Partially Dried and Oxidized Coals. 3. Liquefaction Results. Fuel, 1984, 63, 71-77.

Graff, R.A.; Brandes, S.D. Modification of Coal by Subcritical Steam: Pyrolysis and Extraction Yields. Energy & Fuels, 1987, 1, 84-88.

Gray, M.L.; Lai, R.W.; Wells, A.W. Surface Modification of Oxidized Coal by Methanol Vapor. Am. Chem. Soc. Div. Fuel Chem. Prepr., 1991, 36 (2), 804-813.

Lewan, M.D. Water as a Source of Hydrogen and Oxygen in Petroleum Formation by Hydrous Pyrolysis. Am. Chem. Soc. Div. Fuel Chem. Prepr., 1992, 37 (4), 1643-1649.

Pollack, N.R.; Holder, G.D.; Warzinski, R.P. Pretreatment for Coal Liquefaction. Am. Chem. Soc. Div. Fuel Chem. Prepr., 1991, 36 (1), 15-22.

Ross, D.S.; Hirschon, A.S.; Tse, D.S.; Loo, B.H. The Effects of Hydrothermal Treatment on Wyodak Coal. Am. Chem. Soc. Div. Fuel Chem. Prepr., 1990, 35 (2), 352-363.

Ross, D.S.; Loo, B.H.; Tse, D.S.; Hirschon, A.S. Hydrothermal Treatment and the Oxygen Functionalities in Wyodak Coal. Fuel, 1990, 70, 289-295.

Ruether, J.A.; Mima, J.A.; Kornosky, R.M.; Ha, B.C. Effect of Water and Hydrogen Partial Pressures during Direct Liquefaction in Catalyzed Systems with a Low Solvent-to-Coal Ratio. Energy & Fuels, 1987, 1, 198-202.

Saini, A.K.; Song, C.; Schobert, H.H. Influence of Drying and Oxidation of Coal on Its Catalytic and Thermal Liquefaction. 1. Coal Conversion and Products Distribution. Am. Chem. Soc. Div. Fuel Chem. Prepr., 1993a, 38 (2), 593-600.

Saini, A.K.; Song, C.; Schobert, H.H. Influence of Drying and Oxidation of Coal on Its Catalytic and Thermal Liquefaction. 2. Characterization of Dried and Oxidized Coals and Residues. 1993b, 38 (2), 601-608.

Serio, M.; Solomon, P.R.; Kroo, E.; Bassilakis, R.; Malhotra, R.; McMillen, D.F. Studies of Coal Pretreatment in Direct Liquefaction. Am. Chem. Soc. Div. Fuel Chem. Prepr., 1990, 35 (1), 61-69.

Siskin, M.; Katritzky, A.R.; Balasubramanian, M. Aqueous Organic Chemistry. 4. Cleavage of Diaryl Ethers. Energy & Fuels, 1991, 5, 770-771.

Song, C.; Schobert, H.H. Temperature-Programmed Liquefaction of Low-Rank Coals in H-donor and Non-donor Solvents. Am. Chem. Soc. Div. Fuel Chem. Prepr., 1992, 37 (2), 976-983.

Song, C.; Saini, A.K.; Schobert, H.H. Positive and Negative Impacts of Drying and Oxidation on Low-Severity Liquefaction of Low-Rank Coal. Proc. 7th Int. Conf. Coal Sci., accepted for presentation, Sept. 12-17, 1993.

Suuberg, E.M.; Otake, Y.; Deevi, S.C.; Yun, Y. The Role of Moisture in the Macromolecular Structure of Coals. Proc. 1991 Int. Conf. Coal Sci., pp.36-39.

Tse, D.S.; Hirschon, A.S.; Malhotra, R.; McMillen, D.F.; Ross, D.S. Effect of Hydrothermal Pretreatment for Coprocessing. Am. Chem. Soc. Div. Fuel Chem. Prepr., 1991, 36 (1), 23-28.

Vorres, K.S.; Wertz, D.L.; Malhotra, V.; Dang, Y.; Joseph, J.T.; Fisher, R. Drying of Beulah-Zap Lignite. Fuel, 1992, 71, 1047-1053.

Table 1. Effects of Water Addition on Solvent-Free Liquefaction of DECS-8 Wyodak Coal at 350 °C for 30 min under 6.9 MPa H_2

ID No.	51/63/93	7	26/32	90/139	119	54/66/96	10	29/35	116	113	122/142
Coal Sample[a]	Raw	VD-100°C-2 h	AD-100°C-2 h	VD-100°C-2 h	AD-100°C-2 h	Raw	VD-100°C-2 h	AD-100°C-2 h	Raw	VD-100°C-2 h	AD-100°C-2 h
Solvent	Solvent-free	Solvent-free	Solvent-free	Solvent-free	Solvent-free	Solvent-free	Solvent-free	Solvent-free	Solvent-free	Solvent-free	Solvent-free
Catalyst (ATTM)	–	–	–	–	–	ATTM	ATTM	ATTM	ATTM	ATTM	ATTM
H_2O Addition	Original H_2O	–	–	**H_2O added**	**H_2O added**	–	–	–	**H_2O added**	**H_2O added**	**H_2O added**
Prod. dmmf wt%											
Conversion	25.0	12.5	14.8	22.5	26.1	43.3	29.8	29.2	66.0	66.5	62.3
Gases	7.7[b] (9.52)[c]	3.3 (4.93)	5.0 (6.33)	7.4 (8.64)	8.4 (11.49)	2.2 (4.11)	3.0 (2.78)	3.3 (6.20)	6.2 (8.41)	6.5 (9.20)	6.6 (7.50)
CO	0.37	0.24	0.26	0.12	0.17	0.24	0.19	0.38	0.04	0.04	0.03
CO_2	8.90	4.50	5.93	8.27	11.11	3.52	2.30	5.18	8.18	8.70	7.09
C_1-C_4	0.25	0.19	0.14	0.25	0.21	0.35	0.29	0.59	0.44	0.46	0.38
Oil	5.4 (3.1)[d]	2.1	3.3	5.4 (3.1)	8.5	16.9	10.0	12.6	13.0	13.3	13.4
Asphaltene	2.8	2.6	0.7	2.3	2.1	9.2	5.4	3.2	19.9	21.6	19.5
Preasphaltene	9.1	4.5	5.8	7.6	7.1	14.9	11.4	10.1	26.9	25.1	22.9
H consum, dmmf wt%											
H_2 gas	0.72	0.20	0.28	0.44	0.43	1.92	1.35	1.34	1.64	1.70	1.73
H-donor sol											

a) Including fresh raw coal (Raw); vacuum-dried at 100°C for 2 h (VD); air-dried at 100°C for 2 h (AD). b) The gas yields determined by weighing the microreactor before reaction and after releasing the gaseous products. c) The figures in parenthesis are the gas yields determined by GC and volumetric analyses. d) Yield of physically recovered oil.

Table 2. Effects of Water Addition on Liquefaction of DECS-8 Wyodak Coal at 350 °C for 30 min in 1-Methylnaphthalene under 6.9 MPa H_2

ID No.	53/65/95	9	28/34	92/141	121	56/68/98	12	31/37	118	115	124/144
Coal Sample[a]	Raw	VD-100°C-2 h	AD-100°C-2 h	VD-100°C-2 h	AD-100°C-2 h	Raw	VD-100°C-2 h	AD-100°C-2 h	Raw	VD-100°C-2 h	AD-100°C-2 h
Solvent	1-MN	1-MN	1-MN	1-MN	1-MN	1-MN	1-MN	1-MN	1-MN	1-MN	1-MN
Catalyst (ATTM)	–	–	–	–	–	ATTM	ATTM	ATTM	ATTM	ATTM	ATTM
H_2O Added	Original H_2O	–	–	H_2O added	H_2O added	–	–	–	H_2O added	H_2O added	H_2O added
Prod. dmmf wt%											
Conversion	38.4	18.3	22.7	34.8	36.5	35.9	31.1	37.4	60.0	56.0	51.7
Gas	6.4[b] (7.34)[c]	4.0 (4.66)	5.1 (6.58)	6.4 (7.14)	8.9 (10.93)	3.2 (4.96)	2.6 (3.7)	3.0 (5.8)	5.7 (9.82)	5.8 (10.39)	6.8 ()
CO	0.14	0.16	0.25	0.11	0.16	0.14	0.11	0.19	0.04	0.05	0.04
CO_2	7.02	4.34	6.18	6.84	10.57	4.48	3.37	5.23	9.46	9.99	8.54
C_1-C_4	0.18	0.16	0.15	0.19	0.20	0.34	0.25	0.37	0.32	0.35	0.28
Oil	15.9	1.1	4.2	11.2	12.2	10.4	6.1	10.3	25.3	15.4	15.5
Asphaltene	6.6	5.8	4.0	7.1	6.9	10.4	10.1	8.1	9.6	13.2	9.5
Preasphaltene	11.4	7.4	9.4	10.1	8.4	11.9	12.3	16.0	19.5	21.6	19.9
H consum, dmmf wt%											
H_2 gas	0.58	0.45	0.43	0.44	0.29	1.17	1.00	1.08	0.99	1.02	0.75

a) Including fresh raw coal (Raw); vacuum-dried at 100°C for 2 h (VD); air-dried at 100°C for 2 h (AD). b) The gas yields determined by weighing the microreactor before reaction and after releasing the gaseous products. c) The figures in parenthesis are the gas yields determined by GC and volumetric analyses.

Table 3. Effects of Water Addition on Liquefaction of DECS-8 Wyodak Coal at 350 °C for 30 min in Tetralin under 6.9 MPa H_2

ID No.	52/64/94	8	27/33/33a	91/140	120	55/67/97	11	30/36	117	114	123/143
Coal Sample[a]	Raw	VD-100°C-2 h	AD-100°C-2 h	VD-100°C-2 h	AD-100°C-2 h	Raw	VD-100°C-2 h	AD-100°C-2 h	Raw	VD-100°C-2 h	AD-100°C-2 h
Solvent	Tetralin	Tetralin	Tetralin	Tetralin	Tetralin	Tetralin	Tetralin	Tetralin	Tetralin	Tetralin	Tetralin
Catalyst (ATTM)	–	–	–	–	–	ATTM	ATTM	ATTM	ATTM	ATTM	ATTM
H_2O Addition	Original H_2O	–	–	H_2O added	H_2O added	–	–	–	H_2O added	H_2O added	H_2O added
Prod. dmmf wt%											
Conversion	43.3	25.9	35.1	40.0	40.4	42.2	36.4	45.6	64.1	62.9	60.5
Gas	5.8[b] (7.71)[c]	4.2 (4.4)	5.4 (6.3)	6.0 (7.31)	7.1 (9.60)	2.8 (4.94)	3.0 (2.9)	3.9 (5.47)	5.9 (9.67)	6.2 (8.96)	5.7 (8.10)
CO	0.11	0.19	0.24	0.10	0.19	0.14	0.13	0.21	0.05	0.04	0.03
CO_2	7.41	4.10	5.91	7.01	9.20	4.45	2.58	4.83	9.27	8.57	7.79
C_1-C_4	0.19	0.15	0.19	0.20	0.21	0.35	0.28	0.43	0.35	0.35	0.28
Oil	15.8	4.1	11.7	14.0	16.6	16.0	10.2	15.7	18.2	20.8	18.1
Asphaltene	9.3	7.6	7.4	10.5	5.9	11.5	12.9	11.1	13.9	13.8	9.3
Preasphaltene	12.4	10.0	10.6	7.9	10.8	11.9	10.6	14.9	26.1	22.0	27.4
H consum, dmmf wt%											
H_2 gas	0.67	0.29	0.24	0.48	0.19	1.21	1.35	1.36	1.07	1.37	0.81
H-donor sol	0.28	0.41	0.47	0.36	0.42	0.24	0.08	0.14	0.28	0.22	0.26

a) Including fresh raw coal (Raw); vacuum-dried at 100°C for 2 h (VD); air-dried at 100°C for 2 h (AD). b) The gas yields determined by weighing the microreactor before reaction and after releasing the gaseous products. c) The figures in parenthesis are the gas yields determined by GC and volumetric analyses.

Table 4. Effect of Water Addition on Thermal Liquefaction of DECS-9 Coal at 400 °C

ID No.	73	133/162	60	135/164	59/87	134/163
Coal Sample[a]	VD-100 °C-2h	VD-100 °C-2h	VD-100 °C-2h	VD-100 °C-2h	VD-100 °C-2h	VD-100 °C-2h
Solvent	Solvent-free	Solvent-free	1-MN	1-MN	Tetralin	Tetralin
Catalyst (ATTM)	–	–	–	–	–	–
H_2O Addition	–	H_2O added	–	H_2O added	–	H_2O added
Prod. dmmf wt%						
Conversion[b]	30.3	35.4	38.2	43.1	71.4	73.1
Gas	8.8[b] (7.6)[c]	12.3 (12.54)	8.5 (9.78)	10.3 (12.45)	8.4 (9.37)	10.3 (12.39)
CO	0.41	0.21	0.25	0.25	0.33	0.25
CO_2	6.35	11.26	8.56	10.75	7.80	10.55
C_1-C_4	0.85	1.07	0.97	1.45	1.24	1.59
Oil	10.4 (5.3)[d]	16.1	13.1	20.7	27.3	32.0
Asphaltene	1.8	2.2	7.4	6.1	16.4	16.3
Preasphaltene	10.5	4.8	9.2	6.0	19.3	14.4

a) Including fresh raw coal (Raw); vacuum-dried at 100°C for 2 h (VD); air-dried at 100°C for 2 h (AD).
b) The gas yields determined by weighing the microreactor before reaction and after releasing the gases.
c) The figures in parenthesis are the gas yields determined by GC and volumetric analyses. d) Recovered oil.

Table 5. Effect of Water Addition on Catalytic Liquefaction of DECS-9 Coal at 400 °C

ID No.	148/155	136/165	150/157	138/167	149/156	137/166
Coal Sample[a]	VD-100 °C-2h	VD-100 °C-2h	VD-100 °C-2h	VD-100 °C-2h	VD-100 °C-2h	VD-100 °C-2h
Solvent	Solvent-free	Solvent-free	1-MN	1-MN	Tetralin	Tetralin
Catalyst (ATTM)	ATTM	ATTM	ATTM	ATTM	ATTM	ATTM
H_2O Addition	--	H_2O added	--	H_2O added	--	H_2O added
Prod. dmmf wt%						
Conversion	85.4	62.1	70.9	61.8	83.6	80.3
Gas	7.5[b] (10.1)[c]	11.4 (11.23)	7.3 (9.91)	9.7 (12.82)	7.7 (9.74)	9.7 (12.73)
CO	0.10	0.02	0.18	0.02	0.17	0.03
CO_2	7.39	9.57	7.87	11.31	7.71	11.14
C_1-C_4	2.61	1.64	1.86	1.49	1.86	1.56
Oil	45.8	28.2	34.0	28.1	36.4	34.0
Asphaltene	19.7	10.5	12.8	10.7	16.9	14.9
Preasphaltene	12.4	12.0	16.9	13.3	22.6	21.7
H consum, dmmf wt%						
H_2 gas	2.80	1.38	1.81	0.90	1.75	0.72

a) Including fresh raw coal (Raw); vacuum-dried at 100°C for 2 h (VD); air-dried at 100°C for 2 h (AD).
b) The gas yields determined by weighing the microreactor before reaction and after releasing the gases.
c) The figures in parenthesis are the gas yields determined by GC and volumetric analyses.

SOLVENT AND PRETREATMENT EFFECTS ON COAL SWELLING

Rowena J. Torres-Ordonez, Elaine M. Quinga, and Donald C. Cronauer
Amoco Oil Company, PO Box 3011, Naperville, IL 60566

Keywords: Coal, solvent swelling.

ABSTRACT

Swelling ratios were determined with a wide variety of solvents and solvent blends using pulverized samples of Black Thunder, (WY) subbituminous, Burning Star (IL) bituminous, and Martin Lake (TX) lignite. Experiments were also conducted with 8 x 60 mesh raw and sulfurous acid-treated Black Thunder coal. Only marginal levels of swelling were observed for the hydrocarbon solvents, while hetero-functional solvents enhanced swelling ratios. Oxygenates gave equilibrium swelling ratios, Q, in the range of 1.15 to 1.6, with tetrahydrofuran as the most effective. Selected nitrogen-containing solvents and dimethyl disulfide were also effective, with Q ratios ranging from 1.6 to 2.7. As a result of sulfurous acid-treatment to remove the alkali and alkaline earth ions, the selling of Black Thunder coal was enhanced. The effects of coal type may be attributed to the interaction of the solvent with the bonds present in both the raw and acid-treated coals. Experiments with blends of effective and non-effective solvents gave much greater Q ratios than those expected from an linear combination of the two solvents. The greatest synergisms were observed with Black Thunder and Burning Star coals.

INTRODUCTION

Van Krevelen[1] proposed that coals are three-dimensionally cross-linked macromolecular networks. The area was expanded upon.[2-5] When brought into contact with most organic solvents, coals absorb the solvent and swell. The two factors which control the amount of swelling are the magnitude of the solvent-coal interactions and the cross-link density of the coal. Another aspect is that coals can behave as either a glass or rubber with a transition zone. In a glassy state, the macromolecular chains are constrained and diffusion through the coal matrix is quite slow. In the rubbery state, the macromolecular chains can move relatively freely, and diffusion rates in the solid approach those in liquids. Some solvents can cause a glass-to-rubber transition to occur in coals.

Coal swelling solvents can be divided into two classes: non-hydrogen bonding and hydrogen bonding. The swelling ratios of the coal samples in non-hydrogen bonding solvents are significantly less than those in hydrogen bonding solvents. The most effective solvents are those containing a nitrogen or oxygen atom possessing an unshared pair of electrons. The strong hydrogen bonding solvents replace the coal-coal hydrogen bonds with new coal-solvent hydrogen bonds. If the coal-coal hydrogen bonds are active cross-links, the replacement would result in a lower cross-link density which would cause swelling to increase. The weak hydrogen bonding solvents result in less swelling since more coal-coal hydrogen bonds remain intact.

EXPERIMENTAL

Coal swelling experiments were made using (1) Martin Lake lignite, (2) Black Thunder subbituminous, and (3) Illinois No. 6 bituminous coals. The coals were dryed and handled in nitrogen whenever possible. The coals were either

sieved and ground to -325 mesh under nitrogen, or used as coarse (8 x 60 mesh) material. Samples of raw and SO_2-treated Black Thunder coal, that were partially dried to 8 wt% moisture content at ambient temperature in nitrogen, were also used.

The experimental procedure for the first set of samples consisted of placing samples of dry coal in a 1 mm. o.d. tube followed by centrifuging for 60 minutes. The height of the coal was measured as h_1. After breaking up the column of packed coal, solvent in excess was introduced and the tube was vigorously shaken to ensure thorough mixing. The slurry was centrifuged after specified times and the height was measured as h_2. The swelling ratio was defined as the ratio of the resulting heights of swelled and raw coal ($Q = h_2/h_1$). In the experiments with the coarse coal samples, 10 ml conical centrifuge tubes were used.

RESULTS AND DISCUSSION

Reproducibility: Experiments were made to determine reproducibility using two technicians to make multiple parallel tests. Reproducibility was good. At low swelling ratios, such as those of the methanol runs (average Q of 1.28), the standard deviation averaged about ±0.06. At high swelling ratios (tetrabutyl ammonium hydroxide, Q averaging about 2.5), the standard deviation averaged about ±0.14.

Effect of Solvent Type and the Interaction with Coal Pretreatment: The results of swelling ratio experiments using finely pulverized (through 325 mesh) coal samples are given in Table I. Only marginal levels of coal swelling were observed for the hydrocarbon solvents including hexane, cyclohexane, single-ring aromatics, and tetralin.

Swelling greatly increased with the introduction of hetero-functionality. Equilibrium (96 hour contact) swelling ratios of the three coals with alcohols and ketones fell in the range of 1.15 to 1.4. There appeared to be no consistent effect of the type (molecular weight) of alcohol or ketone, but the Black Thunder coal swelled to a greater extent than the other coals. Cresol was a more effective swelling agent than the above oxygenates in the case of Illinois No. 6 coal, but it was the same for the other coals. The results with methyl acetate were the same as those of the above oxygenates. Tetrahydrofuran (THF) was a significantly more effective coal swelling solvent than the other oxygenates. The Q ratios ranged from 1.38 to 1.63.

The nitrogen-containing compounds varied greatly in their effectiveness to swell these coals. The highly polar compound, tetrabutylammonium hydroxide (TBAH), was very effective with a range of Q ratios of 2.18 to 2.66. Aniline was quite effective for Illinois No. 6 and Black Thunder coals (1.94 and 1.64, respectively), but it was essentially ineffective (1.19) for Martin Lake lignite. Nitrobenzene was poor for all three coals (1.11 to 1.19).

Dimethylsulfoxide was tested due to its unusual solvent properties in other systems. It was found to be particularly effective for the Black Thunder and Illinois No. 6 coals and moderately effective for Martin Lake lignite (2.39, 2.15, and 1.63, respectively).

The results of coal swelling experiments carried out with 8X60 mesh size fractions of both raw and SO_2-treated Black Thunder coal are given in Table II. There appeared to be little or no effect of coal particle size upon the swelling ratio. However, the SO_2-treated coal swelling was significantly

greater than that of the raw coal. The removal of alkali and alkaline earth ions from the subbituminous coal reduced the interaction of coal species with each other.

The above differences in swelling are attributed to the interaction of the solvent with the various bonds present in coal. The low rank coals contain significant amounts of ionic and hydrogen bonds due to the presence of a relatively large number of polar functional groups, while the high rank coals contain more charge transfer complexes because of their higher aromatic content. TBAH, which is a very basic solvent, interacts with the ionic and hydrogen bonds readily, thus swelling the Martin Lake lignite to the greatest extent. This is followed by Black Thunder coal and Illinois No. 6. On the other hand, THF disrupts charge transfer complexes, which are predominant in Illinois No. 6, a higher rank coal, thus resulting in a swelling trend opposite to that of TBAH. The increase of swelling ratio in the case of SO_2 treatment is an obvious extension of this theory, especially with the removal of divalent metal ions, such as calcium.

Effect of Solvent Blends: The results of experiments made with 325 mesh coal samples and blends of tetralin (TET) and isopropanol (IPA) are shown in Table I and Figure 1. There was a high level of synergism with an advantage of using these blends over the pure solvents. In all cases, the swelling ratios were much greater than those derived from a linear correlation between the pure solvents.
As shown in Figures 2 and 3, the synergism of coal swelling solvents also was demonstrated for methanol/water, dimethyl sulfoxide/tetralin, methanol/tetralin, and isopropanol/water. Experimentation was also carried out with the 8X60 mesh fractions of raw and SO_2-treated Black Thunder coal, as given in Table II. Again, there were high levels of synergism of solvent blends with both samples of coal.
There is a distinct advantage of using solvent blends to swell coal, because relatively low levels of swelling agent would be needed to be effective in treating coal feed slurries for a liquefaction plant.

CONCLUSIONS

The following conclusions are drawn from the coal swelling studies:

1. Only marginal levels of coal swelling were observed for the hydrocarbon solvents including paraffins, cycloparaffins, and aromatics.
2. Swelling ratios were greatly increased with the use of solvents having heteroatom functionality.
3. The effectiveness of the oxygenates increased in the following order: alcohols, ketones, methyl acetate < cresol < tetrahydrofuran.
4. The swelling ratios generated by nitrogen-containing compounds increased as follows: nitrobenzene < aniline < tetrabutylammonium hydroxide.
5. High coal swelling ratios were observed with dimethylsulfoxide.
6. Solvent synergism was observed in that the swelling ratios of solvent blends were much greater than those derived from a linear correlation between the pure solvents.

ACKNOWLEDGMENT

This project was supported in part by DOE under Project DE-AC22-91PC91051, entitled "Advanced Liquefaction Using Coal Swelling and Catalyst Dispersion Techniques."

REFERENCES

1. Van Krevelen, D. W., Coal; Elsevier; Amsterdam, 1961, and Fuel 1966 45, 99, 229.
2. Vahrman, M., Fuel 1970, 49, 5.
3. Palmer, T. J., Vahrmen, M., Fuel 1972, 51, 22.
4. Shapiro, L-L. D.; Al'terman, L. S., Solid Fuel Chem. 1977 11(3), 13.
5. Larson, J. W., Lee, D., Shawver, S. E., Fuel Process. Techn. 1986 12, 51.

Table I
SWELLING RATIO OF COAL/SOLVENT BLENDS
(325 Mesh Coal with 1 ml Winthrobe Tubes)

	Black Thunder		Illinois No. 6		Martin Lake Lignite	
Solvent/Time	24 Hr	96 Hr	24 Hr	96 Hr	24 Hr	96 Hr
Hexane	--	1.01	--	1.00	--	0.95
Cyclohexane	--	1.00	1.00	1.00	--	--
Benzene	--	1.12	--	1.06	--	1.14
Toluene	--	1.04	--	1.16	--	1.00
Xylene	--	1.02	--	1.04	--	1.05
Tetralin	1.00	1.04	0.96	1.02	1.02	1.03
Methanol	1.28	1.35	1.16	1.23	1.43	1.36
Ethanol	--	1.31	--	1.26	--	1.24
Isopropanol	1.30	1.39	1.06	1.15	1.14	1.25
Isopropanol	1.30	1.39	1.06	1.15	1.14	1.25
33% Tetralin/67% IPA	1.40	1.53	1.31	1.43	1.18	1.37
67% Tetralin/33% IPA	1.39	1.47	1.34	1.49	1.18	1.36
80% Tetralin/20% IPA	1.34	1.42	1.22	1.35	1.10	1.23
90% Tetralin/10% IPA	1.22	1.33	1.13	1.19	1.10	1.18
Tetralin	1.00	1.04	0.96	1.02	1.02	1.03
Cresol	1.16	1.29	1.28	1.48	1.13	1.20
Acetone	--	1.32	--	1.24	--	1.25
Methyl Ethyl Ketone	1.32	1.34	1.29	1.29	1.27	1.3
Methyl Acetate	1.28	1.34	1.20	1.20	1.25	1.25
Tetrahydrofuran	1.45	1.53	1.50	1.63	1.36	1.38
Chloroform	--	1.17	--	1.19	--	1.03
Chlorobenzene	1.08	1.08	1.07	1.16	1.09	1.12
Nitrobenzene	1.11	1.15	1.18	1.19	1.08	1.11
Aniline	1.41	1.64	1.71	1.94	1.12	1.19
Tetrabutylammonium Hydroxide	2.05	2.45	1.59	2.18	2.04	2.66
Dimethyl Sulfoxide	2.19	2.39	2.08	2.15	1.52	1.63

Table II

SWELLING RATIO OF THREE SAMPLES OF BLACK THUNDER COAL
(10 ml Conical Centrifuge Tubes)

	Untreated -325 Mesh				Untreated 8 x 60 Mesh				SO_2-Treated 8 x 60 Mesh			
Solvent/Time	2 Hr	4 Hr	24 Hr	96 Hr	2 Hr	4 Hr	24 Hr	96 Hr	2 Hr	4 Hr	24 Hr	96 Hr
Isopropanol	--	--	--	--	1.20	--	1.25	--	1.27	--	1.42	--
50% IPA/50% H_2O	--	--	--	1.38	--	--	--	--	--	--	1.40	1.40
20% IPA/80% Tetralin	1.16	--	1.24	--	1.25	--	1.48	--	1.33	1.38	1.41	1.41
20% IPA/80% Toluene	--	--	--	--	1.18	--	1.21	--	1.26	--	1.42	--
30% IPA/70% Toluene	--	--	--	--	1.20	--	1.24	--	1.38	--	1.51	--
40% IPA/60% Toluene	--	--	--	--	1.18	--	1.30	--	1.32	--	1.56	--
Methanol	1.34	1.43	1.43	--	--	--	1.26	1.26	1.24	--	--	--
(repeat)	--	--	1.19	1.33	--	--	--	--	1.18	--	--	--
70% MeOH/30% H_2O	--	--	1.32	1.40	1.24	--	1.24	--	--	--	1.25	--
50% MeOH/50% H_2O	--	--	1.38	1.36	--	--	--	--	--	--	1.21	--
30% MeOH/70% H_2O	--	--	1.21	1.28	--	--	--	--	--	--	--	--
25% MeOH/75% Tetralin	1.43	1.46	1.49	--	--	--	--	--	--	--	--	--
Acetone	--	--	--	--	1.23	--	1.24	--	1.52	--	1.52	--
Tetrahydrofuran	--	--	1.42	1.55	--	--	1.54	1.59	1.83	1.94	2.07	2.08
70% THF/30% H_2O	--	--	1.87	1.91	1.71	--	1.86	--	1.93	--	2.15	--
50% THF/50% H_2O	--	--	1.78	1.85	--	--	--	--	--	--	--	--
30% THF/70% H_2O	--	--	1.52	1.60	1.36	--	1.49	--	1.43	--	1.52	--
20% THF/80% H_2O	1.40	1.46	1.46	--	--	--	--	--	--	--	--	--
10% THF/90% H_2O	1.24	1.24	1.31	--	--	--	--	--	--	--	--	--
5% THF/95% H_2O	1.40	1.38	1.41	--	1.14	--	1.16	--	1.16	--	1.16	--
(repeat)									1.17	--	1.15	--
Aniline	--	--	--	--	1.17	--	1.37	--	1.22	--	1.68	--
(repeat)									1.21	--	1.97	--
Dimethyl Sulfoxide	2.05	2.37	2.37	2.37	1.60	--	2.09	--	2.28	2.35	2.41	2.58
10% DMSO/90% Tetralin	1.39	1.49	1.58	--	1.21	--	1.60	--	1.41	--	1.83	--
5% DMSO/95% Tetralin	1.19	1.27	1.32	--	1.13	--	1.43	--	1.23	--	1.44	--
												--

Figure 1
Swelling Ratios of 325-mesh Coal with the IPA/Tetralin System

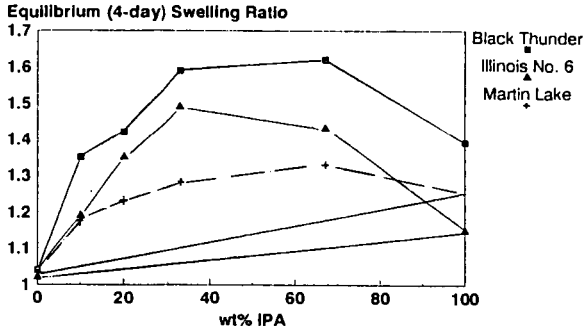

Figure 2
Swelling Ratios of 325-mesh Black Thunder Coal
with the THF/Water System

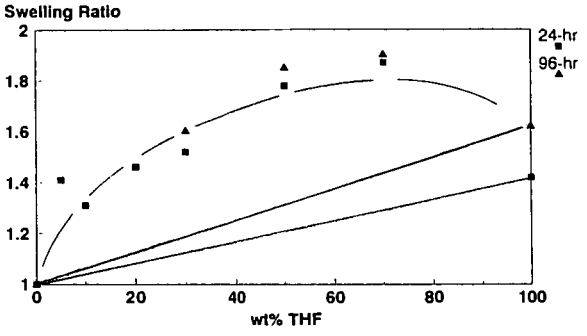

Figure 3
Swelling Ratios of 325-mesh Black Thunder Coal with Solvent Blends

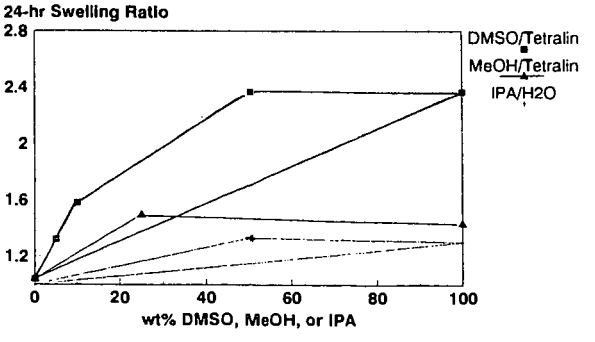

ION EXCHANGE PROPERTIES OF WYODAK PREMIUM COAL SAMPLES

Karl S. Vorres
Chemistry Div., Bldg. 211
Argonne National Laboratory
Argonne, IL 60439

ABSTRACT:
Low rank coals (lignite and subbituminous) contain exchangeable cations. A sample of -20+200 mesh Argonne Premium Wyodak coal was washed with nitric acid in a burette fitted with a coarse glass frit at the base of the graduations to remove the exchangeable cations from the system. The eluent was passed to a flow-through pH electrode and a titration curve was obtained on a computer file. A series of electrodes (pH, calcium, sodium and potassium) were used in separate experiments to follow the elution from the coal. Some implications for coal structure are also indicated.

INTRODUCTION:

The abundant reserves of low rank coals in the United States are potentially useful for the production of synthetic liquid fuels. In addition the structure of these coals is becoming better understood but significant additional information is needed to optimize this use.

The coal structure involves polymers of molecules derived from the lignin in the original plants. This structure is known to contain several reactive functional group types including carboxylate and phenolic. The carboxylates are known to be able to act as ion-exchange materials. The functional groups are frequently linked to a variety of alkali and alkaline earth cations. The inorganic cations can be detrimental due to fouling of boilers during operation or reducing yields for liquefaction.

The latter deleterious effects of calcium in the coal (and any other exchangeable cations) can be overcome by removal of these species. A number of studies have indicated that low rank coals can be treated with acids to exchange the cation species with hydrogen ions (1-3). The cations can then be washed away from the coal to minimize their effect.

Cations with a single charge can be attached to a single carboxylate group. Calcium may be present in either or both of two forms. In one case the doubly charged cation can be bound to one hydroxyl and one carboxylate group. This represents a more easily removed form. The second case involves simultaneous bonding to two nearby carboxylate groups. Removal of this calcium involves releae from one carboxylate, and later from the second. This process is more difficult and would appear more slowly.

EXPERIMENTAL:

The coal sample was the Argonne Premium Wyodak subbituminous (4). This coal contains (dry basis) 8.7% mineral matter from low temperature ashing. The 8.7% is made up of: 2.0% quartz, 0.1% pyrite, 0.4% calcite and 6.2 % clays which may be kaolinite (5). The -20 mesh samples were dry screened to -20+200 mesh. Weighed

amounts (about 30 grams) of the screened samples were slurried with deionized water. Fines (still -200 mesh) were decanted away from the slurry using about 200-600 ml of water. The slurry was washed into a special 50 ml burette. The burette had been fitted with a coarse fritted glass disk at the 50 ml mark to retain the coal but allow solutions to pass. Fine coal particles had to be removed to avoid pluggage of the frit. A peristaltic pump provided a uniform flow of 0.1 N HNO_3 to the sample. Acid flow rates were typically about 1-3 ml/minute and were set according to the ability of the solution to pass through the coal bed. Following the treatment with the acid, the samples were washed with distilled water fed by the peristaltic pump, and the record of pH and ion concentration was obtained in a manner similar to that for the acid treatment. The burette tip was fitted with tubing to connect a flow-through pH electrode from Cole-Parmer, or from Microelectrodes, Inc (Londonderry, NH). For some of the later experiments the pH electrodes were augmented with ion-selective electrodes for Ca^{+2}, and Na^{+}. The electrodes with used with an Orion EA940 pH meter. The pH meter in turn was connected to an IBM model AT computer for data acquisition. A schematic diagram of the equipment is given in Figure 1. A program was written which allowed data points to be acquired at specific intervals in the range of 10-18 seconds. The data files were then manipulated with a word processor and Lotus 123 macros to permit plots to be drawn of the data.

The pH electrodes were calibrated with Cole Parmer standard buffers of pH 4 and 7. The ion selective electrodes were calibrated with standard solutions made up of a series of analyzed reagents salts diluted to give 0.1, 0.01 and 0.001 M solutions for each of the cations. Calibrations were checked at the end of the runs.

This arrangement does give a different approach to an endpoint than a simple titration since the exchanged cations are removed from the system.

RESULTS AND DISCUSSION:

The results for the Wyodak sample with the pH and sodium electrode are shown in Figure 2. A number of features are evident. The pH changes for the Wyodak coal titrated with 0.1 N nitric acid indicate an initial period in which the water in contact with the coal was displaced by the acid (pH about 6.5 to 5). During this time the soluble species were released and contributed to a near neutral state. This period was followed by an extensive period in which the pH was steady at about 5. During this time the other cations associated with carboxylate groups were exchanging with hydrogen ions and being eluted. At the end of this phase a pair of inflections was exhibited before reaching the pH of the input acid.

The Na electrode indicated that the Na was eluted early in the exchange process, and tailed off slowly. The increase near the end of teh acid addition is associated with a change in sensitivity with pH and is not associated with an increase in Na concentration. The most readily released species was released first. The pH remained high after the sodium release indicating that other species were reacting with the acid.

Figure 3 shows the effect of washing the coal with acid and monitoring the calcium ion concentration as well as the pH. A number of features can be seen. The initial pH for this solution is higher than for the sodium, believed to be due to the use of a smaller amount of water to decant the fines, and more of the soluble species were retained in the slurry and eluted in this stage. These species are alkaline as the pH exceeds 7. As the water is displaced from the coal by the acid the pH drops to about 6. During this period an initial calcium species is eluted. There is a slight increase to about pH 6.2 and a long period of very slow decrease to pH 6.1. During this period there is a rapid rise of the calcium concentration (dissolution of calcite is at least partially responsible) and then a slow and consistent increase to a maximum. Just before the maximum calcium concentration the pH drops from about 6.1 to about 4. During this period there is a rapid decrease in the calcium concentration. This is followed by an even more rapid decrease in pH to about 1.15, accompanied by a very rapid decrease in the calcium ion concentration. An instrumental problem caused the discontinuity in the pH curve and compressed the time during that period. The scatter in values for the calcium values at higher concentrations is attributed to the electrode stability.

Figure 4 shows the effects of rinsing the acid washed coal with deionized water. It should be noted that the coal changes character in the process and the rate of passage of the deionized water decreased. Initially the acid was washed out of the column at pH 1.15. A period followed during which the pH changed from 1.15 to about 1.9 with a linear slope. The pH changed more rapidly and then asymptotically approached a value of about 3.3. The shape of the latter part of the curve approached that of a parabola. The initial linear portion is assumed to be due to the mixing of the acid in the space between the particles with the incoming water flow and discharge from the burette. The latter more parabolic shaped curve is believed to be due to diffusional processes from the pores of the particles.

One characteristic of the water washing step is the release of some calcium near the intersection of the linear and the non-linear parts of the pH curves. This is seen in Figure 4 and is reproducible through several stages of acid washing and water rinsing. The shape of the curve is consistent through 3 wash and rinse sequences. In each case the calcium is rinsed out near the intersection of the two segments of the pH versus time plots. The calcium is also washed out in successive acid washes in the same pH range.

The cause of the release of calcium in both the acid wash and water rinse near the same pH is not yet clear. It may be that the physical structure of form of the external surface changes at a certain pH. If that were so, then any calcium which had been freed from internal linkages to carboxylate or other groups might be released in the rearrangement step during the transition between the structures.

A small amount of cloudy material was seen in the supernatant water after the treated coal was removed from the burette. The cloudy material was decanted and allowed to settle. The clear supernatant was discarded. A grey solid was recovered and analyzed with FTIR.

FTIR indicated the presence of clay type minerals. Apparently the acid form of the coal is active and can release very finely divided clay material.

An analysis of the the acid solution which was passed over the coal in the burette for the experiment with the sodium electrode, and the rinse water, was made. The results are given in Table 1.

Table 1. Concentrations of Cationic Species in Wyodak Solutions in ppm (ug/ml)

Cation	Acid Soln	Rinse
Al	56.6	6.80
B	1.04	<.10
Ba	7.94	.37
Ca	908.	14.6
Fe	35.7	4.73
Mg	212.	1.26
Mn	1.21	.04
Ni	.21	<.05
Si	.55	<.30
Sr	16.5	.22
Ti	.07	.04
V	.13	<.10
Zn	.42	.05
K	4.91	<.20
Na	49.8	.19

The estimated accuracy of the ICP AES analysis is +/- 10%.

Be, Cd, Co, Cr, Cu, Mo, Pb, Sn, and Zr were all below the limits of determination.

The release of clay during the acid washing and subsequent water rinsing may indicate that the clay is attracted to negative groups such as the carboxylate in the coal structure. The clay has a number of cations bound in its layer structure. The rinse water following the acid wash contained some additional calcium, indicating the release of this cation during the duration of the contact with the water. It is possible that the coal structure includes coal-matter-to-clay bonds. Acid washing can rupture some of these linkages, permitting the liberation of the clay. The structure of the coal particle would then be weakened. This weakening would limit the useful life of low rank coals for uses such as ion exchange resins.

CONCLUSIONS:

1. some of the ion exchange properties of low rank coals can be understood by titrating with the burette system described.

2. Alkali cations are removed early in the titration, and alkaline earth cations are removed throughout the acid treatment.
3. More acid is consumed in the titration than the equivalent amount of cations which are recovered.
4. Some aluminum is solubilized.
5. Clay is released following the acid treatment. This clay is probably associated with the exchanged cations.

FUTURE WORK:

The potential of application of small amounts of catalysts which can still be useful needs to be explored. The ion exchange capabilities of the low rank coals presents an opportunity to add catalytically active species such as Fe^{+2}, Co^{+2}, Ni^{+2}. Other useful metal species, such as MoO_4^{-2}, can be added by adsorption techniques.

ACKNOWLEDGMENTS:

The author acknowledges support from the U. S. Department of Energy, Office of Fossil Energy for the support which made this work possible.
Thanks are expressed to Joe Gregar for the preparation of the burette, to Robert McBeth for the preparation of standard solutions for the calibration of the ion selective electrodes, and to David French for the FTIR analysis.

REFERENCES:

1. C. Lafferty and M. Hobday, Fuel, 69, 78-83 (1990)

2. C. Lafferty and M. Hobday, Fuel, 69, 84-87 (1990)

3. J. T. Joseph and T. R. Forrai, Fuel, 71, 75-80 (1992)

4. K. S. Vorres, Energy Fuels, 4, 420-426 (1990).

5. R. D. Harvey, Ill. State Geol. Survey, 1988.

FIGURE 1.
DIAGRAM OF EQUIPMENT FOR ACID LEACHING OF COAL SAMPLES

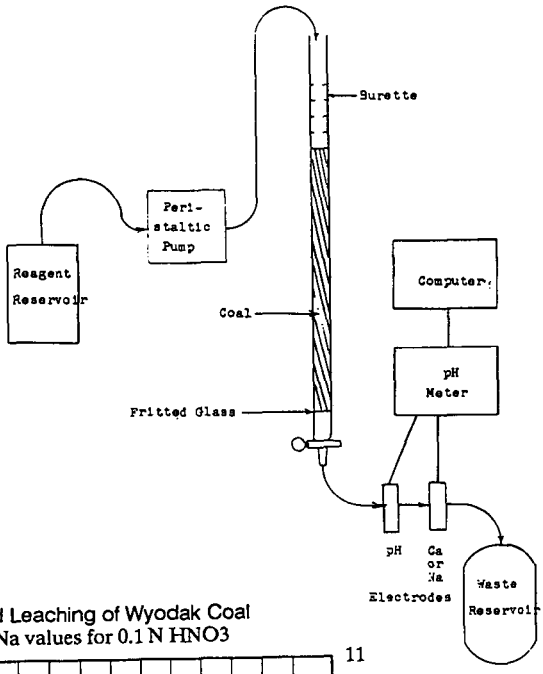

Fig. 2, Acid Leaching of Wyodak Coal
pH and Na values for 0.1 N HNO3

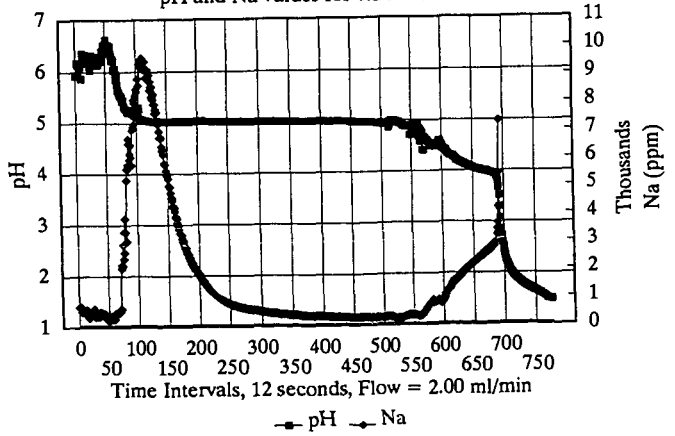

WY427S.wk3

Fig. 3, Wyodak Acid Washed for Comparison
WY521, 0.1 HNO3

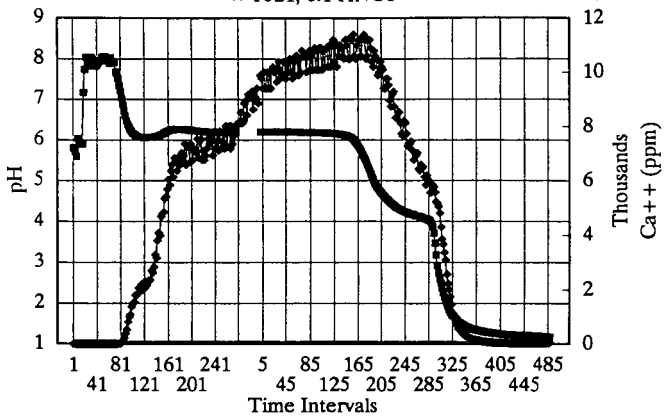

WY521 composite

Fig. 4, Wyodak Rinsed with Water for Comparison

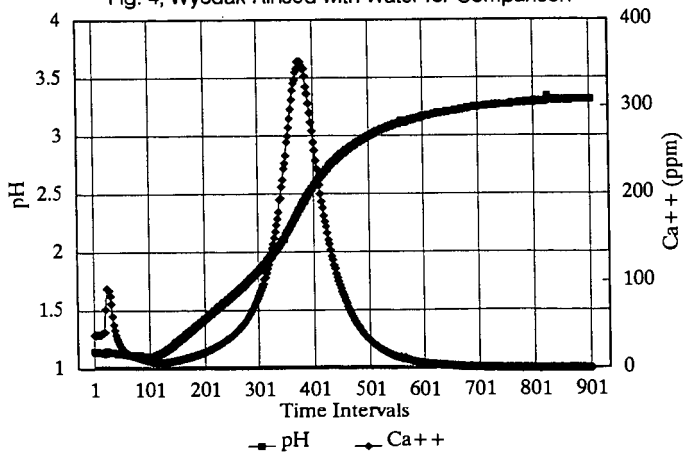

WY521B

DIRECT COAL LIQUEFACTION: A POTENTIAL ROUTE TO THERMALLY STABLE JET FUEL

Caroline E. Burgess and Harold H. Schobert
Fuel Science Program, Department of Materials Science and Engineering
The Pennsylvania State University, University Park, PA 16802

Keywords: coal liquefaction, catalysis, jet fuel

INTRODUCTION

The principal mechanism of fuel degradation at temperatures above 300°C is pyrolytic decomposition. Cycloalkanes are much more resistant to thermal degradation than are *n*-alkanes or alkylaromatics [1]. Indeed, decalin shows remarkable thermal stability even at 450° [1, 2]. Hydroaromatics, such as tetralin, are also quite stable at these temperatures when reacted neat [1, 2] and can suppress the thermal degradation of other compound classes, such as *n*-alkanes, in a process termed hydrogen-transferring pyrolysis [3, 4]. Thus high concentrations of cycloalkanes and hydroaromatics in a real fuel (which of course may contain dozens of components) could provide significant thermal stability.

Direct liquefaction of coal could potentially provide a facile route to liquids boiling in the jet range and containing the desired cycloalkanes and hydroaromatics. The key chemical steps in this process would be the liberation of the aromatic units by cleavage of whatever crosslinks or other interactions hold them in the coal structure, and the hydrogenation of the aromatics to cycloalkanes or hydroaromatics. Clearly, coals showing good reactivity during liquefaction are desirable. To facilitate liberation of the aromatic ring systems, it would be helpful to select coals containing a relatively low population of crosslinks. To minimize downstream processing, it would also be useful to select coals in which a preponderance of the aromatic structures are naphthalene derivatives, to allow direct hydrogenation to decalins and tetralins. Similarly, it would be desirable to have a low content of heteroatoms, also to minimize downstream treatment of the liquids. Not all of these features are available in coals of a given rank. High reactivity and small aromatic units are characteristics of coals at the low end of the rank range. Low crosslink density and relatively low heteroatom content are more likely to be found in the bituminous rank range. Thus the selection of potential feedstocks may involve a compromise to achieve a reasonable balance among these desired characteristics.

We are conducting an exploratory study to test the hypothesis that it is possible to form high yields of cycloalkanes and hydroaromatics boiling in the jet range by selection of feedstocks to contain a high proportion of small aromatic units and relatively few crosslinks; and by choosing catalyst and reaction conditions to liberate the desirable structural features of the coal. In the present paper we report results of reactions of two bituminous coals subjected to temperature-programmed liquefaction, particularly, the effects of coal, solvent, and catalyst on conversion, product slate, and product quality.

EXPERIMENTAL

The coals were obtained from the Penn State Coal Sample Bank and Data Base. The provenance and characteristics of the coals are shown in Table 1. The solvents, catalysts, and reagents used in this work were purchased from commercial vendors and used without further purification.

Liquefaction reactions were conducted in stainless steel microautoclave reactors of nominal 30 mL capacity. Pyrene and 9,10-dihydrophenanthrene (DHP) were used as liquefaction solvents. The reactors were charged with 4 g coal and 4g of the desired solvent. For those reactions in which a catalyst was used, coal was dried and impregnated with ammonium tetrathiomoybdate (ATTM) or $NiCl_2$ as described in previous work [5]. The

reactors were pressurized to 7 MPa with H_2 at ambient temperature. The concept of temperature-programmed liquefaction has been discussed elsewhere [5, 6]. Briefly, the reactor is immersed in a sandbath preheated to 200°C and held for 15 min. The temperature is then ramped to 425° at 7°/min, and is held at 425° for 30 or 60 min. At the end of a reaction, the reactor is quenched by immersion in cold water.

Products were emptied from the tubing bomb into a dry tared thimble using dichloromethane (DCM) and extracted with DCM for about 36-48 h until the extracted solvent appeared clear. The products were then extracted with tetrahydrofuran (THF) for about 24–36 h until the extracted solvent appeared clear. The DCM was rotoevaporated from the DCM-solubles, and then the sample was extracted with hexane. The THF-insoluble portion was rinsed with acetone and pentane and dried at 100°C for 12 h. The THF-soluble fractions were dried for 1 h at 60°C. The hexane-soluble fractions were analyzed by GC/FID and GC/MS. The conditions of the GC used were a rate of 4 °C/min from 40 to 280 °C.

RESULTS AND DISCUSSION

The principal experimental results are summarized in Table 2. The DCM-solubles include gas yields, and gas yields were ≤5% for all reactions. The principal compound classes identified in the hexane-soluble portions of the DCM-soluble products are summarized in Table 3. For convenience, we will occasionally refer to three ratios: a) THF-solubles to the sum of the DCM-solubles expressed as THF/DCM; b) aromatic compounds of one ring to those with two rings or more, (i.e., benzenes + phenols to naphthalenes + phenanthrenes + polynuclear aromatics) expressed as B+P/≥2-ring; and c) the total aromatic compounds to alkanes, expressed as ΣAro/ΣAli.

For reactions without catalyst, conversions to DCM-solubles depend mainly on solvent. For a given solvent, conversions of the two coals are similar. However, DHP is clearly superior to pyrene for increasing conversions. Even though pyrene is well known as a hydrogen shuttler [7], DHP is a potent hydrogen donor [8]. Furthermore, in non-catalytic reactions, most of the hydrogen consumption comes from the solvent rather than gas-phase H_2 [8], so it is not surprising that substantially higher conversions are achieved in DHP. Although the conversions of the two coals in a given solvent are comparable, and the comparative effects of pyrene versus DHP are comparable, the change in product slates with increased conversion is quite different between the two coals. With DECS-6, the increased conversion effected by DHP comes largely via formation of THF-solubles. THF/DCM increases from 0.23 for reaction in pyrene to 0.64 for reaction in DHP. In contrast, THF/DCM is essentially unchanged (and in fact slightly decreases from 0.37 to 0.33) for reactions of DECS-12 in these solvents. DHP reduces the proportion of aromatics with ≥2 rings in the DCP-solubles, and increases the proportion of total aromatics relative to alkanes, relative to results obtained using pyrene. For DECS-6, the B+P/≥2-ring ratio is 0.98 for reaction in pyrene, and 0.73 for reaction in DHP. ΣAro/ΣAli increases from 1.46 to 1.80 for reaction in pyrene and DHP, respectively. The effect of solvent on the B+P/≥2-ring ratio for DECS-12 is quite similar, 1.19 for reaction in pyrene decreasing to 0.83 when DHP is used. A remarkable difference is seen in the ΣAro/ΣAli ratio for DECS-12 relative to DECS-6. For both coals, reaction in DHP increases this ratio relative to reaction in pyrene, but the products from reaction of DECS-12 have so fewer *n*-alkanes that there is an order-of-magnitude difference in the ΣAro/ΣAli ratios. Characterization of these two coals by flash pyrolysis GC/MS has shown the preponderence of *n*-alkanes in DECS-6 relative to DECS-12 [9].

For reactions in pyrene, the addition of catalyst not unexpectedly enhances conversion of both coals. Using either MoS_2 or $NiCl_2$, the conversion of DECS-6 increases by about 30 percentage points (Table 2). Both catalysts increase the conversion in the hydrogen-shuttling solvent pyrene to the same level as obtained by using the strong hydrogen donor solvent DHP without catalyst. However, the two catalysts have quite different effects on the product slate. MoS_2, which could be considered to be a hydrogenation catalyst [10-12], provides a very high yield of light products, THF/DCM being only 0.06. In comparison, $NiCl_2$, a cracking

catalyst [12-13] provides almost the same conversion, but a higher yield of preasphaltenes than attained with MoS_2. Using $NiCl_2$ catalyst, the THF/DCM ratio is about the same as obtained in pyrene but without catalyst, i.e., 0.19 vs. 0.23, respectively. Thus $NiCl_2$ appears to increase the depolymerization of DECS-6, but not to alter the relative proportion of products; in comparison, MoS_2 seems both to increase the depolymerization and shift the product slate toward lighter products.

However, when deductions are drawn based on conversion data, it is important not to lose sight of the fact that these product classifications are based on solubility behavior, which potentially could mask differences in molecular composition. For $NiCl_2$/pyrene reaction of DECS-6, there is a substantial increase in the amount of naphthalenes in the DCM-solubles relative to the MoS_2-catalyzed reaction, which actually decreases the B+P/≥2-ring ratio, from 1.87 for MoS_2 catalysis to 1.32 with $NiCl_2$. With DECS-12, catalytic reaction in pyrene also increases conversion to about the same value as obtained in non-catalytic reaction in DHP. Use of MoS_2 shifts the product slate to lighter products, as occurred with DECS-6, although the effect is not quite so pronounced for DECS-12, THF/DCM decreasing from 0.37 to 0.23. With $NiCl_2$, however, the proportion of preasphaltenes in the product is actually enhanced relative to reaction without catalyst. In this case the effect of $NiCl_2$ catalysis is quite different for the two coals. However, when product composition is examined, a reduction of the B+P/≥2-ring ratio is observed for $NiCl_2$-catalyzed reaction of DECS-12 in pyrene relative to MoS_2, which can, as in the similar case of DECS-6, be attributed to a large increase in naphthalenes and a loss of phenols in the DCM-solubles. It is possible that the reduction of phenols and the concurrent increase in THF/DCM ratio could mean that retrogressive reactions are promoted by the $NiCl_2$ cracking without the stabilization of hydrogen from an H-donor or hydrogenation catalyst.

The effect of reaction time was evaluated only for DECS-6, by comparing reactions with high-temperature holding times of 30 and 60 min for both MoS_2 and $NiCl_2$ in pyrene. Little change was observed in either conversion or product slate. It is unlikely that the slight changes in conversion or product slate observed after 60 min would repay the additional processing costs associated with a doubling of the residence time at 425°.

The combination of the MoS_2 hydrogenation catalyst and DHP donor solvent in reaction of DECS-6 provided the highest conversion observed in the present work, 95%. The product slate was about the same as that obtained for MoS_2 and pyrene, with THF/DCM of 0.06. Liquefaction of DECS-6 in DHP without catalyst actually increased the THF/DCM ratio relative to non-catalytic reaction in pyrene. The catalytic effect of the added MoS_2 thus seems important for shifting the product slate to lighter—on the basis of solubility classifications—products, regardless of whether a hydrogen donor or hydrogen shuttler is used as solvent. Using DHP with $NiCl_2$ produced no increase in conversion relative to that of $NiCl_2$ and pyrene. There is, though, a shifting of the THF/DCM ratio to 0.15, compared with 0.19 for $NiCl_2$/pyrene, and 0.23 for non-catalytic reaction in pyrene. It is noteworthy that the combination of catalyst and donor solvent produces the lowest values of the B+P/≥2-ring ratio observed for this coal, 0.46 for MoS_2-catalysis and 0.53 for $NiCl_2$. Thus 40–43% of the DCM-solubles from DECS-6 for catalytic reaction in DHP are naphthalene derivatives.

For liquefaction of DECS-12 in pyrene, $NiCl_2$ provided higher conversions than MoS_2, 84 vs 77%, respectively. The same superiority of $NiCl_2$ is observed when DHP is used as the solvent, the conversions being 89 and 85%, respectively. For both coals, a change of solvent from pyrene to DHP when MoS_2 is used as the catalyst produces essentially the same effect: an additional 6-8 percentage points of conversion, and a reduction of THF/DCM to 0.06. On the other hand, the change of solvent has different effects for the coals when $NiCl_2$ is used as the catalyst. We discussed the DECS-6 case above; for DECS-12, an increase in conversion and significant shift of THF/DCM is observed when DHP is used instead of pyrene. The combination of a catalyst and donor solvent causes significant reductions in the B+P/≥2-ring ratio, as was seen for DECS-6. Indeed, nearly 50% of the DCM-solubles from MoS_2/DHP reaction of DECS-12 are naphthalene derivatives.

An additional aspect of $NiCl_2$ catalysis is its ability to reduce yields of phenols relative to similar reactions in the presence of MoS_2. For all but one coal/solvent combination, the concentration of phenols in the DCM-solubles is lower for the $NiCl_2$-catalyzed reaction relative to MoS_2, the single exception being DECS-6/DHP. But if there is a reduction in phenols when using $NiCl_2$, and a concurrent increase in THF/DCM, it could be the lost phenols are participating in retrogressive reactions by crosslinking to THF-solubles. Soloman et al. [14] have suggested that functional groups containing oxygen participate in retrogressive reactions. It is also apparent these crosslinking reactions are repressed when a donor solvent or a good hydrogenation catalyst is used.

Attaining the highest conversion with either coal under these reaction conditions clearly requires the presence of the donor solvent in addition to a catalyst. For DECS-6, 95% conversion is achieved for MoS_2/DHP reaction. Any other combination of solvent, catalyst, or both provides conversions in the range 83–89%. For DECS-12, the highest conversion, 89%, was obtained in $NiCl_2$/DHP reaction; the other combinations of solvent and catalyst gave conversions of 77–85%. For either coal and either solvent, the lowest values of THF/DCM are invariably obtained with MoS_2 catalysis. THF/DCM ratios of 0.06 can be achieved for either coal with this catalyst, along with conversions in the 85–95% range. Furthermore, MoS_2/DHP liquefaction produces DCM-solubles that are 40–50% naphthalene derivatives. The subsequent hydrogenation of this product could, in principle, provide a liquid that contains ~50% of the desirable, high-thermal-stability decalins and tetralins.

SUMMARY AND CONCLUSIONS

This paper reports preliminary results of work still in progress. We have so far shown that, with careful selection of the feedstock, it is possible to achieve 85–95% conversions, with THF/DCM ratios <0.1 and 40-50% of the DCM-solubles being naphthalenes. We have not yet attempted to improve these results by optimizing reaction conditions. The DCM-solubles are highly aromatic, with $\Sigma Aro/\Sigma Ali$ approaching 30 for some reactions of DECS-12. It is clear that both a hydrogenation of the product and a hydrodeoxygenation to remove phenols, neither of which is an insignificant operation, still must be investigated. Nevertheless, if these two further transformations can be effected, either by some alteration of reaction strategy such as "reverse temperature staging" [15] or by separate subsequent reactions, the prospect exists for direct conversion of bituminous coals to high yields of liquids containing high concentrations of desirable decalins and tetralins. Such a product could be the foundation of a jet fuel with excellent high-temperature stability characteristics.

ACKNOWLEDGEMENT

The authors are grateful for the financial support for this work provided by the U.S. Department of Energy, the Pittsburgh Energy Technology Center, and the Air Force WL/Aero Propulsion and Power Directorate, Wright-Patterson AFB.

REFERENCES

1. Eser, E., Song, C., Schobert, H., Hatcher, P., Copenhaver, R., Jiang, H., Li, R., Parzynski, M., and Peng, Y. *Advanced Thermally Stable Jet Feuls Deveopment Program Annual Report, Vol. II*, WRDC-TR-90-2079, July 1989 - June 1990.
2. Song, C., Eser, S., Schobert, H.H., Hatcher, P.G., Coleman, M.M., and Walsh, P. *Advanced Thermally Stable Coal-Derived Jet Fuels*, Progress Report, 18-1124-TPR-1, July 1991 - November 1991,
3. Lai, W.C., Song, C., and Schobert, H.H. *Ind. Eng. Chem.* 1993 (submitted).
4. Song, C., Lai, W-C., and Schobert, H.H. *American Chemical Society, Division of Fuel Chemistry, Preprints*, **37** (4), 1655, 1992.
5. Huang, L., Song, C., and Schobert, H.H. *American Chemical Society, Division of Fuel Chemistry, Preprints*, **37** (1), 223, 1992.
6. Song, C., Schobert, H.H., and Hatcher, P.G. *Energy & Fuels*, **6**, 326, 1992.
7. Derbyshire, F.J. and Whitehurst, D.D. *Fuel*, **60**, 655, 1981.
8. Artok, L. and Schobert, H.H. *Fuel Proc. Tech.*, 1993, accepted.
9. Burgess, C., Wenzel, K., Song, C., Hatcher, P., and Schobert, H.H. Proceedings of the 7th International Conference on Coal Science, September, 1993.
10. Weller, S.W. in *Proceedings of the Fourth International Conference on the Chemistry and Uses of Molybdenum*, Eds. H.F. Barry and P.C.H. Mitchell, Climax Molybdenum Co., Ann Arbor, MI, 179, 1982.
11. Naumann, A.W., Behan, A.S., and Thorsteinson, E.M. n *Proceedings of the Fourth International Conference on the Chemistry and Uses of Molybdenum*, Eds. H.F. Barry and P.C.H. Mitchell, Climax Molybdenum Co., Ann Arbor, MI, 313 1982.
12. Derbyshire, F.J. "Catalysis in Coal Liquefaction," IEA CR/08, IEA Coal Research, London, 1988.
13. March, J. *Advanced Organic Chemistry: Reactions, Mechanisms, and Structure, 2nd Edition*, McGraw-Hill, Inc. New York, 1977.
14. Dutta, R. and Schobert, H.H. *American Chemical Society, Division of Fuel Chemistry, Preprints*, this volume, 1993.
15. Solomon, P.R., Serio, M.A., Deshpande, G.V., Kroo, E., Schobert, H.H., and Burgess, C. in *Coal Science II*. Eds. H.H. Schobert, K.D. Bartle, and L.J. Lynch. **ACS Symposium Series No. 461**, American Chemical Society, Washington, D.C., 1991, p 193.

Table 1: Properties of coals.

Coal Number	DECS-6	DECS-12
Seam, State	Blind Canyon	Pittsburgh #8, PA
Rank	hvA b	hvA b
%C	81.72	84.75
%O	10.10	7.37
%H	6.22	5.66
%S	0.40	0.83
%N	1.56	1.40
%Mineral Matter	6.67	11.88
H/C	0.905	0.794

Table 2: Liquefaction conversion data for DECS-6 and DECS-12.

Expt #	Temp	Catalyst	Solvent	TC	THF-Sol	DCM-Sol	THF/DCM
tb 6-8	TPL, 425-30	none	pyrene	55.2	10.5	44.7	0.235
tb 6-9	TPL, 425-30	none	DHP	83.0	32.5	50.5	0.644
tb 6-3	TPL, 425-30	MoS_2	pyrene	89.3	5.1	84.2	0.061
tb 6-4a	TPL, 425-30	$NiCl_2$	pyrene	83.0	13.1	69.9	0.187
tb 6-10	TPL, 425-30	MoS_2	DHP	95.0	5.7	89.3	0.064
tb 6-11	TPL, 425-30	$NiCl_2$	DHP	83.2	11.0	72.2	0.152
tb 6-6	TPL, 425-60	MoS_2	pyrene	88.2	3.6	84.6	0.043
tb 6-7	TPL, 425-60	$NiCl_2$	pyrene	87.3	12.7	74.6	0.170
tb 12-5	TPL, 425-30	none	pyrene	51.9	14.0	37.9	0.369
tb 12-6	TPL, 425-30	none	DHP	81.7	20.1	61.6	0.326
tb 12-3	TPL, 425-30	MoS_2	pyrene	76.8	14.5	62.3	0.233
tb 12-4	TPL, 425-30	$NiCl_2$	pyrene	84.2	28.3	55.9	0.506
tb 12-7	TPL, 425-30	MoS_2	DHP	85.4	5.1	80.3	0.064
tb 12-8	TPL, 425-30	$NiCl_2$	DHP	88.7	13.1	75.6	0.173

TC = total conversion
DCM-Sol = DCM-Solubles + Gas Yield
THF/DCM = ratio of THF-Solubles to DCM-Solubles

Table 3: Percent area of major compounds in GC of hexane-solubles.

Expts	Benzenes	Phenols	2-Ring	3-Ring	4-Ring +	Alkanes	B+P/2-Ring	ΣAro/ΣAli
tb 6-8	3.7	25.6	27.7	2.3	0.0	40.6	0.98	1.46
tb 6-9	8.9	18.2	35.4	n.d.	1.8	35.8	0.73	1.80
tb 6-3	14.6	30.6	21.0	3.2	0.0	30.5	1.87	2.28
tb 6-4	19.2	25.8	29.4	3.8	0.9	21.0	1.32	3.77
tb 6-10	0.5	19.4	40.5	n.d.	3.1	36.6	0.46	1.73
tb 6-11	2.6	20.5	43.4	n.d.	0.0	33.4	0.53	1.99
tb 6-6	2.7	44.7	22.8	3.9	2.9	23.0	1.60	3.35
tb 6-7	8.6	29.5	34.5	3.9	0.0	23.5	0.99	3.26
tb 12-5	8.3	41.8	20.7	20.8	0.6	7.8	1.19	11.8
tb 12-6	15.4	28.3	46.7	n.d.	6.2	3.3	0.83	29.3
tb 12-3	5.0	46.4	29.2	2.2	4.5	12.8	1.43	6.82
tb 12-4	6.3	32.2	38.6	6.6	4.4	11.9	0.78	7.40
tb 12-7	2.4	30.1	48.1	n.d.	10.4	9.1	0.56	10.0
tb12-8	2.6	23.4	39.5	n.d.	31.1	3.4	0.37	28.4

2-Ring = alkylated aromatics and hydroaromatics composed of two rings
3-Ring = alkylated aromatics and hydroaromatics composed of three rings
4-Ring = alkylated aromatics and hydroaromatics composed of four rings and other polynuclear aromatics
n.d. = not determined
B+P/≥2-Ring = Benzenes + Phenols/2-Ring + 3-Ring + 4-Ring+
ΣAro/ΣAli = Total Aromatics/ Total Alkanes

UPGRADING OF DISTILLATE PRODUCTS FROM COAL LIQUEFACTION AND COAL/BITUMEN COPROCESSING

Michael F. Wilson
CANMET, Energy Research Laboratories, Energy, Mines and Resources Canada
555 Booth Street, Ottawa, Ontario K1A 0G1

Key words: hydrotreating, coal liquefaction, coprocessing

INTRODUCTION

Upgrading of heavy coal liquids involves first-stage hydrotreating with the objective of removing heteroatomic species, particularly nitrogen, which can be a serious poison for catalysts in second-stage hydrocracking or FCC. Hydrotreating also achieves molecular weight reduction and increases the hydrogen content of the coal liquid prior to cracking to lighter products suitable for use as transportation fuels.

A major problem in coal liquids upgrading is deactivation of hydrotreating catalysts through fouling of the catalyst surface. Deactivation has been attributed to the strong adsorption of certain feedstock nitrogen and oxygen containing components at acidic catalyst sites, as well as fouling by asphaltenic materials and polynuclear aromatic hydrocarbons. The adsorbed species are believed to act as precursors for the formation of carbonaceous deposits which result in loss of surface area and plugging of catalyst pores. These aspects of coal liquids upgrading have been adequately reviewed by Derbyshire (1). Previous work was undertaken by Chevron Research Company, notably Sullivan and Frumkin (2,3), who identified feedstock properties which were found to most influence the ease of upgrading: boiling point distribution, distillation end-point, heteroatom content and hydrogen content.

The objectives of this work were to undertake experimental hydrotreating of two gas oil feedstocks derived respectively from liquefaction of coal and coprocessing coal/bitumen. The purpose was to compare the upgradeability of the coal derived liquids for use as transportation fuels and to identify solutions to the problem of catalyst fouling and deactivation.

EXPERIMENTAL

The feedstocks used in the program were: Nedol process spent donor solvent, supplied by Sumitomo Metal Mining Co. Ltd., Ichikawa, Japan, and a CANMET coal/bitumen coprocessed heavy gas oil fraction. The latter feedstock was derived from coprocessing 70% Cold Lake bitumen and 30% Forestburg coal. The feedstocks represent two different sources and processing technologies for production of transportation fuels from coal. In both cases the materials require extensive upgrading to produce distillates which meet the required specifications as liquid fuels. The boiling range of both feedstocks was between 200°C-550°C. Approximately 2 wt % of the Nedol process spent donor solvent boiled above 525°C, and the amounts of asphaltenes and preasphaltenes were found to be 4.15 wt % and 0.86 wt % respectively. For the coprocessed gas oil, the +525°C fraction was 1.4 wt % and asphaltenes and preasphaltenes were 1.68 wt % and 0.11 wt %. Since the sulphur content of the spent donor solvent feedstock was low, 3 wt % butanethiol was added to maintain MoS_2 based catalyst activity during screening, following the procedure of Inoue et al. (4).

An automated microreactor unit was used to hydrotreat the coal liquid feedstocks and study the effects of catalyst deactivation. Time on stream catalyst deactivation runs were carried out to establish the extent of fouling by problematical feedstock components. A fixed bed stainless steel tubular reactor, 0.305 m long, 0.635 cm I.D., was operated in the continuous upflow mode. The catalyst bed was 0.14 m long and of volume 4.50 cm^3. The catalyst was presulphided in situ with a mixture of 10% H_2S

in H_2. Operating conditions for carrying out the catalyst deactivation experiments were: temperature 380°C, hydrogen pressure 10.3 MPa (1500 psig), LHSV 1.00, and hydrogen flowrate 1000 L H_2/L liquid feed (5500 scf/bbl).

Hydrotreating experiments were also carried out using a Robinson-Mahoney gradientless stirred tank reactor (5) to determine conversion of heteroatoms and aromatics in coprocessed liquid. The reactor is a continuous flow unit equipped with an annular catalyst basket and internal recycle impeller. The internal reactor volume was approximately 50 cm^3 and the catalyst bed 6.0 cm^3. The catalyst was first presulphided using a mixture of 3 wt % butanethiol in diesel fuel and was then de-edged for three days (72 h) using the same feedstock. De-edging conditions were: temperature 380°C, hydrogen pressure 10.3 MPa (1500 psig), WHSV 0.75 and gas flowrate 1000 mL H_2/mL liquid feed. The coprocessed heavy gas oil was introduced into the reactor and the internal recycle impeller rate was set at 2500 rpm. For each of the catalysts tested, the operating temperatures were 300°C, 340°C, 360°C and 380°C at WHSV 0.75. Three Ni-Mo catalysts were used: AKZO KF-153S, CANMET CER 20 and CANMET CER 24. The physical properties of the catalysts are presented in Table 1.

RESULTS AND DISCUSSION

Feedstock Properties

Figure 1 compares the heteroatom and aromatic content of the two feedstocks. The coprocessed liquid had a significantly lower aromaticity, i.e., f_a = 0.40 compared with 0.58 for the spent donor solvent. There was also a large difference in elemental sulphur. Coprocessed gas oil had a very high sulphur content, i.e., 2.29 wt %, compared with 0.069 wt % for the spent donor solvent. The amounts of elemental nitrogen were about the same, but the coprocessed material had a somewhat lower oxygen content, i.e., 0.80 wt % compared with 1.60 wt % for the Nedol coal liquid. Further characteristics of coprocessed products are given by Rahimi et al. (6).

Catalyst Deactivation Runs For Hydrotreating Coal Liquids - Nitrogen Conversion (Effect of time on Stream)

Commercial catalyst AKZO KF-153S was used to hydrotreat the coal derived liquids at the prescribed operating conditions for between 200-300 h time on stream. Since sulphur was added to the spent donor solvent and oxygen content was difficult to analyze, the two parameters monitored were nitrogen and aromatics conversion. The catalyst was de-edged using the coal derived liquid feedstocks over 80 h time on stream. Plots of per cent nitrogen conversion versus catalyst time on stream are presented in Fig. 3. For both feedstocks the nitrogen conversion declined during the initial 80 h period. The commercial catalyst continued to show a steady decline in activity for the spent Nedol process donor solvent up to 200 h. For this feedstock the catalyst initially demonstrated a nitrogen conversion of greater than 80%. The effect of time on stream on nitrogen conversion in the coprocessed liquid, also plotted in Fig. 3, shows an interesting phenomenon which is observed over the first 200 h. The nitrogen conversion appears to decline during the first 80 h of the experimental run, but then recovers and rises to a maximum at approximately 130 h. Thereafter the catalyst activity appears to stabilize. An examination of this phenomenon suggests that during hydrotreating there is a transition from one type of catalytic site to another. Thus, at first, deactivation of active sites appears to occur, then in situ regeneration of the catalyst appears to take place. This may be the result of accumulation of H_2S in the reactor over the first 80 h, leading to regeneration of the catalyst. For the coprocessed gas oil, between 200-300 h time on stream, the activity of the AKZO catalyst appears to decline slowly.

Aromatics Conversion (Effect of Time on Stream)

The other indicator of catalyst deactivation relates to hydrogenation of aromatic type ring structures in the feedstocks. The fraction of aromatics, f_a, in the feed and products was determined by ^{13}C NMR. Figure 4 plots f_a versus time on stream for hydrogenation of the feedstocks over the commercial

catalyst. For Nedol process spent donor solvent, the catalyst showed a steady rate of deactivation over 200 h. In the case of coprocessed gas oil, the AKZO catalyst showed good hydrogenation activity with some scatter of experimental data but little deactivation. It is important to note that the cyclical deactivation/regeneration phenomenon shown in Fig. 3 for the HDN reaction was not observed in this case. This suggests that different catalytic sites are involved for the hydrogenation reactions and these were unaffected throughout the experimental run.

Determination of Heteroatom and Aromatics Conversion in Coprocessed Gas Oil Using a Gradientless Reactor

To determine meaningful conversion data for hydrotreating the coprocessed heavy gas oil feedstock, experimental runs were carried out using the gradientless stirred tank reactor (5). An insufficient amount of Nedol process spent donor solvent was available, therefore it was not possible to carry out corresponding determinations on that material. Because the gradientless reactor permits determinations under isothermal conditions with uniform reactant concentrations, it provides a means of accumulating reliable feedstock conversion data. Hydrotreating catalysts used were the high surface area commercial catalyst AKZO KF-153S and CANMET catalysts CER 20 and CER 24 for aromatics and heteroatom conversion respectively (see Table 1).

Determination of Nitrogen and Sulphur Conversion in Coprocessed Heavy Gas Oil

Figure 5(i) presents plots of per cent nitrogen conversion in coprocessed gas oil versus reaction temperature over catalysts AKZO KF-153S and CER 24. Both catalysts had high surface areas and reasonably good agreement is observed for nitrogen removal. At the maximum operating temperature, 380°C, the nitrogen conversion was approximately 80%. Plots of per cent sulphur conversion for the coprocessed gas oil versus reaction temperature are presented in Fig.5 (ii). Again, high conversions (approximately 94%) were obtained at the maximum operating temperature. It is also shown that, at low sulphur conversions, a significant difference in conversion was found for the two catalysts tested. It is apparent from the general trends of the two curves plotted, that catalyst AKZO KF-153S had a higher chemical reaction rate at the lower temperatures. However, as the temperature is increased to the maximum, the two plots are seen to converge to a single point. This phenomenon is attributed to the HDS reaction being diffusion controlled at the higher temperatures. Catalyst AKZO KF-153S has a significantly higher surface area and pore volume than CER 24. However, this advantage is lost when the rate of diffusion of sulphur containing molecules into the catalyst pores becomes rate determining and it is observed that the sulphur conversion became the same for both catalysts.

Determination of Aromatics Conversion in Coprocessed Gas Oil

Input of additional hydrogen into the coprocessed liquid should facilitate second-stage upgrading to naphtha and middle distillates by improving product quality and reducing the amount of coke formed on cracking catalysts. Plots of per cent conversion of coprocessed gas oil aromatic carbon (^{13}C NMR) over catalysts AKZO KF-153S and CER 20 versus reaction temperature are presented in Fig. 5(iii). Again, the curvature and convergence of the two plots indicates that aromatics hydrogenation over the Ni-Mo catalysts became diffusion controlled at the higher operating temperatures. These diffusion control effects in coprocessed gas oil were also confirmed by constructing Arrhenius plots for the hydrotreating reactions. As expected, the plots showed curvature in the high temperature region.

CONCLUSIONS

Time on stream hydrotreating runs showed that an overall higher rate of catalyst deactivation occurred during upgrading of the product from coal liquefaction. The limited amount of deactivation shown by the coprocessed liquid is considered acceptable for commercial operations. However, it was also shown that, at the higher operating temperatures, reactions were diffusion controlled.

Figure 2 compares final properties of hydrotreated products in terms of heteroatom and aromatics

content. It is shown that the regenerated Nedol process donor solvent had a significantly higher aromatic content (46.0%) than the corresponding coprocessed liquid product (25.0%). This difference is also reflected in the product atomic H/C ratios which were 1.32 and 1.69 respectively. Concerning nitrogen content, which is a key performance indicator for hydrocracking operations, both coal liquid products had about the same concentration, i.e, 1000-1200 ppm. No final measurements of elemental oxygen content were made, but experience has shown that oxygen is easier to convert. Similarly, Fig. 2 shows that sulphur conversion is not a problem. In summary, since hydrocracking operations usually require a final product nitrogen specification of approximately 10 ppm, and further hydrotreating was shown to consume excessive amounts of hydrogen, problems are anticipated in meeting the hydrocracking specification for both feedstocks. It is therefore concluded that fluid catalytic cracking is a better option than hydrocracking for converting coal derived and coprocessed heavy gas oils to lighter products.

ACKNOWLEDGEMENTS

The author wishes to acknowledge the contributions of personnel from CANMET Catalytic Processing Section, the Fuels Characterization Research Laboratory, and financial support from Sumitomo Metal Mining Co.Ltd. and the Federal Panel on Energy Research and Development.

REFERENCES

1. Derbyshire, F.J. "Catalysis in coal liquefaction: new directions for research", IEA Coal Research, London, England, June 1988.
2. Sullivan, R.F. American Chemical Society, Division of Fuel Chemistry, Preprints 31(4):280-293, September, 1986.
3. Sullivan, R.F. and Frumkin, H.A. American Chemical Society, Division of Fuel Chemistry, Preprints 31(2):325-339, September, 1986.
4. Inoue, Y., Kawamoto, K., Mitarai, Y., Takami, Y. Kurachi, K. and Hayakawa, K. Proceedings International Conference on Coal Science, 193, 1985.
5. Mahoney, J.A., Robinson, K.K. and Myers, E.C. Chemtech 758, December, 1978.
6. Rahimi, P.M., Fouda, S.A., Kelly, J.F., Malhotra, R. and McMillen, D.F. Fuel, 68, 422, 1989.

Table 1 - Physical Properties of Ni-Mo Hydrotreating Catalysts

Catalyst	Surface area (m^2/g)	Pore volume (cm^3/g)
AKZO KF-153S	286	0.43
CANMET CER 20	166	0.21
CANMET CER 24	230	0.34

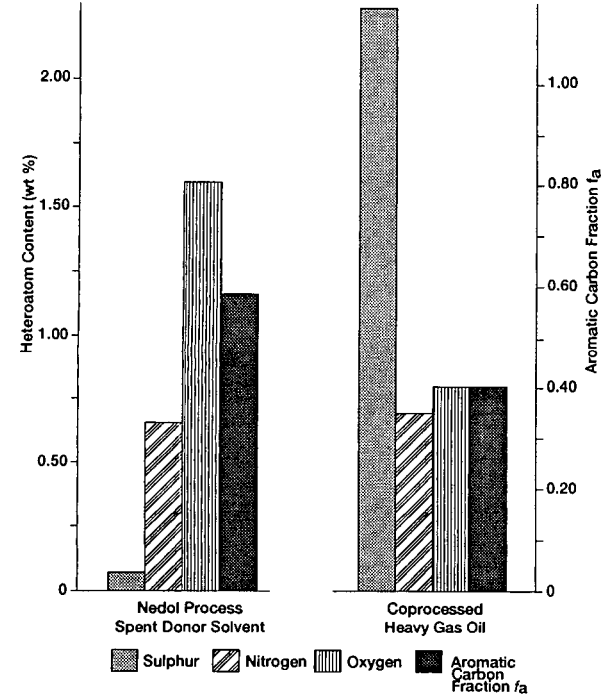

Figure 1 - Heteroatom and Aromatic Content of Coal Derived and Coprocessed Liquid Feedstocks

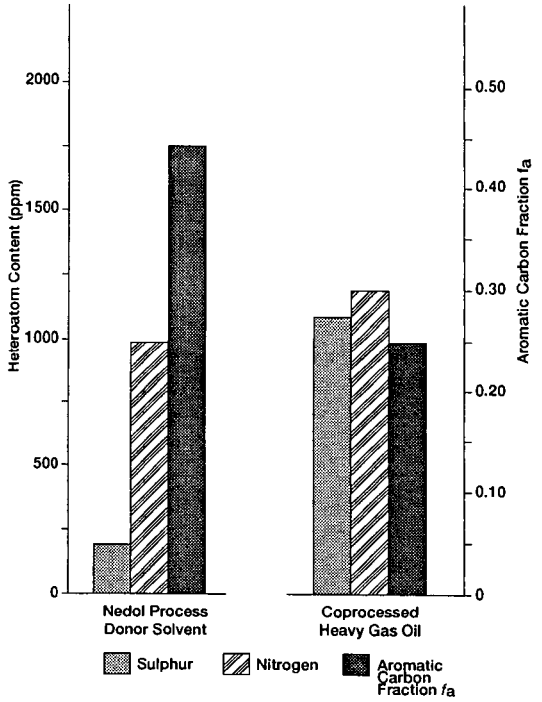

Figure 2 - Heteroatom and Aromatic Content of Hydrotreated Products

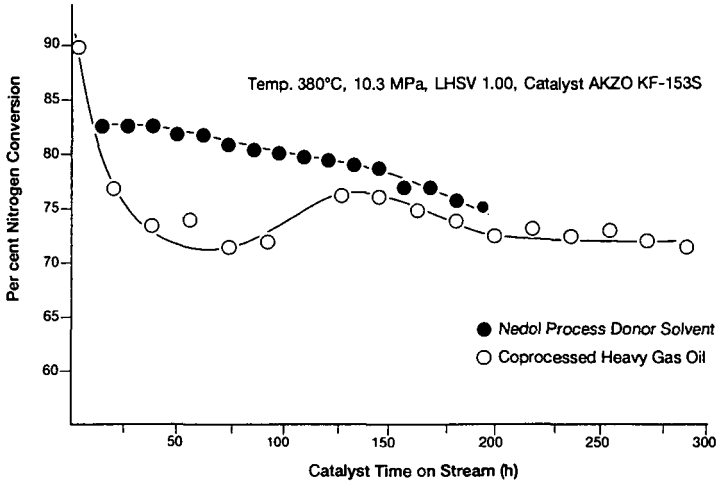

Figure 3 - Nitrogen Conversion in Hydrotreated Products as a Function of Time on Stream

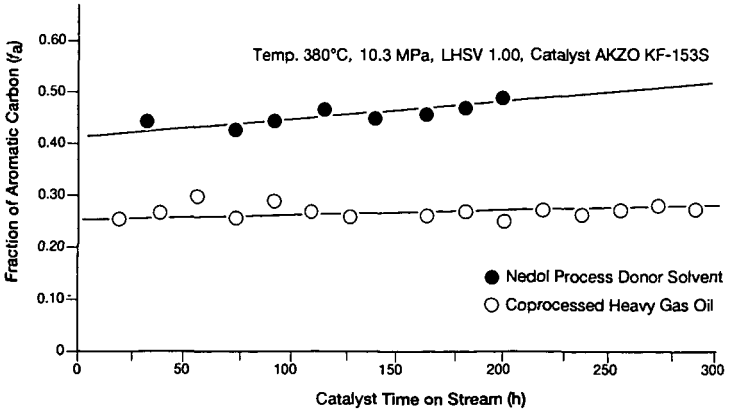

Figure 4 - Hydrotreated Product Aromacity as a Function of Time on Stream

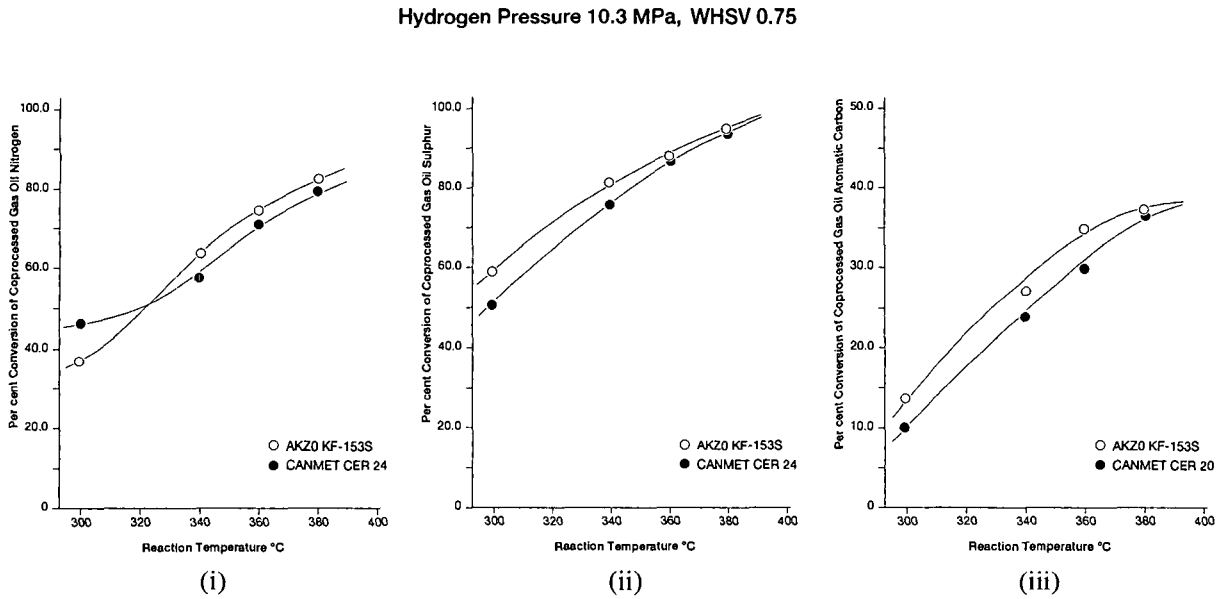

Figure 5 - Effect of Temperature on Conversion of Coprocessed Gas Oil Nitrogen, Sulphur and Aromatic Carbon over Ni-Mo Catalysts Using a Gradientless Reactor

CATALYTIC HYDROTREATMENT OF COAL-DERIVED NAPHTHA USING FIRST ROW TRANSITION METAL SULFIDES

Shuh-Jeng Liaw, Ajoy Raje and Burtron H. Davis

Center for Applied Energy Research
University of Kentucky
3572 Iron Works Pike
Lexington, KY 40511-8433

Keywords: Coal-derived Naphtha, Catalytic Hydrotreatment

ABSTRACT

This study is designed to define the possibility of increasing the rate of heteroatom removal from coal-derived naphtha by an order of magnitude greater than the current hydrodesulfurization catalysts. For the unsupported first row transition metal sulfide catalysts, maxima HDS activity is obtained for chromium sulfide and the minimum HDS activity is obtained for manganese sulfide. This is similar to the results presented by Chianelli et al. for hydrodesulfurization of dibenzothiophene. The maximum HDN activity is obtained for chromium sulfide and the minimum HDN activity is obtained for cobalt sulfide. The effect of substituents on the conversion of nitrogen compounds in the naphtha varied. The HDN of alkyl-substituted pyridine and aniline is dominated by an electronic, rather than a steric, effect. The effect of alkyl-substitution on the reactivity of quinoline is relatively small.

INTRODUCTION

Exxon workers(1) showed that some metal sulfides of the second and third row transition metals were more than 10 times as active as MoS_2 for the hydrodesulfurization of dibenzothiophene. Our study is designed to define the possibility of increasing the rate of heteroatom removal by an order of magnitude over the rate attainable with current Co-Mo-alumina or Ni-Mo-alumina catalysts. It is also designed to define whether heteroatom removal has a common rate for all compounds in each heteroatom class or whether some heteroatom compounds are especially difficult to convert. To characterize a catalyst in terms of its selectivity for individual heteroatom removal reactions for individual compounds in a coal-derived naphtha, methods to determine the amount of each sulfur and nitrogen compounds present in the feed and hydrotreated naphtha is needed. Recently instrumentation with the potential to sample directly from a flame ionization detector to determine the amount of sulfur present in the effluent from a capillary gas chromatograph has become available. Likewise, a nitrogen sensitive GC detector can be utilized for a quantitative determination of individual nitrogen compounds. Thus, the naphtha can be analyzed for composition using a high resolution capillary column gas chromatography.

EXPERIMENTAL

Hydrotreatment of the Ill. # 6 naphtha sample was carried out using the first row unsupport transition metal sulfides at temperatures of 350 and 400°C. The temperature was varied while holding constant the total pressure (660 psig) and weight hourly space velocity (WHSV = 1 g of feedstock / g of catalyst / hour). For each experiment, 3 grams of the row 1 unsupported transition sulfide was used.

Individual nitrogen compounds of the hydrotreated Ill. #6 naphtha were analyzed using a Thermionic Specific Detector (TSD) coupled with an Varian 3700 gas chromatograph containing a carbowax column. Sulfur compounds were analyzed using a Sievers Model 350B Chemiluminescence Sulfur Detector (CSD) coupled with an HP 5890 Series II gas chromatograph containing a SPB-1 column. Identification of the nitrogen and sulfur compounds was accomplished by comparison of the retention time to a standard compound.

RESULTS

The conditions and results for the preparation of the transition metal sulfides are given in Table 1. Transition metal sulfides with intermediate to high surface areas were obtained; these are comparable to the earlier Exxon work. The nitrogen and sulfur content of products and the % HDN and % HDS are shown in Table 2. These catalysts do not exhibit an especially high activity for the removal of sulfur and nitrogen, compared to Ni-Mo-alumina and Co-Mo-alumina catalysts.

For the HDS reaction, the maximum % HDS activity, based on three grams of catalyst, is obtained for chromium sulfide (Figure 1). Increasing the temperature from 350°C to 400°C results an increase of approximately 25 % for sulfur removal. Chianelli et al.(1) reported that chromium sulfide has the highest activity for HDS of dibenzothiophene and manganese sulfide has the lowest activity for the first row transition metals.

The % HDN based on catalyst weight is approximately the same for all of the catalysts, about 40 % (Figure 2). Increasing the temperature from 350 to 400°C results an increase of approximately 10 % for nitrogen removal.

A comparison of the % HDN vs % HDS based on catalyst weight shows that sulfur removal varies while nitrogen removal remains nearly constant (~40%) (Figure 3).

Conversion of Individual Nitrogen Compounds:

The conversion of individual nitrogen compounds was studied at 350°C, 660 psig and a weight hourly space velocity of 1 g/g/hr.

Pyridines

Figure 4 shows the results, as a typical example, for the conversion of compounds in the pyridine class using an iron sulfide catalyst. For this class, pyridine is the easiest compound to convert for all of the catalysts. The rate of conversion of pyridine substituted by a methyl or ethyl group decreases in the order: unsubstituted > 4- > 2- > 3- for all catalysts. Similar results were observed for the commercial Co-Mo-Alumina and Ni-W-Alumina catalysts. Pyridines with substituents of 2 or more carbons are harder to convert than pyridine with a one carbon substituent.

Anilines

The conversion of compounds in the aniline class, using iron sulfide (Figure 5), as a typical example, shows that unsubstituted aniline is the easiest compound to convert; this is analogous to the pyridine class where the unsubstituted compound is easier to convert. For all catalysts, anilines substituted with 2 to 4 carbons are harder to convert than anilines with only a one carbon substituent. These figures also show that the conversion of nitrogen compounds depends on the position the group(s) substituted on the ring. The rate of conversion for the mono-methyl or mono-ethyl substituted anilines are: unsubstituted > 4- ≈ 2- > 3-. This is the case for all catalysts. However, the conversion of mono-methyl and mono-ethyl aniline is not as dependent on substituents or their ring position as the pyridines were.

Quinolines

Figure 6 shows results of the conversion of compounds in the quinoline class using iron sulfide as a typical example. The data show that quinoline is harder to convert than the pyridines were. Unsubstituted quinoline, is converted at about the same rate as one carbon alkyl substituted quinoline with the all catalysts.

DISCUSSION

In general, hydrotreatment of the heavy fractions of coal derived materials is complicated by the molecular weight, and the corresponding large size, of the molecules converted. The large size introduces severe diffusional problems during processing. However, this is not a problem in the hydrotreatment of coal derived naphtha, since the dominant fraction of the material contains only one ring of five or six carbons; two ring components are the largest molecules that will be encountered and these represent only approximately 10 % of the nitrogen compounds and approximately 24 % of the sulfur compounds. Thus, diffusion limitations due to size exclusion should not be a problem in this study.

Alkyl-sustituted heterocyclic compounds were found in the Illinois #6 naphtha. The position of the substituent influences the rate of HDN. For the first row unsupported transition metal catalysts, HDN reactivities of pyridine, aniline and quinoline varies according to the position of substituent added as follows:

pyridine > 4-R-pyridine > 2-R-pyridine > 3-R-pyridine,
Aniline > 4-R-Aniline ≈ 2-R-Aniline > 3-R-Aniline, and
Quinoline ≈ 3-Methyl-Quinoline ≈ 4-Methyl-quinoline,
where R = methyl or ethyl group. 2-Methylquinoline is present in the naphtha in such small quantities that its conversion could not be followed.

Many publications(2-5) have reported that steric and electronic effects may play an important role for the HDS of a number of sulfur compounds. From the point view of steric hindrance by a substituent group, the order of reaction rates for HDN should be 4 > 3 > 2. However, from the point view of electronic effect, the rates should be 4 ≈ 2 > 3. HDN of alkyl-substituted anilines and pyridines show the order expected for an electronic effect. The effect of alkyl substituents on the reactivity of quinoline is relatively insignificat. Gates et. al.(5) reported that HDN conversion of 2,6-, 2,7-, and 2,8-dimethylquinoline is approximatly the same as that of quinoline.

ACKNOWLEDGMENT

This work was supported by the DOE contract #DE-AC22-90PC91058 and the Commonwealth of Kentucky. The authors also thank the personnel at the Wilson liquefaction facility for providing the naphtha samples.

REFERENCES

1. T.A. Pecoraro and R. R. Chianelli, J. Catal., 67, 430(1981).
2. B. C. Gates, J. R. Katzer, and G. C. A. Schuit, "Chemistry of Catalytic Processes," McGraw-Hill, New York, 1979.
3. M. Houalla, D. H. Broderick, A. V. Sapre, N. K. Nag, V. H. J. Beer, B. C. Gates, and H. J. Kwart, J. of Catal., 61, 523(1980).
4. J. H. Singhal, R. L. Espino, and J. E. Sobel, J. Catal., 67, 446(1981).
5. B. C. Gates, J. R. Katzer, J. H. Olson, H. Kwart, and A. B. Stiles, Quarterly Report to DOE, June 21 to September 20, 1978.

Table 1

Row 1 Transition Sulfide Preparation Conditions and Results

	Ti	V	Cr	Mn	Fe	Co	Ni
Metal	20g	20g	25g	25g	25g	30g	25g
Chloride	$TiCl_4$	VCl_4	$CrCl_3$	$MnCl_3$	$FeCl_3$	$CoCl_2$	$NiCl_2$
Li_2S	9.70g	9.53g	10.88g	10.68g	10.83g	5.79g	8.86g
EA, mL	None	None	None	800	800	800	800
THF, mL	800	800	800	None	None	None	None
S_g, m^2/g	4.4	25.82	13.02	1.7	10.18	9.34	1.99

EA = Ethyl Acetate
THF = Tetrahydrofuran
S_g = Surface Area

Table 2

Nitrogen and Sulfur Content of Products from the Hydrotreatment of Illinois #6 Naphtha

Temp. °C	Pressure, psig	Catalyst	Nitrogen, Wt. ppm	Sulfur, Wt. ppm	Nitrogen % HDN	Sulfur % HDS
350	660	VS_x	1030	370	36.6	52.8
350	660	CrS_x	996	385	38.7	50.9
350	660	MnS_x	1058	465	36.4	40.7
350	660	FeS_x	1049	393	36.9	49.9
350	660	CoS_x	1113	301	33.1	61.6
350	660	$Ni2_N$	977	446	39.8	43.1
400	660	VS_x	958	223	41.0	71.6
400	660	CrS_x	953	237	41.3	69.8
400	660	MnS_x	995	385	38.7	50.9
400	660	FeS_x	1047	288	37.0	63.3
400	660	CoS_x	1103	220	33.7	71.9
400	660	$Ni2_N$	970	376	40.3	52.0

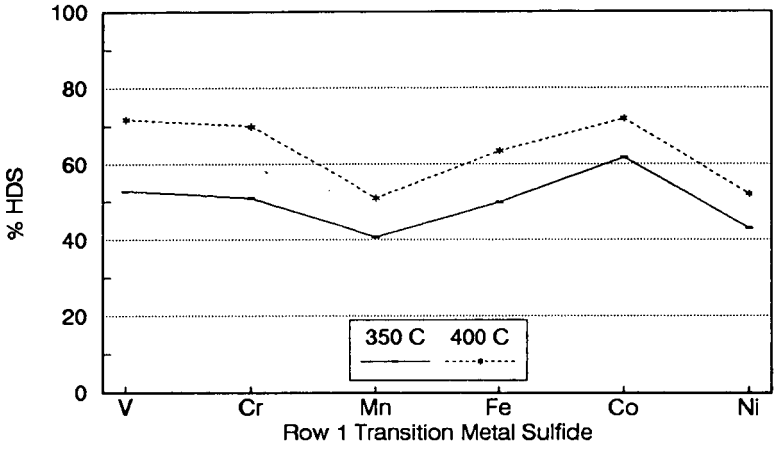

Figure 1. HDS of Illinois #6 Naphtha

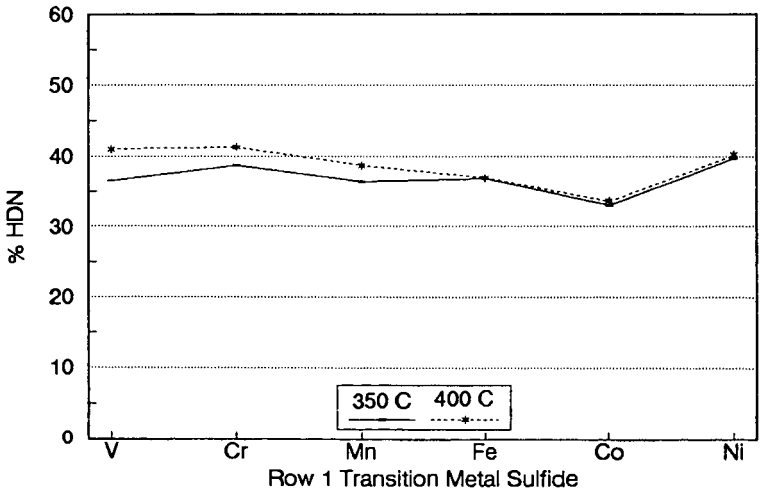

Figure 2. HDN of Illinois #6 Naphtha

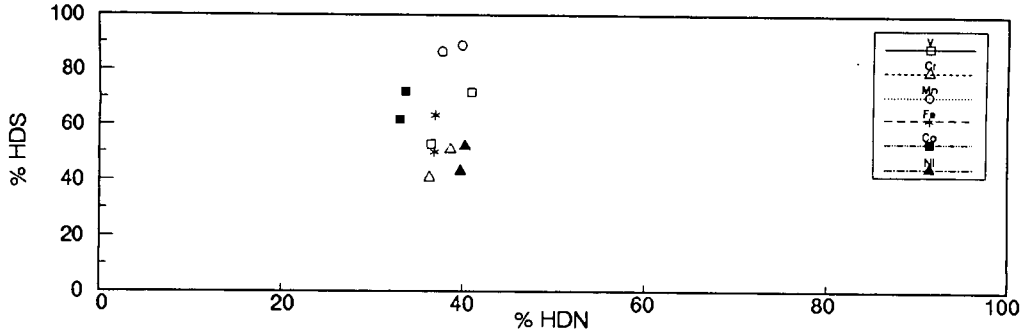

Figure 3. HDS vs HDN

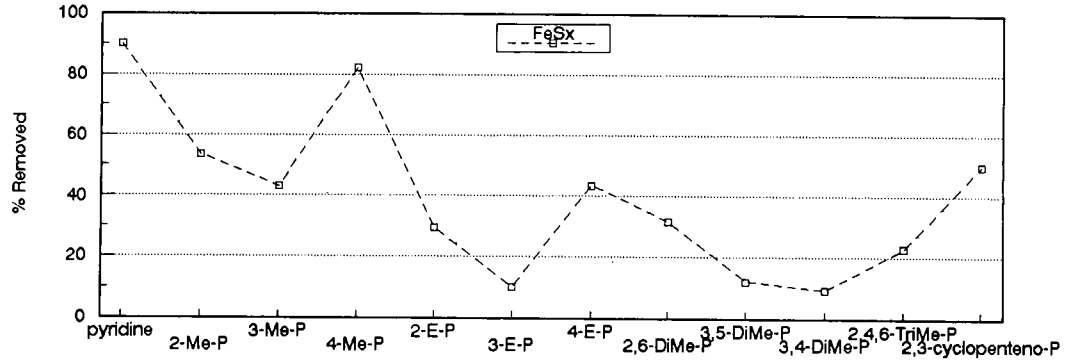

Figure 4. Converted of Pyridine Compounds

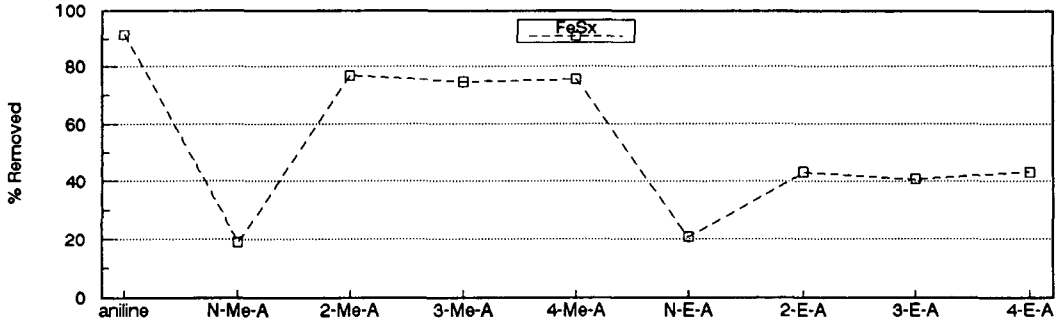

Figure 5. Conversion of Aniline Compounds

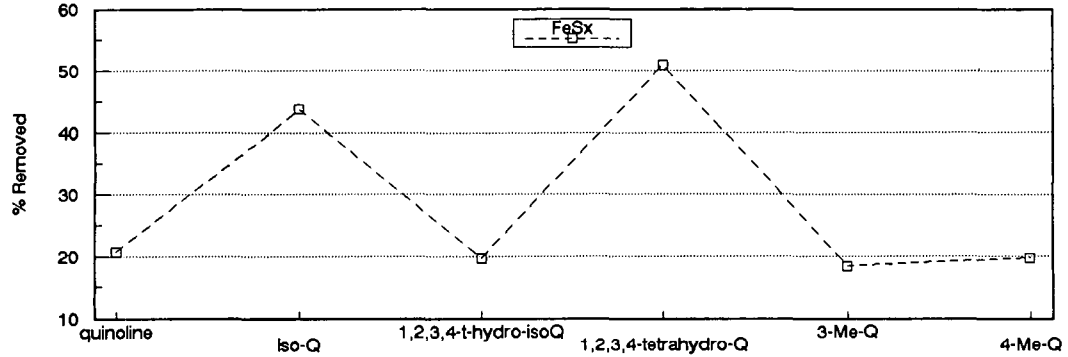

Figure 6. Conversion of Quinoline Compounds

CATALYTIC MULTISTAGE LIQUEFACTION OF BLACK THUNDER MINE COAL USING BOTH SUPPORTED AND SLURRY CATALYSTS.

R. H. Stalzer, A. G. Comolli, L. K. Lee, V. Pradhan
Hydrocarbon Research Inc.
100 Overlook Center, Suite 400
Princeton, NJ 08540

KEYWORDS: Coal Liquefaction, Molybdenum, Iron Impregnated Coal

ABSTRACT

Catalyst cost has a significant impact on the economics of direct coal liquefaction. The catalyst cost is determined by its activity and deactivation. The use of an active slurry catalyst in low concentration, which gives equivalent performance to supported catalyst systems, would be potentially attractive. A slurried molybdenum catalyst, used with both iron impregnated coal and untreated coal, has been found to be an effective catalyst for the liquefaction of a sub-bituminous coal in HRI's Catalytic MultiStage Liquefaction process. The efficacy of the combined molybdenum/iron catalyst system in the first stage was investigated in HRI's ebullated bed bench unit. The combined catalyst system of molybdenum/iron (300 ppm Mo & 5000 ppm Fe) performed better than either iron or molybdenum alone in the first stage. The slurried catalyst, at these low concentrations, appeared to do as well a job of converting coal into liquids as a conventional supported catalyst ($Ni-MO/Al_2O_3$) in the first stage.

INTRODUCTION

The process performance parameters such as total coal conversion, 975+°F resid conversion and c4-975°F distillate yield can be used successfully as a measure of hydrogenation/hydrocracking activities of different catalyst systems. The catalyst activity and its deactivation-behavior can be compared for different catalyst systems by examining the resid conversion and the resid content of the heavy oil products as a function of catalyst age.

EXPERIMENTAL

This paper compares the results of three different bench-scale tests all run with Black Thunder Mine coal. The first test uses supported catalyst in both stages of a two reactor system. The other two tests use supported catalyst in the second stage and two different slurry catalyst additives in the first stage. The iron catalyst precursor was impregnated on the coal matrix using an incipient wetness technique developed by Pittsburgh Energy Technology Center[1] and previously scaled up by HRI for bench run CC-15[2]. Black Thunder Mine coal was impregnated with hydrated iron oxide (FEOOH) at 5000 ppm of iron using this technique. The molybdenum catalyst was added as a 5 wt% solution of ammonium heptamolybdate at 300 ppm of coal.

HRI, Inc's Catalytic MultiStage Liquefaction (CMSL) technology was used as a basis for this test program. The reactor configuration consisted of an initial pre-treater stage, followed by a backmixed slurry reactor and then an ebullated bed reactor. The iron and molybdenum catalyst precursors were first activated to a sulfided form in the pre-treater stage prior to the two liquefaction stages. The first liquefaction stage operated as a slurry reactor (containing no supported catalyst) and the second stage as an ebullated bed containing Shell S-317 1/32" extrudate. Downstream product separation was accomplished by a hot separator and a cold separator. The bottoms from the hot separator were further processed off-line by batch pressure filtration. The pressure filter liquid (PFL) was used to slurry the feed coal and as a flush oil. The two catalyst precursors were activated with H_2S (3 wt% coal) at 300 °C in the pre-treater stage.

RESULTS AND DISCUSSION

Three runs with five different first stage catalyst conditions were compared; second stage catalyst always consisted of Shell S-317 1/32" extrudates (Table 1). Run CMSL-1 used both the slurry molybdenum catalyst with the iron impregnated coal as well as just the slurry molybdenum catalyst. Run CC-15 examined the use of both the iron impregnated coal and using no catalyst additive so that the first stage would be just a thermal reactor. Run CC-1[3] is a base case for a catalytic/catalytic CTSL™ operation. Since each run consisted of a number of operating conditions, the exact periods chosen for comparison were based upon comparable second stage catalyst ages and similar high/low temperature staging of the final two reactors. The major significant difference among the runs is that CMSL-1 was run at a much higher space velocity, 1.45-1.66 times the base condition, giving only 60-69% of the nominal residence time of the base condition. This would normally lead to poorer performance in terms of coal conversion, resid conversion and total distillate yield and a higher level of resid in the pressure filter liquid.

The coal conversion for the four systems using a first stage catalyst are all roughly equal, within 1.5% (Figure 1). The two conditions using the slurried molybdenum catalyst actually have the highest conversion, and the run with only a molybdenum additive has a higher conversion than when the iron is also present. All three slurry catalyst systems, the molybdenum/iron, the molybdenum alone and the iron alone, give favorable coal conversion compared to the base condition with the supported catalyst.

The resid conversion for the four catalytic systems also show only a small variation, with the molybdenum/iron system having the highest conversion and the iron system with the lowest (Figure 1). Both of the systems using the molybdenum additive show at least as good resid conversion as the base system does. Since the resid conversion is strongly dependent on the catalyst age, it is not surprising that the molybdenum/iron system, with a lower catalyst age by almost 1/2, has a higher conversion then the molybdenum

system does.

The total distillate yield (C4-975+F) also shows only small differences among the four catalytic conditions (Figure 1). This is the only measure of performance for which either of the molybdenum containing systems is worse then the base condition, and even then the molybdenum system is only 1.6 WT% lower then the supported catalyst; while the molybdenum/iron system is 1.2 WT% higher.

These three parameters, coal conversion, resid conversion and distillate yield, can be used to determine the performance of a catalyst in the CMSL process. The resid conversion and the total distillate yield being the two more catalyst dependent variables, but the coal conversion is not entirely independent of catalyst. For these three parameters there is little difference among the four different catalytic systems, the condition using no catalyst at all in the first stage having the poorest performance, as would be expected. These four conditions show equivalent performance even though the molybdenum/iron system was run at 1.66 times the reference space velocity and the molybdenum system was run at 1.45 times the reference space velocity. Also, there is little difference in the performance between the run with just a molybdenum catalyst and the run with the molybdenum and iron catalysts.

Another measure of catalyst performance is the distribution of the final products (Figure 2). The molybdenum/iron system gives the best overall product distribution with the highest light distillate yield and the lowest resid yield. Both the iron system and the molybdenum system compare well with the supported catalyst system, demonstrating higher light distillate yields with lower heavy distillate yields while the naphtha and resid yields are very close. The molybdenum and the molybdenum/iron systems both give better distillate distribution than the supported catalyst even though they are at a much higher space velocity, 1.45 and 1.66 times the reference space velocity respectively.

The activity and deactivation of a catalyst system is also critical to the long term operation of a liquefaction process. Figure 3 shows one measure of catalyst deactivation in terms of the resid conversion as a function of catalyst age. The CMSL-1 run using the molybdenum catalyst always gives a higher resid conversion then does CC-15 with the iron catalyst. Additionally the rate of deactivation as measured by the slope of the graph is also lower for the molybdenum system by 54%.

One of the more noticeable effects catalyst has is on the quality of the pressure filter liquid (PFL) used as a recycle oil to slurry the fresh coal feed. This is taken as the liquid bottoms from an atmospheric flash vessel usually operated at 315 °C. The better a catalyst is as a hydrocracker, the slower will the resid content of the PFL increase as the catalyst ages. Figure 4 shows the resid content as a function of catalyst age for the three runs. Run CC-1

data is not appropriate to this comparison past a catalyst age of 168 lbs dry coal/lb catalyst due to various recycle schemes that were used. Both CC-15 with the iron catalyst and CC-1 with the supported Shell S-317 catalyst show the same trend of resid buildup in the PFL. Run CMSL-1 with the molybdenum catalyst initially shows this same trend until a catalyst age of 300 lbs dry coal/lb catalyst is reached. At this point the resid content of the PFL is constant at 27 WT%. The molybdenum catalyst system achieves a steady level of resid content in the PFL sooner and at a lower level then does the iron system. The molybdenum system performs as well as either the supported catalyst system or the iron system does and at a much higher space velocity.

CONCLUSIONS

It has been shown that at comparable operating conditions the use of combined molybdenum/iron slurried catalysts in the first stage of the CMSL process results in an improved process performance for liquefaction of a sub-bituminous coal over that obtained from the use of either iron or molybdenum catalyst alone or the use of the supported Ni-Mo/Al_2O_3 catalyst in the first stage. The slurried catalysts, as compared to the supported catalyst (in the first stage) not only resulted in improvements in coal and resid conversion and C4-975+F distillate yield, they also subsidized the deactivation of the second stage supported catalyst, probably by maintaining the quality of the recycle oil in the first stage. This similar, if not better, overall performance was achieved while maintaining a 66% higher throughput.

REFERENCES

1. Cugini, A.V., et al, DOE/PETC, "A Highly Active Disposable Iron Catalyst for Coal Liquefaction", 201st National ACS Meeting, Atlanta, GA, April 14-19, 1991.

2. Lee, T.L.K., et al, "A Study of Dispersed Additives in Coal Liquefaction", 205th National ACS Meeting, Denver, Co, March 28 - April 2, 1993.

3. Comolli, A., et al, DOE Topical Report #1 Contract # DE-AC22-88PC88818, "Catalytic Two Stage Liquefaction Process (CTSL) Bench Studies and PDU Scale-Up with Sub-Bituminous Coal".

TABLE 1: OPERATING PARAMETERS FOR COMPARISON RUNS					
RUN ID#	CMSL-1	CMSL-1	CC-15	CC-15	CC-1
PERIOD (DAY)	7	14	8	11	16
CATALYST AGE (LB COAL/LB CAT)	168	317	228	316	384
CATALYST 1ST STAGE	MOLY & IRON	MOLY	IRON	NONE	SHELL S-317
2ND STAGE	SHELL S-317	SHELL S-317	SHELL S-317	SHELL S-317	SHELL S-317
TEMP (°C) (°F) RXN 1	444 (832)	440 (824)	427 (801)	427 (801)	436 (817)
RXN 2	413 (775)	413 (775)	412 (774)	413 (775)	408 (767)
SPACE VELOCITY (SV_{REF} = 1.0)	1.66	1.45	0.91	0.96	1.00

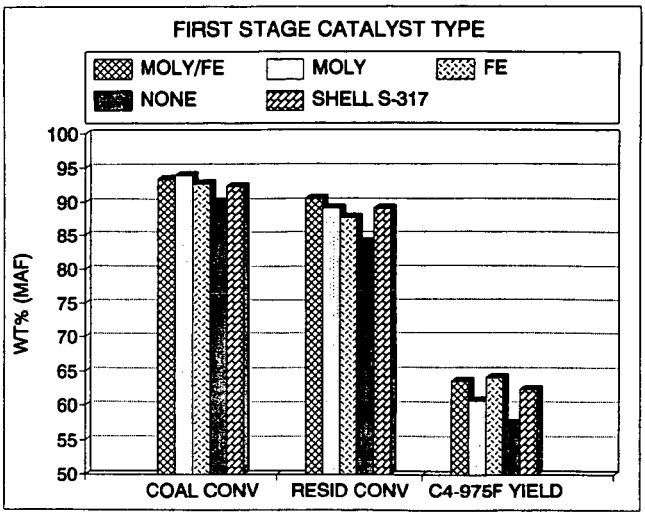

Figure 1. Process performance.

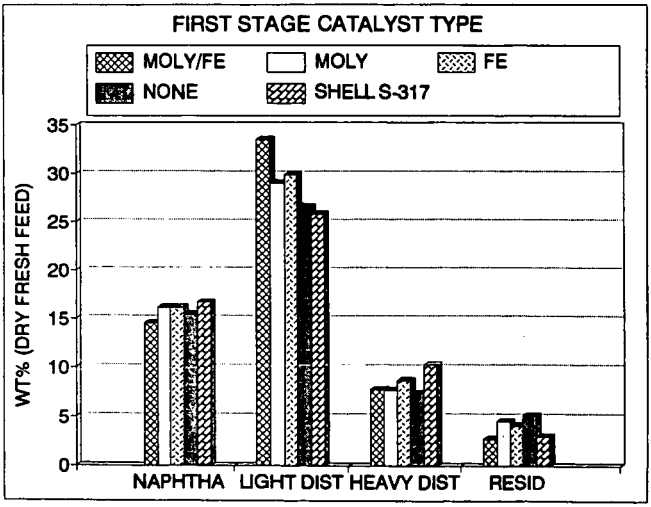

Figure 2. Final Product Distribution.

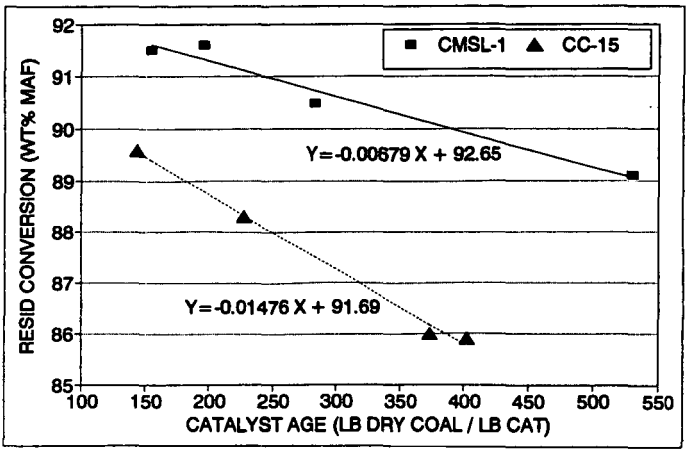

Figure 3. Resid conversion as a function of catalyst age for CMSL-1 and CC-15.

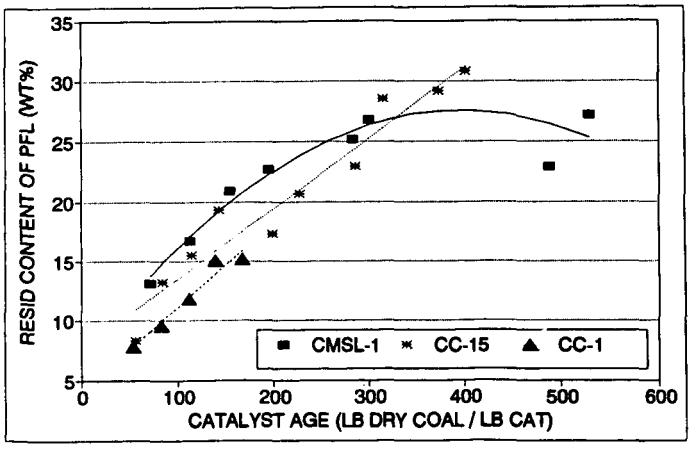

Figure 4. Resid content of the pressure filter liquid as a function of catalyst age.

A NOVEL SHORT TIME REACTOR SYSTEM FOR STUDYING THE INITIAL STAGES OF DIRECT COAL LIQUEFACTION

He Huang, William H. Calkins*, and Michael T. Klein
Department of Chemical Engineering
University of Delaware, Newark, DE 19716

Keywords: short contact time reactor, DBE conversion, coal liquefaction

ABSTRACT

Study of direct coal liquefaction at short contact time can provide insight into the chemical and physical processes involved at low conversions, before the occurrence of significant secondary degradative and retrogressive reactions of the liquefaction products. However, it has been difficult in the past to produce well-defined, short reaction time samples for in-depth analysis. To achieve this, a novel bench scale reactor was designed and built. The characteristics of the reactor system are as follows. The coal-organic solvent liquid slurry is driven into a reactor, which is already at reaction temperature, through preheater tubing using a high-pressure gas. Preliminary tests show that this can be accomplished in less than one second, and the desired reaction temperature of the process stream is achieved within approximately 0.3 seconds. The injected slurry is agitated by gas bubbles introduced through the slurry from the bottom of the reactor. The quenching process is performed in a similar way and accomplished in less than one second. The product stream cools down to about 25 °C in approximately 0.3 seconds. The preliminary operating results on this unit for conversion of model compound, direct coal liquefaction, and conversion of coal-derived resids have been reported in this paper.

INTRODUCTION

In the liquefaction of coal, as in many other high-pressure and high-temperature reactions, important information concerning the controlling chemical and physical processes can be obtained through study at the very early stages, before complicating secondary reactions occur. The major experimental challenge is to bring the system up to the reaction temperature and pressure in a time frame less than that required for the physical and chemical processes to start to occur. It is also important to choose an appropriate method to agitate the reactor contents to maintain uniforms of temperature and concentration.

In most laboratory high pressure equipment used to run direct coal liquefaction, such as tubing bombs or autoclaves, the heat up and cool down times of the massive equipment required to hold the pressure are long compared to the times involved in the reactions themselves. A representative temperature profile for the tubing-bomb reactor is shown in Figure 1. The resulting long heat up and cool down times obscure fundamental interpretation of the results, and do not allow practical process studies to be made at short reaction times. The common ways to agitate the reactor system are either stirring or shaking. To do this requires complicated and expensive equipment, particularly on a very small laboratory scale (ca. 30 grams). This also makes rapid sampling difficult. Thus, a reaction system at constant temperature and pressure, capable of sampling at very short reaction times (a few seconds up to 30 minutes or longer) and agitating in a simple way, is needed. Such a novel Short Time Batch Reactor (STBR) has been devised and built in our

laboratory, and tests of this apparatus for studying conversion kinetics of model compounds, coal-derived resids, and coal liquefaction are underway. Herein we report on the preliminary operating results of this unit.

EXPERIMENTAL

Apparatus

An empty batch reactor illustrated in Figure 2 is immersed in a sand bath and brought up to the desired reaction temperature. Using high pressure gas, the reaction mixture under study is driven into the reactor from a small blow case through preheater tubing, which is also at reaction temperature. Tests show that this can be accomplished in less than one second. Because only small quantity (about 30 grams in our present unit) of the reaction mixture is heated during injection in the relatively massive preheater tubing, the desired reaction temperature is achieved within approximately 0.3 seconds. The reaction mixture is then agitated by gas bubbles injected through the slurry from the bottom of the reactor. The degree of agitation is controlled by the exit gas flow rate from the top of the reactor. At a selected time, the reactor contents are driven out of the reactor into a cold receiver through a precooler with high pressure gas. Both the receiver and precooler are immersed in a water bath. This process is also accomplished in less than one second, and the cooling of the product mixture to about 25°C is achieved in approximately 0.3 seconds.

The details of the reactor system are shown in Figure 3. The heating bath used is a Techne IFB-52 industrial fludized sand bath, which maintains a reaction temperature of ±2°C. The 30 cm^3 reactor is capable of containing 17 MPa (2500 psi) pressure at temperatures up to 550 °C. The tubing used for preheater and precooler was 1/4" 316 stainless steel with wall thickness at 0.035". The lengths of the preheater and precooler were both about 21 feet. Since a gas (e.g. hydrogen or nitrogen) is bubbled through the reaction mixture under pressure and out through a let-down valve, a small, water-cooled condenser above the reactor and a disengaging space above it before the let-down valve are necessary to avoid loss of solvent or other low boiling components.

Reaction Temperature Profile

A time-temperature profile for a mixture of 89% tetralin, 1% biphenyl, and 10% dibenzylether (DBE) is shown in Figure 4. At the time of injection, the reactor temperature dropped 5 - 8 °C, but it recovered to sand bath temperature within 30 seconds. This temperature drop may be reduced by longer preheater tubing.

The excellent time-temperature profile of Figure 4 is due to the preheating of the comparatively massive empty reactor and the preheater tubing and fittings prior to t = 0. This allows the only thermal transient to be focused on the reaction mixture.

Sample Recovery

The amount of material recovered from the reactor when it is driven from the system depends on the surface area of the entire apparatus. This is because surface holds up liquid for wetting. The surface areas of the preheater and precooler are the bulk of that involved, and therefore there is a trade off between the reaction temperature drop on injection and the degree of recovery. For that reason, the longer the preheater, the smaller the reaction temperature drop on injection, but the lower the recovery. The viscosity or fluidity of the sample stream also influences the recovery. For the process streams studied thus far, recoveries have varied from 75 to 85 %. Because of the hold-up of some of the reaction mixture on the walls of the reactor and preheator and precooler tubings, 100% recovery of the reaction mixture is not practical. This means that analytical methods must be available

to follow the course of the reaction with aliquots. This has not been a limitation for the reactions studied thus far. However, if better material balances are required, the first sample can be supplemented with solvent washes of the system, and further quantities of the reactant recovered by solvent removal in a rotovapor.

Cleaning System

The reactor system can be cleaned in place by a series of suitable solvent washes. The number of the washes required will depend on the reactions being studied.

PRELIMINARY RESULTS

Conversion of Model Compound

Solutions of model compounds, such as dibenzylether in tetralin, have been run in this equipment to investigate its performance. A temperature profile of the reaction has already been shown as Figure 4. Approximately 85% of the reaction mixture was recovered. Benzaldehyde, benzyl alcohol and toluene were the principal products as shown by GC-MS. A kinetic curve for the reaction under 1000 psi N_2 at 375 °C is shown in Figure 5. Excellent fit to first-order kinetics with $k_{DBE} = 8.78 \times 10^{-4}\ s^{-1}$ was found.

Coal Liquefaction

Mixtures of 25% Wyodak Black Thunder coal in tetralin were run in this apparatus to begin to study the liquefaction process itself at very low conversions. A typical temperature profile at 380°C over a two minute interval is shown in Figure 6. Samples could be taken at as short a reaction time as 10 seconds, with confidence that the desired reaction time at temperature was achieved. No difficulty was encountered in driving the reaction mixture in and out of the reactor. Recovery of the reaction mixture was about 80%.

Conversion of Coal-Derived Resid

Initial studies with this new reactor are being devoted mainly to investigation of the conversion kinetics of coal-derived resids. The compositions of the coal derived resids being studied are shown in Table 1. Mixtures of the resid, in various concentrations with tetralin, such as 1:2 and 1:3, and sometimes with added catalyst, are heated sufficiently to become fluid, and then charged to the blow case which is maintained sufficiently warm with heating tape to keep them fluid. They are also agitated in the blow case with bubbling hydrogen gas. The charge is then driven into the reactor with 1500 psi hydrogen and the reactor agitated again with bubbling hydrogen. The resids are solid materials at room temperature, and contain up to 20% mineral matter. They therefore present a rather viscous mixture, even when diluted with tetralin and heated to become relatively fluid. Reactions have been run at 1500 psi and 410 °C. Recovery of the reaction mixture has been about 75%.

SUMMARY AND CONCLUSIONS

This reactor system (STBR) should have broad applicability to fuel science problems and many other high-pressure, high-temperature reactions of organic or inorganic systems where small-scale experiments for kinetic measurements are needed. Complex reactions where secondary reactions set in at an early stage can be studied in this type of reaction system at very low conversions.

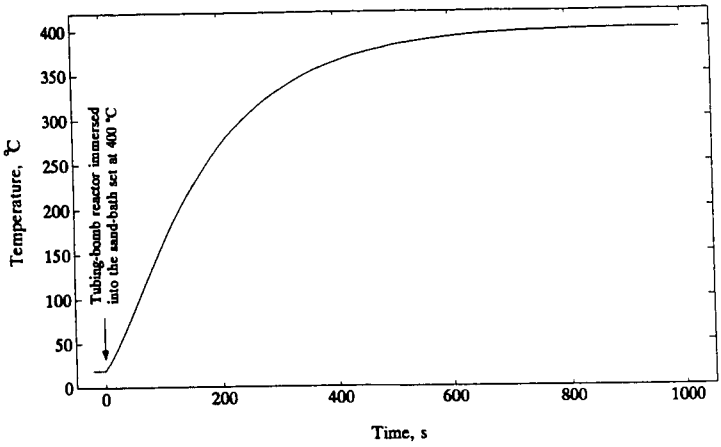

Figure 1 Time-Temperature Profile for a Tubing Bomb Reactor

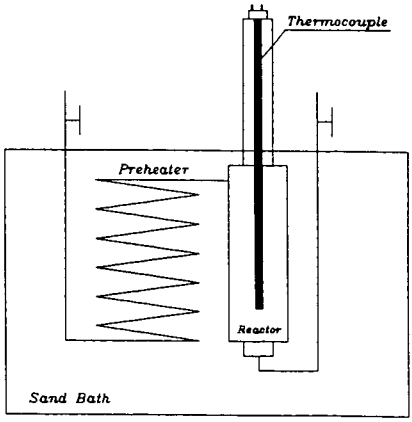

Figure 2 Batch Reactor (STBR) for Studying the Initial Stages of Direct Coal Liquefaction

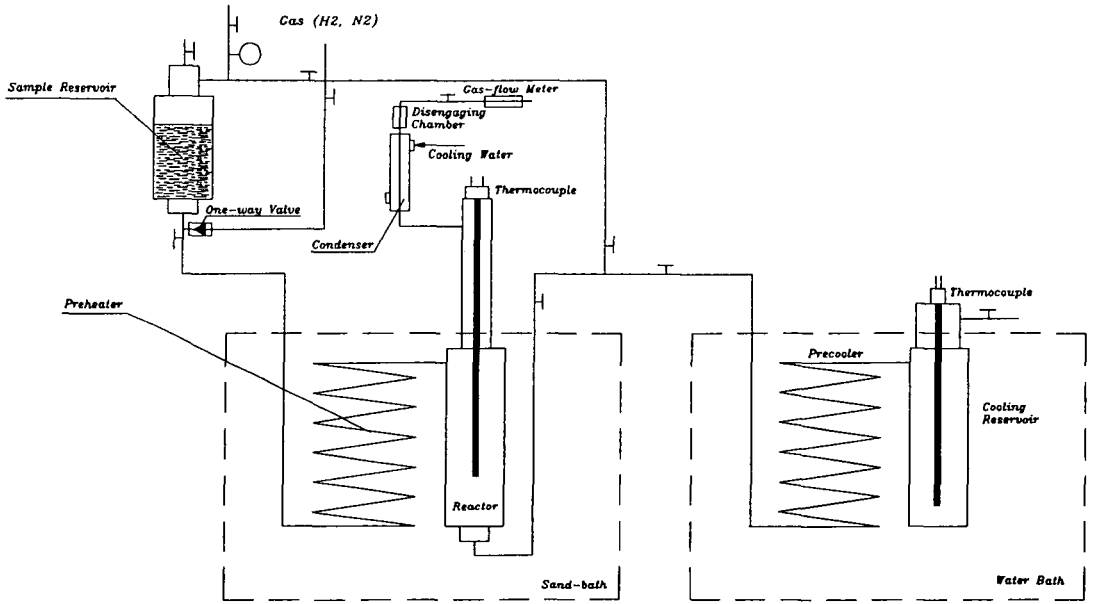

Figure 3 Apparatus for Direct Coal Liquefaction at Short Contact Times

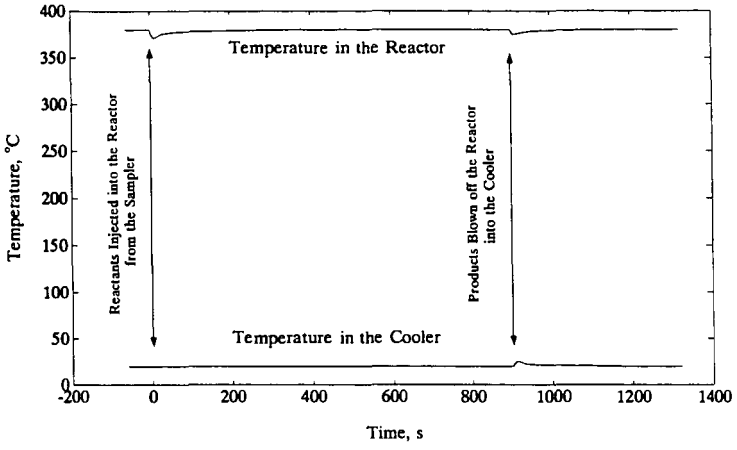

Figure 4 Time-Temperature Profile for a Typical DBE Conversion Run

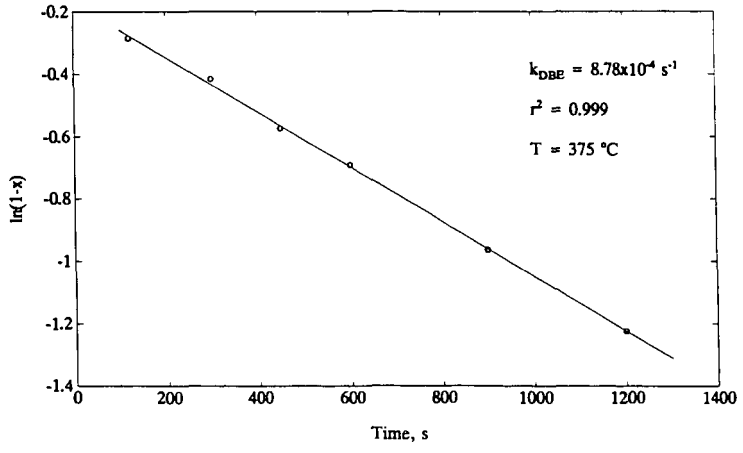

Figure 5 ln(1-x) vs. Time for DBE Conversion in Tetralin

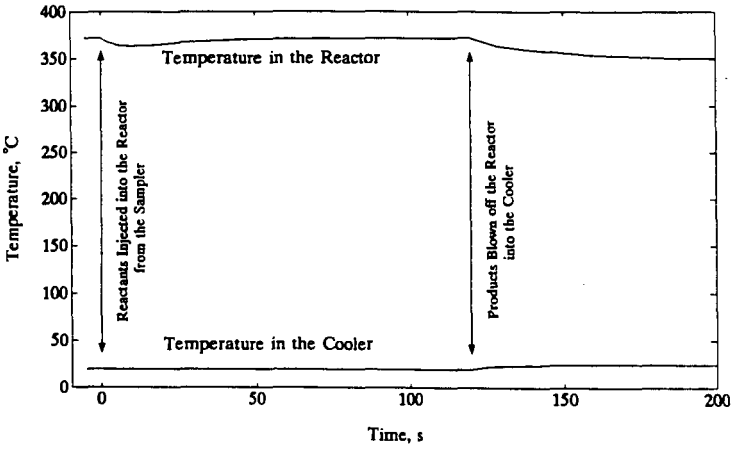

Figure 6 Time-Temperature Profile for a Typical Short Time Coal Liquefaction Run

Table 1 The Compositions of the Coal-Derived Resids

	Resid 1[a)]	Resid 2[b)]
Ultimate:		
Ash, wt%	10.21	16.67
C, wt% MAF	90.24	91.03
H, wt% MAF	6.39	6.56
N, wt% MAF	1.05	1.15
S, wt% MAF	1.49	0.09
O (by diff.), wt% MAF	0.83	1.17
Proton Distribution (%, pyridine-soluble basis):		
Condensed Aromatics	27.8	27.2
Uncondensed Aromatics	3.8	6.8
Cyclic Alpha	21.2	18.3
Alkyl Alpha	9.6	8.8
Cyclic Beta	15.5	13.6
Alkyl Beta	13.4	16.6
Gamma	8.7	8.7
Insoluble Organic Matter in Pyridine (wt%):		
	6.28	13.9

a) Feed coal: Pittsburgh seam Ireland mine, Wilsonville Run 259 of V1067 at 2nd stage product;
b) Feed coal: Wyodak abd Anderson seam Black Thunder mine, Wilsonville Run 260 of V1067 at 2nd stage product;

THE INFLUENCE OF PROMOTER METALS ON THE CATALYTIC ACTIVITY OF A NANOSCALE SULFATED HEMATITE FOR THE LIQUEFACTION OF A SUBBITUMINOUS COAL

G. T. Hager, E. N. Givens, F. J. Derbyshire, The Center for Applied Energy Research, University of Kentucky, 3572 Iron Works Pike, Lexington, KY 40511-8433

Abstract

Nanoscale sulfated hematites ($Fe_2O_3 \cdot SO_4^{2-}$) have been shown to have high catalytic activity both for coal liquefaction and coprocessing of coal with a petroleum resid. The addition of small amounts of molybdenum as a promoter metal significantly enhances this catalytic activity. In this study, several metal promoted hematites have been prepared and characterized. The promoter metals studied include molybdenum, nickel, tungsten, and titanium. Various techniques were utilized to define both the bulk and surface chemistry of these materials, including XRD, SEM, TEM and XPS. The activity of these catalysts for the liquefaction of a subbituminous coal in tetralin will be reported.

Introduction

Several groups have investigated the use of sulfated hematites (Fe_2O_3/SO_4^{2-}) for use as both coal liquefaction and coprocessing catalysts with promising results.[1-8] It is important to note that this formula does not represent a stoichiometric relationship between the sulfate and the iron but rather the sulfate may be considered as SO_3 chemisorbed on the surface of Fe_2O_3. Tanabe et al.[8] found that the sulfated hematite exhibited the highest activity, similar to that of a $Co/Mo/Al_2O_3$ catalyst, for the liquefaction of a bituminous coal. A study by Yokoyama et al [2] showed that the activity of the sulfated hematite was independent of the rank of the coal, yielding high conversions for both bituminous and subbituminous coals. In addition to a high conversion, these catalysts also showed a relatively high selectivity to oils.[1]

More recent work by Pradhan et al. [5-7] has shown the high activity of sulfated hematite for both direct coal liquefaction and coprocessing of coal with a Maya resid. The addition of up to 2 wt% molybdenum as a promoter metal further was found to further increase the activity of the catalyst. The highest conversions were achieved in the presence of added elemental sulfur with the catalyst. The high activities reported were achieved at very low catalyst loadings of <0.4 wt% Fe. This high activity is, in part, due to the small particle size and the associated high dispersion. XRD and TEM have both shown that the average particle diameter is 10-30 nm. The small size of these particles allows better contact with the coal. In addition, the presence of the sulfate group on the surface may inhibit the tendency of the particles to sinter during the liquefaction process. The increased acidity associated with the sulfate group also enhances the activity of the catalyst

for certain reactions.

Experimental

The technique used for production of the sulfated hematite involves the aqueous precipitation of an iron salt in the presence of a source of sulfate ion. There are several techniques used for this purpose. For this project, a urea precipitation of ammonium ferric sulfate was utilized. In this process 25 g of urea were mixed with 17.5 g of iron alum [$(NH_4)Fe(SO_4)_2 \cdot 12\ H_2O$] in 500 ml of distilled deionized water. The initial pH of the solution was ~3. The solution, stirred continuously during the process, was heated to ~95°C and kept at temperature for ~2 hrs. During this time the urea caused the gradual precipitation of the iron and a neutral pH was attained indicating the completion of the reaction.

The precipitate was removed from the solution by vacuum filtration and washed with distilled deionized water to remove unbound sulfate groups. The filter cake was dried to remove any residual moisture. The original technique called for calcination of the filter cake in air at 500°C for ~1 hr. Subsequent testing showed that for the small samples (~3g) generated in each batch calcining at ~475°C for ~10 minutes was sufficient.

Promoter metals may be added to the sulfated hematite by addition of metal containing salts to the solution. Molybdenum has been used, in the form of ammonium molybdate, to produce a sulfated hematite doped with molybdenum. Various concentrations of molybdenum have been added to determine the effect of loading on the activity. Several other metals, including tungsten, nickel, and cobalt were also added using this method. In addition, this procedure may be modified to add multiple promoter metals to the sulfated hematite. Several combination promoted sulfated hematite have been produced by this technique including nickel/molybdenum, cobalt/molybdenum, and tungsten/molybdenum.

XRD was utilized to identify the phase of the precipitated iron particles, both before and after calcination. As shown in Figure 1 the XRD spectra of the as-formed particles closely matches the reported spectra of goethite (α-FeOOH). Also clearly shown in the spectra are the 44.7° and 65.0° peaks identified with α-Fe. The relatively poor resolution in the XRD spectra is due to both the extremely small size and poor crystallinity of the particles. After calcining, the XRD spectra of the particles, shown in Figure 2, can clearly be identified as hematite (α-Fe_2O_3) with the continued presence of the α-Fe peaks at 44.7° and 65°. The sharpness of the peaks in the calcined particles may be attributed to an increase in both the crystallinity and average particle size.

The chemisorbed sulfate group has been reported to have several effects on the catalytic properties of the particles.[5] One of the purposed function is the attainment and maintenance of high dispersion. The sulfate group may inhibit the particle agglomeration and sintering. The quantity of sulfur present was determined by elemental analysis to be 3-5 wt %. There was little effect of calcination on the sulfur content. The slight increase in concentration is easily accounted for by the mass loss which occurs during calcination.

The average crystallite diameter of the particles may be estimated from the XRD spectra. Utilizing this technique, the average particle sizes were shown to be in the 5 - 30 nm range with

most particles ranging from 15-20nm. SEM on the particles reveal that the particles exist as an agglomeration of very small particles below the resolution of the instrument. While this does not directly confirm the estimates made from the XRD spectra, neither does it refute them. TEM on the particles is in progress to validate the XRD derived estimates.

In order to determine the effect of residence time at temperature during calcination on the particle phase and size, a single batch of goethite was split into 4 samples. Each sample was calcined for between 10 and 60 minutes. The resulting catalysts were analyzed by XRD and the spectra were compared to determine phase and particle size. It was found that the transformation from goethite to hematite is complete within 10 minutes. However, the continued exposure to this temperature appeared to have little effect on the average diameter of the particles. There is some loss of surface area associated with the calcination process. Nitrogen BET measurements showed a decrease of the surface areas of ~18% during the calcination process.

The addition of molybdenum to the sulfated hematite as a promoter metal has been reported to improve the activity of the catalyst.[5] It was therefore decided to attempt to add varying amounts of molybdenum to the sulfated hematite to act as a promoter metal. The doping of the sulfated hematite with molybdenum was achieved by addition of ammonium molybdate to the iron alum/urea solution. Elemental analysis of both the product and the waste water indicate that all but a trace amount of the molybdenum is incorporated in the catalyst.

It has been reported that the role of the molybdenum in the catalyst structure is to deposit on the surface as MoO_4[9]. Consequently, elemental analysis shows that the addition of molybdenum results in a decrease in the amount of sulfate present. Since the sulfate group is located primarily on the surface, this further confirms that the molybdenum acts to displace the sulfate group on the surface of the hematite. Further, the XRD spectra indicate that, even at concentrations up to 10 wt% molybdenum, only the hematite and α-Fe spectra were present indicating that the molybdenum is present either in an amorphous phase or on the surface.

The addition of molybdenum had a moderate effect on the particle diameter as determined from XRD spectra. As shown in Figure 3, the increase in the amount of molybdenum added led to a gradual decrease in the particle diameter. However, as the error bars indicate, this trend is somewhat dubious. The significant error is due to inaccuracies associated with the estimation of particle diameter from XRD spectra and also to the amount of noise present in the spectra. The molybdenum promoted sulfated hematites also appear as a loose agglomeration of particles whose size was below the resolution of the SEM.

Surface areas of the molybdenum promoted sulfated hematites were measured by the nitrogen BET method. The effect of increasing molybdenum concentration was to increase the surface area of the particles, as shown in Figure 4. As expected, since there is little to no porosity associated with these particles, the trend in surface area agrees with the trend seen in the particle diameter estimation. The replacement of the sulfur with molybdenum on the surface may lead to further inhibition of agglomeration due to the relative size of the atoms. This would agree well with both the surface area measurements and particle diameter estimations.

The catalysts were tested for use in the liquefaction of a subbituminous Black Thunder coal.

The experiments were carried out in horizontal 50 ml. microautoclave reactors. The conversions were determined by solubility using THF and pentane, into IOM, preasphaltenes + asphaltenes, and oils. The gas yields were determined directly by GC. Two sets of reactions were carried out to determine the effect of severity on catalytic activity. The low severity experiments were conducted at 385°C for 15 minutes while the high severity conditions were carried out at 415°C for 60 minutes. All runs were done in duplicate to assure reproducibility. As shown in Table 1, preliminary results indicate that, for a catalyst loading of 0.7 wt % Fe at high severity conditions, while all catalysts displayed similar total conversions (~89%), the use of molybdenum resulted in the greatest increase in conversion to oils (~39%). The nickel doped sulfated hematite showed a slightly higher total conversion (~90 %) but a lower selectivity to oils (~33 %). Tungsten and cobalt yielded similar total conversions (~89 %) and oil yields (~37 %). These results show that these catalysts compare favorably with a commercially available 30 Å superfine iron oxide, while their lower cost and ease of production make them economically more viable for scale up.

References

1) Hattori, H; Yamaguchi, T; Tanabe, K.; Yokoyama, S; Umematsu, J; Sanada, Y.; *Fuel Proc Tech*, **8**, 117-22, 1984
2) Yokoyama, S; Yamamoto, M; Yoshida, R; Maekawa, Y; Kotanigawa, T; *Fuel*, **70**, 163-8, 1991
3) Kotanigawa, T; Yokoyama, S; Yamamoto, M; Maekawa, Y; *Fuel*, **68**, 618-21, 1989
4) Huffman, G P; Ganguly, B; Taghiei, M; Huggins, F E; Shah, N; *Preprint ACS- Div of Fuel Chem*, **36**(2), 561-9, 1991
5) Pradhan, V R; Herrick, D E; Tierney, J W; Wender, I; *Energy & Fuels*, **5**, 712-20, 1991
6) Pradhan, V R; Tierney, J W; Wender, I; Huffman, G P; *Energy & Fuels*, **5**, 497-507, 1991
7) Pradhan, V R; Tierney, J W; Wender, I; *Preprint ACS- Div of Fuel Chem*, **35**(3), 793-800, 1990
8) Tanabe, K; Hattori, H; Yamaguchi, T; Iizuka, T; Matsuhashi, H; Kimura, A; Nagase, Y; *Fuel Proc tech*, **14**, 247-60, 1986
9) Pradhan, V R; Hu, J; Tierney, J W; Wender, I; *Preprint ACS- Div of Fuel Chem*, 38(1), 8-13, 1993

Table 1. Effect of Catalyst on Liquefaction Yields

	% Total Conversion	% PA&A	% Oils	% Gas
SFIO	87.0	45.2	34.6	7.2
1%Mo/Fe_2O_3/SO_4^{2-}	88.5	43.1	38.9	6.8
5%Co/Fe_2O_3/SO_4^{2-}	88.8	45.6	36.6	6.6
5%W/Fe_2O_3/SO_4^{2-}	88.9	45.3	36.8	6.8
5%Ni/Fe_2O_3/SO_4^{2-}	90.4	49.8	33.4	7.1

Figure 1. XRD Spectra of As-formed Particles with Goethite and alpha Fe

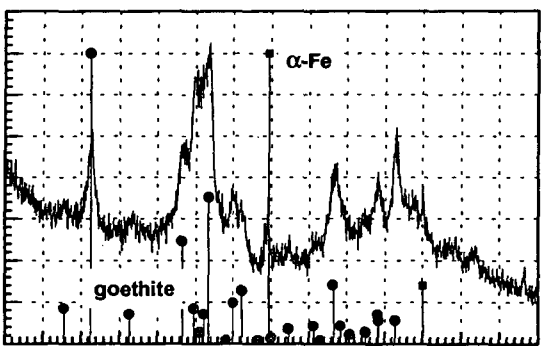

Figure 2. XRD Spectra of Calcined Particles with Hematite and alpha Fe

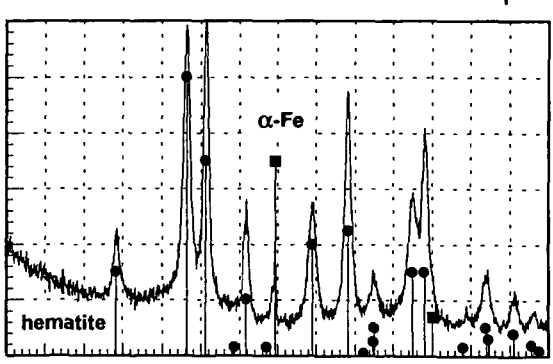

Figure 3. Effect of Molybdenum Concentration on Particle Diameter Estimated from XRD

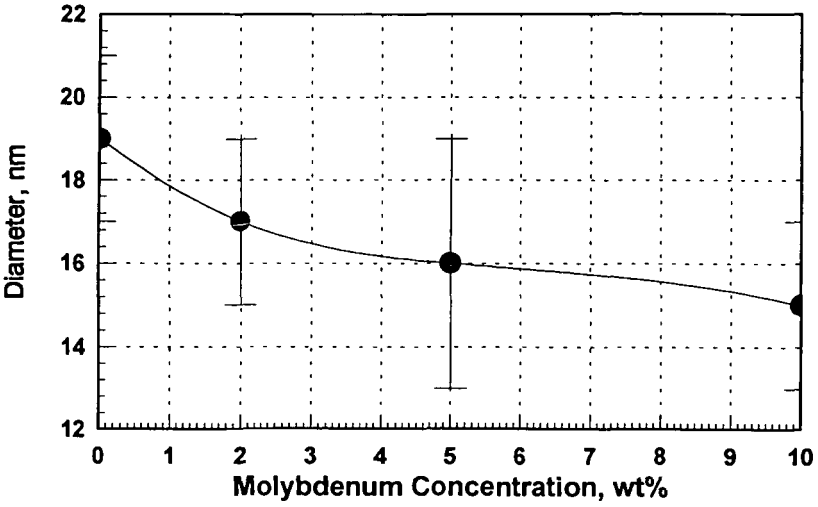

Figure 4. Effect of Molybdenum Concentration on Surface Area

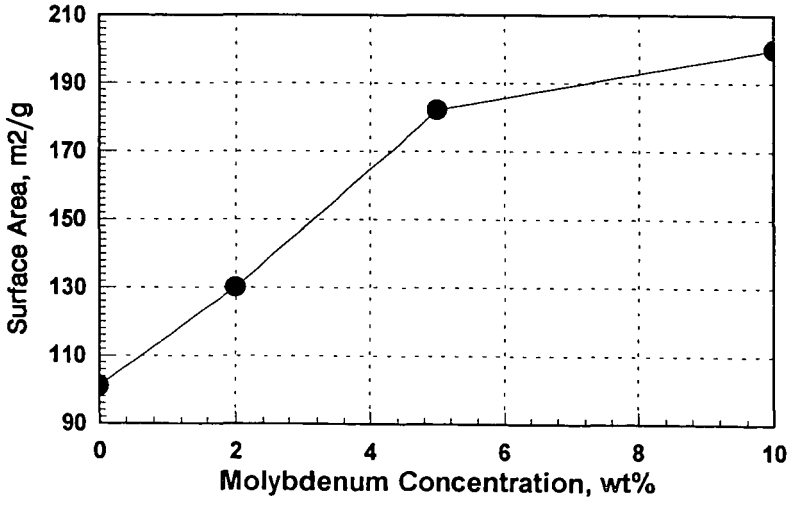

EFFECTS OF SOLVENT AND CATALYST ON LIQUEFACTION CONVERSION AND STRUCTURAL CHANGES OF A TEXAS SUBBITUMINOUS COAL

Lili Huang, Chunshan Song, Harold H. Schobert
Fuel Science Program, Department of Materials and Engineering,
209 Academic Projects Building,
The Pennsylvania State University, University Park, PA 16802

Keywords: liquefaction, conversion, aromaticity

INTRODUCTION

Coal liquefaction involves an initial stage of coal macromolecular break-up driven by thermal energy [1, 2]. The result of this break-up is the formation of free radicals. If these free radicals are stabilized by hydrogenation, a liquid product is formed and the goal of liquefaction is achieved. On the contrary, if the radicals recombine with one another and form more stable and heavier product, the liquefaction has failed. Therefore, hydrogenation is the key in coal liquefaction. In fact, a recent study showed that the more hydrogen consumed in the reaction, the higher conversion would be obtained [3]. There are several ways often used to accelerate the rate of hydrogenation: to use a high pressure of H_2 [4], to use a hydrogen-donor solvent [5], and to use a catalyst.

In this study, a Big Brown Texas subbituminous (DECS-1) coal was used for liquefaction. A low-rank coal like this is characterized by low aromaticity, small ring clusters, abundant aliphatic and hydroaromatic carbon, and high oxygen content [6]. These structural features cause the thermal break-up of the coal over a wide temperature range [7-9], and thus the hydrogenation should be feasible in the same range. The purpose of this work is to investigate the liquefaction of DECS-1 at temperature range from 250°C to 450°C. Two kinds of solvent, a hydrogen-donor solvent (tetralin) and a non-donor solvent (1-methylnaphthalene) were used to compare with the reactions without solvent. An ammonium-tetrathiomolybdate-derived catalyst was used. Liquefaction results are presented to determine the solvent effect and the catalyst effect. The residues from tetrahydrofuran (THF) extraction of the reaction products were studied by CPMAS ^{13}C NMR to obtain their aromaticities. Furthermore, the conversion and the aromaticity data were combined to calculate the amount of aliphatic and aromatic carbon that has reacted and has been removed from the coal during liquefaction.

EXPERIMENTAL

The coal sample was a Big Brown Texas subbituminous (DECS-1) obtained from the Penn State Coal Sample Bank. Its compositional data are summarized as the following on a dry and mineral matter free basis: 76.13% carbon, 5.54% hydrogen, 1.50% nitrogen, 1.05% organic sulfur and 15.78% oxygen (by difference). The reaction solvents were tetralin (Aldrich, 99%), and 1-methylnaphthalene (1-MN, Aldrich, 98%). The catalyst precursor was ammonium tetrathiomolybdate (ATTM, Aldrich, 99.97%). All the chemicals were used without further purification.

The catalyst loading was 1 wt% of Mo based on the dmmf coal. A THF/H_2O (1:1) mixture was used to make the solution of the catalyst precursor, because this binary mixture was superior to H_2O in terms of providing higher conversion and oil yield in subsequent liquefaction [10]. The catalyst precursor was first added to water, of just enough volume to dissolve the desired amount of the precursor. An equal volume of THF was then added to the H_2O solution. After being stirred to achieve a homogeneous mixture, the THF/H_2O/ATTM mixture was added to the dried coal to make a slurry. After 20 minutes of stirring at room temperature under N_2 atmosphere, the excess water and THF was removed by rotary evaporator. The "wet" sample (still containing some residual H_2O and THF) was then dried in a vacuum oven at room temperature for 20 hours, at 45°C for 5 hours and at 95°C for 4 hours, sequentially.

Liquefaction experiments were conducted in 25 ml microautoclaves in a fluidized sandbath. For each reaction, 4 grams of the coal sample and 4 grams of a solvent, if a solvent was applied, were loaded into a microautoclave. The reactor was purged three times with hydrogen and the final H_2 pressure was 1000 psi (7 MPa) at room temperature. For every reaction, the sandbath was preheated to a desired temperature, 250°C, 300°C, 350°C, 400°C, or 450°C. The microautoclave was then plunged into the sandbath and agitated at a rate of 200 cycles per minute. The total time in which a microautoclave was kept in the sandbath was 33 minutes, with 3 minutes being the time for rapid heat up. Finally, after reaction, the microautoclave was taken out of the sandbath and rapidly quenched by dipping into cold water.

After the microautoclave was cooled to room temperature, the reactor was vented, the volume of the gas was measured by the water displacement method, and a sample was collected for further analysis. The liquids and the solids in the microautoclave were washed into a tared ceramic thimble using hexane. Then the products were separated under a nitrogen atmosphere by Soxhlet extraction using hexane, toluene and THF sequentially. The soluble products are classified as oil, asphaltene and preasphaltene, respectively.

The THF insolubles were analyzed by ^{13}C solid state NMR using cross polarization magic angle spinning (CPMAS) technique. All CPMAS spectra were obtained on a Chemagnetics NMR Model M100s. The ^{13}C frequency was 25.15 MHz. The pulse delay was 1 second and the contact time was 1 ms.

RESULTS AND DISCUSSION

The results of liquefaction without catalyst are listed in Table 1. Conversions are in a large range, from 11.7% to 92.2%. At 250°C, the solvents do not show any significant effect on conversion or product distribution. As the temperature increases to 300°C, the solvents start showing their advantage by providing slightly higher conversions than the reaction without solvent. At 350°C, there is a remarkable increase in oil, asphaltene and preasphaltene yields when a solvent is used. This indicates that in this temperature range, the solvents play a role which enhances the conversion, but since there is no difference between the reaction with tetralin and the reaction with 1-MN, this role may not relate to hydrogen donation. In the temperature range from 350°C to 400°C, there is a drastic increase in conversion no matter whether a solvent is applied or not, suggesting that at this temperature range, thermal energy is enough to break down the coal macromolecular matrix. At 400°C, tetralin made a tremendous difference from 1-MN and no solvent. The conversion reaches 82.0%, composed of gas, 9.5%; oil, 36.7%; asphaltene, 16.6%; and preasphaltene, 19.2%. With 1-MN or without solvent, the conversions are much less, 55.5% and 45.0% respectively. The differences of conversion and product distribution imply that tetralin is active in donating hydrogen at temperatures higher than 350°C. 1-MN, on the other hand, shows a very slight advantage over no solvent in gaining higher conversion and oil yield, but as temperature increases to 450°C, this advantage almost disappears.

The results of catalytic liquefaction are presented in Table 2. In the presence of ATTM, the conversion of all experiments increase drastically as the temperature increases from 250°C to 400°C. Comparing the reactions with no solvent, tetralin or 1-MN with the corresponding non-catalytic reactions, the catalyst increased the conversion, especially at temperatures higher than 300°C, suggesting that ATTM was converted to an active catalyst at temperature between 300°C and 350°C [11]. Furthermore, the product distribution shows that the increasing conversion is accompanied by an increasing yield of light materials, such as oil, when the catalyst is added. The other comparison is among the three kinds of catalytic reactions. At temperatures between 250°C and 400°C, there is no significant difference in conversion and product distribution (though at 400°C the reaction without solvent seems to have higher oil yield). In this temperature range, the catalyst has a stronger effect than the solvents; thus any difference caused by the solvents is diminished. However, at 450°C, tetralin gave a slightly higher conversion while both 1-MN and no solvent actually gave a much lower conversion (almost 20 percentage units lower) relative to those at 400°C. In the case of 1-MN at

450°C, the yields of gas, asphaltene and preasphaltene are still very similar to those in tetralin, while the conversion is much lower. The sole cause of this conversion difference is the decrease of the oil yield. With tetralin at 450°C, yields of asphaltene and preasphaltene dropped by 9 percentage units and 17 percentage units respectively , while the yield of oil increased by 22 percentage units compared with that at 400°C. This suggests that at this temperature (450°C), in the presence of both catalyst and a H-donor solvent, the conversion from preasphaltene and asphaltene to oil, or from heavy products to light products, is favorable. With the presence of the catalyst but absence of a donor solvent (meaning with no solvent or a non-donor solvent), the conversion drops as well as all of the product yields, except gas, suggesting that retrogressive reactions take place and form heavier and more stable materials.

In coal liquefaction, once the free radicals are formed, the reactions that they undergo are the result of a competition between radical stabilization by hydrogenation to form light products and recombination of the radicals to form heavy products. Since the free radical formation is a pyrolytic break-up of coal matrix, it is a thermally driven reaction [1]. At low temperatures (up to 400°C), the rate of radical formation is so slow that the hydrogenation rate can catch up, regardless of whether the hydrogen radicals are from the donor solvent or from the gaseous H_2. However, at 450°C, radical formation from the coal is very fast, but the H radical from catalytic decomposition of gaseous H_2 is not as fast, and therefore radical recombination is more likely to take place. Since tetralin has intimate contact with these radicals and is able to donate H, hydrogenation can still take place to form light products.

The gas yields from all liquefaction experiments are plotted versus temperature in Figure 1. All the yields are in the range from 0% to 20%. Regardless of the solvents and the catalyst used in the reactions, they all fall on one line. Therefore, the amount of gas produced in the reactions is a function only of temperature. Since neither a solvent nor a catalyst has any effect, gas formation is a reaction driven by thermal energy.

Examples of the spectra of CPMAS ^{13}C NMR of residues are shown in Figure 2. The spectra were curve-fitted using LabCalc program and the area of each peak was integrated. The aromaticities of the raw coal and the dried coal are both 0.48. This shows that before reaction, the aromaticity is not affected by vacuum drying at 95°C. The aromaticities of residues from all runs are summarized in Table 3. It is observed that as temperature increases, the aromaticity increases from 0.50 to 0.94. There are two possible explanations of this increase: one is that as reaction temperature increases, more and more aliphatic carbons are cracked from the macrostructure of the coal while the aromatic carbon may not react as much; the other is that dehydrogenation and condensation reactions take place during the reaction increasing the amount of aromatics in the coal. Comparing the aromaticities of the residues from the non-catalytic reactions, it is found that the solvents do not have a significant effect. Furthermore, in the case of catalytic reactions, the solvents have no significant effect either. In order to determine the influence of the catalyst on the aromaticities, all the data are plotted versus conversion in Figure 3. A general trend is that the aromaticities of residues increase with conversion, but the data fall into two separate sets: those from reactions with and without the catalyst, regardless of the solvent used. Generally, f_a of the residue from a catalytic reaction is lower than that from a non-catalytic reaction, and the difference between the two increases with increasing conversion. At the most severe conditions, 450°C with the catalyst, the aromaticities deviate from the line of catalytic reaction. The higher aromaticities are caused by more aromatic carbon, which indicates the retrogressive reactions at this temperature. In non-catalytic reactions, the use of tetralin at 400°C and 450°C results in lower aromaticities, suggesting that tetralin helps to convert aromatic carbons from coal to THF solubles.

To achieve a general idea on what kinds of structure have been converted to THF solubles, or what kinds of reactions are actually catalyzed by the catalyst during the liquefaction, the percentages of aliphatic and aromatic carbon that have been reacted are calculated from the amounts of dry, mineral-matter-free coal charged, aromaticity of the dried coal, the conversions, and the aromaticities of the residues. In Figure 4, the extent of reacted aliphatic carbon is shown as a function of temperature. At each temperature, the lowest point always corresponds to the reactions with no

solvent and no catalyst. As expected, these reactions with the worst liquefaction conditions result in the lowest conversion of aliphatic carbon. Comparing the effects of the solvents, the catalyst and temperature, the latter is shown to be the most significant by the fact that highest conversion of aliphatic carbon at one temperature is always lower than the lowest conversion at the next temperature (except that between 400°C and 450°C). Roughly speaking, all the points stay on one curve, regardless of the use of solvent or catalyst. The amount of reacted aliphatic carbon increases nearly linearly when the temperature increases, up to 400°C. At 400°C, about 90% of the aliphatic carbon has been converted to THF solubles. When the reaction temperature was further increased to 450°C, the increase of the reacted aliphatic carbon became insignificant, from 90% to about 95%. This study suggests that, like the yields of the gases, the conversion of aliphatic carbon from coal to THF solubles is a function mainly of temperature, neither solvent nor catalyst has any influence on it. In Figure 5, the amount of aromatic carbon converted to THF solubles is plotted versus the temperature. Unlike those in Figure 4, the data are much more scattered in Figure 5. In non-catalytic liquefaction reactions, tetralin made a remarkable difference from 1-MN and no solvent. When the temperature was 350°C or higher, much more of the aromatic carbon reacted in the presence of tetralin. At 450°C, the conversion of aromatics reached 86% with tetralin, while it only reached 15% and 10% with 1-MN and without solvent respectively. In catalytic liquefaction reactions, the difference caused by the solvents is diminished when the temperature increases to 400°C, indicating that the catalyst is sufficiently active in converting the aromatics into THF solubles and that solvent is no longer a major determining factor. However, when the temperature increased to 450°C, with the presence of the catalyst, reactions with 1-MN or without a solvent have a large decrease from 77% to 36% and from 93% to 42% respectively, while that with tetralin increased from 87% to 92%. At temperature as high as 450°C, the thermal cracking of the coal matrix is very fast, and the hydrogenation from the gaseous H_2 catalyzed by the added catalyst is no longer able to catch up. Therefore at 450°C in the presence of the catalyst, tetralin is no longer a minor factor. In fact , the only way to prevent the retrogressive reaction is to have a donor solvent, such as tetralin.

The study of reacted aliphatic and aromatic carbon helps to explain why a non-catalytic reaction always produces residues with higher aromaticity than a catalytic reaction even though the conversion can be the same. In the former case, the conversion is achieved by having more aliphatic carbon reacted and in the latter case, it is achieved by having a greater proportion of aromatic carbon reacted. For example, in experiment no. 331, the conversion is 44.0%, there is -8% aromatic (i. e. implying retrogressive aromatization reactions) and 79% aliphatic carbon reacted; while in experiment no. 327, the conversion is 45%, there are 23% aromatic and 63% aliphatic carbon reacted.

SUMMARY

Liquefaction of a Big Brown Texas subbituminous coal was studied in the temperature range from 250°C to 450°C. Tetralin and 1-MN were used as reaction solvents to compare with the reactions without solvent. Ammonium tetrathiomolybdate was used as the catalyst precursor. In thermal experiments, tetralin, a H-donor solvent, was beneficial not only in gaining high conversion but, most importantly, also in gaining high yield of oil at temperatures higher than 350°C. In catalytic experiments, conversions are very similar regardless of solvent used at temperatures up to 400°C, and tetralin does not have an advantage. However, at 450°C, conversions with 1-MN or with no solvent dropped while that with tetralin increased, as well as the oil yield. The gas yields appears to be independent of solvent and catalyst but dependent on temperature.

Cross polarization magic angle spinning of ^{13}C NMR was performed to obtain aromaticities of reaction residues. It is found that in the plot of aromaticity versus conversion, the data fall into two sets: the non-catalytic reactions and the catalytic reactions. With the same conversion, a residue from a catalytic reaction always has lower aromaticity. This is because in a catalytic reaction, more aromatic carbon has been reacted. The study of the amount of aliphatic carbon converted from the coal to THF solubles shows that neither the catalyst nor the solvents has influence on it, but it is a function of temperature. In the case of conversion of aromatic carbon from coal to THF solubles, both the catalyst and the solvents have strong effects. For non-catalytic reactions, tetralin gave much

higher conversions of aromatic carbon than 1-MN or no solvent. For catalytic reactions, there is no difference among the solvents (or no solvent) at temperatures up to 400°C. At temperatures higher than 400°C, tetralin again gave a much higher conversion than the other two cases, indicating that the hydrogen donation by the solvent played a significant role. As for 1-MN and no solvent, compared with the results at 400°C, the conversion of aromatic carbon at 450°C did not increase, in fact it decreased drastically, suggesting that retrogressive reactions occur in these situations.

ACKNOWLEDGEMENT

The authors gratefully thank the United States Department of Energy for the financial support for this work.

REFERENCES

1. Gates, B. C., *Chemtech*, **1979**, 9, 97-102
2. Artok, L., Davis, A., Mitchell, G., Schobert, H. H., *Energy & Fuel*, **1993**, 7, 67-77
3. Artok, L., Schobert, H. H. Energy & Fuel, in press
4. Vernon, L. W., *Fuel*, **1980**, 59, 102
5. Neavel, R. C., *Fuel*, **1976**, 55, 237
6. Schobert, H. H., *Resources, Conservation and Recycling*, **1990**, 3, 111-123
7. Neavel, R. C., in "*Coal Science*", Vol. 1, Academic Press, New York, **1982**, 313
8. Suuberg, E. M., Lee, D., Larsen, J. H., *Fuel*, **1985**, 64, 1688
9. Suuberg, E. M., Unger, P.E, Larsen, J. W., *Energy & Fuel*, **1987**, 1, 305
10. Huang, L., Song, C., Schobert, H. H. *Am. Chem. Soc., Div. Fuel Chem. Prepr.*, **1992**, 37(1), 223-227
11. Garia, A. B., Schobert, H. H., *Fuel*, **1989**, 68, 1613-1615

Table 1. Conversion and yield of non-catalytic reactions

Expt.#	Description	Conv.	Gas	Oil	Asph.	Preasph.
317	250C, NC, NS	11.7	1.9	8.2	0.8	0.8
318	250C, NC, TE	13.3	0.6	6.0	3.7	3.1
319	250C, NC, MN	11.9	2.8	5.6	2.4	1.2
335	300C, NC, NS	16.2	3.5	7.9	0.9	3.9
336	300C, NC, TE	20.8	3.5	9.8	3.5	4.0
337	300C, NC, MN	22.2	3.5	10.2	2.0	6.5
320	350C, NC,NS	19.1	6.5	7.4	1.2	4.1
307	350C, NC,TE	38.2	4.4	18.2	8.3	7.4
309	350C, NC, MN	33.8	5.0	14.8	7.4	6.7
331	400C, NC, NS	45.0	11.6	19.8	3.4	10.2
332	400C, NC, TE	82.0	9.5	36.7	16.6	19.2
334	400C, NC, MN	55.5	9.7	24.4	10.4	11.0
349	450C, NC, NS	51.5	17.6	28.8	0.9	4.2
350	450C, NC, TE	92.2	19.2	49.0	8.4	15.6
351	450C, NC, MN	57.0	16.3	31.8	4.3	4.6

Table 2. Conversion and yield of catalytic reactions

Expt. #	Description	Conv.	Gas	Oil	Asph.	Preasph.
322	250C, ATTM, NS	5.0	0.9	0.0	3.1	3.8
323	250C, ATTM, TE	3.8	0.9	0.0	2.3	1.7
324	250C, ATTM, MN	3.6	0.6	6.0	2.3	2.5
338	300C, ATTM, NS	17.2	2.5	9.3	1.8	3.6
339	300C, ATTM, TE	22.0	0.9	12.4	5.5	3.2
340	300C, ATTM, MN	22.9	2.4	10.2	6.0	4.3
325	350C, ATTM, NS	39.4	4.0	23.2	6.2	6.0
326	350C, ATTM, TE	46.6	3.7	23.9	11.4	7.6
327	350C, ATTM, MN	44.0	3.4	18.5	9.9	12.2
328	400C, ATTM, NS	95.5	7.4	58.9	24.0	5.2
329	400C, ATTM, TE	92.0	6.8	44.3	19.3	21.6
330	400C, ATTM, MN	84.8	8.1	41.6	16.4	18.7
352	450C, ATTM, NS	69.4	18.0	44.6	5.2	1.6
353	450C, ATTM, TE	95.8	14.2	66.1	10.4	5.1
354	450C, ATTM, MN	67.2	16.1	37.4	8.4	5.3

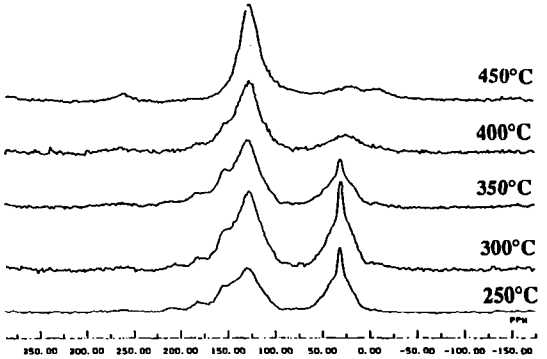

Figure 2. NMR spectra of residues from non-catalytic reactions with tetralin

Table 3. Aromaticity of residues from all liquefaction experiments

T (°C)	nc/ns	nc/tetr.	nc/1-mn	attm/ns	attm/tetr.	attm/1-mn
250.0	0.52	0.50	0.53	0.50	0.52	0.52
300.0	0.55	0.63	0.60	0.45	0.57	0.58
350.0	0.64	0.69	0.74	0.59	0.62	0.66
400.0	0.80	0.85	0.86	0.78	0.76	0.72
450.0	0.89	0.91	0.94	0.85	0.94	0.93

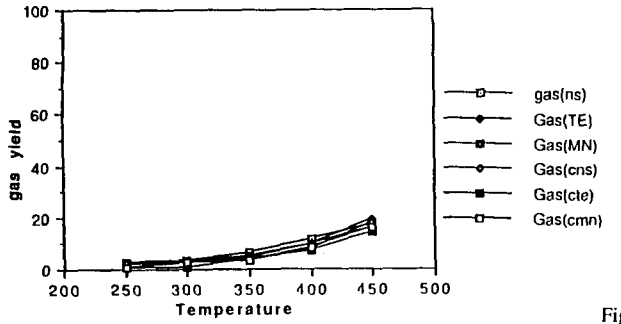

Figure 1. Gas yield of all liquefaction experiments

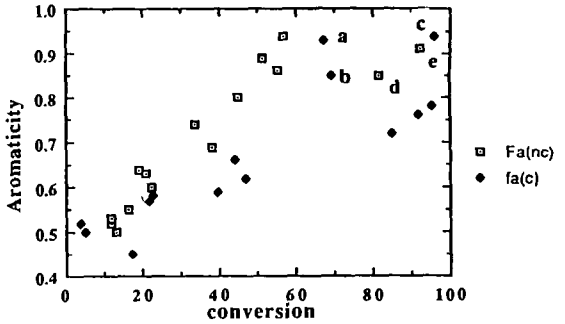

Figure 3. Aromaticity of residues from all experiments as a function of conversion a, b, c, aromaticities of catalytic reaction at 450°C with 1-MN, no solvent and tetralin respectively; d, e, aromaticities of residue from non-catalytic reactions with tetralin at 400°C and 450°C.

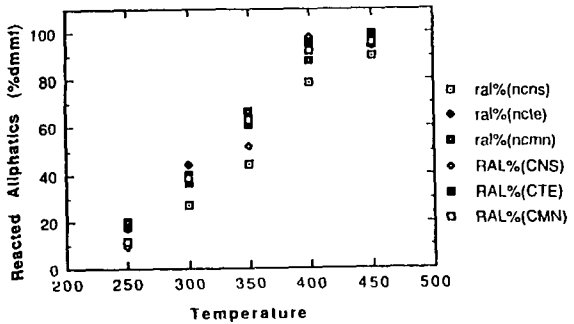

Figure 4. Reacted aliphatic carbon as a function of temperature

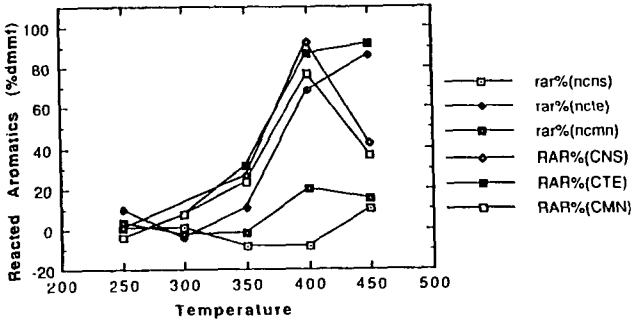

Figure 5. Reacted aromatic carbon as a function of temperature

A Novel Synthesis Route for Liquid Fuels from Coal-derived Syngas

Makarand Gogate, Conrad J. Kulik#, and Sunggyu Lee
Process Research Center
Department of Chemical Engineering
The University of Akron
Akron, Ohio 44325-3906

#Fuel Science Program
Electric Power Research Institute
Palo Alto, California 94303

Keywords: MTG Process, Methanol, Indirect Coal Liquefaction, Synthetic Fuels

Abstract

Coal-derived syngas can be converted to methanol using Liquid Phase Methanol Synthesis Process. Methanol can be further converted to gasoline using the Mobil Methanol-To-Gasoline (MTG) process. The combination of commercial syngas-to-methanol technology with the MTG Process thus provides a ready synthetic route for liquid hydrocarbon fuels. We have developed a novel process for one-step synthesis of Dimethyl Ether (DME) from syngas. This DME Synthesis improves the reactor productivity and syngas conversion, by as much as 100%, over LPMeOH Process. One-step DME synthesis is thus an ideal front-end for further conversion to gasoline. This substitution is justified not only because DME yields an identical product distribution as methanol, DME is also a true intermediate in the Mobil MTG process. The novel integration scheme has been termed as the Dimethyl Ether-to-Gasoline (DTG) process. The advantages of the UA/EPRI DTG Process over the conventional Methanol-to-Gasoline Process are in (a) enhanced syngas conversion, (b) superior hydrocarbon yield, (c) superior product selectivity, (d) alleviated heat duties, and (e) integrated energy efficiency. These and other salient features of this novel synthesis route for liquid fuels have been discussed.

Introduction

The conversion of syngas to gasoline occurs typically in two stages. Syngas is first converted to methanol over a copper-based hydrogenation catalyst. In the second stage, methanol is converted to gasoline over a ZSM-5 catalyst. These two process steps form the basis for the Mobil Methanol-To-Gasoline (MTG) Process [1-3, 12, 15]. Dimethyl Ether (DME) is a key intermediate chemical species in the second stage. Mobil's MTG process in combination with the commercial syngas to methanol technology thus provide a ready route to synthetic gasoline, i.e., with feedstocks other than petroleum.

The first stage of the MTG process is the synthesis of methanol from syngas. In a typical Liquid Phase Methanol Synthesis (LPMeOH^{TM}) process, the synthesis catalyst (composed of CuO, ZnO, and Al_2O_3) is slurried in an inert hydrocarbon oil [14, 16]. Syngas (H_2, CO, and CO_2) reacts over the active catalyst to produce methanol in-situ. The reaction chemistry for methanol synthesis in the liquid phase from CO-rich syngas has been well-established to be [4-6, 8, 9, 13, 16, 17]:

$$CO_2 + 3\,H_2 = CH_3OH + H_2O \quad (1)$$
$$CO + H_2O = CO_2 + H_2 \quad (2)$$

Syngas-to-methanol conversion technology has recently been modified and improved to synthesize Dimethyl Ether (DME) directly from syngas in a single reactor stage [4-7, 10]. This process augments the per-pass syngas conversion and volumetric reactor productivity as a result of reduced chemical

equilibrium limitation governing the syngas-to-DME conversion. The reaction chemistry for typical single-stage DME synthesis from CO-rich syngas can be written as [7]:

$$CO_2 + 3\,H_2 = CH_3OH + H_2O \quad (3)$$
$$CO + H_2O = CO_2 + H_2 \quad (4)$$
$$2\,CH_3OH = CH_3OCH_3 + H_2O \quad (5)$$

In the Liquid Phase DME Synthesis (LP-DME) process, DME is thus directly produced from syngas, in a single reactor stage. As seen from the reaction sequence, the reaction scheme is a combination of an equilibrium limited reaction (#3, methanol synthesis) and an equilibrium unlimited reaction (#5, DME synthesis, or, methanol dehydration). Reactions #3 and #4 occur over the coprecipitated $Cu/ZnO/Al_2O_3$ catalyst, while reaction #5 occurs over gamma-alumina. The LP-DME synthesis is thus based on the application of dual catalysis in the liquid phase [10, 11].

This process can be an effective substitute for the syngas-to-methanol step in the Mobil MTG Process. This substitution is justified based on the following facts (a) DME results in virtually identical hydrocarbon product distribution as methanol and (b) DME is a true intermediate in the Mobil MTG process. The single-stage conversion of syngas to DME (and methanol) thus provides an ideal front-end for further conversion to gasoline.

A novel syngas-to-gasoline process based on this unique integration scheme (Syngas-to-DME and DME-to-Gasoline) has been proven to be superior to the Mobil MTG process. Block diagrams of the conventional Syngas-to-Methanol-to-Gasoline and our novel Syngas-to-DME-to-Gasoline have been shown in Figures 1 and 2. Our novel synthesis process for hydrocarbon fuels has been termed as the UA/EPRI Dimethyl Ether -To- Gasoline (DTG) process. The DTG process merits over the Mobil MTG are in the areas of heat duty, heat of reaction, adiabatic temperature rise, space time and velocity, reactor size, hydrocarbon product yield, and selectivity. These have been conclusively validated in the following sections.

Results and Discussion

1. Heat of Reaction:

The conversion of methanol to hydrocarbons is an exothermic reaction. Depending on the nature and spectrum of the hydrocarbon product, the heat of reaction will vary. In the simple case when water is the only byproduct, the conversion can be represented stoichiometrically as:

$$CH_3OH \Longrightarrow [CH_2] + H_2O \quad (6)$$

The heat of reaction of methanol conversion to hydrocarbons is a function of the product distribution, or alternately, that of space velocity. Thus, to calculate the heat of reaction of methanol (or, DME) conversion to hydrocarbons, the product distribution spectrum at a fixed space time is necessary. These have been summarized elsewhere [1, 2]. Based on these calculations (at one sample space velocity of 108), the heat of reaction for DME conversion to hydrocarbons (-142 cal/g) was found to be 32% less than that for methanol conversion to hydrocarbons (-211 cal/g). Overall, since methanol dehydration to DME contributes about 25% to the total heat of reaction of the methanol conversion to hydrocarbons, it is expected that the heat of reaction for DME conversion to hydrocarbons at complete conversion would be about 25% lower than that for methanol conversion.

2. Selectivity and Product yield:

The conversion of methanol to water and hydrocarbons is essentially stoichiometric and complete. The stoichiometric representation of the reaction is:

$$CH_3OH \Longrightarrow [CH_2] + H_2O \quad (7)$$

where $[CH_2]$ is the average composition of the hydrocarbon product comprising of paraffins and aromatics. Water is the only co-product. The final stoichiometric composition for methanol conversion then would be [12+2 = 14] gatoms of $[CH_2]$ and [2+16 = 18] gatoms of $[H_2O]$. The stoichiometric

product ratio then becomes 14 g to 18 g. This translates to a 44:56 weight ratio basis of the hydrocarbons to water. The selectivity towards hydrocarbons for methanol conversion is then 0.44 g of hydrocarbons / g methanol.

For the conversion of DME to hydrocarbons and water, the stoichiometric representation of the reaction is:

$$CH_3OCH_3 \Longrightarrow [CH_2.CH_2] + H_2O \qquad (8)$$

where $[CH_2.CH_2]$ is the average composition of the hydrocarbon product. The final stoichiometric composition for DME conversion would then be [12+2+12+2 = 28 gatoms] of hydrocarbons and [2+16 = 18 gatoms] of water. This stoichiometric ratio then becomes 28 g to 18 g. This translates to a product ratio of 60.8 : 39.2 weight basis ratio of hydrocarbons to water. The selectivity towards hydrocarbons is then 0.61 g hydrocarbons/ g DME. The reactor productivity would then be 0.61 g/unit volume of the reactor, when compared 0.44 g for methanol case, this is 38% higher for the DME conversion.

3. Space Velocity and Reactor Size:

The conversion of methanol and DME to hydrocarbons is a function of space velocity (or, space time in the reactor). The reaction paths for methanol and DME conversion [2] bring out this fact in greater detail. A substantially more space time (or, contact time) is needed for complete and stoichiometric conversion of methanol to hydrocarbons when compared to that needed for DME conversion to hydrocarbons. The relative difference between the space times for these two cases is estimated at 1 magnitude of space time (1/ [g reactant/g cat. h]). Based on the reaction paths given in [1], it is estimated that for identical space time, the DTG reactor size can be about 25% lower than of the MTG reactor, for complete and stoichiometric conversion. Conversely, for identical MTG and DTG reactor size, the DTG reactor will be 25% more productive (i.e., reactor productivity per unit volume) than the MTG reactor.

4. Overall Comparison and Analysis:

Sections (1-3) have elucidated the rationale and the philosophy behind operating the novel Syngas-to-DME-to-Gasoline process, as against the conventional Syngas-to-Methanol-to-Gasoline process. The conclusive advantages of this novel synthesis route (DTG) have been summarized as follows. These advantages have also been summarized in Table I.

[1] One-step conversion of syngas to DME improves the per-pass syngas conversion and reactor productivity over syngas to methanol. The comparison of our experimental results are as follows. At 250 ^{o}C, 70 atm, 1-liter slurry reactor, per-pass syngas conversion to methanol is 53%. At nominally identical operating conditions, per-pass syngas conversion to DME is at 74%. Starting with 1 gmol of syngas, this translates to about 0.47 gmol of recycle / gmol of syngas for syngas to methanol case. The recycle load is reduced to only 0.26 gmol / gmol of syngas for the syngas to DME case. The recycle load is thus reduced by about 46%.

[2] The conversion of syngas to methanol uses copper-based $Cu/ZnO/Al_2O_3$ catalyst. This catalyst is susceptible to deactivation by crystal growth in the liquid phase rich in methanol and water. However, the conversion of syngas to DME uses a dual catalyst system based on a combination of $Cu/ZnO/Al_2O_3$ catalyst and gamma-alumina catalyst. This conversion offers a favorable scenario for crystal growth of copper catalyst because of two reasons. First, the liquid phase is lean in methanol because of in-situ conversion to DME over gamma-alumina. Second, water produced by both methanol synthesis (CO_2 hydrogenation) and DME synthesis (methanol dehydration) constantly is shifted by the forward water gas shift reaction. This is perhaps the most significant merit of the one-step conversion of syngas to DME, a fact well-proven by the research at the University of Akron. The reaction chemistry of syngas to DME conversion is as follows, starting with CO-rich or the so-called unbalanced syngas:

$$CO_2 + 3\,H_2 = CH_3OH + H_2O \qquad (9)$$
$$CO + H_2 = CO_2 + H_2 \qquad (10)$$
$$2\,CH_3OH = CH_3OCH_3 + H_2O \qquad (11)$$

[3] The one-step conversion of syngas to DME improves the volumetric reactor productivity by as much as 100%, over that of syngas to methanol conversion. This is because of conversion of syngas to DME is not nearly limited by chemical equilibrium as syngas to methanol. This fact has been well-proven by the research at the University of Akron. For example, at 250 ^{o}C at 70 atm, starting with 1 gmol of unbalanced syngas, methanol yield is about 0.14 gmol, or, 0.14 gmol (CH_3) equivalent. At identical conditions, the yield of DME is about 0.12 gmol, or, 0.24 gmol of (CH_3) equivalent. This corresponds to an increase of about 72% in the reactor productivity, at identical conditions.

[4] The conversion of methanol to gasoline is highly exothermic with a heat of reaction of 398 cal/g of methanol converted. For this reason, the conversion is usually split in two parts, for exothermic heat management. In the first, methanol is converted to an equilibrium mixture of DME, water (and unconverted methanol). In the second, this mixture of methanol, DME, and water is converted to gasoline. The first step contributes to about 25% of the total exothermic heat of reaction. The conversion of DME to gasoline is thus about 25% less exothermic, with a heat of reaction of about 300 cal/g of DME converted.

[5] . As elucidated in point [4], the conversion of methanol to gasoline requires the conversion of methanol to methanol, DME, and water first, to manage the exothermic heat of reaction. The one-step conversion of syngas-to-DME followed by DME conversion to gasoline thus obviates the need for a separate methanol dehydration reactor. This contributes to significant savings in capital and operating cost.

[6] The adiabatic temperature rise in the conversion of methanol to gasoline is estimated at about 650 ^{o}C, while that for the conversion of DME to gasoline is only at about 475 ^{o}C.

[7] In methanol to gasoline conversion, equilibrium mixture of DME, water, and methanol is usually fed to the gasoline synthesis reactor. The ZSM-5 based zeolite catalyst is extremely sensitive to water in the feed (water is a catalyst poison). For this reason, water is removed from the feed. In the conversion of DME to gasoline, very little to no water is fed to the gasoline synthesis reactor, because the single-step syngas-to-DME conversion produces DME with extremely high selectivity (>99%). Catalyst life cycle in the gasoline synthesis reactor is favorable in the direct conversion of DME-to-gasoline because of (a) lower concentrations of water in the reactor and (b) about 25% reduced exothermicity of the reaction.

[8] The stoichiometric conversion of methanol to gasoline produces 44 % (w/w) to 56 % (w/w) mixture of hydrocarbons to water. For example, 1 g of methanol yields 0.44 g hydrocarbons [CH_2] and 0.56 g water, at complete and stoichiometric conversion. On the contrary, 1 g DME yields 0.61 g hydrocarbons [CH_2] and only 0.39 g water. The yield of gasoline hydrocarbons for DME conversion is thus 38 % higher than that for methanol conversion. The yield of water is concomitantly 30 % lower for the DME conversion case.

[9] Hydrocarbon product distribution is directly related to the space time for both methanol and DME conversion. For methanol conversion, the reactor space time is estimated to be 20% higher than that for DME conversion, to achieve a stable hydrocarbon product distribution. Intuitively also, this can be immediately validated considering that reaction path of methanol conversion to hydrocarbons involves DME as the intermediate. At identical space time, the DTG reactor size can be 25% lower than the conventional MTG reactor.

[10] Finally, there are important differences between two cases of syngas-to-DME-to-gasoline process, where syngas is derived from coal or from natural gas. Syngas derived from coal is CO-rich (or, unbalanced), while that derived from natural gas is H_2-rich (or, stoichiometric). These differences are in the areas of:

(a) recycle load (about 0.34 gmol / gmol for coal vs 0.52 for NG case).
(b) CO_2 rejection is mandatory in coal-based syngas. CO addition is necessary for NG.
(c) overall [CH_2] productivity is about 30% higher for coal-based syngas.
(d) overall, coal-based syngas process is more attractive. However, the availability and price of coal in comparison to NG remains a primary concern.

Conclusions

Process comparison and analysis of Syngas-to-Methanol-to-Gasoline and Syngas-to-DME-to-Gasoline conclusively proves that synthesis of gasoline via direct DME route has definitive process advantages over the synthesis via methanol route. These process merits are in the areas of higher gasoline yield, higher syngas conversion, good adaptability to coal-based syngas, and integrated energy efficiency. Further experimental investigation to establish these merits is currently underway at the University of Akron.

Acknowledgments

This work was completely supported by the Electric Power Research Institute, via the research contract RP317-6. The authors (Makarand Gogate and Sunggyu Lee) are also thankful to Conrad J. Kulik for his continued support and help throughout the course of this project.

References

1 Chang, C. D. and Silvestri, A. J., "The Conversion of Methanol and other O-Compounds to Hydrocarbons over Zeolite Catalysts", J. Catal., 47, 249-259, 1977.

2. Chang, C. D., "Hydrocarbons from Methanol", Cat. Rev. - Sci. Eng., 25 (1), 1-118, 1983.

3. Chang, C. D. and Silvestri, A. J., "MTG Origin and Operation, CHEMTECH, 10, 624-631, 1987.

4. Gogate, M. R., Lee, S., and Kulik, C. J., "A Single-Stage, Liquid-Phase Dimethyl Ether (DME) Synthesis Process from Syngas I. Dual Catalytic Activity and Process Feasibility", Fuel Sci. Tech. Int'l, 9(6), 653-679, 1991.

5. Gogate, M. R., Lee, S., and Kulik, C. J., "A Single-Stage, Liquid-Phase Dimethyl Ether (DME) Synthesis Process from Syngas II. Comparison of Per-pass Syngas Conversion, Reactor Productivity, and Hydrogenation Extent", Fuel Sci. Tech. Int'l, 9(7), 889-912, 1991.

6. Gogate, M. R., Lee, S., and Kulik, C. J., "Synthesis of Hydrocarbons Via Single-Stage DME Route", Paper Presented at AIChE National Meeting, New Orleans, Louisiana, March 29 - April 2, 1992.

7. Gogate, M. R., "A Novel Single-Step Dimethyl Ether (DME) Synthesis from Syngas", Ph.D. Dissertation, The University of Akron, Akron, Ohio, 1992.

8. Lee, S., Methanol Synthesis Technology, CRC Press, Boca Raton, Florida, 1990.

9. Lee, S. and Parameswaran, V. R., "Reaction Mechanisms in Liquid Phase Methanol Synthesis Process", Interim Report ER/GS-6715, Electric Power Research Institute, Palo Alto, California, 1991.

10. Lee, S., Gogate, M. R., and Kulik, C. J., "A Novel Single-Stage Dimethyl Ether (DME) Synthesis Process over Dual Catalyst System from CO-rich Syngas", Chem. Eng. Sci., 47(13/14), 3769-3776, 1992.

11. Lewnard, J. J., Hsiung, T. H., White, J. F., and Brown, D. M., "Single-Step Synthesis of Dimethyl Ether in a Slurry Reactor", Chem. Eng. Sci., 45 (8), 2735-2741, 1990.

12. Meisel, S. L., "Catalysis Research Bears Fruit", CHEMTECH, 1, 32-37, 1988.

13. Parameswaran, V. R., "Roles of Carbon Dioxide and Water in Liquid Phase Methanol Synthesis", Ph. D. Dissertation, The University of Akron, Akron, Ohio, 1987.

14. Parasmeswaran, V. R., Gogate, M. R., Lee, B. G., and Lee, S., "Mass Transfer in the Liquid Phase Methanol Synthesis Process", Fuel Sci. Tech. Int'l, 9(6), 653-679, 1991.

15. Sardesai, A., Gogate, M. R., Fullerton, K. L., and Lee, S., "Fluidized Bed Synthesis of Hydrocarbons from Dimethyl Ether - Design and Operation", Fuel Sci. and Tech. Int'l, In Press, 1993.

16. Sawant, A. V., "The Effects of Carbon Dioxide, Water, and Thermal Aging on the Liquid Phase Methanol Synthesis Catalyst", Ph. D. Dissertation, The University of Akron, Akron, Ohio, 1987.

17. Sherwin, M. and Blum D., "Liquid Phase Methanol", Final Report EPRI AF-1291, Electric Power Research Institute, Palo Alto, California, 1979.

Table I

Syngas-to-Methanol-to-Gasoline Vs.Syngas-to-DME-to-Gasoline

		MTG	DTG
Syngas-to-Methanol Vs. Syngas-to-DME			
1)	productivity, g product#	10.9	11.8
2)	hydrogen conversion, %	72.4	87.7
3)	CO conversion, %	38.2	62.3
4)	syngas conversion, %	53.0	73.4
5)	recycle, gmol / gmol feed syngas	0.47	0.27
6)	heat of reaction, cal (exothermic)	8008	13745
7)	catalyst life	good	better
Methanol-to-Gasoline Vs. DME-to-Gasoline			
8)	productivity, g [CH_2]#	4.79	7.46
9)	conversion, %	100	100
10)	heat of reaction, cal / g (exothermic)	398	300
11)	adiabatic temperature rise, °C	600	475
12)	reactor size at identical WHSV	1.25	1
13)	catalyst life	poor	better
14)	methanol dehydration reactor	necessary	not nec.
15)	water concentration in the reactor	high	low
16)	overall water production, g [H_2O]	6.16	5.15
17)	[CH_2] selectivity, g / g converted	0.44	0.61
18)	[H_2O] selectivity, g / g converted	0.56	0.39
19)	Overall hydrogen consumption, g [CH_2] / g	3.42	4.31

#On basis of experimental data, 2.68 mol (= 50 g) syngas feed, 250 °C, 70 atm, 1-Lit Autoclave.

#On basis of complete and stoichiometric conversion, 375 °C, 1 atm, feed item (1).

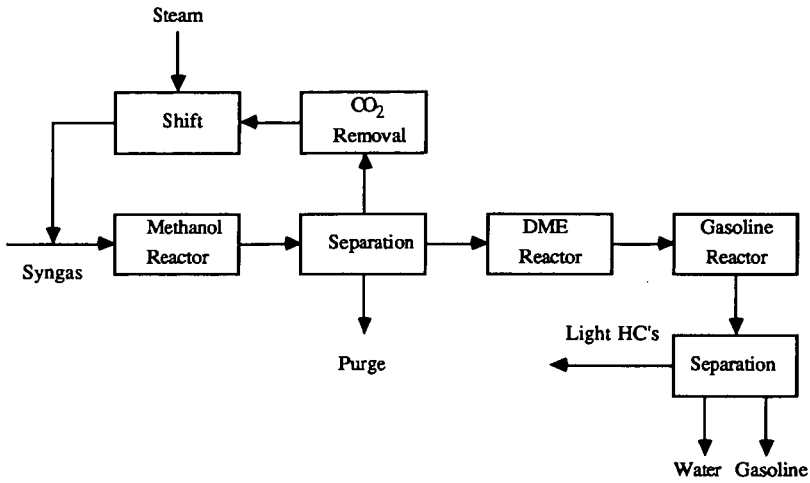

Figure 1. Syngas-to-Methanol-to-Gasoline-Methanol Condensation -Low Pressure Gasoline Reactor.

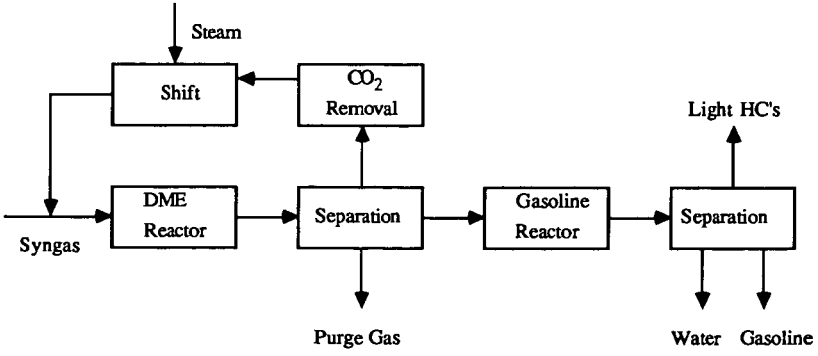

Figure 2. Syngas-to-DME-to-Gasoline-DME Condensation -Low Pressure Gasoline Reactor.

SURFACE CHARACTERIZATION OF IRON OXIDE DISPERSED ON SUBBITUMINOUS COAL.

H. Ni, R. K. Anderson, E. N. Givens and J. M. Stencel
University of Kentucky Center for Applied Energy Research
3572 Iron Works Pike, Lexington, KY 40511-8433

Keywords: Iron oxide, coal liquefaction, X-ray photoelectron spectroscopy

ABSTRACT
The preparation and characterization of Wyodak subbituminous coal impregnated with 0.1-1.0 wt% iron by the incipient wetness technique have been studied. X-ray photoelectron spectroscopy (XPS) was used to examine the surface chemistry versus the bulk composition of the iron oxide loaded on the coal particles. The effects of Fe concentration, NH_4OH/Fe ratios and coal drying on the speciation of Fe are reported. The relative concentration of FeOOH and Fe_2O_3 on the surface is a function of coal drying. The direct liquefaction performance of the different Fe loaded coal samples is related to the specific Fe concentrations.

INTRODUCTION
Small particle iron oxide catalyst precursor deposited on coal by an incipient wetness (IW) technique provided improved conversion and distillate yields in direct liquefaction.[1] In this technique coal is impregnated with a metal salt solution which when added to the coal reaches the point where unbound moisture begins to form drops.[2] In the case of iron salts, addition of base produces finely divided iron oxyhydroxide. SEM analysis showed that iron impregnated by IW using $FeCl_3 \cdot 6H_2O$ was primarily deposited on the surface of the coal.[3] Subsequently, coal is dried to remove the excess moisture before subjecting it to liquefaction. Sulfidation that occurs during liquefaction presumably does not result in any significant growth of the iron particles upon conversion to pyrrhotite,[4] although recent results indicate that pretreatment at lower temperatures provide increased liquefaction performance because of more efficient conversion of the precursor oxide to pyrrhotite.[5] Distillate yields from liquefaction of 5000 ppm Fe-impregnated Wyodak coal were greater than from the corresponding liquefaction when using pigment grade iron oxide plus added sulfur.[6]

Impregnating coals by IW is a multi-step process involving first the distribution of the metal solution onto the coal, after which the oxide is formed, presumably at the point of contact with the base material. Since preparation proceeds through a series of steps involving coal preparation, metals impregnation, base precipitation, filtration, washing, and drying, all which may alter the subsequent liquefaction performance of the impregnated coal.

This paper describes the results of a study to evaluate the performance of an Fe-impregnated Wyodak coal. The effects of several independent variables in the preparation scheme on metal dispersion and chemical form were investigated using XPS. This technique has been used not only to analyze the surface composition of coals[7] but also to characterize the surface composition, elemental distribution and chemical state of the Fe-O system, including Fe_2O_3, Fe_3O_4, FeO, and FeOOH.[8] In addition, the conversion and product distribution from liquefaction of several of

these Fe-impregnated coals are discussed.

EXPERIMENTAL

Impregnated Coals - Wyodak coal from the Black Thunder Mine in Wright, Wyoming, which was provided by CONSOL, Inc., was ground to -200 mesh, riffled and stored under nitrogen at 4°C. Proximate and ultimate analyses of the coal are presented in Table 1. IW-coal samples were prepared starting with either as-received coal or coal predried at 110°C/10 Torr/20 hrs. The moisture content and the volume of water used in the IW-impregnation of as-received coal were 21 wt% and 0.75 ml/g dry coal, respectively, and for impregnation of predried coal were 2-3 wt% and 0.90 ml/g dry coal, respectively. Solutions containing $Fe(NO_3)_3 \cdot 9H_2O$, purchased from Aldrich Chemical Co., were slowly added in a dropwise manner to the coal while mixing to assure even distribution. 1.5M NH_4OH was added to these samples at a NH_4OH/Fe mole ratio from 31 to 138. The aqueous slurries were filtered and the samples were dried at 40°C/20 hrs/10 Torr, unless otherwise specified. Water washing, if performed, preceded the drying step.

XPS Measurements - The XPS of the various samples of Fe impregnated coal was carried out with the LHS-10 Leybold-Heraeus Spectroscope using Mg K_α radiation with 15 Kv, 20 mA and pass energy of 100 ev. The powdered samples were mounted on the XPS sample probe with Double-Stick Scotch tape. The sample powders were gently pressed and covered all of the Scotch tape attached on the stainless steel foil. The analysis chamber vacuum was about 5×10^{-9} Torr. The C_{1s}, O_{1s}, Fe_{2p}, Fe_{3p}, N_{1s}, Ca_{2p}, Al_{2p}, Si_{2p}, and S_{2p} elemental spectra and the survey spectra of the coal samples were obtained under the above working conditions and corrected with the hydrocarbon C_{1s} binding energy 284.6 ev. The elemental concentrations were calculated and the peak deconvoluted with a computer aided program of damped non-linear least squares curve fitting, using mixed Gaussian/Lorentzian profiles.[9]

Equipment and Procedures - Liquefaction experiments were performed in 50 ml microautoclaves to which were added 3 grams of coal, 5.4 grams of tetralin, and 1.2 mol dimethyl disulfide/mole added Fe. The reactors were sealed, pressurized with hydrogen to 1000 psig, and leak tested. Reactions were carried out in a fluidized sandbath set at the specified temperature while the reactors were continuously agitated at a rate of 400 cycles per minute. Reactors were then quenched to ambient temperature, the gaseous products collected and analyzed, and the products separated into THF insoluble (IOM), THF soluble-pentane insoluble (PA+A), and pentane soluble (oils+water) fractions. The product distribution was calculated assuming complete recovery of ash and conversion of catalyst to pyrrhotite ($Fe_{0.9}S$). The total of the net products equals the amount of maf coal in the feed and reflects the net make of each of the solubility fractions; coal conversion equals 100 minus the yield of IOM.

RESULTS AND DISCUSSION

The volume of water used in the IW-impregnation of as-received coal containing 21 wt% moisture was 0.75 ml/g, which was 20% less than for dry coal (0.90 ml/g). Ferric nitrate has sufficient solubility that this difference in the volume of water was not limiting. The incorporation of the metal onto the coal was essentially quantitative as determined by analysis of filtrates collected during preparation. The analysis of filtrates from addition of 1.5M NH_4OH, which causes precipitation of Fe as FeOOH, and filtrates from subsequent water

washes, indicated negligible Ca exchange and Fe bypass (see Table 2). In the NH_4OH treatment, only 0.1 wt% of the Ca originally in the coal was removed with about the same amount recovered in a subsequent water wash. Less than 0.01 wt% of the Fe added to the coal was found in both filtrates. The extent of NH_4^+ exchange corresponding with formation of ammonium carboxylates is presumably quite small. NO_3^- recoveries in the NH_4OH filtrates ranged from 83 wt% up to 119 wt% and were accurate only to ±20%. The absence of NO_3^- ions in the washwater filtrate indicates substantially complete removal in the NH_4OH filtrate which makes water washing unnecessary.

Fe Distribution - Surface and bulk concentrations determined for metals (Fe, Ca, Al, Si), C, O, N and S for both impregnated as-received and predried coals are presented in Table 3. The surface of the dry as-received Black Thunder coal without any added Fe is enriched in the concentration of Fe, O, Al and Si, which reflects particle fracturing along the mineral surfaces during grinding. In the impregnated samples, the Fe concentration on the surface was significantly higher than in the bulk and increased with the amount of added Fe. In those samples that were final dried at 40°C/10 Torr/20 hrs, the concentration on the surface reached 6.3 wt% (CH-41) at the 1.0 wt% Fe addition level versus 12.5 wt% (CH-45) in the sample dried in flowing nitrogen at 40°C/20 hrs, the maximum observed in this study. This difference in surface Fe concentration suggests significant penetration of the iron within the cracks, crevices and pores of the coal particles. For each of these samples the relative concentration of oxygen on the surface increased as the iron concentration increased. Carbon fluctuated between samples and sulfur was generally lower at the surface relative to the bulk.

The increased surface Fe concentration of two impregnated predried samples suggests that diffusion of the Fe salt into these coals was hindered. Thermal pretreatment apparently results in sufficient transformation within the coal structure to block diffusion of the Fe-containing aqueous phase into the particle. Maintaining the integrity of the aqueous phase within the particle, as in the as-received samples, promotes diffusion of the Fe ions into the particle.

Surface Chemistry - Fe-IW impregnated coals show XPS spectra with Fe_{2p} peaks appearing at 711.2 ev ($Fe_{2p\ 3/2}$) and 725.1 ev ($Fe_{2p\ 1/2}$), Fe_{3p} at 56.6 ev and O_{1s} at 531.3 ev. The known spectra of FeOOH provides a good fit with the observed spectra. For those coals having low Fe loadings the O_{1s} peak is shifted to a higher binding energy of 532.4 (CH-20, CH-11) which approaches that of the O_{1s} binding energy in the spectra of the starting coal. This higher binding energy is consistent with greater participation of the O_{1s} peaks for Al_2O_3 and SiO_2, which are located at 531.8 and 532.8 ev, respectively. The binding energy of the N_{1s} peak was found to be 399.5 ev which is consistent with organic nitrogen in the coal which precludes the presence of any significant amount of NH^+ or NO_3^-. Interpretation of the form of the added Fe is not complicated by the iron in the original coal since the $Fe_{2p\ 3/2}$ peak at 709.3 ev and a Fe_{3p} peak at 52.3 ev are considerably lower than observed. These lower binding energies are consistent with Fe-O and Fe-S structures. For the samples dried at about 110°C (CH-2), the decrease in the Fe_{3p} binding energy to 56.0 ev indicates the appearance of Fe_2O_3 that occurs as the FeOOH particles on the surface agglomerate. Likewise, deconvolution of the O_{1s} envelope indicates a lower binding energy peak at 530.0 ev consistent with the presence of the Fe_2O_3 species. In general, the Fe_{2p} spectra are broadened and highly complex due to multiplet splitting

effects which are characteristic of oxides. The samples developed significant electrical charge during analysis consistent with the low electrical conductivity of Fe oxyhydroxide.

Liquefaction of Impregnated Coals - No significant effect on THF conversion or product distribution was observed as a result of varying the NH_4OH treatment over a range of NH_4^+/Fe ratios from 31 to 138. Likewise, subjecting the coals to a final wash also had no effect on liquefaction. Fe, however, had a definite effect on both oil yield and THF conversion as shown in Table 4. A sharp increase in both THF conversion and oil yield occurred with addition of 2800 ppm Fe; conversion increased from 81 wt% to 86 wt% while oils+water increased from 38 wt% to 44 wt%. Further addition of Fe up to 1.0 wt% resulted in smaller increases in both conversion and oil+water yields.

CONCLUSIONS

XPS spectra show a high degree of Fe dispersion on the coal surface with significant diffusion of Fe into the cracks, crevices and pore structure of the coal. The surface Fe concentration was higher on coals predried at 110°C before adding the Fe salt, indicating reduced metal diffusion into the coal. XPS supports Fe being present both as FeOOH and Fe_2O_3. Addition of 2800 ppm Fe causes a sizable increase in both THF conversion and oils+water yield. Increasing the Fe concentration up to 1 wt% causes still further increases in both conversion and oil+water yield, though to a lesser extent.

ACKNOWLEDGEMENT

Financial support was provided by the Commonwealth of Kentucky and the U.S. Department of Energy under contract number DE-AC22-91PC91040.

REFERENCES

1. B. R. Utz, A. V. Cugini and E. A. Frommell, ACS Fuel Div Preprints, 1989, 34(4), p1423; B. R. Utz and A. V. Cugini, "Method for Dispersing Catalyst onto Particulate Material," U.S. Patent 5,096,570, Mar. 17, 1992.
2. D. R. Milburn, B. D. Adkins, and B. H. Davis, Am. Chem. Soc. Div. Fuel Chem. Preprints, 1989, 34(4), p1439
3. D. A. Sommerfield, J. Jaturapitpornsakul, L. Anderson and E. M. Eyring, Am. Chem. Soc. Div. Fuel Chem. Preprints, 1992, 37(2), p749.
4. M. Andres, H. Charcosset, P. Chiche, L. Davignon, G. Djega-Mariadassou, J. P. Joly and S. Pregermain, Fuel, 1983, 62, p69.
5. A. V. Cugini, B. R. Utz, D. Krastman, and R. F. Hickey, ACS Fuel Div Preprints, 1991, 36(1), p91.
6. T. L. K. Lee, A. Comolli, E. Johanson and R. Stalzer, Am. Chem. Soc. Div. Fuel Chem. Preprints, 1993, 38(1), p107.
7. N. S. McIntyre, R. R. Martin, W. J. Chauvin, C. G. Winder, J. R. Brown and J. A. Macphee, Fuel, 1985, 64, p1705; C. Frost, W. R. Leeder, R. L. Tapping and B. W. Bank, Fuel 1977, 55, p277.
8. N. S. McIntyre and D. G. Zetarak, Analytical Chemistry, 1977, 49, p1521; G. C. Allen, M. T. Curtis, A. J. Hooper, P. M. Tucker, J. Chem. Soc., Dalton Trans., 1974, 14, p1525; C. S. Kuivila, J. Catalysis, 1989, 118, p299-311.
9. A. Proctor, FRYFIT Software, Surface Science Center, Univ of Pittsburgh, Pittsburgh, PA 15260, Version Jan 3, 1992.

Table 1. Proximate, Ultimate and Ash Analysis of Black Thunder Wyodak Coal

	As Received[a]	Dry[b]
Proximate, as-received basis		
Moisture	22.4	2.63
Ash	5.46	5.66
Volatile Matter	34.4[c]	45.47
Fixed Carbon	39.8[c]	46.2
Ultimate, Dry		
Carbon	70.32	72.15
Hydrogen	4.68	4.34
Nitrogen	1.04	1.23
Sulfur	0.50	0.53
Chlorine	0.035	-
Oxygen	16.74	15.93
Ash	6.69	5.81
Ash Composition, wt%		
Fe_2O_3	5.48	-
CaO	21.34	-
Al_2O_3	15.76	-
SiO_2	31.48	-
MgO	4.3	-
Na_2O	0.48	-
K_2O	0.49	-
TiO_2	1.14	-
P_2O_5	0.96	-
SO_3	17.26	-

[a] Analysis provided by Consol, Inc. [b] Dried 110°C/20 hrs/10 Torr. [c]Determined at UK/CAER.

Table 2. Filtrate Analysis[a]

	NH_4OH Filtrate		Washwater Filtrate	
Coal Sample No.	CH-3	CH-21	CH-4[b]	CH-22[c]
Fe^{+3} Added, wt% dry coal	1.0	0.55	1.0	0.55
Ca, wt% dry coal	1.0	1.0	-	-
Calcium Recovery, wt% Ca in dry coal	0.10	0.11	0.12	0.02
Fe Recovery, wt% Added Fe ($\times 10^2$)	0.1	3.0	9.8	3.1
NO_3^- Recovery, wt%[d]	83	93	[e]	[e]

[a] Direct Current Plasma Emission Spectrometry (DCP). [b] CH-4 originated from CH-3. [c] CH-22 originated from CH-21. [d] Measured using ion specific electrode; values ±18%. [e] NO_3^- was not detected in these solutions.

Table 3. Surface Concentration of Elements as Determined by XPS[a,b]

	Starting Coal[c]	Moisture wt%	Added Fe	Fe	C	O[d]	N	Ca	Al	Si	S
As Received	-	22.4		- (0.19)	- (57.8)	- (29.6)	- (1.2)	- (0.75)	- (0.56)	- (1.1)	- (0.46)
CH-BT	AR	2.6	0	0.33	71.1 (70.3)	20.6 (17.8)	1.3 (1.2)	0.5	2.0	4.0	0.2 (0.5)
CH-10	AR	3.6	0.15	1.0	62.3	25.5	1.4	1.0	3.4	3.5	n.a.[e]
CH-11	AR	1.8	0.28	1.4	66.2	23.5	1.7	1.0	2.4	3.5	0.3
CH-13[f]	AR	5.4	0.28	1.9	64.1	23.9	1.7	1.2	3.1	3.8	0.3
CH-1	PD	1.4	0.28	2.7	63.5 (67.4)	24.7 (19.4)	1.7 (1.5)	1.0	2.5	3.6	0.4 (0.4)
CH-20	AR	0	0.55	2.4	63.5	25.2	1.5	1.0	2.9	3.3	0.2
CH-8[g]	AR	5.4	0.77	3.2	66.8 (68.1)	20.2 (19.2)	0.8 (1.8)	0.7	1.9	4.6	n.a. (0.4)
CH-31	AR	2.9	0.77	4.2	62.4	24.8	1.2	1.0	2.5	3.3	0.6
CH-41	AR	2.7	1.0	6.3	59.6	25.6	1.6	1.0	3.8	3.4	0.3
CH-3	PD	3.9	1.0	8.3	54.2 (65.4)	28.2 (21.2)	1.0 (1.6)	0.8	3.8	3.1	0.4 (0.5)
CH-45[f]	AR	6.1	1.0	12.5	49.3	30.7	0.8	0.3	3.8	2.5	0.1

a. ( )Bulk composition, wt% of sample.
b. Starting coal impregnated with $Fe(NO_3)_3 \cdot 9H_2O$ in 0.74 ml water/g for as-received coal and 0.90 ml/g for predried coal, treated with 1.54M NH_4OH at 138 NH_4^+/Fe ratio, vacuum filtered, and dried at 40°C/10 Torr/20 hrs.
c. AR is as-received coal, PD is predried coal at 110°C/10 Torr/20 hrs.
d. Includes oxygen associated with moisture in sample.
e. n.a., not available
f. Dried at 40°C/1 atm/flowing N_2/20 hrs.
g. Washed with 1.54M NH_4OH at 31 NH_4^+/Fe ratio.

Table 4. Product Distribution from Liquefaction of Fe IW-Impregnated Coals

Sample No.		CH-11	CH-20	CH-8	CH-41	CH-45
Fe Added, wt% dry coal	0[a]	0.28	0.55	0.77	1.0	1.0
S/Fe[b]	0	2.9	1.0	1.3	1.2	1.3
Moisture, wt%	1.8	2.5	0	3.4	2.7	6.1
Product, wt% maf coal						
HC Gases	1.0	1.1	1.1	1.1	1.2	1.2
CO_2+CO	4.0	3.7	3.6	4.1	3.9	3.8
Oils + Water	38.3	44.1	44.9	45.1	46.4	48.0
PA + A	37.9	37.5	37.0	38.7	37.9	36.1
IOM	18.8	13.6	13.4	11.0	10.6	10.9
THF Conv	81.2	86.4	86.6	89.0	89.4	89.1
mg H_2/g maf coal	26	38	40	36	40	45

a. Coal dried 90°C/125 Torr/20 hrs.
b. Mole ratio of added S in DMDS to added Fe.

REACTION OF DEUTERIUM-LABELED 1,2-DIPHENYLETHANE WITH H_2

Venkatsubramanian Rajagopal
Robert D. Guthrie
Department of Chemistry
University of Kentucky
Lexington, KY 40506

Buchang Shi
Burtron H. Davis
Kentucky Center for Applied Energy Research
3572 Iron Works Pike, Lexington, KY 40511

Keywords: Scrambling, Isotope Effects

INTRODUCTION

In a previous report, we described experiments carried out in a glass reactor in which 1,2-diphenylethane, **DPE**, was observed to react with D_2 at 450 °C to give extensive deuterium incorporation in both starting **DPE** and reaction products.[1] Examination of compounds present by ^1H and ^2H NMR showed the presence of deuterium in both aliphatic and aromatic positions with somewhat more aromatic D than aliphatic D. Toluene and recovered **DPE** contained similiar amounts of D, 10 - 20% of one atom of D per molecule at low conversions of **DPE** but increasing with increasing conversion. Certain products, benzene, ethylbenzene, and 1,1-diphenylethane, contained initially higher amounts of deuterium, 50% of one atom or greater, signalling distinct mechanistic pathways.

It was thus suggested that benzyl radicals formed through homolysis of the 1,2-bond in **DPE** react mainly with unconverted **DPE** to give toluene and 1,2-diphenylethyl radicals, accounting for the fact that 80% of the initially formed toluene contained no deuterium. The 1,2-diphenylethyl radicals produced were implicated in the removal of D atoms from D_2. Recently we have shown that 1,2-diphenylethyl radicals generated by an alternate path at lower temperatures are, indeed, capable of promoting reaction with D_2.[2] Our earlier work also supported the suggestion of Vernon[3] that H atoms produced through the reaction of radicals with H_2 are responsible for the hydrocracking of **DPE** to give benzene and 2-phenylethyl radicals in that the reaction under D_2 gave ethylbenzene with a relatively high D content in the methyl group and D-enriched benzene.

Because the literature contains abundant evidence that exchange of hydrogens is facile between benzylic positions,[4] we undertook to determine the extent to which transfer of deuterium between various positions in **DPE** might complicate our mechanistic conclusions. To this end we have carried out experiments with **DPE-1,1-d_2** (two aliphatic hydrogens replaced) and **DPE-d_{10}** (aromatic hydrogens replaced). The results force modification of our earlier scheme and lead to important new insights.

RESULTS AND DISCUSSION

1,2-Diphenylethane-1,1-d_2, DPE-d_2. This compound was prepared as described in the Experimental Section. Tables I and II present data obtained by GC/MS on recovered diphenylethane and product toluene from the thermolysis of **DPE-d_2** at 450 °C under N_2 and under H_2. As will be

noted, at short time periods, listed at < 5 min, 96 to 98% of all diphenylethane molecules contain two atoms of D. This is essentially identical to the composition of starting material. The two D atoms in this material and in the starting material are shown to be positioned on the same atom by the mass spectral fragmentation pattern which shows fragments at m/z of 91 and 93 with very little spectral intensity at m/z = 92. After 10 or 15 min at 450 °C, redistribution is evident both under H_2 and under N_2. It is also apparent that the distribution of D atoms does not change significantly with additional heating (30 min). This indicates that equilibrium is reached after roughly 10 min at 450 °C. Significantly, none of the mass spectra show molecular ions containing more than four atoms of D as would be the case if exchange included the aromatic positions.

One experiment was also carried out with a mixture of toluene-1,1,1-d_3 and **DPE**-d_0 for 20 min at 450 °C under H_2. Deuterium transfer to **DPE** was observed, but this was not extensive, indicating that toluene is a less active partner in the exchange process than is **DPE**. This is expected based on the relative stabilities of benzyl radicals and 1,2-diphenylethyl radicals.

The non involvement of the aromatic hydrogens was confirmed by NMR measurements combining ^1H and ^2H NMR in the manner described in our earlier report. These data, shown in Table III, show a small amount of D transfer to the aromatic ring positions under N_2. Aromatic D in the H_2 experiments is too small to detect. NMR experiments on toluene produced showed no significant aromatic D, however, detection limits for toluene were higher because of small sample size. NMR determination of aliphatic D in toluene gave results in agreement with those obtained by MS.

Importantly, it was also observed that the benzene produced in the H_2 runs contained no significant amount of D by MS measurement. The benzene produced in the N_2 runs, albeit formed in very small amount, showed about 25% of one atom of D per molecule. This suggests that a mechanism exists for the expulsion of D atoms from the benzylic positions but that they react with the aromatic ring only in the absence of H_2. This clearly indicates that the reaction $D^{\cdot} + H_2 \rightarrow H^{\cdot} + HD$ is rapid under the reaction conditions.

Comparison of the runs carried out under H_2 shows that there is a gradual removal of D from **DPE** molecules such that approximately half of the original D content of the starting **DPE** is lost after 30 min at 450 °C. This process is partly due to the reaction of benzyl or 1,2-diphenylethyl radicals with H_2 to add H atoms to the mixture of starting materials and products. This dilutes the aliphatic D present in diphenylethane after its hydrogens are mixed with other aliphatic hydrogens, presumably including those of toluene. However, this is not the entire story because there appears to be a net loss of D from the system and this can also be explained by the expulsion of D atoms from the 1,2 diphenylethylradical as discussed above.

The reaction described above was carried out at a lower temperature to allow observation of the exchange process with greater precision. The results are presented in Tables IV and V. In Table IV it is clear that the exchange of D atoms between **DPE** molecules is proceeding, but even after 40 min is some distance from the equilibrium situation reached in Table I. It will be noted that in recovered **DPE**, d_1 molecules accumulate more rapidly than do d_3 molecules despite the fact that at equilibrium (Table I - N_2) they become equal. As the formation of **DPE**-d_1 involves removal of D and replacement with H

whereas **DPE-d_3** requires removal of H and replacement by D, the observed distribution suggests a larger isotopic preference in the replacement process. It is not obvious why this should be so, but the situation is complicated because isotope effects on two reactions are involved.

The deuterium content of the toluene produced from **DPE-1,1-d_2** at 420 °C, presented in Table V, is particularly interesting. The total of d_0 plus d_1 toluene molecules is nearly equal to that of d_2 plus d_3, indicating that roughly half of the toluene arises from d_2 benzyl radicals and half from d_0 benzyl radicals. It is also clear that each of these radicals pick up H atoms in preference to D atoms. At least in the experiment carried out under N_2, the only source of hydrogen would appear to be the **DPE** molecules themselves. Thus it would appear that there is a average isotope effect for the removal of H from **DPE** by benzyl radicals of roughly $k_H/k_D = 4.6$. It is curious that benzyl-d_2 radicals and benzyl-d_0 appear to be showing somewhat different isotope effects, but this could be an artifact of the analysis of the mass spectral data which is complicated in the case of toluene by facile fragmentation. Also, at longer times, significant scrambling within the **DPE** occurs prior to conversion to toluene. Nevertheless, the observed isotope effect is almost certainly real and is consistent with studies by Bockrath who found values of 6.5 to 8.0 for the reaction of benzyl radical with a variety hydrogen atom donors at 170 °C in solution.[5] Comparing the H_2 and N_2 data for toluene shows that there is slightly more D in the toluene from the N_2 runs, but it is not clear whether this comes from H_2 or whether it simply reflects the loss of D from **DPE**. We are attempting to analyze this situation in greater detail. It seems clear that the major source of H atoms in the toluene formed is the **DPE** molecule and, at most, about 10 % comes from H_2.

1,2-Di(phenyl-d_5)ethane. This compound was prepared by reaction of 2-phenylethyl chloride with benzene-$\underline{d}_6$ and $AlCl_3$. As it turned out, aromatic exchange with reaction-generated DCl is quite facile giving 1,2-diphenylethane with more than 5 D atoms. By treating the product with more benzene-d_6, $AlCl_3$ and a trace of D_2O we were able to obtain material which was largely d_{10}. NMR experiments showed no D in aliphatic positions. Preliminary data for the thermolysis of the d_{10} compound at 450 °C is shown in Table VI. The composition of the diphenylethane recovered after thermolysis under N_2 is essentially that of the synthesized material. The data thus strongly suggest that there is very little transfer of hydrogen from aliphatic to aromatic positions. We presume there is a small amount, based on the experiments with d_2 material, but the present experiment is too insensitive to measure it. Because there is no significant amount of d_{11} material, it seems probable that there is little or no transfer of D from aromatic to aliphatic positions. This is confirmed by ^2H NMR which shows that the amount of aliphatic D is undetectably small in the N_2 experiment (<0.1 atom of D per molecule) and barely measurable in the H_2 experiment (0.15 atom of D per molecule).

These results are particularly important in that they rule out termination steps involving aromatic H-atom adducts. In our previous analysis of the overall process for the thermolysis of diphenylethane under D_2,[1] we suggested a scheme in which H- or D-atom adducts transferred H or D atoms to the various benzylic radicals in termination steps. The experiments with $\underline{d}_{10}$ material rule out any significant contribution from such processes. This leaves us without termination steps for the sequence. As it is clear that long chains are not involved (D incorporation does not greatly exceed the amount of conversion to products in D_2 reactions) we need to invoke a

different termination process. The evidence of facile disproportionation of 1,2-diphenylethyl radicals shown in the tetraphenylbutane experiments,[2] suggests that this is the most important termination step in the **DPE** reactions.

SUMMARY AND CONCLUSIONS

What is now known about the reaction of diphenylethane with hydrogen?

The first and second steps in Figure 1 are well precedented and general accepted. They are also supported by our work in that we have shown that the dominant reaction of benzyl radicals is with unreacted **DPE**. The generation of H atoms by the reaction of benzylic radicals with H_2 also is accepted and our work suggests that the 1,2-diphenylethyl radical may be the dominant participant in this process as shown in the fourth reaction in Figure 1.

What now happens to the H atom? Clearly it adds to aromatic rings as evidenced by the incorporation of D when D_2 is used. However, the adducts must be too unstable to survive at concentrations high enough to react with either benzyl or diphenylethyl radicals as shown by the experiments with d_{10} material. Thus when an H atom reacts with an aromatic ring, it simply generates another H atom (or occasionally a 2-phenylethyl radical but this most likely reacts with H_2 to give another H atom). Because the reverse of the fourth reaction is an energetically downhill reaction, it seems likely that most H atoms will simply give back 1,2-diphenylethyl radicals by H-atom extraction from **DPE**. If, however, stilbene is present, another option presents itself, that of the fifth reaction in Figure 1 which also gives a diphenylethyl radical. With disproportionation of 1,2-diphenylethyl radicals included as shown in the third equation in Figure 1, the third and fifth steps constitute a route for disposal of H atoms. Combining the five processes in Figure 1, in proper proportion totals to a stoichiometrically correct result for the conversion of diphenylethane to toluene.

The mechanism would then work as follows. Benzyl radicals are formed and equilibrate with 1,2-diphenylethyl radicals. This process is clearly demonstrated by scrambling, etc. 1,2-diphenylethyl radicals having no exothermic reaction available other than reversible dimerization to a species which is unstable at 450 °C (tetraphenylbutane) or disproportionation, build to relatively high concentrations and disproportionate. When the occasional H atom is formed, it adds reversibly to aromatic rings, extracts H atoms from benzylic positions and reacts with stilbene formed in the disproportionation. At low substrate concentrations, the reaction of radicals with H_2, present at high concentration is favored and relatively little stilbene accumulates.

If this sequence is correct, it would explain the relatively high amounts of deuterium incorporated in **DPE** which is formed as a side reaction in the thermolysis of 2,2,5,5-tetramethyl-3,4-diphenylhexane.[6] We have found that stilbene is formed as a side reaction in thermolysis of this compound. If it is serving as a D-atom scavenger, this would explain not only why **DPE** enriched in D_2 is found, but also why there is relatively little aromatic D incorporation in other products. Considering that we now know that D-atom adducts of phenyl rings do not build up in these systems, it is reasonable to presume that the reaction of D atoms with phenyl rings is somewhat endothermic. This being the case, stilbene may be an effective scavenger of wandering H

(or D) atoms. We are presently trying to design experiments to demonstrate the role of stilbene.

There are a number of potentially important implications of this analysis. It would, for example, suggest that a role of catalyst in promoting cleavage of Ar-R bonds in coal liquefaction and related model studies could be simply to facilitate hydrogenation of species which might otherwise trap H atoms. In coal, the role of H-atom trap would likely be played by various polynuclear aromatic compounds as well as various reaction-produced elimination products. A paper by Bockrath, Schroeder and Keldsen reports an effect of 9-methylanthracene which could be interpreted in this way.[7] A thorough understanding of this phenomenon might lead to a better design for catalysts. We are excited about the relative simplicity and the potential implications of this model.

EXPERIMENTAL

2-Phenylethanol-1,1-$\underline{d}_2$. Methyl phenylacetate (3.5 g, 23.2 mmol) was dissolved in ether to make a ca. 1 M solution and this was added to a 1 M ether solution containing 1 g of $LiAlD_4$ at 25 °C. This was allowed to stir under N_2 for 30 min. This was treated with a saturated solution of NH_4Cl in water and the ether layer separated. The ether layer was dried with anh Na_2SO_4 and the solvent removed by rotary evaporation. ^1H NMR ($CDCl_3$) δ 2.85 (s, 2.0 H), 7.2 (m, 5 H). This was used without further purification.

2-Phenylethyl chloride-1,1-$\underline{d}_2$. The alcohol prepared above (2.0 g, 16 mmol) was treated with 10 mL $SOCl_2$ and 4 mL pyridine and the reaction mixture was stirred at 25 °C for 30 min followed by cautious treatment with about 10 mL water. The resultant mixture was extracted with 50 mL ether. The ether was dried and evaporated as above. This was used without purification in the following reaction.

1,2-Diphenylethane-1,1-$\underline{d}_2$. The crude chloride prepared above (1.4 g, 9.9 mmol) was dissolved in 10 mL of spectrometric grade benzene and this was added to anhydrous aluminum chloride (1.5 g, 11.3 mmol) at 0 °C. The reaction mixture was stirred for 40 min followed by treatment with water and extraction with ether (ca. 75 mL of each). Drying and removal of ether as before gave crude product. This was purified by column chromatography on silica gel in hexane to give 1.02 g of product mp 48-50 °C, ^1H NMR ($CDCl_3$) δ 2.91 (s, 2.0 H), 7.2 (m, 10 H). MS gave m/z 184, 93, 91.

1,2-Di(phenyl-$\underline{d}_5$)ethane. 2-Phenylethyl chloride (2.0 g, 14.2 mmol) was dissolved in benzene-$\underline{d}_6$ (5 g, 58 mmol) and the solution added to aluminum chloride (2.8 g, 22.6 mmol) following the procedure described above. The crude product was redissolved in fresh benzene-$\underline{d}_6$ and treated with fresh $AlCl_3$ and a drop of D_2O. Work-up and purification as described above gave product mp 48-50 °C. ^1H NMR ($CDCl_3$) δ 2.92 (s), aromatic resonance was less than 5% of the aliphatic resonance. MS gave m/z 192, 96.

REFERENCES

1. Guthrie, R. D.; Shi, B.; Sharipov, R.; Davis, B. H. Prepr., Div. Fuel Chem., Am. Chem. Soc. **1993**, 38, 526-533.

2. Ramakrishnan, S.; Guthrie, R. D.; Shi, B.; Davis, B. H. Prepr., Div. Fuel Chem., Am. Chem. Soc. **1993**, 38, this volume.

3. Vernon, L. W. FUEL **1980**, 59, 102-106.

4. (a) Poutsma, M. L.; Dyer, C. W. J. Org. Chem. **1982**, 42, 4903. (b) Buchanan, A. C.; Dunstan, T. S. J.; Douglas, E. C.; Poutsma, M. L. J. Am. Chem. Soc. **1986**, 108, 7703. (d) Bockrath, B.; Bittner, D.; McGrew, J. J. Am. Chem. Soc. **1984**, 106, 135-138. (e) McMillen, D. G.; Malhotra, R.; Chang, S.-J.; Ogier, W. C.; Nigenda, S. E.; Fleming, R. H. FUEL, **1987**, 66, 1611-1620.

5. Bockrath, B. C.; Bittner, E. W.; Marecic, T. C. J. Org. Chem. **1986**, 51, 15-19.

6. Sharipov, R.; Guthrie, R. D.; Shi, B.; Davis, B. H. Prepr.,Div. Fuel Chem., Am. Chem. Soc. **1993**, 38, this volume.

7. Bockrath, B. C.; Schroeder, K. T.; Keldsen, G. L. Proceedings of the 1985 International Conference on Coal Science, 28 -31 October, 1985, Sydney, N. S. W., Pergamon Press, 1985, pp 83-86.

ACKNOWLEDGEMENT

The authors wish to thank the United States Department of Energy, Pittsburgh for a grant: DE-FG22-91-PC9129 supporting this work.

Table I. Composition of 1,2-Diphenylethane after Thermolysis of 1,2-Diphenylethans-1,1-d_2 at 450 °C.

	d_0	d_1	d_2	d_3	d_4
<5 min (H_2)	1.75	1.49	96.4	0.12	0.15
10 min (H_2)	26.3	29.8	32.3	11.3	0.4
30 min (H_2)	29.7	41.7	22.5	5.5	0.6
<5 min (N_2)	1.6	0.7	97.5	0.1	0.1
15 min (N_2)	5.6	22.9	46.3	21.7	3.0
30 min (N_2)	7.8	23.8	42.2	22.4	3.8

Table II. Toluene from Thermolysis of Diphenylethane-1,1-d_2 at 450 °C.

	d_0	d_1	d_2	d_3
<5 min (H_2)	44.3	4.8	50.1	0.8
10 min (H_2)	34.0	32.5	30.1	3.4
30 min (H_2)	42.1	43.3	13.1	1.5
<5 min (N_2)	---	---	---	---
15 min (N_2)	26.2	30.1	35.9	7.8
30 min (N_2)	25.4	31.9	35.3	7.5

Table III. NMR Analysis of Recovered Diphenylethane from Thermolysis of 1,2-Diphenylethane-1,1-$\underline{d}_2$.

Conditions	D atoms/molecule aliphatic	aromatic
H_2 (10 min)	1.96	<0.09
H_2 (30 min)	1.19	<0.09
N_2 (15 min)	1.98	0.09
N_2 (30 min)	1.84	0.16

Table IV. Composition of 1,2-Diphenylethane after Thermolysis of 1,2-Diphenylethane-1,1-d_2 at 420 °C.

	d_0	d_1	d_2	d_3	d_4
10 min (H_2)	0.4	12.0	86.0	1.5	0.17
20 min (H_2)	2.3	19.6	73.6	4.2	0.18
40 min (H_2)	5.9	29.5	59.5	5.0	0.20
10 min (N_2)	1.6	4.8	91.6	2.0	0.1
20 min (N_2)	1.6	11.1	83.1	4.0	0.1
40 min (N_2)	2.9	16.5	71.6	8.7	0.3

Table V. Toluene from Thermolysis of Diphenylethane-1,1-d_2 at 420 °C.

	d_0	d_1	d_2	d_3
10 min (H_2)	42.8	7.6	46.7	3.0
20 min (H_2)	40.3	12.4	42.8	4.5
40 min (H_2)	41.2	16.3	39.4	3.0
10 min (N_2)	37.3	10.9	45.0	6.7
20 min (N_2)	37.1	13.2	41.9	7.8
40 min (N_2)	33.5	17.1	39.6	9.8

Table VI. Thermolysis of 1,2-Di(phenyl-$\underline{d}_5$)ethane (DPE) at 450° C (20 min).

Composition	Reaction under N_2		Reaction under H_2	
	DPE %	Toluene %	DPE %	Toluene %
$\underline{d}_{10}$	55	--	2	--
$\underline{d}_9$	22	--	8.5	--
$\underline{d}_8$	8	--	17.4	--
$\underline{d}_7$	3.2	--	22.3	--
$\underline{d}_6$	2.6	--	20.2	--
$\underline{d}_5$	2.2	59	13.2	11.4
$\underline{d}_4$	--	32	7.0	31.8
$\underline{d}_3$	--	9	3.6	33.8
$\underline{d}_2$	--	--	2.4	13.8
$\underline{d}_1$	--	--	1.8	6.8
$\underline{d}_0$	--	--	1.5	2.4

Figure 1

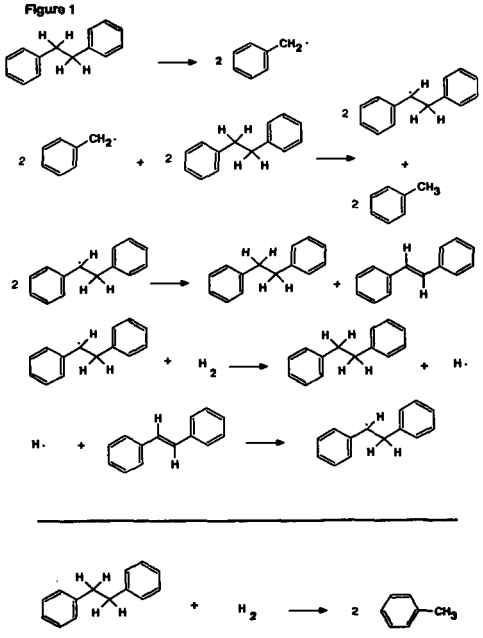

REACTION OF 1,2,3,4-TETRAPHENYLBUTANE WITH D_2 AT 400 °C

Shreekumar Ramakrishnan
Robert D. Guthrie
Department of Chemistry
University of Kentucky
Lexington, KY 40506

Buchang Shi
Burtron H. Davis
Kentucky Center for Applied Energy Research
3572 Iron Works Pike, Lexington, KY 40511

Keywords: Radicals, thermolysis, liquefaction

INTRODUCTION

In an earlier preprint,[1] we have described the reaction of diphenylethane, **DPE**, with D_2 at 450 °C to promote D incorporation in both starting **DPE** and reaction products. A previous study by Vernon[2] had suggested that when the reaction is carried out under H_2 with tetralin present, benzyl radicals produced in the thermolysis react with H_2 to give toluene and H-atoms and that the H atoms react with **DPE** to give 2-phenylethyl radicals and benzene. Our earlier results are consistent with this suggestion in that the Vernon process would provoke D incorporation for the reaction under D_2. However, in our experiments, the amount of D in initially formed toluene as well as in benzene and ethylbenzene was substantially less than one atom of D per molecule demanding the conclusion that radicals present also react with **DPE** to give 1,2-diphenylethyl radicals. In fact, the amount of aliphatic deuterium present in unreacted **DPE** was quite similiar to that in the formed toluene. The similarity was then explained by further experiments in which **DPE**-1,1-$\underline{d}_2$ was shown to undergo extensive scrambling under the reaction conditions and that toluene-1,1,1-$\underline{d}_3$ undergoes exchange with **DPE** under the reaction conditions.[3] As this agreed with existing literature which provided a number of examples of exchange of H atoms between benzylic positions,[4] it was clear that it would be difficult to identify the radical primarily responsible for removing D atoms from D_2 because the initial landing sites of D-atoms become obscured by exchange.

Although it seemed reasonable that both benzyl and 1,2-diphenylethyl radicals were capable of carrying out this reaction, the roles played by each were not separable. It seemed likely that the 1,2-diphenylethyl radical being rendered more stable by its "secondary" structure would be less reactive. On the other hand, the equilibrium between the benzyl and diphenylethyl radicals would allow the latter to accumulate in the reaction mixture for the same reason. To establish the 1,2-diphenylethyl radical as a candidate for reaction with D_2 we undertook to produce it by a route which did not also generate benzyl radicals. We thus secured 1,2,3,4-tetraphenylbutane, **TPB**, by a literature preparation,[5] and undertook to study its thermolysis in the presence of D_2.

RESULTS AND DISCUSSION

1,2,3,4-Tetraphenylbutane

TPB underwent thermolytic reaction at 400 °C to give 1,2-diphenylethane, **1**, and stilbene, **2**, as major products. Small amounts of 1,2,3-triphenylpropane, **3**, toluene, **4**, and smaller amounts of benzene, **5**, ethylbenzene, **6**, and styrene, **7**, were observed at high conversions. The product distribution is presented in Table I. It seems clear that the major reaction pathway for thermolysis of TPB is homolysis of the 2,3 bond to give two 1,2-diphenylethyl radicals, **8**, which then react, predominantly, by disproportionation to give **1** and **2**. Compounds **3** and **4** are presumeably formed via homolysis of the 1,2 bond to give benzyl radicals, **9**, and 1,2,3-triphenylprop-1-yl radicals, **10**. Interestingly, the amount of **3** + **4** increases relative to **1** + **2** as the reaction progresses suggesting the possible production of some of **3** and **4** from **1** and **2**. It is clear that the formation of **2** constitutes the only source of hydrogen atoms. Formation of two molecules of **1** from one **TBP** requires that two atoms of H be provided externally unless **2** is formed concurrently. The formation of **3** and **4** also requires a source of H or D.

As the reaction proceeds, the total moles of **1**, **3**, and **4** formed exceeds the moles of **2**. This fact alone, in the absence of other unsaturated products, clearly predicts the consumption of D_2. Products were analyzed for deuterium content by gas chromatography/mass spectrometry (GC/MS) and, indeed, contained substantial amounts of deuterium as detailed in Table II.

Interpretation of GC/MS data obtained for recovered **TPB** is rendered difficult by the fact that the original molecular ion (m/z = 362) fragments readily to give daughter ions at (m/z = 181). However, the pattern of ion intensities in the m/z = 181 region is, within experimental error, identical to that for starting **TPB** suggesting that no deuterium has been incorporated. This is confirmed by ^{2}H NMR experiments which fail to detect the presence of D atoms (upper limit of 5%). In previous experiments with more volatile substrates, we have usually found significant amounts of deuterium in all aromatic compounds present. Apparently the reaction with *D* atoms occurs largely in the gas phase and unreacted liquid **TPB** is protected in this instance by its low vapor pressure.

Most of the deuterium atoms predicted to be present are found in the diphenylethane, **1**, formed. Roughly 50% of the molecules of **1** contain one or more atoms of D. Rough calculation suggests that the amount of D present in **1**, plus small amounts present in other components of the reaction mixture, is sufficient to explain the excess of **1**, **3**, and **4** over **2**. Interestingly, the stilbene present contains a relatively small amount of D. Although we have not yet been able to determine its exact location by NMR, earlier experiments suggest that this amount of *D* is roughly that expected for the aromatic ring exchange reaction associated with D-atom production and D-atom addition to the double bond of **2** would incorporate some D at the vinyl positions after disproportionation.

Thus, it seems clear that one-third to one-half of the 1,2-diphenylethyl radicals produced through scission of the 2,3-bond in **TPB** react with D_2 to give **1-d$_1$** plus a D-atom. The remainder disproportionate to give **1** plus **2**. The D-atoms formed react with all gas-phase aromatic compounds to give ring exchange. We find that these results make it difficult to avoid the conclusion that 1,2-

diphenylethyl radical is a viable partner in the reaction with D_2.

Interestingly, the small amount of toluene, **4**, produced in this reaction contains about the same level of D as does **1**. While we cannot say unequivocally that benzyl radicals also react with D_2 in this system, it seems unlikely that the relatively high levels of D in **4** could arise through D-atom removal from **1**.

As might be expected, triphenylpropane, **3**, formed also contains D. The amount is somewhat less, for reasons that are not clearly understood. One possible explanation is that the 1,2,3-triphenylprop-1-yl radical remains in the liquid phase and therefore has less ready access to gaseous D_2.

The processes which seem likely to explain the data described are given in equations 1,2,3 and 4 in Figure 1. It will be noted that the only termination steps suggested are those in eq 2. It is clear that the amount of **2** produced is insufficient to account for all of the necessary termination processes. Whether termination reactions involving $R^{\cdot}$ + $D^{\cdot}$ are involved or other processes must be invoked, is not clear at the present time. It will be noted that in runs to high conversion, we do not list 100% of the material balance. This is because a large assortment of minor products are formed, not all of which have been identified.

2,3-Dimethyl-2,3-diphenylbutane

From the results described above as well as those in the following paper in this series, it seemed likely that the reaction with D_2 is general for radicals of a variety of structural types. To this point the radicals studied were either monosubstituted (primary) or disubstituted (secondary). It was thus of interest to extend the scope to tertiary radicals and preliminary experiments have now been carried out with 2,3-dimethyl-2,3-diphenylbutane (bicumyl), **11**. When 11 was subjected to thermolysis at 450 °C under D_2 for 30 min, the products were found to be cumene, **12**, (70%) and 2-phenylpropene, **13**, (30%), the latter clearly arising from disproportionation of 2-phenylprop-2-yl radical (cumyl), **14**. Thus about 40% excess **12** is produced and this presumably is obtaining D from D_2.

GC/MS studies showed that molecules of **12** were 62% d_0, 26% d_1 and 11% d_2. ^1H and ^2H NMR studies show that deuterium is being incorporated at both aliphatic positions in **12**. About 55% of the aliphatic D is at the methine (CH) position and 45% is in the CH_3 groups. This suggests that when cumyl radicals react with D_2, the D atoms produced react to a significant extent at the methylene (CH_2) group in **13**, rather than at aromatic positions as observed with the diphenylethane system. The resultant deuterated cumyl radicals disproportionate and place deuterium at all positions in both **12** and **13**. The sequence of events for the reaction of **11** is shown in Figure 2.

EXPERIMENTAL SECTION

Synthesis of 1,2,3,4-Tetraphenylbutane, TPB. The synthesis was carried out as described in the literature.[5] The product was a white crystalline solid, mp 183 °C. ^1H NMR δ ($CDCl_3$) 2.8 (m, 2 H), 3.1 (m, 4 H), 7.4 (m, 20 H).

Synthesis of 2,3-Dimethyl-2,3-diphenylbutane, 11. This compound was prepared by a literature procedure.[6] The product was sublimed to give white crystals, mp 119 °C. ^1H NMR δ ($CDCl_3$) 1.25 (s, 12 H), 7.10

(m, 10 H).

Thermolysis of 1,2,3,4-Tetraphenylbutane, TPB, and 2,3-Dimethyl-2,3-diphenylbutane, 11, under D2 gas pressure. The experiments with D2 gas were conducted in a reaction bulb with a long capillary neck described earlier.[1] Normally 100 mg of model compound was placed in the reaction vessel. The reaction products were dissolved in 0.6 mL of carbon disulfide analyzed by GC and GC-MS then separated by preparative gas chromatography. Isolated compounds were analyzed by ^{1}H and ^{2}H NMR, mass spectrometry and comparison with authentic samples.

REFERENCES

1. Guthrie, R. D.; Shi, B.; Sharipov, R.; Davis, B. H. Prepr., Div. Fuel Chem., Am. Chem. Soc. **1993**, 38, 526-533.

2. Vernon, L. W. FUEL **1980**, 59, 102-106.

3. Rajagopal, V.; Guthrie, R. D.; Shi, B.; Davis, B. H. Prepr.,Div. Fuel Chem., Am. Chem. Soc. **1993**, 38, this volume.

4. (a) Poutsma, M. L.; Dyer, C. W. J. Org. Chem. **1982**, 42, 4903. (b) Buchanan, A. C.; Dunstan, T. S. J.; Douglas, E. C.; Poutsma, M. L. J. Am. Chem. Soc. **1986**, 108, 7703. (d) Bockrath, B.; Bittner, D.; McGrew, J. J. Am. Chem. Soc. **1984**, 106, 135-138. (e) McMillen, D. G.; Malhotra, R.; Chang, S.-J.; Ogier, W. C.; Nigenda, S. E.; Fleming, R. H. FUEL, **1987**, 66, 1611-1620.

5. Wyman, D. P. J. Org. Chem. **1962**, 27, 3712. See also, Brook, A. G.; Tai, K. N.; Gilman, H. J. Am. Chem. Soc. **1955**, 77, 6219, and Smith, L. I.; Hoehn, H. H. J. Am. Chem. Soc. **1941**, 63, 1184.

6. Bors, D.; Kaufman, M. J.; Streitwieser, A., Jr. J. Am. Chem. Soc. **1985**, 107, 6975-6982.

ACKNOWLEDGEMENT

The authors wish to thank the United States Department of Energy, Pittsburgh for a grant: DE-FG22-91-PC9129 supporting this work.

Table I. Weight % of Products from the Thermolysis of 1,2,3,4-Tetraphenylbutane under D_2 at 400 °C.

	Time (min)				
Compound	5	10	15	20	30
TPB	92	71	41	29	16
1	2.1	16.2	22.6	26.3	33.6
2	3.5	7.4	15.2	12.4	12.7
3	0.2	3.2	3.3	11	9.6
4	<0.1	0.5	1.1	1.6	3.3
5	<0.1	0.2	0.2	--	0.4
6	<0.1	0.1	0.1	--	0.5
7	<0.1	0.1	0.1	--	0.2

Table II. Deuterium Content of Products from Thermolysis of **TPB** under D_2 at 400 °C.

	% of d_n at Time (min)				
Product	5	10	15	20	30
TPB-d_0	>95	>95	>95		>95
TBP-d_1	<5	<5	<5		<5
1-d_0	50.5	49.8	43.8	28.6	29.8
1-d_1	40.6	41.5	44.0	46.2	44.1
1-d_2	8.0	7.8	10.4	20.5	20.7
1-d_3	0.8	0.7	1.5	4.7	4.9
2-d_0	88.0	88.5	83.1	61.6	63.0
2-d_1	11.6	10.7	14.2	29.2	31.0
2-d_2	0.3	0.8	1.9	6.6	6.6
3-d_0	75	74	68		
3-d_1	25	26	32		
4-d_0			43.2	25.6	30.5
4-d_1			46.2	57.7	55.3
4-d_2			8.4	16.7	14.3

Figure 1

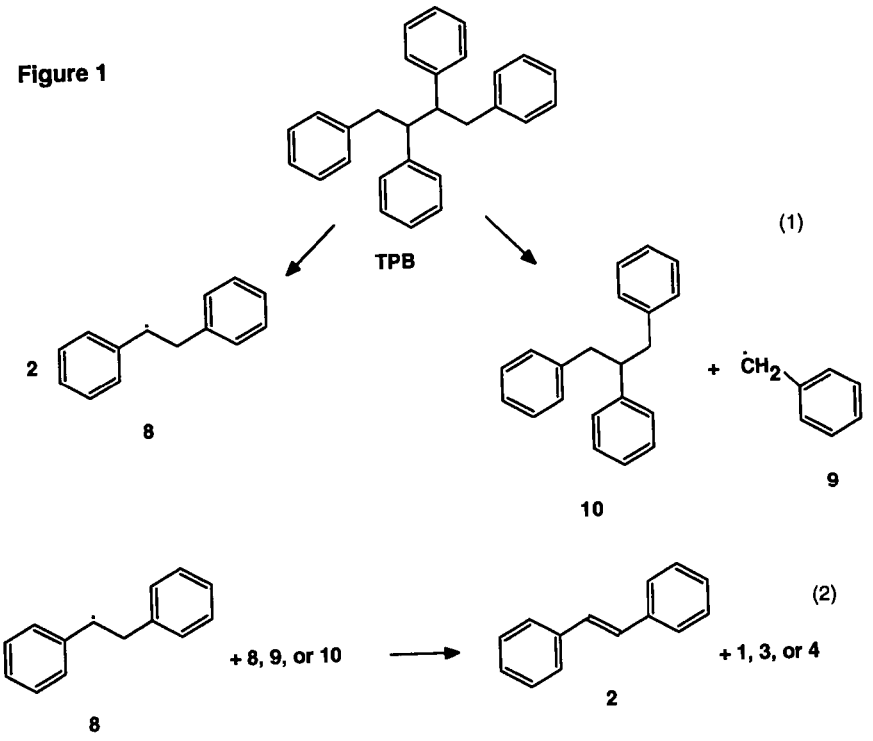
TPB
(1)
2
8
10
9
CH2
(2)
+ 8, 9, or 10
8
2
+ 1, 3, or 4
8, 9, or 10 + D 2
1-d, 3-d, or 4-d + D ·
(3)
D ·
H
R
D
R
+ H ·
(4)

Figure 2

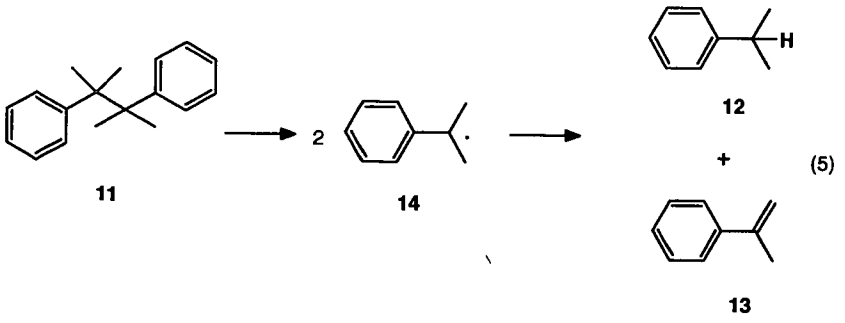

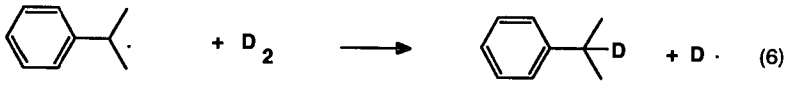

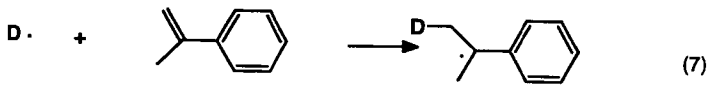

REACTION OF 2,2,5,5-TETRAMETHYL-3,4-DIPHENYLHEXANE WITH D_2 AT 300-350 °C

Rustem Sharipov
Robert D. Guthrie
Department of Chemistry
University of Kentucky
Lexington, KY 40506

Buchang Shi
Burtron H. Davis
Kentucky Center for Applied Energy Research
3572 Iron Works Pike, Lexington, KY 40511

Keywords: radicals, liquefaction, hydrogen atoms

INTRODUCTION

In previous preprints we have described the thermolysis of 1,2-diphenylethane (bibenzyl)[1,2] and 1,2,3,4-tetraphenylbutane under D_2.[3] We have also described preliminary results with 2,3-diphenyl-2,3-dimethylbutane (bicumyl).[3] In these cases the resulting pattern of deuterium incorporation into reaction products and recovered starting materials was interpreted in terms of benzylic radicals reacting with D_2 to produce D atoms which then reacted both to reverse the processes involved in their formation and also to add to unsaturated centers in the molecules present. An important mechanistic consideration for reactions of the compounds listed turned out to be the availability of a disproportionation process as the probable dominant termination step in each case. For both diphenylethane and tetraphenylbutane, a 1,2-diphenylethyl radical is formed which disproportionates to stilbene and diphenylethane. Cumyl radical can similarly give cumene and α-methylstyrene. It was thus of interest to see what might happen in a system where this option was missing. We also wished to explore temperature limitations for the reaction with D_2.

For these and other reasons, we decided to investigate the thermolysis of 2,2,5,5-tetramethyl-3,4-diphenylhexane (**TMDH**) under D_2. This substrate had been synthesized earlier and its thermolysis kinetics studied by Ruchardt.[4] Thermolysis of this compound produced a rich assortment of products suggesting a complex network of reaction steps. The situation was somewhat simpler in the presence of D_2 and led to some interesting mechanistic conclusions as described below.

RESULTS AND DISCUSSION

meso-**TMDH** undergoes thermolysis at 300 °C, and the most abundant product after 30 min is the d,l-isomer (approx. 55 Wt%). Other products are 1-phenyl-2,2-dimethylpropane (neopentylbenzene),**1**, stilbene, **2**, 1-phenyl-2-methylprop-1-ene,**3**, 2,2,4,4-tetramethyl-3-phenylpentane, **4**, 1,2-diphenyl-3,3-dimethylbutane, **5**, 1,1-diphenyl-3,3-dimethylbutane, **6**, and other minor products. Amounts of neopentylbenzene and stilbene in the products mixture suggest the possibility of two paths for isomerization of **TMDH**. First by cleavage of the central C-C bond (as anticipated from the work of Ruchardt[4]) and second by cleavage of the

C-C bond between alpha and beta carbons. On further heating (at 350°C) either in vacuum or under N_2, the mixture of meso- and d,l-**TMDH** is completely converted to the mixture of products indicated above. The distribution of products for the reaction carried out in vacuum is given in Table I.

When the 350 °C reaction of **TMDH** is carried out under D_2, the proportion of neopentylbenzene in the product mixture becomes quite large: 63% as compared to 13% when run in vacuum, strongly suggesting that 1-phenylneopentyl radicals are being intercepted by D_2. It is also significant that while there is no significant amount of 1,2-diphenylethane, **7**, present in the vacuum or N_2 reactions, this product develops in the D_2 reaction. The amount of stilbene, **2**, formed under D_2 is smaller than the amount formed under N_2 and **7** grows in as the reaction proceeds. This suggests the possibility that **7** is formed from **2**. Similarly, 1-phenyl-2-methylpropane, **8**, is formed under D_2 at the expense of **3**. The product **6**, which is likely the rearrangement product of 1,2-diphenyl-3,3-dimethylbutyl radical, is also greatly diminished under D_2. The product distribution for the D_2 reaction is given in Table III. The results are compared graphically in Figures 1 and 2.

Mass spectrometric analysis of the major reaction product, **1**, gives the results shown in Table II. Results of ^1H and ^2H NMR for this compound are shown in Table IV. It will be noted that even after 5 min, at which time about 35% of the mixture of meso- and d,l-**11** remains, the amount of deuterium in the 1-position of neopentylbenzene is 50% of one atom of D. The distribution does not change significantly with time. We see little alternative to the conclusion that the phenylneopentyl radical formed from dissociation of **TMDH** removes D from D_2 making this the clearest example so far of the reaction $R^{\cdot} + D_2 \rightarrow R\text{-}D + D^{\cdot}$. We have no information to indicate the source of the H atoms which are required to produce the **1**-d_0 produced. The most likely possibility is a termination process involving H atom removal from the tert-butyl radicals which would seem likely side products to the formation of **2**, **5**, and **7**. The presence of compound **4** in substantial amounts in the vacuum and N_2 reactions indicate the presence of tert-butyl radicals and demonstrate the viability of a coupling with phenylneopentyl radicals. As H atom removal is an expected companion reaction to coupling, this makes the tert-butyl radical a logical source of H.

It is interesting that the level of incorporation of D in the aromatic rings of **1** and recovered **TMDH** is much lower relative to the aliphatic D when compared with results from the diphenylethane system. This suggests the possibility that D atoms are being scavenged by species present in the reaction mixture. A logical possibility is the 2-methylpropene expected as a product of the reaction of tert-butyl radicals with H-atom acceptors and the observance of D in the methyl groups of **4**, but not of **1** confirms this suggestion. Reaction of D atoms with stilbene, **2**, and **3** also seemed likely. This would seem to explain the unexpectedly high levels of D found in diphenylethane, **7**, both at aromatic and aliphatic positions as shown in Table V. The possibility that stilbene can serve as an efficient scavenger for D atoms is presently under investigation. The stilbene present in the D_2 reaction was also found to contain high levels of D.

The various observations described above lead us to suggest the reaction scheme shown in Figure 3 as representing the most significant processes involved in the thermolysis of **TMDH** under D_2. In addition to demonstrating the viability of a number of processes having basic importance in the understanding of hydroliquefaction chemistry, this

study documents the uncatalyzed reaction of an organic compound with D_2 at an unusually low temperature.

EXPERIMENTAL SECTION

Equipment and Procedures. These have been described elsewhere.[1,2,3]

Synthesis of 1-phenyl-2,2-dimethylpropanol. This material was synthesized by a literature method.[5] The product was a colorless liquid, 17.5 g (53.7 %) with pleasant honey smell. ^{1}H NMR (CDCl3), : 0.93 (9H,s, t-Bu); 2.65 (1H, -OH); 4.35 (1H,s, C-H); 7.3 (5H,s, -Ph).

1-Bromo-1-phenyl-2,2-dimethylpropane. This material was prepared by a literature synthesis.[6] ^{1}H NMR (CDCl3), : 1.1 (9H,s, t-Bu); 4.9 (1H,s,C-H); 7.3-7.5 (5H,m, -Ph).

meso-2,2,5,5-Tetramethyl-3,4-diphenylhexane,(1) This material was prepared by a literature synthesis.[4] For use in the reaction with D2 it was twice recrystallized from acetic acid, then twice from petroleum ether - stout prisms, m.p. 181 °C , ^{1}H NMR (CDCl3), : 0.53 (18H,s, t-Bu); 3.05 (2H,d,-CH-); 7.15-7.3,7.5 (10H,m, -Ph).

Thermolysis of 2,2,5,5-tetramethyl-3,4-diphenylhexane. Thermolysis of the model compound was conducted in sealed evacuated 4 mL Pyrex ampules in a silicone oil bath at 300-320 °C and in a sand bath at 330-400 °C. For each experiment 5 mg of compound was used. After pyrolysis, reaction mixture was analyzed by GC-MS.

Thermolysis of 2,2,5,5-tetramethyl-3,4-diphenylhexane under D2 gas pressure. The experiments with D2 gas were conducted in a reaction bulb with a long capillary neck described earlier.[1] Normally 100 mg of model compound was placed in the reaction vessel. The reaction products were dissolved in 0.6 mL of carbon disulfide analyzed by GC and GC-MS then separated by preparative gas chromatography. Isolated compounds were analyzed by ^{1}H and ^{2}H NMR, mass spectrometry and, where possible, comparison with authentic samples. Details of identification will be presented elsewhere.

REFERENCES

1. Guthrie, R. D.; Shi, B.; Sharipov, R.; Davis, B. H. Prepr., Div. Fuel Chem., Am. Chem. Soc. **1993**, 38, 526-533.

2. Rajagopal, V.; Guthrie, R. D.; Shi, B.; Davis, B. H. Prepr.,Div. Fuel Chem., Am. Chem. Soc. **1993**, 38, this volume.

3. Ramakrishnan, S.; Guthrie, R. D.; Shi, B.; Davis, B. H. Prepr.,Div. Fuel Chem., Am. Chem. Soc. **1993**, 38, this volume.

4. (a) Hellmann, G.; Beckhaus, H.-D.; Ruchardt, C. Chemishe Berichte **1979**, 112, pp.1808-1834. (b) Beckhaus, H.-D.; Ruchardt, C. Chemishe Berichte **1977**, 110, pp. 878-895. (c) Kratt, G.; Beckhaus, H.-D.; Lindner, H. J.; Ruchardt, C. Chemishe Berichte **1983**, 116, pp. 3265-3263. (d) Kratt, G.; Beckhaus, H.-D.; H. J.; Ruchardt, C. Chemishe Berichte **1984**, 117, pp. 1748-1764.

5. Conant, J.B.; Blatt, A.T. J. Am. Chem. Soc. **1928**, 50, p.554.

6. Masada, H.; Murotani, Y. Bull. Chem. Soc. Jpn. **1980**, 53, 1181.

ACKNOWLEDGEMENT

The authors wish to thank the United States Department of Energy, Pittsburgh for a grant: DE-FG22-91-PC9129 supporting this work.

Table I. Product Distribution from the Reaction of meso-TMDH at 350 °C in Vacuum.

Product	Time(min)				
	5	10	20	30	40
meso-TMDH	30.0	10.0	5.3	2.2	1.3
d,l-TMDH	37.0	16.0	6.1	2.6	2.0
1	3.7	12.7	13.6	13.2	12.9
2	4.5	11.7	12.1	12.6	12.6
3	3.5	13.0	13.3	13.6	13.8
4	3.8	11.4	12.4	12.6	12.6
5	3.4	7.0	9.1	6.1	2.0
6	6.3	10.3	12.4	8.3	3.1
7	--	--	--	--	--
8	--	--	--	--	--

Table II. Deuterium Distribution in 1-Phenyl-2,2-dimethylpropane Formed from Thermolysis of TMDH under D_2 at 350 °C (from GC/MS)

Time (min)	d_0	d_1	d_2	d_3
5	38	51	11	--
10	39	46	13	2
20	40	47	11	2
30	31	51	15	3
40	33	50	15	2

Table III. Product Distribution from the Reaction of meso-**TMDH** at 350 °C under D_2.

Product	Time(min)				
	5	10	20	30	40
meso-**TMDH**	16.7	2.3	1.0	0.5	0.3
d,l-**TMDH**	18.6	9.1	4.5	2.9	1.7
1	38.7	58.4	64.7	62.9	62.7
2	7.7	7.6	7.0	6.7	7.4
3	3.0	2.9	3.3	3.7	3.5
4	4.1	3.9	3.8	3.4	3.6
5	2.1	2.2	2.0	2.3	2.5
6	--	--	--	--	--
7	0.7	3.2	4.4	5.5	6.9
8	1.3	2.4	2.6	3.9	4.1

Table IV. Deuterium Incorporation in 1-Phenyl-2,2-dimethylpropane Formed from Thermolysis of TMDH under D_2 at 350 °C.

Time (min)	D/molecule (GC/MS)	D/molecule (NMR)	Aliphatic D (1-position)	Aromatic D
5	0.73	0.86	0.53	0.33
10	0.78	0.82	0.52	0.30
20	0.74			
30	0.89			
40	0.87	0.86	0.55	0.31

Table V. Deuterium Incorporation in 1,2-Diphenylethane Formed from Thermolysis of TMDH under D_2 at 350 °C.

Time (min)	D/molecule[a] (GC/MS)	D/molecule (NMR)	Aliphatic D	Aromatic D
5	2.02	2.04	0.44	1.60
10	1.95	1.98	0.67	1.31
20	2.6			
30	3.2			
40	3.3	3.37	1.55	1.82

[a] Because the amount of DPE formed was small, it was difficult to get reliable data. A good mass spectral analysis was produced only in the 20 min run. The distribution for this run was d_0 = 22%, d_1 = 32%, d_2 = 28%, d_3 = 13%, d_4 = 4%. The 30 and 40 min runs showed comparable distributions, but the experimental error was judged to be rather large.

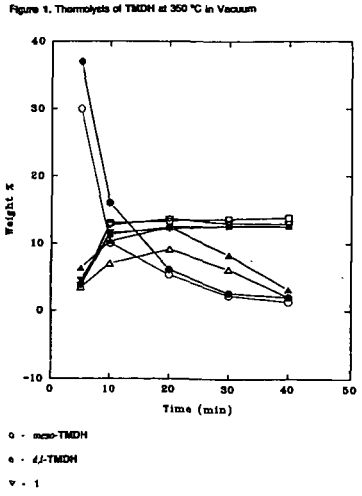

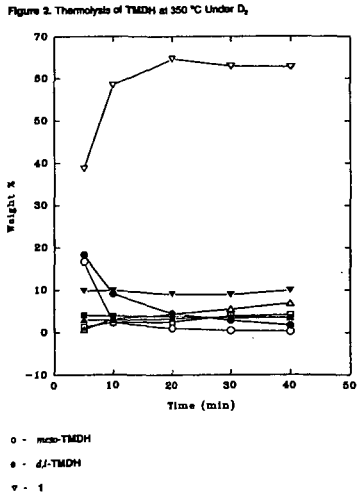

Figure 3

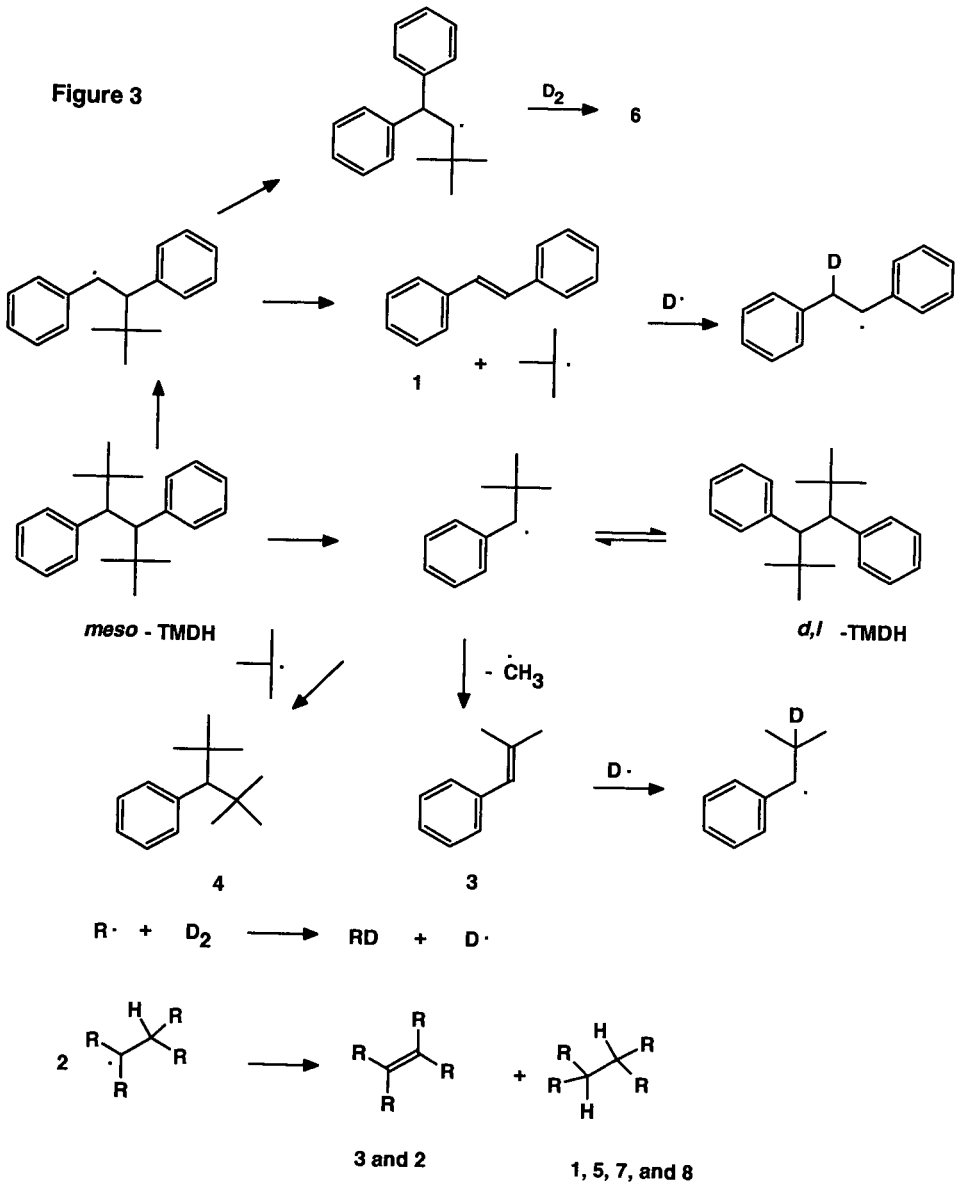

A MECHANISM FOR SULFUR-SPECIFIC BACTERIAL DESULFURIZATION

Edwin S. Olson, Daniel C. Stanley, and John R. Gallagher

Energy & Environmental Research Center
University of North Dakota
Grand Forks, ND 58201-9018

ABSTRACT

The desulfurization of dibenzothiophene by *Rhodococcus rhodochrous* IGTS8 was recently demonstrated to result in formation of 2-hydroxybiphenyl or of 2,2′-dihydroxybiphenyl, depending on whether growth or nongrowth conditions are used in the desulfurization experiments. The key intermediate in the bacterial degradation under nongrowth conditions is 2′-hydroxybiphenyl-2-sulfinic acid (or the corresponding cyclic sultine), which is the immediate precursor of 2-hydroxybiphenyl. Addition of either dibenzothiophene or the sulfinic acid (sultine) to pregrown cells that are using ethanol-d_6 resulted in the formation of only unlabeled 2-hydroxybiphenyl. Therefore, formation of the carbon–hydrogen bond that accompanies cleavage of the carbon–sulfur bond of the sulfinic acid was demonstrated not to require hydrogen transfer from a reducing cofactor. A mechanism consistent with proton incorporation at the ipso carbon is proposed.

Key Words: bacterial desulfurization, sulfur-specific degradation

INTRODUCTION

Because of their potential commercial use in removing sulfur from high-sulfur coals and sour crude oil, microbial systems that desulfurize organosulfur compounds have been intensively studied for several years. Some organisms utilize a catabolic pathway that results in excision of the sulfur from dibenzothiophene (DBT). Intermediates corresponding to this thiophenic-ring scission (4S) pathway have been isolated and characterized (1). Recent results obtained in feeding the various intermediates to *Rhodococcus* IGTS8 elucidated two pathways for the thiophenic scission of DBT (2). Under nongrowth conditions, the DBT is oxidized to 2′-hydroxybiphenyl-2-sulfinate **1** via the DBT 5-oxide (or the corresponding cyclic sultine ester form), and the sulfinate is subsequently cleaved to 2-hydroxybiphenyl **2** (Scheme 1). Under growth conditions, very little of the 2′-hydroxybiphenyl-2-sulfinate is converted to 2-hydroxybiphenyl, and instead most is oxidized to 2′-hydroxybiphenyl-2-sulfonate **3** (or the corresponding sultone), and 2,2′-dihydroxybiphenyl **4** is the major product. The oxidation of the sulfinate to the sulfonate occurs spontaneously (nonenzymatically) in aqueous buffer exposed to air. Further understanding of the details of the enzymes and mechanisms of the various steps in the pathways is needed.

The desulfurization of 2′-hydroxybiphenyl-2-sulfinate to 2-hydroxybiphenyl, which occurs in the last step of the *Rhodococcus* degradation of DBT under nongrowth conditions, involves replacement of the carbon-sulfur bond by a carbon-hydrogen bond. Thus the carbon appears in a reduced state in the final product, but the oxidation state of the sulfur resulting from the last step is not known with certainty. Only sulfate was found in the culture medium (2), but initially formed sulfite could have been converted to sulfate in a subsequent reaction. To elucidate the mechanism for sulfur cleavage of the sulfinate intermediate, a labeling experiment was needed to determine whether the hydrogen that is added to the carbon is

derived from a reducing cofactor, such as NADH or NADPH, or instead from a hydrogen ion derived from water.

Since ethanol is an excellent energy source for the *Rhodococcus* bacterium, deuterium-enriched ethanol was used to generate in vivo the deuterated reducing cofactor (NADH-d) that might be postulated to be involved in the carbon reduction. The 2-hydroxybiphenyl produced in this reaction was examined by mass spectrometry (MS) to determine whether a significant amount of 2-hydroxybiphenyl-2′-d was formed via a mechanism involving an addition of deuterium from the reducing cofactor. The results of the experiment can then be used to infer what kind of redox reactions occur during the last reaction of the desulfurization.

RESULTS AND DISCUSSION

Two sulfur-containing substrates (DBT and the intermediate sultine) were utilized in the desulfurization experiments with ethanol-d_6 as the energy (or potential reduction equivalent) source as well as carbon source for the cells. As expected, both substrates were converted by the bacterium *Rhodococcus rhodocrous* (ATCC #53968) to 2-hydroxybiphenyl. Gas chromatography/mass spectrometry (GC/MS) analysis of the products showed that the 2-hydroxybiphenyl produced from both substrates contained no deuterated product.

Since 2-hydroxybiphenyl-2′-d was not formed in the *Rhodococcus* desulfurization reaction of 2′-hydroxybiphenyl-2-sulfinic acid in the presence of ethanol-d_6, where reducing cofactors would have been enriched in deuterium, the mechanism of carbon–sulfur bond cleavage in the final reaction is unlikely to have occurred via transfer of a hydrogen from a reducing cofactor (as a hydride equivalent) to the ipso carbon. Thus a mechanism involving simple displacement of hydride for the sulfonyl group or a mechanism involving addition of hydride to a positive carbon intermediate cannot be used in modeling this reaction.

Thus, addition of a proton to the ipso carbon is demanded by the results, but a simple hydrolysis mechanism is not likely here. The 2′-hydroxybiphenyl-2-sulfinic acid is not hydrolytically cleaved to the aromatic compound plus sulfite in the buffered culture media. Such a cleavage of the carbon–sulfur bond would require a very strong acidic site on the enzyme that could protonate the sulfinic acid ipso ring carbon. Any very acidic site would be unstable in the buffered media. We can find no precedent for this type of enzyme activity.

The reactions of dibenzothiophenes and sulfinic acids with basic reagents have been investigated, but these studies do not appear to be applicable to the enzyme-catalyzed degradation to hydroxybiphenyl. Attack of nucleophilic oxygen has been reported to occur at the ring carbon of biphenylsulfinic acid at high temperatures in the presence of crown ether, not at the sulfur atom, resulting in the formation of 2-hydroxybiphenyl rather than biphenyl (3).

An oxidase-catalysis mechanism for the transformation of 2′-hydroxybiphenyl-2-sulfinic acid to 2-hydroxybiphenyl is the more likely alternative. The biological cleavage of aliphatic sulfoxides is known to occur via hydroxyl attack (4). Several oxidative enzymes degrade aromatics by one-electron oxidation followed by attack of hydroxide. This mechanism can produce the same intermediate, however, and the mechanism is essentially equivalent to the hydroxyl radical attack. Addition of hydroxyl radical to the arylsulfinate anion, as shown in Scheme 2, or its equivalent would result in the sulfonate radical anion 5 with substantial

anionic character in the ring. An alternative to the hydroxyl radical attack on the sulfinate sulfur is the adjacent phenol group forming the phenoxy radical **7** that adds to the sulfinate group to give the analogous cyclic sulfonate (sultone) radical anion **8**. Subsequent protonation of the ipso ring carbon of either radical anion intermediate would form protonated sulfonate radical intermediates **6** or **9**. In the addition reactions of the analogous sulfur ylids (sulfenes) in a hydroxylic medium, hydrogen adds to the carbon, and oxygen to the sulfur to form the sulfonate (5).

The intermediate radicals formed by this addition across the arylsulfinyl system resemble those implicated in the ipso substitution reaction investigated by Motherwell (6). In that reaction, a similar radical intermediate was formed by addition of an adjacent radical to the ipso carbon, and the sulfonyl radical was then eliminated. A similar displacement of the sulfonyl radical is proposed here in the microbial oxidase mechanism.

Depending on whether the final step involves gain or loss of an electron, either sulfite or sulfate will be formed. Or possibly disproportionation will give a mixture of the sulfite and sulfate forms. If an aryl sulfate ester forms, then an arylsulfatase enzyme may be required to complete the transformation to sulfate.

As shown in Scheme I, the reductive sulfur cleavage actually involves use of a sulfinate electron to "internally reduce" the ring carbon, the sulfinyl sulfur being converted to a sulfonate group in the process. Thus reducing cofactors are not required, as demanded by the lack of deuterium incorporation. Attack at the sulfur must be prevented in the enzyme that forms the 2-hydroxybiphenyl, or else the sulfur is simply oxidized, as it is in the formation of DBT 5-oxide and DBT 5,5-dioxide from DBT or in the formation of 2'-hydroxybiphenyl-2-sulfonic acid from 2'-hydroxybiphenyl-2-sulfinic acid.

REFERENCES

1. Olson, E.S.; Stanley, D.C.; Gallagher, J.R. *Energy Fuels* **1993**, *7*, 159-164.

2. Gallagher, J.R.; Olson, E.S.; Stanley, D.C. *FEMS Microbiol. Lett.* **1993**, *107*, 31-36.

3. Squires, T.G.; Venier, C.G.; Hodgson, B.A.; Chang, L.W. *J. Org. Chem.* **1981**, *46*, 2373-2376.

4. Klein, S.M.; Cohen, G.; Cederbaum, A.I. *Biochem.* **1981**, *20*, 6006-6012.

5. Langendries, R.F.J.; de Schryver, F.C. *Tetrahedron Lett.* **1972**, 4781.

6. Motherwell, W.B.; Pennell, A.M.K.; Ujjainwalla, F.J. *J. Chem. Soc., Chem. Commun.* **1991**, 877.

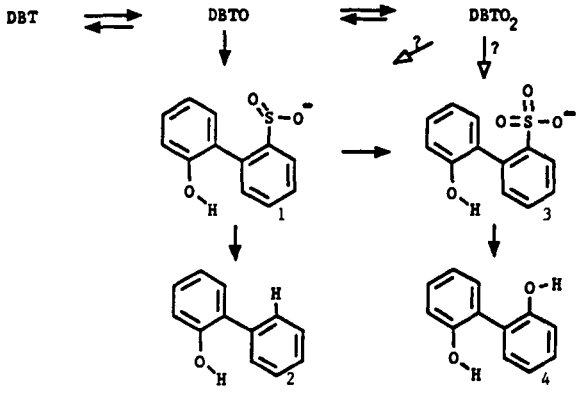

Scheme 1. Desulfurization Pathways in *Rhodoccus*.

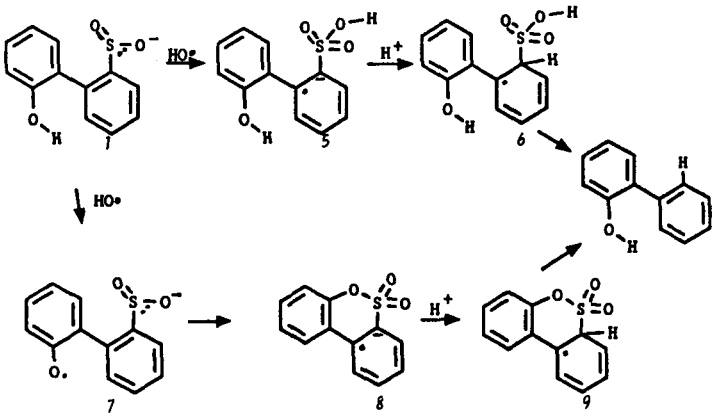

Scheme 2. Mechanism of Sulfinate Desulfurization.

HYDROGENATION/DEHYDROGENATION REACTIONS OF ROSIN

Richard P. Dutta and Harold H. Schobert
Fuel Science Program, Pennsylvania State University, University Park, Pa 16802.

Keywords: Liquefaction, Rosin, Hydrogenation-dehydrogenation

INTRODUCTION

One of the most important factors controlling the high-temperature thermal stability of jet fuels is their chemical composition [1]. At high temperatures, pyrolysis reactions of certain components in the fuel become significant and result in the formation of gums and insoluble solids. These materials will reduce heat transfer efficiency, degrade valve performance and deposit solids in the fuel pipeline and in fuel combustor nozzles. Cycloalkanes are desirable components of advanced jet fuels because of their high thermal stability. If cycloalkanes can be produced in high yield by direct coal liquefaction, downstream processing of the product would be reduced. In order to obtain a high quality product, selection of a good feedstock is vital. Therefore, if cycloalkanes are to be produced from coal, it is reasonable to choose coals with high concentrations of these compounds already present or structures that could be easily converted to cycloalkanes

The higher plants contain terpenoid-based substances commonly known as resins. These resins may polymerize on exposure to air, and the polymerization in situ in dead plants gives rise to the resinite maceral found in almost all coals. Several recent publications on resins in coal [2-6] have indicated that the resins are composed of oxidatively polymerized sesquiterpenoids and diterpenoids. Certain coals from Canada, the Far East and Australia contain diterpenoid resinites in high concentration. Western United States coals contain sesquiterpenoid resinite in high concentration (up to 5wt%) [5,6]. This paper will deal with modeling of diterpenoid resinite reactions, although the results obtained do have some relevance to sesquiterpenoid resinites. If the behavior of resinite under liquefaction conditions can be determined and understood, a highly efficient liquefaction system can be developed. Coals with high resinite concentration can be liquefied, and the cycloparaffinic products from resinite can be extracted into the oil fraction, producing liquids that are thermally stable and could be a source of high-quality jet fuel. However, because resinite is a complex mixture of polymerized compounds, it is advisable to study model compounds. This makes analysis of products easier and evaluation of reaction pathways less complicated. Rosin is commercially available and contains 90% diterpenoids (isomeric with abietic acid). In a sense, rosin is a simplified analogue of certain resinite structures and its hydrogenation-dehydrogenation behavior should give an insight into resinite liquefaction.

Because of the dwindling supply of petroleum and the possible environmental effects of fossil fuel conversion, alternative fuel sources have been sought. Biomass has emerged as a possible alternative to produce liquid fuels and chemicals. The environmental effects of the conversion of biomass should be less than those of fossil fuels. With careful process development and investigation into the chemistry of biomass conversion, the use of this renewable energy source should be realized. Tall oil is a by-product of the Kraft wood-pulping process. It contains fatty acids and rosin acids in approximately equal proportions. The use of tall oil to produce liquid fuels has been discussed in the literature [7,8] although the chemistry of the hydrocracking of the rosin acids has not been addressed. To maximize efficiency of a process to produce fuel components from tall oil or rosin, it is necessary to investigate the hydrocracking behavior of the rosin acids.

This paper will discuss the aromatisation/cracking/isomerisation reactions of rosin compounds with various catalysts. The relevance of these reactions to jet fuel production and biomass conversion will be discussed.

EXPERIMENTAL

Rosin was hydrogenated under different conditions with $NiMo/Al_2O_3$, Ni-Y zeolite and ammonium tetrathiomolybdate. All reactions were carried out in 25ml capacity microautoclave

reactors with cold hydrogen pressure of 7MPa. The reactors were brought to the desired temperature using a preheated sandbath. The products were analysed by GC/MS using a HP5890A GC with 5971A mass selective detector and quantified using heptadecane as an external standard.

RESULTS AND DISCUSSION

Figure 1 shows the concentration of reaction products and how they vary with temperature. At 350°C the major products of reaction are tricyclic compounds, e.g. norabietatriene. This compound is formed by decarboxylation and dehydrogenation of abietic acid (a major component of rosin). Norabietatriene is further dehydrogenated to tetrahydroretene and retene. At this low temperature, only a small amount of retene is formed. Cracking of the 3-ring compounds is minimal, with only C_4-benzene and isopropyltetralin being formed in large concentration.

At 400°C the concentration of norabietatriene increases with increasing dehydrogenation/decarboxylation of abietic acid. This increase also yields an increase in tetrahydroretene and retene in the reaction products. The concentration of alkylbenzenes triples in the products at the higher temperature. This can be accounted for by cracking of the saturated ring of isopropyltetralin seen at 350°C. The concentration of naphthalenes has not increased. This is because the temperature is not yet high enough for major cracking of the 3-ring compounds. In theory, cracking of norabietatriene will occur at the saturated terminal ring, as in hydrogenated phenanthrene, giving naphthalenes [9,10]. This does not occur at 400°C.

At 450°C naphthalenes and benzenes are now being formed. These naphthalenes are cracking products of norabietatriene, tetrahydroretene, and other partially saturated 3-ring compounds. It is unlikely that the fully aromatic retene has cracked. It is widely held that all hydrocracking reactions go in two stages: first, hydrogenation of the terminal ring and then cracking of the saturated ring [10]. Figure 1 shows the concentration of norabietatriene and tetrahydroretene decreasing after 400°C. This is in line with the thoughts that it is these compounds that are cracking to benzenes and naphthalenes, and not retene, which continues to increase.

If we interpret the chromatograms purely from the point of view of wanting to produce a good quality jet fuel, it appears that hydrocracking of the tricyclic compounds is the route to take. Naphthalenes and benzenes are produced by cracking of the diterpenes in rosin. These compounds can form the "backbone" for subsequent hydrogenation to produce desirable cycloalkanes and tetralins. Unfortunately these cracking reactions occur at high temperatures, which is accompanied by increasing dehydrogenation of the cycloparaffinic diterpenoids. In a sense, we are destroying the major property of these compounds that they were selected for — their cycloparaffinic nature. The fully aromatic retene seen in large concentration at 450°C will give rise to solid deposits in thermally stressed jet fuel. The reaction at 500°C has almost totally cracked the 3-ring compounds in rosin to naphthalenes and benzenes. Cleavage of side chains has also occured. This may seem a good reaction if jet fuel is to be produced, but the amount of dehydrogenation makes the feasibility of this reaction being of any use small. Continuing work may prove otherwise; i.e., is it possible to re-hydrogenate the aromatic compounds to compounds that are desirable and can be hydrocracked? It is likely that in going to such a high temperature, we are simply "going backwards to go forwards".

Figure 2a shows how the concentrations of the products vary with reaction time for the non-catalytic run. It can be seen that cracking does not occur to a great extent until after 30 minutes. This is simultaneous with the disappearance of norabietatriene and tetrahydroretene. The concentration of retene continues to increase even as the concentration of naphthalenes increases from 0.4-3.6 mg/ml. This is further evidence that retene does not crack, although its concentration may be kept down due the fact that tetrahydroretene is being hydrocracked. To produce thermally stable cycloalkanes from diterpenoid structures, it is necessary to hydrocrack the 3-ring compounds to naphthalenes and benzenes. This needs a high temperature which also promotes dehydrogenation of cycloparaffinic compounds to unwanted fully aromatic compounds. Therefore, a two stage reaction is envisaged: 1) A high temperature cracking reaction to yield a 'backbone' of naphthalenes and benzenes. This means a reaction temperature of at least 450°C, and maybe as

high as 500°C, and a reaction time of at least 45 minutes. 2) A low temperature hydrogenation stage. The naphthalenes and benzenes from stage 1 would be catalytically hydrogenated to cycloalkanes and tetralins. The final products should fall into the jet fuel boiling range, yielding a highly thermally stable fuel.

In order to establish the optimum conditions for a temperature-staged catalytic hydrogenation, the product distribution of rosin hydrogenation was investigated using three catalysts: $NiMo/Al_2O_3$, Ni-Y(zeolite), and ammonium tetrathiomolybdate (ATTM).

Figure 3 shows a histogram of the product distribution of rosin hydrogenation with various catalysts (reaction temperature 400°C, reaction time 60 min.). All three of the catalysts caused a major reduction in the concentration of retene. ATTM did not crack the tricyclic compounds in rosin. In fact, it can be seen that the non-catalytic run produced more benzenes than the run with ATTM. This can be explained by the formation of dehydroabietane in the ATTM experiment. This compound is more stable than norabietatriene, due to the methyl-group substitution of the carboxyl group. Therefore, dehydroabietane does not crack and shows less tendency to dehydrogenate. Because of the low hydrocracking effectiveness of ATTM it was decided not to continue with this catalyst in this investigation. Supported NiMo shows good hydrocracking effectiveness and the Ni-Y catalyst shows an even greater cracking capability. This preliminary investigation into catalytic reactions of rosin led into a more detailed look at how product distribution would vary with time. This would help in determining the best temperature program for the two-stage reaction postulated previously.

Figure 2b shows the product distribution vs time for rosin hydrogenation with NiMo at 450°C. Three major points arise from this graph: 1) From 5-60 minutes, there is no overall increase in retene, but after 20 minutes, methylphenanthrene is formed by dehydrogenation/ dealkylation of terahydroretene. 2) The major cracking reactions occur after 10 minutes. Secondary cracking of naphthalenes to benzenes occurs after 20 minutes. This can be seen by the increase in concentration of benzenes after 20 minutes but naphthalenes show a 'slowing down' of formation. 3) After 40 minutes there is a maximum in the benzenes concentration. This could be explained two ways—formation of gases or coking of the catalyst. The appearance of methylphenanthrene tends to support the latter explanation but dealkylation would lead to hydrocarbon gas formation.

1-Methyl-4-isopropylbenzene (p-cymene) reaches a maximum in concentration at 40 minutes. Toluene increases slowly throughout the reaction times. The isopropyl group is quite stable but will be cleaved after 40 minutes at 450°C. This could also explain the decrease in benzenes concentration seen in Figure 2b. This is due to C_2-C_3 hydrocarbon gases being produced by cleavage of side chains. Isopropyltetralin reaches a maximum at approximately 30 minutes. The disappearance of isopropyltetralin is simultaneous with the increase in concentration of methylindene. This is due to dealkylation/isomerisation of isopropyltetralin.

As mentioned in the introduction, this work does have some application to sesquiterpenoid resinite. The proposed pathway of dealkylation to tetralin would probably occur in sesquiterpenoid structures. The isomerisation reaction could probably be controlled by tailoring the reaction temperature, and the possibility of producing tetralin is good.

Figure 2c shows the product distribution of rosin hydrogenation vs time with Ni-Y catalyst at 450°C. It can be seen that after 10 minutes of reaction, the tricyclic compounds in rosin have almost totally been cracked. Benzenes, naphthalenes and indenes are produced in high concentration and continue to increase up to 60 minutes of reaction. Isopropylteralin is completely dealkylated and isomerized after 60 minutes. The isomerisation reaction seems to be the major cause of loss of isopropyltetralin. This was observed with the simultaneous increase of dihydromethylindene. p-Cymene is dealkylated to toluene after 10 minutes of reaction.

In order to find a relationship between the cracking of tricyclic compounds and the appearance of mono and bicyclic compounds, a plot of the ratio of 1+2 ring to 3-ring compounds is shown in Figure 4. It can be seen that Ni-Y is the most effective hydrocracking catalyst. The maximum at 20 minutes is probably due to secondary cracking of side chains producing gases or coke formation on the catalyst. This would cause a decrease in the calculated ratio. This result also suggests a reverse-temperature-stage-program would be effective in this situation. Most of the

cracking of 3-ring compounds has taken place in the first 20 minutes at 450°C. Therefore, to continue at this high temperature would give no effective increase in the components desired for a high-quality jet fuel, and would cause excess gas formation and an increase in aromaticity.

From the above results, reaction pathways have been proposed (Scheme 1 and 2). Scheme 1 shows the dehydrogenation pathway of abietic acid in rosin. Scheme 2 deals with the possible route of cracking and isomerisation of the 3-ring compounds.

CONCLUSIONS

Diterpenoid compounds can be successfully hydrogenated and cracked to cycloalkanes and hydroaromatics using supported NiMo and Ni-Y catalysts. With careful tailoring of the process temperature and time of reaction, high quality distillate could be obtained. A reverse temperature-staged reaction with optimum conditions chosen from the plots of product distribution could yield maximum concentration of cycloalkanes and hydronaphthalenes. Fully aromatic compounds would be kept to a minimum. Diterpenoids are the most common resins in the geosphere. As well as appearing in some coal resinites, they can be found as ambers or as modern pine resins, e.g. rosin. Their chemical properties can be used in developing high quality fuels, either by direct hydrocracking or as a blending additive in a coal liquefaction process. Some of the reactions occuring in rosin hydrocracking, e.g. dealkylation and isomerisation of substituted tetralins, could be useful in determining the best way to study the liquefaction behavior of sesquiterpenoid resinites, e.g. as found in some Utah coals.

ACKNOWLEDGMENT.

This project was supported by the U.S. Department of Energy, Pittsburgh Energy Technology Center, and the Air Force WL/Aero Propulsion and Power Directorate, Wright-Patterson AFB.

REFERENCES

[1] Song, C.; Hatcher, P.G. *Prepr. Pap.-Am. Chem. Soc., Div. Pet. Chem.* 1992, **37**(2), 529.
[2] Simoneit, B.R.T., Grimalt, J.O., Wang, T.G., Cox, R.E., Hatcher, P.G. and Nissenbaum, A., *Organic Geochemistry*, 1988, **13**, 677.
[3] Wilson, M.A., Collin, P.J., Vassallo, A.M., Russel, N.J. *J. Org. Geochem.* 1986, **7**, 161.
[4] Hatcher, P.G., Breger, I.A., Dennis, L.W., Maciel, G.E. Prepr. Pap.-*Am. Chem. Soc., Div. Fuel. Chem.* 1982, **27**, 172.
[5] Meuzelaar, H.L. , Huai, H., Lo, R., and Dworzanski, J., *Fuel Process Tech.* 1991, **28**, 119.
[6] Crelling, J.C., Pugmire, R.J., Meuzelaar, H.L., McClennen, W.H., Huai, H., and Karas, J., *Energy Fuels*, 1991, **5**, 688.
[7] Sharma, R.K. and Bakhshi, N.N. *Can. J. Chem. Eng.* 1991, **69**, 1071.
[8] Sharma, R.K. and Bakhshi, N.N. *Can. J. Chem. Eng.* 1991, **69**, 1082.
[9] Wu, W.L. and Haynes, H.W. Jr. *ACS Symposium Series*; Washington D.C. 1975, **20**, 65.
[10] Lemberton, J.L. and Guisnet, M. *Appl. Cat.* 1984, **13**, 181.

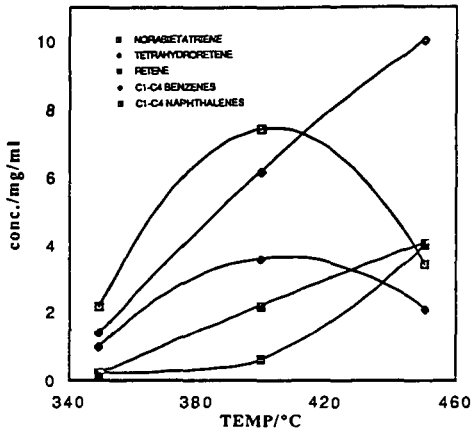

Fig.1 Concentration vs temp:no catalyst

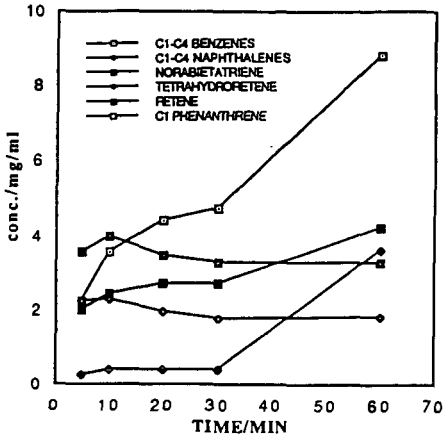

Fig.2a Concentration vs time:no catalyst

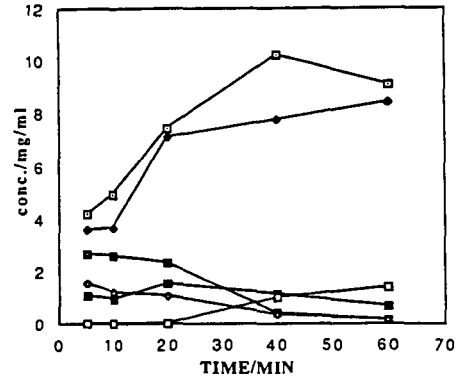

Fig.2b Concentration vs time:NiMo

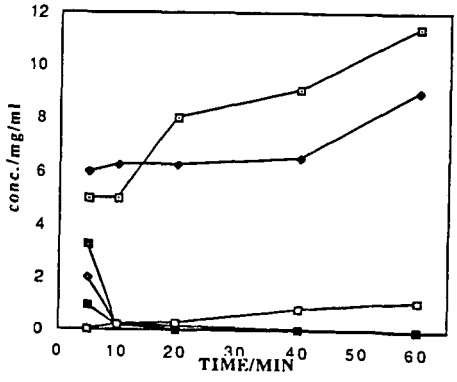

Fig.2c Concentration vs time:Ni-Y

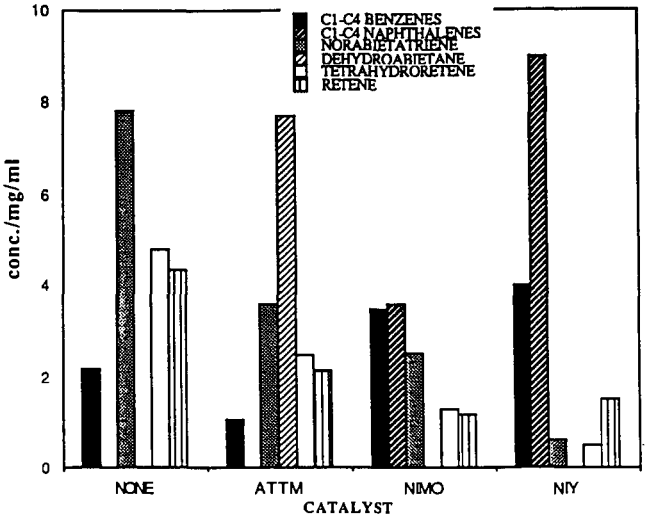

Fig.3 Concentration vs catalyst : 400°C

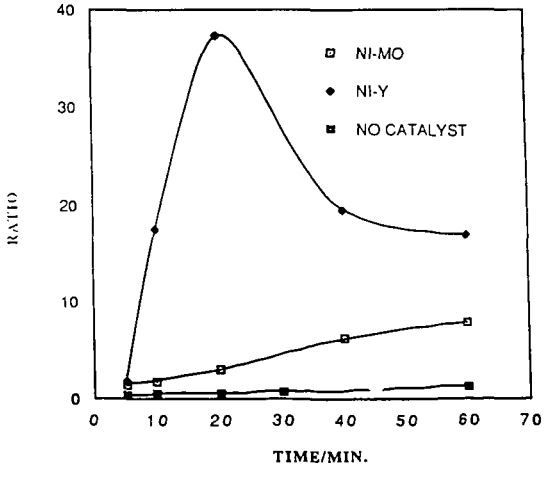

Fig.4 1+2 ring/3-ring compounds vs time

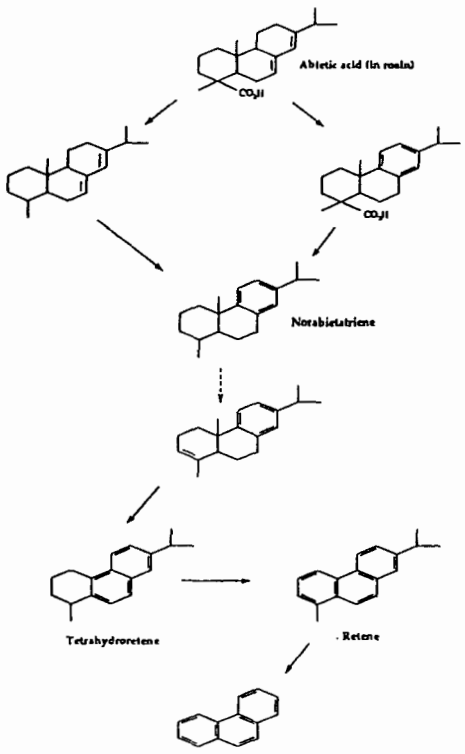

Scheme 1. Dehydrogenation of rosin

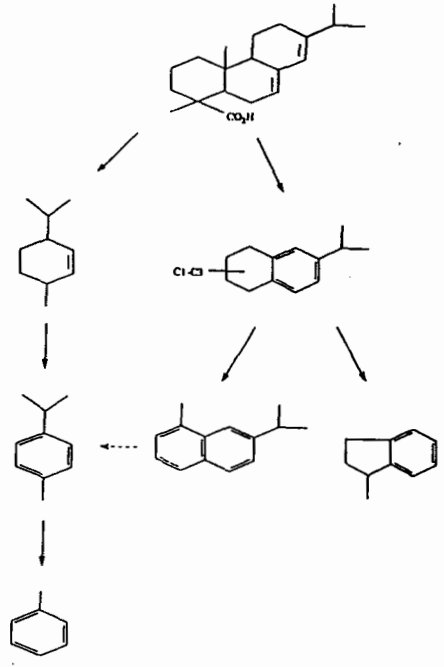

Scheme 2. Cracking/isomerisation of rosin